

# **Circuit Formation in the Striatum in Health and Disease**

Noorya Yasmin Ahmed

April 2023

A thesis submitted for the degree of Doctor of Philosophy  
of The Australian National University



**Australian  
National  
University**

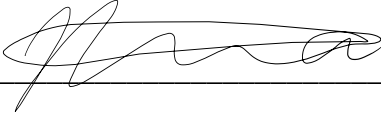
Eccles Institute of Neuroscience,  
John Curtin School of Medical Research

© Copyright by Noorya Yasmin Ahmed, 2023

All Rights Reserved

## **Statement of Originality**

I hereby state that the work presented in this thesis is my own, unless otherwise stated. Details of contributions and collaborations are detailed throughout the thesis and in Appendix D.



---

Noorya Yasmin Ahmed

## **Acknowledgements**

There are many people I must thank for their support throughout the course of my PhD, both professionally and personally.

First and foremost, to my supervisor and mentor Dr Nathalie Dehorter, words cannot express how much I have enjoyed being a student under your supervision, nor how grateful I am to you. Your endless passion and enthusiasm for science and discovery alongside your steadfast encouragement have pushed me through some of the most difficult parts of this PhD. Thank you for all the support and opportunities you have given me.

To my advisory panel: Professor John Bekkers, Assistant Professor Isabel del Pino, and Dr Assistant Professor Robin Broersen. Thank you for your invaluable advice, teachings, and support over the course of this PhD. I have learnt a great deal from each of you and am grateful to have had such a wonderful panel.

I would also like to thank our collaborators and those who have contributed to this research. Firstly, thank you to Assistant Professor Da Mi, Associate Professor Riccardo Natoli, Associate Professor Jean Wen, Dr Ulrike Schumann, and Ema Liu for the collaboration that formed the beginning of our most recent paper. Thank you to Professor Silvia Arber for the use of the Er81 antibody, and to Professor Greg Stuart for the mice used to generate the *Pet-cre* colonies.

To the Dehorter Lab, members past and present, thank you all for your passion, collaboration, ideas, and friendship.

To Shaam, thank you for being such a wonderful friend and bringing me back to reality when I started to lose focus and motivation. Your enthusiasm for science is infectious, and I hope you never lose it. You'll always be welcome at my house for rice salad.

To Nathan, it's been such a brilliant journey going through honours and into our PhDs these last five years. I'm so glad I got to do it alongside you, and I will really miss your presence down the hall, across from me, and behind me in the lab. You have a wonderful analytical mind, and amazing ideas, I can't wait to see what you will do in life.

To Rhys Knowles, thank you for your friendship and support. You have always made me laugh and enjoy being at the lab, even when it was difficult to be there. Talking science with you was always fun. I know you will make a brilliant doctor, and I am excited to see where your future takes you. I'm going to miss our Enigma runs and the weirdness that too much chocolate and sugar brings out in you.

To Becky, you have been a beacon of positivity since day one, and I'm somewhat glad to see that our efforts to make you more cynical haven't really worked. I'm so excited to continue this research journey alongside you in Brisbane. Thank you for being such a rock during my writing this thesis; for your edits and also for reminding me that I would eventually get it done.

To Alex and Yovina, thank you for teaching me so much throughout my honours and PhD, and for all your advice and help over the years. To Yumeng, thank you for all your hard work kickstarting the *Cntnap2* project, along with Yovina.

To my students: Yilan, Melissa, Lochie, and Anna, thank you for your hard work on the projects I gave you and for your contributions to this research.

To all of the members of the Eccles Institute of Neuroscience, it has been my absolute delight to be a part of this community and to know each and every one of you. Thank you for all of the wonderful scientific (and non-scientific) conversations we have all had over the years, I look forward to seeing the paths we all take in life.

To my beautiful friends: Jess, Arti, Kiran, Punna, and Maha, girls, I could not have done this without you all. Thank you for always listening, and always being there for me. Jess and Arti, I am honestly so lucky to have gone through this PhD with the two of you so nearby me.

To my family, I cannot thank you enough for your love and support. To my sister Fatima and my brother Hassan, you were always there to keep me sane and to listen to all of my gossip and stories. You are both brilliant and I look forward to seeing your futures bloom before you.

Finally to my Mum and Dad. You have supported me in whatever I have wanted to do from day one, and I am so privileged and grateful for that. Thank you for giving me this life to be able to work in a field that I am passionate about, and for teaching me how to value the parts of life that really matter. And thank you for your encouragement and love throughout this journey.

“With opportunity the world is very interesting.”

*Beatrix Potter, Mycologist*

## Abstract

Developing circuits form in a highly specific manner, reliant on a number of steps including proliferation, differentiation, and synapse formation. However, developmental connection specificity is still poorly understood, particularly in subcortical structures such as the striatum, which represents a fundamental processing hub in the brain, as we explore in chapter one. Since developing striatal circuitry is vastly susceptible to alterations in genetic programming, any perturbations in network configuration can last into adulthood, and underlie the pathogenesis of a number of disorders, including autism spectrum disorder (ASD). In this thesis we hypothesised that certain cell populations critically shape the formation of functional striatal circuits, such that manipulating their genetic identity will cause abnormal wiring and network activity.

In chapter two, we aimed to describe how genetic regulation of developing striatal interneuron circuitry is vital for maintaining developmental trajectory. We show that both cholinergic interneurons (CINs) and parvalbumin positive inhibitory interneurons (PV-INs) express the *ETV1/Er81* transcription factor, which has a key role in regulating cell identity and activity. In the absence of *Er81*, we discovered developmental changes to striatal interneuron morphology, electrophysiology, and connectivity, which impacts striatal function and associated behaviour.

In the third chapter, we demonstrated how striatal circuitry is highly dependent on neuromodulatory inputs. Very little is known about serotonergic inputs to the striatum and how their specific targeting is regulated during development, as well as how this innervation is important for behaviour. We found that *Er81* is expressed in serotonergic neurons in the dorsal raphe nucleus, and is a key regulator of neuromodulatory signalling. We show that the absence of *Er81* alters serotonergic cell function and raphe-striatal innervation, as well as motor and anxiety-like behaviour.

Striatal circuitry is susceptible to reshaping following altered genetic programming, which is reminiscent of many neuropathological disorders. As very little is known about the contribution of interneurons to ASD, in chapter four we investigated how these cells are impacted in the *Cntnap2* knockout mouse model of ASD. We followed their maturation across embryonic and early postnatal stages and found increased cell proliferation and apoptosis, as well as further molecular and functional changes specifically to cholinergic interneurons. This unveils some of the mechanisms underlying the shift in the developmental trajectory of striatal interneurons, which greatly contribute to ASD pathogenesis.

Together, we have found that striatal interneuron development is a highly intricate and regulated process; and show for the first time that deviations from typical genetic programming cascades and developmental trajectory cause the reshaping of striatal circuitry, leading to subsequent functional and behavioural alterations. This is especially pertinent in neuropathological disorders such as ASD, where perturbations to network formation and the excitation-inhibition balance are hallmarks of the disorder.

## Table of Contents

Statement of Originality .....	i
Acknowledgements .....	ii
Abstract .....	iv
Table of Contents .....	vi
Table of Figures .....	viii
Chapter 1: Introduction .....	1
1.1 Genetic and Activity-Dependent Mechanisms Regulating Development.....	1
1.2 Regulation of the Excitation and Inhibition Balance in the Brain.....	12
1.3 The Impact of Neuromodulatory Control on Circuit Function.....	14
1.4 The Striatum .....	15
Chapter 2: Molecular Regulation of the Function and Connectivity of Developing Striatal Circuits .....	23
2.1 Preamble .....	23
2.2 Er81 is Expressed in Striatal Interneuron Populations .....	27
2.3 Er81 Regulates the Morpho-Functional Properties and Circuit Integration of Cholinergic Interneurons.....	29
2.4 Er81 is not Implicated in the Proliferation and Migration of MGE-derived Interneurons.....	37
2.5 Er81 Regulates the Excitability of Parvalbumin and Cholinergic Interneurons .....	39
2.6 Lhx6+ Interneuron Connectivity is Not Dependent on Er81 Expression.....	46
2.7 Discussion.....	59
Chapter 3: Diversity in Serotonergic Modulation of the Striatum in Response to Early Genetic Insult.....	64
3.1 Preamble .....	64
3.2 Er81 is expressed in serotonergic neurons .....	70
3.3 <i>Er81</i> Ablation Causes Behavioural Alterations in Male and Female Mice .....	72
3.4 Long Range Serotonergic Innervation of the Striatum.....	76
3.5 Sex-Specific Alterations to the Functional Properties of Serotonergic Neurons .....	78
3.6 The ablation of Er81 alters serotonergic cell numbers .....	83
3.7 Discussion.....	85
Chapter 4: Developmental Deficits of MGE-Derived Interneurons in a Mouse Model of Autism Spectrum Disorder.....	90
4.1 Preamble .....	90
4.2 <i>Cntnap2</i> expression maps to enrichment in striatal interneuron populations.....	97
4.3 The proliferative and apoptotic trajectory of the Lhx6 cell population is shifted ...	100
4.4 Alterations to Striatal Cholinergic Interneuron Number .....	103
4.5 Changes to the Molecular Profile of Striatal Cholinergic Interneurons .....	106

4.6	Striatal Interneuron Morphology is Altered in ASD .....	109
4.7	Electrophysiological alterations .....	111
4.8	Discussion.....	119
Chapter 5: Discussion.....		128
Methods.....		138
6.1	Mice .....	138
6.2	Tissue Collection .....	140
6.3	Stereo-seq .....	141
6.4	RNA Analysis.....	141
6.5	Immunohistochemical Staining .....	144
6.6	Image Acquisition and Analysis.....	147
6.7	Electrophysiology Recordings.....	153
6.8	Electrophysiology analysis .....	156
6.9	Behavioural Tests .....	160
6.10	Statistical Analysis .....	161
Appendices .....		163
Appendix A: Literature Review (Ahmed et al. 2019).....		163
Appendix B: Research Paper (Ahmed et al. 2021) .....		164
Appendix C: Research Paper (Ahmed et al. 2023) .....		165
Appendix D: Details of contributions .....		166
Appendix E: Electrophysiology Result Tables .....		167
Appendix F: Fiji/ImageJ Macros.....		171
References .....		173



## Table of Figures

Figure 1.1: Mechanisms of Development .....	3
Figure 1.2: Connection formation and maintenance during development .....	11
Figure 1.3: The excitation-inhibition balance in the brain is maintained at various levels.....	13
Figure 1.4: The striatum and its circuitry .....	17
Figure 1.5: Connections in the striatal microcircuit .....	21
Figure 2.1: Developmental roles of Er81 in neuronal circuitry .....	25
Figure 2.2: Er81 expression levels differ across striatal interneuron subtypes .....	28
Figure 2.3: Cholinergic interneuron morphology is dependent on <i>Er81</i> expression .....	31
Figure 2.4: Inputs to cholinergic interneurons are rewired in the absence of <i>Er81</i> .....	33
Figure 2.5: Cholinergic output is shifted in the absence of <i>Er81</i> .....	35
Figure 2.6: <i>Er81</i> ablation does not alter the composition of the Lhx6+ interneuron population .....	38
Figure 2.7: CIN evoked activity is decreased in the mature <i>Lhx6</i> -dependent knockout of <i>Er81</i> .....	40
Figure 2.8: Putative Fast Spiking Interneurons are less excitable in the absence of <i>Er81</i> during early development .....	42
Figure 2.9: Developmental versus mature ablation of Er81 from PV-INs produces different electrophysiological phenotypes .....	44
Figure 2.10: <i>Er81</i> ablation may strengthen the connectivity between PV-INs and CINs in the mature striatum.....	47
Figure 2.11: <i>Er81</i> ablation does not severely affect the synaptic connectivity of Lhx6+ interneurons .....	51
Figure 2.12: Gap junction connectivity is decreased in the absence of <i>Er81</i> .....	55
Figure 2.13: Evidence of characteristic developmental activity in striatal interneurons .....	58
Figure 3.1: Serotonergic projections throughout the brain .....	65
Figure 3.2: Overlap of Striatum- and Serotonin-mediated behaviours .....	66
Figure 3.3: Serotonergic innervation of the striatum. ....	68
Figure 3.4: Er81 expression in Pet-positive neurons in the Dorsal Raphe Nucleus.....	71
Figure 3.5: Female behaviour in an open field is altered following <i>Er81</i> ablation.....	73
Figure 3.6: Anxiety and locomotive behaviour are shifted following <i>Er81</i> ablation .....	75
Figure 3.7: Impacts on serotonergic innervation of the striatum .....	77
Figure 3.8: Serotonergic neuron electrophysiological properties .....	79
Figure 3.9: Excitatory inputs to serotonergic neurons in the DRN .....	82
Figure 3.10: Evidence of developmental role for Er81 in Pet+ serotonergic neurons .....	84
Figure 3.11: Summary of findings in females and males following <i>Er81</i> ablation from serotonergic neurons .....	85
Figure 4.1: The role of the striatum in autism spectrum disorder. ....	92

Figure 4.2: <i>Cntnap2</i> mRNA levels are enriched in cholinergic interneurons in the adult striatum .....	99
Figure 4.3: MGE-derived interneuron cell numbers at early stages of development .....	103
Figure 4.4: Specific alterations to the striatal cholinergic interneuron population .....	105
Figure 4.5: Molecular identity of developing striatal Lhx6+ interneurons .....	108
Figure 4.6: Morphological alterations to cholinergic and putative parvalbumin interneurons .....	110
Figure 4.7: Functional alterations in Lhx6+ cholinergic interneurons in the developing striatum .....	114
Figure 4.8: Functional alterations in Lhx6+ putative fast spiking interneurons in the developing striatum.....	116
Figure 4.9: Glutamatergic and GABAergic synaptic inputs onto Lhx6+ GABAergic interneuron in the <i>Cntnap2</i> KO mice.....	118
Figure 4.10: Summary of results .....	121
Figure 5.1: Links between the various levels of the relationship between genetic identity and behaviour.....	130
Figure 1: RNA Analysis Workflow .....	142
Figure 3: Analysis of Neuropil.....	151
Figure 4: Axonal Bouton Reconstruction.....	152
Figure 5: General Dual Patch Stimulus Protocols.....	155
Figure 6: Action potential kinetics measurements. ....	158
Figure 7: Current kinetics measurements.....	159

## List of Common Abbreviations

<i>Abbreviation</i>	<i>Definition</i>
5-HT	Serotonin
ACh	Acetylcholine
AMPA	$\alpha$ -amino-3-hydroxy-5-methyl-4-isoxazolepropionic acid
AP	Action Potential
ASD	Autism Spectrum Disorder
CGE	Caudal Ganglionic Eminence
ChAT	Choline Acetyltransferase
CIN	Cholinergic Interneuron
cKO	Conditional Knockout
CTX	Cortex
DA	Dopamine
DLS	Dorsolateral Striatum
DMS	Dorsomedial Striatum
DNA	Deoxyribonucleic Acid
E	Embryonic day
E/I	Excitation-Inhibition
GABA	$\gamma$ -aminobutyric acid
GDP	Giant Depolarising Potentials
IN	Interneuron
KO	Knockout
LGE	Lateral Ganglionic Eminence
LTD	Long Term Depression
LTP	Long Term Potentiation
MGE	Medial Ganglionic Eminence
mRNA	Messenger Ribonucleic Acid
NMDA	N-Methyl-D-aspartic acid
NPY	Neuropeptide-Y
P	Postnatal day
PLTS	Persistent Low Threshold Spiking
PV	Parvalbumin
PV-IN	Parvalbumin positive Interneuron
RNA	Ribonucleic Acid
SPA	Synchronous Plateau Assemblies
SPN	Spiny Projection Neuron
SST	Somatostatin
STR	Striatum
TAN	Tonically Active Neuron
TH	Tyrosine Hydroxylase
THAL	Thalamus

## **Chapter 1:**

### **Introduction**

One of the greatest questions in neuroscience is how the brain develops from single cells to a vast, highly specific, and functional neuronal network. During the early stages of life, the brain passes through many states, from hyperconnectivity within an overpopulated system to a restricted population of neurons that connect precisely and form circuitry capable of facilitating complex behaviours and higher order processing (Stiles and Jernigan 2010). Throughout this entire process, the brain remains highly plastic, susceptible to both its surroundings and intrinsic gene expression (Kolb and Gibb 2011). We still do not fully understand the mechanisms by which these vast genetic networks control the progression of development, and there is still an element of complexity regarding the interaction between genetic regulation, intrinsic neuronal and brain activity, and resulting alterations in behaviour, including the emergence of neuropathological disorders. Dissecting the genetic networks regulating neuron activity within specific circuits, and subsequently how shifted circuit formation can regulate behaviour is vital for our understanding of brain development and will give insights into both mechanisms of typical development and those underlying pathology.

#### **1.1 Genetic and Activity-Dependent Mechanisms Regulating Development**

Developmental processes are highly regulated, comprising a series of scheduled events that are governed by intrinsic genetic cascades and a dynamic external molecular signalling environment (**Figure 1.1A**) (Fox et al. 2010). Gene expression in the developing brain is tightly regulated, eventuating in a highly specific spatiotemporal map of protein expression across the developing brain that acts to control network formation (Dillman and Cookson 2014). The specific pattern of expression of these molecular factors is reliant on a number of pre- and post-transcriptional mechanisms, including transcription factor mediated control of gene transcription, post-transcriptional control of gene translation, and epigenetic mechanisms (Dillman and Cookson 2014). Furthermore, the influence of activity in conjunction with genetic regulation has been long established, and electrical activity is known to regulate all stages of development, both directly, and via influencing activity-dependent gene expression (Spitzer 2006, Flavell and Greenberg 2008, Kolb and Gibb 2011). The correct progression and timing of developmental events is vital (Dehorter and Del Pino 2020), and the balance and interaction of activity and genetic factors in regulating developmental processes, and subsequent behaviour are still relatively unknown, though it has been suggested that activity-dependent genes are what links cell and circuit activity with behaviour (Yap and Greenberg 2018). Recent studies

have found that several early response genes are upregulated following neuron membrane depolarisation, some of which are associated with neuropsychiatric disorders (Boulting et al. 2021). Similarly, sensory experiences can induce neuronal circuit remodelling, mediated by the expression of specific molecular factors (Cheadle et al. 2020). As such, variations to signalling cascades and fluctuations in activity levels can lead to the malformation and dysfunction of neuronal circuits and can thus result in neurodevelopmental disorders (Marsh et al. 2008, Fleiss et al. 2019), emphasising the importance of understanding these basic mechanisms for uncovering disease aetiology.

### **1.1.1 Embryonic Proliferation**

Cell proliferation occurs during the earliest stages of development to produce neurons that will populate the brain. In the embryonic brain, pools of neural progenitor cells exist in transitory structures (from approximately embryonic day (E)11-E18) lining the major lateral ventricle (Martinez-Cerdeno and Noctor 2018). Some of the major pools are known as the medial, lateral, and caudal ganglionic eminences (MGE, LGE, CGE; **Figure 1.1B**). There are also cortical proliferative zones, which lie dorsal to the ganglionic eminences, and more ventral zones such as the pre-optic area (PoA) and septal epithelium. The ganglionic eminences are known to be neurochemically diverse, with heterogenous combinatorial molecular expression patterns (Flames and Hobert 2009). Thus specific classes of neurons are known to arise from these different regions, as they are already somewhat fate determined. For example, it is known that the majority of cortical and striatal interneurons originate in the MGE (**Figure 1.1B**), whilst striatum-fated projection neurons originate in the LGE (Marin et al. 2000, Butt et al. 2005, Waclaw et al. 2009). Furthermore, proliferative processes are tightly transcriptionally regulated; for example, the expression of the transcriptional coregulator Prdm16 (PR domain containing 16) in the MGE is essential for maintaining proliferative ability and producing the correct number of interneurons (Turrero Garcia et al. 2020). This is one of many genetic factors that function as part of signalling cascades to control proliferation during embryogenesis.

In addition to genetic programs already in place, the surrounding environment in the transient structures also governs neurogenesis. Excitatory neurotransmitter-mediated signalling can regulate proliferation by depolarising progenitor cells via calcium transients, inhibiting DNA synthesis and limiting proliferation in some cases (LoTurco et al. 1995, Liu et al. 2005), whilst doing the opposite and stimulating proliferation in others (Fiszman et al. 1999, Spitzer 2006).

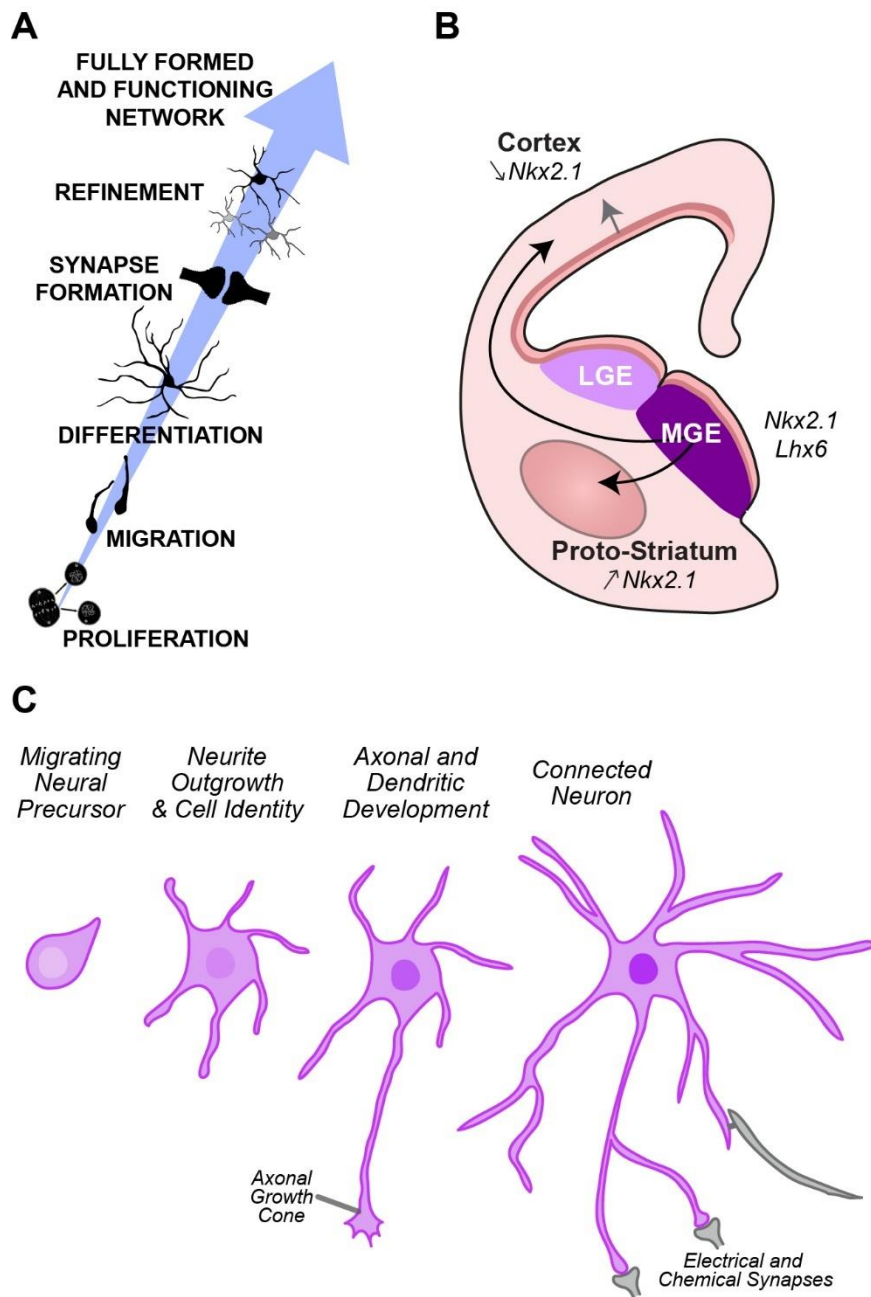


**Figure 1.1: Mechanisms of Development**

**A.** Stages of development occur chronologically, comprising of conserved events necessary for building a functional neuronal network. **B.** Interneurons migrate from the medial ganglionic eminence (MGE), where they are born, to their final positions in the cortex and striatum. Selection of these structures coincides with the cells' upregulation or downregulation of the *Nkx2.1* transcription factor. **C.** Generalised morphological development of a neuron, including dendritic and axonal maturation and connection formation.

### 1.1.2 Migration

Neuronal migration is a highly coordinated process that involves the movement of post-mitotic neurons from their site of origin in proliferative zones to their appropriate position in the brain (Stiles and Jernigan 2010, Martinez-Cerdeno and Noctor 2018). Migration occurs during mid-embryonic stages and is guided by both intrinsic molecular identifiers and extrinsic signalling factors that determine a neuron's target destination. A key example is the tangential migration of interneurons derived in the MGE to their final positions in the cortex and striatum, which generally begins at E12 (Nadarajah et al. 2001, Guo and Anton 2014, Deans et al. 2015). Genetic factor expression in the developing MGE determines both the overall ability of post-mitotic neurons to migrate and also specifies their final location. The LIM homeobox domain 6 (*Lhx6*) transcription factor is expressed in post-mitotic MGE-derived neurons; its expression is necessary for the migration of these cells, and ablating it severely disrupts their localisation across cortical layers (Liodis et al. 2007). *Nkx2.1* is a homeodomain transcription factor that is expressed in MGE-derived progenitor cells and is necessary for correct mature neuron fate (Butt et al. 2008). Postmitotic neurons fated to migrate to the cortex will downregulate *Nkx2.1* expression, whereas those fated for the striatum will maintain their expression of *Nkx2.1* (Nobrega-Pereira and Marin 2009) (**Figure 1.1B**). This is also in conjunction with guidance receptors, whereby *Nkx2.1* expression regulates the expression of neuropilin-2, a receptor for chemorepulsive Semaphorin molecules. Migrating neurons downregulating *Nkx2.1* increase their expression of the Neuropilin 2 receptor and are susceptible to Semaphorin molecules present in the striatum, thus guiding them away and towards the cortex (Nobrega-Pereira and Marin 2009, Villar-Cervino et al. 2015). A reciprocal mechanism also guides striatum-fated cells away from the cortex, as they express Ephrin receptors sensitive to chemorepulsion from the Ephrins expressed in the cortex (Villar-Cervino et al. 2015). In addition to molecular signalling, migratory processes also rely on activity levels. It is known that migrating interneurons are directed to their final position by electrical activity cues (De Marco Garcia et al. 2011, De Marco Garcia et al. 2015). Survivability and circuit integration are also determined by the intrinsic activity levels of migrating neurons (Lim et al. 2018). Together, both intrinsic and environmental molecular signalling alongside intrinsic and environmental electrical activity regulate migration to enable neurons to arrive to the correct position and begin further maturation processes.

### 1.1.3 Differentiation

A diverse population of neurons is a key feature of a neural network, vital for supporting information transmission and higher order processing (Fishell and Rudy 2011, Kepecs and Fishell 2014). Stages of differentiation finely organise molecular, morphological, and functional properties of neurons (Stiles and Jernigan 2010); these processes are fundamentally regulated by complex genetic signalling cascades, however other factors can also play a role. Diversity begins to arise as neurons are born throughout proliferative periods, governed by when and where neurons are generated from progenitors (Kao and Lee 2010, Telley et al. 2019). The temporal specification of neuronal identity is evident in a number of examples. The birthdate of cortical projection neurons in the neocortical proliferative zone dictates their final position within the laminar structure of the cortex, with early-born (E10-13) neurons occupying the deeper layers and late-born (E13-17) neurons migrating past these cells and populating the upper cortical layers (Molyneaux et al. 2007). Similarly, early- and late-born striatum-fated interneurons generated in the MGE are under separate transcriptional regulation; the transcription factors *Mash1* (proneural basic helix-loop-helix transcription factor) and *Dlx1/2* (distal-less homeobox 1/2) regulate the differentiation of early-born and late-born interneurons respectively (Marin et al. 2000).

Precise progenitor location also contributes to differentiation. Combinatorial gene expression in proliferative regions translates to progenitor sub-domains that govern cellular diversity (Flames et al. 2007). For example, the LGE produces both striatal projection neurons and olfactory bulb interneurons; the expression of the LIM homeobox protein *Islet1* (*Isl1*) and the ETS transcription factor *Etv1/Er81* (E-twenty-six translocation variant 1) within separate progenitor subdomains respectively delineate the fate of these two neuronal populations (Stenman et al. 2003).

In addition to molecular mechanisms, environmental influences play a crucial role in neuronal differentiation. The excitability of cells across their developmental trajectory plays a role in determining their identity, particularly in regards to neurotransmitter specification (Spitzer 2006). Characteristics of spontaneous calcium activity in developing neurons regulate their expression of excitatory versus inhibitory neurotransmitters; with shifts towards more excitation following the suppression of activity, and vice-versa (Borodinsky et al. 2004). Thus, as neurons mature, they are susceptible to a number of influences governing their identity, both genetic and activity-dependent. However, some stages of development are more plastic than others; the localisation of cells within the brain is established by early postnatal stages (P0-P2),



and yet other aspects of differentiation, such as the morphological development and refinement of neurons, are changeable until even adulthood (Jabaudon 2017).

#### **1.1.4 Morphological Development**

The morphological development of neurons is essential for the maturation of neural circuitry, and correlates with physiological changes in neurons (Allene et al. 2012). These processes are complex and reliant on coordination between intrinsic and extrinsic signalling to occur correctly. Specific patterns of regulatory and terminal selector genes that identify individual neuron populations, as discussed above, also govern the morphological and functional properties of these neurons (Hobert et al. 2010).

Immature neurons have simple morphology, generally only exhibiting a leading process and a developing axon (Kawauchi 2015). In order to form connections with other neurons, be it locally or distally, the axon must elongate and find its target. Axon elongation is mediated by the growth cone, a structure located at the end of a growing axon, which is highly dynamic and responsive to both intrinsic and extrinsic cues. Extrinsic guidance cues in the surrounding extracellular environment can repel or attract the axonal growth cone via receptors on the growth cone membrane (Tamariz and Varela-Echavarría 2015). In response to these molecular cues, the growth cone and axon will adjust by changing their cytoskeletal organisation to mediate growth and direction of elongation (Tamariz and Varela-Echavarría 2015). In addition, dendritic arborisation must occur at the same time. Neurons have type-specific diverse dendritic properties, and many structures rely on morphological diversity for circuit function (Jan and Jan 2010, Reimann et al. 2017). Dendritic arborisation and organisation have been found to be dependent on a number of factors: transcription factor signalling, receptor activation and activity, extrinsic signalling cues, and local environmental factors are all implicated in regulating the development of the dendritic tree (Jan and Jan 2010). For example, *Dlx1* and *Dlx2* regulate the morphology of cortical interneurons, whereby ablating both of these transcription factors results in impaired neurite outgrowth (Butt et al. 2007). Similarly, enhancing the excitability of olfactory bulb adult-born neurons downregulates the expression of activity-dependent genes regulating neuron morphology, resulting in decreased dendrite complexity and outgrowth (Li et al. 2023). Neuron morphology subsequently contributes to cell connectivity and network formation, dependent on the extent of axonal and dendritic overlap (Reimann et al. 2017).

### 1.1.5 Connection Formation

The formation of connections between cells is a finely-tuned process and is especially reliant on both genetic instructions and cellular activity (West and Greenberg 2011). Studies in a number of brain structures have shown a conserved series of events to establish connections via synchronous activity that begins as early as embryonic stages, before any circuitry is being established, when immature cells display intrinsic waves of spontaneous calcium dependent activity (Kerschensteiner 2014, Luhmann et al. 2016). During late embryonic and perinatal developmental stages, connections between neurons begin to form. During the first two postnatal weeks, a high prevalence of electrical synapses known as gap junctions, that connect adjacent cells physically, occur across the brain (Peinado et al. 1993, Eugenin et al. 2012, Belousov and Fontes 2013) (**Figure 1.2A**). Gap junctions during early development are necessary for future circuit development and maturation, as they are the first form of connectivity between neurons, and thus vital for activity synchronisation. Gap junctions allow for the rapid exchange of signalling ions such as calcium and sodium, and molecules such as cyclic AMP (adenosine monophosphate) and IP3 (inositol triphosphate) (Belousov and Fontes 2013), and are composed of two connexin subunit hemichannels forming an intercellular channel (**Figure 1.2A**). As such, the presence of gap junctions at early stages of development has also been confirmed by increased connexin 36 expression, a protein specific for neuronal gap junctions (Belousov and Fontes 2013). During development, electrically connected small assemblies of neurons exhibit synchronised calcium plateaus that are mediated by voltage gated calcium currents (Crepel et al. 2007). These are referred to as synchronous plateau assemblies (SPAs) and have been documented in the cortex (Allene and Cossart 2010), hippocampus (Allene et al. 2012), and the striatum (Dehorter et al. 2011), and are postulated to be global to the central nervous system (Dehorter et al. 2012).

Later in development, most gap junction connections are removed to be replaced and augmented by chemical synapses, although up to 50% of cells can remain electrically connected. There is a period of overlap in this process, including the uncoupling of gap junction connections, which is regulated by the excitatory neurotransmitter glutamate and the activation of NMDA (N-Methyl-D-aspartic acid) receptors (Arumugam et al. 2005, Belousov and Fontes 2013). This process is important, as it has also been shown that electrical coupling is necessary for chemical synapse formation, and the inhibition of gap junction formation early in development causes a decrease in chemical synapses, which never recovers, even into maturity (Todd et al. 2010). The formation of chemical synapses is reliant on the selection of appropriate

connections and the elimination of inappropriate ones, dependent on existing electrical connections. For example, sister neurons born from the same lineage preferentially form strong electrical coupling with each other, as opposed to with other adjacent cells; this coupling regulates and promotes subsequent chemical synapse formation between these same cells (Yu et al. 2012). In addition, genetic factors control the balanced selectivity of chemical synapse formation between excitatory and inhibitory synapses (Gatto and Broadie 2010, Favuzzi and Rico 2018).

Chemical synapse formation (**Figure 1.2B**) begins with target selection, as synapses are only formed between specific cells. This is mediated in part by extrinsic guidance molecules directing axon elongation (Jabeen and Thirumalai 2018) and is also governed by the diversity of the expression of cell type specific surface receptors to aid in cell identification during connection formation (de Wit and Ghosh 2016). These surface molecules, including Cadherins and Neurexins, support the formation of initial contact, following which the synapse begins to form. Molecular control over presynaptic and postsynaptic specialisation occurs, with synaptic cell adhesion molecules present both presynaptically and postsynaptically, forming trans-synaptic connections (Sudhof 2018). In addition, presynaptic Neurexins and postsynaptic Neuroligins bind and have a role in inducing various synaptic features such as recruiting synaptic vesicles and inducing postsynaptic receptor expression (Jabeen and Thirumalai 2018). Following synapse formation, there is a stage of maturation and refinement (**Figure 1.2C**). Changes to the probability of neurotransmitter release occur to strengthen synapses, and dendritic spines begin to form (Jabeen and Thirumalai 2018). Chemically connected networks continue to generate synchronous calcium waves of activity, known as giant depolarising potentials (GDPs). These are the first synapse driven circuit activities, and have been observed in a number of structures *in vitro* (Kasyanov et al. 2004, Mohajerani and Cherubini 2006, Dehorter et al. 2011). GDPs are mediated by depolarising glutamatergic and GABAergic ( $\gamma$ -Aminobutyric acid, an inhibitory neurotransmitter) currents (Dehorter et al. 2012), and are necessary for further circuit formation as they strengthen synaptic connections (Griguoli and Cherubini 2017). This developmental activity; *i.e.* calcium plateaus followed by GDPs, are purely for the purpose of facilitating neurons to fire together and form functional circuitry. The halting of this activity later in development thus signifies circuitry moving towards making functional synaptic assemblies, and often correlates with behavioural developmental milestones, such as the onset of locomotion (Dehorter et al. 2012).

### 1.1.6 Refinement

The first waves of refinement occur as cells undergo programmed cell death, or apoptosis. Apoptosis is thought to be part of the processes re-balancing the neuronal network and removing cells unable to integrate with circuitry. Developmental apoptosis typically occurs within the first 10 postnatal days of life (Heumann and Leuba 1983, Ferrer et al. 1990, Spreafico et al. 1995), though the timing and incidence is structure specific (White and Barone 2001). The cascades of gene expression inducing apoptosis are well known, however the factors regulating which cells undergo cell death are still being discovered today (Fricker et al. 2018, Hollville et al. 2019). Cell death occurs in both projection neurons and interneurons, and in the cortex it has been shown that this occurs at different timepoints within the first two postnatal weeks for these two populations (Wong et al. 2018). Generally, intrinsic mechanisms determine cell death, however activity has also been found to influence the number of cells undergoing apoptosis, as well as which cells undergo apoptosis. For example, elevating the activity of Lhx6-expressing cortical interneurons promoted their survivability during apoptotic stages (Denaxa et al. 2018). Similarly, activation of cortico-striatal pathways and intrinsic striatal cells promoted the survivability of striatal interneurons (Sreenivasan et al. 2022). Apoptosis is a key tool for network refinement and the formation of functional circuitry, with many genetic and activity-dependent mechanisms regulating its incidence.

Subsequent to connection formation, there are also stages of refinement in the second and third postnatal weeks during which synaptic pruning occurs (**Figure 1.2C**). Connections form in overabundance during development, but the final form of neuronal circuitry is specific. Synaptic pruning is largely driven by activity levels and this process is necessary for circuit flexibility (Tierney and Nelson 2009). It is well established that changes in neuronal activity can cause developmental rewiring; classic experiments by Hubel and Wiesel (1963) showed monocular deprivation during development results in the weakening of synapses corresponding to the deprived eye and strengthening of synapses corresponding to the open eye. Similarly, long-term depression (LTD) is a key mechanism of plasticity contributing to pruning, and also occurs in response to activity changes (Faust et al. 2021). The susceptibility of synaptic pruning to genetic manipulation and shifts in neuronal activity is largely unknown at the fine scale, with some of the only knowledge in this area arising from evidence of abnormal connectivity in neurodevelopmental disorders, such as autism spectrum disorder (ASD) and schizophrenia.

The theory of ASD arising due to the miswiring of the brain has been suggested throughout literature (Gatto and Broadie 2010, Long et al. 2016, Vasa et al. 2016, Ajram et al. 2017, Abbott

et al. 2018). Most studies contribute to this theory at a global scale, looking at whole brain effects and structure connectivity, however, there is some evidence for fine scale alterations to circuit formation leading to ASD. For example, shifts in the number of synapses observed in ASD compared to controls has been linked to abnormal synaptic pruning mechanisms (Faust et al. 2021). Similarly, abnormal microcircuit formation contributes to shifted excitation-inhibition balance in circuits, which is thought to be another hallmark of ASD (Culotta and Penzes 2020).

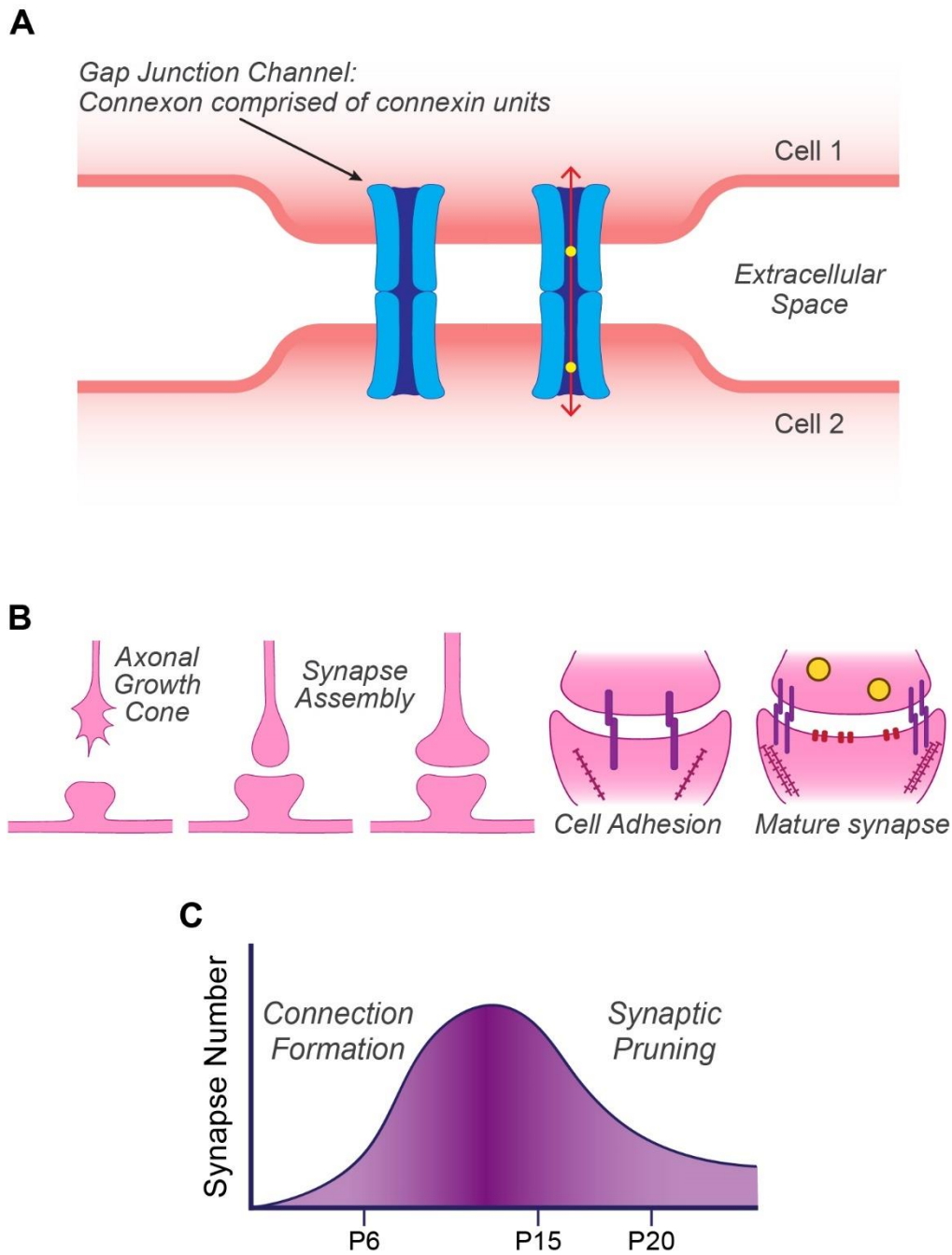


**Figure 1.2: Connection formation and maintenance during development**

**A.** Gap junctions facilitate a direct open pore between two cells, causing an electrical connection between neurons. This is formed by connexin channels (a connexon comprised of connexin subunits). **B.** The process of synapse formation, from the exploratory extension of the axonal growth cone, to initial synapse assembly, culminating in the expression of cell adhesion molecules at the synapse, facilitating a mature and functioning chemical connection. **C.** Schematic of the fluctuations in the number of synapses in the brain across time. Connection formation occurs heavily during the first two postnatal weeks (Postnatal day P1-14). This is followed by synaptic pruning, where connections are removed to refine the network during the second and third postnatal weeks (P14-21).

## 1.2 Regulation of the Excitation and Inhibition Balance in the Brain

Proper neuronal circuit function is reliant on a delicate balance between excitation and inhibition. This balance is achieved through mechanisms at cellular, synaptic, and whole network levels (He and Cline 2019), and determines the firing rates, patterns, and spatial distributions of neuronal activity, which in turn shape the output of neuronal circuitry.

At the cellular level, intrinsic electrical properties contribute to regulating the excitability of neurons, regardless of their identity as excitatory or inhibitory. The combination of intrinsic properties, including a cell's resting membrane potential, input resistance, and action potential threshold, all contribute to the responsiveness of cells to excitatory and inhibitory inputs, as well as their own ability to fire spontaneously (Dunn and Kaczorowski 2019). Neurons can subsequently shift their intrinsic excitability in response to changes in surrounding activity to maintain a balance within the cell; for example, reducing their excitability in response to the overstimulation of excitatory inputs (Campanac et al. 2013). As such, cells have adaptable responses to try to maintain the excitation-inhibition balance. Another example is the response of cells to decreasing excitatory neurotransmitter receptor expression, which results in less excitatory input to cells as expected, but also causes a cell autonomous equal reduction in the integration of inhibitory inputs (He and Cline 2019), thus maintaining the overall state of the cell. Together, excitatory and inhibitory signals interact to regulate the activity of neurons and shape their output, facilitating their role in wider circuitry (**Figure 1.3**).

At the level of circuitry, the number of cells, their spatial arrangement, and their connectivity governs the excitation-inhibition balance. Balance is maintained not only between the number of excitatory and inhibitory cells, but also between the strength of excitatory and inhibitory transmitter influence in the circuit (Sohal and Rubenstein 2019). There are of course exceptions; neuromodulatory transmitters such as acetylcholine, serotonin, dopamine, and norepinephrine that have variable effects on post-synaptic cells, as well as developmental shifts in excitation and inhibition. In addition, synaptic balance and plasticity contribute to maintaining equilibrium within circuitry. Excitatory neurons, which are typically projection neurons, must balance their activity with local inhibitory and modulatory interneurons (**Figure 1.3**). As such, interneurons are vital regulators of the excitation-inhibition balance (Ferguson and Gao 2018). Yet, these mechanisms taken together are complex, particularly when considering the vast array of interneuron subtypes (Tepper et al. 2010, Tepper et al. 2018).

If local neuronal circuitry is imbalanced, this can likely impact the function of whole brain structures. The shifted output of a single brain region can break the flow of information and lead to behavioural alterations and pathologies. For example a loss in the balance between long-range corticostriatal excitatory inputs and local striatal inhibitory feedforward inhibition can lead to a break down in striatal circuitry and tremors typical of basal ganglia disorders, such as Parkinson’s Disease (Oran and Bar-Gad 2018). In addition, excitation-inhibition imbalance is a hallmark of ASD (Culotta and Penzes 2020). Elevated excitation, compared to inhibition has been described in a number of mouse models of ASD (**Figure 1.3**) (Antoine et al. 2019, Sohal and Rubenstein 2019). Furthermore, the rectification of this imbalance has been shown to rescue ASD symptomology and is considered a potential clinical treatment option (Selimbeyoglu et al. 2017, Canitano and Palumbi 2021). Yet, mechanisms contributing to this imbalance in ASD have not been fully described, particularly in the context of neuromodulatory contributions (**Figure 1.3**).

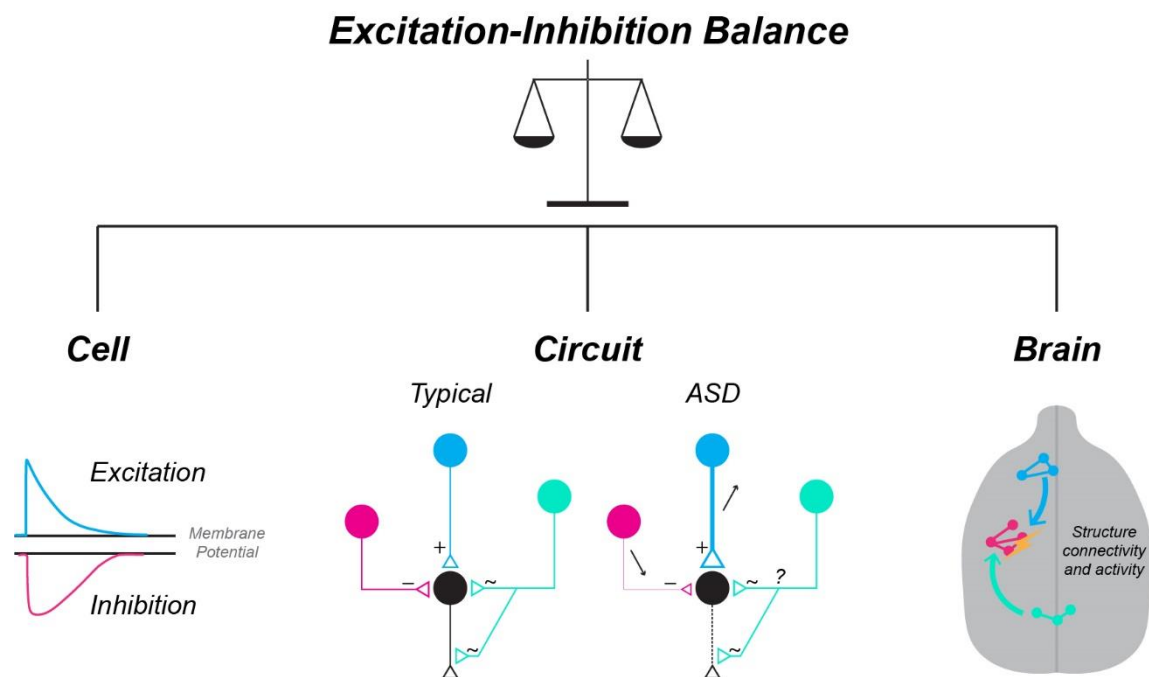


**Figure 1.3: The excitation-inhibition balance in the brain is maintained at various levels**

The balance between excitation and inhibition is maintained at a cellular level by balanced excitatory and inhibitory inputs to a single cell, controlling its inherent excitability (left). It is also preserved at a circuit level, by balanced excitation (blue) and inhibition (pink) in the whole network. This balance is also controlled by neuromodulatory cell populations (green). This balance can be altered by the miswiring of neurons which is known to occur in ASD, where there is excessive excitation and decreased inhibition. However, we are still unsure of the effect of neuromodulators on this balance in ASD (middle). This circuit balance contributes to whole brain equilibrium, where structures interact to maintain balance (right).



Whilst maintaining the excitation-inhibition balance is crucial in mature circuits, it is even more important during development. Several characteristics of the developing brain make its excitation-inhibition balance unique. During early development, high intracellular chloride concentrations, mediated by chloride co-transporters, mean that GABA receptor activation leads to an efflux of chloride and a subsequent depolarisation of the cell (Ben-Ari et al. 2012). It is therefore considered an excitatory neurotransmitter, as opposed to inhibitory, as it is in mature circuits; GABA does eventually shift to being inhibitory, with low intracellular chloride concentrations corresponding to GABA causing the hyperpolarisation of the post-synaptic cell (Ben-Ari 2012). Similarly, neurotransmitter switching during development also contributes to the excitation-inhibition balance. A cell has the capacity to lose one neurotransmitter, which is then replaced by another, for example a GABA releasing cell loses the GABA transmitter and gains the ability to release glutamate (Spitzer 2017). This process is dynamic and activity-dependent, highlighting the complex interplay between excitation and inhibition during development. With such intricate regulatory mechanisms, understanding how the excitation-inhibition balance can shift during development, and the potential repercussions of this, is crucial for understanding typical developmental processes and neurodevelopmental pathology.

### **1.3 The Impact of Neuromodulatory Control on Circuit Function**

Neuromodulation shapes the overall activity and output of neuronal circuits through complex mechanisms. Neuromodulators are a diverse class of signalling molecules that act on specific receptors, and can alter the excitability, synaptic strength, and plasticity of neurons. In the central nervous system, discrete cell populations are classified as neuromodulatory, dependent on their expression of a neuromodulatory neurotransmitter, such as acetylcholine, serotonin, and dopamine amongst others. Some key populations are cholinergic neurons, which are present in various nuclei throughout the brain (Ahmed et al. 2019), and serotonergic neurons, which localise to caudal midbrain and brainstem nuclei (Charnay and Leger 2010). These neurons act both locally and via long range projections to regulate various levels of the network, particularly during development. The typical impact of neuromodulatory signals is the modulation of cell excitability. For example, the application of neuromodulatory transmitters, such as acetylcholine and serotonin, during *in vitro* recordings of neurons results in prolonged alterations to the membrane potential (Gadsby et al. 1978, Celada et al. 2013, Ko et al. 2016). Additionally, neuromodulatory signals target pre-synaptic probability release and post-synaptic receptor expression, via activity-dependent mechanisms, to influence activity at a circuit level (Nadim and Bucher 2014, Nelson et al. 2014). Furthermore, direct current responses in post-

synaptic cells have also been observed (Kassam et al. 2008, Goodfellow et al. 2009). This highlights the variety of ways in which neuromodulation can occur to control neuronal networks. Subsequently, neuromodulatory influences can also lead to behavioural modifications (McCormick et al. 2020). For example, high levels of acetylcholine, compared to dopamine, in the striatum have been found to bias excitatory inputs onto indirect-pathway spiny projection neurons (SPNs) towards long-term potentiation (LTP), which has been suggested to induce a behavioural state of inactivity (Lerner and Kreitzer 2011).

Whilst neuromodulation widely affects nearly all brain structures, one region that is particularly under the influence of various neuromodulatory inputs is the striatum. The striatum receives extensive dopaminergic inputs from the substantia nigra (Aosaki et al. 2010, Straub et al. 2014), serotonergic inputs from the dorsal raphe nucleus (Waselus et al. 2006, Ren et al. 2019), and contains both intrinsic and external acetylcholine (cholinergic interneurons and inputs from the pedunculopontine nucleus, respectively), contributing to the striatum having the highest levels of acetylcholine in the brain (Macintosh 1941, Lim et al. 2014). As such, the striatum can be considered as a hub of neuromodulation.

#### **1.4 The Striatum**

The striatum has a major role in regulating behaviour (Graybiel and Grafton 2015), and is the input structure of the basal ganglia, which is crucial for maintaining the overall excitation-inhibition balance in the brain (Radulescu et al. 2017). Excitatory commands from the cortex and thalamus are relayed to the striatum, which gates and controls these inputs to ensure correct balance, before conveying information to the rest of the basal ganglia (Hunnicutt et al. 2016).

The striatum can be anatomically divided into sections with diverse and specialised roles in striatal processing. The dorsal and ventral regions of the striatum, representative of the human caudate nucleus and putamen, and the nucleus accumbens, respectively, have entirely distinct anatomical circuits, that are involved in separate learning processes (Balleine et al. 2009). In addition, the dorsomedial (DMS) and dorsolateral (DLS) striatal areas show further distinction in both their anatomy and role. The DMS is attributed with motor learning and goal directed behaviour, whereas the DLS is involved with habit formation and action execution (Lim et al. 2014, Ito and Doya 2015).

The striatum is composed mainly of inhibitory GABA-releasing spiny projection neurons (SPNs, 95%), which project out of the striatum to further areas of the basal ganglia via two pathways: the direct and indirect pathways, mediated by the select expression of the D1 or D2

dopamine receptors (Calabresi et al. 2014). D1-expressing SPNs project to the globus pallidus interna and the substantia nigra pars reticula, forming the direct pathway. The indirect pathway is formed by D2-expressing SPN projections to the globus pallidus externa (Calabresi et al. 2014) (**Figure 1.4A**). The activation of these two pathways was thought to have opposing effects on movement, whereby activating the direct pathway increases movement and activating the indirect pathway inhibits movement, however more evidence is pointing to a structural and functional overlap between these pathways, likely facilitated by striatal interneuron microcircuitry (Calabresi et al. 2014).

The remaining cells in the striatum (*i.e.* 5%) are interneurons. These cells innervate locally and are categorised into different subtypes based on their molecular identity and their morphological and electrophysiological properties (Tepper et al. 2018). Generally, striatal interneurons can be either GABAergic or cholinergic (releasing acetylcholine as a neurotransmitter) (**Figure 1.4B**). Within the GABAergic interneuron population, the most common are parvalbumin (PV) positive fast spiking interneurons (FSI), which alone account for 1% of the total striatal population (Tepper et al. 2010). Also present in the striatum are neuropeptide-Y positive (NPY) and somatostatin (SST) positive persistent and low threshold spiking (PLTS) GABAergic interneurons (Tepper et al. 2010), which together account for approximately 2% of all striatal neurons. In addition, there are further smaller populations of interneurons, including tyrosine hydroxylase (TH) positive interneurons, amongst others, which are still being fully classified (Xenias et al. 2015, Tepper et al. 2018). These inhibitory interneurons have diverse roles in modulating the activity of SPNs and surrounding interneurons.

Striatal cholinergic interneurons (CINs) make up 2-3% of the striatal population. These interneurons are the largest in the striatum, and also have unique continuous firing properties. They are known as large aspiny interneurons and tonically active neurons (TANs; **Figure 1.4C**) (Atallah et al. 2014). An important aspect of their functionality is that they pause their tonic firing in response to a salient stimulus, which is thought to be important for encoding information in reward based learning (Kim et al. 2019). Although these neurons have long been described as a single population both molecularly and functionally, they are indeed quite diverse (Ahmed et al. 2019) (Appendix A).

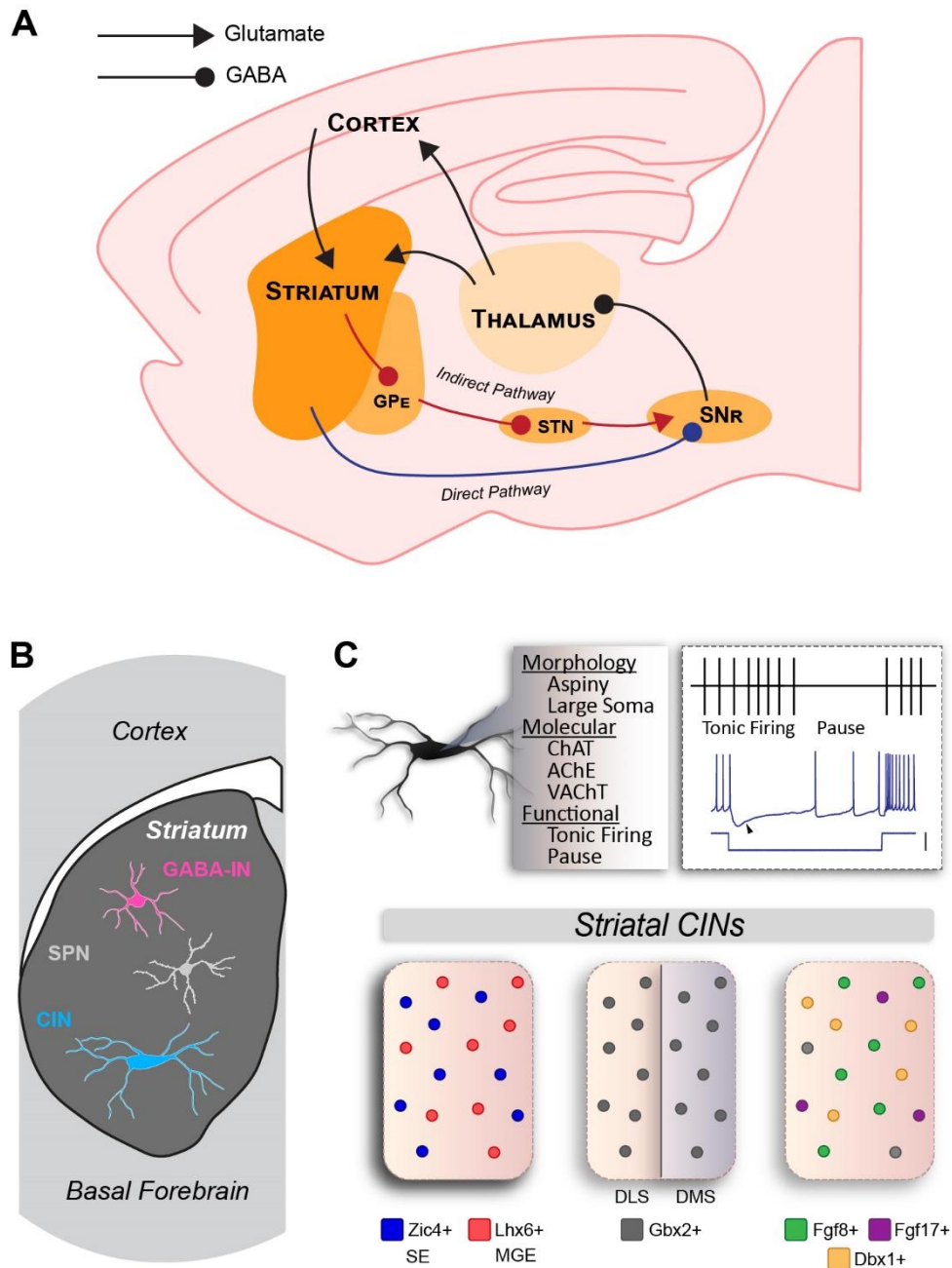


### Figure 1.4: The striatum and its circuitry

**A.** Excitatory (glutamate) inputs to the striatum from the cortex and thalamus and inhibitory (GABA) outputs via the direct and indirect pathways. Direct pathway spiny projection neurons (SPNs) project to the substantia nigra pars reticula (SNr) or the globus pallidus interna (not shown). Indirect pathway SPNs project to the SNr via the globus pallidus externa (GPe) and subthalamic nucleus (STN). These pathways enact opposing control over the SNr (excitatory versus inhibitory), which sends projections to loop back to the cortex via the thalamus. **B.** The general division of the striatal cell population is into SPNs, GABAergic interneurons, and cholinergic interneurons (CINs). **C.** Striatal CINs have distinct morphological, molecular, and functional properties (top). They are molecularly diverse, based on their developmental origin being either the septal epithelium (SE) or the medial ganglionic eminence (MGE) (bottom left). Diversity is also dependent on the expression of other molecular factors (bottom right). Figure adapted from Ahmed et al. (2019).

### 1.4.1 Cholinergic Interneuron Diversity

Striatal CINs were long considered as a single homogeneous population. Despite sharing some identifying commonalities, such as the expression of choline acetyl-transferase (ChAT) which is necessary for the synthesis of acetylcholine, striatal CINs in fact comprise a diverse population. The first aspect of their developmental diversity relates to their embryonic origin. Striatal CINs arise from the MGE, PoA, and septal epithelium (Marin et al. 2000, Fragkouli et al. 2009, Magno et al. 2017). It is likely that the origin of different CIN populations governs aspects of their identity and delineates their diversity. For example, the *Dbx1* (developing brain homeobox protein 1) transcription factor defines a sub-domain of the embryonic PoA which gives rise to a subset of cholinergic striatal interneurons (Gelman et al. 2011). Similarly, fibroblast growth factor 8 (*Fgf8*) and fibroblast growth factor 17 (*Fgf17*) expressing progenitors in the ventral MGE and ventral embryonic septal epithelium give rise to individual subsets of cholinergic interneuron in the striatum (Hoch et al. 2015). Further examples delineate 50% of striatal CINs expressing the transcription factor *Zic4*, marking their origin in the septal epithelium (Magno et al. 2017) (**Figure 1.4C**).

However, as many progenitor regions have genetically defined sub-domains (Flames et al. 2007), neurons originating from the same regions may also display further genetic diversity. The transcription factors *Lhx8* and *Isl1* drive cholinergic identity in MGE/PoA- derived CINs, and the ablation of *Isl1* leads to the loss of 40% of the *Nkx2.1* expressing CINs in the striatum (Cho et al. 2014). It was previously thought that striatal CIN identity was exclusively defined by the upregulation of *Lhx8* and coordinated downregulation of *Lhx6* (Liodis et al. 2007, Fragkouli et al. 2009, Lopes et al. 2012). However, a subset of CINs was recently found to maintain *Lhx6* expression alongside cholinergic markers, resulting in *Lhx6* positive (53%) and negative (47%) CIN populations in the adult striatum (Lozovaya et al. 2018) (**Figure 1.4C**).

As previously mentioned, another element to consider regarding cell specification and diversity is the fact that during development, neurons acquire different identities according to their time of birth (Kao and Lee 2010). Striatal CINs are amongst the earliest cells born (Semba et al. 1988); early- and late-born CINs migrate at stages relative to their birth (<E13: early born, E13-17: late born)(Marin et al. 2000) and populate lateral and medial regions of the striatum, respectively (Chen et al. 2010). The *Gbx2* transcription factor is implicated in the distinction between these early- and late-born cells; its absence almost entirely ablates the late-born population, thus also delineating a cholinergic subpopulation in the striatum (Chen et al. 2010). Furthermore, striatal CINs present with diverse genetic patterning, even extending to

cholinergic markers. Individual CINs express different levels of ChAT and choline transporters, indicating a level of functional heterogeneity (Munoz-Manchado et al. 2018). Differential striatal CIN activity has been previously described, with higher levels of CIN baseline activity in the dorsomedial region compared to the ventrolateral region of the striatum, marked by a gradient in the expression of the phosphorylated ribosomal protein S6 (p-rpS6), a specific marker of cholinergic activity (Bertran-Gonzalez et al. 2012, Matamales et al. 2016).

In addition, diverse morphological and electrophysiological properties were recently described in striatal CINs, dependent on the *Lhx6* transcription factor. Lhx6-negative CINs present with a vaster and more complex dendritic arbour, as well as a higher firing frequency and less prominent pause response than Lhx6-positive CINs, which are considered to be dual GABAergic-cholinergic interneurons.

Furthermore, the pattern of connectivity surrounding striatal CINs is fundamental to their function. It is known that the cortical and thalamic innervation of the striatum follows an approximate topographical gradient, whereby the dorsomedial and dorsolateral striatum receive inputs from different regions of the cortex, thalamus, and brainstem (McGeorge and Faull 1989, Berendse et al. 1992, Bolam et al. 2000, Dautan et al. 2014, Assous et al. 2019). This trend may also extend to influencing CINs, as they receive afferents from the cortex and thalamus (Doig et al. 2014, Klug et al. 2018), and dorsomedial CINs have higher levels of activity than dorsolateral ones (Matamales et al. 2016). This functional cell diversity implies a fine control of information processing from cholinergic neuron subtypes and suggests that the regulation of striatal output via CIN activity is heterogeneous.

#### **1.4.2 Striatal Microcircuit Connectivity**

Whilst striatal interneurons have a primary role of modulating SPNs and the output of the striatum, their connectivity with one another is also important, and yet many intricacies of interneuron microcircuitry remain unknown. The striatum receives glutamatergic inputs from the cortex and thalamus (Bolam et al. 2000), as well as dopaminergic and serotonergic inputs from the substantia nigra and dorsal raphe nucleus, respectively (Ren et al. 2019, Zhai et al. 2019). These have been shown to influence the function of SPNs, as well as cholinergic and GABAergic interneurons (Blomeley and Bracci 2009, Lim et al. 2014, Bang et al. 2020, Dorst et al. 2020, Poppi et al. 2021).

Within striatal interneuron microcircuitry, the connections surrounding CINs, as well as the primary GABAergic population, the PV interneurons (PV-INs) is of great interest, as both enact

strong control over SPNs, correlating strongly with behaviour (Koos and Tepper 1999, Szydlowski et al. 2013, Gritton et al. 2019), whilst also integrating with other interneurons. CINs have a dense axonal field, innervating their surrounding neurons (Lim et al. 2014). They project robustly to NPY interneurons via nicotinic receptors (English et al. 2011, Assous et al. 2017), and also receive reciprocal connections from these neurons (Straub et al. 2016, Abudukeyoumu et al. 2019). In addition, CINs receive dense synaptic inputs from other CINs, forming microcircuitry that then modulates the overall striatal output via dense innervation of the spiny projection neurons (English et al. 2011, Straub et al. 2016, Abudukeyoumu et al. 2019). Furthermore, CINs have been shown to enact presynaptic control over glutamatergic and dopaminergic inputs to the striatum (Abudukeyoumu et al. 2019, Mallet et al. 2019). CINs also innervate PV-INs, and this has been shown both descriptively (Chang and Kita 1992), and functionally (Koos and Tepper 2002, Nelson et al. 2014). As such, CINs connect extensively within the striatum. Yet, interestingly, PV-IN to CIN connectivity has not been found in previous studies (Chang and Kita 1992, Szydlowski et al. 2013), apart from some instances of weak post synaptic responses after PV-IN activation (Straub et al. 2016). PV-INs are fast spiking and enact powerful inhibitory control over their target neurons (Koos and Tepper 1999), which include other inhibitory interneurons in the striatum, including other PV-INs (Fukuda 2009, Szydlowski et al. 2013) (See **Figure 1.5** for summary of striatal connectivity). Whilst connectivity within the striatum appears ubiquitous at first glance, the prominent absence of PV-IN mediated inhibition over CINs highlights the specificity of connections between interneurons in the striatum and raises questions regarding how this arises during development.

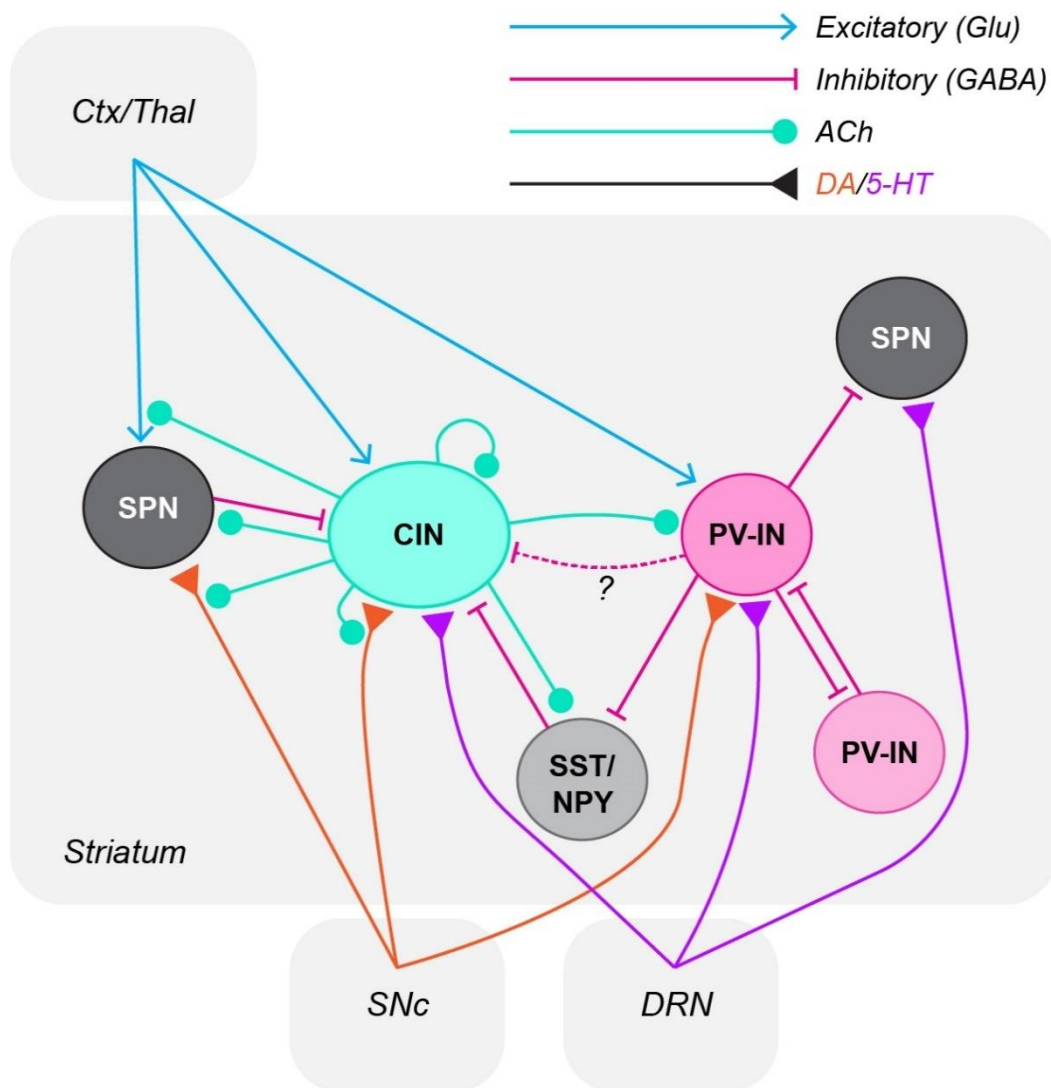


**Figure 1.5: Connections in the striatal microcircuit**

The integration of cholinergic interneurons (CINs) and parvalbumin positive interneurons (PV-INs) into the striatal microcircuit. Excitatory inputs from the cortex (Ctx) and thalamus (Thal) innervate interneurons as well as striatal spiny projection neurons (SPNs). Dopaminergic inputs from the substantia nigra pars compacta (SNc) and serotonergic inputs from the dorsal raphe nucleus (DRN) supply neuromodulatory inputs to the whole striatum. CINs and PV-INs also send projections to and receive input from SPNs and somatostatin (SST) and neuropeptide-Y (NPY) expressing interneurons. Figure adapted using information and figures from (Blomeley and Bracci 2009, Lim et al. 2014, Klug et al. 2018, Abudukeyoumu et al. 2019, Poppi et al. 2021).



The developmental trajectory of striatal microcircuitry is largely unknown, as previous research has focussed on other structures or on elucidating the connectivity of the developed striatum. It is therefore critical to understand the interplay between activity and genetic regulation of interneurons during development in this structure.

In this thesis, we will explore how shifting the molecular identity of neurons influences the formation of functional striatal microcircuits and long-range input circuitry, as well as its importance in regulating the activity and role of neuromodulatory cell populations. Furthermore, we will study how the gene-activity balance is disrupted in a neurodevelopmental conditions such as Autism Spectrum Disorder.

We will address the following aims:

1. To probe the result of specific molecular alterations on striatal cholinergic interneuron function and the connectivity between striatal interneurons.
2. To manipulate neuromodulatory inputs to the striatum and determine links to behaviour.
3. To investigate alterations to the developmental trajectory and functionality of the striatal interneuron population in a mouse model of Autism Spectrum Disorder.

Researching the mechanisms underlying striatal development, particularly circuit formation, is crucial not only for our general understanding of developmental processes, but also for determining the deviations from developmental trajectory that contribute to behavioural alterations, such as in neurodevelopmental disorders.

## Chapter 2: Molecular Regulation of the Function and Connectivity of Developing Striatal Circuits

### 2.1 Preamble

Transcription factors are finely tuned regulators of development, and in conjunction with activity, they are responsible for maintaining correct neuronal developmental trajectory. The mechanisms underlying transcription factor mediated control of circuit formation are still emerging, largely due to the complexity of gene-activity interactions. The formation of neuronal circuits involves several steps, including morphological development (*i.e.*, axon and dendrite formation), synapse formation, as well as the establishment of electrophysiological properties such as the maturation firing properties and the hyperpolarisation of the resting membrane potential over time (McGuirt et al. 2021). In addition, the intrinsic activity of neurons during development governs whether they remain in the network or are removed via apoptosis (Denaxa et al. 2018), as well as their connectivity within the neuronal network (Andreae and Burrone 2014, Kim et al. 2018). However, how connections between neurons are specified and selected for is largely unknown.

Despite not knowing the specific underlying mechanisms, it has been shown that aberrant connectivity, essentially resulting in the mis-wiring of the brain, is a key marker of altered behaviour and neuropsychiatric pathologies, including Autism Spectrum Disorder (Di Martino et al. 2014, Vasa et al. 2016). Dissecting the genetic mechanisms regulating developmental neuronal activity and connectivity is essential for understanding how circuitry is built and maintained particularly in sub-cortical structures such as the striatum where very little is known about developmental connection formation.

A key unexplored gene that may potentially influence circuit formation in the developing striatum is the ETS (E-twenty-six) transcription factor *Etv1/Er81* (ETS translocation variant 1; herein referred to as *Er81*). *Er81* has been characterised as having a number of roles in various contexts, with many contributing to developmental processes. For example, *Er81* has been studied in terms of its involvement in various molecular pathways, particularly as an oncogenic factor regulating cell division in cancer (Eid and Abdel-Rehim 2019). It has also been found that the transcriptional targets of *Er81* are correlated with neural developmental processes, including neurogenesis, axon development, and synaptogenesis (Eid and Abdel-Rehim 2019). Classically, *Er81* is a target of the RAS/ERK signalling pathway (Janknecht 1996, Hollenhorst

2012), which is important in many developmental processes including differentiation (Cruz and Cruz 2007), the regulation of neuron fate (Li et al. 2014), and axon elongation (Zhong 2016).

*Er81* has also been studied in regards to neuronal identity and differentiation. *Er81* expression has been found to segregate olfactory bulb interneurons in anatomical and phenotypic subsets (Saino-Saito et al. 2007), a subset of cortical layer 5 pyramidal neuron population (Yoneshima et al. 2006), as well as a subpopulation of facial motor neurons during late embryonic developmental stages (~E16.5) (Tenney et al. 2019). *Er81* also has roles in later developmental processes, including regulating the maturation of genetic profiles and morphological development. For example, *Er81* regulates the maturation program of cerebellar granule cells, and does so in an activity-dependent manner (Abe et al. 2011). It also transcriptionally controls the Nuclear Factor One (NFI) group of transcription factors, which are required for dendritogenesis and synaptogenesis via their occupancy of specific genetic promoter regions (Ding et al. 2016). In addition, *Er81* expression in dorsal root ganglion neurons is temporally important for late neuronal differentiation including branching and target invasion (Hippenmeyer et al. 2005). These examples highlight the diversity of actions undertaken by *Er81* during development. Both genetic and morphological maturation are critical for circuit formation; and there are some examples of *Er81* being a vital regulator of connection formation. Notably, *Er81* was found to regulate the formation of a monosynaptic connection between parvalbumin and cholinergic neurons in the spinal cord (Arber et al. 2000). In this study, when *Er81* was ablated, the parvalbumin positive sensory neuron axon was unable to form correctly and synapse with the cholinergic motor neuron. Furthermore, *Er81* has been shown to be involved in the regulation of gap junction channels. As developmental precursors to synaptic connectivity (Todd et al. 2010), gap junction connectivity is a key aspect of circuit formation (see Chapter 1 for more detail). *Er81* is necessary for the expression of specific connexin gap junction hemichannels (cardiovascular connexin 40) (Shekhar et al. 2016, Shekhar et al. 2018), implicating a possible role in early cell connectivity through neuronal gap junctions, and thus activity dependent development trajectories. Taken together, it is possible that *Er81* is a master regulator of processes underlying circuit formation by regulating the connectivity between specific neuronal populations in the brain. Elucidating the role of *Er81* in neuronal connectivity will uncover general mechanisms for the susceptibility of neuronal connectivity to intrinsic molecular factor expression.

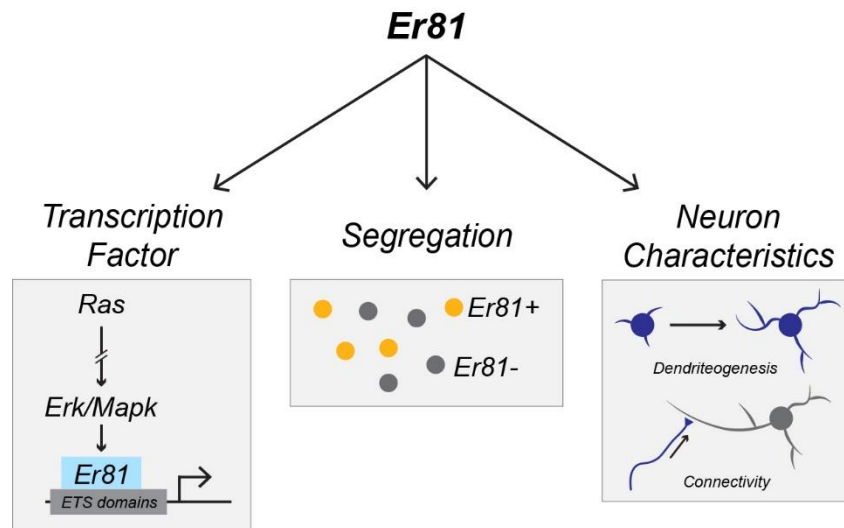


**Figure 2.1: Developmental roles of Er81 in neuronal circuitry**

Er81 has been shown to have several roles in neurons, particularly during development. As a transcriptional regulator, Er81 is activated by the Ras-Raf-Erk/Mapk signalling pathway where Ras binds guanosine triphosphate (GTP) when active and subsequently activates downstream effector kinases culminating in the activation of extracellular signal related kinases (ERK), which are also known as mitogen activated protein kinases (MAPK). These then stimulate Er81 (via phosphorylation), causing it to localise to ETS binding motifs and regulate gene transcription. Er81 expression in certain neuronal populations segregates subgroups. Er81 has also been found to regulate morphological characteristics of neurons, including dendritogenesis and synaptogenesis.

Striatal interneurons have a specific pattern of connectivity to facilitate feedforward inhibition and neuromodulatory control over the surrounding circuitry (Szydlowski et al. 2013). As outlined in Chapter 1, the striatum has a unique interneuron population including both inhibitory and cholinergic neuromodulatory interneurons. However, their connectivity within the striatal microcircuit, particularly during development has remained uncharacterised, as has the molecular pathways governing this. Interestingly, *Er81* has been found to be expressed in striatal neurons (Chen et al. 2020), and particularly in parvalbumin expressing neurons (Dehorter et al. 2015). We therefore wondered whether *Er81*-dependent transcriptional regulation can affect the formation of the striatal microcircuit, particularly the establishment and maintenance of interneuron connections and their specificity. As the maintenance of developmental trajectory relies on these processes occurring correctly, and pathological states can arise when they do not, understanding the genetic patterning that underlies the maintenance of striatal network connectivity and activity is crucial for linking molecular identity with cell and circuit function and identifying mechanisms altered in disease states. As such, we hypothesised that *Er81* maintains control over the striatal microcircuit, via the regulation of factors contributing to circuit formation, such as morphological development, cellular activity, and electrical and chemical synapse formation.

In this study, we aimed to:

1. Characterise the role of *Er81* in specific striatal interneuron populations.
2. Determine how *Er81* can influence striatal interneuron microcircuit connectivity via:
  1. A cell-type specific knockout of *Er81*
  2. A knockout of *Er81* affecting the entire interneuron population
3. Explore the role of *Er81* in the developmental activity of striatal interneurons.

## 2.2 Er81 is Expressed in Striatal Interneuron Populations

Whether Er81 is expressed in striatal interneuron subtypes, other than parvalbumin positive interneurons (Dehorter et al. 2015), is unknown. To address this, we first characterised the expression of Er81 in three striatal interneuron subtypes: parvalbumin positive interneurons (PV-INs), cholinergic interneurons (CINs), and neuropeptide-Y (NPY) expressing interneurons. These subtypes cover most interneuron subpopulations in the striatum, including somatostatin (SST) positive interneurons, which are included in the NPY-IN population (Munoz-Manchado et al. 2018), but do not cover the tyrosine hydroxylase (TH) positive and cholecystokinin (Cck) positive populations, however these are quite small populations *i.e.* less than 1% of the total cell population; (Munoz-Manchado et al. 2018). Quantification of Er81 protein expression via immunofluorescent staining revealed strong nuclear staining in PV-INs (**Figure 2.2A, D**), as has been described previously in the cortex (Dehorter et al. 2015). Conversely, Er81 is expressed at lower levels in CINs, with a different pattern of expression as well (**Figure 2.2B, D**); Er81 expression appears far more cytoplasmic in CINs than in PV-INs, potentially indicating a difference in protein regulation and/or the function of the transcription factor in these two cell types. NPY-INs show very low expression of Er81 in comparison to PV-INs and CINs (**Figure 2.2C, D**).

We observed a continuous spectrum of Er81 protein levels in PV-INs and CINs. As such, we quantified the number of putative Er81 positive cells within these populations (see Methods) and found that almost all PV-INs expressed Er81 (90%), most CINs express Er81 (70%), and very few NPY-INs (14%; **Figure 2.2E**). Due to the higher expression levels and higher proportion of positive cells in the PV-IN and CIN populations, we focussed our study on understanding the role of Er81 in these cells.

The role of Er81 in mature cortical PV-INs has been previously described (Dehorter et al. 2015). However, this has not been explored in maturing striatal PV-INs and CINs. We first aimed to understand the direct role of Er81 in CINs in the context of regulating their maturation and activity.

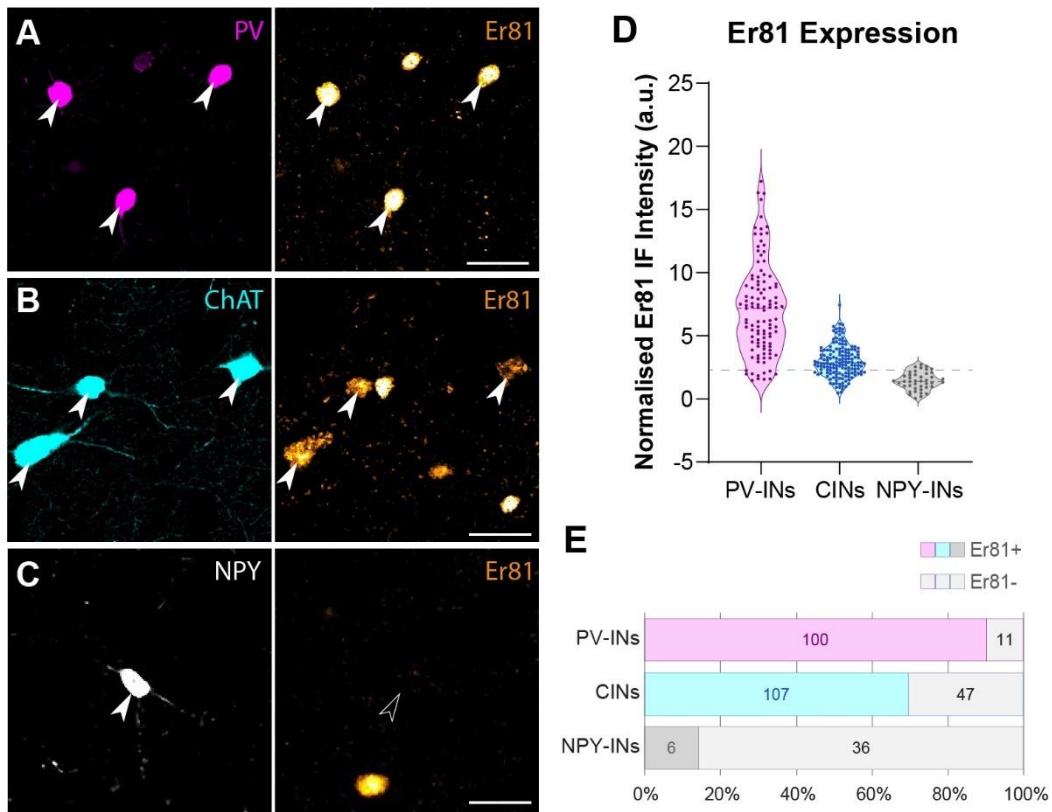


**Figure 2.2: Er81 expression levels differ across striatal interneuron subtypes**

**A.** Er81 expression (orange, right) in striatal parvalbumin (PV) positive interneurons (magenta, left). **B.** Er81 expression (orange, right) in striatal cholinergic interneurons stained with choline acetyltransferase (ChAT, cyan, left). **C.** Er81 expression (orange, right) in striatal neuropeptide-Y (NPY) positive interneurons (white, left). Scale: 40  $\mu$ m. **D.** Quantification of Er81 immunofluorescence intensity in striatal PV interneurons (PV-INs, n = 111 cells), cholinergic interneurons (CINs, n = 154 cells), and NPY interneurons (NPY-INs, n = 42 cells), normalised to background intensity (n = 4 mice). **E.** Division of PV-INs, CINs, and NPY-INs into positive and negative cells, thresholding above (Er81+) and below (Er81-) 2.3 times the Er81 background immunofluorescence.

### 2.3 Er81 Regulates the Morpho-Functional Properties and Circuit Integration of Cholinergic Interneurons<sup>1</sup>

Er81 has been shown to regulate cell morphology and excitability in the cortex and cerebellum in a cell-type specific manner (Dehorter et al. 2015, Ding et al. 2016). As we observed a unique cytoplasmic pattern of Er81 expression in CINs, we wanted to determine its role in these cells. We therefore generated a conditional cre-dependent knockout under the choline acetyltransferase (ChAT) promoter (*Er81<sup>lox/lox</sup>;ChAT-cre;RCE-GFP*; control: *ChAT-cre;RCE-GFP* mice) to specifically ablate Er81 from CINs and study resulting alterations. We first verified that Er81 was removed in the conditional knockout (**Figure 2.3A**). Since Er81 appears to be expressed at higher levels in developmental stages compared to adults (data not shown, Ahmed et al. 2021, Appendix B), we then wanted to determine whether Er81 had a role in cholinergic cell proliferation and migration. We quantified CIN cell numbers during early postnatal development, shortly following migration and prior to developmental apoptosis (P2) and at a mature (P30) stage in the control and conditional knockout. We found no change in cell density at either stage, showing that Er81 does not regulate the migration processes of CINs (**Figure 2.3B**).

We next compared the morphology and electrophysiological properties of CINs between control and knockout conditions. Morphological deficits of neurons could arise as either a direct repercussion of genetic expression regulating development and refinement, or from compensatory or activity-mediated changes, resulting from altered network state (Ghiretti and Paradis 2014). To determine the direct, cell-autonomous role of Er81 ablation in CINs, and to label CINs sparsely for reconstruction, we utilised a cre-dependent inducible expression model under the *Nkx2.1* promoter, whereby a low-titre Tamoxifen dose at P0 was used to label (control: *Nkx2.1-creER;RCE*) and ablate Er81 (*Er81<sup>lox/lox</sup>;Nkx2.1-creER;RCE*) from interneurons derived from the MGE/Poa (*i.e.* CINs and PV-INs) (Marin et al. 2000).

The reconstruction of CINs (**Figure 2.3C**) revealed that there was no change in the spread of the dendritic field (**Figure 2.3D**), however dendritic volume and the number of branch points were significantly decreased in the knockout at P30 (**Figure 2.3E-F**). Additionally, Sholl analysis (see Methods) confirmed that the overall dendritic complexity was decreased in the knockout condition (**Figure 2.3G**). Axonal morphology was then analysed by measuring the

---

<sup>1</sup> Data in this section went towards the completion of an Honours thesis (Noorya Ahmed, 2018), and was completed in collaboration with Yadollah Ranjbar-Slamloo. This work has also been published (Ahmed et al. 2021, Appendix B). See Appendix E for details of contribution.



area occupied by cholinergic neuropil, which comprises dense CIN axonal projections that extend in a complex manner and innervate large regions surrounding each cell (Lim et al. 2014). The neuropil was labelled robustly via GFP under the ChAT promoter (**Figure 2.3H**). Neuropil area was significantly less in the knockout condition (*Er81<sup>flox/flox</sup>;ChAT-cre;RCE*) compared to the control (*ChAT-cre;RCE*), indicating that the axonal field of striatal CINs is less extensive when Er81 is removed from the cholinergic population (**Figure 2.3I**).

Together these results indicate that Er81 has a direct role in regulating both dendritic and axonal cell morphology of CINs. With this knowledge, we next aimed to determine the functional repercussion of Er81 ablation.

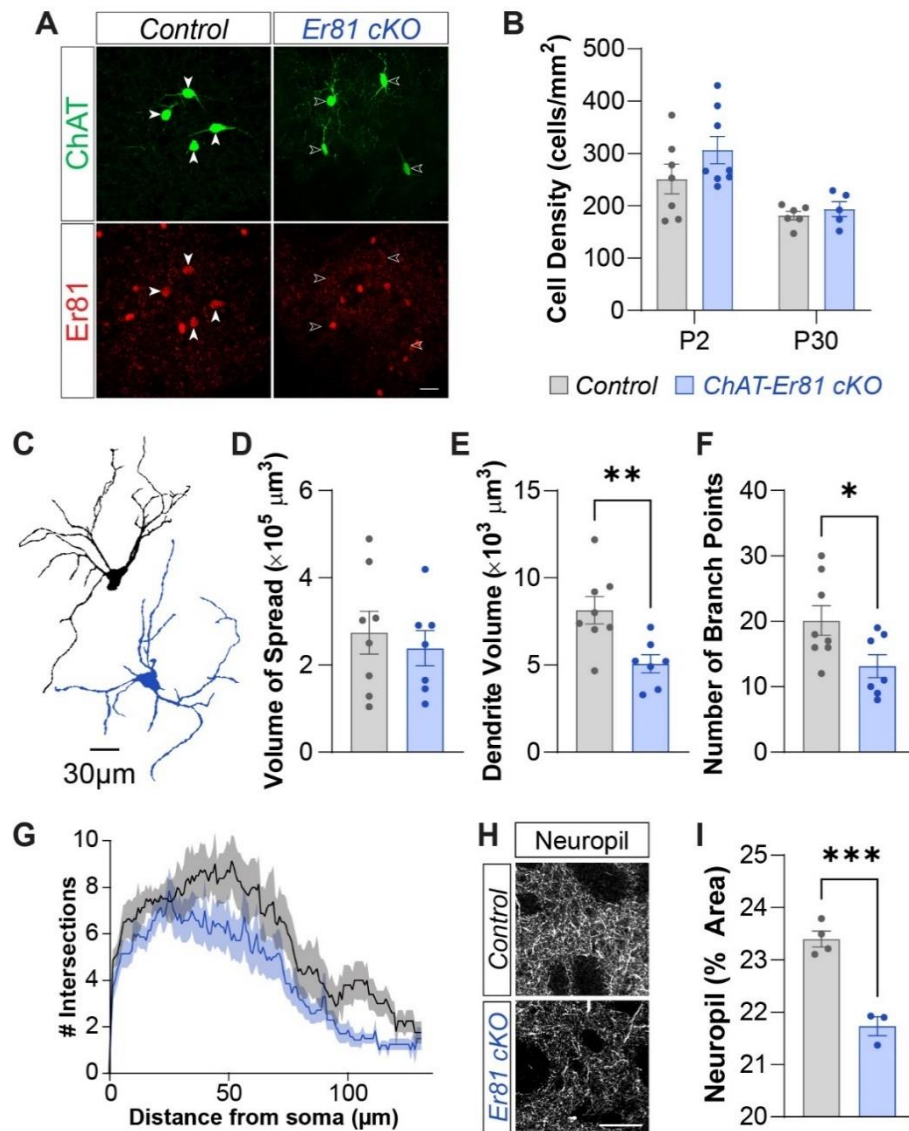


**Figure 2.3: Cholinergic interneuron morphology is dependent on *Er81* expression**

**A.** *Er81* expression in ChAT<sup>+</sup> interneurons in the mature striatum of control (*ChAT-Cre*) and *Er81* conditional knockout (cKO; *Er81<sup>fl/fl</sup>;ChAT-Cre*) mice, scale: 25  $\mu\text{m}$ . **B.** CIN density at P2 ad P30+ in the control and *Er81* cKO striatum (P2:  $n = 4011$  cells, 6 control mice,  $n = 1050$  cells, 6 cKO mice,  $p = 0.871$ ; P30:  $n = 1084$  cells, 6 control mice,  $n = 1050$  cells, 6 mice,  $p = 0.784$ ). **C.** Somato-dendritic reconstruction of control (black,  $n = 8$ ) and cKO (blue,  $n = 7$ ) striatal CINs, scale: 30  $\mu\text{m}$ . **D.** Volume of dendritic spread of control and *Er81* cKO CINs ( $p = 0.5911$ ). **E.** Total dendritic volume of control and *Er81* cKO CINs ( $p = 0.0072$ ). **F.** Number of dendritic branch points in control and *Er81* cKO CINs ( $p = 0.0337$ ). **G.** Sholl analysis representing the complexity of the dendritic field of control and *Er81* cKO CINs (two-way ANOVA:  $F_{(1, 2262, \text{genotype})} = 167.2$ ,  $p < 0.0001$ ;  $F_{(173, 2262, \text{interaction})} = 0.5176$ ,  $p > 0.9999$ ). **H.** ChAT<sup>+</sup> neuropil in the control and *Er81* cKO striatum, scale: 50  $\mu\text{m}$ . **I.** Quantification of the area occupied by ChAT<sup>+</sup> neuropil in the striatum ( $n = 4$  control mice, 3 cKO mice,  $p = 0.0009$ ). Unless otherwise specified, Student's t-test:  $p < 0.05$ :\*,  $p < 0.01$ :\*\*,  $p < 0.001$ :\*\*\*,  $p < 0.0001$ :\*\*\*\*.

Electrophysiological recordings from CINs revealed decreased excitability and activity in mature knockout conditions (data not shown, Ahmed et al 2021, Appendix B). Specifically, we observed slower afterhyperpolarisation (AHP) kinetics and larger delayed rectifier and inward rectifier currents, both contributing to decreased evoked excitability, with no changes to baseline firing. These altered currents were thought to be attributed to shifted calcium signalling perhaps mediated by the metabotropic Glutamate Receptor 5 (mGluR5), as we observed a significant increase in its expression in knockout conditions. As morphological and functional properties of neurons govern their connectivity (Reimann et al. 2017), we anticipated that these functional changes would impact the synaptic integration of CINs within striatal circuitry.

We therefore compared the connectivity pattern of the striatal circuit in the control and Er81 conditional knockout by staining and quantifying synaptic terminal markers specific to cell subpopulations, combined with recordings of current inputs to CINs (**Figure 2.4A**). We found no changes to spontaneous excitatory post-synaptic currents (EPSCs, **Figure 2.4B**, data not shown) or the density of boutons expressing markers of glutamatergic inputs from either the cortex (VGluT1; **Figure 2.4D, E**) or thalamus (VgluT2; **Figure 2.4F, G**) on the soma, proximal dendrites, and distal dendrites of CINs. However, we did observe an increase in the amplitude of spontaneous inhibitory post-synaptic currents (IPSCs, **Figure 2.4C**, data not shown) in the Er81 knockout, indicating possible changes to the inhibitory innervation of CINs mediated by  $\gamma$ -aminobutyric acid (GABA). We therefore quantified bouton densities representing innervation from GABAergic striatal interneuron subtypes. As CINs primarily receive innervation from striatal NPY-INs (English et al. 2011, Straub et al. 2016) and receive some very sparse innervation from PV-INs (Chang and Kita 1992, Straub et al. 2016), we analysed the density of NPY and PV positive synaptic boutons on CINs in control and knockout conditions. We did not observe any differences in NPY bouton density (**Figure 2.4H, I**), however we did see a significant increase in PV bouton density in the knockout (**Figure 2.4J, K**). This implies that the increase in GABAergic innervation could derive specifically from PV-INs. However, it is known that CINs are able to co release GABA in the striatum (Nelson et al. 2014, Lozovaya et al. 2018), therefore we also quantified cholinergic inputs to CINs by labelling the specific cholinergic vesicular glutamate transporter VgluT3 (Higley et al. 2011, Nelson et al. 2014). We found a significant increase in cholinergic bouton density on CINs in the knockout (**Figure 2.4L, M**), indicating that there are some alterations also occurring within the cholinergic microcircuitry. As we previously saw shifts in CIN axonal morphology, these results indicated that the outputs of CINs may also be altered.

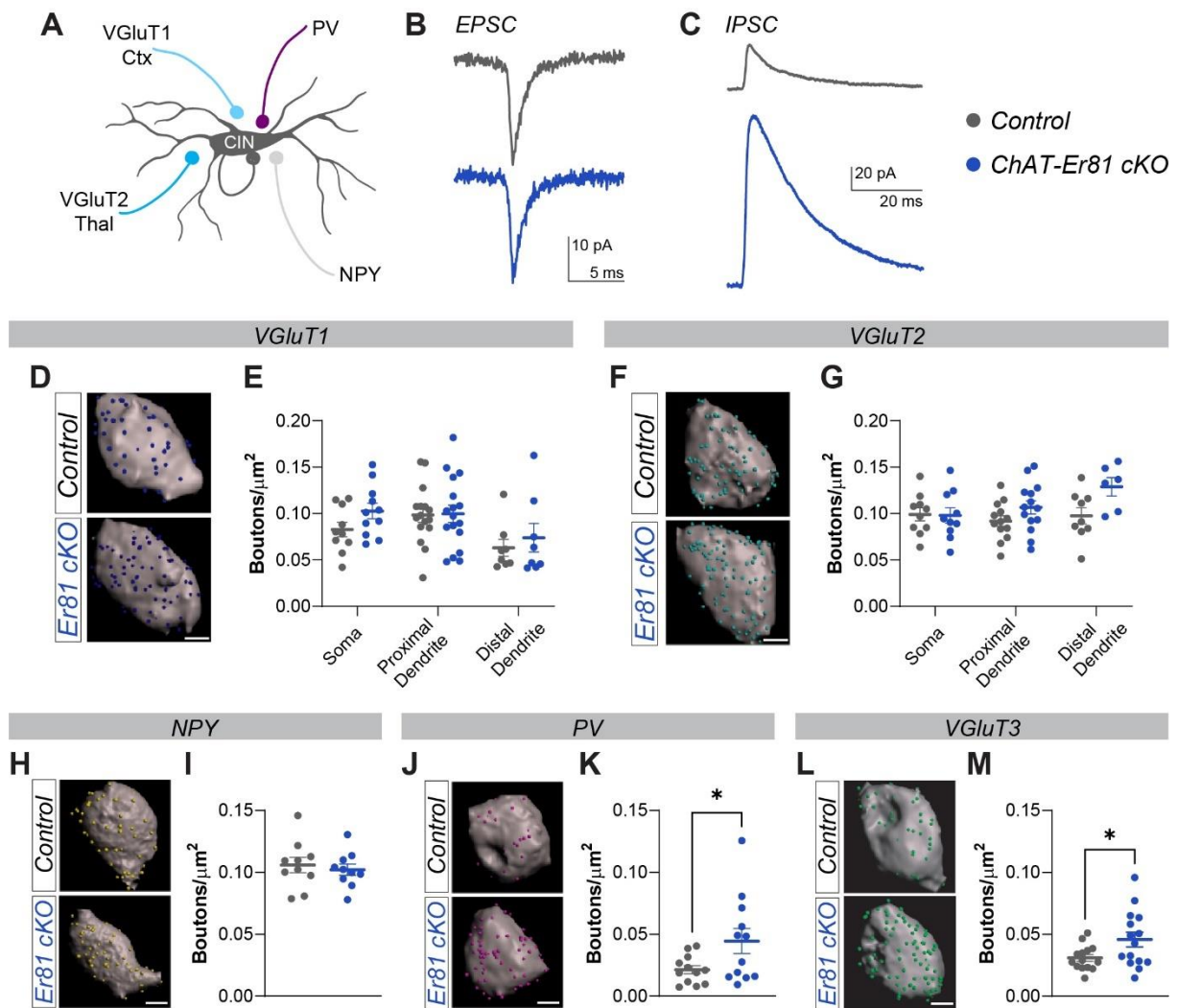


**Figure 2.4: Inputs to cholinergic interneurons are rewired in the absence of *Er81***

**A.** Schematic of inputs to striatal cholinergic interneurons (CINs): vesicular glutamate transporter 1 (VGLuT1) is expressed in cortical inputs (ctx), vesicular glutamate transporter 2 (VGLuT2) is expressed in thalamic inputs (thal), parvalbumin (PV), neuropeptide-Y (NPY), and cholinergic inputs labelled with vesicular glutamate transporter 3 (VGLuT3). **B.** Excitatory post-synaptic current (EPSC) examples in control and Er81 cKO CINs. **C.** Inhibitory post-synaptic current (IPSC) examples in control and Er81 cKO CINs. **D.** Reconstruction of VGLuT1+ boutons contacting a control and Er81 cKO CIN, scale: 5  $\mu\text{m}$ . **E.** VGLuT1+ bouton density quantification across the soma (n = 10 control, 11 cKO cells), proximal dendrites (n = 16 control, 17 cKO cells), and distal dendrites (n = 8 control, 8 cKO cells) of control and Er81 cKO CINs (two-way ANOVA:  $F_{(1, 64, \text{genotype})} = 1.705$ ,  $p = 0.1963$ ;  $F_{(2, 64, \text{interaction})} = 0.522$ ,  $p = 0.5958$ ). **F.** Reconstruction of VGLuT2+ boutons contacting a control and Er81 cKO CIN, scale: 5  $\mu\text{m}$ . **G.** VGLuT2+ bouton density quantification across the soma (n = 10 control, 10 cKO cells), proximal dendrites (n = 13 control, 14 cKO cells), and distal dendrites (n = 9 control, 6 cKO cells) of control and Er81 cKO CINs (two-way ANOVA:  $F_{(1, 56, \text{genotype})} = 5.525$ ,  $p = 0.0223$ ;  $F_{(2, 56, \text{interaction})} = 1.890$ ,  $p = 0.1606$ ; post-hoc Bonferroni's multiple comparisons: soma  $p > 0.9999$ , proximal dendrites  $p = 0.3611$ , distal dendrites  $p = 0.0513$ ). **H.** Reconstruction of NPY+ boutons contacting a control and Er81 cKO CIN, scale: 5  $\mu\text{m}$ . **I.** Somatic NPY+ bouton density quantification (n = 10 control, 10 cKO cells,  $p = 0.6272$ ). **J.** Reconstruction of PV+ boutons contacting a control and Er81 cKO CIN, scale: 5  $\mu\text{m}$ . **K.** Somatic PV+ bouton density quantification (n = 12 control, 12 cKO cells,  $p = 0.0403$ ). **L.** Reconstruction of VGLuT3+ boutons contacting a control and Er81 cKO CIN, scale: 5  $\mu\text{m}$ . **M.** Somatic VGLuT3+ bouton density quantification (n = 14 control, 15 cKO cells,  $p = 0.0334$ ). Unless otherwise specified, Student's t-test:  $p < 0.05$ :\*,  $p < 0.01$ :\*\*,  $p < 0.001$ :\*\*\*,  $p < 0.0001$ :\*\*\*\*.

To further test whether reciprocal cholinergic innervation of other striatal neurons was also altered in the *Er81* conditional knockout, we characterised ChAT or VGluT3 expressing bouton densities on striatal interneurons and projection neurons (English et al. 2011, Nelson et al. 2014) (**Figure 2.5A, D**). We first characterised VGluT3 boutons on other interneuron subtypes in the *Er81* conditional knockout. We found no change in the density of cholinergic boutons on NPY-INs (**Figure 2.5B**) alongside a significant decrease in the output to PV-INs (**Figure 2.5C**). Combined with the specific increase in PV innervation of CINs, this decrease indicates a shift in the connectivity between PV-INs and CINs when *Er81* is ablated from CINs. This is interesting, particularly as the connection from PV-INs to CINs is canonically weak (Chang and Kita 1992, Straub et al. 2016), thus a strengthening of this connection, combined with a weakening of cholinergic regulation of PV-INs suggests that the activity of these neurons could be modulated in the *Er81* conditional knockout, and thus result in changes to striatal output.

We thus wondered if these alterations could culminate in the rewiring of cholinergic inputs to the spiny projection neurons (SPNs) of the striatum. CINs generally enhance SPN activity, primarily via the activation of muscarinic acetylcholine receptors (mAChRs) (Lim et al. 2014, Mamaligas et al. 2019), although SPNs do also express nicotinic acetylcholine receptors (nAChRs), which are also important for regulating SPN properties (Ehlinger et al. 2017). We therefore labelled SPNs via a GFP viral infection in the striatum (**Figure 2.5E**, see Methods) and quantified cholinergic boutons on the soma and proximal dendrites. We found an increase in bouton density in the *Er81<sup>fl/fl</sup>;ChAT-cre* knockout, compared to controls (**Figure 2.5F**). This may correlate to increased acetylcholine release onto SPNs and modulate their function, and thus the overall striatal output.

It has been previously shown that increases in cholinergic signalling can induce dendritic expansion in SPNs (Ehlinger et al. 2017). As we observed increased cholinergic input density on SPNs, which could represent increased cholinergic signalling, we decided to compare the morphological characteristics in the *Er81* conditional knockout, compared to control. We therefore reconstructed SPNs and quantified measures of dendritic complexity. There was no change in the Sholl intersections (**Figure 2.5G**), size of the neuron (**Figure H, I**), or the number of dendritic branch points (**Figure 2.5J**). Despite the apparent change in cholinergic innervation of SPNs, we anticipate that this does not equate to the drastic alterations induced in Ehlinger et al. (2017), and therefore did not result in any alterations to SPN morphology.

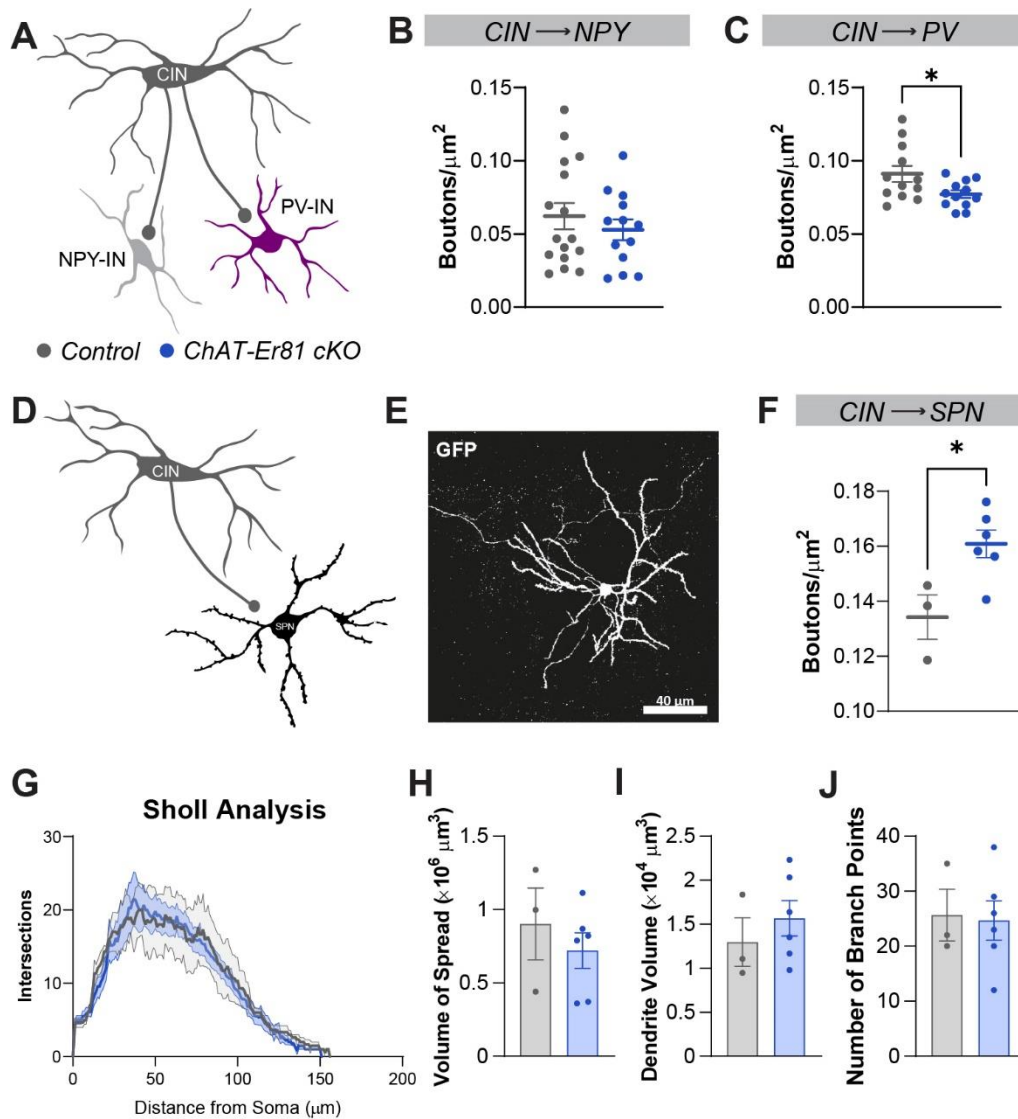


**Figure 2.5: Cholinergic output is shifted in the absence of *Er81***

**A.** Schematic of CIN outputs to NPY+ and PV+ interneurons. **B.** Somatic VGluT3+ bouton density quantification on control and Er81 cKO NPY+ interneurons ( $n = 16$  control,  $13$  cKO cells,  $p = 0.4385$ ). **C.** Somatic VGluT3+ bouton density quantification on control and Er81 cKO PV+ interneurons ( $n = 12$  control,  $12$  cKO cells,  $p = 0.0319$ ). **D.** Schematic of cholinergic outputs innervating striatal spiny projection neurons (SPNs). **E.** A SPN labelled with virally infected green fluorescent protein (GFP; see Methods) for bouton and morphological reconstruction ( $n = 3$  control,  $6$  cKO cells), scale:  $40 \mu\text{m}$ . **F.** ChAT+ bouton density quantification across the soma and proximal dendrites of control and Er81 cKO SPNs ( $p = 0.0218$ ). **G.** Sholl analysis representing the complexity of the dendritic field of control and Er81 cKO SPNs (two-way ANOVA:  $F(1, 1099, \text{genotype}) = 2.768, p = 0.0964$ ;  $F(156, 1099, \text{interaction}) = 0.1362, p > 0.9999$ ). **H.** Volume of dendritic spread of control and Er81 cKO SPNs ( $p = 0.4731$ ). **I.** Total dendritic volume of control and Er81 cKO SPNs ( $p = 0.4593$ ). **J.** Number of dendritic branch points in control and Er81 cKO SPNs ( $p = 0.8738$ ). Unless otherwise specified, Student's t-test:  $p < 0.05$ :\*,  $p < 0.01$ :\*\*,  $p < 0.001$ :\*\*\*,  $p < 0.0001$ :\*\*\*\*.

Together these results indicate a specific perturbation to the connection between CINs and PV-INs in the striatum when *Er81* is ablated from CINs. Interestingly, PV-INs also express *Er81*, as we have shown above, thus raising the question of *Er81* expression regulating the connectivity between specific neuronal subtypes. Based on the results observed thus far, the lack of *Er81* in CINs appears to promote PV-IN innervation of CINs, but also redirect cholinergic outputs from PV-INs to other CINs and SPNs. It is possible that some of these mechanisms are compensatory, potentially in response to the morphological alterations observed. Decreased dendrite availability could result in a higher clustering of the same number of boutons, resulting in a higher density. In addition, the decrease in axonal neuropil may underlie the decreased innervation of PV-INs, however this is not a global effect, with increased innervation of other neuron types. This could implicate *Er81* expression in CINs as necessary for connection specificity, particularly in relation to PV-INs. This is of great interest as *Er81* expression could link these two cell populations together within striatal circuitry.

Interestingly, both PV-INs and most CINs express the *Lhx6* (LIM Homeobox 6) transcription factor, signifying that they are born in a common location, the medial ganglionic eminence (MGE), which does have a subdomain expressing *Er81* during embryonic development and neurogenesis (Marin et al. 2000, Flames et al. 2007). Whether *Er81* is expressed in striatum-fated PV-INs and CINs from embryonic stages is not known, regardless, their common birthplace and altered circuitry in the absence of *Er81* in CINs implicates *Er81* as a regulator of connectivity between cells born in the MGE. This concept has been shown before in cortical circuits, whereby daughter cells originating from a common radial glial progenitor are more likely to form synaptic connections with one another than cells from a different lineage (Yu et al. 2009, He et al. 2015, Lin et al. 2023). We hypothesised that *Er81* may be necessary for controlling a similar mechanism in striatal MGE-derived interneurons. We therefore utilised a conditional genetic model under the *Lhx6* transcription factor promoter to target and remove *Er81*. *Lhx6* is expressed in MGE derived interneurons from the stage that they are post-mitotic; as such, *Lhx6* interneurons comprise most striatal interneurons, including almost all PV-INs (Liodis et al. 2007), and a proportion of CINs, reported as approximately 50% (Lozovaya et al. 2018). We anticipate that the *Lhx6*-dependent *Er81* knockout will cause further dysregulation of striatal interneuron connectivity, and potentially reshape the wiring of the network. Understanding this would give us further knowledge about factors regulating circuit development, and how these processes are vulnerable to perturbation, and thus pathological alterations.

## 2.4 Er81 is not Implicated in the Proliferation and Migration of MGE-derived Interneurons

The *Er81<sup>fllox/fllox</sup>;Lhx6-cre;TdTomato* knockout model ablates Er81 from interneurons originating in the MGE during post-mitotic, embryonic stages. We first confirmed the efficacy of the knockout in removing Er81 (**Figure 2.6A, B**). To determine whether any early embryonic or postnatal changes had occurred to affect the Lhx6+ interneuron population, we quantified cell number and subtype composition at mature stages. As previously mentioned in Chapter 1, striatal interneurons are not a homogeneous population, and a key functional divide reflected in both behavioural control and interneuron identity and function, is the division between the dorsomedial (DMS) and dorsolateral (DLS) striatum. As MGE-derived interneurons populate the striatum, they follow a conserved order of migration; early born interneurons inhabit the DLS and late born interneurons populate the DMS, this has been shown particularly in the case of CINs (Chen et al. 2010). In addition, PV-INs in the DMS and DLS are functionally different and integrate with circuitry separately (Monteiro et al. 2018). Overall, we found no change in the density of Lhx6+ interneurons in both the DMS and DLS (**Figure 2.6C**). Within the striatal CIN population, there are both Lhx6-expressing and non-expressing neurons, thought to be evenly split (Lozovaya et al. 2018). Here, we found approximately 80% of CINs were Lhx6+ (data not shown), with a much higher proportion in the DMS compared to the DLS (**Figure 2.6G**). We therefore analysed the proportion of the whole Lhx6+ population that expressed choline acetyltransferase (ChAT; indicates CINs, **Figure 2.6D**), which was unchanged in the *Er81* conditional knockout in both the DMS and DLS (**Figure 2.6E**). The proportion of the whole CIN population that was Lhx6+ (**Figure 2.6F**) was also unchanged (**Figure 2.6G**). PV+ and SST+ cells make up the majority of the remaining Lhx6+ interneuron population (Gittis et al. 2010), and Lhx6 is necessary for the specification of both of these cell types (Liodis et al. 2007). We similarly quantified the proportion of the Lhx6+ population expressing either PV or SST in both the DMS and DLS and found no differences between the control and conditional knockout (**Figure 2.6H-K**).

Overall, the composition of the Lhx6+ interneuron population remains consistent between the control and *Er81* conditional knockout, implying that despite the fact that *Er81* is ablated during migratory embryonic stages, it does not regulate the overall migration, differentiation, and survivability of Lhx6+ interneurons in the striatum. However, it is entirely possible that postnatal developmental factors such as intrinsic electrophysiological activity and connection formation are under the control of *Er81* regulation.



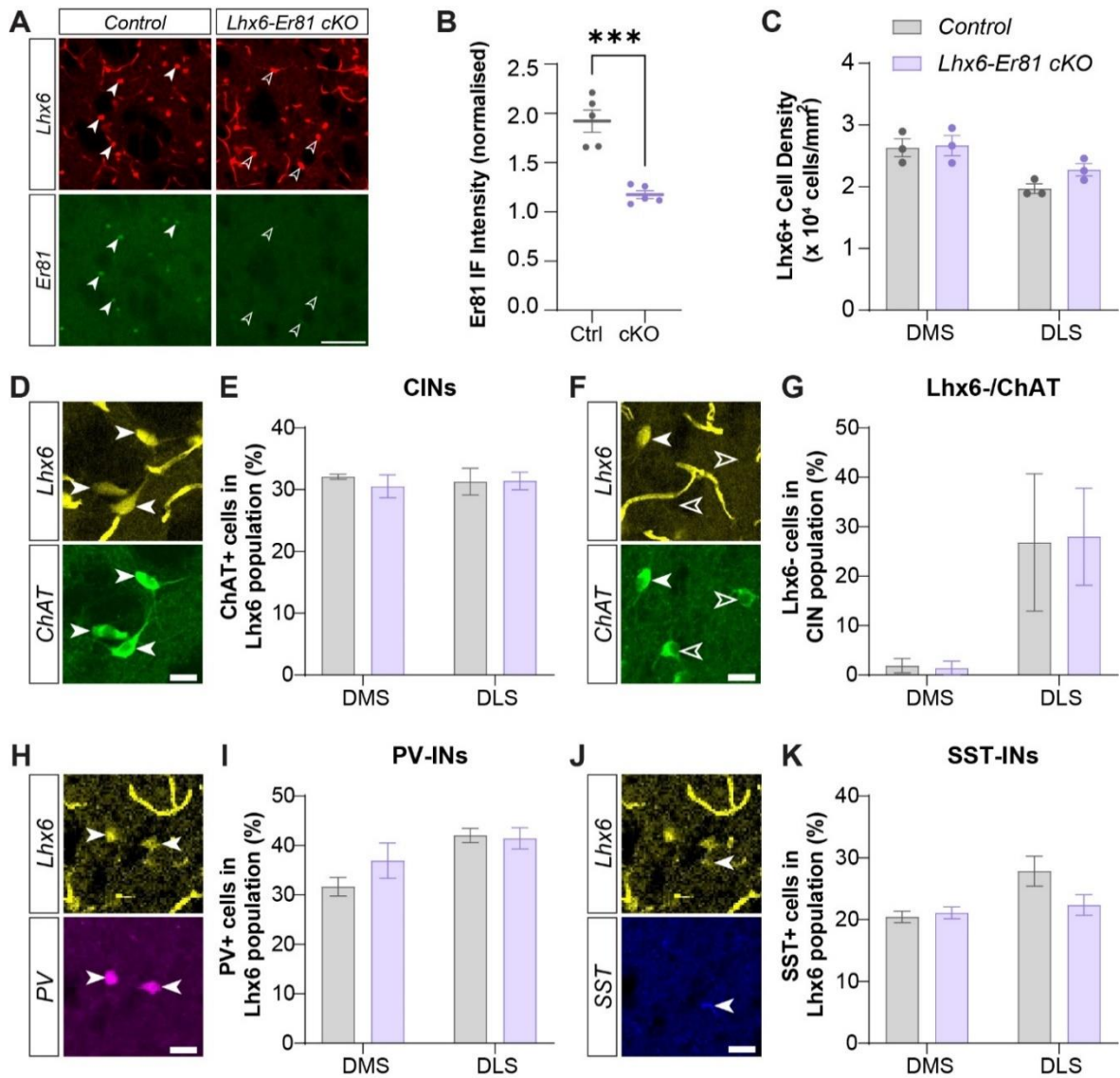


**Figure 2.6: *Er1* ablation does not alter the composition of the *Lhx6*+ interneuron population**

**A.** *Er1* expression (green) in *Lhx6*+ cells (red) in the control (*Lhx6-Cre;TdTomato*) and *Lhx6-Er1* cKO (*Er1<sup>fl/fl</sup>;Lhx6-Cre;TdTomato*) adult striatum, scale: 100  $\mu$ m. **B.** Quantification of relative *Er1* intensity in control and *Er1* cKO *Lhx6*+ interneurons (n = 245 cells, 5 control mice, 168 cells, 5 cKO mice, p = 0.0002). **C.** *Lhx6*+ cell density in the control and *Er1* cKO dorsomedial and dorsolateral striatum (DMS, DLS; n = 3 control, 3 cKO mice, two-way ANOVA:  $F_{(1, 8, genotype)} = 1.795$ , p = 0.2171;  $F_{(1, 8, interaction)} = 1.141$ , p = 0.3167). **D.** *Lhx6*+ cells expressing ChAT, scale: 25  $\mu$ m. **E.** The proportion of the *Lhx6*+ population made up of CINs in the control and *Er1* cKO DMS and DLS (n = 3 control, 3 cKO mice, two-way ANOVA:  $F_{(1, 8, genotype)} = 0.2041$ , p = 0.6635;  $F_{(1, 8, interaction)} = 0.2728$ , p = 0.6156). **F.** *Lhx6* positive and negative ChAT+ cells, scale: 25  $\mu$ m. **G.** The proportion of the ChAT+ population made up of *Lhx6*+ cells in the control and *Er1* cKO DMS and DLS (n = 3 control, 3 cKO mice, two-way ANOVA:  $F_{(1, 8, genotype)} = 0.0016$ , p = 0.9691;  $F_{(1, 8, interaction)} = 0.0090$ , p = 0.9268). **H.** *Lhx6*+ cells expressing PV, scale: 25  $\mu$ m. **I.** The proportion of the *Lhx6*+ population made up of PV+ cells in the control and *Er1* cKO DMS and DLS (n = 3 control, 3 cKO mice, two-way ANOVA:  $F_{(1, 8, genotype)} = 0.9466$ , p = 0.3591;  $F_{(1, 8, interaction)} = 1.500$ , p = 0.2555). **J.** *Lhx6*+ cells expressing SST, scale: 25  $\mu$ m. **K.** The proportion of the *Lhx6*+ population made up of SST+ cells in the control and *Er1* cKO DMS and DLS (n = 3 control, 3 cKO mice, two-way ANOVA:  $F_{(1, 8, genotype)} = 2.185$ , p = 0.1776;  $F_{(1, 8, interaction)} = 3.552$ , p = 0.0962). Unless otherwise specified, Student's t-test: p<0.05:\*, p<0.01:\*\*, p<0.001:\*\*\*, p<0.0001:\*\*\*\*.

## 2.5 Er81 Regulates the Excitability of Parvalbumin and Cholinergic Interneurons

Since neuronal activity is a key regulator of circuit development, we compared electrophysiological properties of CINs and PV-INs in control and *Lhx6*-dependent *Er81* conditional knockout conditions at early postnatal (P5-7; a key critical period of striatal maturation (Dehorter et al. 2011)) and developed stages (P30+). Despite our previous findings in a CIN specific knockout of *Er81* (Chapter 2.3, Ahmed et al. (2021), Appendix B), and the alterations found in cortical PV-INs (Dehorter et al. 2015), we anticipate that an *Lhx6*-dependent knockout will affect wider interneuron microcircuitry, and therefore may present with separate alterations to interneuron intrinsic properties.

### 2.5.1 Cholinergic Interneuron Properties

As we outlined previously, not all CINs are included within the *Lhx6*+ interneuron population. Therefore, not all CINs are affected in the knockout condition. This poses the question whether any resulting phenotypes are dependent on cell autonomous alterations to CINs, or circuit dynamics adjusting CIN activity and function. *In vitro* electrophysiological recordings revealed that during postnatal development (P5-7), there were no differences between control and conditional knockout cell properties. There was no change in the resting membrane potential or input resistance (**Figure 2.7B, C**), and no changes to action potential (AP) kinetics, including AP threshold (**Figure 2.7D**, Table 4, Appendix E). In addition, there were no changes to characteristic CIN properties, such as the rate of spontaneous tonic firing (**Figure 2.7E**), or the regularity of firing (**Figure 2.7F**). When stimulated with hyperpolarising to depolarising current steps, we found no difference in the evoked firing rate (**Figure 2.7G**), initial hyperpolarising sag (**Figure 2.7H**) or the adaptation of evoked spiking (**Figure 2.7I**).

Similarly, we observed no changes to basic CIN electrophysiological properties in mature conditional knockout cells compared to controls. Resting membrane potential (**Figure 2.7K**) and input resistance (**Figure 2.7L**) remained consistent. However, we did observe a slight trend towards a more depolarised AP threshold (**Figure 2.7M**), as well as a significant increase in AP afterhyperpolarisation (AHP) amplitude (Table 5, Appendix E). Spontaneous firing rate and regularity remained unchanged (**Figure 2.7N, O**), but we did observe a decrease in evoked firing rate (**Figure 2.7P**), with no change to the sag ratio and adaptation of evoked spikes (**Figure 2.7Q, R**). This indicates similar results to what we found in the ChAT-dependent knockout of *Er81*. The increased AHP, with no change in baseline firing, but deficits at higher depolarised steps that we have found in the *Lhx6*-dependent *Er81* knockout suggest that these factors are under the cell autonomous control of *Er81*.

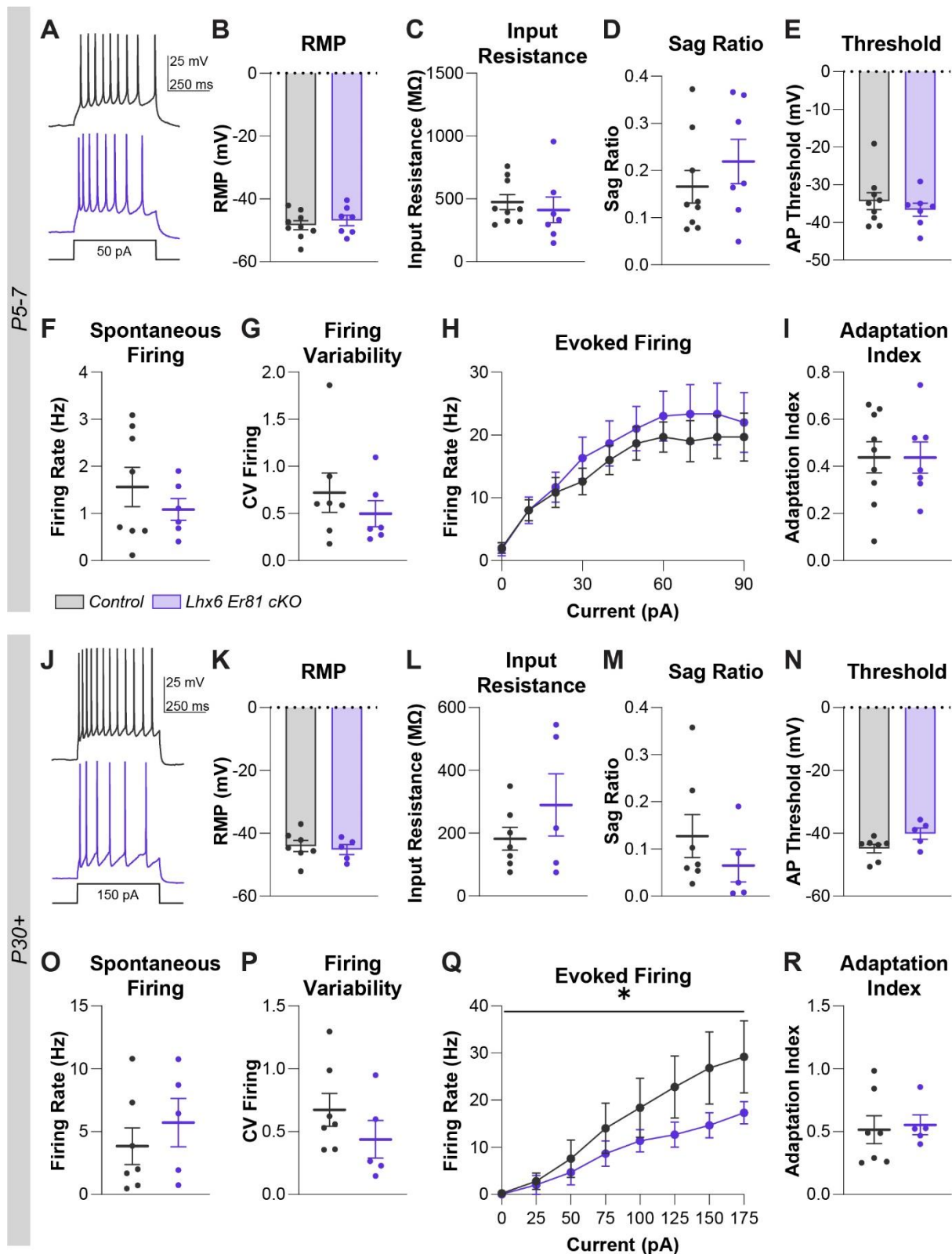


**Figure 2.7: CIN evoked activity is decreased in the mature *Lhx6*-dependent knockout of *Er1***

**A-I.** Electrophysiological characteristics of developing striatal CINs in control and *Er1* cKO conditions at P5-7. **A.** Example traces of evoked firing in response to a 50 pA depolarising current step in a control and *Er1* cKO CIN at P5-7. **B.** Resting membrane potential (n = 9 control, 7 cKO cells, p = 0.5095). **C.** Input resistance (n = 9

control, 7 cKO cells,  $p = 0.5872$ ). **D.** Sag ratio ( $n = 9$  control, 7 cKO cells,  $p = 0.4698$ , Mann-Whitney test). **E.** Action potential threshold ( $n = 9$  control, 7 cKO cells,  $p = 0.4591$ ). **F.** Spontaneous firing rate ( $n = 8$  control, 6 cKO cells,  $p = 0.3779$ ). **G.** The coefficient of variation of spike timing (CV of inter-spike intervals;  $n = 7$  control, 6 cKO cells,  $p = 0.4069$ ). **H.** F-I curve showing firing rate across increasing current steps ( $n = 7$  control, 6 cKO cells, two-way ANOVA:  $F_{(1, 111, \text{genotype})} = 2.991$ ,  $p = 0.0865$ ;  $F_{(9, 111, \text{interaction})} = 0.1629$ ,  $p = 0.9971$ ). **I.** Adaptation index of evoked firing ( $n = 9$  control, 7 cKO cells,  $p = 0.9906$ ). **J-R.** Electrophysiological characteristics of mature striatal CINs in control and Er81 cKO conditions at P30+. **J.** Example traces of evoked firing in response to a 150 pA depolarising current step in a control and Er81 cKO CIN at P30+. **K.** Resting membrane potential ( $n = 7$  control, 5 cKO cells,  $p = 0.6628$ ). **L.** Input resistance ( $n = 7$  control, 5 cKO cells,  $p = 0.2727$ ). **M.** Sag ratio ( $n = 7$  control, 5 cKO cells,  $p = 0.3352$ ). **N.** Action potential threshold ( $n = 7$  control, 5 cKO cells,  $p = 0.0588$ ). **O.** Spontaneous firing rate ( $n = 7$  control, 7 cKO cells,  $p = 0.4458$ ). **P.** The coefficient of variation of spike timing (CV of inter-spike intervals;  $n = 7$  control, 5 cKO cells,  $p = 0.2670$ ). **Q.** F-I curve showing firing rate across increasing current steps ( $n = 5$  control, 3 cKO cells, two-way ANOVA:  $F_{(1, 48, \text{genotype})} = 5.482$ ,  $p = 0.0234$ ;  $F_{(7, 48, \text{interaction})} = 0.3937$ ,  $p = 0.9015$ ). **R.** Adaptation index of evoked firing ( $n = 7$  control, 5 cKO cells,  $p = 0.7986$ ). Unless otherwise specified, Student's t-test:  $p < 0.05$ :\*,  $p < 0.01$ :\*\*,  $p < 0.001$ :\*\*\*,  $p < 0.0001$ :\*\*\*\*.

---

## 2.5.2 Parvalbumin Positive Interneuron Properties

The dependence of PV-IN activity and function on Er81 expression has been previously studied in the cortex, where approximately two-thirds of layer 2/3 PV-INs express Er81. The electrophysiological properties of these neurons correlate with their expression of Er81, and the ablation of Er81 leads to altered excitability gating in these cells, as they present with a shortened latency to the first evoked spike (Dehorter et al. 2015).

We do not expect the exact same mechanisms to be in effect in the striatum. Apart from the fact that the expression profile of Er81 is different in the striatum, with nearly all PV-INs expressing Er81 (**Figure 2.2**), PV-INs integrate into striatal circuitry differently from the cortex. Despite being born in a common location, the MGE, cortical and striatal PV-INs undergo segregated developmental processes from the point at which they divert their migratory paths (Villar-Cervino et al. 2015). We therefore anticipate that the role of Er81 in regulating PV-IN properties will be distinct in the striatum.

We therefore first probed PV-IN functional properties during development (P5-7). PV expression does not arise until later stages of development (Vogt Weisenhorn et al. 1998), however their expression of Lhx6, combined with post-hoc staining showing that they express neither SST nor ChAT can determine cells at putative PV-INs. In addition, we observed that PV-INs during early development already exhibit fast-spiking characteristics and can also be identified thusly. We observed no change to baseline characteristics in putative PV-INs such as the resting membrane potential (**Figure 2.8B**) and action potential characteristics (**Figure 2.8D**, Table 6, Appendix E). However, input resistance was significantly lower in the conditional knockout (**Figure 2.8C**), and subsequently, rheobase (the smallest current required to elicit a response) was significantly greater in the knockout (**Figure 2.8F**). These changes indicate a

decrease in excitability, as a decrease in input resistance results in greater current inputs required to elicit voltage depolarisations (Kernell 1966). Despite this, there was no change in spike latency (**Figure 2.8G**) or maximum firing frequency (**Figure 2.8H**), signifying that cells showed similar activity upon stimulation, but required greater input for activation.

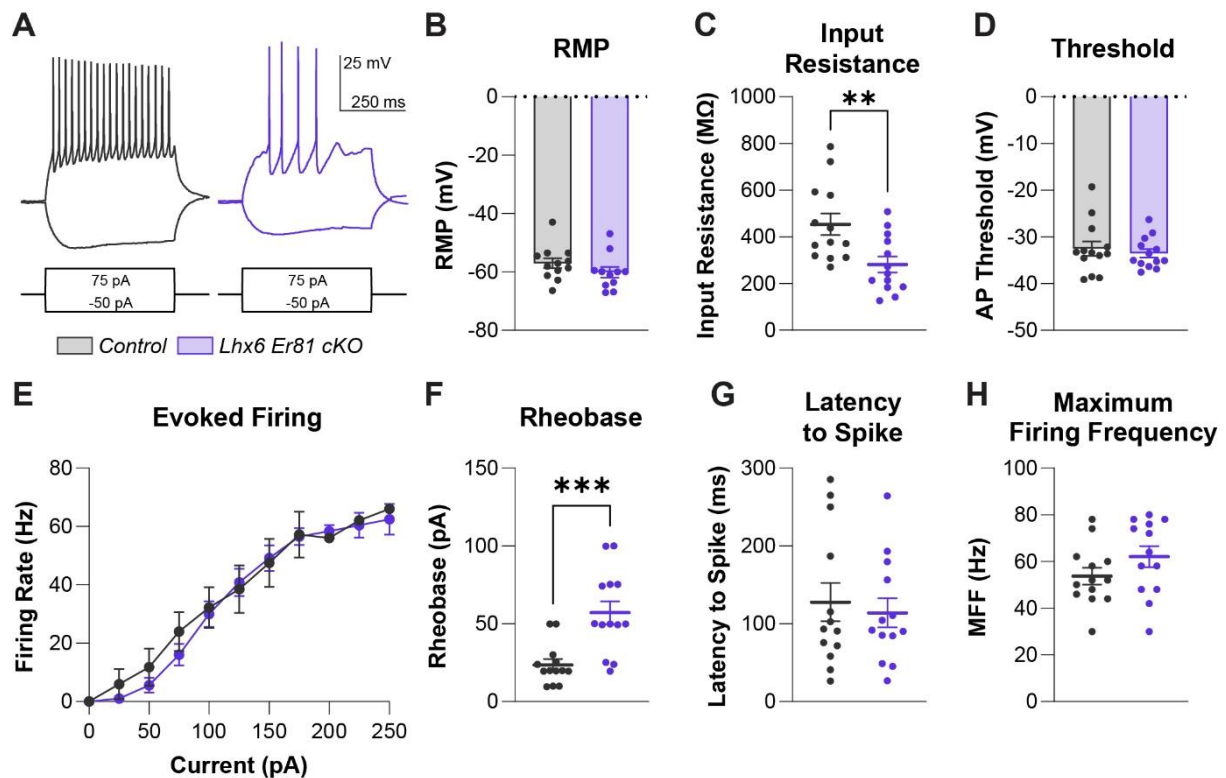


**Figure 2.8: Putative Fast Spiking Interneurons are less excitable in the absence of *Er81* during early development**

**A.** Example traces of hyperpolarisation and evoked firing in response to -50 and 75 pA current step stimulations in a control and *Er81* cKO putative FSI/PV-IN at P5-7. **B.** Resting membrane potential ( $n = 12$  control, 11 cKO cells,  $p = 0.2334$ ). **C.** Input resistance ( $n = 13$  control, 13 cKO cells,  $p = 0.006$ ). **D.** Action potential threshold ( $n = 13$  control, 13 cKO cells,  $p = 0.5861$ ). **E.** F-I curve showing firing rate across increasing current steps ( $n = 8$  control, 14 cKO cells, two-way ANOVA:  $F_{(1, 171, \text{genotype})} = 0.3967$ ,  $p = 0.5296$ ;  $F_{(10, 171, \text{interaction})} = 0.1629$ ,  $p = 0.9911$ ). **F.** Rheobase ( $n = 13$  control, 13 cKO cells,  $p = 0.0010$ , Mann-Whitney test). **G.** Latency to the first spike at rheobase ( $n = 13$  control, 13 cKO cells,  $p = 0.8798$ , Mann-Whitney test). **H.** Maximum firing rate achievable ( $n = 13$  control, 13 cKO cells,  $p = 0.1599$ ). Unless otherwise specified, Student's t-test:  $p < 0.05$ :\*,  $p < 0.01$ :\*\*,  $p < 0.001$ :\*\*\*,  $p < 0.0001$ :\*\*\*\*.

Decreased excitability at this early stage may impact the ability of PV-INs to regulate striatal circuitry in the *Er81* knockout, and as a result, they may not have the capacity to integrate into

the striatal network due to their decreased activity (Allene et al. 2012, Denaxa et al. 2018). This could result in aberrant connectivity with the rest of the striatal circuit. We therefore wanted to confirm whether these alterations persist into adulthood.

We found that PV-INs in the *Lhx6*-dependent *Er81* conditional knockout had properties completely resembling control cells. There was no change in resting membrane potential (**Figure 2.9B**), action potential kinetics (**Figure 2.9C**, Table 7, Appendix E), rheobase (**Figure 2.9D**), spike latency (**Figure 2.9E**), or firing ability (**Figure 2.9F**). Despite developmental alterations in these cells, PV-IN properties had rectified by adulthood. We wondered whether this might be due to developmental compensation within the striatal network (Tien and Kerschensteiner 2018), perhaps via rewiring of the circuitry to modulate PV-IN activity. To probe this, we utilised a PV-dependent knockout of *Er81* (*Er81<sup>fl/fl</sup>;PV-Cre;TdTomato*). As mentioned above, PV is not expressed until P12-15, therefore alterations to PV-INs in this condition do not occur until after the P5-7 critical period of plasticity, and only within the PV-IN population, without affecting CINs. We therefore anticipate that *Er81* has a more cell autonomous effect in this knockout than in the *Lhx6*-dependent knockout.

PV-INs in the *PV*-dependent *Er81* knockout displayed deficits in line with what has been shown previously in the cortex (Dehorter et al. 2015). Despite no change to resting membrane potential (**Figure 2.9H**), action potential kinetics (**Figure 2.9I**, Table 8, Appendix E), or rheobase (**Figure 2.9J**), there was a decrease in the latency to the first spike on evoked firing (**Figure 2.9K**). This indicates that when *Er81* is ablated from PV-INs at a later stage of development, the observed increase in near threshold excitability may be under the control of similar mechanisms as in the cortex. Cortical PV-INs present with a shift in near threshold excitability in the absence of *Er81* which is mediated by the expression of *Kv1.1* potassium channels (Dehorter et al. 2015). It is possible that striatal PV-INs in the *PV*-dependent knockout of *Er81* are under the same mechanistic control.

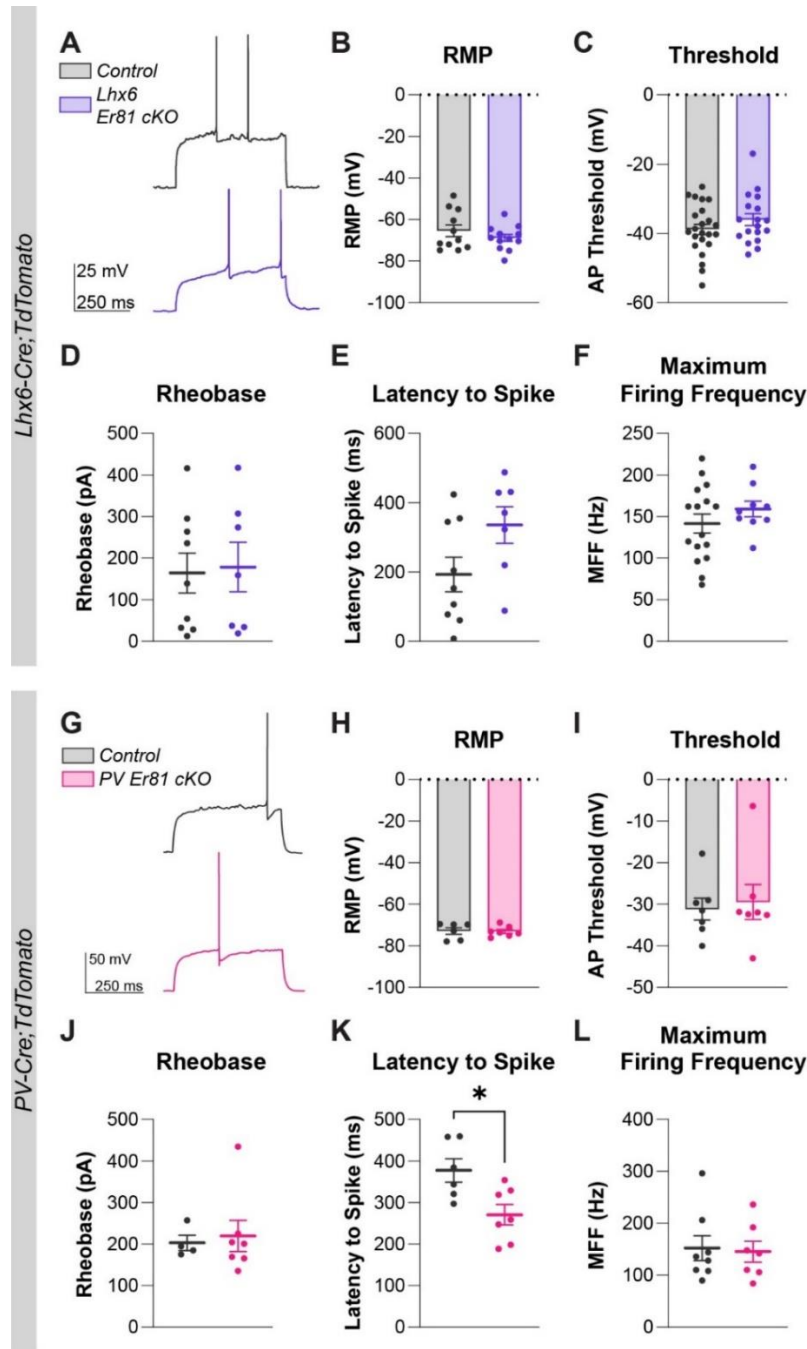


**Figure 2.9: Developmental versus mature ablation of Er81 from PV-INs produces different electrophysiological phenotypes**

**A-F.** Electrophysiological properties of mature (P30+) striatal FSIs/PV-INs in control (*Lhx6-Cre;TdTTomato*) and *Lhx6-Er81* cKO (*Er81<sup>fl/fl</sup>;Lhx6-Cre;TdTTomato*) mice. **A.** Example traces of near threshold spiking in a control and *Lhx6-Er81* cKO FSI. **B.** Resting membrane potential (n = 11 control, 12 cKO cells, p = 0.2949). **C.** Action potential threshold (n = 23 control, 18 cKO cells, p = 0.2192). **D.** Rheobase (n = 9 control, 7 cKO cells, p = 0.8541). **E.** Latency to the first spike at rheobase (n = 9 control, 7 cKO cells, p = 0.0704). **F.** Maximum firing rate achievable (n = 16 control, 9 cKO cells, p = 0.3058). **G-L.** Electrophysiological properties of mature (P30+) striatal FSIs/PV-INs in control (*PV-Cre;TdTTomato*) and *PV-Er81* cKO (*Er81<sup>fl/fl</sup>;PV-Cre;TdTTomato*) mice. **G.** Example traces of near threshold spiking in a control and *PV-Er81* cKO FSI. **H.** Resting membrane potential (n = 6 control, 7 cKO cells, p = 0.9051). **I.** Action potential threshold (n = 7 control, 7 cKO cells, p > 0.9999, Mann-Whitney test). **J.** Rheobase (n = 4 control, 7 cKO cells, p = 0.9273, Mann-Whitney test). **K.** Latency to the first spike at rheobase (n = 6 control, 7 cKO cells, p = 0.0155). **L.** Maximum firing rate achievable (n = 8 control, 7 cKO cells, p = 0.9795, Mann-Whitney test). Unless otherwise specified, Student's t-test: p<0.05:\*, p<0.01:\*\*, p<0.001:\*\*\*, p<0.0001:\*\*\*\*.

The role of Er81, and transcription factors in general, in both cell autonomous and network mediated manners is difficult to differentiate. Using sparse knockout techniques (see Methods), we did find that single PV-INs with Er81 ablated did have significantly lower expression levels of PV (data not shown). This suggests that Er81 has a key role in regulating the intrinsic properties of PV-INs, including their activity, as parvalbumin functions as a calcium buffer and mediates PV-IN activity (Caillard et al. 2000). However, in a vaster knockout condition such as the Lhx6-dependent knockout, compensatory mechanisms to account for the loss of Er81 can normalise circuitry, especially through modulation during high plasticity critical periods.



## 2.6 Lhx6+ Interneuron Connectivity is Not Dependent on Er81 Expression

We previously questioned the molecular regulation of the connectivity of striatal interneurons, and focussed on connections surrounding CINs in a specific knockout of the *Er81* transcription factor targeting only these cells. Our findings indicated a potential specific perturbation in the connectivity between CINs and PV-INs, two cell populations that primarily originate from the MGE (Marin et al. 2000). *Lhx6*<sup>+</sup> MGE-derived interneurons may have an affinity to form connections with one another as opposed to interneurons with different origins, as this has been shown previously in the cortex (Yu et al. 2009, He et al. 2015, Lin et al. 2023). We therefore questioned whether the connectivity between *Lhx6* interneurons, and specifically between PV-INs and CINs was altered upon ablation of *Er81* from the whole *Lhx6*<sup>+</sup> interneuron population. To address that, we probed measures of connectivity between *Lhx6* interneurons.

### 2.6.1 Descriptive measures of connectivity in the *Lhx6* interneuron circuit

We first quantified bouton density between PV-INs and CINs in control and the *Lhx6*-dependent *Er81* knockout and found a significant increase in PV bouton density on all CINs (**Figure 2.10B**). When we segregated CINs into *Lhx6*<sup>+</sup> and *Lhx6*<sup>-</sup>, we found that this was driven by an increase in the PV innervation of *Lhx6*<sup>-</sup> CINs (**Figure 2.10C, D**). We also found no change in the density of overall ChAT labelled cholinergic boutons on PV-INs (**Figure 2.10F**). This lack of change could be due to the pooling of all cholinergic input, including those from *Lhx6*<sup>-</sup> CINs.

Comparing these findings to the results observed in the CIN-dependent knockout of *Er81*, we do see a similar overall phenotype. However, in the *Lhx6*-dependent *Er81* knockout, we only affect *Er81* in a subpopulation of CINs, and therefore were able to more closely probe the relationship between *Er81* expression and connectivity by comparing *Lhx6*<sup>+</sup> and *Lhx6*<sup>-</sup> CINs. However, bouton quantification is simply a measure of descriptive connectivity, as boutons do not always signify functional synapses. We therefore decided to study the functional connectivity of *Lhx6*<sup>+</sup> interneurons.

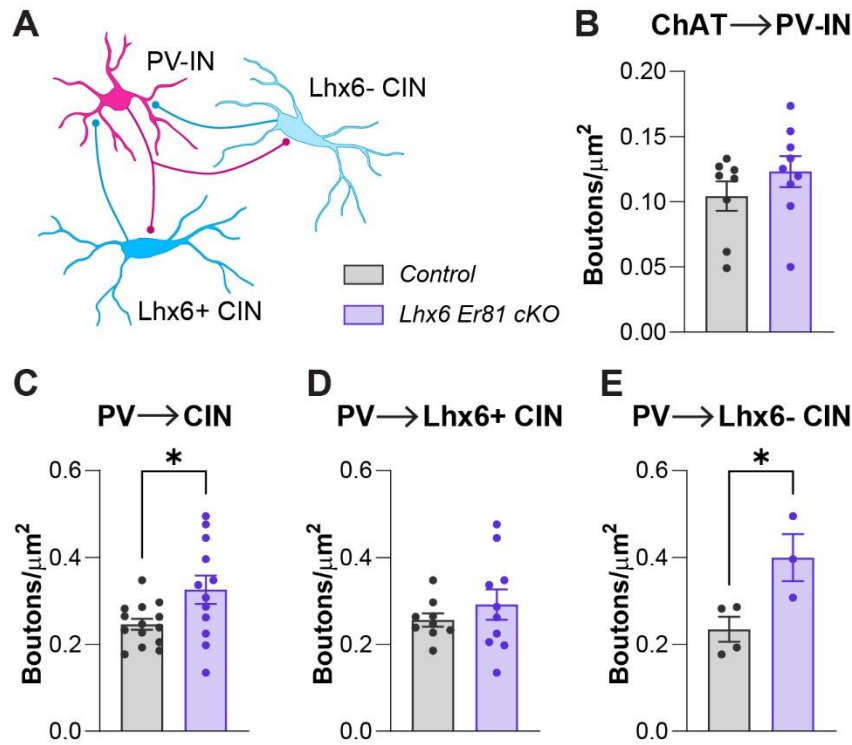


**Figure 2.10: *Er81* ablation may strengthen the connectivity between PV-INs and CINs in the mature striatum**

**A.** Scheme of connections between PV-INs and Lhx6+ and Lhx6- CINs. Connectivity from PV-INs to CINs is functionally weak. **B.** ChAT+ bouton density quantification on the soma of control and Er81 cKO PV-INs (n = 8 control, 9 cKO cells, p = 0.2766, Mann-Whitney test). **C.** PV+ bouton density quantification on the soma of all control and Er81 cKO CINs (n = 14 control, 12 cKO cells, p = 0.0240). **D.** PV+ bouton density quantification on the soma of Lhx6+ control and Er81 cKO CINs (n = 9 control, 10 cKO cells, p = 0.3773). **E.** PV+ bouton density quantification on the soma of Lhx6- control and Er81 cKO CINs (n = 4 control, 3 cKO cells, p = 0.0332). Unless otherwise specified, Student's t-test: p<0.05:\*, p<0.01:\*\*, p<0.001:\*\*\*, p<0.0001:\*\*\*\*.

### 2.6.2 Probing the synaptic connectivity of the Lhx6 interneuron circuit

Synaptic connections are established and refined throughout development. During early development, there is a large increase in connections that are then refined during synaptic pruning stages (Faust et al. 2021). We therefore decided to probe functional connectivity in the MGE-derived Lhx6<sup>+</sup> interneuron population, both during early development whilst connection formation is occurring (P5-7) and following stages of refinement (P30+).

We performed dual whole-cell patch clamp recordings from Lhx6<sup>+</sup> interneurons in the striatum at these two stages (**Figure 2.11A**). We quantified both the presence and the strength of synaptic connectivity (**Figure 2.11C**) in recorded pairs in general, as well as in identified subpopulation pairs; *i.e.* cells identified as either PV-INs or CINs (or unknown Lhx6<sup>+</sup> cells) (**Figure 2.11B, G**). We found a general decreasing trend in connected Lhx6<sup>+</sup> pairs in the P5-7 knockout condition compared to control (58% to 35%; **Figure 2.11D**), but no change in the response rate of the post-synaptic cell across trials (**Figure 2.11E**) or the amplitude of the evoked response current (**Figure 2.11F**). When we segregated pairs based on the putative identity of cells (**Figure 2.11G**), we found no difference in the connectivity of PV-IN/CIN pairs (**Figure 2.11H**). The overall incidence of confirmed PV-IN/CIN pairs was low, contributed to by the fact that many cells at this stage either still exhibited immature characteristics or were not retained for post-hoc staining, and therefore could not be identified. We therefore compared the overall connectivity of PV-INs and CINs with any other Lhx6<sup>+</sup> interneuron (including other interneurons of the same subclass and unidentified Lhx6<sup>+</sup> interneurons). We found no difference in connectivity between the control and knockout conditions in either case but did notice that PV-INs seem to more connected overall compared to CINs (**Figure 2.11I, J**). These results show no major differences in developmental connectivity between the control and *Er81* conditional knockout. However, as we are only targeting a specific time point, there is still a possibility that shifts in connectivity persist past developmental stages, therefore we performed similar paired recordings at mature stages (P30+). Once again, we found no difference in connectivity between control and knockout conditions, and an overall low incidence of connectivity between Lhx6<sup>+</sup> interneuron pairs (**Figure 2.11L**). Connected pairs were all PV-IN/PV-IN (FSI/FSI) pairs, and we observed no PV-IN/CIN connected pairs, which is unsurprising as previous studies have also shown a very low incidence of connectivity between PV-INs and CINs (Gittis et al. 2010, Straub et al. 2016). Interestingly, we did observe some connectivity between these two interneuron subtypes during developmental stages (**Figure 2.11H**). This raises a key question of whether this connection is developmentally relevant for

circuit formation but with no functional purpose later in life and is therefore pruned. Further probing into the incidence of this connectivity during development is necessary, perhaps via the use of retrograde viral labelling to determine the expanse of PV-INs connecting to CINs and vice-versa during stages of circuit formation.

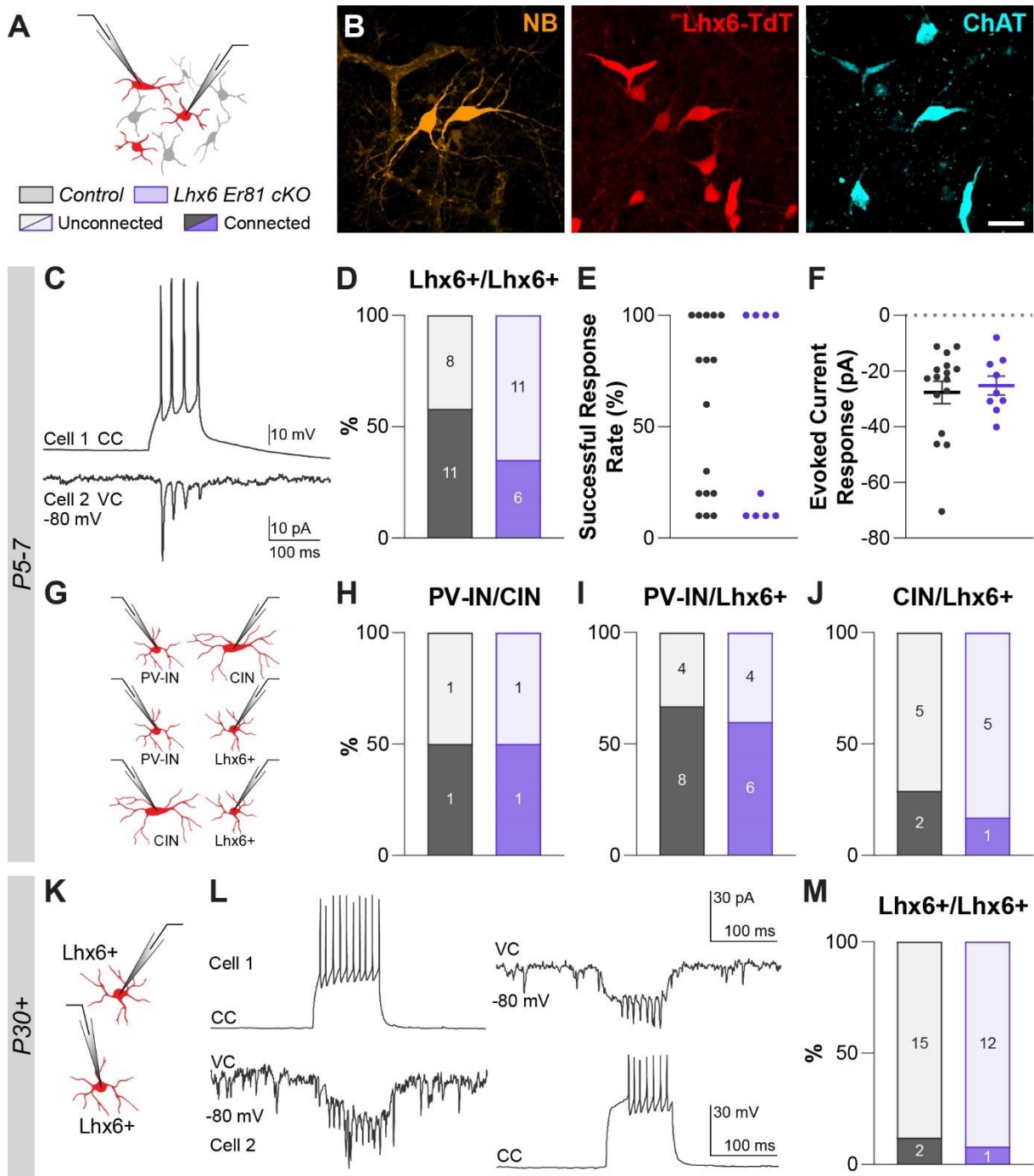


**Figure 2.11: *Er81* ablation does not severely affect the synaptic connectivity of Lhx6+ interneurons**

**A.** Dual patch recordings were done of Lhx6-TdTomato+ pairs in the striatal circuit at P5-7 and P30+. **B.** Example of a P5-7 Lhx6-TdTomato+ (red) pair loaded with neurobiotin (orange) during recording, with one cell expressing ChAT (cyan), identifying it as a CIN, scale 50  $\mu\text{m}$ . **C.** Recording trace from a synaptically connected pair, where cell 1 was stimulated to generate action potentials in current clamp (CC) mode, whilst cell 2 was held at -80 mV in voltage clamp (VC) mode to record post-synaptic currents. **D.** The proportion of all recorded pairs connected at P5-7 in the control and Er81 cKO striatum ( $n = 12$  control, 10 cKO mice,  $p = 0.1751$ , Chi-Square test). **E.** The proportion of trials where a successful post-synaptic current response was recorded (out of ten trials, for each pair direction). **F.** The average response current amplitude for each pair direction ( $p > 0.9999$ , Mann-Whitney t-test). **G.** Lhx6+ interneuron pair identity configurations: pairs were classified as either PV-IN/CIN, PV-IN/any other Lhx6+ interneuron, and CIN/any other Lhx6+ interneuron. **H.** The proportion of confirmed PV-IN/CIN pairs connected at P5-7 in the control and Er81 cKO striatum. **I.** The proportion of pairs including a PV-IN connected at P5-7 in the control and Er81 cKO striatum ( $p = 0.7462$ , Chi-Square test). **J.** The proportion of pairs including a CIN connected at P5-7 in the control and Er81 cKO striatum ( $p = 0.6115$ , Chi-Square test). **K.** Lhx6+ interneurons pairs were recorded in the adult (P30+) striatum. **L.** Recording trace of a pair connected both via gap junction and synaptically. Left: cell 1 held in CC, with action potentials evoked, cell 2 held in VC at -80 mV; then conditions switched, right: cell 1 held in VC at -80 mV, cell 2 held in CC, with action potentials evoked. **M.** The proportion of all recorded pairs connected at P30+ in the control and Er81 cKO striatum ( $n = 9$  control, 7 cKO mice,  $p = 0.7125$ , Chi-Square test).

---

The detection of synaptic connectivity in this study relies on the integration of post-synaptic responses to pre-synaptic stimulation to be strong enough to elicit a response in the soma of the post-synaptic cell. It is possible that pairs that were synaptically connected remained undetected as the stimulation of the pre-synaptic cell generated a response that was attenuated in dendritic compartments (Spruston et al. 1994). Indeed, it is possible that synchronous inputs are needed to generate a response between interneuron pairs. Synchronous firing is common within the CIN population and is important for regulating dopamine release in the striatum and enacting feedforward inhibition onto SPNs (Dorst et al. 2020). Conversely, synchronous firing in striatal PV-INs is uncommon (Klaus et al. 2011), but has been predicted in FSI pairs that are electrically connected via gap junctions.

### **2.6.3 Electrical connectivity of striatal interneurons**

During development, and even persisting into adulthood, electrical or gap junction connectivity between neurons is a critical form of cell communication. Neuronal coupling via gap junctions peaks during a transient increase during development, increasing during the first two postnatal weeks and peaking around P15, before decreasing in adulthood (Belousov and Fontes 2013). As such, gap junctions in neuronal circuits have a vital role in the regulation of circuit formation and refinement.

We have previously mentioned that sister neurons have an affinity for forming chemical synapses with each other as opposed to neurons from other lineages (Yu et al. 2009, He et al. 2015, Lin et al. 2023). Further studies revealed that these chemical synapses are preceded by

electrical connections. Excitatory cortical sister neurons arising from radial glial cells form gap junction connections with each other, but not with neurons from separate lineages (Yu et al. 2012). This electrical connectivity largely disappeared after P6 and was replaced by chemical synapses. The same study found that the presence of the electrical connection early during development was necessary for the future formation of a chemical synapse between sister neurons (Yu et al. 2012). This concept has been shown in a number of contexts, and multiple studies provide evidence for the presence of electrical connections being essential for chemical synapse formation (Todd et al. 2010, Jabeen and Thirumalai 2018).

However, it appears that gap junction connectivity may have a separate role in interneurons. A similar study focussing on cortical interneurons originating from the MGE and PoA found that neurons originating from a single progenitor form preferential electrical connections with one another as opposed to the progeny of another neural progenitor cell (Zhang et al. 2017). Interestingly, the characteristics of gap junction connectivity in inhibitory interneurons was very different from that in cortical excitatory neurons. Electrical synapses between interneurons continued to form throughout development, and did not dictate the presence or formation of chemical synapses between interneurons (Zhang et al. 2017). Instead, it is suggested that interneuron electrical coupling serves an important functional purpose for synchronising inhibitory control of the surrounding circuitry. Indeed, electrically connected interneurons preferentially form coordinated synaptic connections with the same excitatory neuron and thus suggests that interneuron origin is linked to the precise microcircuit assembly between inhibitory and excitatory neurons in the cortex (Zhang et al. 2017).

In general, interneurons appear to have a high affinity for forming gap junction connections, and this has been shown in various brain regions other than the cortex, including the striatum (Fukuda 2009). Although a dependence of connectivity on developmental lineage has not been shown in the striatum, as the majority of striatal interneurons are derived from the MGE, it is expected that they will follow similar developmental mechanisms. Whilst gap junctions have been shown between various interneuron subtypes, the most commonly reported coupling, particularly in the striatum, is between PV+ FSIs (Koos and Tepper 1999, Galarreta and Hestrin 2001, Yang et al. 2014). Early studies indicated that FSI-FSI gap junction connected pairs occur with approximately a 30% incidence in adults (Koos and Tepper 1999). Network model studies have indicated that these FSI gap junction connected pairs strongly enact synchronous inhibitory control over striatal SPNs (Hjorth et al. 2009), and are therefore vital for striatal output regulation.

We hypothesised that Er81 has a role in the promotion of gap junction connectivity between fast spiking interneurons in the striatum. Gap junctions are facilitated by two hemichannels known as connexins (Belousov and Fontes 2013). Connexin expression is under tight transcriptional control, with increasingly more regulatory transcription factors being identified (Oyamada et al. 2005). Amongst these, Er81 has been shown to regulate transcriptional programs necessary for the expression of the cardiovascular Cx40 (Shekhar et al. 2016, Shekhar et al. 2018). Although Cx40 is not expressed in neuronal cells, which instead primarily express connexin 36 (Cx36) (Condorelli et al. 1998, Rash et al. 2000), most connexins share a common genetic structure and are therefore likely to be susceptible to similar transcriptional regulation (Condorelli et al. 1998, Dbouk et al. 2009).

We saw no changes to the synaptic coupling of striatal interneurons in the absence of Er81 (**Figure 2.11**), however previous studies outlined above show that synaptic connectivity in interneurons may not be reliant on electrical connectivity, as it is in excitatory neurons. Therefore it is possible that gap junction connectivity between striatal FSIs is mediated by Er81, without then influencing synaptic connectivity. We therefore compared the number and characteristics of gap junction connected FSIs in control and Lhx6-dependent Er81 knockout conditions. This was done across three age points; P5-7, P15-18, and P30+. The addition of P15-18 was due to evidence of this stage being the peak of gap junction prevalence in interneurons, and also the peak of coupling strength between gap junction connected FSI pairs (Belousov and Fontes 2013, Yang et al. 2014).

Paired electrophysiological recordings consisted of a hyperpolarising stimulation being applied to each neuron, and the subsequent response recorded in the other neuron (**Figure 2.12A**, see Methods). From this and depolarising current steps (**Figure 2.12B**), we were able to identify electrically connected pairs with corresponding responses in both cells. We found no difference in the proportion of pairs connected at P5-7 and a low overall incidence of connected pairs (25% control, 25% conditional knockout; **Figure 2.12C**). This proportion increased in the P15-18 control (83%) but was significantly lower in knockout conditions at this stage (41%; **Figure 2.12D**). By mature (P30+) stages the prevalence of connected pairs decreased and was equivalent between control and knockout conditions (14% control, 10% conditional knockout; **Figure 2.12E**). We also compared the coupling coefficient between connected pairs and found no differences at any stage between control and knockout conditions (data not shown).



To further test this, we loaded single patched FSIs at P15-18 with neurobiotin to facilitate the loading of nearby gap junction connected cells (**Figure 2.12F**). We compared the number of loaded cells between control and knockout conditions to determine whether the overall number of connected cells showed a similar decrease. Whilst we saw no significant difference in the number of loaded cells (**Figure 2.12G**), there was a decreasing trend. There was also no difference at mature stages (0-2 cells connected control and conditional knockout, data not shown).

Together, we show that gap junction connectivity during later stages of development is significantly impeded by the lack of *Er81* in Lhx6+ interneurons. This has potential impacts on the overall formation and function of the circuit. Although FSI function is not altered in the Lhx6-dependent knockout at mature stages, it is possible that their overall control over and connectivity with SPNs is affected and impacts other aspects of basal ganglia circuit formation. Whilst we observed no differences in gap junction connectivity between individual pairs during early development (P5-7), this does not reflect the overall connectivity of the striatal network.

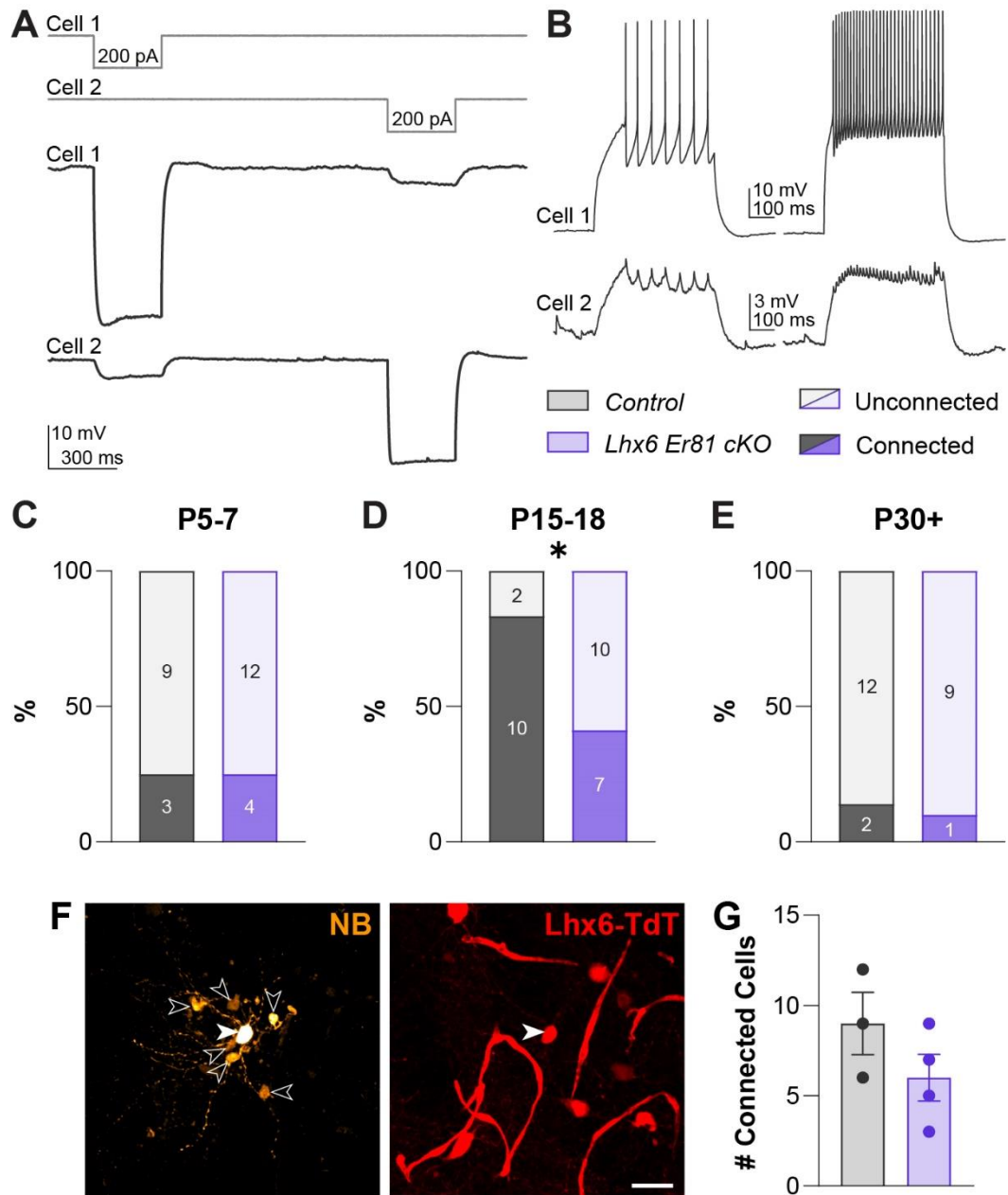


**Figure 2.12: Gap junction connectivity is decreased in the absence of *Er81***

A. The stimulation protocol to test for gap junction connectivity and cell responses in a connected pair. Each cell was stimulated by a 200 pA hyperpolarising 300 ms pulse in sequence. The stimulated cell response and the gap junction mediated response in the other cell were compared to determine the strength of connectivity. B. Example traces of a gap junction connected PV-IN pair, where both cells were held in current clamp mode. C. The proportion of PV-IN/FSI pairs connected via gap junction at P5-7 (n = 12 control, 10 cKO mice, p = 1.000, Chi-Square test). D. The proportion of PV-IN/FSI pairs connected via gap junction at P15-18 (n = 5 control, 6 cKO mice, p = 0.0232, Chi-Square test). E. The proportion of PV-IN/FSI pairs connected via gap junction at P30+ (n = 9 control, 7 cKO mice, p = 0.7543, Chi-Square test). F. A single Lhx6+ (red) cell loaded with neurobiotin (orange) *in vitro*, surrounded by cells loaded via gap junction connections at P15-18, scale: 25 μm. G. The number of connected cells surrounding the single loaded cell in the control and cKO striatum at P15-18 (n = 3 control, 3 cKO mice, p = 0.2135, Student's t-test).

#### **2.6.4 Evidence of characteristic developmental activity shifts in the absence of *Er81***

During early stages of development, characteristic waves of activity are known to be crucial for driving circuit formation. Electrically connected neurons engage in synchronised calcium plateaus (SPAs; synchronous plateau assemblies) from as early as embryonic stages (Allene and Cossart 2010, Dehorter et al. 2011, Allene et al. 2012). Connectivity between cells engaging in SPAs shifts from electrical to chemical, and SPAs are then replaced by synchronous waves of calcium activity, known as giant depolarising potentials (GDPs; **Figure 2.13A**) (Kasyanov et al. 2004, Mohajerani and Cherubini 2006, Dehorter et al. 2011). GDPs are highly necessary for further circuit formation as they strengthen synaptic connections between participating neurons (Griguoli and Cherubini 2017), and occur in the striatum from P5-7 (Dehorter et al. 2011). Given our hypothesis for both aberrant neuronal development and aberrant circuit formation in the absence of *Er81*, we investigated the incidence and characteristics of cells that appeared to be participating in either SPA or GDP activity.

Due to their nature as network wide events, identifying SPAs and GDPs is not possible in a whole-cell patch clamp configuration. Optimally, calcium imaging is the best method for capturing these events. Due to technical issues, we were unable to perform calcium imaging to visualise activity in developing striatal interneuron, however, we were able to classify cells as either SPA-like or GDP-like during whole-cell patch clamp recordings. This was dependent on them exhibiting properties indicative of a cell in a SPA (calcium plateaus; **Figure 2.13C**) or GDP network (large, regular, non-action potential depolarisations; **Figure 2.13H**). As SPAs precede GDPs, we first wondered whether the number of cells engaging in this developmental activity differed between the control and conditional knockout of *Er81*, potentially indicating a shift in the speed of maturation. Overall, we did not see a difference in the proportion of immature cells recorded from between P5 and P7 (healthy cells unable to sustain action potential firing further than a single spike, data not shown). We also saw no difference in the proportion of cells engaged in SPA-like or GDP-like activity (**Figure 2.13B**). We then determined whether features of SPA-like and GDP-like events were different between control and conditional knockout cells. Cells engaging in SPA-like behaviour did present with a hyperpolarised resting membrane potential in the conditional knockout (**Figure 2.13D**). This indicates a decrease in excitability, which could be linked with *Er81*-dependent regulation of specific channel expression. *Er81* regulates the expression of the Kv1.1 potassium channel (Dehorter et al. 2015), which is also known to regulate resting membrane potential in the early postnatal hippocampus (Chou et al. 2021). In addition, it has been suggested that a

hyperpolarisation of the membrane potential indicates the retraction from spontaneous calcium transients (Watari et al. 2013), which in this case, could signify an early maturation. However, as we saw no difference in the frequency at which SPA-like events were occurring (**Figure 2.13E**), or the proportion of cells that had SPA-like and GDP-like characteristics, we assumed that SPA-like activity was not retracting earlier in the Er81 knockout condition, and there was no difference in the speed of maturation.

Upon comparing the characteristics of SPA-like events, we found that conditional knockout cells presented with calcium plateaus with a significantly smaller amplitude of depolarisation than control cells (**Figure 2.13F**), with no change to the average duration (**Figure 2.13G**). This correlates with both the observed hyperpolarisation of RMP causing a decrease in excitability, but also the observed decrease in input resistance observed in FSIs at P5-7 (**Figure 2.8C**). Overall, these results indicate a decrease in excitability, with less power behind SPA-like calcium plateaus. It is a possibility that this could decrease the coupling between the gap-junction connected neurons in the SPA network, and could decrease the overall connectivity of the network. Combined with our findings of decreased gap-junction connectivity at P15-18, this indicates that these early decreases in excitability, potentially stemming from potassium or calcium channel or receptor mediated changes to resting membrane potential and input resistance, could be the cause of decreased electrical coupling in late postnatal developmental stages.

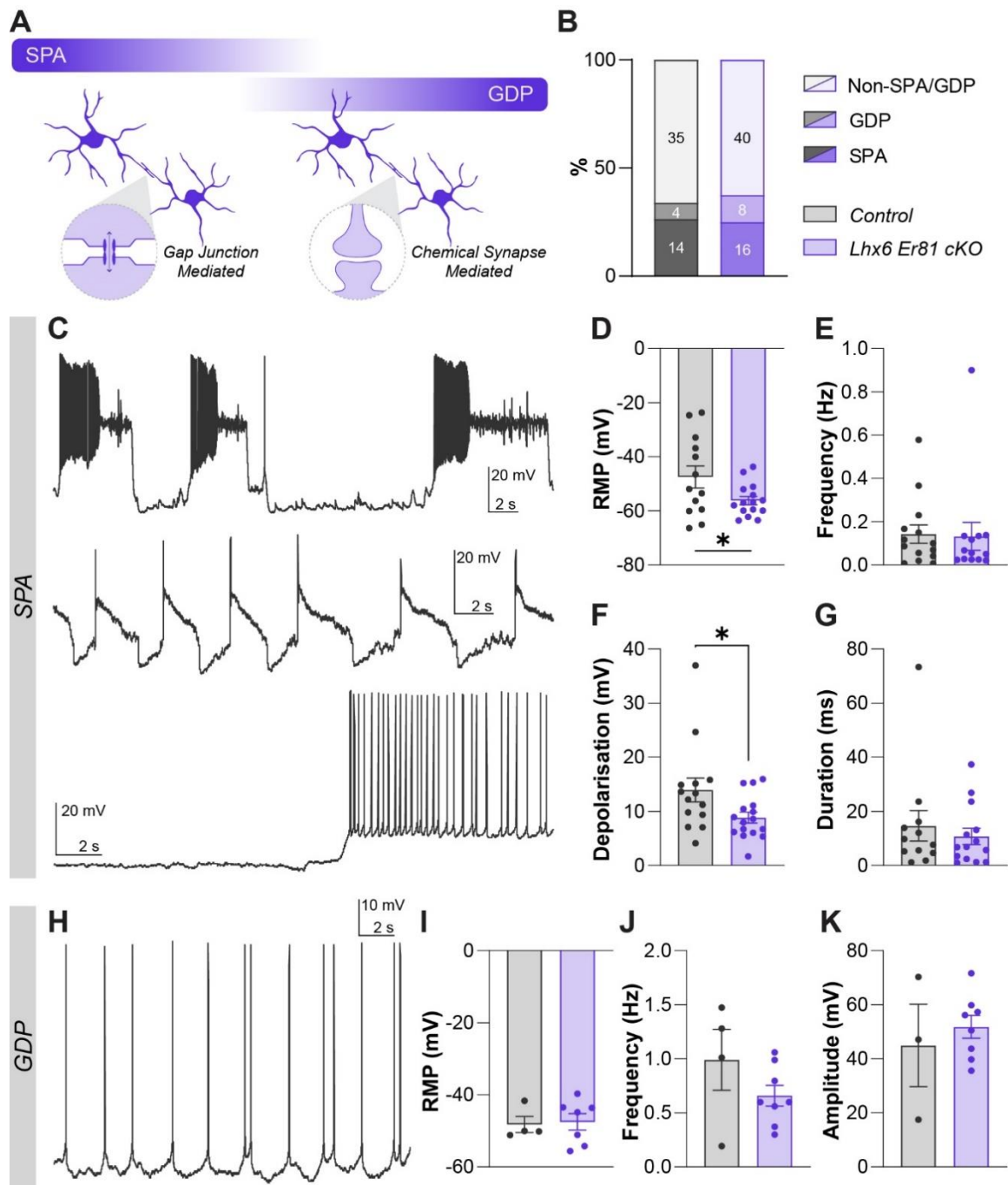


### Figure 2.13: Evidence of characteristic developmental activity in striatal interneurons

**A.** SPAs are driven by gap junction connected networks; GDP activity is driven by synaptically connected networks. **B.** The proportion of P5-7 Lhx6+ neurons expressing SPA-like or GDP-like activity in control and Er81 cKO conditions. **C.** Examples of three different presentations of SPA-like activity. **D.** The resting membrane potential (RMP) of cells displaying SPA-like activity in control and cKO cells ( $n = 13$  control,  $15$  cKO;  $p = 0.0449$ ). **E.** The frequency of SPA-like events in control and Er81 cKO cells ( $n = 14$  control,  $13$  cKO;  $p = 0.5580$ , Mann-Whitney test). **F.** The average amplitude of SPA-like depolarisation plateaus in control and Er81 cKO cells ( $n = 14$  control,  $16$  cKO;  $p = 0.0472$ , Mann-Whitney test). **G.** The average duration of SPA-like events in control and Er81 cKO cells ( $n = 12$  control,  $14$  cKO;  $p = 0.6308$ , Mann-Whitney test). **H.** Example of GDP-like activity. **I.** The resting membrane potential (RMP) of cells displaying GDP-like activity in control and Er81 cKO cells ( $n = 4$  control,  $7$  cKO;  $p > 0.9999$ , Mann-Whitney test). **J.** The frequency of GDP-like events in control and conditional knockout cells ( $n = 4$  control,  $8$  cKO;  $p = 0.1905$ ). **K.** The average amplitude of GDP-like events in control and conditional knockout cells ( $n = 3$  control,  $8$  cKO;  $p = 0.5487$ ). Unless otherwise specified, Student's t-test:  $p < 0.05$ :\*,  $p < 0.01$ :\*\*,  $p < 0.001$ :\*\*\*,  $p < 0.0001$ :\*\*\*\*.

## 2.7 Discussion

In this study, we probed the role of Er81 in striatal interneurons and their connectivity with one another. Our findings show that Er81 can exact cell-type specific control over neuron function, with separate alterations to PV-INs and CINs in developing and mature stages. Crucially, we also found deficits in striatal interneuron circuit formation in response to the modulation of striatal interneuron genetic patterning. Together this raises questions regarding the susceptibility of the developing network to change, its reliance on cellular diversity, and the fine-tuned actions of molecular factors to control neuronal characteristics.

### *Er81 has diverse roles in different neuronal populations*

Er81 is expressed in a subregion of the medial ganglionic eminence (MGE) during neurogenesis (Flames et al. 2007), hence we questioned whether Er81 regulates lineage-dependent connectivity during development and into adulthood. Er81 expression persists into adulthood in both PV-INs and CINs, but with differing expression patterns. Our results confirmed diverse effects of Er81 ablation in PV-INs and CINs, that are likely mediated by separate transcriptional pathways (Dehorter et al. 2015, Ahmed et al. 2021).

The main role of transcription factors is to regulate their target genes by interacting with DNA, as such, they are generally localised to the nucleus when active. Nuclear localisation is a process that is influenced by a number of environmental factors (Vandromme et al. 1996). In particular, Er81 has been shown to act in an activity-dependent manner; its localisation to the nucleus and regulation of maturation genes in cerebellar granule cells is triggered by action potentials leading to a calcium influx (Abe et al. 2011) and enhanced in cortical PV-INs upon network activity decrease, corresponding to increased PV-IN activity (Dehorter et al. 2015).

Transcription factors can exist both in the nucleus, ready for activation, and in the cytoplasm of cells, localising to the nucleus following activation signals (Vandromme et al. 1996). This process is mediated by the binding of a nuclear localisation sequence (NLS) (Vandromme et al. 1996, Lu et al. 2021). Here we have found that Er81 can exist in both of these configurations, dependent on cell type. Er81 expression in striatal PV-INs appears nuclear, as it is the case in cortical PV-INs (Dehorter et al. 2015), where it is likely that it acts as an active transcriptional regulator in these cells. Interestingly, CINs exhibit both nuclear and cytoplasmic Er81 expression, which could imply that Er81 does not have an active transcriptional role in these cells. There is evidence of protein-protein interactions being a key secondary aspect of transcription factor function (Goos et al. 2022). Er81 has been shown to form protein-protein

complexes with other transcription factors such as SMAD4 (Mothers against decapentaplegic homolog 4), which is both a transcription factor and tumour suppressor (Oh et al. 2019), and Tpit (T-box transcription factor), a highly restrictive regulator of differentiation in pituitary gland (Budry et al. 2011). Indeed, cytoplasmic Er81 expression has been shown before in cortical layer five pyramidal neurons, and in this study it was suggested that Er81 may have a developmental role, during which time it is active, and then it remains less active at later adult stages (Yoneshima et al. 2006). Further research is needed to determine if Er81 engages in protein coupling interactions in striatal CINs, such as via coimmunoprecipitation (Co-IP) assays, and whether this might influence its role in these cells. In addition, probing the responsiveness of Er81 localisation to signalling pathway stimulation and increased cellular activity in CINs may indicate whether Er81 can take on the role of a transcriptional regulator in these cells at all, or whether its ability to localise to the nucleus is blocked by inhibition of the NLS (Lu et al. 2021). Understanding whether the purpose of Er81 expression in the cytoplasm of CINs is representative of inactivity or a separate functional role will be important for understanding the factors governing the maturation of these cells throughout development. Tools such as single cell or spatial RNA sequencing will be critical for studying this.

When Er81 was ablated from both CINs and PV-INs, via an Lhx6-dependent knockout, some alterations to electrophysiological properties that were observed in specific knockouts (*PV* and *ChAT* dependent) were no longer seen. This is evidence for Er81 having separate cell autonomous and network wide roles. Whether the phenotypes observed are indeed due to the lack of Er81 within individual cells, (*i.e.*, a cell autonomous role) or a flow-on effect of whole network alterations due to the knockout impacting activity levels, remains to be determined. Whilst we do have some evidence that Er81 can regulate cell morphology and PV expression in a cell autonomous manner, future studies should attempt to ablate Er81 from select neurons at early stages and study whether these cells lose their place in the network due to cell intrinsic deficits.

When Er81 was removed from the larger interneuron microcircuit (*i.e.* the Lhx6+ interneuron population), we observed deficits in electrical connectivity. This is another example where the mechanisms of Er81 regulation is unclear. Er81 may potentially control the overall excitability of the network, via its control of interneuron excitability, and thus impact connectivity. Indeed, it is known that activity levels influence connectivity between neurons (Zarei et al. 2022). However, we do also have some evidence of Er81 directly regulating the expression of gap

junction channel proteins, and its ablation could downregulate the overall presence of gap junctions in the network (Shekhar et al. 2016, Shekhar et al. 2018).

*Er81*-mediated regulation of cells and circuitry is complex, and elucidating its mechanisms of action will require further studies to fully characterise the expression pattern of *Er81* in striatal interneurons and the purpose of this diversity.

### ***The contribution of striatal interneuron diversity to building functional circuitry***

Diversity within neuron populations has been thought to contribute to the formation of specialised circuitry, underlying the rich range of functions that the brain is capable of (Thivierge 2008, Miterko et al. 2018). Striatal interneurons are a heterogeneous population; both CINs and PV-INs are heterogeneous populations, genetically, morphologically, and functionally (Koos and Tepper 1999, Tepper et al. 2018, Ahmed et al. 2019). In Chapter 1, we explored the diversity of cholinergic interneurons in the striatum (Ahmed et al. 2019); there are several sub-populations of CIN, which result from diverse birth-places and times (Chen et al. 2010, Magno et al. 2017). In this chapter, we have investigated the CIN population as a whole and have also focussed on the *Lhx6*<sup>+</sup> CIN subpopulation. Adult *Lhx6*<sup>+</sup> and *Lhx6*<sup>-</sup> CIN characteristics have been well described, and they differ in cell morphology and function (Lozovaya et al. 2018). *Er81* expression does not segregate *Lhx6*<sup>+</sup> and *Lhx6*<sup>-</sup> CINs (Ahmed et al. 2021), and therefore, even in the *Lhx6*-dependent knockout condition, in which we investigated key aspects of connectivity, we have not ablated *Er81* from all CINs. Indeed, we did find a discrepancy between the innervation of PV boutons targeting *Lhx6*<sup>+</sup> versus *Lhx6*<sup>-</sup> CINs. In the *Lhx6*-dependent *Er81* conditional knockout, we observed a potential redirection of PV axonal boutons towards *Lhx6*<sup>-</sup> CINs. These are the cells that were not affected by the *Er81* knockout, and therefore some of which may still express *Er81*.

We also show for the first time a potential upregulation of connectivity between PV-INs and CINs during development. Discrepancies between *Lhx6*<sup>+</sup> and *Lhx6*<sup>-</sup> CINs in terms of their integration into the striatal network remains to be elucidated by future studies. These would include simultaneous recordings from PV-INs with either *Lhx6*<sup>+</sup> or *Lhx6*<sup>-</sup> CINs, to determine whether they have different connectivity, particularly during development. Importantly, we saw low levels of connectivity between PV-IN/CIN pairings in this current study, therefore utilising optogenetic mechanisms to stimulate the vast PV-IN or CIN network may overcome issues of low connectivity between single cells. These experiments would confirm whether PV-INs and *Lhx6*<sup>+</sup> CINs, which are born in the MGE, preferentially connect to one another during



development compared to connections between PV-INs and Lhx6- CINs, which are born elsewhere, such as the septal epithelium. As we have discussed previously, cells from a common neurogenic origin are more likely to form connections (Yu et al. 2009, Yu et al. 2012, He et al. 2015, Zhang et al. 2017, Lin et al. 2023), therefore it is possible that the presence of PV-IN/CIN connectivity during development is specific to Lhx6+ circuitry and not found in Lhx6- CINs. An additional point is to recognise that this current study only looks at functional cell-cell connectivity. The striatum appears to rely heavily on synchrony as a structure that stabilises and filters inputs from other regions (Stern et al. 1998, Dorst et al. 2020). In addition, the two cell types we have focussed on have unique properties that contradict the idea of them being strongly connected at a single cell level. CINs rely primarily of the volume transmission of acetylcholine to the whole striatum (Taber et al. 2011, Nosaka and Wickens 2022), and whilst they do have direct connections with other neurons, their tonic firing pattern also makes it unlikely that a single action potential elucidates a strong response in the post-synaptic cell. In addition, there is evidence that PV-INs fire synchronously in the striatum to enact control over other cells (Damodaran et al. 2014), similarly this also indicates that a strong influence of many PV-INs may be necessary to elucidate post-synaptic responses, particularly in the mature circuit. Previous studies to investigate striatal connectivity have utilised optogenetic approaches to stimulate many interneurons simultaneously, and then record the resulting response in the postsynaptic cell (Nelson et al. 2014, Straub et al. 2016). A future aim to confirm connectivity deficits in the Er81 knockout model would be to use a similar approach.

We described a continuous spectrum of Er81 expression in striatal interneurons, particularly CINs. In this study, we ablated Er81 and investigated the resulting alterations to circuitry. A key future experiment would be to facilitate the overexpression of Er81 and test whether the circuit responds in an equal and opposite manner or engages in a different form of regulation. Whether Er81 overexpression would change the identity of some neurons from non-expressing to expressing and shift the wiring of the network to be overconnected is a distinct possibility.

### ***How a transcription factor can influence connectivity and network building***

Defects in neuronal circuitry, from decreased or increased connectivity, to miswiring, have been linked to subsequent behavioural alterations, to the point of neuropsychiatric pathologies (Vasa et al. 2016). During early stages of development, excessive connections form in the brain. Whether this has a functional purpose, other than to guarantee that enough connections are present in the brain, is unknown. It is possible that even these excessive connections form in a specific manner, and that they facilitate key processes during developmental critical periods.

Refinement of neuronal circuits occurs later, by way of synaptic pruning (Kolb and Gibb 2011). The removal of certain synapses is specific and activity dependent, reliant on spontaneous neuronal activity, such as SPA and GDP activity (Faust et al. 2021). Here we show for the first time that striatal PV-INs and CINs are bidirectionally connected during early development. PV-INs and CINs are thought to be poorly connected in adulthood, with little to no PV-IN to CIN connections (Chang and Kita 1992, English et al. 2011, Szydlowski et al. 2013, Straub et al. 2016). These findings indicate that the connection between PV-INs and CINs is not functionally relevant for refined circuitry and is likely removed during synaptic pruning. However, it is also possible that this connection has a key role in regulating striatal circuitry during development and even facilitating the establishment of neuronal properties.

The susceptibility of neuronal connection specificity to be under transcriptional control is a complex question, with no clear answer based on the current literature. Synaptogenesis in the brain is far too vast to be reliant on a single transcription factor, or even a single family of transcription factors (Shen and Scheiffele 2010). Instead, it is possible that different transcription factors regulate circuit formation and connectivity in certain brain regions, and in various sub-circuits. In this study, we wanted to determine the direct and indirect roles that the *Er81* transcription factor could play in regulating striatal microcircuit formation and function.

In the absence of *Er81*, we found a severe deficit in the number of FSI-FSI gap junctions during late postnatal development. Developmental gap junction connectivity is vital for establishing future functional circuitry. It is well known, in many structures, that electrical synapses are prominent between FSIs, and occur in a dendrito-dendritic fashion (Galarreta and Hestrin 2001). In addition, the input resistance of cells influences their ability to respond stimulations through gap junctions (Galarreta and Hestrin 2001), and we observed a significant decrease in input resistance during early development. This decreased responsivity of cells could have led to a weakening of gap junction connection reinforcement, therefore resulting in the decreased proportion of connected pairs. However, this relationship is complex, as we explore further in Chapter 5.

Overall, whilst we have observed developmental alterations to circuitry, it is crucial to understand the impact of shifts in developmental trajectory. Future studies will link these findings to behavioural alterations.

## Chapter 3: Diversity in Serotonergic Modulation of the Striatum in Response to Early Genetic Insult

### 3.1 Preamble

Circuit development not only depends on specific genetic programming, but also activity levels in the surrounding environment, which is maintained via an excitation-inhibition balance (Sohal and Rubenstein 2019). Several genetic and activity dependent factors then regulate circuit maintenance and function, essentially controlling how neuronal circuits facilitate behaviour and cognition. We have previously focussed on manipulating microcircuitry within a structure, however long range innervation from distant structures can carry crucial information and modulate circuit function. Serotonin (5-HT) has been found to have a role in the vast majority of behavioural and physiological functions, such as motor control, emotion and mood, and reward control (Lucki 1998), and is implicated in many neuropsychiatric disorders, including schizophrenia, anxiety, and depression (Schwartz et al. 1998, Charnay and Leger 2010). Serotonin enacts this control via massive innervation of nearly all structures in the brain, where it is released generally via volume transmission (Quentin et al. 2018). Serotonergic neurons are located in select, small nuclei in the midbrain and brainstem (Charnay and Leger 2010). The major nucleus sending projections to the forebrain is the Dorsal Raphe Nucleus (DRN), whilst caudal nuclei in the brainstem innervate the spinal cord. The DRN is not a homogeneous structure, diversity in anatomical sub-regions and along the rostro-caudal axis contribute to the selective innervation of downstream target structures and functional relevance (Ren et al. 2018, Huang et al. 2019, Ren et al. 2019).

The role of some genetic factors in regulating the differentiation of serotonergic identity is known, such as the necessity of the *Nkx2.2* and *Pet-1* transcription factors for serotonergic identity (Gaspar et al. 2003). *Pet-1* is an ETS transcription factor (also known as *FEV*: Fifth Ewing Variant) that is known to segregate the vast majority of serotonergic neurons in the DRN, and is expressed from early stages (Hendricks et al. 1999, Liu et al. 2010). It is a terminal selector of serotonergic identity that also regulates serotonergic neuron excitability and functional maturation (Spencer and Deneris 2017). Other ETS factors have also been shown to be linked to serotonergic identity and function; *Etv5* is required for hypothalamic serotonergic neuron differentiation (Bosco et al. 2013), and an orthologue of *Etv1/Er81* (*Ast-1*) has been identified as a terminal selector of serotonergic neuron identity in the *C. elegans* animal model (Lloret-Fernandez et al. 2018). *Er81* has a very similar molecular structure to its ETS family

member Pet-1 and has been shown to also be expressed from early stages in other structures such as the MGE (Flames et al. 2007). We therefore wondered whether Er81 could regulate the identity and function of DRN serotonergic neurons, as it does in other neuromodulatory populations (see Chapter 2).

As mentioned above, DRN serotonergic neurons innervate nearly all brain structures, this includes the striatum. The striatum is a primarily inhibitory structure, acting almost as a filter in the basal ganglia circuitry (Calabresi et al. 2014). Whilst much of the innervation it receives is excitatory (Hunnicuttt et al. 2016), it also receives heavy neuromodulatory inputs from midbrain structures (Guo et al. 2015), including the DRN. Approximately a third of all serotonergic neurons in the DRN send projections to innervate the striatum (Steinbusch et al. 1981, Waselus et al. 2006, Huang et al. 2019), and there is a vast network of serotonergic receptors expressed on spiny projection neurons (SPNs) and interneurons (Navailles and De Deurwaerdere 2011), indicating their widespread influence. However, their specific role and effect on striatal circuitry is still being established.

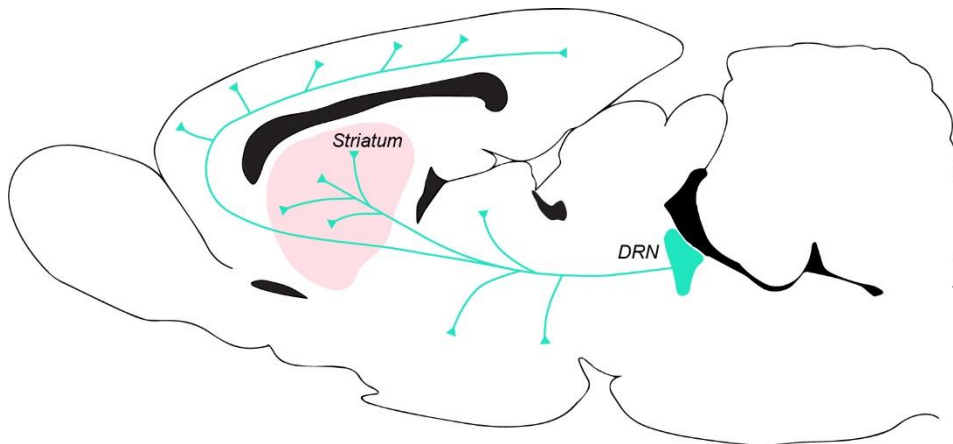


**Figure 3.1: Serotonergic projections throughout the brain**

Long range projections from serotonergic neurons in the Dorsal Raphe Nucleus (DRN) innervate many structures throughout the brain (sagittal view), including the striatum (pink).

Serotonin has been shown to influence striatum-dependent behaviour. Serotonin regulates motor behaviour in the dorsal striatum (Nair et al. 2020), but has also been shown to be involved in other behaviours such as anxiety and depression, via the striatum (Schwartz et al. 1998). For example, striatal serotonin levels in mice are elevated following a high stress experience (Takahashi et al. 1998, Strong et al. 2011), and mice subsequently show depression-like behaviour; this depressive state can then be rescued by inhibition of a specific serotonin receptor type (5-HT<sub>2C</sub>) (Strong et al. 2011). Interestingly, it has also been shown that this relationship is sensitive to environmental influence, such as exercise, which reduces 5-HT<sub>2C</sub> expression in the striatum and attenuates the previously observed receptor mediated depressive state (Greenwood et al. 2012). Similarly, modulation of serotonin levels via selective serotonin reuptake inhibitor (SSRI) application rescues OCD-like behaviour in an orbitofrontal cortex lesion induced model of OCD (Schilman et al. 2010). In terms of human studies and more complex emotional responses, striatal serotonin activity has been linked with reward processing as well as decision making in humans (Tanaka et al. 2007, Bang et al. 2020). Serotonin depletion also affects the behavioural response to fairness and punishment, whereby subjects had decreased ventral striatum responses to fairness and increased dorsal striatum responses to punishment (Crockett et al. 2013). With such diverse roles, additional even to those outlined above, serotonin is considered a fine-tuned regulator of many behavioural processes, with a great number of them involving the striatum (Lucki 1998).

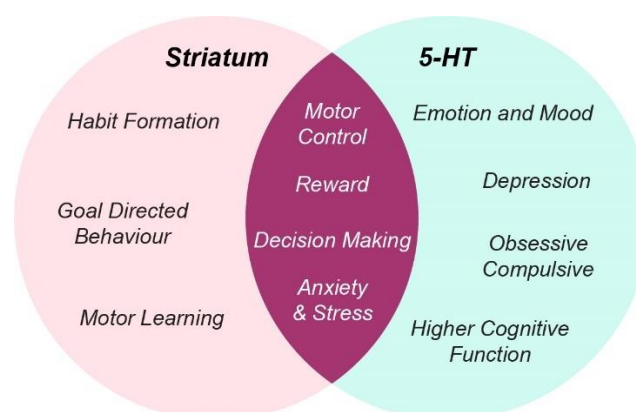


**Figure 3.2: Overlap of Striatum- and Serotonin-mediated behaviours**

Several behaviours under the control of the striatum are also regulated by serotonin (5-HT), and vice versa: several serotonin-mediated behaviours have been found to act via the striatum.

Behavioural alterations must be rooted somewhere in neuronal circuitry, as such, a number of studies have attempted to link the function of serotonin-mediated striatal circuits with behavioural characteristics. As the striatum is heavily innervated by serotonergic projections, and there is evidence for ubiquitous serotonin receptor expression across the various striatal neuron populations (Nair et al. 2020), serotonin signalling has a key role in regulating the striatum, both at the level of single cells as well as the circuitry as a whole.

Inputs to the striatum are somewhat dispersed throughout the dorsal DRN, and functional circuits involving the DRN and the striatum are not specific to a single sub-region (Huang et al. 2019). Yet, it has been shown that striatum projecting cells localise mostly in the dorsomedial and lateral wing regions of the DRN (Huang et al. 2019). In the striatum, serotonergic afferents have been found to generally appose dendritic and axonal compartments rather than cell somas and seem to have a low incidence of direct functional synaptic contacts (Soghomonian et al. 1989, Cover and Mathur 2021). This suggests that there is indeed a large component of volume transmission mediated serotonergic modulation of striatal circuitry.

Not many studies have explored direct wired connections between serotonergic afferents from the DRN and post-synaptic striatal projection neurons or interneurons. Instead, many have focussed on the result of serotonin receptor modulation on the activity and function of striatal cells. Serotonergic modulation of striatal spiny projection neurons (SPNs) is thought to influence their reciprocal and lateral inhibition of each other, whereby the activation of the 5-HT<sub>1B</sub> receptor whilst stimulating SPN activity resulted in decreased lateral inhibition strength (Pommer et al. 2021). In addition, serotonin application induces slow depolarisations and increased excitability in fast spiking interneurons (FSIs), mediated specifically by the 5-HT<sub>2C</sub> receptor via suppressing the inward rectifying potassium current (Blomeley and Bracci 2009). Similarly, serotonin application, as well as blockade of serotonin re-uptake, induced membrane depolarisation alongside increased firing rate in striatal cholinergic interneurons (CINs) (Bonsi et al. 2007, Virk et al. 2016). Modulation of 5-HT receptor expression (conditional knockout of 5-HT<sub>1B</sub>) on CINs resulted in decreased depressive behaviour (Virk et al. 2016). Whether the modulatory activity described above functions via direct synaptic innervation of striatal neurons or via volume transmission remains to be seen.

There is, however, some evidence of axo-axonic and presynaptic regulation by serotonin in the striatum. Approximately 30% of serotonin terminal appositions are with axons and axon terminals (Cover and Mathur 2021). Serotonin is thought to mediate striatal dopamine through

presynaptic innervation of dopaminergic terminals, whereby serotonin release in the striatum leads to increased dopamine release (Navailles and De Deurwaerdere 2011). Additionally, serotonin has been found to regulate the plasticity of glutamatergic inputs to striatal SPNs. Serotonin signalling induces long term depression (LTD), a mechanism for the weakening of synapses, at cortico-striatal SPN synapses via activation of the 5-HT<sub>1B</sub> receptor, resulting in an overall decrease in striatal (Mathur et al. 2011). On the contrary, at thalamo-striatal SPN synapses, decreased serotonin signalling results in LTD via reduced activation of the 5-HT<sub>4</sub> receptor subtype (Cavaccini et al. 2018). In addition, there is some evidence for serotonin regulating connection formation and specificity. Serotonin has been shown to act as a guidance cue regulating the direction of axonal growth cone extension, in a dose-dependent manner (Vicenzi et al. 2021). This may be enacted at axo-axonic synapses.

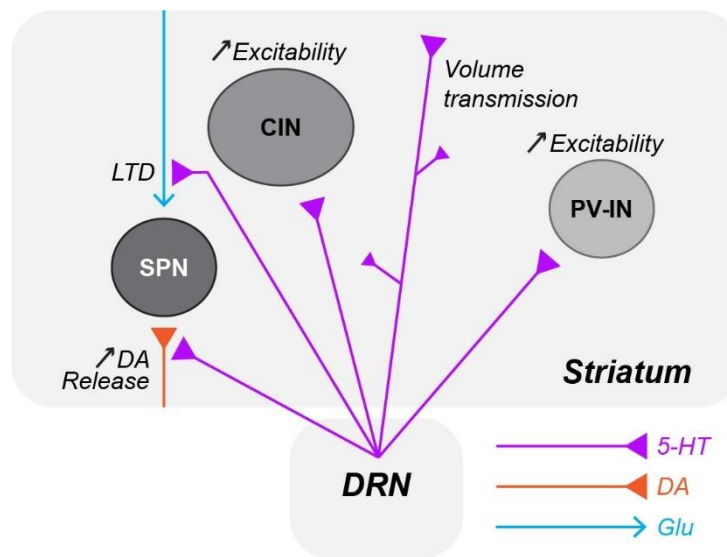


**Figure 3.3: Serotonergic innervation of the striatum.**

Serotonergic projections (5-HT) from the Dorsal Raphe Nucleus (DRN) to striatal cells and connections. Axo-axonic connections to glutamatergic inputs to spiny projection neurons (SPNs) induce long term depression (LTD) at these synapses. Axo-axonic connections to dopaminergic inputs to SPNs induce dopamine (DA) release. Serotonin causes increased excitability of both cholinergic interneurons (CINs) and parvalbumin-positive interneurons (PV-INs). Overall, serotonin release into the striatum is via volume transmission over direct connections.

Overall, whilst we have some knowledge of the role and regulation of serotonin in the striatum, we still lack an understanding of how these long-range connections are regulated and how serotonergic signalling in the striatum links specifically to behaviour. The susceptibility of the serotonergic neuronal population in the DRN to molecular regulation is somewhat known (Hendricks et al. 1999, Ren et al. 2018, Baretino et al. 2021), but largely unstudied in the context of how this can affect striatal projections and subsequently striatal circuitry and behaviour.

We therefore hypothesised that long range serotonergic inputs to the striatum are susceptible to the state of DRN serotonergic circuitry, and shifting the molecular identity of these cells can hence alter striatal function.

We aimed to:

1. Determine the pattern of expression of Er81 in the serotonergic neurons of the DRN.
2. Understand how Er81 mediated regulation of serotonergic neurons can affect striatum-dependent behaviour.
3. Elucidate functional alterations in serotonergic circuitry underlying behavioural regulation.



### 3.2 Er81 is expressed in serotonergic neurons

The expression of Er81 in the Dorsal Raphe Nucleus (DRN) has never been quantified. We therefore characterised Er81 expression in Pet-1 positive (Pet+) serotonergic cells at adult (P60+) stages in three subregions of the DRN; the dorsomedial (DM), ventromedial (VM), and lateral wing (LW) aspects (**Figure 3.4A**). We found Er81 expression in Pet+ cells (**Figure 3.4B**) in all subregions (95% of Pet+ cells were classified as Er81+, see Methods), but specifically higher in the lateral wing regions (**Figure 3.4C**). This enhancement of Er81 in a specific DRN region could indicate its more prominent role in these cells, potentially segregating specific projections to downstream structures.

In addition, we noted that Er81 had a specific expression pattern that appeared to be more cytoplasmic than nuclear (**Figure 3.4D, E**). Interestingly, this was similar to what we observed in striatal cholinergic interneurons, another neuromodulatory population, and different to non-modulatory striatal parvalbumin positive interneurons (Chapter 2). This indicates that Er81 has diverse roles in cell populations, dependent on their identity, and suggests expression mechanisms specific to neuromodulatory neurons facilitate the cytoplasmic localisation of Er81.

To determine whether Er81 expression in serotonergic neurons is necessary for facilitating their long range projections and integration into the striatal network, we generated a conditional knockout under the Pet promoter (*Er81<sup>fl/fl</sup>;ePet-cre;RCE-GFP*) to remove Er81 from serotonergic Pet+ cells, and confirmed the ablation of Er81 from DRN neurons (**Figure 3.4F**).

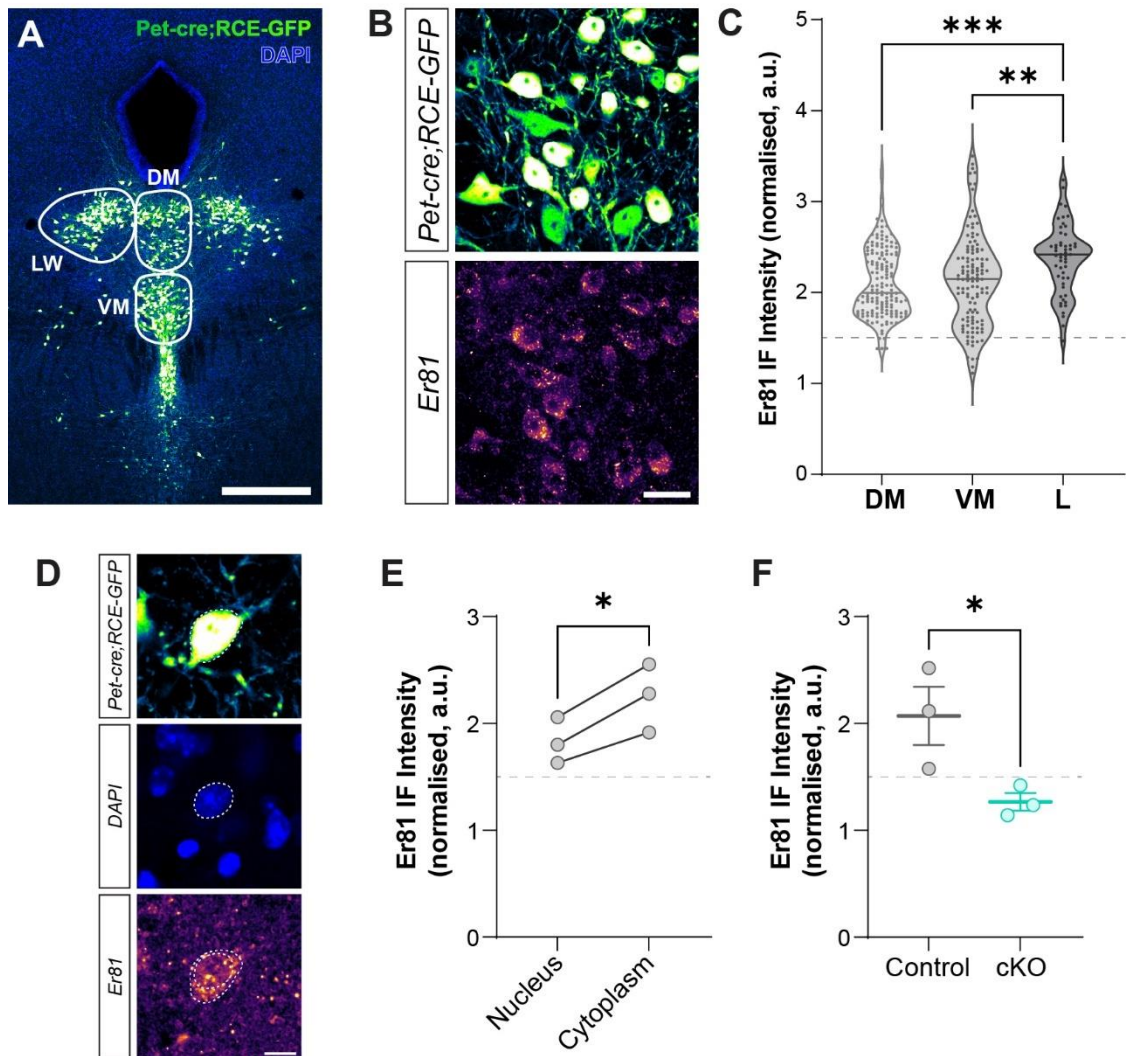


**Figure 3.4: Er81 expression in Pet-positive neurons in the Dorsal Raphe Nucleus**

**A.** Cells expressing GFP in subregions of the Dorsal Raphe Nucleus (DRN) in the *Pet-cre;RCE-GFP* mouse model. Subregions outlined are the dorsomedial (DM), ventromedial (VM), and lateral wing (LW) aspects of the DRN. Scale: 500  $\mu\text{m}$ . **B.** Expression of the Er81 transcription factor in Pet positive (Pet+) cells in the DRN. Scale: 30  $\mu\text{m}$ . **C.** Quantification of Er81 expression levels in Pet+ cells in the DM, VM, and LW aspects of the DRN, normalised to background Er81 (n = 157 cells DM, 123 cells VM, 53 cells LW, 3 mice; 1-way ANOVA:  $F_{(2,330)} = 7.547$ ,  $p = 0.0006$ ; Bonferroni post-hoc comparisons: DM vs VM:  $p > 0.9999$ , VM vs LW:  $p = 0.0034$ , DM vs LW:  $p = 0.0005$ ). Line: 1.5x background fluorescence, distinction between positive and negative cells. **D.** Nuclear and cytoplasmic expression of Er81. Scale: 10  $\mu\text{m}$ . **E.** Quantification of Er81 expression in nuclear and cytoplasmic compartments of Pet+ cells (n = 3 mice,  $p = 0.0252$ ). Line: 1.5x background fluorescence, distinction between positive and negative cells. **F.** Confirmation of Er81 ablation in Pet+ cells in *Er81<sup>fl/fl</sup>;Pet-cre;RCE-GFP* (cKO) mice compared to control *Pet-cre;RCE-GFP* mice (n = 3 control, 3 cKO mice,  $p = 0.0477$ ). Line: 1.5x background fluorescence, distinction between positive and negative cells. Unless otherwise specified, Student's t-test:  $p < 0.05$ :\*,  $p < 0.01$ :\*\*,  $p < 0.001$ :\*\*\*,  $p < 0.0001$ :\*\*\*\*.

### 3.3 *Er81* Ablation Causes Behavioural Alterations in Male and Female Mice

As the serotonergic system is heavily implicated in both mouse and human behavioural state, including motor control via the striatum (Lucki 1998), we characterised behavioural characteristics of the conditional knockout mice compared to controls. This would reveal whether the removal of *Er81* from Pet+ serotonergic neurons had lasting effects on brain circuitry, and whether *Er81* has a role in the regulation of the function of these cells.

To monitor general locomotor activity and exploratory behaviour, we first placed the mice in an open field paradigm, where they were left to roam a circular arena freely for five minutes and their movements tracked (**Figure 3.5A**). During experimentation, we noted stark differences in the responses of males and females. Taking into consideration known sex differences in the mouse serotonergic system (Carlsson and Carlsson 1988, Jones and Lucki 2005), we therefore separated animals by sex for behavioural purposes. We found specific deficits in female knockout mice in the open field. Female mice travelled less total distance (**Figure 3.5B**), moved significantly slower (**Figure 3.5C**), with greater resting time (**Figure 3.5D**). Together, this represents a potential female specific deficit in motor ability, which could be related to alterations to raphe-striatal circuitry as the striatum is heavily related in movement initiation and control (Gittis and Kreitzer 2012). However, we also observed a decrease in thigmotaxis behaviour in female conditional knockout mice (**Figure 3.5E**); thigmotaxis is the tendency of mice to remain on the outer edges of an open field, and is an indicator of anxiety like behaviour, particularly in a novel environment (Simon et al. 1994). With a decrease in thigmotaxis, female knockout mice travelled more to the centre of the arena and were therefore less anxious than controls. On the other hand, *Er81* conditional knockout males showed no differences from controls in any locomotive measures (**Figure 3.5B-D**) or thigmotaxis (**Figure 3.5E**). Together these results suggest a sex-specific role for *Er81* in regulating motor and anxiety-like behaviour via serotonergic function.

Although anxiety is heavily associated with brain regions such as the amygdala and prefrontal cortex, there are some links with the striatum. Thigmotaxis incidence can be modulated in opposing directions by general activation of D1 and D2 dopamine receptors, which segregate the two opposing basal ganglia pathways in the striatum by their expression on separate populations of SPNs (Simon et al. 1994). In addition, lower striatal serotonin and serotonin receptor expression has been linked with higher anxiety-like behaviour (Schwartz et al. 1998, Greenwood et al. 2012), further implicating raphe-striatal circuitry being altered in knockout conditions, and possibly specifically in females.

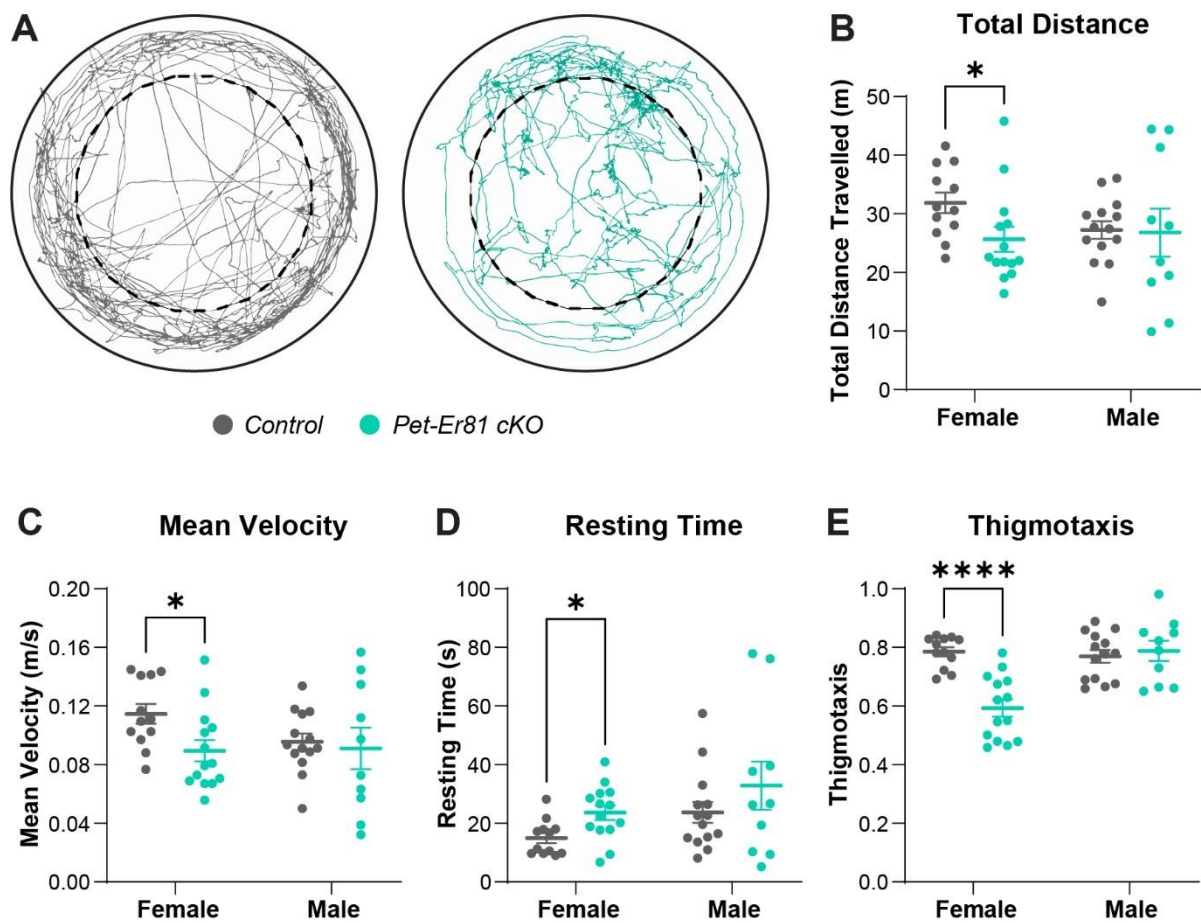


**Figure 3.5: Female behaviour in an open field is altered following *Er81* ablation**

**A.** Traced movement of an example control (*Pet-cre;RCE-GFP*) and conditional knockout (*Er81<sup>fl/fl</sup>;Pet-cre;RCE-GFP*) mouse around a circular open field. The field is divided into inner and outer regions for thigmotaxis measurement. **B-E.** Characteristics of male and female control and conditional knockout mice travelling around a circular open field ( $n = 12$  control, 14 cKO female mice; 14 control, 10 cKO male mice;). **B.** Total distance travelled over five minutes in the open field arena ( $p_{\text{female}} = 0.0373$ ,  $p_{\text{male}} = 0.9114$ ). **C.** Mean velocity at which mice travelled around the open field ( $p_{\text{female}} = 0.0192$ ,  $p_{\text{male}} = 0.7376$ ). **D.** Time spent by mice resting ( $p_{\text{female}} = 0.0113$ ,  $p_{\text{male}} = 0.2711$ ). **E.** Thigmotaxis (tendency to remain in the outer section of the open field arena;  $p_{\text{female}} = 0.00001$ ,  $p_{\text{male}} = 0.6351$ ). Unless otherwise specified, Student's t-test:  $p < 0.05$ :\*,  $p < 0.01$ :\*\*,  $p < 0.001$ :\*\*\*,  $p < 0.0001$ :\*\*\*\*.

To corroborate this phenotype, we performed the light-dark box anxiety test. Mice were placed into a darkened box, joined to a lit box by an open doorway (**Figure 3.6A**), and their time spent in each box was compared. High anxiety mice will spend more time in the darkened box, without exploring the lit box, as they ensure they remain in the safer (dark) environment (Bourin and Hascoet 2003). We once again found that female knockout mice displayed less anxiety-like behaviour, and explored the light box nearly as much as the dark, whereas control mice preferred remaining in the dark box (**Figure 3.6B**). There was no significant difference in the number of transitions between the two boxes, however knockout mice tended to switch between boxes more (**Figure 3.6C**). This result confirmed that female mice lacking *Er81* in Pet+ serotonergic neurons display less anxiety-like behaviour, with males displaying no differences.

To then further explore the motor deficits observed in the open field, mice were tested on the Digigait treadmill to measure their gait and gait properties<sup>2</sup>. Both males and females showed differences across various properties, in both fore- and hindlimbs, relating to their ability to walk (**Figure 3.6D-I**). Males showed specific forelimb in-toeing (**Figure 3.6D**), with increased stride length (**Figure 3.6E**), and more forelimb and hindlimb paw overlap along the midline (**Figure 3.6F**). Males also were faster to propel into their hindlimb stride (**Figure 3.6H**) but were dragging their paws more (**Figure 3.6I**). Females on the other hand showed more forelimb and hindlimb paw overlap, similar to males (**Figure 3.6F**), as well as significantly more hindlimb in-toeing (**Figure 3.6G**) and increased hindlimb paw dragging (**Figure 3.6I**).

Whilst when taken together these results do not implicate a specific gait trait being affected in the knockout, they do show a severe instability in gait, that male mice in particular appear to be trying to compensate for. Males showed no difference in distance travelled or velocity in the open field task, and we therefore expected no alterations to their gait. However, what we observe is instability, evidenced by the in-toeing, overlapping, and dragging, which males appear to be compensating for by increasing their stride length and the speed of their propulsion. Females on the other hand, do not show differences in these measures of compensation, but have similar gait deficits which could explain the female specific results from the open field test. This poses an interesting relationship between neuromodulatory control in the striatum and pathological gait phenotypes. For example, gait deficits are a hallmark of Parkinson's Disease, which has a higher incidence in males and is heavily related to decreased dopaminergic neuromodulation in the striatum (Hausdorff 2009).

---

<sup>2</sup> Digigait experiments and analysis were performed in collaboration with Rebekah Parkinson.

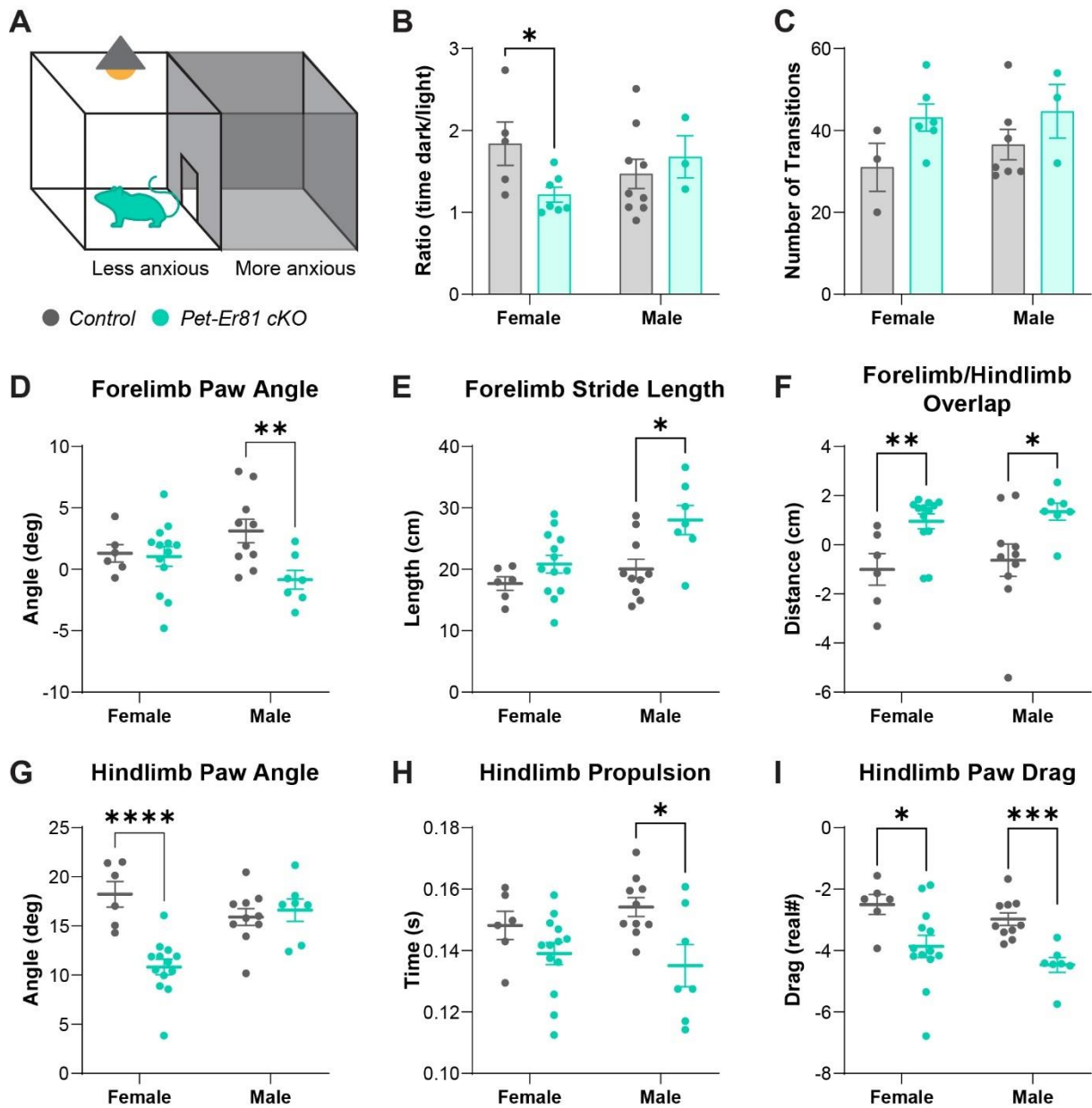


**Figure 3.6: Anxiety and locomotive behaviour are shifted following *Er81* ablation**

**A.** Schematic of the light-dark box anxiety test, containing a lit box (left) and a dark box (right) that a mouse can travel between. **B.** The ratio of time spent in the dark box to the light box (dark:light) by female and male control and conditional knockout mice ( $n = 5$  control, 7 cKO female mice; 9 control, 3 cKO male mice;  $p_{\text{female}} = 0.0290$ ,  $p_{\text{male}} = 0.5617$ ). **C.** The number of transitions between the light and dark box during the task ( $n = 3$  control, 6 cKO female mice; 7 control, 3 cKO male mice;  $p_{\text{female}} = 0.0897$ ,  $p_{\text{male}} = 0.2860$ ). **D-I.** Measurements of gait from Digigait treadmill task in female and male control and conditional knockout mice ( $n = 6$  control, 13 cKO female mice; 10 control, 7 cKO male mice). **D.** Angle of forelimb paws with the long axis of the direction of motion (*i.e.* from the paw midline; positive angle: external rotation, negative angle: internal rotation;  $p_{\text{female}} > 0.9999$ ,  $p_{\text{male}} = 0.0087$ ). **E.** Forelimb stride length ( $p_{\text{female}} = 0.4307$ ,  $p_{\text{male}} = 0.0065$ ). **F.** The overlap distance of ipsilateral fore and hind paws ( $p_{\text{female}} = 0.0242$ ,  $p_{\text{male}} = 0.0231$ ). **G.** Angle of hindlimb paws with the long axis of the direction of motion ( $p_{\text{female}} < 0.0001$ ,  $p_{\text{male}} > 0.9999$ ). **H.** The time duration of the propulsion phase of a stride ( $p_{\text{female}} = 0.3355$ ,  $p_{\text{male}} = 0.0118$ ). **I.** Quantification of paw dragging of hindlimbs, larger value indicates greater drag ( $p_{\text{female}} = 0.0151$ ,  $p_{\text{male}} = 0.0074$ ). Unless otherwise specified, Student's t-test:  $p < 0.05$ :\*,  $p < 0.01$ :\*\*,  $p < 0.001$ :\*\*\*,  $p < 0.0001$ :\*\*\*\*.

### 3.4 Long Range Serotonergic Innervation of the Striatum

We then wished to determine whether projections to the striatum were altered and might explain the behavioural phenotypes observed. We began by quantifying the density of serotonergic Pet+ neuropil in the striatum. As described previously, serotonergic innervation of the dorsomedial (DMS), dorsolateral (DLS), and ventral region of the dorsal (V) striatum is specifically implicated in different behaviours. By quantifying the neuropil, which is comprised of serotonergic axons and axon terminals (**Figure 3.7A**), we were able to compare the physical innervation of the striatum in control and knockout conditions.

We found that females showed no significant differences in serotonergic neuropil in all striatal subregions (**Figure 3.7B**), however there were slight increasing trends across all three regions which would require increased sampling, particularly from control females. Conversely, males had significant decreases in serotonergic neuropil in the dorsomedial and ventral striatum (**Figure 3.7C**). We did see male specific gait alterations, which could be linked to this change in innervation, as decreased serotonergic input to the striatal circuit may result in motor deficits, as serotonergic function and striatal function both intersect on motor control (Mathur et al. 2011, Cavaccini et al. 2018, Nair et al. 2020).

However physical alterations to innervation do not cover the full possibilities, indeed, functional alterations to the serotonergic neurons in the DRN could affect downstream circuitry similar to changes in axonal innervation. In addition, we have shown in the previous chapter that Er81 can affect intrinsic cell properties, including overall cell function, particularly in striatal cholinergic interneurons, which are also neuromodulatory.

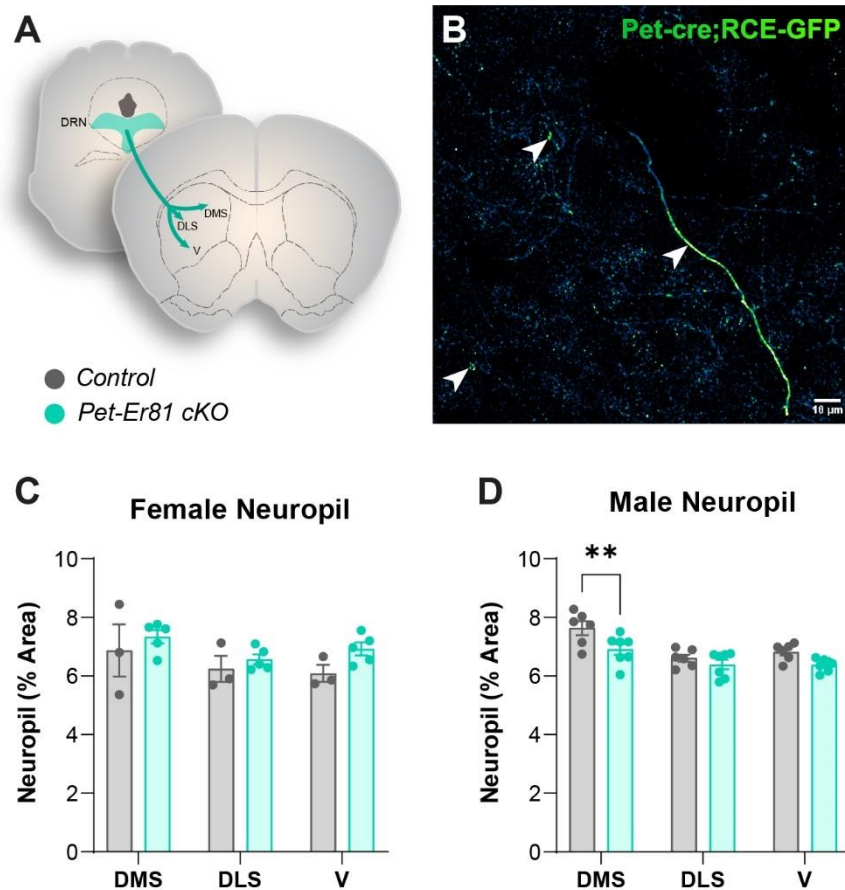


### Figure 3.7: Impacts on serotonergic innervation of the striatum

**A.** Schematic of serotonergic afferents from the dorsal raphe nucleus (DRN) to the striatum in three striatal regions: the dorsomedial (DMS), dorsolateral (DLS), and ventral region of the dorsal (V) striatum. **B.** Serotonergic neuropil in the striatum visualised in the *Pet-cre;RCE-GFP* model. Arrows indicate an axon and axon terminals. Scale: 10  $\mu$ m. **C.** Quantification of the area occupied by serotonergic neuropil in striatal subregions in female control and conditional knockout mice (n = 3 control, 5 cKO mice, two-way ANOVA:  $F(1, 18, \text{genotype}) = 3.281, p = 0.0868$ ;  $F(2, 18, \text{interaction}) = 0.2604, p = 0.7736$ ). **D.** Quantification of the area occupied by serotonergic neuropil in striatal subregions in male control and conditional knockout mice (n = 6 control, 7 cKO mice, two-way ANOVA:  $F(1, 33, \text{genotype}) = 12.81, p = 0.0011$ ;  $F(2, 33, \text{interaction}) = 1.251, p = 0.2995$ ; post-hoc Bonferroni multiple comparison tests: DMS:  $p = 0.0086$ , DLS:  $p = 0.9923$ , V:  $p = 0.1640$ ).



### 3.5 Sex-Specific Alterations to the Functional Properties of Serotonergic Neurons

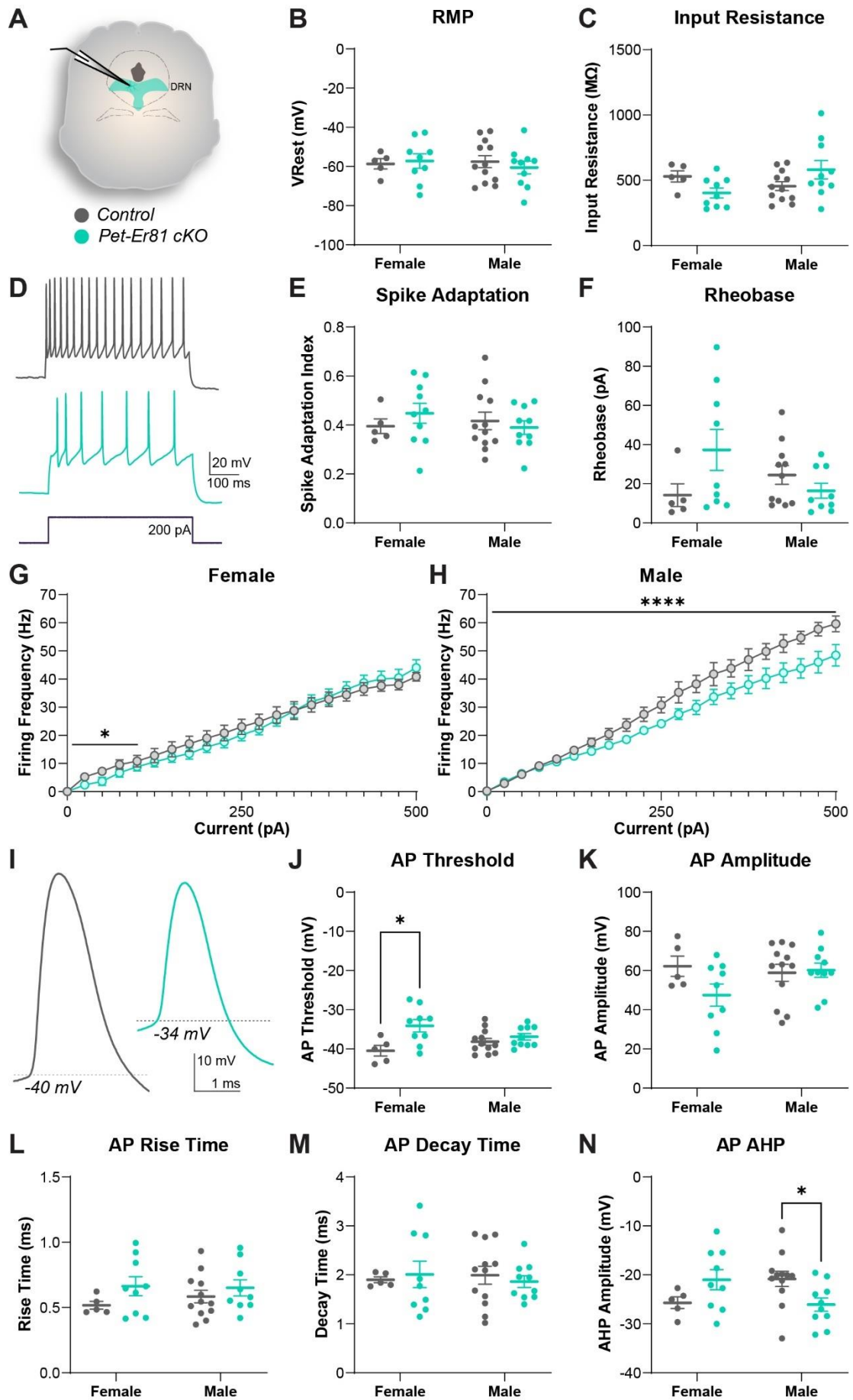
We performed whole-cell electrophysiology on Pet+ serotonergic neurons in the DRN to assess their overall functionality and whether it corresponds with our observed behavioural phenotypes (**Figure 3.8A**). We anticipated that some form of functional alteration in both males and females, as behaviour has been closely linked to serotonergic tone throughout the brain (Lucki 1998), and we saw behavioural deficits in both. However, we also expected differing presentations that may explain the behavioural heterogeneity. We found no changes to general cell electrical properties (Tables 9 & 10, Appendix E), such as resting membrane potential (RMP, **Figure 3.8B**), input resistance (**Figure 3.8C**). However, evoked firing properties (**Figure 3.8D**) were altered, in a sex-specific manner. Despite no changes to spike adaptation or rheobase (**Figure 3.8E, F**), we did observe a significant decrease in action potential firing rate with increasing current steps in both female and male knockout conditions, compared to controls (**Figure 3.8G, H**), but with different presentations. Evoked firing in female cells was only decreased at lower current step stimulations, near threshold (**Figure 3.8G**). On the other hand, male conditional knockout cells showed a persistent reduction in firing rate, across increasing current steps (**Figure 3.8H**). This shows a potential dichotomy of cell functionality between males and females, with both resulting in decreased firing in the Er81 conditional knockout. To determine possible action potential alterations that may explain the decrease in firing, we compared their properties (**Figure 3.8I**). Whilst there was no change to the threshold potential in males, it was more depolarised in females (**Figure 3.8J**), corroborating our observations of decreased near threshold firing (**Figure 3.8G**). There were no changes to the action potential amplitude, rise time, or decay time (**Figure 3.8K-M**), but a significant increase in the afterhyperpolarisation (AHP) amplitude in male conditional knockout mice (**Figure 3.8N**), which correlates with decreased firing as a larger AHP decreases the overall excitability of the cell. The sex-specific deficits, whereby Pet+ serotonergic cells in the Er81 conditional knockout are hypofunctional, but with differences in presentation, may indeed explain the observed behavioural alterations. Female mice displayed decreased firing near threshold, due to a depolarisation of the threshold potential. Action potential threshold has been shown to be dependent on sodium and potassium channel activity (Platkiewicz and Brette 2010), the expression of which could be under the control of Er81, particularly the Kv1.1 potassium channel, which has been shown before (Dehorter et al. 2015). Conversely, male mice presented with a larger AHP in the Er81 conditional knockout, similar to our observations in other neuromodulatory populations (Chapter 2), which likely contributes to the persistent decrease in action potential frequency at increasing stimulus amplitudes.

Consequently, decreased serotonergic function, for example via a knockout of the serotonin precursor enzyme tryptophan hydroxylase 2 (Tph2), has been shown to lead to decreased anxiety, corresponding to our observations in female *Er81* knockout mice (Ren et al. 2018).

---

**Figure 3.8: Serotonergic neuron electrophysiological properties**

**A.** Schematic of electrophysiological recordings in the DRN. *Pet*<sup>+</sup> cells in the DRN were recorded under whole-cell patch clamp in control (*Pet-Cre;RCE-GFP*) and conditional knockout (*Er81<sup>fl/fl</sup>;Pet-Cre;RCE-GFP*) mice (n = 5 control, 9 cKO female cells; 12 control, 10 cKO male cells). **B.** Resting membrane potential (female: p = 0.7865, male: p = 0.5160). **C.** Input resistance (female: p = 0.0992, Mann-Whitney test, male: p = 0.1024). **D.** Firing responses to a 200 pA current stimulus in control and conditional knockout males. **E.** Spike adaptation (female: p = 0.4107, male: p = 0.5664). **F.** Rheobase (n = 5 control, 9 cKO female cells, p = 0.111p, Mann-Whitney test; 11 control, 9 cKO male cells, p = 0.1943, Mann-Whitney test). **G.** Female firing frequency in response to increasing current input (two-way ANOVA (0-100 pA):  $F_{(1, 45, \text{genotype})} = 6.837$ , p = 0.0121;  $F_{(4, 45, \text{interaction})} = 0.5111$ , p = 0.7278). **H.** Male firing frequency in response to increasing current input (two-way ANOVA:  $F_{(1, 338, \text{genotype})} = 68.58$ , p < 0.0001;  $F_{(20, 338, \text{interaction})} = 1.614$ , p = 0.0473). **I.** Action potentials in the female cells. Lines indicate threshold. **J.** Action potential threshold (female: p = 0.0203, male: p = 0.3092). **K.** Action potential amplitude (female: p = 0.1117, male: p = 0.9229, Mann-Whitney test). **L.** Action potential rise time (female: p = 0.1722, male: p = 0.2276, Mann-Whitney test). **M.** Action potential decay time (female: p = 0.7713, male: p = 0.5752). **N.** Afterhyperpolarisation amplitude (female: p = 0.1397, male: p = 0.0217). Unless otherwise specified, Student's t-test: p<0.05:\*, p<0.01:\*\*, p<0.001:\*\*\*, p<0.0001:\*\*\*\*.



Whilst changes in serotonergic neuron activity can be attributed to intrinsic alterations to ionic channel composition and subsequent membrane properties, synaptic inputs also have a role (Maejima et al. 2013). Serotonergic neurons in the DRN receive extensive excitatory glutamatergic inputs from other brain structures such as the prefrontal cortex and lateral habenula (Pollak Dorocic et al. 2014). However, it has also been shown that DRN serotonergic neurons can co-release glutamate and serotonin, evidenced by the expression of the vesicular glutamate transporter 3 (VGluT3) in some DRN neurons and at serotonergic axon terminals (Wang et al. 2019, Okaty et al. 2020). Importantly, serotonergic neuron activity is thought to be partly regulated by autoregulation mediated by serotonin receptors on both somatodendritic compartments and at axon terminals (Stamford et al. 2000, McDevitt and Neumaier 2011). To determine whether altered excitatory inputs (*i.e.* circuit dysfunction) could be influencing the excitability of serotonergic neurons, we recorded excitatory post-synaptic currents (EPSCs) in serotonergic Pet<sup>+</sup> neurons in the DRN (**Figure 3.9A**) and compared male and female control and conditional knockout cells. There was no alteration to the frequency or kinetics of EPSCs in male cells (**Figure 3.9B-E**), however there was a decreasing trend in EPSC frequency (**Figure 3.9B**) and a significant decrease in amplitude (**Figure 3.9C**) in female conditional knockout cells compared to controls. This difference in excitatory tone could modulate overall excitability of cells and explain the previously observed differences in female near threshold excitability. However, changes to EPSCs can be attributed to pre-synaptic or post-synaptic mechanisms; to further determine the origin of this shift in glutamatergic signalling, recordings under synaptic blockade will be necessary. In addition, determining whether these alterations are due to shifts in long range glutamatergic signalling or glutamate mediated serotonergic neuron autoregulation is necessary. Serotonergic cell excitability, which appears to be decreased as a result of Er81 ablation, may contribute directly to the decrease in glutamatergic signalling in females. Disruptions to this feedback circuitry can exacerbate deficits in long range signalling, impacting serotonergic release in downstream structures. As such, dissecting the mechanisms behind the decreased excitability of serotonergic neurons in both male and female conditional knockouts of Er81 is a vital future direction.

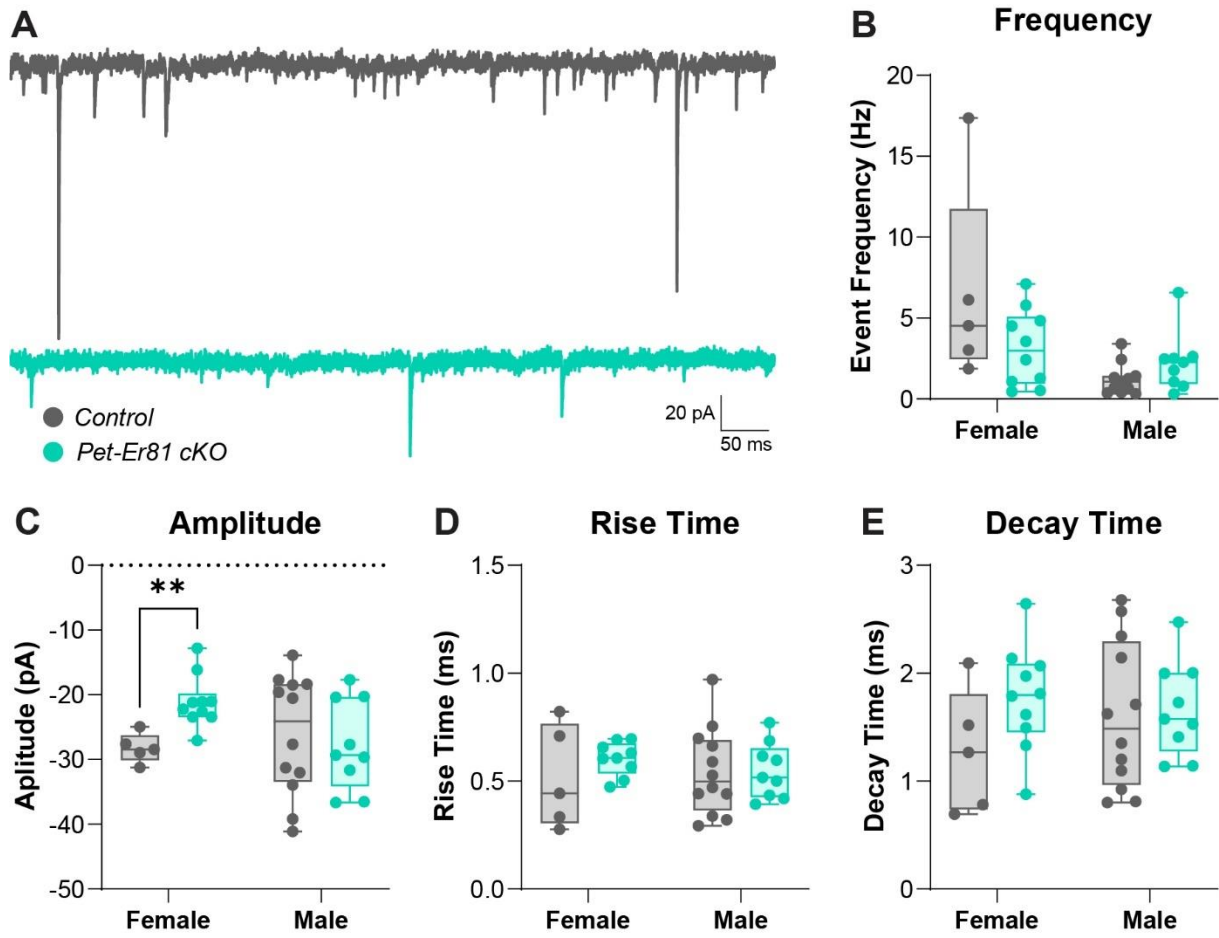


**Figure 3.9: Excitatory inputs to serotonergic neurons in the DRN**

**A.** Example traces of excitatory post-synaptic currents (EPSCs) recorded in control (*Pet-Cre;RCE-GFP*) and conditional knockout (*Er81<sup>fl/fl</sup>;Pet-Cre;RCE-GFP*) mice (n = 5 control, 10 cKO female cells, n = 11 control, 9 cKO male cells). **B.** EPSC event frequency (female: p = 0.1394, male: p = 0.1519). **C.** EPSC amplitude (female: p = 0.0029, male: p = 0.6649). **D.** EPSC rise time (female: p = 0.3273, male: p = 0.9402). **E.** EPSC decay time (female: p = 0.0969, male: p = 0.8172). Unless otherwise specified, Student's t-test: p<0.05:\*, p<0.01:\*\*, p<0.001:\*\*\*, p<0.0001:\*\*\*\*.

### 3.6 The ablation of Er81 alters serotonergic cell numbers

To determine alterations to serotonergic circuitry within the DRN that might contribute to the functional differences we observed, we decided to determine whether there were any prevalent alterations to the *Pet*<sup>+</sup> cellular population. Whilst we are unsure when Er81 is first expressed in *Pet*<sup>+</sup> serotonergic neurons, *Pet* expression begins from E12.5, and serotonergic neurons are amongst the earliest born (Hendricks et al. 1999), in addition, Er81 expression has been characterised in other embryonic domains (Flames et al. 2007). We therefore considered the possibility that Er81 is necessary for early developmental processes, such as proliferation and migration, and hence quantified the number of *Pet*<sup>+</sup> cells in the DRN across the rostro-caudal axis (**Figure 3.10A**)<sup>3</sup>. We found a significant decrease in the number of cells in the rostral aspect of the DRN in the female conditional knockout with no changes in the caudal aspects, and no changes in male mice (**Figure 3.10B, C**). This female specific decrease in cell number may indeed explain the decrease in excitatory input, if it can in fact be attributed to serotonergic autoregulation. It also correlates with decreased serotonergic signalling in downstream structures, which has been shown in other studies to lead to decreased anxiety (Ren et al. 2018), similar to our observations (**Figure 3.5E, 3.6A-C**). Considering these results, it is likely that developmental alterations underlie disrupted serotonergic circuitry and function in the Er81 conditional knockout. To determine whether Er81 may have a developmental role, which has been demonstrated by its enhanced expression at early postnatal stages (Ahmed et al. 2021), we quantified Er81 expression in *Pet*<sup>+</sup> neurons at P5 (**Figure 3.10D**). We found that Er81 is expressed approximately 1.5 times higher during development than in adult (**Figure 3.10E**), suggesting transient changes in expression that may signify when Er81 is the most transcriptionally active.

---

<sup>3</sup> Cell counting analysis was performed by Melissa Ritchie and Lachlan Kimpton, see Appendix X.

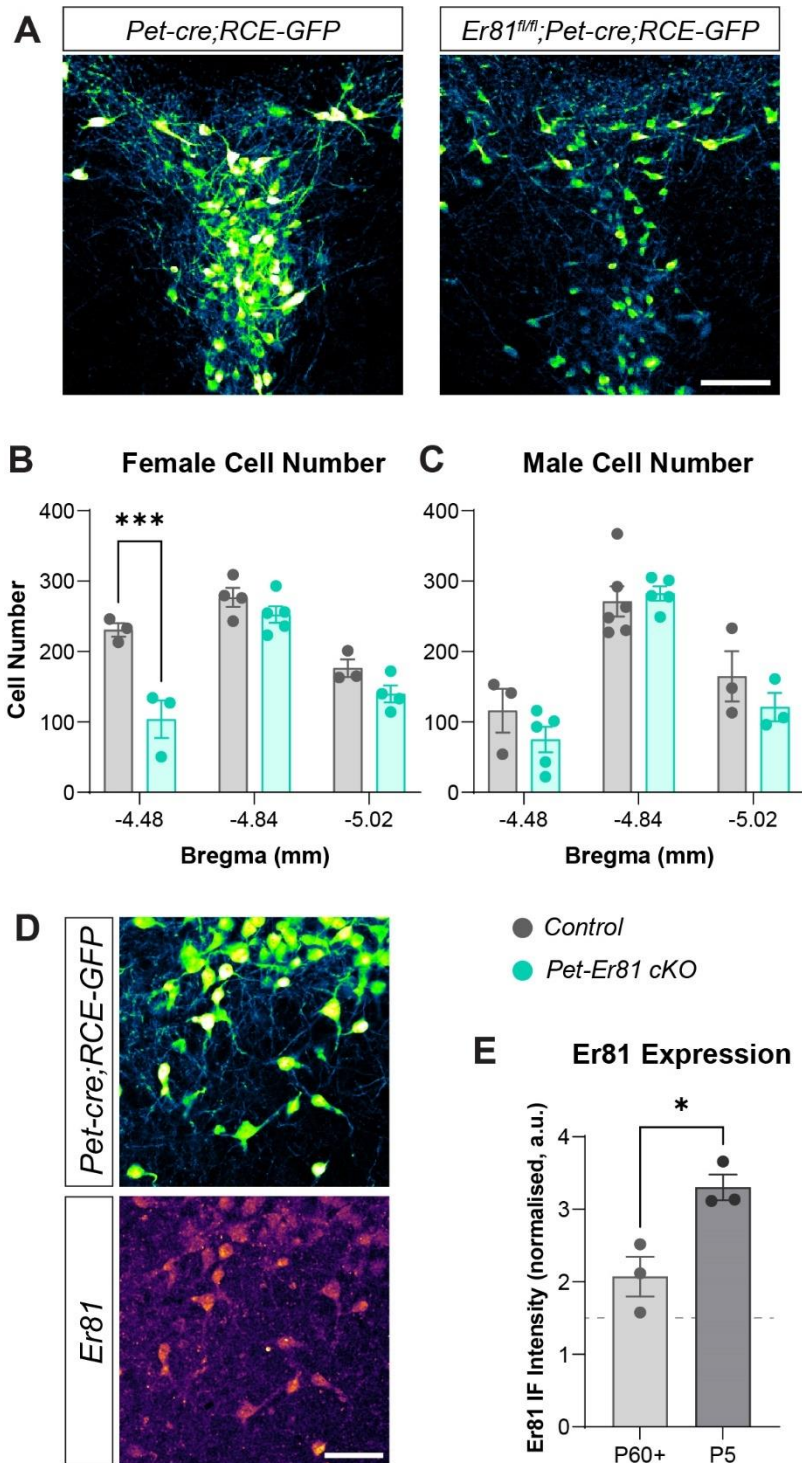


**Figure 3.10: Evidence of developmental role for Er81 in Pet+ serotonergic neurons**

**A.** Pet+ cells in the rostral DRN of a control and a conditional knockout mouse. Scale: 100  $\mu$ m. **B-C.** Pet+ cell number quantification across three rostro-caudal axis points (Bregma -4.48, -4.84, -5.02) in **(B)** female (-4.48: n = 3 control, 3 cKO mice, -4.84: n = 4 control, 5 cKO mice, -5.02: n = 3 control, 4 cKO mice; two-way ANOVA: F(1, 16, genotype) = 26.59, p < 0.0001, F(2, 16, interaction) = 6.648, p = 0.0079; post-hoc Bonferroni multiple comparison tests: -4.48: p = 0.0001, -4.84: p = 0.6312, -5.02: p = 0.3174) and **(C)** male (-4.48: n = 3 control, 4 cKO mice, -4.84: n = 6 control, 5 cKO mice, -5.02: n = 3 control, 3 cKO mice; two-way ANOVA: F(1, 19, genotype) = 1.717, p = 0.2057, F(2, 19, interaction) = 1.069, p = 0.3631; post-hoc Bonferroni multiple comparison tests: -4.48: p = 0.6786, -4.84: p > 0.9999, -5.02: p = 0.7409) mice. **D.** Er81 expression in Pet+ cells at postnatal day 5 (P5). Scale: 50  $\mu$ m. **E.** Comparison of Er81 expression in Pet+ cells at adult (P60+) and developmental (P5) stages (n = 3 P60+ mice, 3 P5 mice; p = 0.0194, Student's t-test).

### 3.7 Discussion

The striatum is influenced by long-range neuromodulatory inputs, making it a key neuromodulatory hub in the brain. Here we have shown that serotonergic input to the striatum is physically and functionally altered when *Er81* is lacking from *Pet+* serotonergic neurons in the DRN. This is correlated with behavioural alterations, including motor deficits and decreased anxiety-like behaviour, indicating long lasting alterations to circuitry that we anticipate occur during developmental stages. These results occur in a sex-specific manner, which highlights the complex interaction of sex-specific mechanisms in development, circuitry, and behaviour.

#### *Sexual dimorphism in serotonergic regulation of circuitry and behaviour*

In this study, we found differences between males and females following the ablation of *Er81* in *Pet+* serotonergic neurons of the DRN, thus showing evidence of sex specific responses to an early insult to genetic programming in the serotonergic system. This includes differing behavioural responses, circuit and cell function, and changes in the serotonergic cell population itself.

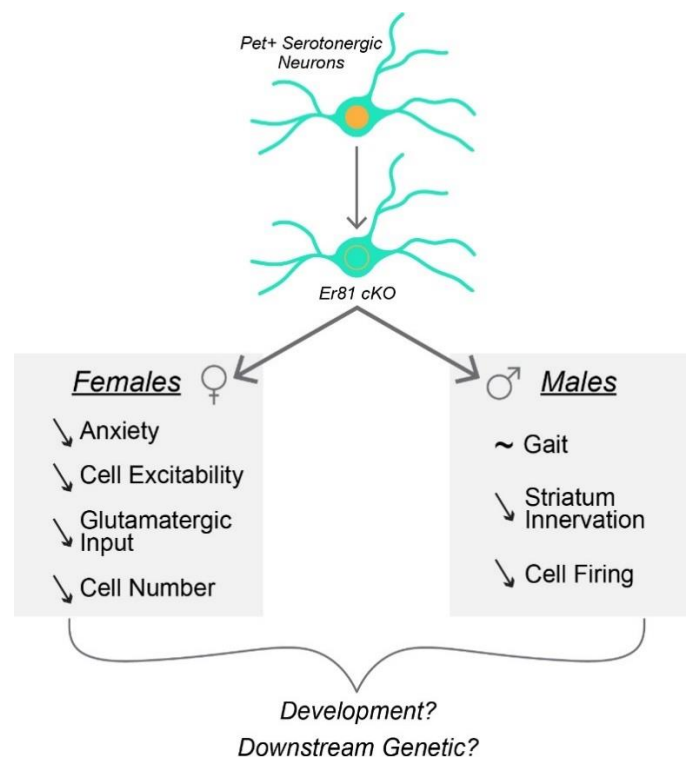


**Figure 3.11: Summary of findings in females and males following *Er81* ablation from serotonergic neurons**

Female mice in the *Er81<sup>fl/fl</sup>;Pet-Cre;RCE-GFP* conditional knockout presented with decreased anxiety, decreased serotonergic neuron excitability, decreased glutamatergic inputs to serotonergic neurons, and decreased serotonergic cell number compared to control *Pet-Cre;RCE-GFP* mice. Male mice in the conditional knockout presented with altered gait, decreased serotonergic innervation of the striatum and decreased firing in serotonergic cells compared to controls. These alterations could be rooted in early alterations to serotonergic cell development and circuit formation or downstream genetic factors under the control of *Er81*.



Current research is exploring the concept of sexual dimorphism from the behavioural level down to the genetic level. For example, it has been shown that males have a predisposition for early onset disorders, such as autism spectrum disorder and Tourette's syndrome, whereas females are susceptible for disorders with a later onset, including anxiety and mood disorders (Rutter et al. 2003). Further studies have shown that this is reliant on genetics; in the case of major depressive disorder, females are much more likely to develop it, and there are sex specific transcriptional networks underlying this predisposition (Labonte et al. 2017). Generally, differences in gene and protein expression between males and females have been described and highlight the molecular complexities that underlie sex differences in baseline brain function (Block et al. 2015).

Sex differences have also been studied specifically in the serotonergic system. There is evidence for differences between sexes in the rate of serotonin synthesis, whereby males have a higher rate of synthesis than females, and thus have more serotonin (Nishizawa et al. 1997). This indeed correlates with observed higher rates of depressive disorders (which present with decreased serotonin) in females. In addition, select studies have shown that modulating the serotonergic system is effective in a sex dependent manner. For example, a knockout of the 5-HT<sub>1B</sub> receptor resulted in behavioural alterations related to mobility and a higher baseline of serotonin, caused by the disinhibition of serotonin release specifically in females, but not in males (Jones and Lucki 2005). Furthermore, sex differences in 5-HT<sub>1A</sub> receptor binding and the current elicited in cortical pyramidal neurons following serotonin application show that sex-dependent serotonin receptor expression may mediate dimorphic circuitry and behaviour (Goodfellow et al. 2009). Here, we showed differential innervation of the striatum in male and female Er81 conditional knockout mice. Whilst these alterations can correlate with the behavioural phenotypes we observed, we cannot rule out altered innervation of other brain regions with links to these behaviours. For example, the amygdala has close ties with anxiety, in fact decreased serotonergic signalling to the amygdala has been shown to decrease anxiety in mice, with the opposite occurring with increased signalling (Ren et al. 2018). Similarly, the gait deficits observed may be striatum related, as the striatum regulates motor decisions, but may also be a result of aberrant serotonergic signalling to the spinal cord, which is involved in locomotion (Ghosh and Pearse 2014). We did not observe high Er81 expression in the medial raphe nucleus or other caudal nuclei containing serotonergic neurons, however we cannot discard the possibility that these populations are also affected in the Er81 knockout, with changes to their projections mediating the behavioural responses we observed.

Therefore determining the serotonergic regions affected when Er81 is ablated from Pet+ serotonergic cells and studying other downstream structures to identify regions altered will lead to a more comprehensive dissection of the behavioural deficits. With new techniques, there are possibilities for genetically manipulating the identity of only serotonergic neurons projecting to specific structures. The use of retrograde *Cre* expressing viruses injected into the structure of interest (*i.e.* the striatum) could then label and conditionally knock out Er81 from striatum-projecting cells. This type of study would show the specific functional and behavioural roles of serotonergic signalling in the striatum and how it is impacted upon Er81 ablation in a cell-autonomous manner.

In this study, we affected the expression of the transcription factor Er81 in serotonergic neurons. Many transcription factors do have sex-biased regulatory targeting patterns, which have been linked to pathology presentation. For example, Parkinson's and Alzheimer's disease genes are targeted by different transcription factors in each sex (Lopes-Ramos et al. 2020). As such, we expect that Er81 may be regulating different downstream targets within serotonergic cells in males and females. Therefore, future experiments must explore gene targets associated with Er81 regulation in both sexes to understand the genetic mechanisms underlying the developmental and functional cellular alterations we have observed, as well as linking genetic processes to behavioural presentation. Employing RNA sequencing methods will allow us to determine the molecular pathways affected in females versus males; using novel spatial transcriptomics would also give a better spatial resolution to link to cell diversity.

Sexual dimorphism highlights one level of diversity in the serotonergic system, however with such varied functions and targets in the brain, the serotonergic cells themselves are a highly heterogeneous population.

### ***The heterogeneous serotonergic neuron population***

Serotonergic neurons are heterogeneous across sub-structures, projections, and genetic identity. Transcriptional analysis has found genetic diversity and clustering of serotonergic cells into sub-groups (Ren et al. 2018, Huang et al. 2019, Okaty et al. 2020, Baretino et al. 2021). This leads to heterogeneity in downstream innervation targets (Ren et al. 2019), as well as functional diversity (Okaty et al. 2020).

In this study, we focussed on the Er81 transcription factor, which we found to be expressed in all Pet+ serotonergic neurons. Er81 expression has been shown to segregate neuronal subpopulations before, such as in cortical pyramidal neurons (Yoneshima et al. 2006) and

parvalbumin positive interneurons (Dehorter et al. 2015), as well as striatal cholinergic interneurons (Ahmed et al. 2021). As opposed to a marker of a specific subtype of serotonergic neuron, Er81 appears to have the potential to regulate the whole population. This is somewhat unsurprising given its close relationship and similarities with Pet-1 (Cooper et al. 2015).

It is true that when considering properties of the serotonergic population, such as in electrophysiology, we do not consider the different subtypes of serotonergic neuron and how they may be affected by the lack of Er81. That is, we are unsure how Er81 interactions with the transcriptional environment in different subpopulations. For example, a subset of the serotonergic neuron population expresses the tyrosine kinase receptor Erbb4, the expression of which facilitates serotonergic innervation of thalamic nuclei, and contributes to memory processing (Barettino et al. 2021). Er81 has been shown to have some transcriptional influence over Erbb4 (Yamaguchi et al. 2021), thus posing the question of whether a knockout of Er81 would affect the Erbb4+ serotonergic population in a different manner to the Erbb4- population. Future studies must therefore take into account the diversity of the serotonergic neuron population when looking at the functional result of genetic manipulation. Employing techniques such as patch-seq, where the contents of single cells are collected following patch-clamp electrophysiology for RNA sequencing, is a viable solution for correlating molecular identity and alterations with cell functionality.

### ***Diverting the developmental trajectory of the serotonergic system***

Serotonergic signalling throughout the brain is highly important during development. Serotonergic cells are differentiated early during development, from embryonic day (E)10 to 12 in rodents, and the first month of gestation in humans (Gaspar et al. 2003). As such they are functional from early stages, and serotonergic signalling in downstream structures is known to regulate developmental processes from early, embryonic stages up to morphological establishment and circuit formation (Daubert and Condrón 2010, Migliarini et al. 2013). For example, serotonergic axons arising from the DRN have been shown to reach the rodent cortex by E17 (Wallace and Lauder 1983), and serotonin activity here impacted interneuron migration into the cortex (Ricchio et al. 2009). In addition, altered serotonin levels during development have been shown to contribute to the cortical abnormalities, such as aberrant structure formation (Cases et al. 1996, Daubert and Condrón 2010), and cell morphology deficits (Vitalis et al. 2007).

In this study, we suggest a link between decreased serotonin signalling and behavioural alterations. We anticipate that this result is rooted in developmental alterations; the Er81 knockout occurs from the stages of *Pet* expression, which is early in embryonic development. Therefore, future experiments must first focus on determining whether serotonergic signalling is altered during developmental and adult stages under the Pet-dependent Er81 knockout. This can be done through measuring serotonin expression in the striatum, but also through the use of new sensor technology that allows for *in vitro* and *in vivo* temporal measurements of serotonin release. G-protein-coupled receptor-activation-based (GRAB) sensors are recently developed molecules that exhibit large increases in fluorescence in response to extracellular neurotransmitter signalling (Sun et al. 2020). A sensor specific for serotonin signalling (GRAB<sub>5-HT</sub>) is highly sensitive and detects serotonin via a modified 5-HT receptor with an attached green fluorescent protein (GFP), which fluoresces upon activation of the receptor by serotonin (Wan et al. 2021). These powerful sensors would enable recordings of serotonin dynamics in the striatum *in vivo* during behaviour, and *in vitro* with pharmacological manipulation.

Further work must then be done to understand whether serotonin signalling in the striatum during early developmental stages regulates circuit formation, and whether behavioural alterations arise during development. Tracking both serotonergic and downstream striatal circuit function during developmental stages via calcium imaging and electrophysiology in control and Er81 knockout conditions would elucidate whether aberrations in striatal circuits mediated by altered serotonin signalling underlie behavioural regulation.

**Chapter 4:**  
**Developmental Deficits of MGE-Derived Interneurons**  
**in a Mouse Model of Autism Spectrum Disorder<sup>4</sup>**

**4.1 Preamble**

Circuit development is an intricate process, susceptible to changes in both genetic programming and shifts in the surrounding environment, as we have explored in previous chapters. It is well established in literature that variations in developmental processes, at nearly all stages, lead to neuropsychiatric disorders with distinctive and detrimental behavioural symptoms, such as deficits in motor control, intellectual disability, and impaired communication (Taber et al. 2011, Bassett et al. 2018). In fact, some researchers have postulated that neurodevelopmental disorders are differentiated by the time point at which brain development deviates from its canonical trajectory (Del Pino et al. 2018). Autism Spectrum Disorder (ASD) is one such neurodevelopmental pathology that is governed by both genetic and environmental factors during various developmental stages (Del Pino et al. 2018).

Studies regarding early alterations to the autistic brain have been in progress for the last 20+ years in an effort to corroborate these developmental behavioural symptoms with shifted brain states. Alterations to brain volume in ASD have been well documented via magnetic resonance imaging (MRI) (Courchesne et al. 2001, Vaccarino and Smith 2009, Ha et al. 2015, Prigge et al. 2021) and have attributed to incorrect organ growth during early stages. Similarly, neuronal migration defects have been posited as a general characteristic of ASD (Reiner et al. 2016, Pan et al. 2019), however this is still debated due to a lack of direct evidence and a heterogenous presentation. Functional connectivity alterations have been characterised via MRI studies in patients however findings remain inconsistent, with both enhanced and decreased connectivity at both short and long ranges having been observed (Long et al. 2016), once again likely due to the heterogeneity of ASD presentation, and finer studies into network connectivity at a cellular level are still lacking. The generation of mouse models recapitulating ASD-like symptoms via manipulation of ASD-related genes have greatly advanced autism research, as behavioural characteristics can be correlated with cellular alterations (Abrahams and Geschwind 2008, Kazdoba et al. 2016).

ASD has not been linked to a single brain structure; multiple brain regions show alterations in ASD patients and models. Indeed, some regions are now gaining additional interest, including

---

<sup>4</sup> Work presented in this chapter has been published as Ahmed et al. (2023), *Frontiers in Cell and Developmental Biology*.

the striatum. Whilst altered striatal circuit formation and function has been linked primarily to movement disorders (Gittis and Kreitzer 2012), such as Tourettes Syndrome (Wang et al. 2011, Hienert et al. 2018, Schilke et al. 2022), and Huntington's Disease (Lebouc et al. 2020), its role in ASD is of particular interest. The intersection between core symptoms of ASD: impaired social interaction and communication, and repetitive behaviours (DSM-5), as well as imbalanced reward processing (Scott-Van Zeeland et al. 2010), remains unexplained, however all can be linked with striatal function (**Figure 4.1A**) (Kohls et al. 2014, Fuccillo 2016). For instance, the severity of repetitive behaviours has been linked to the developmental growth rate of the striatum, which is elevated in ASD patients compared to controls (Langen et al. 2014). Similarly, imbalanced activity in response to reward stimuli observed in ASD is also localised to the dorsal striatum (Kohls et al. 2018). Subsequent research has focussed on both cortico-striatal circuitry and striatal microcircuitry. Cortico-striatal connectivity has been found to be imbalanced in ASD in both functional MRI studies in humans (Abbott et al. 2018) and in ASD risk gene mouse model studies (Li and Pozzo-Miller 2020). For example, *FMRI* (Fragile X messenger ribonucleoprotein 1; associated with Fragile X Syndrome, a severe form of ASD) knockout mice display hypoactive cortico-striatal connectivity (Zerbi et al. 2018). Similarly, *TSHZ3* (teashirt zinc finger homeobox 3) has been identified as a susceptibility gene for ASD (Hussman et al. 2011), and a heterozygous deletion mouse model displays ASD-like behaviour and presents with increased release probability and enhanced long-term potentiation (LTP) at cortico-striatal synapses (Caubit et al. 2016).

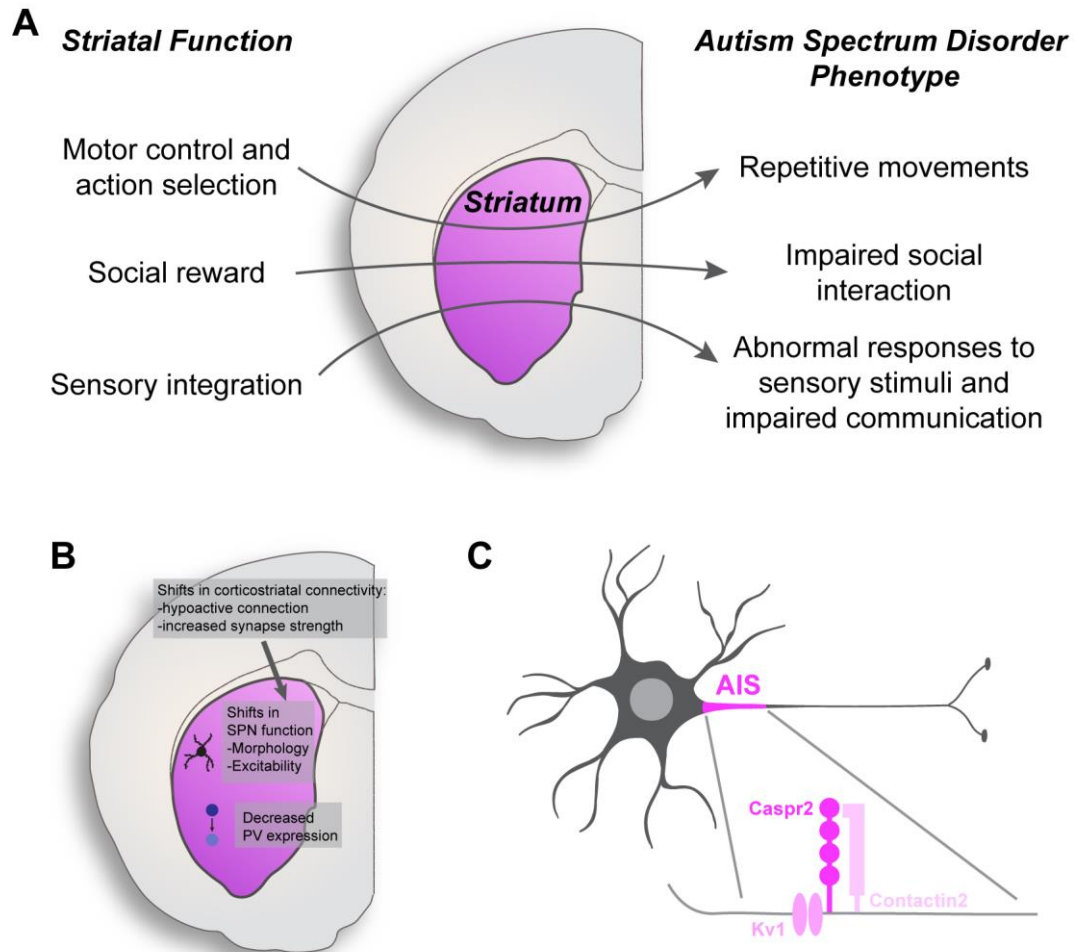


**Figure 4.1: The role of the striatum in autism spectrum disorder.**

**A.** The link between striatum-mediated behaviours and core symptoms of autism spectrum disorder (ASD). **B.** Well-known cortico-striatal, striatal spiny projection neuron (SPN), and striatal parvalbumin (PV) interneuron alterations in ASD. **C.** The location of Caspr2 (contactin-associated protein-like 2), the protein product of the ASD risk gene *Cntnap2*, at the axon initial segment (AIS) of neurons. Caspr2 anchors potassium channels (Kv1) to the cell membrane and is associated with contactin2.

In addition, striatal microcircuit specific deficits have also been observed, often linked to changes in cortico-striatal connectivity (**Figure 4.1B**). For example, *Shank3* (SH3 and multiple ankyrin repeat domains 3) is an ASD risk gene (Moessner et al. 2007, Uchino and Waga 2013), and knockout mice for this gene are well-established models of ASD (Peca et al. 2011, Zhou et al. 2016). *Shank3B* knockout mice show increased striatal spiny projection neuron (SPN) dendritic complexity and post-synaptic alterations leading to reduced cortico-striatal synaptic transmission in SPNs (Peca et al. 2011). A further study linked these changes to developmental deficits whereby cortico-striatal connection hyperactivity at early stages contributes to altered SPN development (Peixoto et al. 2019). Changes in SPN functionality have also been characterised in the context of the basal ganglia direct and indirect pathways, which are each modulated by separate SPN populations (D1 and D2 expression, see Chapter 1). D1- and D2-SPNs in mice exposed to valproic acid (VPA; an environmental model of ASD) showed opposite alterations to excitability, morphology, and responsiveness to a social interaction task (Di et al. 2022). This suggests that overall striatal circuitry is shifted in ASD, presenting deficits in the principal cells of the striatum. However, SPNs are heavily regulated and influenced by diverse striatal interneuron populations, as we have described in Chapter 1. Interneurons have been implicated as key risk populations in ASD, in various brain structures (Lunden et al. 2019, Contractor et al. 2021), thus the contribution of striatal interneuron populations to ASD aetiology is of keen interest.

In the striatum, a decrease in the number of parvalbumin (PV) positive interneurons was first described in the *Cntnap2* (contactin-associated protein-like 2) knockout model of ASD (Penagarikano et al. 2011). However, this was later attributed to a decrease in PV expression, leading to a lack of detection, and was also confirmed in the *Shank3* knockout model (**Figure 4.1B**) (Filice et al. 2016, Lauber et al. 2018). Regardless, another paper showed that the downregulation of PV leads to ASD-like behavioural deficits, including impaired social interaction and increased repetitive movements, as well as a shift in the cellular excitation-inhibition balance (Wohr et al. 2015). In fact, several studies have specifically altered interneuron populations in the striatum and found resulting behavioural and cellular phenotypes indicative of ASD. The deletion of *Mecp2*, the gene causing Rett Syndrome (a severe form of ASD), specifically from PV interneurons leads to sensory and motor deficits which could be attributed to striatal dysfunction (Ito-Ishida et al. 2015). Additionally, the depletion of both PV interneurons and cholinergic interneurons (CINs) in the striatum led to stereotypic spontaneous ASD-like behaviour (grooming, repetitive movements) and decreased social interaction, as well



as elevated activity dependent signalling in SPNs (Rapanelli et al. 2017). Together, these findings indicate decreased PV interneuron function, rather than decreased cell number, as a key contributor to striatal circuit imbalances in ASD. This is supported by the above study, as the depletion of PV interneurons alone was not sufficient to cause ASD-like symptoms, the depletion of CINs was also necessary (Rapanelli et al. 2017).

CINs are also essential in striatal circuitry, as we have explored in Chapter 3. However, the role and susceptibility of striatal CINs in ASD pathophysiology remains largely unknown. ASD has been associated with decreased cholinergic tone (Nagy et al. 2017), and elevating acetylcholine levels relieves cognitive and social symptoms in a BTBR (Black and Tan Brachyury; mutation within the *Itpr3* gene) mouse model of ASD (Karvat and Kimchi 2014). Yet, only one study has concretely linked striatal CINs to ASD; a conditional knockout of the aforementioned *TSHZ3* gene, specific to CINs in the striatum, results in electrophysiological alterations to these cells, including decreased spontaneous firing and increased firing irregularity, and was also associated with increased repetitive behaviours (Caubit et al. 2022). This type of disruption can result in dysfunctional regulation of the striatal inhibitory and output circuitry, affecting other striatal interneurons and SPNs (Oldenburg and Ding 2011).

Overall, striatal function has been implicated in contributing to ASD aetiology in human patients, however this has not been explored at a cellular level. Despite some sparse studies into striatal interneuron properties in the adult ASD brain, there has been no research on their developmental trajectory and how it may be altered in ASD. Striatal interneuron function is critical during developmental stages for facilitating circuit development and activity, as we have shown in Chapter 2. This presents a key question to answer this gap in current knowledge: Do striatal interneurons present with a shifted developmental trajectory in ASD compared to typically developing controls, and could this underlie ASD pathophysiology?

Answering these intricate circuitry questions is near impossible in human patients with current technology. Therefore, mouse models with mutations of ASD-risk and ASD-related genes are a powerful tool (Abrahams and Geschwind 2008, Kazdoba et al. 2016). There is a vast range of mouse models currently being used to study ASD, and we have referenced many of these above. This includes both genetic and environmental models; and studies have emerged exploring new genetic risk factors, epigenetic contributions, and interactions between genetic and environmental systems in ASD (Lim et al. 2022). However, in order to investigate striatal interneuron development, we selected one particular mouse model that has been used

extensively, and presents with both cellular and behavioural alterations: the *Cntnap2* knockout model of ASD.

The transmembrane, neurexin family, *Cntnap2* scaffolding protein (also known as Caspr2) has a vital role in anchoring potassium channels at the axon initial segment (Strauss et al. 2006, Duflocq et al. 2011)(**Figure 4.1C**), and has been identified as an ASD risk gene (Alarcon et al. 2008). *CNTNAP2* alterations were first observed in human patients with severe ASD symptoms, including epilepsy (Strauss et al. 2006, Rodenas-Cuadrado et al. 2016), and variants have been found in human individuals with confirmed ASD (Egger et al. 2014). A homozygous *Cntnap2* knockout mouse model was established by Penagarikano et al. (2011), and was described to have behavioural deficits characteristic of ASD, including increased repetitive movements, decreased social interaction, decreased communication, and epileptic seizures. Following this, further studies described additional details regarding molecular and cellular alterations in this model. Impaired function and excitation-inhibition balance of neurons at adult stages has been described in *Cntnap2* knockout conditions; in cortical pyramidal neurons (Varea et al. 2015, Antoine et al. 2019) and in cortical PV interneurons (Vogt et al. 2018). However, the Caspr2 protein has been shown to be expressed as early as embryonic day 13.5 (E13.5) (Penagarikano et al. 2011, Vogt et al. 2018), and thus we anticipate that cellular and network alterations occurring in this mouse model must occur from early stages, particularly given the importance of Caspr2 during development (Penagarikano et al. 2011, Poot 2015, Rodenas-Cuadrado et al. 2016, Canali et al. 2018, Scott et al. 2019, Lu et al. 2021). Despite our current knowledge of *Cntnap2* and its role in inducing ASD, the specific pattern of its expression in the brain is still unknown. In addition, very little is known about how the absence of *Cntnap2* could perturb striatal circuitry, particularly during development.

To track striatal interneurons during development in the *Cntnap2* knockout model of ASD, we targeted the major population of striatal interneurons with a common developmental origin, the medial ganglionic eminence (MGE). As previously shown, these interneurons can be labelled with the transcription factor *Lhx6* (LIM homeobox 6), which is expressed from the time these cells are post-mitotic.

Parvalbumin positive and cholinergic interneurons comprise the majority of the *Lhx6*<sup>+</sup> interneuron population in the striatum (Gittis et al. 2010, Lozovaya et al. 2018). Both of these subpopulations of neurons contribute to the excitation-inhibition balance in the striatum (Pakhotin and Bracci 2007, Ferguson and Gao 2018, Nahar et al. 2021, Poppi et al. 2021), and

we hypothesise that functional alterations may be present early in development, leading to imbalances in striatal circuitry, thus contributing to ASD aetiology. As such, this chapter has the following aims.

1. To characterise *Cntnap2* expression in the control brain through the use of novel techniques, providing higher resolution and higher throughput information than current literature.
2. To track the development of MGE-derived interneurons populating the striatum from embryonic stages through to early postnatal stages in control and in the *Cntnap2* knockout model of ASD.
3. To probe alterations to the identity and functional properties of MGE-derived striatal interneurons in the *Cntnap2* knockout model of ASD.

Studying early alterations to striatal interneurons in ASD will hopefully provide insights into the shifted developmental trajectory occurring in this condition, and elucidate potential therapeutic targets, but also highlight general mechanisms behind striatal circuit development, allowing us to understand the delicate balance between typical and atypical circuitry in the striatum.

## 4.2 *Cntnap2* expression maps to enrichment in striatal interneuron populations

Caspr2, the protein product of *Cntnap2*, is expressed ubiquitously throughout the brain (Rodenas-Cuadrado et al. 2014). However, as *Cntnap2*/Caspr2 is a scaffolding protein, involved in anchoring potassium channels to the cell membrane (Strauss et al. 2006, Duflocq et al. 2011), quantifying its expression in specific neuronal subtypes has not been done. Previous studies have relied on mRNA and protein expression levels in whole tissue samples (Penagarikano et al. 2011), or on high resolution imaging of single neurons (Scott et al. 2019). Recent advances in sequencing technology have begun to include spatial components, to essentially map mRNA presence onto tissue samples, and this new technology has the potential to reveal previously unknown details about gene expression across brain regions and in specific cell types. To elucidate the intricacies of *Cntnap2* expression in the adult mouse brain, we performed spatial transcriptomics, also known as stereo-seq, on a sagittally sectioned tissue sample<sup>5</sup>. This technique is based on DNA nanoball technology, whereby a grid of probes on a chip synthesise cDNA upon interaction with the tissue sample, which is then sequenced and can be correlated with the spatial coordinates of the individual probes (more information on this protocol can be found in the Methods section).

Initial unbiased clustering generated 23 clusters that when mapped back onto the tissue, mostly corresponded to known brain regions (**Figure 4.2A**). Evident key structures were the striatum (cluster 7), and the deep (cluster 3) and superficial (cluster 4) layers of the cortex (**Figure 4.2A**). Further clustering including spatial information and co-expressed genes generated a separate set of 12 modules corresponding more directly to brain structures (**Figure 4.2B**). Of key interest for this project was module 5, corresponding to the striatum. As expected, genes enriched in this module corresponded to learning, locomotion, and developmental biological pathways (**Figure 4.2C**), correlating to some of the main known functions of this structure (Graybiel and Grafton 2015). One of the genes particularly enriched in the striatum was *Cntnap2* (**Figure 4.2D**), and it was significantly higher there than cortical regions (**Figure 4.2E**), which are highly studied in ASD. The stereo-seq technology used was powerful enough (*i.e.* 500 nm distance between probes) to generate readouts at a single cell resolution level. As such, we were able to separate each probe readout into groups based on expression of interneuron subtype specific factors, such as somatostatin (SST) and choline acetyltransferase (ChAT, marking cholinergic interneurons). We quantified *Cntnap2* expression levels in putative cells expressing SST or ChAT, compared to the remaining population. We found no difference between SST

---

<sup>5</sup> Performed in collaboration with Ulrike Schumann, Lixinyu Liu.

positive and negative cells (data not shown), but interestingly saw higher levels of *Cntnap2* in ChAT positive cells, compared to ChAT negative cells (**Figure 4.2F, G**). Unfortunately, detection of parvalbumin (PV) was unsuccessful; this could potentially be due to its expression within putative PV+ interneurons not being statistically enriched.

These results indicate not only a potential role for *Cntnap2* in regulating striatal cholinergic interneuron function, but also the potential for striatal cholinergic interneurons to be significantly altered in the absence of *Cntnap2* and therefore, to contribute to circuit dysfunction and behavioural alterations in autism. In fact, very little is known about how cholinergic interneurons are affected in this condition. We therefore explored how MGE-derived interneurons, which include a population of cholinergic interneurons, are affected in the absence of *Cntnap2*.

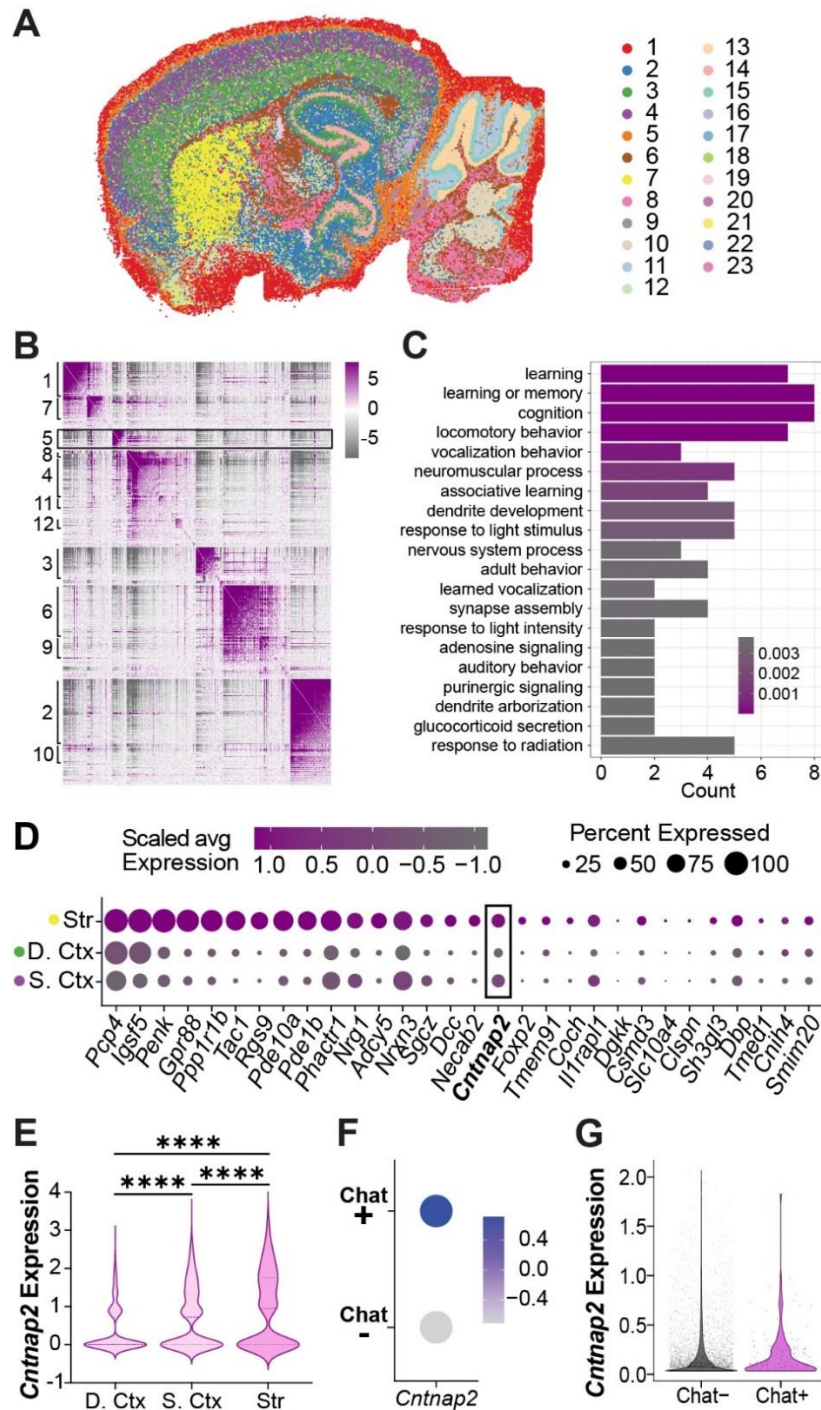


**Figure 4.2: *Cntnap2* mRNA levels are enriched in cholinergic interneurons in the adult striatum**

**A.** Unsupervised clustering in a sagittal adult mouse brain slice identified 23 clusters following stereo-seq analysis at a 50 bin resolution. **B.** Genes with significant spatial autocorrelation (FDR < 0.05) grouped into 12 distinct modules. **C.** Biological pathways related to genes enriched in Module 5, *i.e.* striatum. **D.** Relative expression of module 5 genes in striatum and cortex clusters (Str: striatum, cluster 7, D. Ctx: deep cortex, cluster 3, S. Ctx: superficial cortex: cluster 4). **E.** *Cntnap2* mRNA expression levels in the deep and superficial cortex, and striatum clusters. Log<sub>2</sub> fold change and adjusted p values were calculated pairwise (deep ctx vs sup. ctx: log<sub>2</sub>FC = 0.31, p < 0.0001; sup. ctx vs str: log<sub>2</sub>FC = 0.17, p < 0.0001; deep ctx vs str: log<sub>2</sub>FC = 0.48, p < 0.0001). **F.** *Cntnap2* expression in two populations segregated based on Choline Acetyltransferase (ChAT, marker of cholinergic interneurons). Scale: average expression. **G.** Violin plots showing *Cntnap2* expression levels in cholinergic (ChAT+) and non-cholinergic (ChAT-) cell populations (n = 3927 ChAT-, 143 ChAT+, p = 0.812).

### 4.3 The proliferative and apoptotic trajectory of the Lhx6 cell population is shifted

Previous studies have shown *Cntnap2* expression from as early as E14 (Penagarikano et al. 2011), however its expression in specific embryonic regions and whether it is expressed in the MGE was unknown. We utilised previously published single cell RNA sequencing data (Mi et al. 2018) to answer this question<sup>6</sup>. It was found that *Cntnap2* is expressed in the MGE, and specifically enhanced in putative cholinergic interneurons originating there (data not shown, Ahmed et al. 2023; Appendix C).

During these early stages, the main cellular processes occurring are the proliferation of neural progenitor cells, and the differentiation, and migration of post-mitotic neurons. For *Cntnap2* to be expressed at such early stages indicates that it may have a role in these processes, potentially through establishing early activity-based cues for proliferation (Borodinsky et al. 2015). We therefore expected possible early alterations to the proliferative and migratory processes of MGE-derived interneurons in the *Cntnap2* knockout mice. Indeed, when we investigated proliferative markers and characteristics of embryonic structures, we found an increase in the number of progenitor cells, and a greater size of the proliferative ventricular zone in the MGE of the *Cntnap2* knockout mice (data not shown, Ahmed et al. 2023; Appendix C)<sup>7</sup>. This was followed by an early decrease in the thickness of the proliferative zones, signifying a reduction in the progenitor pools typical of later embryonic stages (E14+; Turrero Garcia and Harwell 2017), and thus an early maturation in the knockout (data not shown, Ahmed et al. 2023; Appendix C). Knowing that there were embryonic alterations leaning towards more interneurons being produced, we then aimed to follow this through to postnatal stages.

Previous work in ASD has revealed that increased brain structure size is a key marker in early postnatal stages (Courchesne et al. 2001). As our previous findings indicate a potential specialised role of *Cntnap2* in the striatum, we first measured the size of the striatum across four postnatal stages (P0, P4, P6, P10), and compared control and *Cntnap2* knockout conditions (**Figure 4.3A**). These stages were chosen as they are key timepoints for critical moments during early postnatal development; P0 being birth, P4 the beginning of apoptotic processes, P6 a key age for the peak of circuit development and maturation, and P10 around when the primary stages of network development have finished (Semple et al. 2013, Lo et al. 2017, Dehorter and Del Pino 2020). We found a transient increase in striatum size at P4 and 6, which was then normalised by P10 (**Figure 4.3B**). This finding is consistent with human observations, where

---

<sup>6</sup> This work was done in collaboration with Mi Da

<sup>7</sup> This work was done in collaboration with Rhys Knowles

enhanced brain growth has been shown at early developmental stages (Courchesne et al. 2001, Courchesne 2002), but with no difference or even decreased brain volume at later stages (Courchesne 2002, Ha et al. 2015). As a result of increased striatal size, combined with evidence of more proliferation observed at embryonic stages, we expected a higher number of striatal Lhx6+ cells in *Cntnap2* knockout conditions. Quantification revealed an enhanced cell number at P0 and P4 in the knockout, however this was normalised to control levels by P6 and P10 (**Figure 4.3C, D**). Due to the increase in both striatum size and cell number, overall striatal Lhx6+ cell density remained unchanged across age points (**Figure 4.3E**). We next explored mechanisms underlying the rectification of cell number to control levels by P6. Postnatal mechanisms for regulating cell number include apoptosis, which occurs during the first two postnatal weeks (Dehorter and Del Pino 2020). We hypothesised that this process is perturbed in the absence of *Cntnap2*. To measure apoptosis, we quantified the number of cells expressing the cell death specific marker caspase-3 (Lossi et al. 2018, Sreenivasan et al. 2022) in striatal Lhx6+ interneurons. We found a significant increase in the number of cells expressing caspase-3 in the striatum at P6 in the *Cntnap2* KO, with no changes at P4 or P10 (**Figure 4.3F, G**). This eventuated in a ~58% cell loss in the knockout, compared to only ~49% in the control. This indicated an increase in the canonical window of apoptosis (described in Chapter 1), reducing the exaggerated number of cells back to control levels. Although cell number is normalised, and we see no difference at mature stages (data not shown), the observed shift in the Lhx6 population during this important developmental period could lead to alterations in the establishment of striatal circuitry, which could contribute to an excitation-inhibition imbalance, and thus ASD aetiology.

To determine whether what we observed was unique to the striatum or could indeed be conserved across brain structures, we investigated structure size, Lhx6+ cell number, and cell death in the prefrontal cortex (PFC), another key structure susceptible to network alterations in ASD (Selimbeyoglu et al. 2017). We found no change in the thickness of the PFC across all postnatal stages (**Figure 4.3H, I**), and subsequently, only observed a change in the number of Lhx6+ cells at P0 in the deeper layers of the PFC (**Figure 4.3J, K**). This can be explained by embryonic data revealing that the number of cells migrating towards cortical areas via the cortical migratory streams was significantly higher in the *Cntnap2* knockout (data not shown, Ahmed et al. 2023; Appendix C).



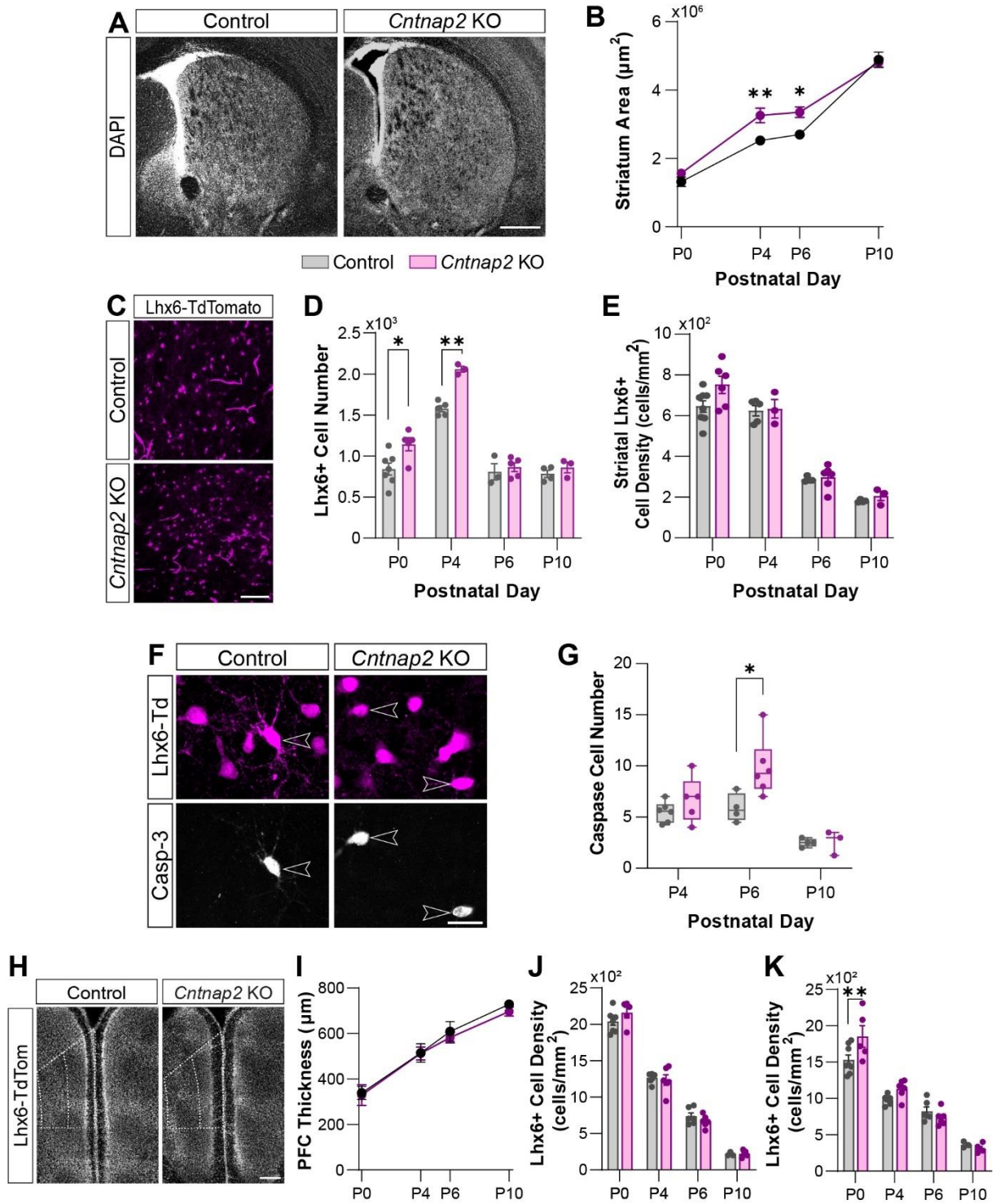


### Figure 4.3: MGE-derived interneuron cell numbers at early stages of development

**A.** DAPI staining of the striatum in Control and *Cntnap2* KO, scale: 500  $\mu$ m. **B.** Quantification of the striatum area across early postnatal stages in Control and *Cntnap2* KO (P0: n = 8 Control, 5 KO, p = 0.195; P4: n = 5 Control, 3 KO, p = 0.007; P6: n = 3 Control, 5 KO, p = 0.027; P10: n = 4 Control, 4 KO, p = 0.768). **C.** Lhx6 positive interneurons in the striatum, scale: 100 $\mu$ m. **D.** The number of Lhx6 positive interneurons in the Control and *Cntnap2* KO striatum across early postnatal stages (P0: n = 7 Control, 5 KO, p = 0.019; P4: n = 5 Control, 3 KO, p = 0.0001; P6: n = 3 Control, 5 KO, p = 0.606; P10: n = 4 Control, 3 KO, p = 0.343). **E.** Density of Lhx6+ striatal interneurons across postnatal stages in Control and *Cntnap2* KO conditions (P0: n = 8 Control, 6 KO, p = 0.051; P4: n = 5 Control, 3 KO, p = 0.856; P6: n = 4 Control, 6 KO, p = 0.738; P10: n = 4 Control, 3 KO, p = 0.253). **F.** Expression of the cell death marker Caspase-3 in striatal Lhx6 positive interneurons, scale: 20  $\mu$ m. **G.** Quantification of Lhx6 positive interneurons expressing Caspase-3 across early postnatal stages in the Control and *Cntnap2* KO conditions (P4: n = 6 Control, 5 KO, p = 0.259; P6: n = 4 Control, 5 KO, p = 0.033; P10: n = 4 Control, 3 KO, p = 0.898). **H.** The prefrontal cortex (PFC, DAPI) in Control and *Cntnap2* KO conditions, separated into upper (nearest to midline) and deeper layers, scale: 200  $\mu$ m. **I.** Quantification of the thickness of the PFC in Control and *Cntnap2* KO conditions (P0: n = 8 Control, 4 KO; P4: n = 6 Control, 6 KO; P6: n = 5 Control, 5 KO; P10: n = 4 Control, 4 KO;  $p_{\text{genotype}} = 0.490$ ,  $p_{\text{interaction}} = 0.968$ , 2-way ANOVA). **J-K.** Quantification of cell density in the upper (**J**) and deeper (**K**) layers of the prefrontal cortex in Control and *Cntnap2* KO conditions (P0: n = 8 Control, 5 KO; P4: n = 6 Control, 6 KO; P6: n = 6 Control, 6 KO; P10: n = 3 Control, 5 KO; upper:  $p_{\text{genotype}} = 0.854$ ,  $p_{\text{interaction}} = 0.250$ ; deeper:  $p_{\text{genotype}} = 0.106$ ,  $p_{\text{interaction}} = 0.015$ , 2-way ANOVA; P0<sub>deeper</sub>: p = 0.005, P4<sub>deeper</sub>: p = 0.487, P6<sub>deeper</sub>: p = 0.999, P10<sub>deeper</sub>: p = 0.999, Bonferroni post-hoc multiple comparisons). Unless otherwise specified, Student's t-test was used to determine significance, p<0.05:\*, p<0.01:\*\*, p<0.001:\*\*\*, p<0.0001:\*\*\*\*.

#### 4.4 Alterations to Striatal Cholinergic Interneuron Number

As we have shown that *Cntnap2* expression is enriched in striatal cholinergic interneurons (CINs), when compared with other interneuron types, we investigated whether the number of CINs within the Lhx6+ interneuron population could be preferentially altered in the absence of *Cntnap2* (**Figure 4.4A**). At P0, we found a significant increase in CIN density in the *Cntnap2* KO, with no change to the putative GABAergic, ChAT negative Lhx6+ interneuron population (**Figure 4.4B**). At P6, we quantified CIN numbers in the dorsomedial (DMS) and dorsolateral (DLS) regions of the striatum separately. These regions were segregated as the migration pathways of CINs populating the DLS and DMS is known to segregate early- and late-born CINs, respectively (Chen et al. 2010). There is also a known difference in behavioural regulation and CIN network activity between these two subregions (Matamales et al. 2016, Lipton et al. 2019, Ahmed et al. 2021), suggesting differential regulation of CINs in the DMS versus the DLS. Whilst there was no change in the DMS (**Figure 4.4C, left**), we did find significantly fewer CINs in the DLS, and once again no change in the ChAT negative Lhx6+ population (**Figure 4.4C, right**). This indicates that the increase and normalisation of Lhx6+ interneurons observed previously could be attributed to CINs, as opposed to non-cholinergic Lhx6+ interneurons.

However, there are also cholinergic interneurons that do not express Lhx6 and therefore are not derived from the MGE (Lozovaya et al. 2018, Ahmed et al. 2019). To explore whether these neurons were also affected via a general CIN-specific mechanism, we quantified Lhx6+ versus

Lhx6- CIN densities in the striatum at P0 and P6. We once again found a significant increase in the density of Lhx6+ CINs in the *Cntnap2* KO at P0, with no change in Lhx6- CIN density (**Figure 4.4D**). In addition, at P6, there was no change in the DMS (**Figure 4.4E, left**), and a significant decrease in the density of Lhx6+ CINs with no change to Lhx6- CINs in the DLS (**Figure 4.4E, right**). Overall, these results show that shifted cell numbers in the *Cntnap2* knockout model are specific to MGE-derived cholinergic interneurons. The specific decrease in Lhx6+ CIN number compared to other populations in the knockout DLS suggests a potential specificity for apoptotic processes to target early-born Lhx6+ CINs. We do not know whether this population has a higher expression of *Cntnap2* mRNA or protein in this population as opposed to the Lhx6-negative CINs, as this may explain the enhanced differences. We have established in previous chapters that cholinergic interneurons in the striatum are a diverse population, as such a difference in the expression of *Cntnap2* between these two is not improbable. Indeed, the distribution of *Cntnap2* expression within CINs does indicate the presence of both high-expressing and low-expressing cells (**Figure 4.2G**), which may correspond to segregating MGE-derived CINs versus those originating elsewhere. We anticipate that mechanisms specific to the embryonic and early postnatal developmental trajectory of MGE-derived CINs is affected in the absence of *Cntnap2*, thus causing alterations to their cell number without affecting other populations.

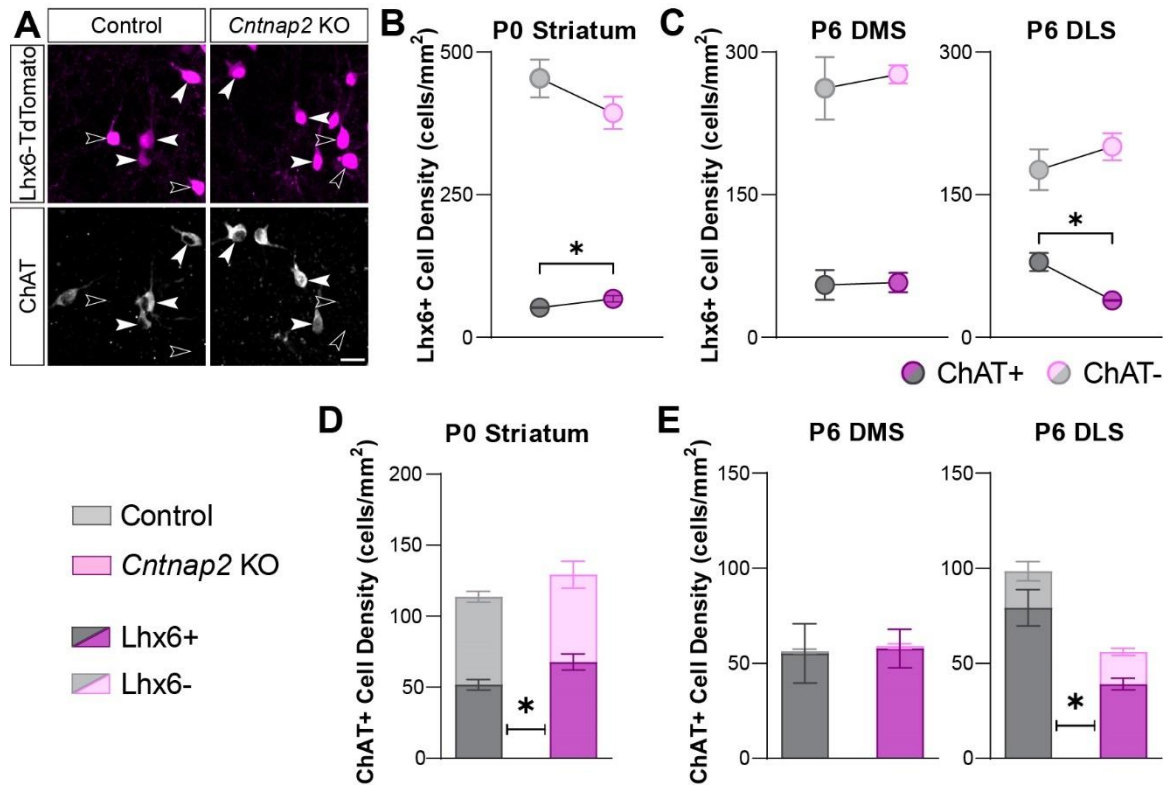


**Figure 4.4: Specific alterations to the striatal cholinergic interneuron population**

**A.** Expression of the cholinergic marker ChAT in the Lhx6+ interneurons of the striatum at P6, scale: 20  $\mu$ m. **B.** Density of ChAT positive and ChAT negative Lhx6+ interneurons in the Control and *Cntnap2* KO striatum at P0 (n = 5 Control, 3 KO, p = 0.043 ChAT+, p = 0.259 ChAT-). **C.** Density of ChAT positive and ChAT negative Lhx6+ interneurons in the Control and *Cntnap2* KO at P6, in the dorsomedial (DMS, n = 3 Control, 4 KO, p = 0.893 ChAT+, p = 0.644 ChAT-) and dorsolateral (DLS, n = 3 Control, 3 KO, p = 0.016 ChAT+, p = 0.398 ChAT-) striatum. **D.** Cell density of Lhx6+ ChAT+ and Lhx6- ChAT+ cells, showing the distribution of Lhx6 positive and negative cells within the cholinergic interneuron population, in the striatum at P0 (n = 6 Control, 3 KO, Lhx6+ p = 0.042, Lhx6- p = 0.960). **E.** Cell density of Lhx6+ ChAT+ and Lhx6- ChAT+ cells in the dorsomedial (DMS; n = 3 Control, 4 KO, p = 0.893 Lhx6+, p = 0.940 Lhx6-) and dorsolateral (DLS; n = 3 Control, 4 KO, p = 0.016 Lhx6+, p = 0.652 Lhx6-) striatum at P6 in Control and *Cntnap2* KO conditions. Student's t-test: p<0.05:\*, p<0.01:\*\*, p<0.001:\*\*\*, p<0.0001:\*\*\*\*.

#### 4.5 Changes to the Molecular Profile of Striatal Cholinergic Interneurons

With the previously explored changes in cell number in the striatum and PFC, resulting from early alterations to proliferation, it is possible that subsequent processes such as differentiation and the establishment of cell identity could also be perturbed. We thus questioned whether the molecular characteristics governing certain aspects of cell function were altered. To examine this, we performed mRNA (qRT-PCR) and protein analyses for several factors relevant for cholinergic cell identity and function.

We first investigated factors relating to MGE derived interneuron identity. As we have been using expression of the transcription factor *Lhx6* to identify MGE derived interneurons, and have observed significant alterations specifically to this population, we wondered whether the genetic and molecular expression of *Lhx6* at P6 was affected, and subsequently the identity and composition of the striatal interneuron population. Quantification of the whole striatum revealed significantly less *Lhx6* mRNA levels in the knockout condition (**Figure 4.5A**). In contrast, relative *Lhx6* protein immunofluorescence in *Lhx6*<sup>+</sup> interneurons (combining cre-dependent expression of TdTomato in *Lhx6*<sup>+</sup> interneurons with *Lhx6* staining via immunofluorescent antibodies), showed no difference between control and knockout (**Figure 4.5B**). This indicates that although there is no change in protein expression of *Lhx6*, and thus no functional differences, there is a possible change in the genetic identity of these cells due to the decrease in mRNA. We expect this to be specific to cholinergic interneurons, as we previously showed alterations to this population. We therefore investigated molecular factors involved in cholinergic interneuron identity. As previously described, CINs can be discerned by their expression of the enzyme Choline Acetyltransferase (ChAT), a precursor of acetylcholine production. We quantified *ChAT* mRNA levels at P6 in the striatum and found no difference (**Figure 4.5C**). However, we did observe a significant increase in ChAT protein levels in *Lhx6*<sup>+</sup> CINs (**Figure 4.5D**), but with no changes in *Lhx6*<sup>-</sup> CINs (**Figure 4.5E**). This indicates an *Lhx6*<sup>+</sup> CIN specific mechanism, whereby acetylcholine production, and therefore the functionality of these cells, is likely to be altered (Lim et al. 2014). Upon quantification of other molecular factors related to CIN identity, including *Lhx8* (LIM homeobox 8; a transcription factor specific to CIN identity (Zhao et al. 2003, Lopes et al. 2012)), *AChE* (Acetylcholine esterase; another precursor of acetylcholine production), *Gbx2* (Gastrulation Brain Homeobox 2; required for the development of striatal CINs (Chen et al. 2010)), and *Zic4* (Zinc finger protein 4; expressed by a CIN subpopulation (Ahmed et al. 2019)), we found no changes to mRNA levels (**Figure 4.5F**). This suggests that intrinsic, genetic cholinergic cell

identity is not perturbed in the absence of *Cntnap2*, however this does not account for other markers, protein expression regulation, and functional properties.

We also considered a possible genetic mechanism behind the increase in apoptosis described previously. *Pten* (Phosphatase and tensin homolog) is a key marker known to regulate apoptotic processes; it has been shown that PTEN expression in cortical pyramidal neurons influences the survivability of interneurons (Wong et al. 2018). We therefore probed *Pten* expression in the striatum and PFC, to determine if this apoptotic pathway was altered in the *Cntnap2* knockout. This was also of particular interest as mutations in the *PTEN* gene in humans have been associated with ASD (Busch et al. 2019, Cummings et al. 2022), and a knockout mouse model recapitulates ASD-like behavioural deficits (Lugo et al. 2014); hence, shifted *Pten* expression in the *Cntnap2* knockout model of ASD could contribute to behavioural phenotypes as well as the shifted developmental trajectory. There was no difference in *Pten* mRNA levels in the *Cntnap2* knockout striatum (**Figure 4.5G**), however we did find a significant decrease in the PFC (**Figure 4.5H**). This indicates that *Pten* may not have a conserved role in the striatum, as in the cortex, and that the slight alterations in PFC cell number might be due to apoptosis mechanisms controlled by *Pten*. However, these results are relevant for the whole striatum, and are not specific to the cell types that are known to regulate this process (*i.e.* whole tissue analysis as opposed to analysis on single cells).

Together, these results indicate some activity-dependent molecular alterations to cholinergic interneuron identity that may subsequently lead to functional alterations.

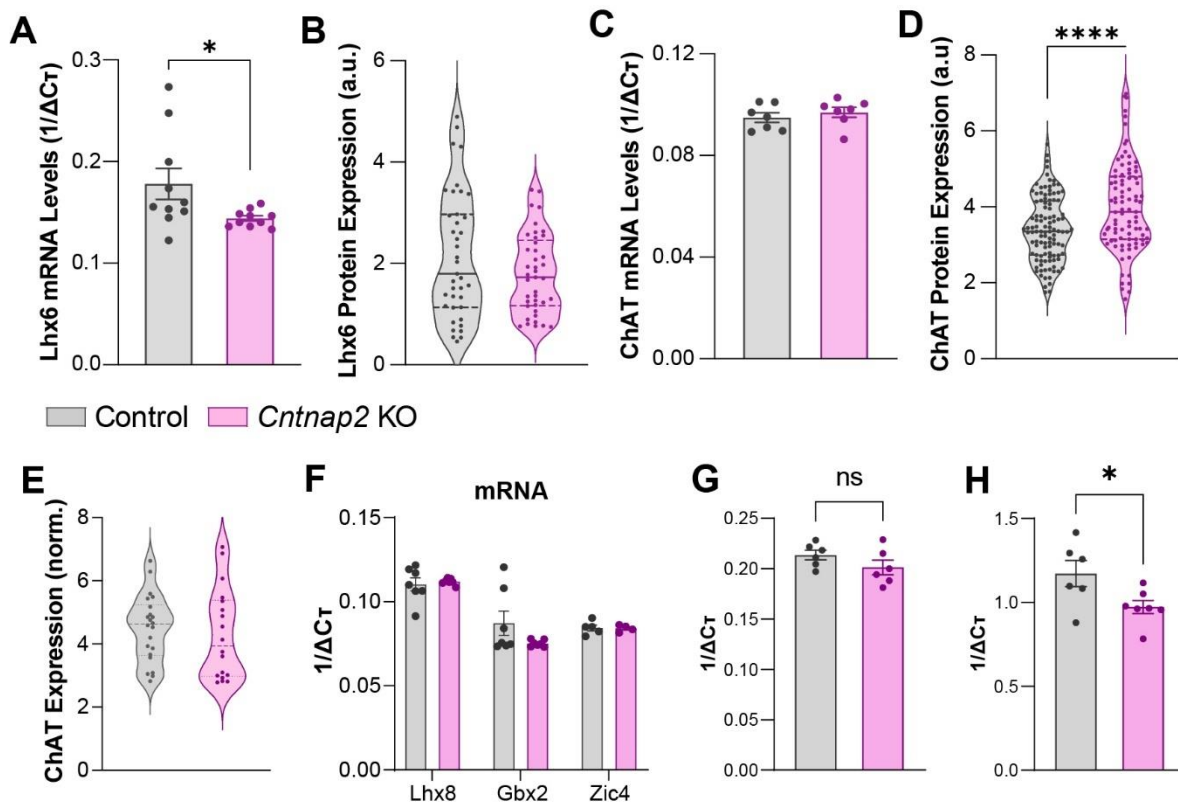


**Figure 4.5: Molecular identity of developing striatal Lhx6+ interneurons**

**A.** Relative *Lhx6* mRNA expression in the striatum in control and *Cntnap2* KO conditions at P6 (n = 10 control, 10 KO, p = 0.041). **B.** Normalised *Lhx6* protein levels at P6 in striatal interneurons, in control and *Cntnap2* KO conditions (n = 40 cells, 4 mice control; 42 cells, 3 mice KO, p = 0.129). **C.** Relative *ChAT* mRNA expression in the striatum in control and *Cntnap2* KO conditions at P6 (n = 7 control, 7 KO, p = 0.465). **D.** Normalised ChAT protein levels in striatal Lhx6+ cholinergic interneurons, in control and *Cntnap2* KO conditions (n = 110 cells, 4 mice control, 91 cells, 3 mice KO, p = 0.00005). **E.** Normalised ChAT protein levels in striatal Lhx6- cholinergic interneurons, in control and *Cntnap2* KO conditions (n = 22 cells, 4 mice control, 18 cells, 3 mice KO, p = 0.609). **F.** Relative mRNA expression of cholinergic neuron identity related factors: *Lhx8* (n = 7 control, n = 7 KO, p = 0.695), *Gbx2* (n = 7 control, n = 7 KO, p = 0.126), *Zic4* (n = 5 control, n = 4 KO, p = 0.894) in the P6 striatum in control and *Cntnap2* KO conditions. **G.** Relative *PTEN* mRNA in the striatum in control and *Cntnap2* KO conditions at P6 (n = 6 control, 6 KO, p = 0.192). **H.** Relative *PTEN* mRNA in the prefrontal cortex in control and *Cntnap2* KO conditions at P6 (n = 6 control, 7 KO, p = 0.036). Student's t-test: p<0.05:\*, p<0.01:\*\*, p<0.001:\*\*\*, p<0.0001:\*\*\*\*.

#### 4.6 Striatal Interneuron Morphology is Altered in ASD

Neuron morphology is important for regulating cell function within circuitry, and morphological development is a key marker of circuit maturation and is dependent on the state of the surrounding network (De Marco Garcia et al. 2011). Alterations to dendritic arborisation in ASD have been previously described at mature stages (Gao et al. 2018), but it is unknown whether a shifted developmental trajectory in ASD can impact developing interneuron morphology. To assess this, we reconstructed cholinergic and putative fast-spiking interneurons that had been filled with Neurobiotin during electrophysiological recordings at P5-7 in the control and *Cntnap2* knockout striatum (**Figure 4.6A, G**). We found substantial differences in morphology in both interneuron types. Cholinergic interneurons were significantly more complex, with increased branch points, and dendrite segments (**Figure 4.6B, C**), and trends to an increase in the overall volume occupied by the dendritic field (convex hull) and the total dendrite length (**Figure 4.6D, E**). In addition, upon Sholl analysis, an increase in the number of intersecting dendrites was observed (**Figure 4.6F**). Axonal morphology was difficult to quantify in this configuration because of low optical power combined with the thickness of the slices, particularly for CINs, which have a dense and complex axonal field. However, we anticipate similar changes as axonal perturbations have been shown before in the *Cntnap2* knockout model of ASD (Scott et al. 2019).

Putative FSIs also appeared more complex; with an increasing trend in the number of branch points and dendrite segments (**Figure 4.6H, I**), a significantly larger volume of spread (**Figure 4.6J**), and an increasing trend in dendrite length (**Figure 4.6K**). Sholl analysis also revealed a similar significant increase in dendritic complexity as CINs, however this was not as closely localised to intermediate dendrites, and extended to distal dendrites in FSIs (**Figure 4.6L**).

These alterations in morphology indicate early cell maturation, which is a known characteristic of ASD (Courchesne 2004, Whitehouse et al. 2011, Hazlett et al. 2017). However, it is possible that interneuron morphology is altered into adulthood as a result of this developmental change; this remains to be determined.



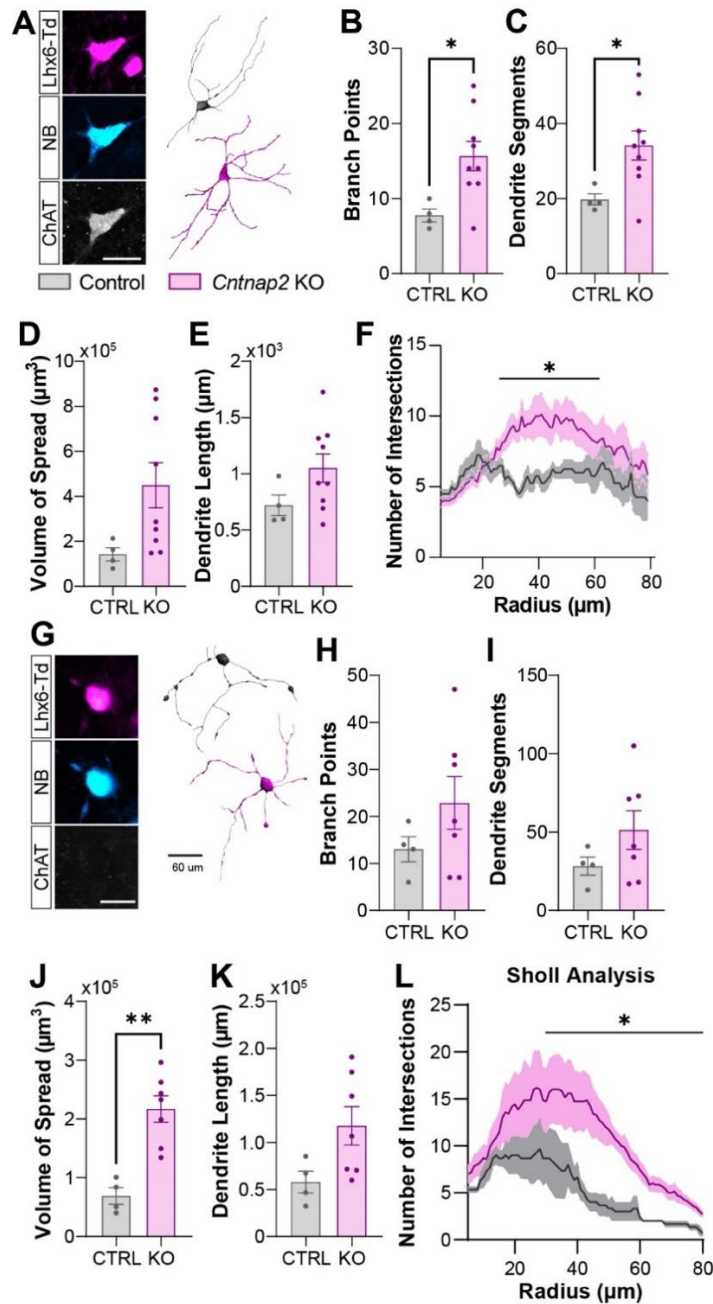


**Figure 4.6: Morphological alterations to cholinergic and putative parvalbumin interneurons**

**A.** Patched cholinergic interneurons loaded with neurobiotin (left) used for morphological reconstruction (right) in control and *Cntnap2* KO conditions, scale = 20  $\mu\text{m}$ . **B-F.** Characterisation of dendritic morphology of striatal cholinergic interneurons at P6 in control (n = 4) and *Cntnap2* KO (n = 9) conditions. **B.** Number of branching points ( $p = 0.025$ ). **C.** Number of dendritic segments ( $p = 0.037$ ). **D.** Volume occupied by dendritic spread ( $p = 0.075$ ). **E.** Total dendritic length ( $p = 0.131$ ) **F.** Sholl analysis measuring the number of dendrites intersecting circles increasing in radius by 1  $\mu\text{m}$  ( $p = 0.049$ , two-way ANOVA). **G.** Patched ChAT negative, Lhx6+ striatal fast spiking interneurons (*i.e.* putative parvalbumin interneurons) loaded with neurobiotin (left) used for morphological reconstruction (right) in control and *Cntnap2* KO conditions, scale = 60  $\mu\text{m}$ . **H-L.** Characterisation of dendritic morphology of striatal putative parvalbumin interneurons at P6 in control (n = 4) and *Cntnap2* KO (n = 7) conditions. **H.** Number of branching points ( $p = 0.240$ ). **I.** Number of dendritic segments ( $p = 0.215$ ). **J.** Volume occupied by dendritic spread ( $p = 0.001$ ). **K.** Total dendritic length ( $p = 0.068$ ). **L.** Sholl analysis ( $p = 0.040$ , two-way ANOVA). Student's t-test:  $p < 0.05$ :\*,  $p < 0.01$ :\*\*,  $p < 0.001$ :\*\*\*,  $p < 0.0001$ :\*\*\*\*.

#### 4.7 Electrophysiological alterations

Alterations to neuron activity have been shown in ASD in previous studies (Caubit et al. 2022), however, this has not been explored during earlier stages of development, when electrophysiological properties are still in the process of maturing. In particular, the electrophysiological properties of developing striatal interneurons in ASD is unknown. At these early stages, functional properties determine a neuron's ability to survive (Pfisterer and Khodosevich 2017) and integrate within the network (Munakata and Pfaffly 2004, Dekkers et al. 2013). We recorded intrinsic electrophysiological properties and synaptic inputs to Lhx6+ tonically active neurons (TANs) and fast spiking interneurons (FSIs) at P6. As described previously, striatal cholinergic interneurons are tonically active, and can therefore be identified by their firing properties and size. In addition, fast spiking interneurons that fire above 50 Hz, even at early developmental stages, are considered to be putative parvalbumin interneurons. These can also be identified by a rounder soma morphology (Tepper et al. 2010, Tepper et al. 2018). Other striatal Lhx6+ interneuron types display persistent low threshold spiking (PLTS, commonly somatostatin interneurons, which have a distinct oblong soma shape).

We found differences to excitability of CINs, including a decrease in spontaneous/tonic firing rate (**Figure 4.7A, B**), and an increase in the irregularity of spontaneous firing (**Figure 4.7C**). We then applied negative to positive incremental current steps to evoke firing. Following a hyperpolarising current injection, CINs are known to display a depolarising sag, mediated by prominent inward rectifying current ( $I_h$ ; Ahmed et al., 2021). We found no difference in the sag ratio between control and knockout (**Figure 4.7D**), indicating no contribution of this current to the altered firing rate. In addition, evoked firing following depolarising current steps was also decreased (**Figure 4.7E, F**), but with no change to the adaptation index (**Figure 4.7G**), indicating a mechanism non-specific to the resting state of the cell. As such, we did not see any difference in the resting membrane potential or capacitance (**Figure 4.7H, I**), however there was a decrease in the input resistance (**Figure 4.7J**), which could potentially indicate altered expression of ion channels, such as the potassium channels Kv1.1 and Kv1.2, which Caspr2 regulates the clustering of (Poliak et al. 2003, Tzimourakas et al. 2007). Potassium conductance has been shown to contribute to the input resistance of neurons (Cameron et al. 2000), hence it is possible that a decrease in input resistance could correlate to aberrant expression patterns of potassium channels across the membrane culminating in increased potassium conductance. This reduction in input resistance likely underlies the decreased firing profile of CINs, due to a decrease in cell excitability (Kernell 1966). We then compared action potential kinetics, and

found no difference in the threshold or amplitude, but a significant decrease in rise time and a trend to a decrease in decay time (**Figure 4.7K-N**, Table 11, Appendix E). This corroborates possible alterations to potassium channel expression, which is essential for repolarisation of the membrane during the decay phase of the action potential (Abudukeyoumu et al. 2019). Disrupted potassium channel expression and distribution remains to be seen in striatal CINs in the *Cntnap2* knockout, however abnormal Kv1.2 clustering has been shown in cortical pyramidal neurons, contributing to altered action potential decay kinetics (Scott et al. 2019). Together these findings show alterations to cholinergic interneuron function, indicating less activity, which could potentially be detrimental for striatal circuit development and function, as cholinergic innervation of the striatum is established early during development (Aznavour et al. 2003), and is highly important for the regulation of striatal circuits (Abudukeyoumu et al. 2019).

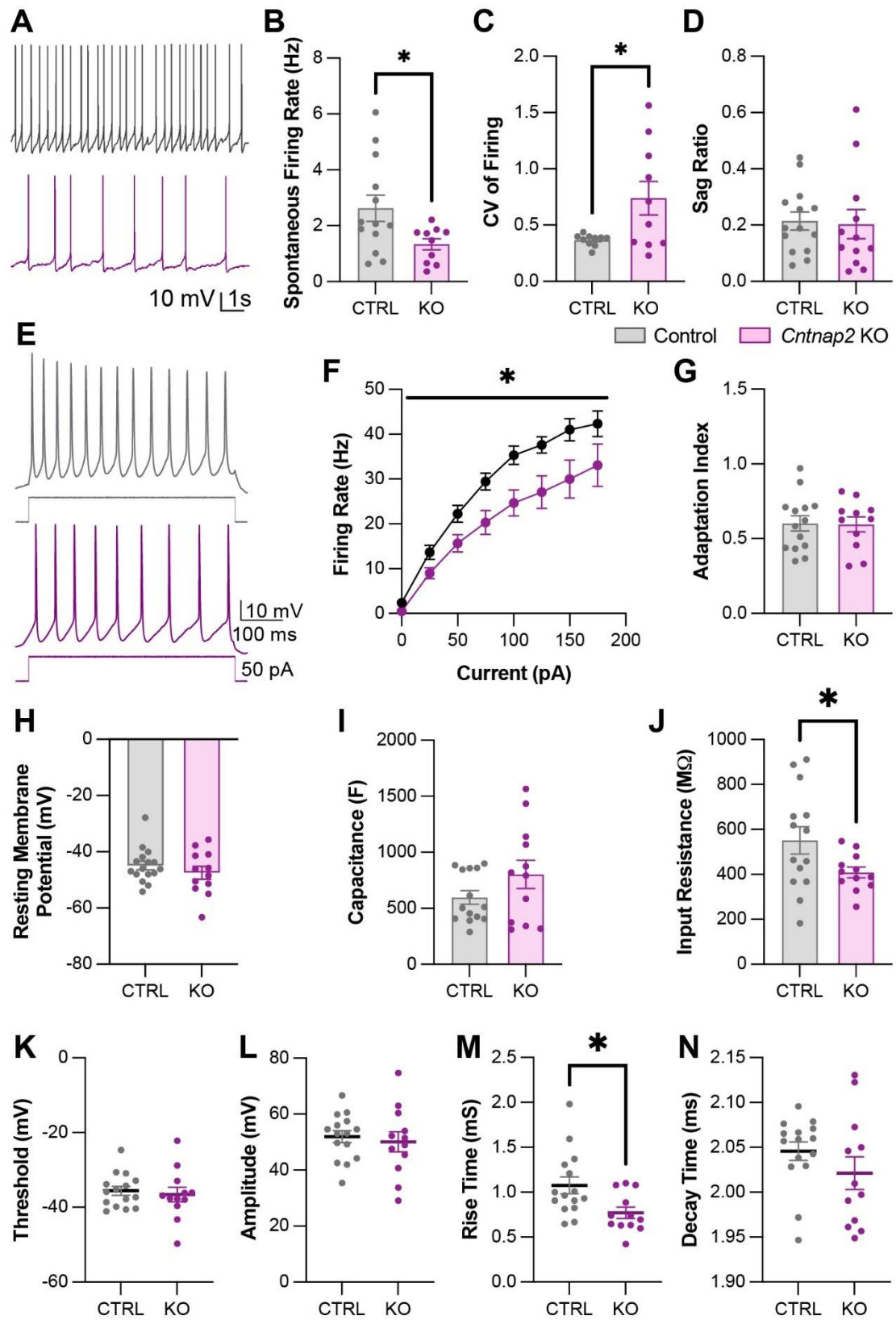


**Figure 4.7: Functional alterations in Lhx6+ cholinergic interneurons in the developing striatum**

**A.** Spontaneous tonic firing of Lhx6+ striatal cholinergic interneurons (CINs) at resting membrane potential at P5-7 in a control and *Cntnap2* KO cell. **B.** Quantification of the spontaneous firing rate of CINs in control and *Cntnap2* KO conditions (n = 13 control, 10 KO cells, p = 0.034). **C.** Coefficient of spike variation of CIN firing in control and KO conditions (n = 11 control, 10 KO cells, p = 0.026). **D.** The sag ratio of CINs from hyperpolarising current steps in control and KO conditions (n = 13 control, 11 KO cells, p = 0.462, Mann-Whitney test). **E.** Evoked firing of Lhx6+ CINs at P5-7 in response to a 50 pA stimulus step. **F.** Evoked firing rate in control and *Cntnap2* KO conditions across increasing current inputs (n = 8 control, 12 KO cells, two-way ANOVA:  $F_{(1, 121, \text{genotype})} = 26.87$ ,  $p < 0.0001$ ,  $F_{(7, 121, \text{interaction})} = 0.6758$ , p = 0.6922). **G.** The index of firing adaptation upon a 50 pA current injection (n = 14 control, 11 KO cells, p = 0.9258). **H.** Resting membrane potential of control and KO CINs (n = 16 control, 12 KO cells, p = 0.3488). **I.** Capacitance of control and KO CINs (n = 14 control, 12 KO cells, p = 0.4940, Mann-Whitney test). **J.** Input resistance of control and KO CINs (n = 14 control, 12 KO cells, p = 0.0490). **K.** Action potential threshold of control and KO CINs (n = 15 control, 12 KO cells, p = 0.6551). **L.** Action potential amplitude of control and KO CINs (n = 15 control, 12 KO cells, p = 0.6542). **M.** Action potential rise time of control and KO CINs (n = 15 control, 12 KO cells, p = 0.0169). **N.** Action potential decay time of control and KO CINs (n = 15 control, 12 KO cells, p = 0.2174, Mann-Whitney test). Unless otherwise specified, Student's t-test: p<0.05:\*, p<0.01:\*\*, p<0.001:\*\*\*, p<0.0001:\*\*\*\*.

---

Recordings from putative FSIs (Lhx6+ ChAT-, with non-adaptive firing over 50 Hz) revealed a similar decrease in excitability as in CINs. We observed a decrease in evoked firing upon depolarising current steps (**Figure 4.8A, B**), as well as an increase in rheobase, the smallest current required to elicit an action potential (**Figure 4.8C, D**). Both of these results indicate a similar decrease in excitability as seen in CINs. However, there was no change in the latency to the first spike at rheobase (**Figure 4.8E**), indicating no difference in the physiological properties of FSIs at a near threshold potential. Similarly to CINs, we saw no difference in resting membrane potential and capacitance and a significant decrease in input resistance (**Figure 4.8F-H**), implying a phenotype common across the MGE-derived, Lhx6+ interneuron population. We then compared action potential kinetics (Table 12, Appendix E) and found a higher action potential threshold (**Figure 4.8I**), further consolidating the decrease in excitability. With no change in amplitude, but a decreasing trend in rise time and significant decrease in decay time (**Figure 4.8J-L**), FSI action potential kinetics display similar deficits to CINs in the knockout condition. This shows that the *Cntnap2* knockout may affect all Lhx6+ interneurons at this specific developmental stage, possibly altering their role within the network.

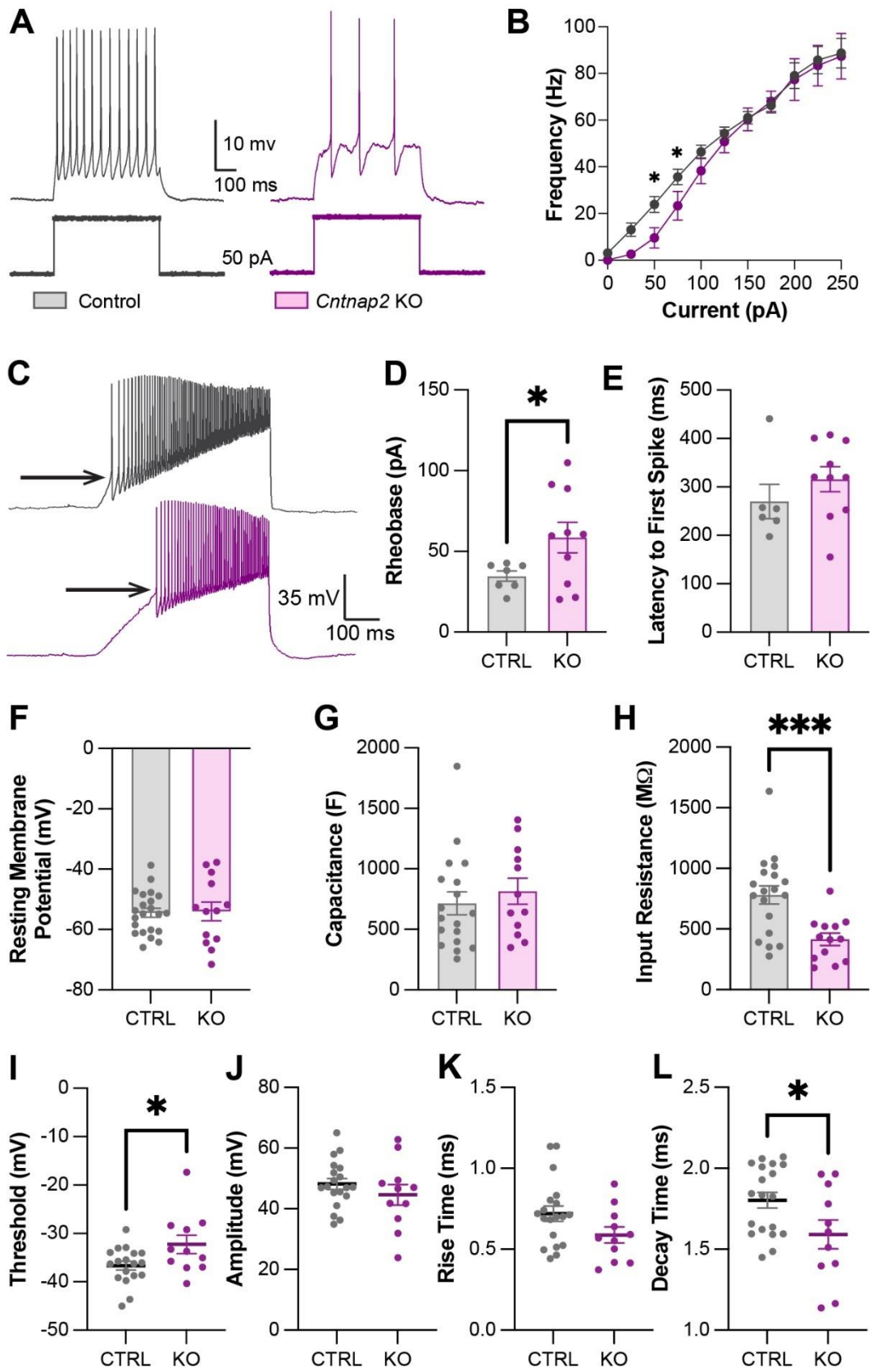


### Figure 4.8: Functional alterations in Lhx6+ putative fast spiking interneurons in the developing striatum

Electrophysiological properties of striatal fast spiking interneurons (FSIs) at P5-7 in control and *Cntnap2* knockout conditions **A.** Traces showing evoked firing of a control and *Cntnap2* KO cell upon a 50 pA stimulation. **B.** Evoked firing rate in control and *Cntnap2* KO conditions across increasing current inputs (n = 13 control, 8 KO cells, two-way ANOVA: F(1, 151, genotype) = 19.32, p < 0.0001, F(7, 151, interaction) = 1.699, p = 0.1132; post-hoc Bonferroni multiple comparisons: 50 pA p = 0.0093, 75 pA p = 0.0230). **C.** Traces reflecting ramp stimulations in a control and *Cntnap2* KO cell, with rheobase shown by arrows. **D.** FSI rheobase (n = 7 control, 10 KO cells, p = 0.0349). **E.** Latency to the first spike evoked at rheobase (n = 6 control, 10 KO cells, p = 0.2635). **F.** Resting membrane potential (n = 22 control, 13 KO cells, p = 0.8797). **G.** Capacitance (n = 18 control, 12 KO cells, p = 0.3684, Mann-Whitney test). **H.** Input resistance (n = 19 control, 13 KO cells, p = 0.0010). **I.** Action potential threshold (n = 18 control, 11 KO cells, p = 0.0269). **J.** Action potential amplitude (n = 19 control, 11 KO cells, p = 0.3198). **K.** Action potential rise time (n = 19 control, 11 KO cells, p = 0.0781) **L.** Action potential decay time (n = 19 control, 11 KO cells, p = 0.0465, Mann-Whitney test). Unless otherwise specified, Student's t-test: p<0.05:\*, p<0.01:\*\*, p<0.001:\*\*\*, p<0.0001:\*\*\*\*.

---

We have discussed previously the expected shift in excitation and inhibition in the striatal circuit in ASD. With these alterations to intrinsic electrophysiological properties of striatal interneurons, we subsequently expect that inputs to these cells will shift to reflect an E/I imbalance (He and Cline 2019). To investigate this, we recorded excitatory and inhibitory post-synaptic currents in Lhx6+ striatal interneurons in voltage-clamp configuration. The frequency and amplitude of inhibitory GABAergic currents were unchanged (**Figure 4.9A-C**). Despite no difference in the rise time of GABAergic events, we observed a decrease in the decay time (**Figure 4.9D, E**). This could reflect alterations to GABA<sub>A</sub> receptor subunit configurations responsible for elongating GABA mediated current decay (*i.e.* a predominance of  $\alpha 1$  over  $\alpha 2$ ) (Dixon et al. 2014). Indeed, some shifts in GABA receptor subunits have been observed in ASD (Fatemi et al. 2009), however this remains unknown in the *Cntnap2* knockout.

Similarly,  $\alpha$ -Amino-3-hydroxy-5-methyl-4-isoxazolepropionic acid (AMPA)/Kainate-driven glutamatergic inputs were unchanged between control and knockout conditions (**Figure 4.9F-J**). However, we did find that Lhx6+ interneurons receive more N-methyl-D-aspartate (NMDA) receptor driven glutamatergic inputs in the *Cntnap2* knockout at P6, as the frequency of events was significantly greater (**Figure 4.9K, L**), and the amplitude of these events was significantly larger as well (**Figure 4.9M**). There was no change in the rise and decay kinetics of these NMDAR mediated currents (**Figure 4.9N, O**). This result could either be due to pre-synaptic cortico-striatal activity enhancement or post-synaptic NMDA receptor expression alteration. Regardless, this shift in glutamatergic signalling, with no alteration to inhibitory signalling indicates an excitation-inhibition imbalance. This is a key characteristic of ASD, and an overabundance of excitation has been explored before in humans (Canitano and Palumbi 2021)

and the *Cntnap2* knockout model (Selimbeyoglu et al. 2017). Here, we show this for the first time in the striatal microcircuitry.

As we observed no change in AMPA/Kainate receptor driven glutamatergic inputs, it is more likely that the enhanced NMDA receptor mediated responses were due to a shift in the expression of glutamate receptors, particularly receptors known to be involved in canonical developmental critical periods, such as the metabotropic glutamate receptor mGluR5 and the NMDA receptor subunits 2C and 2D. mGluR5 is highly important during development and is involved in proliferation, synaptogenesis and neuronal circuit establishment (Piers et al. 2012). Altered mGluR5 regulation has been associated with E/I imbalance and subsequently ASD, among other pathologies (Piers et al. 2012, Wang et al. 2016, Carey et al. 2022). We found increased mRNA and protein expression of mGluR5 in the *Cntnap2* knockout at P6 (**Figure 4.9P, Q**), contributing to increased excitatory signalling, and consistent with the concept of early maturation in ASD.

NMDA receptors are also important during development (Ewald and Cline 2009, Hou and Zhang 2017), and as we saw increased NMDA signalling, we anticipate alterations to these receptors potentially mediating this result. During development, NMDA receptor subunits, including 2C (NR2C) and 2D (NR2D), are vital for synaptic regulation and are susceptible to upregulation in the striatum following an environmental insult (Chen et al. 2021, Jing et al. 2022). NR2C/D are of interest as they mediate striatal network activity during development, including cortico-striatal EPSCs and giant depolarising potentials, and are downregulated by P10 (Dehorter et al. 2011), highlighting a specialised developmental function in the striatum. We observed an increase in *Grin2D* mRNA (**Figure 4.9R**), but a decrease in NR2C/D protein particles (**Figure 4.9S**), indicating abnormal post-transcriptional regulation of NMDA receptor subunits that may underlie the alterations observed in current frequency and amplitude. Together, these results reveal altered synaptic connectivity in the Lhx6+ striatal interneuron population at P6 in the *Cntnap2* knockout.



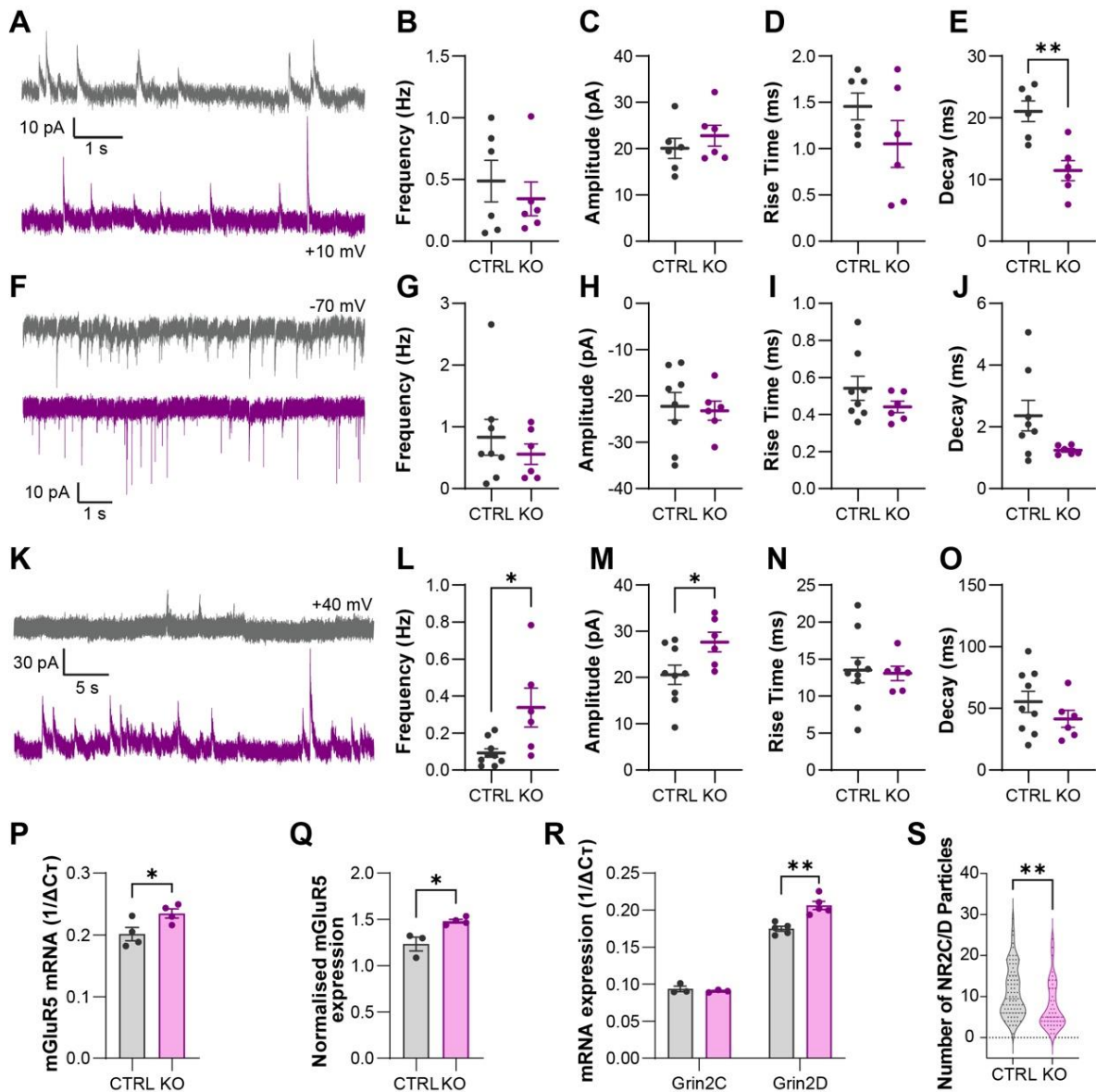


**Figure 4.9: Glutamatergic and GABAergic synaptic inputs onto Lhx6+ GABAergic interneuron in the *Cntnap2* KO mice.**

**A.** Example trace of spontaneous GABA<sub>A</sub>-driven inhibitory post-synaptic currents (sIPSC) recorded in voltage-clamp at 0 mV in Lhx6+ interneurons in control and *Cntnap2* KO conditions (n = 6 Control, 6 KO cells). **B.** sIPSC Frequency (p = 0.522). **C.** sIPSC Amplitude (p = 0.406). **D.** sIPSC Rise time (p = 0.194). **E.** sIPSC Decay time (p = 0.002). **F.** Example trace of spontaneous AMPA/KA-driven excitatory post-synaptic currents (sEPSC) recorded in voltage-clamp at -60 mV in Lhx6+ interneurons in control and *Cntnap2* KO conditions (n = 8 Control, 6 KO cells). **G.** sEPSC Frequency (p = 0.976). **H.** sEPSC Amplitude (p = 0.478). **I.** sEPSC Rise time (p = 0.153). **J.** sEPSC Decay time (p = 0.097). **K.** Example trace of spontaneous NMDA-driven excitatory post-synaptic currents (sEPSC) recorded in voltage-clamp at +40 mV in Lhx6+ interneurons in control and *Cntnap2* KO conditions (n = 9 Control, 6 KO cells). **L.** sEPSC Frequency (p = 0.016). **M.** sEPSC Amplitude (p = 0.038). **N.** sEPSC Rise time (p = 0.847). **O.** sIPSC Decay time (p = 0.268). **P.** *Grm5* mRNA levels in FACS-sorted Lhx6+ interneurons in control and *Cntnap2* KO conditions (n = 4 control, 4 KO; p = 0.045). **Q.** mGluR5 protein levels from immunostaining (n = 3 control, 4 KO; p = 0.014). **R.** *Grin2C* (n = 3 control, 3 KO; p = 0.0484) and *Grin2D* mRNA levels (n = 5 control, 5 KO; p = 0.001) in FACS-sorted Lhx6+ interneurons in control and *Cntnap2* KO conditions. **S.** NMDAR2C/D protein expression from immunostaining analysis (n = 78 control cells, 43 KO cells; p = 0.004). Student's t-test: p<0.05:\*, p<0.01:\*\*, p<0.001:\*\*\*, p<0.0001:\*\*\*\*.

## 4.8 Discussion

Striatal circuit development is reliant on genetic programming and activity levels. How interneurons factor into this process and regulatory mechanisms influencing their state during brain maturation has been a key question in understanding striatal development. In this chapter, we explored circuit development from a pathological perspective, where behavioural alterations are established, but the developmental striatal contributions are unknown.

It has been well established that autism spectrum disorders can be characterised by alterations to microcircuitry (Culotta and Penzes 2020). However, this was largely confirmed in cortical circuits, with very little research having been done in the striatum because of its complex circuitry. Therefore, in this study we aimed to describe the developmental trajectory of striatal interneurons and their role within the developing striatal circuit in the *Cntnap2* mouse model of ASD. This also allowed us to gain a better understanding of typical striatal microcircuit development by comparing it to atypical development in a mouse model of ASD.

### *Implications of preferential Cntnap2 expression in striatal cholinergic interneurons*

The expression pattern of *Cntnap2* mRNA across the whole brain was largely unknown, despite the value this information would bring to understanding the mechanisms behind the recapitulation of ASD symptoms in the knockout model, and in the subset of human cases presenting the mutations to the *CNTNAP2* gene. Whether *Cntnap2* mRNA expression levels in the mouse brain are dependent on cell type was unknown. In this study we presented results utilising new stereo-seq spatial transcriptomics technology, which is able to overcome previous obstacles of single-cell and bulk RNA sequencing, and map mRNA expression to brain regions and even cell types. We show that *Cntnap2* mRNA in the adult mouse brain is enriched in the striatum compared with cortical regions, and with sub-cellular resolution, were able to localise its enhanced expression to choline-acetyltransferase (ChAT) expressing cells (**Figure 4.10**). These novel findings present an avenue for further research into the intricacies of mRNA localisation within neuronal populations across the whole brain. However, there are limitations to this approach, as we only consider mRNA levels here, and do not take into account post-transcriptional regulatory mechanisms that could affect both the abundance of protein and its functional localisation. Studies have explored the intricacies of Caspr2 protein expression within single cells; generally showing its localisation to the axon initial segment and juxtaparanode to facilitate the clustering of voltage-gated potassium channels, as well at synaptic terminals (Poliak et al. 2003, Strauss et al. 2006, Duflocq et al. 2011, Pinatel et al. 2015, Scott et al. 2019). Its expression has also been described in somato-dendritic

compartments of cultured cortical and hippocampal inhibitory neurons (Pinatel et al. 2015, Gao et al. 2018). In fact, cultured hippocampal neurons displayed preferential Caspr2 expression in glutamate decarboxylase (GAD65) positive inhibitory neurons (over 50%) compared to GAD65 negative excitatory neurons (less than 5%) (Pinatel et al. 2015, Saint-Martin et al. 2018). This suggests that despite Caspr2 expression being ubiquitous in the brain, there may be some mechanisms facilitating differential expression based on cell subtype. This example is of particular relevance as Lhx6+ CINs express GAD65, and are considered to have some inhibitory features (Lozovaya et al. 2018). Furthermore, when tracking the expression of Caspr2 across the maturation of cultured neurons, a redistribution was observed via endocytic retrieval of Caspr2 from somato-dendritic compartments, resulting in preferential localisation along axons in mature cells (Bel et al. 2009, Pinatel et al. 2015, Saint-Martin et al. 2018). This indicates a differential developmental role for Caspr2, which may facilitate the developmental alterations observed in the *Cntnap2* knockout.

We observed specific developmental deficits in the MGE-derived, Lhx6+ CIN population of the striatum. The tonic activity of CINs requires Kv1 channels at the axon initial segment to generate their tonic firing pattern (Tubert et al. 2016, McGuirt et al. 2021), thus Kv1 alterations resulting directly from a loss of Caspr2 expression could explain the decrease in activity observed in Lhx6+ CINs. In addition, further elucidating whether Lhx6+ versus Lhx6- CINs have different expression levels of *Cntnap2* and the Caspr2 protein will support the specific alterations observed in the Lhx6+ CINs compared to other populations. This will subsequently shine a light on possible mechanisms behind the alterations to striatal cholinergic neurons we have observed in this study.

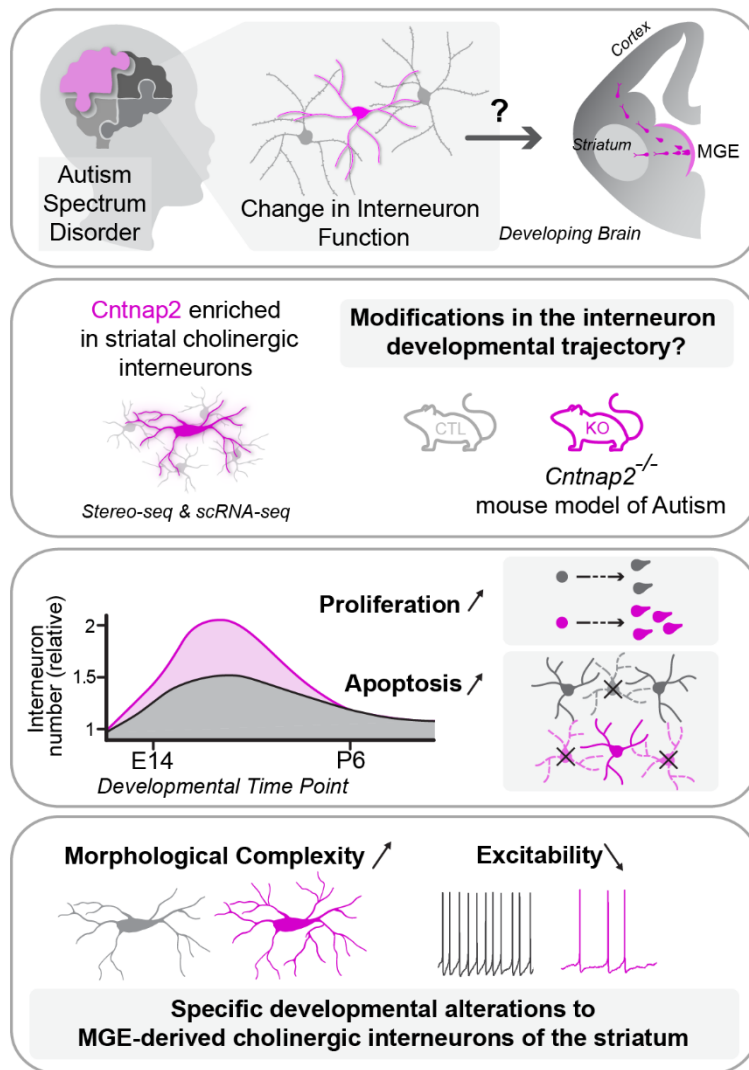


### Figure 4.10: Summary of results

Summarised findings regarding the changes in interneuron properties and function in the developing brain that contribute to ASD aetiology. *Cntnap2* was enriched in striatal cholinergic interneurons. In the *Cntnap2* knockout model of ASD, we observed increased proliferation and increased apoptosis, as well as increased morphological complexity and decreased excitability of MGE-derived striatal cholinergic interneurons.

### ***The impact of a transient shift in the ASD brain on developed striatal circuitry and behaviour***

Our findings in this study reveal key alterations to striatal characteristics during early stages of development in the *Cntnap2* mouse model of ASD, that are then normalised by a later stage. This transient shift in striatal development is likely to contribute to alterations in striatal circuitry and function, and thus could have a causative role in ASD symptomology. We uncovered an increase in striatum size in the *Cntnap2* knockout during early postnatal stages (P0-6), which was then normalised completely by P10. As described previously, increased brain volume early in ASD, with a later normalisation, is well established (Courchesne et al. 2001), and this has also been shown specifically in the striatum (Langen et al. 2009, Langen et al. 2014). In fact, alterations to the size of the human striatum in ASD have been closely correlated with the presence and severity of stereotyped repetitive movement behaviours (Sears et al. 1999, Calderoni et al. 2014, Langen et al. 2014). There is also an important relationship between brain structure volume and circuit formation and maintenance. This has been explored in the context of typical brain development (Tau and Peterson 2010), and in pathologies such as Huntington's Disease, where the degradation of striatal circuitry is associated with a smaller structure size (Lebouc et al. 2020). General consensus and logic rests on increased brain volume requiring more neurons to fill the network. Indeed, when combined with our findings of a transient increase in cell number in the *Cntnap2* knockout (**Figure 4.10**), we can conclude that we see a rapid, early expansion of striatal circuitry that is then rectified to control levels. This considerable perturbation of the striatal circuit during critical developmental stages (migration, differentiation, synaptogenesis, apoptosis) is expected to cause lasting effects to the wiring of the striatum (*e.g.* aberrant synapse formation between neuronal subtypes) and contribute to its role in inducing ASD symptoms (Tang et al. 2014).

The idea of autism being an alternative trajectory of development has been discussed in literature before, raising a key question of whether autism can result from only a transient developmental disturbance (Johnson 2017). It is true that ASD is currently defined not by an underlying mechanism, but by the resulting alterations to behaviour. Thus there are various overlapping and separate mechanisms that could contribute to ASD aetiology, simply by shifting the typical developmental trajectory to an atypical one. We have shown that transient developmental striatal alterations arise in a mouse model of ASD, and we speculate that this is a contributing factor to the occurrence of ASD-like behaviour in the model. Studies have shown that abnormal development of cortico-striatal circuitry may have functional and behavioural implications (particularly in regards to repetitive behaviours) that differ depending on the

timing and nature of the alteration (Del Pino et al. 2018). However, proof of this relationship must be provided through direct causative studies, altering only striatal development (*i.e.* striatal size and interneuron number) without affecting other aspects of development, and observing resulting behavioural changes, which is highly difficult with current technology. Therefore, with our current knowledge and the results obtained in this study, we can postulate that transient diversions of the striatum from its typical developmental trajectory are correlated with ASD. Additional studies are necessary to investigate further into alterations to the functional and anatomical aspects of striatal circuitry.

The dorsomedial (DMS) and dorsolateral (DLS) portions of the striatum have very different behavioural roles and are even completely opposing in some cases (Lipton et al. 2019, Ahmed et al. 2021, Turner et al. 2022). Underlying these differing roles is a substantial difference in circuitry, including differences in neuronal identity and activity (Matamales et al. 2016, Ahmed et al. 2019, Vandaele et al. 2019, Alegre-Cortes et al. 2021). The effect of shifts in circuitry in ASD have not been investigated yet in the context of the DMS and DLS, and this could provide key insights into the circuits behind the core symptoms of ASD.

In addition, the mosaic striosome-matrix chemical divisions of the striatum, which we discussed in Chapter 3, have been largely overlooked, although potential deficits in the compartmentalisation or activity contributing to ASD pathogenesis have been raised as a possibility. It has been shown that in human ASD brains, the boundaries between striosomal and matrix regions were obscured compared to controls (Kuo and Liu 2020). Furthermore, recent evidence from the *Tshz3* ChAT dependent conditional knockout model of ASD shows a shift in the proportion of CINs populating striosomes and the matrix (Molitor 2022). In control conditions, early born CINs populate striosomes, whilst late born CINs localise within the matrix (van Vulpen and van der Kooy 1998). In the knockout condition, more CINs localise to striosomal regions, corresponding to a shift towards early born CIN identity (Molitor 2022). With studies showing that the striosome and matrix contain separate circuits (Banghart et al. 2015, Brimblecombe and Cragg 2017), it is essential to probe further in to the effect of knocking out *Cntnap2* and changes in cell number we observed in the context of these subdivisions.

The striatum has a complex composition. Whilst in this chapter we present alterations to cell number, regulated by increased proliferation and apoptosis, we have not yet probed deeper into some aspects of striatal circuitry in ASD, and whether transient shifts are present there, and also in the functional properties we observed. Future investigating this could reveal specificity

amongst striatal circuits for alteration in the *Cntnap2* knockout (potentially surrounding the Lhx6+ CIN population) and thus elucidate a more precise mechanism underlying ASD symptoms that centre around the striatum.

### ***The role of striatal Lhx6+ cholinergic interneurons in maintaining E/I balance in ASD***

Here, we show for the first time a specificity for alterations to the MGE-derived cholinergic interneuron population in the striatum in the *Cntnap2* knockout model, adding to previously described parvalbumin interneurons or spiny projection neurons. As CINs are among the first cells born during neurogenesis and are the first to populate and be active in the striatum (Knowles et al. 2021, Poppi et al. 2021), they do pose a vulnerable target for dysfunction in disease. We show a specific increase in the number of Lhx6+ CINs, followed by a decrease in the same population, with no change in the non-cholinergic Lhx6+ interneurons or the Lhx6- CINs. Whilst further investigation is needed to fully elucidate mechanisms underlying this specificity, such as tracking striatal CIN development from neurogenesis in the MGE to maturity, our findings implicate them as a potential risk population in ASD. This is unsurprising as cholinergic interneurons have been implicated in a number of other neuropsychiatric and neurodevelopmental disorders, such as Tourette's syndrome (Rapanelli et al. 2017, Poppi et al. 2021). In addition, recent studies have also shown that specific alterations to CIN identity and function via genetic manipulation drives ASD-like behaviour (Molitor 2022).

In terms of striatal circuitry, it is highly likely that MGE-derived Lhx6+ CINs segregate into separate striatal microcircuits from Lhx6- CINs. Lhx6+ CINs have GABA-ergic properties and segregate from Lhx6- CINs morphologically and functionally, including their response to cortical stimulation (Lozovaya et al. 2018). Whilst in our study, we did not compare Lhx6+ and Lhx6- CIN morphology and activity in the *Cntnap2* knockout, we did find a decrease in the activity of Lhx6+ CINs that correlated with increased ChAT levels as a possible compensation to normalise cholinergic tone, with no change in Lhx6- CINs. Not only does this highlight the separation of these two CIN subpopulations, but it also suggests that Lhx6+ CINs are plastic and engage in compensatory mechanisms to normalise circuit function.

The mechanisms underlying the decreased activity Lhx6+ interneurons are not clear. It is likely to be a direct role resulting from aberrant potassium channel expression and clustering, as these channels have direct roles in regulating cell excitability. However, we cannot rule out the contribution of reciprocal relationships between activity dependent gene expression and factors regulating cell excitability. Yet, activity changes in the *Cntnap2* knockout may influence the

other observed phenotypes. The activity levels of Lhx6+ interneurons and cortico-striatal circuitry influence the survivability of cells (Denaxa et al. 2018, Wong et al. 2018), and could influence the increase in apoptosis, with decreased activity correlating with decreased survivability. In addition, morphological development is activity dependent, and it has been shown that NMDA receptor activation facilitates activity driven dendritic expansion (Kalb 1994, Sin et al. 2002). We observed increased NMDA receptor mediated glutamatergic inputs to Lhx6+ interneurons in the *Cntnap2* knockout which may contribute to increase in dendritic complexity of both Lhx6+ CINs and putative FSIs.

Moreover, shifted interneuron activity largely implicates an excitation-inhibition (E/I) imbalance. E/I imbalance is increasingly accepted as hallmark of ASD, as it provides an explanation for decreased GABAergic signalling observed in ASD and cortical circuit hyper-excitation (Rubenstein and Merzenich 2003, Cellot and Cherubini 2014). Our findings in the developing striatum reflect this, with increased glutamatergic inputs to Lhx6+ interneurons, and decreases in the excitability of these interneurons, likely resulting in an overexcitation of the striatal SPNs, which is known to contribute to ASD-like behaviours (Gandhi and Lee 2020).

As neuromodulators, CINs have a unique role in maintaining the excitation-inhibition balance in the striatum. The striatum itself is a mostly inhibitory structure with large excitatory inputs to inhibitory SPNs, which are regulated by the surrounding interneurons, including CINs. CINs are known to innervate and exert direct control over both SPNs and inhibitory interneurons, as well as maintain an axo-axonic connection with excitatory cortico-striatal inputs (Poppi et al. 2021). As such, they can be considered as master regulators of the E/I balance and the selective alterations that we observed in the *Cntnap2* knockout may indeed be the causal break in network balance that causes ASD-like phenotypes.

Future studies should investigate whether this is conserved across other models of ASD, and whether modification of striatal cholinergic neurons could rescue the functional alterations observed. For instance, the *Shank3B* knockout model has presented with striatal alterations and perturbed mGluR5 signalling, similar to what we observed in the *Cntnap2* knockout (Wang et al. 2016). Increases in mGluR5 has been shown to activate the direct striatal pathway, leading to repetitive behaviours underlying ASD (Gandhi and Lee 2020). Similarly, the deletion of neuroligin-1 (NLG-1), which has been linked to ASD, leads to an altered NMDA/AMPA ratio in the striatum, as well as repetitive movements that were rescued upon the rectification of the imbalance (Blundell et al. 2010). In addition, studying these cells in an environmental model



of ASD such as the valproic acid (VPA) induction model would confirm a conserved ASD mechanism versus a phenotype resulting from genetic reprogramming and network imbalance.

In order to fully determine the susceptibility of CINs in ASD, and the specific role of *Cntnap2* in these cells, future studies should generate conditional knockouts whereby *Cntnap2* is ablated from specific neuronal populations. Removing *Cntnap2* from the Lhx6 interneuron population, or from the CIN population, and probing for ASD phenotypes in these conditional knockouts would give key information about the neuronal populations contributing to ASD and provide evidence for a specific neuronal population having a causal role in ASD.

### ***Establishing treatments for ASD- the future of interneurons as a therapeutic target***

As the name suggests, autism spectrum disorders are highly heterogeneous, in both presentation, severity, and cause (Lenroot and Yeung 2013, Masi et al. 2017). As a result, establishing effective pharmacological therapeutics has proven challenging, particularly as a conserved cellular population or mechanism has not been implicated in ASD.

Nevertheless, there are some proposed therapies for ASD. Generalised drugs such as risperidone have been shown to reduce ASD-typical aggression in an ASD mouse model from a mutation in the neuroligin-3 gene (Burrows et al. 2015), and have been used in clinical settings for the treatment of ASD as well (Aishworiya et al. 2022). In addition to drugs, environmental treatments have also been explored for ASD. For example, increased handling during juvenile stages in the VPA induced mouse model rescues some ASD-related behaviours, including repetitive behaviours and impaired sociability (Seiffe et al. 2022). Similarly, environmental enrichment in the neuroligin-3 mutation ASD model can also modulate aggression and social behaviour (Burrows et al. 2020).

Direct interventions targeting the E/I balance in ASD has proven effective in mouse models and also in some human studies. During development, high levels of intracellular chloride can modulate GABA receptor activity from inhibitory to excitatory, and this excitatory transmission has been shown to contribute to ASD (Ben-Ari 2002). Bumetanide, a chloride importer (NKCC1) antagonist, is expected to reduce intracellular chloride and therefore reverse the E/I imbalance in ASD (Ben-Ari and Lemonnier 2021). Indeed, Bumetanide treatment rescued symptoms of ASD in children (Lemonnier et al. 2012). Despite some side effects and off-target effects, this drug is still in clinical trials as a potential ASD therapeutic.

Similarly targeting E/I balance, optogenetic modulation of excitatory pyramidal neurons or inhibitory PV interneurons in the medial prefrontal cortex resulting in decreased excitability

(decreasing pyramidal neuron activity, increasing PV interneuron activity) rescued social deficits in adult *Cntnap2* knockout mice (Selimbeyoglu et al. 2017). This proved an interesting point we have previously discussed; the causal relationship between the excitation-inhibition balance and the core symptoms of ASD.

Following this, the possibility of targeting cholinergic interneurons in the striatum to rectify the E/I imbalance must be considered. Interestingly, as we previously discussed, we observed decreased excitability in the Lhx6+ CIN population. When compared to Lhx6- CINs, Lhx6+ CINs already present with lower excitability (*i.e.* less spontaneous and evoked firing) (Lozovaya et al. 2018). Employing cell type specific DREADDs (Designer Receptors Exclusively Activated by Designer Drugs) to increase activity of Lhx6+ CINs, or even cell type specific knockouts such as removing Lhx6 from CINs (under the Lhx7 promoter) could restore CIN activity in the *Cntnap2* knockout, and potentially rectify the E/I imbalance and ASD core symptoms.

In fact, some research has been done into targeting the cholinergic system in ASD. Low acetylcholine (ACh) levels have been observed in the BTBR (Black and Tan Brachyury; mutation within the *Itpr3* gene) mouse model of ASD. Treatment with Donepezil, an acetylcholinesterase inhibitor, resulted in decreased cognitive rigidity and improved social preference and interaction when mice were treated both generally and directly in the dorsomedial striatum (Karvat and Kimchi 2014). In the same ASD model, nicotine treatment resulted in dose dependent amelioration of either social interaction or repetitive behaviour symptoms (Wang et al. 2015). Whilst CINs or the cholinergic system have not been directly targeted in the *Cntnap2* model, these results indicate that increasing CIN activity, as we previously suggested, may in fact be a viable treatment for ASD.

Whilst effective treatments for ASD in humans are still quite far in the future, due to the heterogeneity in underlying genetic and environmental causes, the work presented in this chapter provides evidence for striatal cholinergic interneurons being a risk population in ASD. With an altered E/I balance in the striatum, and striatal CIN dysfunction as a possible contributing factor, we have opened a new avenue for further studies into the link between striatal neuromodulation in mouse models as well as in humans.

## Chapter 5:

### Discussion

#### *Main Findings*

In this thesis, we investigated how shifting the molecular identity and developmental trajectory of neurons influences the formation of functional microcircuitry and structure innervation via long range circuits. Understanding how molecular alterations, such as differential gene expression, regulated by epigenetics or environmental factors, can regulate various aspects of circuitry and subsequently contribute to behavioural regulation is a crucial goal of neuroscience research.

In Chapter 2 we perturbed the identity of medial ganglionic eminence (MGE)-derived interneurons at post-mitotic stages by ablating the *Er81* transcription factor specifically from these cells; particularly as *Er81* is a key candidate for developmentally regulating interneuron identity and function. We observed alterations to intrinsic functional properties, culminating in decreased excitability of both developing putative PV-INs and mature CINs, as well as disrupted physical connectivity between these two interneuron subtypes in the absence of *Er81*. We also explored the functional connectivity of striatal MGE-derived interneurons throughout development. We found evidence for the prevalence of a PV-IN/CIN connection that is not present in mature circuits and observed decreased electrical connectivity between putative PV-INs during late postnatal developmental stages in the *Er81* knockout condition. Overall, these results highlight the importance of maintained developmental molecular identity for striatal neuronal activity and circuit formation and maintenance and show for the first time key aspects of developmental striatal circuitry.

In Chapter 3 we studied the role of *Er81* in another neuromodulatory population, the serotonergic system. Serotonergic inputs to the striatum heavily influence striatal circuitry and striatum-mediated behaviour. We ablated *Er81* conditionally from serotonergic neurons in the Dorsal Raphe Nucleus (DRN) and observed sexually dimorphic alterations to behaviour and serotonergic circuitry. We found that female mice in the *Er81* knockout condition presented with decreased locomotion and anxiety-like behaviour compared to controls, which correlated with decreased neuron excitability and a reduction of the serotonergic population in the DRN. Male *Er81* knockout mice showed gait deficits, alongside decreased physical innervation of the striatum and decreased serotonergic neuron activity. Thus, we uncover a link between *Er81* transcriptional control and long-range circuitry and behavioural modulation, likely mediated by neuronal activity and excitability.

In Chapter 4 we explored the contribution of striatal interneurons and their associated circuits to the Autism Spectrum Disorder (ASD) pathophysiology. We found significant striatal perturbations in the *Cntnap2* mouse model of ASD; including a transient increase in striatum size across early postnatal development, and in the number of MGE-derived striatal interneurons, mediated by increased embryonic proliferation and early postnatal apoptosis. We also identified striatal CINs as a potentially vulnerable population, with higher *Cntnap2* mRNA levels, and an emphasised increase and decrease in cell number across early development, showing they were primarily affected compared to other subpopulations. We then found that MGE-derived interneurons had developmental morpho-functional deficits in the *Cntnap2* knockout condition compared to controls, with excessive dendritic arborisation and decreased excitability. Together, these alterations likely contribute to developmental shifts in the excitation-inhibition balance that underlie ASD aetiology.

The findings in this thesis culminate in several key concepts: the importance of understanding the gene-activity balance and how this influences development and behaviour; the unknown unique circuitry of the developing striatum; and the vulnerability of neuromodulatory systems in disease via their extensive links with behaviour. Moreover, these findings shine light on potential conserved mechanisms in human systems and how we can use animal studies for advancing our knowledge of the human brain and creating therapeutic treatments for neuropathological disorders.

### ***Understanding the balance between genetics and activity and its influence on development and behaviour***

A common thread we observed throughout all of our findings in this thesis was the observation that genetic manipulation, whether via the ablation of Er81 or in the *Cntnap2* knockout condition, resulted in decreased neuronal activity, and culminated in some measure of shifted downstream functionality. The question then arises whether downstream alterations are directly due to genetic manipulation, for example where the transcriptional control of genetic factors influencing cell morphology or connectivity is altered following Er81 ablation; or if the genetic manipulation affects cell function, which then influences circuit formation, morphology, or behaviour. This issue forms a loop of causality and potentially perpetuating effects, which proves to be very difficult in dissecting molecular and activity dependent mechanisms (**Figure 5.1**).

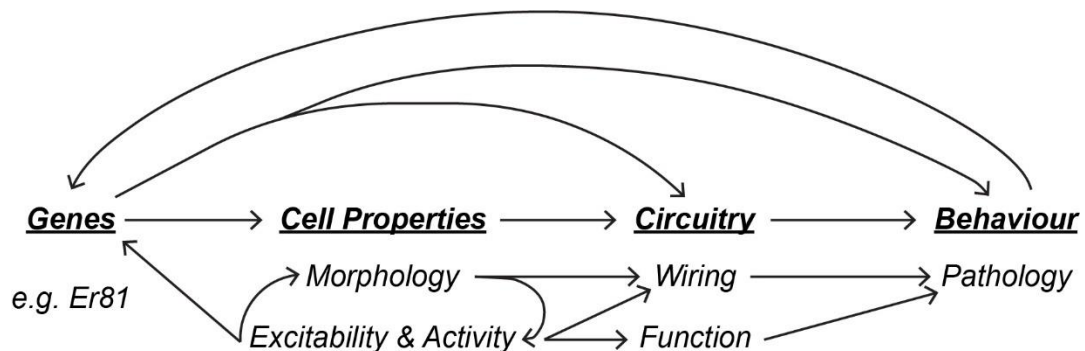


**Figure 5.1: Links between the various levels of the relationship between genetic identity and behaviour**

Map of the interactions between genetic factors, cell properties, circuitry, and behaviour. Arrows represent direction of control that has been shown in literature.

For example, in Chapter 2 we found decreased cell excitability in striatal putative fast spiking interneurons (FSIs, PV-INs) at P5-7 in the Er81 conditional knockout. Subsequently, the characteristics of spontaneous SPA-like events indicated decreased excitability and decreased calcium depolarisation strength at this same age in the knockout. Finally, we observed decreased gap-junction-mediated connectivity at later developmental stages. The causal links between these observations with each other and with Er81 transcriptional regulation is difficult to determine: decreased cell activity could contribute to decreased coupling (Haas et al. 2016, Stampanoni Bassi et al. 2019), however Er81 has been shown to transcriptionally regulate the connexin channels that mediate gap junctions (Shekhar et al. 2018), as such decreased coupling could simply be due to a reduction in channels present.

Similarly, the mouse model of ASD we studied in Chapter 4 knocks out Caspr2, a protein essential for the localisation and clustering of potassium channels, which are crucial for maintaining cell membrane properties, excitability, and action potential generation (Cameron et al. 2000, Platkiewicz and Brette 2010). We observed decreased cell excitability in striatal interneurons that may have been due to aberrant potassium channel expression, but could also be attributed to the morphological defects we observed. A study showed that constraining dendritic morphology in cultured cells to have fewer dendrites correlated with increased excitability and less integrative power (Zhu et al. 2016). In this case, the dendritic field of striatal interneurons in the ASD mouse model were more complex than controls, perhaps causing the alterations to excitability.

Molecular factors influencing cell activity is not a novel concept. Of course, modulating the expression of channels and receptors links directly to changes in cell excitability. For example a knockdown of *Nkcc1* (Na-K-Cl cotransporter) decreases GABA<sub>A</sub> receptor mediated depolarisation of neural precursor cells in the developing brain, subsequently affecting the proliferation and dendritogenesis of neurons, which can be rescued by the expression of NMDA receptors to restore membrane depolarisation (LoTurco et al. 1995, Wang and Kriegstein 2008).

More complex examples are those where the modification of a transcription factor (such as *Er81*) can cause downstream effects, potentially altering multiple cell properties including morphology and connectivity. For example, the specific ablation of the *Foxp1* transcription factor from striatal spiny projection neurons (SPNs) results in increased excitability, with potential contributions from inward rectifying and leak potassium currents, but also from differences in the membrane surface area, which can influence cell excitability (Khandelwal et al. 2021). *Er81* has been shown to have multiple roles in various cell populations: regulating long range axonal connections (Arber et al. 2000), fine-tuning cell excitability (Dehorter et al. 2015), and the promotion of morphology regulating genes (Ding et al. 2016). It's role also seems to be specific to neuronal type, as in some populations it seems to simply segregate a subpopulation (Yoneshima et al. 2006, Tenney et al. 2019). Therefore, whilst we can correlate changes in cell activity, cell connectivity, and behaviour with genetic manipulation, establishing causality is difficult. In order to bridge these gaps to fully understand mechanisms linking our observations, we can suggest several future directions.

Primarily, potential mechanisms can be determined via the identification of changes in gene expression. RNA sequencing techniques across development in control and mutant conditions can illuminate altered molecular pathways and factors that may contribute to observed alterations. For example, using spatial transcriptomics in Chapter 4, we observed in control conditions that enhanced *Cntnap2* expression in the striatum correlated with enhanced molecular pathways relating to ASD-like behavioural presentation, including locomotor behaviour, vocalisation, and cognition. *Cntnap2* was also enhanced in striatal CINs, and we subsequently found these cells to be particularly affected in the knockout condition. However, more powerful studies including sequential analyses across development in both control and mutated conditions will give far more information. To determine the transcriptional control that *Er81* enacts in developing and mature striatal interneurons, single-cell sequencing comparisons between controls and *Er81* conditional knockouts may elucidate factors that regulate cell excitability, such as potassium channels, or channels facilitating gap junction connections, such

as connexins. This could also identify altered activity-dependent genes, evidence for *Er81* integrating with both activity-dependent mechanisms as well as transcriptional ones.

Other methods for dissecting the roles of activity and genes relies on directly manipulating them. Here, we show the effects of knockouts, where a genetic factor is ablated either from the whole brain or in a cell-type specific manner. However, overexpressing the gene of interest to determine whether we see an opposite reaction from the circuit would solidify the proposed mechanisms. This can be done via tetracycline-controlled (tet-on) doxycycline-inducible gene expression (Das et al. 2016), whereby gene transcription is activated only when doxycycline is administered, and also via CRISPR-Cas9 activation of transcription factors (Di Maria et al. 2020). Additionally, directly modulating neuronal activity can also elucidate mechanisms underlying the relationship between cell activity and circuit function and formation. Recent studies have begun to elucidate the presence and identity of early response genes that are activated following membrane depolarisation, particularly in human derived GABAergic cells (Boulting et al. 2021). Utilising Designer Receptors Exclusively Activated by Designer Drugs (DREADDS) to chemically excite cells in a subtype-specific manner, or optogenetic activation of specifically expressed channelrhodopsins, can enhance (or deplete) the activity of a cell population of interest and subsequent analyses of molecular identity and circuit characteristics. In this way we can determine whether *Er81* expression in striatal interneurons during development is activity dependent, and also whether manipulating activity levels in control versus *Er81* knockout conditions has different downstream effects. This would confirm if *Er81* mediates activity dependent mechanisms controlling cell function and connectivity. Similarly, these techniques also pose a potential for rescuing observed deficits in cell excitability; for example, enhancing serotonergic cell activity the *Er81* knockout may rescue the behavioural alterations we observed, linking serotonergic cell function directly with behaviour. However, modulating the activity of single cell populations can imbalance the proportion of excitation and inhibition in the network.

Throughout our findings in this thesis, we have described our findings in the context of shifting the balance between excitation and inhibition in the network. Modulating the function of individual cell populations contributes to shifting this balance, but the brain is plastic and compensatory mechanisms do attempt to rectify this imbalance, particularly during development.

For example, the decrease in excitability observed in striatal interneurons in the *Cntnap2* knockout model of ASD was balanced by increased NMDA receptor mediated excitatory inputs to cells, perhaps as a mechanism to attempt to rectify the excitation-inhibition imbalance. Similarly, we observed decreased striatal PV-IN excitability in the absence of *Er81* during developmental stages, but not at mature stages in Chapter 2. By some mechanism, either the individual cells or the network as a whole was able to rectify this developmental deficit, showing that a transient alteration during development may not last into adulthood. This sort of developmental alteration during critical periods of development may appear to have no resulting effects in our findings in Chapter 2, yet wider circuit dysfunction and behavioural deficits are not out of the question. In fact, our results in Chapter 4 emphasise this; transient alterations to the cell population and developing environment may contribute to the lasting behavioural deficits in the *Cntnap2* mouse model of ASD.

Moreover, we also present evidence for the importance of neuromodulation in regulating the excitation-inhibition balance. Both serotonergic and cholinergic cell populations responded to genetic insult by altering their excitability and function, shifting circuit balance and resulting in behavioural alterations. Whilst the precise effects of neuromodulation are diverse and remain mostly unknown, we can postulate their importance during development for influencing the excitation-inhibition balance and regulating circuit formation.

### ***New insights into the unique circuitry of the developing striatum***

Striatal development, particularly in the context of interneuron activity and connectivity, is largely understudied. Whilst a great amount of research has been done into understanding the developmental origins of striatal interneurons (Marin et al. 2000, Magno et al. 2017), and their migratory pathways (Chen et al. 2010, Villar-Cervino et al. 2015), as well as the diversity and identity of the different subtypes (Fragkouli et al. 2009, Tepper et al. 2010, Tepper et al. 2018, Ahmed et al. 2019), research into later stages of development is limited.

Brain structures do not mature at the same rate, and this is particularly prevalent in human brains. Generally, subcortical structures, including the striatum, mature more rapidly compared to cortical regions (Mills et al. 2014). At a cellular level, we have some sparse evidence of this. Developmental cell loss (apoptosis) occurs at different times dependent on structure and activity, and can be considered a marker for network maturation. In the upper layers of the cortex (L1-4), interneuron cell death occurs from approximately P7-P10 (Wong et al. 2018), whereas, it is markedly earlier in the striatum, occurring from P5-7 (Sreenivasan et al. 2022).



Here, we show similar findings (Chapter 4), with striatal cell loss between P4 and P6, as opposed to cortical cell loss, which appears to continue until P10. We also show that the timing of cell death processes is the same in the *Cntnap2* knockout model of ASD.

PV-INs are common across many brain regions. Our findings indicate the functional identity of putative PV-INs as fast-spiking interneurons (FSIs) is established earlier in the striatum than other structures. There has been some investigation into the maturation of cortical PV-IN electrophysiological properties across development, and they have shown that PV-INs at P7 do not fire much higher than 50 Hz, and even P10 they do not fire at a very high rate (Okaty et al. 2009, Pouchelon et al. 2021). Contrastingly, striatal PV-INs fire as high as 80 Hz at P5-7, and was similar in control, *Er81* conditional knockout, and *Cntnap2* knockout (Chapter 2, Chapter 4). Together, this suggests that striatal circuitry itself matures at a faster rate in the striatum compared to the cortex, and the timing of this process is unchanged in ASD. In addition, it has been suggested that striatal interneurons mature earlier than SPNs (Chesselet et al. 2007). This positions the striatal interneuron network as crucial early regulators of striatal circuit formation and function.

As we outlined in Chapter 1, developing circuitry is overconnected, before refinement occurs in the second and third postnatal weeks. We did indeed observe far more synaptically connected interneuron pairs in the striatum at P5-7 compared to mature stages (P30+). Remarkably, we observed the incidence of bidirectional connections between PV-INs and CINs (Chapter 2). This is particularly interesting because previous literature conducted in adult mice has found little to no connectivity between PV-INs and CINs (specifically PV-INs functionally projecting to CINs). Early staining of PV axon terminals on CINs showed little to no contact (Chang and Kita 1992). Furthermore, optogenetic activation of striatal PV-INs elicited either no response or a very small post-synaptic current in CINs, indicating that they are poorly connected (Straub et al. 2016). Considering this, the likelihood of finding connectivity between a single PV-IN and CIN was low, and indeed we saw no connected PV-IN/CIN pairs in the mature striatum. Therefore the relatively high incidence of this connection at P5-7 may either be the result of excessive connectivity during development, or it is possible that PV-IN inhibitory activity on CINs is involved in the development of striatal circuitry, potentially regulating CIN activity during early stages. Dissecting this developmental circuit will require further studies to isolate and determine the extent of functional inputs from striatal PV-INs to CINs, and what purpose they serve.

There are also several unexplored aspects of the striatum that highlight its complex circuitry, particularly in development. We have previously discussed the striosome and matrix chemical divisions of the striatum, and how they may be rearranged in ASD (Chapter 4). It has also been shown that molecular alterations during development can affect the organisation of these compartments (Anderson et al. 2020). Further studies into striatal development must take these divisions into account, as it is highly likely that striosome and matrix located circuits connect in a segregated manner.

Our findings bring light to previously unexplored aspects of striatal interneuron function and precise circuitry during development. With further studies, we may be able to elucidate the developmental trajectory of the striatum and how it can be altered in diseased states.

### ***Neuromodulatory systems as mediators of behaviour and their vulnerability in disordered states***

Throughout this thesis, we have explored the role of neuromodulatory neurons in regulating circuitry and behaviour. Whilst this has been explored quite extensively (Chapter 1), there are still some aspects, particularly relating to the characteristics of neuromodulatory populations, that remain unresolved.

Neuromodulatory neurons, particularly those we have investigated in this thesis, are highly heterogeneous populations (Munoz-Manchado et al. 2018, Ahmed et al. 2019, Okaty et al. 2020). In particular, the diversity of serotonergic neurons in the dorsal raphe is of particular interest as it correlates with circuitry and behaviour. Yet, we show here that *Er81* seems to be expressed in nearly all DRN Pet+ serotonergic neurons, as opposed to segregating a subpopulation as might have been expected. This combined with its expression in most striatal CINs and in dopaminergic neurons of the substantia nigra pars compacta (unpublished observations, data not shown) suggests that *Er81* may have a specific role in neuromodulatory cell populations. In addition, we have observed particular patterns of expression of *Er81* in neuromodulatory neurons compared to other interneuron subtypes. As we discussed in Chapter 3, cytoplasmic expression of a transcription factor can indicate a protein interaction dependent role.

Neuromodulation has been largely overlooked in ASD, as many studies focus on cortical excitatory and inhibitory neurons. However, there are some known links between neuromodulatory systems and ASD, as we have explored in Chapter 4. The involvement of the serotonergic system in ASD is complex. Elevated whole blood serotonin was an early

biomarker of ASD, and changes to serotonin in the central nervous system have also been documented in ASD (Muller et al. 2016). In addition, there are several studies regarding the interaction of serotonin with other systems contributing to ASD. For example, haploinsufficiency for the *Pten* gene is known to result in ASD (Clipperton-Allen et al. 2019), but introducing haploinsufficiency for the serotonin transporter (SERT) alongside this exacerbates brain overgrowth and leads to female specific deficits in social approach behaviours (Page et al. 2009).

Similarly, our findings alongside recent studies (Caubit et al. 2022, Molitor 2022) have identified striatal CINs as a risk population, prominently contributing to ASD pathophysiology. We show enhanced expression of the ASD risk gene *Cntnap2* in striatal CINs, and the specific alteration of cell number, as well as morphological and functional deficits in CINs in the *Cntnap2* knockout mouse model of ASD. In particular, we show these alterations during developmental stages.

It is essential to further understand and characterise alterations to these populations, particularly as both are now being established as therapeutic targets. Decreased serotonin receptors have been observed in human incidences of ASD, as such several serotonin receptor subtypes have been investigated as potential targets for small molecule modulators in the treatment of ASD (Lee et al. 2022). As we discussed in Chapter 4, modulation of the cholinergic system to alleviate ASD behavioural phenotypes has also been tested, via the acetylcholinesterase inhibitory Donepezil (Karvat and Kimchi 2014). As such, linking alterations to neuromodulatory systems in animal studies with human systems to establish effective therapeutics for ASD is vital, as they pose key target systems for effective treatments.

### ***Making links to the human brain***

Most current research is undertaken in mouse models to gain a better understanding of human mechanisms and pathology. As many of the studies conducted in mice cannot be done in humans, we must instead attempt to link our findings in mice with human systems.

In this study we have focussed quite heavily on striatal interneurons. We have described their alterations in response to direct genetic perturbation (Chapter 2), and in a model of ASD (Chapter 4), emphasising their functional importance within the striatum. These findings are highly relevant for human systems; whilst interneurons comprise approximately 5% of striatal neurons in rodents, with the remainder being spiny projection neurons, this is far higher in the human striatum, with up to 26% of striatal neurons being identified as innervating local circuitry

(Bernacer et al. 2007). Therefore, it is likely that striatal interneurons enact a higher degree of influence over striatal circuits, suggesting their involvement in regulating higher-order processes unique to primates and humans. This is also relevant in the context of therapeutics for pathological conditions. As we have discussed previously, targeting the cholinergic system via a cholinesterase inhibitor (Donepezil) in ASD patients has proven somewhat successful (Handen et al. 2011), opening avenues for novel therapeutics targeting this same system. Our results further associate cholinergic neurons as a vulnerable system to be altered in ASD. As such, determining whether decreased cholinergic cell number and decreased cell activity is consistent in human patients with ASD is necessary, and may subsequently lead to the identification of drugs able to rectify developmental alterations to this system.

In Chapters 2 & 3 of this thesis, we focussed on genetic perturbation of the *Etv1/Er81* transcription factor. Our findings in this context are applicable to the human brain as *Etv1* has a similar pattern of expression in the primate medial ganglionic eminence (Schmitz et al. 2022), and is in fact highly expressed during foetal development (Ding et al. 2022). Therefore, alterations to the developing brain that mirror our findings here may be due to alterations in the *Etv1* gene and may underlie unexplained developmental pathologies. This extends to our findings in Chapter 3 regarding our observations of decreased anxiety following *Er81* ablation from serotonergic neurons. It is entirely possible for this mechanism to be conserved in the human brain. Understanding the mechanisms underlying these changes in anxiety could lead us to possible explanations for the increased prominence of anxiety in females (Bahrami and Yousefi 2011), and present possible treatments.

### ***Conclusions***

Whilst human studies dissecting neuronal circuitry and cell function are part of a distant future, neuroscientists must utilise animal models to make assumptions regarding how the human brain works. Whilst it may not always be correct, it is vital to continue uncovering basic biological and neurological mechanisms underlying neuron function and integration within neuronal networks and behavioural processes. In conclusion, in this thesis we have uncovered crucial mechanisms of brain development; finding novel relationships between genetic factors and neuronal circuitry during development and in the mature brain, with critical links to neurodevelopmental pathology.

## Methods

### 6.1 Mice

Mouse lines used for this project (**Table 1**) were bred and housed at the Australian Phenomics Facility, the Australian National University, with strains sourced from The Jackson Laboratory (JAX® Mice). Control mouse lines were generated by breeding sourced mouse lines with fluorescent reporter lines (**Table 1**); knockout mouse lines were generated by breeding control and reporter lines with either the *Er81<sup>fl/fl</sup>:RCE*, *Er81<sup>fl/fl</sup>:TdTomato*, or *Cntnap2<sup>-/-</sup>* knockout line (Jax: *B6.129(Cg)-Cntnap2<sup>tm1Pele</sup>/J*) to generate homozygous flox or knockout lines (**Table 1**).

Mice were housed in same sex groups up to five mice with water and food *ad libitum*. Due to the nature of the mouse lines used (an autism model and a model with anxiety/aggression phenotype), single housing of mice was avoided whenever possible to ensure that social isolation did not contribute to behavioural alterations. All experiments were conducted with ethical approval from the Australian National University Animal Experimentation Ethics Committee (Protocols 2016/43, 2019/46, 2021/43). Male and female mice were used at embryonic (E12-16), early postnatal (P2-10 and P15-18), and adult stages (P30+).

**Table 1: Mouse Lines**

<i>Control Line</i>	<i>Control Line JAX Nomenclature</i>	<i>Mutation/ Knockout Line</i>	<i>Chapter</i>
<i>ChAT-Cre<sup>+/-</sup>;RCE<sup>+/-</sup></i>	<i>B6;129S6-Chat<sup>tm2(cre)Lowl</sup>/J</i>	<i>Er81<sup>flox/flox</sup>;ChAT-Cre<sup>+/-</sup>;RCE<sup>+/-</sup></i>	2
<i>PV-Cre<sup>+/-</sup>;TdTomato<sup>+/-</sup></i>	<i>B6;129P2-Pvalb<sup>tm1(cre)Arbr</sup>/J</i>	<i>Er81<sup>flox/flox</sup>;PV-Cre<sup>+/-</sup>;TdTomato<sup>+/-</sup></i>	2
<i>Lhx6-iCre<sup>+/-</sup>;TdTomato<sup>+/+</sup></i>	<i>B6;CBA-Tg(Lhx6-icre)IKess/J</i>	<i>Er81<sup>flox/flox</sup>;Lhx6-iCre<sup>+/-</sup>;TdTomato<sup>+/+</sup></i>	2
<i>Lhx6-iCre<sup>+/-</sup>;RCE<sup>+/+</sup></i>	<i>B6;CBA-Tg(Lhx6-icre)IKess/J</i>	<i>Er81<sup>flox/flox</sup>;Lhx6-iCre<sup>+/-</sup>;RCE<sup>+/+</sup></i>	2
<i>Nkx2.1-CreER<sup>+/-</sup>;RCE<sup>+/+</sup></i>	<i>Nkx2-1<sup>tm1.1(cre/ERT2)Zjh</sup>/J</i>	<i>Er81<sup>flox/flox</sup>;Nkx2.1-CreER<sup>+/-</sup>;RCE<sup>+/+</sup></i>	2
<i>Pet-Cre<sup>+/-</sup>;RCE<sup>+/+</sup></i>	<i>B6.Cg-Tg(Fev-cre)IEsd/J</i>	<i>Er81<sup>flox/flox</sup>;Pet-Cre<sup>+/-</sup>;RCE<sup>+/+</sup></i>	3
<i>Lhx6-iCre<sup>+/-</sup>;TdTomato<sup>+/+</sup></i>	<i>B6;CBA-Tg(Lhx6-icre)IKess/J</i>	<i>Cntnap2<sup>-/-</sup>;Lhx6-iCre<sup>+/-</sup>;TdTomato<sup>+/+</sup></i>	4

#### 6.1.1 Breeding

Mice in the *Lhx6-iCre* and *Pet-Cre* dependent strains were bred to ensure *Cre* expression remained heterozygous. As the *Pet-Cre* dependent knockout of *Er81* affects the serotonergic system, which is highly involved in hormone regulation and behaviour (Lucki 1998, Rybaczyk et al. 2005), breeder pairs were kept in the same configuration; a *Cre* negative female (no genetic mutation) and a *Cre* positive male, to reduce the risk of impaired maternal care.

### 6.1.2 Timed Mating

Mice required at embryonic or early postnatal stages (Chapters 2 & 4) were generated using timed mates. A male and 1-2 females were placed together overnight, and the females checked for vaginal plugs the following morning. Presence of a vaginal plug placed the female at 0.5 days post conception as of the discovery, to account for conception occurring during the night. Females were checked for weight gain throughout the pregnancy and were considered not pregnant if there was no weight gain or a weight loss by E10. If females had no vaginal plug or were not pregnant, they were placed back into breeding.

### 6.1.3 Tamoxifen Induction<sup>8</sup>

To sparsely label striatal interneurons for morphological reconstruction in control and Er81 knockout conditions (Chapter 2), mice in the *Nkx2.1-CreER;RCE* and *Er81<sup>flx/flx</sup>;Nkx2.1-CreER<sup>+</sup>;RCE* lines were used and required the activation of *Cre* expression via Tamoxifen induction. Induction in P0 pups was administered via intraperitoneal injection of 25  $\mu$ L low titer Tamoxifen (Sigma, T5648) in corn oil (Sigma, C8267) at 10 mg/mL. Pups were then monitored for seven days post induction and sacrificed at P30.

### 6.1.4 Viral *in vivo* Labelling

To label spiny projection neurons (SPNs) in the striatum for morphological reconstruction (Methods section 6.6.5; Chapter 2) and synaptic bouton quantification (Methods section 6.6.7; Chapter 2), heterozygous littermate control and knockout pups in the *Er81<sup>fl/fl</sup>;ChAT-Cre* strain were virally infected on their day of birth. Micropipettes for infection were pulled from borosilicate glass capillary tubes (100 mm, outer diameter 1.5 mm, filament 0.84, World Precision Instruments, 1B150F-4) pulled with a Narishige PC-10 pipette puller. Pipette tips were gently modified after pulling using tweezers to approximately 50  $\mu$ m in diameter. Pups were anaesthetised on ice until completely unconscious (*i.e.* no response to physical stimulation and no breathing), and then placed into a holding frame and the head secured using 27 gauge needles placed through skin near the ears, where low blood supply prevents lasting damage. The striatum was targeted with a micromanipulator (coordinates: 1.5 mm anterior from bregma, 1 mm lateral from the midline, 1.5 mm depth from skull surface), and bilateral injections of AAV1:hSyn:eGFP:WPRE:bGH (University of Pennsylvania) at a dilution of 1:100,000 in sterile 0.01M PBS were performed with a World Precision Instruments Micro-2T injector. The pipette was plunged to just below the target area and then pulled up to the correct depth to allow

---

<sup>8</sup> Tamoxifen induction injections were performed by Alexandre RCom-H'cheo-Gauthier

a small region for the injected virus to pool. 500 nL of virus was injected, and the pipette removed after a 30 second pause to allow for diffusion. After infection, the pups were placed on a heat pad to recover. Pups were considered revived once they were able to gasp for air and regained a healthy pink colour and temperature. They were then placed back into the home cage. Pups were monitored for the following week to observe any ill effects caused by the infection.

After tissue collection, brain slices were stained with the Cre antibody (see section 6.5) to determine which mice were control and which were Cre-positive and therefore knockout.

## **6.2 Tissue Collection**

### **6.2.1 Fixed Tissue Collection**

To collect fixed tissue samples, mice were first anaesthetised under either ice (P0-P3 pups) or 4-4.5% isoflurane ( $\geq$ P3). Once judged to be under deep anaesthesia, and non-responsive to physical stimulation, animals were perfused transcardially with 0.01M phosphate buffered saline (PBS, Sigma-Aldrich, P38135), followed by 4% paraformaldehyde in PBS (PFA, Sigma-Aldrich, P6148). This was done by opening the thoracic cavity, creating an incision in the right atrium, and applying a constant flow of solution via a needle and syringe (P2-5) or peristaltic pump ( $\geq$ P6) to the left ventricle. PBS was allowed to perfuse through until blood was no longer flowing from the right atrium (approximately 5-6 minutes in adult mice). PFA was allowed to perfuse for 15 minutes, and mice were checked for tail stiffness, indicating the efficacy of fixation. Mice were then decapitated and the brain dissected out and placed in 4% PFA. The tissue was left to post-fixate for between 2-5 hours or overnight in PFA, dependent on the age and condition of the brain, and kept consistent within datasets. The fixative was then removed from the tissue and washed in 0.01M PBS for 15 minutes three times.

For the collection of embryonic brain tissue, the pregnant mother was cervically dislocated, and the embryonic sac extracted from the abdomen and placed into ice-cold 0.01M PBS. Embryos were removed from the sac, and the brain was dissected under a microscope (Zeiss Stemi 305 LAB Microscope, 435063-9020-100) and placed into 4% PFA to fix overnight. A single overnight wash of 0.01M PBS was applied to remove the fixative. Before sectioning, embryonic brains were embedded into 4% bacto-agar (Becton Dickinson, 214010) to protect and maintain the integrity of the tissue.

Brains were sectioned in 0.01M PBS at a thickness of 60  $\mu\text{m}$  (general immunostaining) or 100  $\mu\text{m}$  (for morphological reconstruction) using a Leica 1000S vibratome, and then preserved in an ethylene glycol solution (33% Ethylene glycol (Sigma, 324558), 33% Glycerol (Sigma, G5516), 33% 0.01M PBS) and stored at  $-20^{\circ}\text{C}$ .

### 6.2.2 Fresh Tissue Collection

Fresh tissue was collected from early postnatal mice for RNA extraction. Mouse pups were decapitated and the brains removed into cold 0.01M PBS. The brains were dissected under a microscope to obtain specific regions: the prefrontal cortex and striatum (**Figure 1**). The tissue was placed into an RNase and DNase free tube and flash-frozen on dry ice, then stored at  $-80^{\circ}\text{C}$ .

### 6.3 Stereo-seq<sup>9</sup>

Spatial Enhanced Resolution Omics-Sequencing (Stereo-seq) technology from BGI, in beta testing (V1.0, not commercially available) was used to perform spatial transcriptomics on a sagittal brain slice taken from an adult male mouse (Chapter 4). Briefly, the mouse was sacrificed and the brain removed and embedded in optimal cutting temperature compound (OCT) to be frozen and then sectioned sagittally via cryostat at a thickness of 10  $\mu\text{m}$ . A selected slice was mounted onto a STOmics-GeneExpression-S1 chip (1  $\text{cm}^2$ ), which are patterned grids of probes containing spatial coordinates. The tissue was fixed in methanol, permeabilized, and the reverse transcription was performed. Subsequent analysis of DNA library preparation and sequencing, as well as further data analysis, including clustering, was performed. For full methodology, see methods section of Ahmed et al. (2023) (Appendix C).

### 6.4 RNA Analysis

To determine changes in RNA expression in the *Cntnap2*<sup>-/-</sup>; *Lhx6-iCre*; *TdTomato* mouse model of Autism Spectrum Disorder (ASD) compared to controls (*Lhx6-iCre*; *TdTomato*; Chapter 4), RNA extractions were performed for the purposes of qRT-PCR analysis (**Figure 1**).

---

<sup>9</sup> Stereo-seq was performed in collaboration with Ulrike Schumann, Lixinyu Liu, Riccardo Natoli, and Jean Wen.



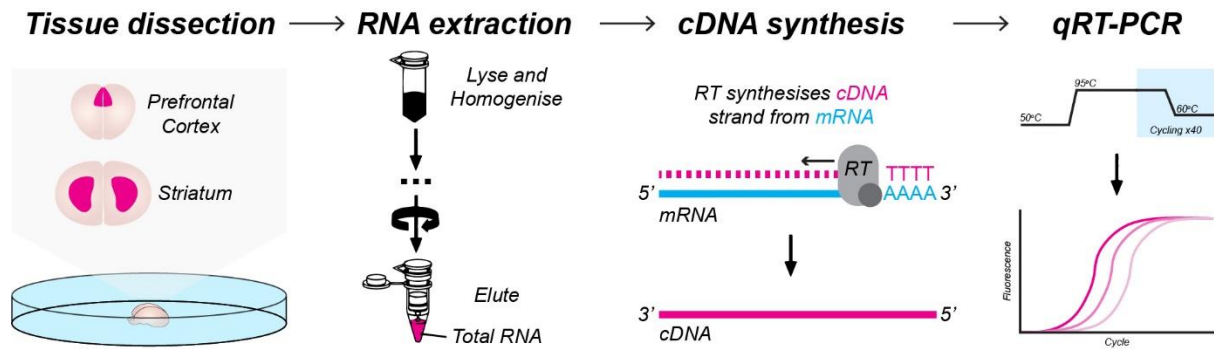


**Figure 1: RNA Analysis Workflow**

The process of RNA level analysis: Tissue is dissected (section 6.2.2), total RNA is extracted (section 6.4.1), retro-transcription generates cDNA (section 6.4.2), which is then analysed via qRT-PCR probing for target genes (section 6.4.3).

### 6.4.1 RNA Extraction from Tissue Samples

Total RNA was extracted using the RNeasy Micro kit (Qiagen) for tissue samples according to manufacturer's instructions (no DNase digestion). Briefly, the tissue (collected as in section 6.2.2) was disrupted within its tube using scissors treated with RNaseZAP (Sigma-Aldrich, R2020), following which Buffer RLT was added, and the tissue homogenised using a 25 gauge needle and a 1 mL syringe. This was centrifuged at full speed for 3 minutes, and the supernatant (lysate) transferred to a new microcentrifuge tube. 70% ethanol was added to the lysate and mixed via pipetting, and this was transferred to a RNeasy MinElute spin column and centrifuged for 15 seconds at 8000 x g. The flow-through was discarded, and Buffer RW1 was added, and the tubes centrifuged once more for 15 seconds at 8000 x g; the flow-through was once again discarded. Buffer RPE was added to the spin column and centrifuged for 15 seconds at 8000 x g, and the flow-through discarded. 80% ethanol was then added to the spin column and centrifuged for 2 minutes at 8000 x g, the flow-through was discarded. The columns were then centrifuged at full speed (15000 x g) for 5 minutes with lids open, after which the flow-through and collection tubes were discarded. The columns were placed into a new 1.5 mL collection tube, and RNase-free water applied directly to the centre of the spin column membrane. They were then centrifuged at full speed for 1 minute to elute RNA (**Figure 1**). The collection tube containing the final RNA sample was retrieved and stored at -80°C. A second elution was performed by applying more RNase-free water and repeating centrifugation, producing a secondary RNA sample.

RNA concentration and purity were determined using a NanoDrop spectrophotometer (ND-1000, Thermo Fisher Scientific). RNA yield was considered optimal if the concentration was

above 100 ng/ $\mu$ L, and purity was assessed by comparing the ratio of absorption at 260 nm over 230 nm (260/230) to acceptable values of 2.0-2.2.

#### **6.4.2 cDNA Synthesis from RNA Samples**

RNA obtained via processes in section 6.4.1 was reverse transcribed into cDNA (**Figure 1**) using the SuperScriptIII First Strand Synthesis System (Invitrogen, 18080093) according to manufacturer instructions. Cycling was done with the use of a ThermoMix (Eppendorf, 5382000066). Briefly, 50  $\mu$ M oligo(dT), 10 mM dNTP mix, and DEPC-treated water were combined in a ratio of 1:1:2, to an amount allowing for 4  $\mu$ L of the final mix per sample. To this, 6  $\mu$ L of RNA was added (calculated based upon measured RNA concentration, to ensure up to 5  $\mu$ g of total RNA was added). This was then incubated at 65°C for 5 minutes, and then placed on ice for at least 1 minute. A cDNA synthesis mix was then prepared containing: 2  $\mu$ L 10X RT buffer, 4  $\mu$ L 25 mM MgCl<sub>2</sub>, 2  $\mu$ L 0.1 M DTT, 1  $\mu$ L RNaseOUT (40 U/ $\mu$ L), 1  $\mu$ L SuperScript III RT (200 U/ $\mu$ L) per reaction. 10  $\mu$ L of this mix was added to each RNA/primer tube and incubated at 50°C for 50 minutes. Reactions were then terminated at 85°C for 5 minutes, and tubes were chilled on ice; cDNA samples were then stored at -20°C.

cDNA was diluted with DNase/Rnase free water to contain 10 ng of cDNA for each reaction required; this solution was used for qRT-PCR.

#### **6.4.3 Quantitative Real Time Polymerase Chain Reaction (qRT-PCR)**

qRT-PCR was used to analyse cDNA samples via the TaqMan™ Gene Expression Assay. PCR reactions were performed on MicroAmp™ Fast Optical 96-Well Reaction Plates (0.1 mL, Applied Biosystems™), run using the StepOnePlus™ Real-Time PCR System (Applied Biosystems™). Samples were run in triplicate, with each 20  $\mu$ L reaction containing 1  $\mu$ L of 20X TaqMan® Gene Expression Assay (*i.e.* the relevant probe), 10  $\mu$ L 2X TaqMan® Universal PCR Master Mix (Applied Biosystems™), 4  $\mu$ L of cDNA sample (containing 10 ng RNA), and 5  $\mu$ L of Rnase-free water. Briefly, a mix of the Rnase-free water, 2X TaqMan® Universal PCR Master Mix, and 20X TaqMan® Gene Expression Probe was prepared in the correct proportions, for all reactions to be performed; this mix was prepared for each Assay Probe. 16  $\mu$ L of this mix was added to each relevant well, and then 4  $\mu$ L of cDNA sample was added to each relevant well.

Thermal cycling was run under standard settings on the StepOnePlus™ software, with incubation at 50°C for 2 minutes, 95°C for 10 minutes to allow for polymerase activation,

followed by 40 cycles of 95°C for 15 seconds (denaturation) and 60°C for 1 minute (annealing and extension) (**Figure 1**).

For analysis, the comparative Ct method (Schmittgen and Livak 2008) was used ( $\Delta(\Delta Ct)$ ) to normalise expression to the reference gene glyceraldehyde-3-phosphate dehydrogenase (Gapdh), and the fold-change in gene expression between experimental and control groups was calculated as  $2^{-\Delta(\Delta Ct)}$ .

## 6.5 Immunohistochemical Staining

To visualise neurons and protein expression in mouse brain slices, immunohistochemical staining was performed (Chapter 2, 3, 4). Brain slices were first washed twice for 5 minutes with 0.01M PBS and permeabilised using a 10% triton (PBS-T, Sigma, T8787) solution twice for 5 minutes (these times were increased to 10 minutes for 400  $\mu$ m slices collected after electrophysiology). Non-specific binding sites were then blocked for 2 hours (increased to 3-4 hours for post-electrophysiology slices) in a 10% normal donkey serum (Merck, S30), 2% bovine serum albumin (BSA, Sigma, A7906) in PBS-T solution. Staining using primary antibodies (**Table 2**) was performed overnight, followed by three 15 minute PBS washes, and secondary antibodies (**Table 3**) for 2-3 hours, followed by another three 15 minute washes. If tertiary antibodies (**Table 3**) were required (*i.e.* a biotin-streptavidin combination) these were applied for 1 hour, and followed by three 15 minute PBS washes. Slices were then incubated in DAPI (5  $\mu$ M 4',6-diamidino-2-phenylindole, Sigma, D9542) for 10 minutes for nuclear staining, which was washed out with four 5 minute PBS washes. Slices were then mounted onto slides in gelatine (0.1 g in 50 mL water), allowed to dry and then coverslipped with a Mowiol (10 g Mowiol (Sigma, 81381), 2.5 g DABCO (Diazabicyclo[2.2.2]octane, Sigma, D27802), 90 mL 0.01M PBS, 40 mL Glycerol) solution.

**Table 2: Primary Antibodies**

<i>Protein Target</i>	<i>Host</i>	<i>Concentration Used</i>	<i>Vendor; Catalogue #</i>
ETS Translocation Variant 1 (Etv1/Er81)	Rabbit	1:5000	Arber Lab; 1704
Green Fluorescent Protein (GFP)	Chicken	1:3000	Aves Labs; GFP-1020
Parvalbumin (PV)	Mouse	1:3000	Sigma; P3088
Parvalbumin (PV)	Goat	1:5000	SWANT; PVG-214
Choline Acetyltransferase (ChAT)	Goat	1:200	Chemicon; AB144P
Neuropeptide-Y (NPY)	Sheep	1:1000	Merck; AB1583
Vesicular Glutamate Transporter 1 (VGluT1)	Guinea-Pig	1:2000	Chemicon; AB5905
Vesicular Glutamate Transporter 2 (VGluT2)	Guinea-Pig	1:2000	Chemicon; MAB5504
Vesicular Glutamate Transporter 3 (VGluT3)	Guinea-Pig	1:2000	Merck; AB5421-I
Cre Recombinase	Guinea-Pig	1:500	Synaptic Systems; 257004
Somatostatin (SST)	Rat	1:200	Chemicon/Merck; MAB354
Caspase-3	Rabbit	1:500	Cell Signalling Technology; 9661
LIM Homeobox 6 (Lhx6)	Mouse	1:300	Santa Cruz Biotechnology; SC271433

**Table 3: Secondary and Tertiary Antibodies**

<i>Primary Antibody Host Target – Fluorescence Excitation Wavelength/Biotin</i>	<i>Host</i>	<i>Concentration Used</i>	<i>Vendor; Catalogue #</i>
Rabbit-488	Donkey	1:200	Molecular Probes; A21206
Rabbit-555	Donkey	1:200	Molecular Probes; A31572
Rabbit-Biotin	Goat	1:200	Vector Laboratories; BA-1000
Mouse-488	Donkey	1:200	Molecular Probes; A21202
Mouse-Cy3	Donkey	1:250	Jackson; 715-165-150
Mouse-Biotin	Horse	1:200	Vector Laboratories; BA-2000
Goat-405	Donkey	1:250	Abcam; AB175664
Goat-488	Donkey	1:200	Molecular Probes; A11055
Goat-555	Donkey	1:400	Molecular Probes; A21432
Goat-647	Donkey	1:200	Thermo Fisher; A21447
Goat-Biotin	Horse	1:200	Vector Laboratories; BA-9500
Chicken-488	Goat	1:400	Molecular Probes; A11039
Chicken-FITC	Donkey	1:250	Merck Millipore; AP194F
Rat-Cy2	Donkey	1:250	Jackson; 712-225-150
Rat-633	Goat	1:200	Molecular Probes; A21094
Rat-Biotin	Goat	1:200	Vector Laboratories; BA-9400
Sheep-Biotin	Donkey	1:200	Life Technology; A16045
Guinea-Pig-Biotin	Donkey	1:200	Jackson; 706-065-148
Streptavidin-Cy2	-	1:200	Jackson; 012-220-084
Streptavidin-555	-	1:200	Molecular Probes; 521381
Streptavidin-647	-	1:200	Jackson; 012-600-084

## 6.6 Image Acquisition and Analysis

Following immunohistochemical staining, images of stained brain slices were captured and analysed to visualise structures, neurons, and protein expression (Chapter 2, 3, 4).

### 6.6.1 Image Capture

Images were captured on a Nikon A1 Confocal, using Nikon Instruments Elements software. Images were captured at a resolution of 1024 x 1024 pixels, with a 2x line average. Factors such as pinhole aperture, laser power, gain, and offset were kept consistent throughout the imaging of a single dataset and multiple channels were always imaged in series. Images were either captured on a single plane or as a z-stack of images: for bouton and morphology reconstruction, stacks were taken 1  $\mu\text{m}$  apart across the entire neuron, for Er81 expression in the striatum, stacks were taken of 3 images 2  $\mu\text{m}$  apart. Large images of the whole striatum were generated via Nikon Instruments image stitching, with 10% overlap and stitching via blending. Images were analysed using either Fiji/ImageJ or IMARIS (Oxford Instruments).

### 6.6.2 Striatal Area

Striatal area in the *Cntnap2;Lhx6-iCre;TdTomato* mouse model of ASD compared to *Lhx6-iCre;TdTomato* controls (Chapter 5) was measured to test brain size across developmental stages. This was determined by tracing the outline of the striatum from rostro-caudally matched images, taken at low magnification to visualise the entire striatum, at P0, 4, 6, and 10. The traced shape was confirmed by the striatal outline shown in the Allen Brain Atlas ([atlas.brain-map.org](http://atlas.brain-map.org)). These values were averaged over the striata from both hemispheres at similar rostro-caudal positions within each animal.

### 6.6.3 Cell Counting

Cell number was determined via various methods, dependent on the nature of the structure being analysed and the marker used to identify cells. Cholinergic interneurons (CINs), which were sparsely present, were counted using a threshold based particle analysis in Fiji/ImageJ (Chapter 3; *ChAT-Cre;RCE* and *Er81<sup>fl/fl</sup>;ChAT-Cre;RCE*). Briefly, ChAT-Cre dependent GFP expression localised to CINs was separated by applying a binary threshold. To this, the ‘Analyse Particles’ tool identified cells and automatically counted them. Lhx6-Cre dependent TdTomato+ cells in the adult striatum were counted manually, using the ‘Count’ tool in Fiji/ImageJ and their density extrapolated (Chapter 3; *Lhx6-iCre;TdTomato* and *Er81<sup>fl/fl</sup>;Lhx6-iCre;TdTomato*).

Pet-Cre dependent GFP expressing cells in the Dorsal Raphe Nucleus (DRN) were also manually counted (Chapter 4; *Pet-Cre;RCE* and *Er81<sup>fl/fl</sup>;Pet-Cre;RCE*), due to the high density of cells. The number of cells was quantified across three rostro-caudal bregma points, based on anatomical characteristics identified from the Allen Brain Atlas ([atlas.brain-map.org](http://atlas.brain-map.org)) and Paxinos Mouse Brain Atlas (Paxinos and Franklin 2001).

Lhx6-Cre dependent TdTomato+ cells were counted across developmental stages (Chapter 4; *Lhx6-iCre;TdTomato* and *Cntnap2<sup>-/-</sup>;Lhx6-iCre;TdTomato*) using an automated macro<sup>10</sup>, as described in Ahmed et al. (2023) (see Appendix C). Caspase-3 expressing cells in the striatum were visually identified and manually counted using the ‘Count’ tool in Fiji/ImageJ (Chapter 4; *Lhx6-iCre;TdTomato* and *Cntnap2<sup>-/-</sup>;Lhx6-iCre;TdTomato*).

## 6.6.4 Analysis of Protein Expression

### 6.6.4.1 Er81 Expression

Images for Er81 protein analysis were taken at 40x or 60x magnification. Protein expression analysis was done using a Fiji/ImageJ macro written specifically for this analysis (Appendix F). Briefly, thresholding was performed on the cell marker channel (*i.e.* GFP, TdTomato), and the expression of Er81 measured within cells identified upon masking and particle analysis. Nuclear versus cytoplasmic expression was determined via a secondary threshold and mask upon the DAPI channel. Er81 expression was normalised to background fluorescence (Er81 expression divided by background fluorescence), which was taken as the average of three regions determined to have no cells present. Relative expression was compared for a clearly positive, low positive, and negative cell to determine the positive-negative threshold value, which was relative for each dataset (threshold = 2.3 in Chapter 2, 1.5 in Chapter 3).

### 6.6.4.2 Other Protein Analyses

The analysis of Choline Acetyltransferase (ChAT) and Lhx6 protein expression (Chapter 4; *Lhx6-iCre;TdTomato* and *Cntnap2<sup>-/-</sup>;Lhx6-iCre;TdTomato*) was completed semi-manually. Lhx6-TdTomato cells expressing ChAT were masked on the TdTomato channel, and the expression levels of ChAT within each cell, relative to background, was determined. This was done similarly for Lhx6 protein expression. ChAT cells not expressing TdTomato were identified and masked on the ChAT channel and ChAT expression measured relative to the background.

---

<sup>10</sup> Fiji/ImageJ macro written by Rhys Knowles

### 6.6.5 Morphological Reconstructions

To determine neuronal morphological characteristics, neurons were visualised and imaged as described above (section 6.1.3, 6.1.4, 6.5, 6.6.1). Striatal CINs were identified by their expression of ChAT. Striatal SPNs were identified by their spiny morphology, as opposed to the aspiny, less common interneurons.

Morphological quantification was done using the Surface and Filament tools in the IMARIS software (**Figure 2**). Reconstruction of the neuronal dendritic field was either done with the automatic component of the filament tool with the dendrite beginning point set to 15  $\mu\text{m}$  and the end point set to 1  $\mu\text{m}$ , or with the autopath and autodepth tools to semi-manually trace the dendrites. Following a semi-manual reconstruction (**Figure 2A<sub>2</sub>**), the dendrite volume was computed surrounding the path of manual reconstruction (**Figure 2B<sub>2</sub>**). Measures such as the dendrite length, number of branch points (**Figure 2A<sub>3</sub>**), and Sholl analysis were saved at this point. The volume of dendritic spread was found by using the Convex Hull Xtension of IMARIS (**Figure 2A<sub>4</sub>**). A reconstruction of the neuron soma was then generated using the Surface tool with 0.5 surface detailing (**Figure 2B<sub>2</sub>**), following which, the parts of the dendrite filament contained within the soma surface were deleted so that the volume of the dendrite filament and soma surface could be measured accurately.



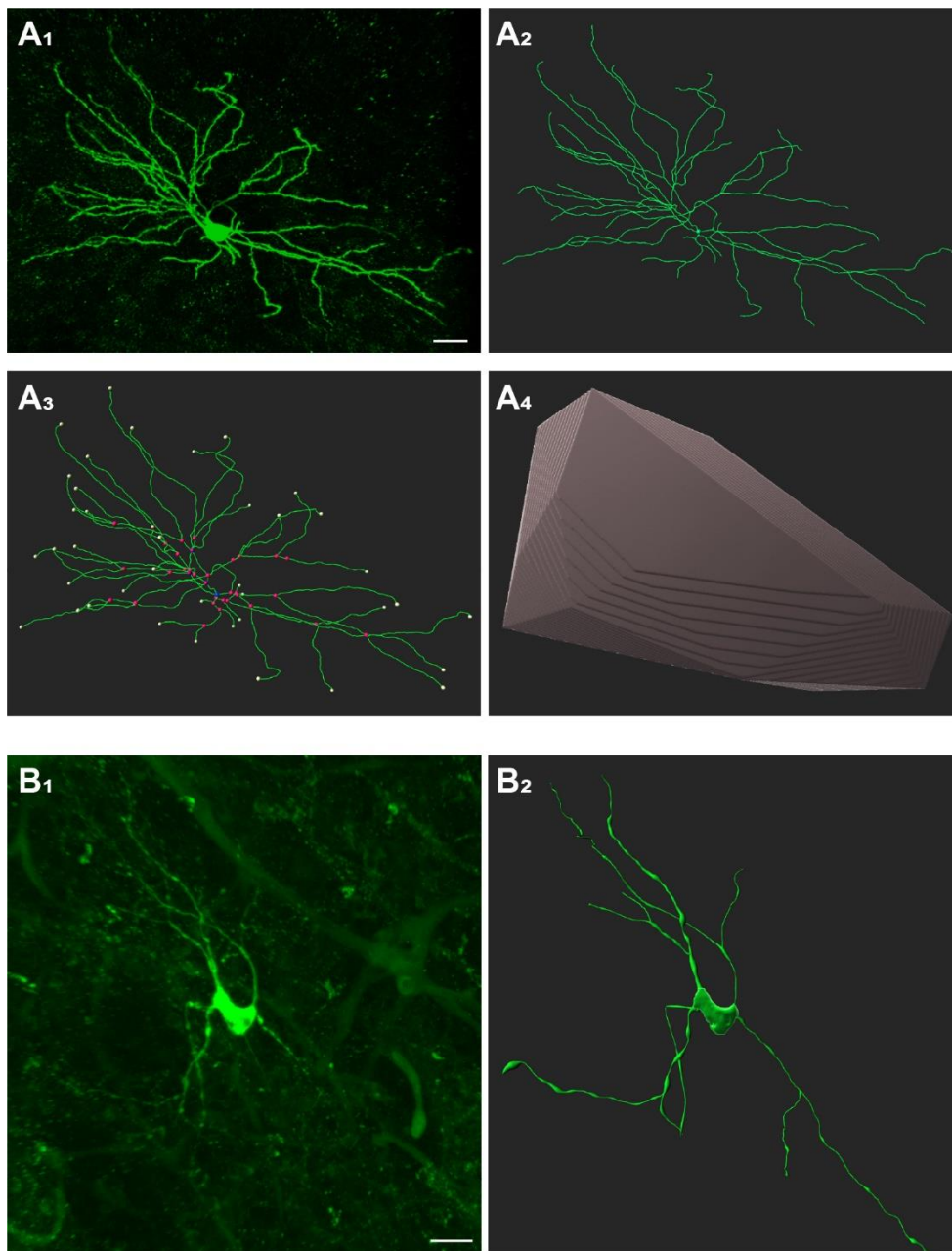


### Figure 2: Morphological Reconstruction of Neurons

Two examples of neuron morphology reconstruction using IMARIS software. **A1.** An example of the raw image of a virally labelled SPN for reconstruction (see section 2.1.4), scale: 20  $\mu\text{m}$ . **A2.** The direct tracing of the dendritic field of the neuron in A1. **A3.** Dendrite start point (blue), branch points (pink), and terminal points (white) mapped onto the dendritic trace. **A4.** A convex hull surface covering the dendritic field, representing the volume of dendritic spread. **B1.** An example of the raw image of a striatal interneuron at P6 for reconstruction, scale: 20  $\mu\text{m}$ . **B2.** Reconstructed dendritic field and soma surface, with dendrite diameter reconstruction.

### 6.6.6 Neuropil

Neuropil density analysis was done to quantify the axonal field of CINs (Chapter 2; *ChAT-Cre;RCE* and *Er81<sup>fl/fl</sup>;ChAT-Cre;RCE*) and serotonergic Pet-positive (Pet+) neurons (Chapter 3; *Pet-Cre;RCE* and *Er81<sup>fl/fl</sup>;Pet-Cre;RCE*) in the striatum, as single axon reconstruction was not possible. Analysis was done on images not containing any neurons or obvious dendrites. The percentage of total analysable area in the image occupied by neuropil stained with the appropriate marker (ChAT-GFP or Pet-GFP) was determined automatically via a Fiji/ImageJ macro written specifically for this analysis (**Figure 3**; Appendix F).

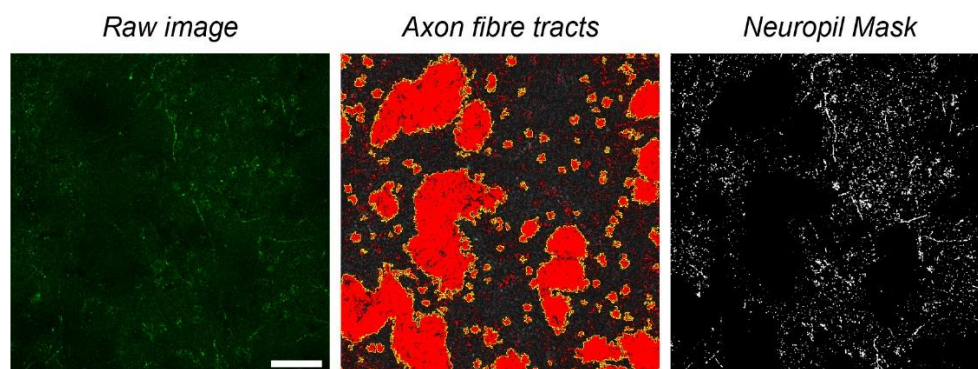


**Figure 3: Analysis of Neuropil**

Left: Raw image example of neuropil (*Pet-cre;RCE-GFP*) in the striatum, scale: 50  $\mu\text{m}$ . Middle: masking of striatal axon fibre tracts to remove from analysis area. Right: final mask of neuropil, the area of this mask was taken as a percentage of the total analysable area as the measure of neuropil.

### 6.6.7 Bouton Analysis

Physical inputs to neurons were visualised in *Er81* conditional mutants and controls (Chapter 2; *ChAT-Cre;RCE* and *Er81<sup>fl/fl</sup>;ChAT-Cre;RCE*; *Lhx6-iCre;TdTomato* and *Er81<sup>fl/fl</sup>;Lhx6-iCre;TdTomato*) as axonal boutons, the aggregation of presynaptic markers contacting the dendrites or soma of the post-synaptic cell. Bouton analysis was done using the Surface and Spots tools in IMARIS (**Figure 4**). The neuron soma or dendrite were reconstructed using the surface tool with 0.5 surface detailing, and the surface area measure recorded. Boutons were identified and quantified depending on the marker used, as the expression pattern and strength of the markers were different, meaning common analysis parameters could not be used across all bouton subtypes. A co-localisation channel was created to identify individual boutons labelled with vesicular glutamate transporters (VGluT1, 2, 3); this channel was then passed by a threshold to filter weak co-localisations. The brightest 30% of co-localised particles

(determined as the threshold accurately representing stained particles) were selected as boutons. For other labels (PV, NPY, ChAT), the brightest 15-30% particles were selected as boutons. Spots further than 1.5  $\mu\text{m}$  away from the neuron surface were excluded, as boutons are typically 0.5-1  $\mu\text{m}$  in diameter. Bouton density was calculated as the number of boutons divided by the surface area of the soma.

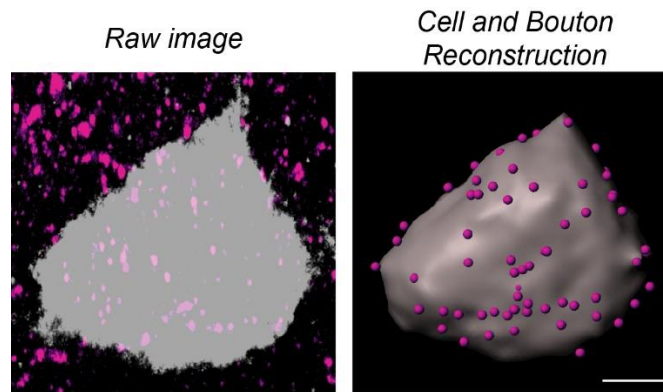


**Figure 4: Axonal Bouton Reconstruction**

Left: Raw image (maximum intensity projection of a z-stack) depicting a labelled neuron (CIN, grey) and stained axonal boutons (PV, magenta). Right: 3D IMARIS reconstruction of cell surface and boutons, scale: 5  $\mu\text{m}$ . Adapted from Ahmed et al. (2021).

## 6.7 Electrophysiology Recordings

To determine the functional electrophysiological properties of neurons whole cell patch-clamp recordings were performed in various configurations (Chapter 2: *ChAT-Cre;RCE* and *Er81<sup>fl/fl</sup>;ChAT-Cre;RCE*; *Lhx6-iCre;TdTomato* and *Er81<sup>fl/fl</sup>;Lhx6-iCre;TdTomato*; Chapter 3: *Pet-Cre;RCE* and *Er81<sup>fl/fl</sup>;Pet-Cre;RCE*; Chapter 4: *Lhx6-iCre;TdTomato* and *Cntnap2<sup>-/-</sup>;Lhx6-iCre;TdTomato*). Both young (P6-18) and adult (P30+) mice were anaesthetised under isoflurane and then perfused with an ice-cold (0-4°C), oxygenated sucrose based cutting solution (containing (in mM): 70 sucrose, 86 NaCl, 4 KCl, 1 CaCl<sub>2</sub>, 7 MgCl<sub>2</sub>, 1 NaH<sub>2</sub>PO<sub>4</sub>, 26 NaHCO<sub>3</sub>, and 25 glucose, saturated with 95% O<sub>2</sub> and 5% CO<sub>2</sub>). The brain was removed and placed into the same solution (sucrose cutting solution maintained at 0-4°C), and 400 µm coronal slices were cut using a Leica VT1200S vibratome. Slices were maintained at room temperature in an artificial cerebrospinal fluid (ACSF) solution (containing (in mM): 127 NaCl, 2.5 KCl, 2 CaCl<sub>2</sub>, 1.298 MgSO<sub>4</sub>.7H, 0.625 NaH<sub>2</sub>PO<sub>4</sub>, 26 NaHCO<sub>3</sub> and 13 glucose saturated with 95% O<sub>2</sub> and 5% CO<sub>2</sub>) for at least 30 minutes for recovery. Slices containing fluorescent markers such as GFP or TdTomato were kept in the dark to preserve fluorescence.

Slices were transferred to a chamber with flowing ACSF saturated with 95% O<sub>2</sub> and 5% CO<sub>2</sub> at 34-35°C. Micropipettes for recording electrodes were pulled from Borosilicate capillary tubes (100 mm, outer diameter 1.5 mm, filament 0.84, World Precision Instruments, 1B150F-4) with a Narishige PC-10 pipette puller (4-7 MΩ final pipette resistance). Cells of interest were located using fluorescence and/or morphological characteristics. A pipette containing either a potassium-gluconate (containing (in mM): 120 K-gluconate (C<sub>6</sub>H<sub>11</sub>KO<sub>7</sub>), 5 KCl, 10 HEPES, 10 di-tris-Phosphocreatine, 4 MgCl<sub>2</sub>, 4 Na<sub>2</sub>-ATP, 0.4 Na-GTP) or caesium-gluconate (containing (in mM): 130 Cs-gluconate (prepared from D-Gluconic acid and Caesium Hydroxide), 13 CsCl, 0.1 CaCl<sub>2</sub>, 10 HEPES, 1 ethylene glycol N-N tetra acetic acid (EGTA)) solution was lowered to the slice and the target cell. If cell labelling for post-hoc analysis was required, the internal solution also contained neurobiotin (1 mg/mL, Vector Laboratories, SP-1120).

Recordings were performed using an Axon Instruments 700B amplifier with a 10 kHz low-pass filter, a HEKA LIH-8+8 digitiser with a sampling rate of 20 kHz, and the WinWCP software (Dr John Dempster, University of Strathclyde, Scotland). During the process of gaining access to a cell, a 10 mV test pulse was applied to the pipette in voltage clamp configuration to monitor pipette resistance. Outward pressure was applied to the pipette whilst in the bath and descending to avoid blockage. The pipette was considered close enough to the target cell when pipette resistance increased and/or a dimple was visible in the cell surface. The pressure in the pipette

was released to form a strong seal with the cell membrane ( $\geq 1000 \text{ M}\Omega$  in resistance). The cell membrane attached to the pipette was then broken with sharp inward pressure. Access resistance was monitored throughout the recording.

### **6.7.1 Current Clamp Recordings**

Current clamp recordings were performed to record intrinsic properties and action potential (AP) kinetics (Chapter 2, 3, 4). Resting membrane potential (RMP,  $V_{\text{rest}}$ ) was recorded when the cell was given no holding current input (0 pA). Spontaneous/tonic firing was recorded at this point as well. All other recordings were performed with the cell held at -60 mV (cholinergic interneurons) or -70 mV (parvalbumin interneurons, serotonergic interneurons). Incremental current steps, beginning from a hyperpolarising pulse (generally beginning at -50 pA, with a 25 pA incremental step), were applied to elicit APs and halted once the depolarisation firing block was reached. Cells that were not spontaneously active were also stimulated with 1 pA steps close to threshold to determine the rheobase (the smallest amount of current required to elicit an AP response in a cell). Some cell types were also stimulated with a current ramp (0-250 pA), as another measure of the rheobase.

### **6.7.2 Voltage Clamp Recordings**

Voltage clamp recordings to record spontaneous post-synaptic currents were performed in all cells (Chapter 2, 3, 4). Cells were held at -60 mV (the chloride reversal potential, calculated from internal and external solution concentrations via Nernst equation) to record excitatory post synaptic glutamatergic currents (EPSCs), then held at -80 - -90 mV to record both glutamatergic and inhibitory GABA-ergic currents (IPSCs). To then separate excitatory and inhibitory currents, the cell was held at -30 mV for inward EPSCs and outward IPSCs.

To record specific receptor mediated post-synaptic currents (Chapter 4), receptor blockers were applied in a specific sequence whilst recording with a caesium-gluconate internal to block potassium channels and produce more stable recordings. AMPA ( $\alpha$ -amino-3-hydroxy-5-methyl-4-isoxazolepropionic acid)/Kainate receptor mediated glutamatergic currents were recorded at a holding potential of -70 mV, after which 10  $\mu\text{M}$  NBQX (2,3-dioxo-6-nitro-7-sulfamoyl-benzo[f]quinoxaline, a blocker of AMPA receptors, Abcam, AB120046) was applied. The cell was then held at +10 mV to record GABA<sub>A</sub> receptor mediated IPSCs under NBQX, following which 10  $\mu\text{M}$  Gabazine (GABA receptor blocker, Abcam, AB120042) was applied. The cell was finally held at +40 mV with 10  $\mu\text{M}$  4-AP (4-Aminopyridine, blocker of

Kv1 channels, Sigma) also applied to record NMDA (N-methyl-D-aspartate) receptor mediated glutamatergic currents. Currents were recorded for three minutes at each holding potential.

### 6.7.3 Simultaneous Paired Recordings

To determine whether two cells were connected, dual patch simultaneous recordings were performed (Chapter 2; *Lhx6-iCre;TdTomato* and *Er81<sup>fl/fl</sup>;Lhx6-iCre;TdTomato*). Protocols were first run to obtain voltage clamp and current clamp recordings from individual cells for intrinsic property analysis, followed by stimulations applied to one cell whilst responses were recorded in the other cell. Briefly, one cell in the pair was kept in current-clamp mode to elicit an action potential (AP) response with a depolarising current step, either to evoke a train of APs or a single AP (**Figure 5**). The other cell was held in voltage clamp at either -60 mV (for glutamatergic current responses), -80 mV (both glutamatergic and GABAergic current responses), or -30 mV (separation of glutamatergic and GABAergic current responses) to simultaneously record currents evoked by the activation of the other cell (**Figure 5**). Cells were recorded in both configurations to determine bi-directional connectivity. Pairs being tested for gap-junction connectivity were recorded with both cells in current-clamp mode, and a strong hyperpolarising current pulse (-200 pA) was applied to each cell, whilst recording any hyperpolarisation response in the other cell (**Figure 5**) (Galarreta and Hestrin 2001, Yang et al. 2014).

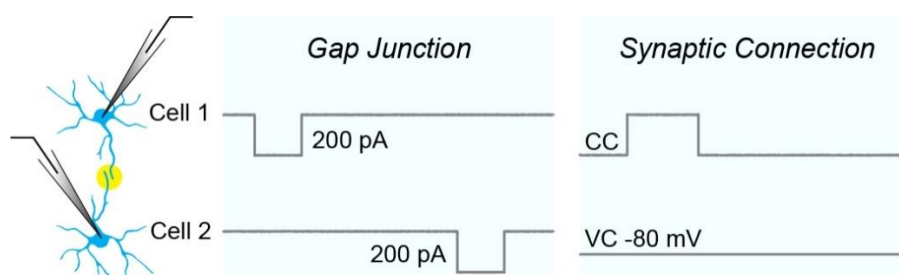


**Figure 5: General Dual Patch Stimulus Protocols**

Connectivity between neurons was tested to be either gap junction mediated or synaptically mediated. Gap junction connectivity protocols maintained both cells in current clamp mode, stimulating both in succession. Synaptic connectivity protocols maintained one cell in current clamp mode (CC) and the other in voltage clamp mode (VC) with a holding potential of -80 mV, -60 mV, or -30 mV.

#### **6.7.4 Dye Loading**

Dye loading to label surrounding cells connected via gap junctions (Chapter 2; *Lhx6-iCre;TdTomato* and *Er81<sup>fl/fl</sup>;Lhx6-iCre;TdTomato*) was done as in Yang et al. (2014). A single cell was patched under potassium-gluconate internal solution containing neurobiotin, and intrinsic property recordings were performed. Following this, the cell was held in current clamp at -60 to -70 mV whilst subthreshold 100 ms depolarising rectangular pulses at 4 Hz were applied for 10 minutes to electrically facilitate dye diffusion. The cell was then held in voltage-clamp at -70 mV for 20-30 minutes. The pipette was then removed from the cell. A second cell was patched and loaded in the contralateral hemisphere (one cell per striatum hemisphere). After leaving the second cell, the slice was allowed to remain in the perfusion chamber for a further 30 for further dye diffusion. With this method, the two patched cells per slice do indeed experience different diffusion times, however Yang et al. (2014) does state that increased diffusion time at this stage did not affect dye loading. For analysis, loaded cells were counted following post-hoc staining of neurobiotin expression.

#### **6.7.5 Slice Fixation for Immunostaining**

Slices required for post-hoc staining were marked with a small cut in the left or right cortex to determine the orientation of the slice (*i.e.* which side of the slice was recorded from). Slices were then placed in 4% PFA and kept gently shaking overnight to allow for fixation, after which they were washed in PBS three times for 30 minutes. Slices were then cryopreserved in 30% sucrose in PBS for staining at a later date; briefly, slices were placed in 30% sucrose in a tube, allowed to sink to the bottom of the tube (either over the course of 1-4 hours or overnight), before being flash-frozen in dry ice and stored at -80°C.

### **6.8 Electrophysiology analysis**

All electrophysiology analysis was either completed in WinWCP or Easy Electrophysiology (RRID:SCR\_021190).

#### **6.8.1 Cell Characteristics and Passive Membrane Properties**

The resting membrane potential (RMP) of cells was determined using the baseline measurement in Easy Electrophysiology. The input resistance and capacitance were measured from hyperpolarising current steps. The input resistance tool in Easy Electrophysiology was used to determine the  $V_m$  and  $I_m$  change across negative current inputs (-50 pA and -25 pA), and the input resistance calculated as either the slope of a linear ordinary least squares fit if more than

one record was analysed, or as  $V/I$  if only one record was analysed. This was kept consistent within datasets. The sag ratio was also measured; calculated as the sag amplitude (the difference between the negative peak and the steady state hyperpolarised response) divided by the total pulse amplitude. To calculate capacitance, a tau value was calculated from a hyperpolarising (-50 pA) pulse using an exponential decay fit; the capacitance was calculated as tau divided by the input resistance (McGuirt et al. 2021).

### **6.8.2 Action Potential Characteristics**

Action potential (AP) counting was done using the Action Potential Counting analysis tool in Easy Electrophysiology. This detected APs based on the spike amplitude, first derivative of the rise and repolarisation of the AP, and the width of the spike. Spikes not detected were manually added, and additional events detected that were clearly not APs were manually removed. The number of spontaneous APs occurring at RMP and the number of APs across depolarising current pulses was measured to calculate the spontaneous and evoked firing rates. Characteristics such as the rheobase (the smallest current at which an AP occurs) and latency to the first spike were measured within the AP Counting tool. Similarly, spike adaptation was measured using the Spike Frequency Accommodation (SFA) option within the AP Counting tool. This was done using the divisor method, where the first inter-spike interval (ISI) is divided by the final ISI in the evoked spike train to generate an adaptation index. To determine the regularity of tonic/spontaneous firing, the coefficient of variation was calculated by dividing the standard deviation of all ISIs by the mean ISI.

AP kinetics were calculated in Easy Electrophysiology with the Action Potential Kinetics analysis tool. Spikes were automatically detected and then manually checked for consistency of the placement of the measurement points (**Figure 6**). Measurements were automatically calculated for each AP and averaged across each cell.



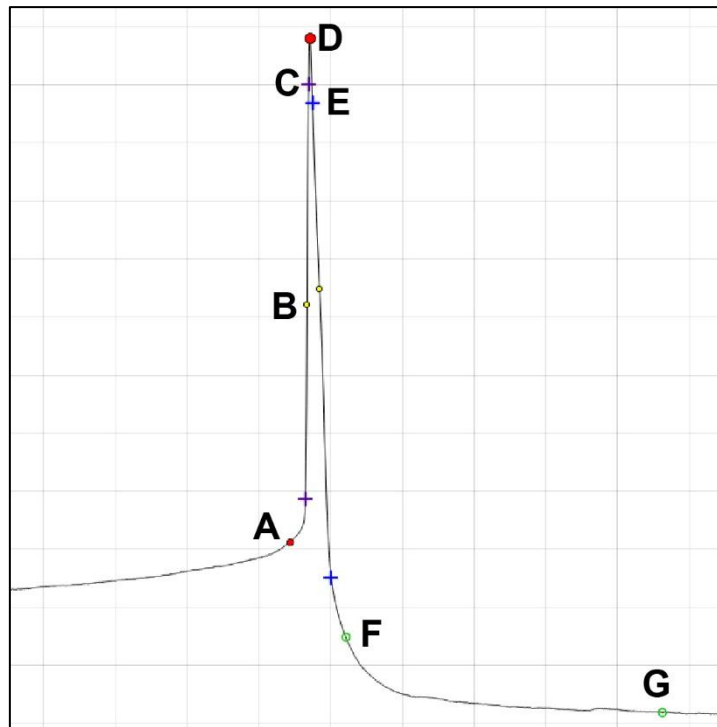


**Figure 6: Action potential kinetics measurements.**

**A.** Threshold, detected as the point of greatest inflection (mV). **B.** Half-width (ms). **C.** Rise time, 10-90% of the AP amplitude, purple crosses (ms). **D.** Peak (mV). **E.** Decay time, blue crosses (ms). **F.** Fast and **G.** medium afterhyperpolarisation (mV). Adapted from the Easy Electrophysiology User Manual.

### 6.8.3 Spontaneous Post-Synaptic Current Analysis

Currents (Chapter 3 & 4) were analysed with the event detection tool in Easy Electrophysiology with detection via thresholding. Currents greater than 1.5 times the background were detected and were filtered manually for correct kinetics (*i.e.* correct rise and decay properties based on the shape of the event, **Figure 7**).

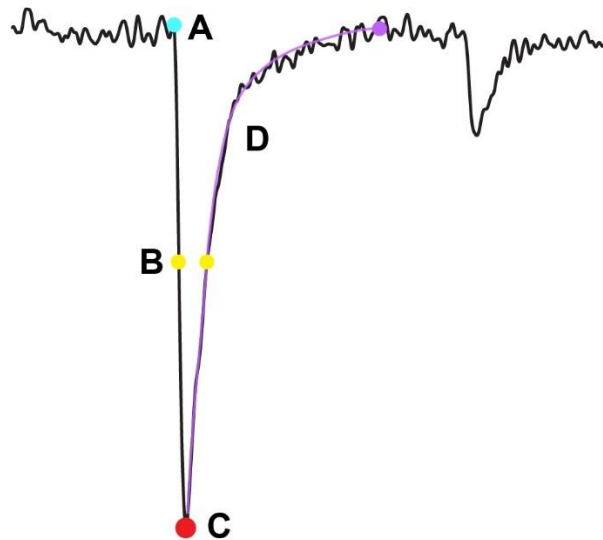


**Figure 7: Current kinetics measurements.**

**A.** Baseline (pA). **B.** Half-width (ms). **C.** Peak (pA). **D.** Decay fit, with decay endpoint (pA). Rise slope and time were calculated as 10-90% from baseline to peak. Adapted from the Easy Electrophysiology User Manual.

### 6.8.4 Synaptic Connectivity

Paired recordings (Chapter 2) were evaluated using the curve fitting tool in Easy Electrophysiology. Current responses in the post-synaptic cell within a 10 ms window following the onset of the AP in the pre-synaptic cell were considered a true connected response. The success rate was recorded as the proportion of trials eliciting a current response. The response amplitude was measured as the amplitude of the current response relative to baseline preceding the stimulus.

### 6.8.5 Gap Junction Connectivity

Cells connected by gap junctions (Chapter 2) were determined by the detection of a hyperpolarising response in one cell to a -200 pA stimulus in the other cell. This was visually assessed. Once cells were considered to be gap junction connected, the coupling coefficient was

determined as the amplitude of the gap junction mediated response divided by the amplitude of the cell's response to the -200 pA stimulus.

### **6.8.6 SPA-like and GDP-like Activity (P5-7 only)**

Single cell activity recapitulating characteristics of development spontaneous network events were analysed to extrapolate characteristics of the developing striatal circuitry (Chapter 2). Synchronous plateau assemblies (SPA)-like calcium plateaus were identified as consistent shifts in membrane potential, that could result in AP trains. SPA-like event frequency (*i.e.* the number of events across the recording), duration (the average duration of SPA-like events), and amplitude (the average amplitude of SPA-like events) was measured. Spike frequency was analysed in SPA-like events containing spike trains. Global depolarising potential (GDP)-like events were classified as regularly occurring, large depolarising potentials approximately 800 ms in duration, 1-2 s apart. These were distinguished from tonically firing cells by the characteristics of the depolarisation (non-AP characteristics, *i.e.* no threshold or hyperpolarisation) GDP-like event frequency and amplitude were analysed.

## **6.9 Behavioural Tests**

To determine behavioural alterations in the novel *Er81<sup>fl/fl</sup>;Pet-Cre;RCE* strain, compared to *Pet-Cre;RCE* controls (Chapter 3), several behavioural assays were performed on male and female adult mice (P50+). Tests were performed in the order listed below, and mice were sex separated at analysis stages.

### **6.9.1 Open Field Recordings**

Open field recordings were conducted in a circular arena (39 cm in diameter). Mice were habituated in the room with the open field at low light for 1 hour, then placed into the arena and recorded for 5 minutes from above as they freely roamed. The arena was cleaned with 70% ethanol between mice. Tracking analysis to determine parameters such as distance travelled and thigmotaxis (propensity to remain near the outer edge of the arena) was done via a MATLAB (Mathworks) code (Zhang et al. 2020) modified for this specific open field arena<sup>11</sup>. Briefly, the code masks the position of the mouse based on its binary contrast to the background arena. Distance was calculated by measuring the difference in the mask centroid position between each frame (Euclidean distance), then summated for the entire recording. Thigmotaxis was calculated by the ratio of time spent within the periphery of the arena compared to the centre,

---

<sup>11</sup> MATLAB code modified by Rebekah Parkinson.

which was defined as an inner circle 5 cm away from the circumference (Seibenhener and Wooten 2015).

### **6.9.2 Light-Dark Box Test**

Light-dark box tests (Bourin and Hascoet 2003) were performed in Imetronic Fear Cages (France). The dark box was in near darkness, and the light box was exposed to 400 lux light. Mice were placed into the dark box, with the door closed. The door was then opened, and the mouse allowed to roam freely between the rooms for 5 minutes. After the mouse completed the task and was removed from the chamber, the chamber was cleaned with a Virkon solution to remove excrement and odour cues. Time spent in each chamber within the 5 minutes was measured from videos or live whilst the mice were completing the task.

### **6.9.3 DigiGait™ Gait Analysis<sup>12</sup>**

The measurement of mouse gait kinematics was performed via the DigiGait™ system (Mouse Specifics Inc.). Mice were placed on the DigiGait™ treadmill and allowed to run for 1 minute at a speed of 20 cm/s (as in Akula et al. (2020), for testing forced gait), whilst video recordings from the underside of the mouse were acquired via the DigiGait imaging software. Videos were processed on the system's automated software to generate several gait parameters based off the orientation and motion of each paw detected. Fine paw measurements were recorded, including paw angle (the angle between the centre of the paw and the axis of the direction in which the paw was moving) and overlap distance (the distance between the ipsilateral forelimb and hindlimb paws). The ability of the mouse to propel or brake was quantified as the duration (s) of the total stride and the percentage of the stride during which the paw was in contact with the belt. Limb drag was also used as a more specific propulsion metric; this was the mean of the slope between the time of full stance and the point when the paw lifts off the belt.

### **6.10 Statistical Analysis**

Statistical analysis was tailored for each dataset. Datasets were tested for outliers using the ROUT method in GraphPad Prism (Motulsky and Brown 2006), and any confirmed outliers discarded. All datasets were tested for normal Gaussian distribution using the Shapiro-Wilk normality test in Prism. Datasets where both comparable groups passed the normality test were treated with parametric tests; datasets where one or both groups failed the test were treated with non-parametric tests. For single variables with numerical data compared between two groups

---

<sup>12</sup> DigiGait tests were performed in collaboration with Rebekah Parkinson and analysed in full by Rebekah Parkinson.

(*i.e.* control versus knockout, with  $n$  values in each) a parametric Student's t-test or non-parametric Mann-Whitney test was used. For datasets with three or more groups for comparison, a one-way ANOVA was used. If a second variable was present (*e.g.* distance, region), with numerical data still compared between two groups, a two-way ANOVA was used. Post-hoc multiple comparisons were done with Bonferroni correction. Where categorical measures were being compared with another set of categorical measures (*e.g.* number of connected neurons versus unconnected neurons in control and knockout), the Chi-Square ( $\chi^2$ ) test was used. Significance was determined below an  $\alpha$  value of 0.05. The statistical test performed is assumed to be a Student's t-test unless otherwise listed in figure legends. Statistical significance is denoted as: \*:  $p < 0.05$ , \*\*:  $p < 0.01$ , \*\*\*:  $p < 0.001$ .

## Appendices

### Appendix A: Literature Review (Ahmed et al. 2019)

Literature Review published in Frontiers in Molecular Neuroscience

**N. Y. Ahmed**, R. Knowles and N. Dehorter (2019). "New Insights Into Cholinergic Neuron Diversity." *Front Mol Neurosci* 12: 204.



# New Insights Into Cholinergic Neuron Diversity

Noorya Yasmin Ahmed, Rhys Knowles and Nathalie Dehorter\*

*Eccles Institute of Neuroscience, John Curtin School of Medical Research, Australian National University, Canberra, ACT, Australia*

Cholinergic neurons comprise a small population of cells in the striatum but have fundamental roles in fine tuning brain function, and in the etiology of neurological and psychiatric disorders such as Parkinson's disease (PD) or schizophrenia. The process of developmental cell specification underlying neuronal identity and function is an area of great current interest. There has been significant progress in identifying the developmental origins, commonalities in molecular markers, and physiological properties of the cholinergic neurons. Currently, we are aware of a number of key factors that promote cholinergic fate during development. However, the extent of cholinergic cell diversity is still largely underestimated. New insights into the biological basis of their specification indicate that cholinergic neurons may be far more diverse than previously thought. This review article, highlights the physiological features and the synaptic properties that segregate cholinergic cell subtypes. It provides an accurate picture of cholinergic cell diversity underlying their organization and function in neuronal networks. This review article, also discusses current challenges in deciphering the logic of the cholinergic cell heterogeneity that plays a fundamental role in the control of neural processes in health and disease.

**Keywords:** interneurons, acetylcholine, diversity, striatum, development

## OPEN ACCESS

### Edited by:

Christopher Alan Reid,  
Florey Institute of Neuroscience and  
Mental Health,  
Australia

### Reviewed by:

Allan T. Gullledge,  
Dartmouth College, United States  
Juan Mena-Segovia,  
Rutgers University, The State  
University of New Jersey,  
United States

### \*Correspondence:

Nathalie Dehorter  
nathalie.dehorter@anu.edu.au

**Received:** 19 May 2019

**Accepted:** 05 August 2019

**Published:** 27 August 2019

### Citation:

Ahmed NY, Knowles R and  
Dehorter N (2019) New Insights Into  
Cholinergic Neuron Diversity.  
*Front. Mol. Neurosci.* 12:204.  
doi: 10.3389/fnmol.2019.00204

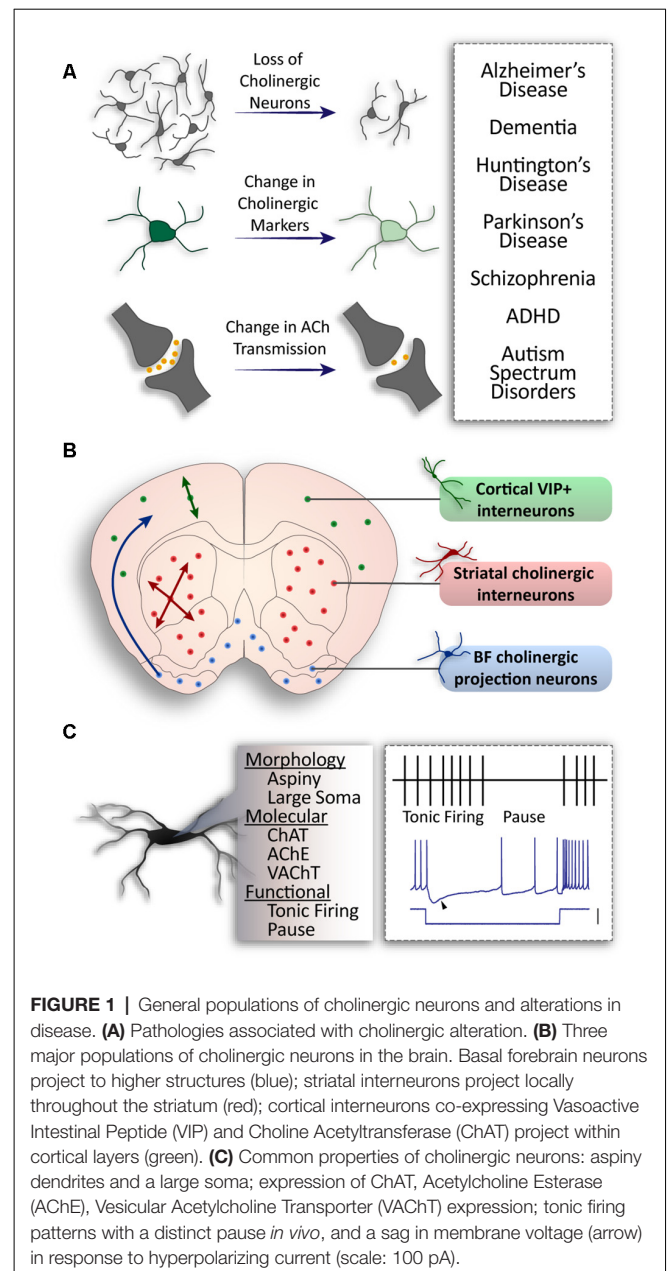
## INTRODUCTION

Cholinergic neurons are highly integral for fine tuning brain function (for review, see Bonsi et al., 2011) and maintaining the excitation-inhibition balance within neural circuits (Zhou et al., 2017). Although cholinergic neurons are distributed in various discrete regions, they can project to almost all parts of the brain (Dautan et al., 2016). These cells release acetylcholine (ACh), which plays a crucial role in the regulation of sensory function (Minces et al., 2017; for review, see Ballinger et al., 2016), and actions (Bradfield et al., 2013; Markowitz et al., 2018). ACh also attunes motivation (Marche et al., 2017), behavioral flexibility (Aoki et al., 2015, 2018; Okada et al., 2018), and associative learning (Atallah et al., 2014; for review, see Yamanaka et al., 2018). A major population is found in the striatum, which contains the highest levels of ACh in the brain (Macintosh, 1941; for review, see Lim et al., 2014). Cholinergic neurons are also found in the basal forebrain, which is classically segregated into four main regions: the Medial Septal Nucleus (MSN), the vertical and horizontal limbs of the Diagonal Band of Broca (DB), and the Nucleus Basalis (NB) of Meynert. Within the brainstem, cholinergic neurons are found in the

pedunculopontine nucleus (PPN) and the laterodorsal tegmentum (for review, see Mesulam et al., 1983). In addition to these groups, smaller cholinergic populations are located in the medial habenula (López et al., 2019), parabigeminal nucleus (Mufson et al., 1986), cerebral cortex (von Engelhardt et al., 2007), hypothalamus (Jeong et al., 2016), and olfactory bulb (Krosnowski et al., 2012).

It has been shown that changes in the activity of striatal cholinergic interneurons (CINs) play a critical role in motor control (Bordia et al., 2016), as well as behavioral flexibility (Okada et al., 2014), memory (Albert-Gascó et al., 2017), and social behavior (Martos et al., 2017). Alterations to the cholinergic system can lead to severe dysfunction of neuronal circuits (Figure 1A). For example, cholinergic neuron loss from the forebrain causes cognitive deficits associated with Parkinson's (PD; for review, see Pepeu and Grazia Giovannini, 2017) and Alzheimer's Disease (AD; for review, see Hampel et al., 2018). In the striatum, a decrease in cholinergic markers is a phenotypic consequence of Parkinson's (Maurice et al., 2015; Ztaou et al., 2016) and Huntington's diseases (HD; Smith et al., 2006). Cholinergic neuron populations are also linked to neuropsychiatric and neurodevelopmental pathologies. For instance, the activity of CINs through the expression and function of the hyperpolarization-activated cyclic nucleotide-gated channel 2 (HCN2) is decreased in the Nucleus Accumbens (NAc) in stress and depression (Cheng et al., 2019). There is also an established link between the cholinergic system and autism spectrum disorders, whereby autism is associated with decreased cholinergic tone and reduced neurite arborization (Nagy et al., 2017). Genetic alterations of the choline transporter cause attention deficit hyperactivity disorder (ADHD) and result in the promotion of ACh synthesis (English et al., 2009). Moreover, elevating ACh levels can relieve cognitive and social symptoms in a mouse model of autism (Karvat and Kimchi, 2014). Aberrant cholinergic signaling has also been reported in schizophrenia (for review, see Terry, 2008; Higley and Picciotto, 2014). However, there is still much debate over the mechanisms underlying cholinergic dysfunction in this disease (for review, see Hyde and Crook, 2001; Scarr et al., 2013). Considering that cholinergic dysfunction is associated with a diverse group of diseases, it is important to understand the functional intricacies of these cells.

Complex and dense cholinergic innervation is achieved in the brain from two categories of cholinergic neurons: the CINs—which synapse locally within a brain structure, and projecting cholinergic neurons—which send their axons to other structures (for review, see Allaway and Machold, 2017). CINs are present in a number of structures where they are important for local modulation. For example, cortical CINs, known for their expression of Vasoactive Intestinal Peptide (VIP), comprise approximately 12% of cortical inhibitory neurons (von Engelhardt et al., 2007; for review, see Rudy et al., 2011). They are primarily bi-tufted and found in layer 2/3 of the cortex (von Engelhardt et al., 2007). However, bipolar and multipolar CINs are also present and populate lower cortical layers (Li et al., 2018). On the contrary, striatal CINs are much larger, with extensive axonal fields (for review, see Lim et al., 2014)



to control the output of the striatal projection neurons (SPNs). Projecting cholinergic neurons are found in the basal forebrain, hypothalamus and medial habenula (Li et al., 2018) and send long-range axonal projections to various cortical and subcortical regions (Figure 1B). Moreover, cholinergic neurons found in the PPN project to the basal ganglia, thalamus, and hypothalamus (for review, see Mena-Segovia and Bolam, 2017; French and Muthusamy, 2018).

In addition to their different projection patterns, cholinergic neurons can also be characterized by their firing properties. PPN cholinergic neurons display phasic and short-latency responses and provide a fast and transient response to sensory events (Petzold et al., 2015), whereas CINs of the striatum switch from



tonic firing to a transient pause (**Figure 1C**; Shimo and Hikosaka, 2001; Atallah et al., 2014). CINs precisely control striatal output (Goldberg and Reynolds, 2011; Faust et al., 2015; Zucca et al., 2018) by inhibiting the firing of SPNs *via* neuropeptide-Y expressing inhibitory interneurons (English et al., 2011). They also drive spontaneous activation of SPNs *via* muscarinic (Mamaligas and Ford, 2016) and glutamatergic transmission (Higley et al., 2011). The spontaneous firing patterns of striatal CINs are sculpted by the widely studied delayed rectifier (IKr) and hyperpolarized activated current (Ih; Oswald et al., 2009). Calcium-dependent potassium conductances also give rise to prominent afterhyperpolarizations, and striatal CIN firing includes two periodic patterns: single spiking and rhythmic bursting (Bennett et al., 2000; Goldberg and Wilson, 2005; **Figure 1C**).

In addition to physiological characteristics, cholinergic neurons share genetic commonalities. The expression of choline acetyl-transferase (ChAT) and acetylcholine esterase (AChE) are markers of all cholinergic neurons, as they are involved in the synthesis and degradation of ACh respectively (Taylor and Brown, 1999). During development, they express common transcription factors that are conserved across neuronal populations. For instance, the homeobox-encoding Nkx2.1 transcription factor is expressed in many sites of neurogenesis within the developing brain such as the Medial Ganglionic Eminence (MGE), preoptic area (POA), septal neuroepithelium (SE). It has been shown that most cholinergic neurons arise from Nkx2.1<sup>+</sup> progenitors (for review, see Allaway and Machold, 2017), and that cells expressing Nkx2.1 that upregulate the LIM homeobox transcription factors Islet-1 (Isl1) and Lhx8 become cholinergic (Zhao et al., 2003; Cho et al., 2014). As these transcription factors are expressed early during development, their co-expression is likely to be one of the earliest traits of cholinergic fated neurons (Fragkouli et al., 2009). Moreover, a loss of Nkx2.1 expression during development halts the maturation and specification of cholinergic cells (Sussel et al., 1999; Du et al., 2008).

Developmental cell specification is an area of great current interest for uncovering how neurons are able to integrate information in a highly complex neural circuit (Tasic et al., 2018; for review, see Fishell and Heintz, 2013). The interplay between the expression of specific genetic factors and neuronal activity are essential contributors to the establishment of cell identity (Dehorter et al., 2015; Jabaudon, 2017) and function (for review, see Yap and Greenberg, 2018). Therefore, the concept of specification leads to diversity among neuronal populations and acts as an important foundation for circuit formation and overall brain function (for review, see Breunig et al., 2011; Dehorter et al., 2017; Wamsley and Fishell, 2017). The cholinergic cell population was believed to be relatively homogenous, despite spanning across various brain regions. However, recent studies have shed light on the diversity within these populations, and the importance of cholinergic subpopulations for brain function. This review article highlights developmental origins of cholinergic neurons and explores recent evidence for genetic, morphological, and electrophysiological diversity of the CINs of the striatum.

## GENETIC DIVERSITY OF CHOLINERGIC INTERNEURONS

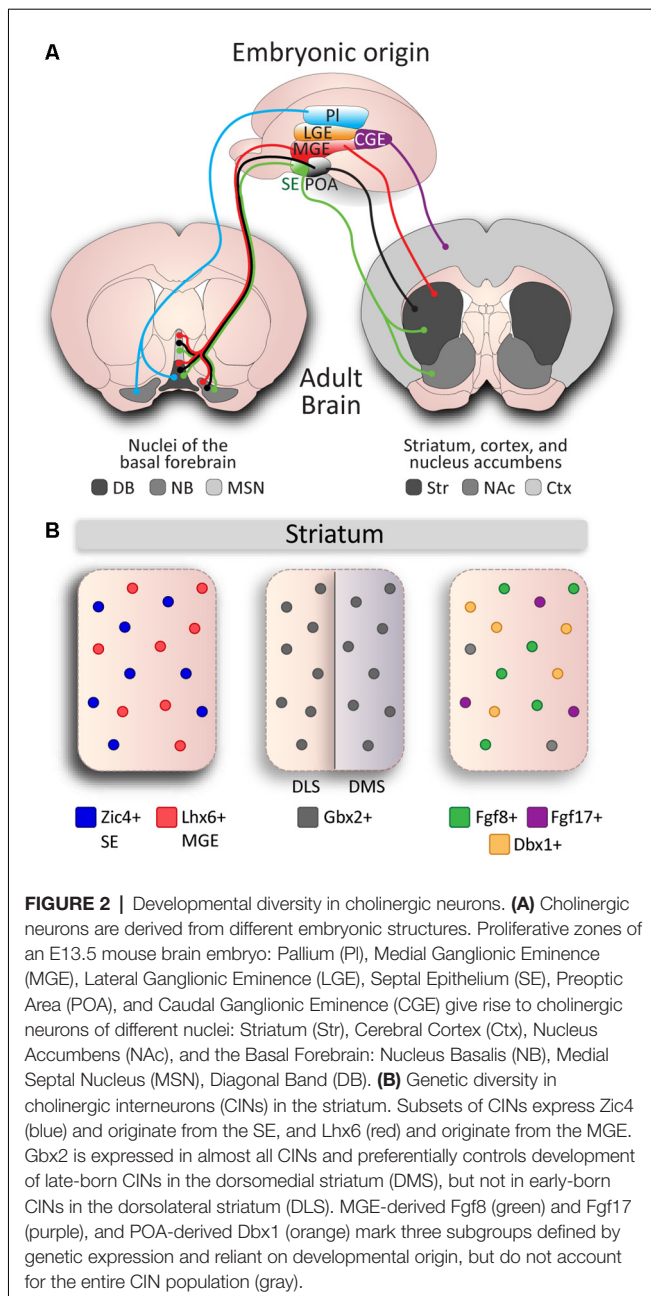
### Cholinergic Cell Diversity Arises From Their Developmental Origin

It is reasonable to expect that cholinergic neurons in a single structure would originate and migrate from a single developmental zone. However, VIP-positive interneurons in the cortex are the only cholinergic population thought to originate from a single developmental proliferative zone, the caudal ganglionic eminence (CGE; Vogt et al., 2014). Cholinergic neurons within a single structure can arise from multiple developmental origins (Nóbrega-Pereira et al., 2010), and conversely, these proliferative areas can also give rise to cholinergic neurons fated to multiple structures in the brain (Marin et al., 2000; Pombero et al., 2011; Magno et al., 2017; **Figure 2A**). Most basal forebrain cholinergic neurons originate from the MGE, POA (for review, see Ballinger et al., 2016), and SE (Magno et al., 2017). Furthermore, subsets of neurons in the diagonal band and NB originate from the ventral area of the pallial telencephalon (pallium), which is located adjacent to the pallium/subpallium border (Pombero et al., 2011; Ceci et al., 2012; **Figure 2A**). Similarly, striatal CINs originate from the MGE and POA (Marin et al., 2000; Fragkouli et al., 2009), as well as the SE (Magno et al., 2017). Therefore, to fully appreciate the diversity within cholinergic populations, their developmental origins must be considered. However, as many progenitor regions have genetically defined sub-domains (Flames et al., 2007), neurons originating in the same region may display further genetic diversity.

### Cholinergic Cell Diversity Is Controlled by Genetic Factors

Combinatorial gene expression during early developmental stages can translate to diversity within the mature striatum (Flames et al., 2007). For example, the Dbx1 transcription factor defines a sub-domain of the POA which gives rise to a subset of cholinergic striatal interneurons (Gelman et al., 2011). Similarly, fibroblast growth factor 8 (Fgf8) and fibroblast growth factor 17 (Fgf17) expressing progenitors in the ventral MGE and ventral SE give rise to individual subsets of CINs in the striatum (Hoch et al., 2015a).

A number of studies have also investigated the effect of gene expression on cholinergic cell specification and identity. The transcription factors Lhx8 and Isl1 drive cholinergic identity in MGE/POA-derived neurons that are fated to populate the basal forebrain and striatum (Zhao et al., 2003; Cho et al., 2014). The ablation of either of these genes results in a loss of most cholinergic neurons in the NB, diagonal band and septum (Zhao et al., 2003; Mori et al., 2004; Elshatory and Gan, 2008; Cho et al., 2014). Moreover, it has been shown that Isl1 is required for the specification of a subset of Nkx2.1+/Lhx8+ interneurons, as Isl1 ablation leads to a ~40% of the Nkx2.1-expressing cells in the striatum (Cho et al., 2014). This partial loss of cholinergic cells suggests that the basal forebrain and striatal neuroepithelium contain Lhx8/Isl1-independent cholinergic fated cells. While the



basal forebrain is divided into different nuclei, striatal CINs are spread throughout the striatum and were long considered as a single homogeneous population. However, studies into specific genetic factors have shown the diverse origins of CINs in the striatum. For instance, the expression of the transcription factor *Zic4* in the SE defines septal cholinergic neurons but also 50% of the striatal CINs, which migrate from the SE (Magno et al., 2017). On the other hand, expression of the *Otx2* transcription factor regulates the development of cholinergic neurons derived from the MGE and POA, and the specific ablation of the *Otx2* gene from the *Nkx2.1* domain results in a loss of some cholinergic neurons of the basal ganglia (Hoch et al., 2015b). It was previously thought that striatal cholinergic

cell identity was exclusively defined by the upregulation of *Lhx8* and coordinated downregulation of *Lhx6* transcription factor (Fragkouli et al., 2009; Lopes et al., 2012), a developmental marker of MGE-derived striatal interneurons (Liodis et al., 2007). However, a subset of CINs was recently found to maintain *Lhx6* expression alongside cholinergic markers, resulting in *Lhx6* positive (53%) and negative (47%) populations in the striatum (Lozovaya et al., 2018). In addition, a proportion of striatal neurons express the *Er81* transcription factor (Dehorter et al., 2015), and these are likely to also be derivatives of *Er81*-positive progenitor domains from the MGE/POA (Flames et al., 2007).

Another factor to consider to fully appreciate cholinergic cell specification is that during development, neurons acquire different identities according to their time of birth (Kao and Lee, 2010). CINs of the striatum are among the earliest cells born (between E12 and E15) along the caudal-rostral gradient respectively (Semba et al., 1988). Early- and late-born CINs migrate at different time points (Marin et al., 2000) and populate lateral and medial regions of the striatum, respectively (Chen et al., 2010). The *Gbx2* transcription factor is implicated in the distinction between these early- and late-born cells and is expressed in almost all CINs. The absence of *Gbx2* almost entirely ablates the late-born population (Chen et al., 2010; **Figure 2B**), and thus may also mark a cholinergic subpopulation in the striatum. These studies demonstrate the presence of diverse genetic patterning during development that is required for the control of cholinergic cell identity. The interactions and overlaying domains of these subgroups has yet to be determined; we are unaware whether they are discrete cholinergic populations or if they arise from combinatorial gene expression that leads to further diversity. In addition, our understanding of the developmental mechanisms behind the regulation of these crucial genetic factors is still limited.

## Advances in Technology Point to Even More Genetic Diversity Within Populations Than First Imagined

An important advancement has been the introduction of single-cell sequencing of neuronal populations to identify patterns of genetic expression (Liu et al., 2018; Zeisel et al., 2018). Using this technique, a number of studies have found substantial genetic diversity among cholinergic neuron populations. For example, the neurochemical patterning of hypothalamic cholinergic neurons in the arcuate nucleus is heterogeneous. These cells show clustering of certain genes coding for POMC-derived peptides, enzymes responsible for the synthesis and release of GABA, glutamate and catecholamines. This heterogeneity has been proposed to be linked to the function of the arcuate nucleus in regulating feeding behavior. Indeed a subset of these cholinergic neurons was found to express leptin and insulin receptors alongside their downstream targets, indicating their specificity (Jeong et al., 2016). In addition, cortical VIP cholinergic neurons also appear genetically diverse when analyzed on a single-cell basis (Zeisel et al., 2015;

Tasic et al., 2016). Striatal CINs present diverse genetic patterning and this even extends to cholinergic markers. Individual CINs express different levels of ChAT and choline transporters, such as vesicular acetylcholine transporter (VAChT) and the high-affinity choline transporter (ChT; Muñoz-Manchado et al., 2018). Such genetic variation points to subsequent functional heterogeneity.

## GENETIC DIVERSITY MAY LEAD TO FUNCTIONAL SUBGROUPS IN CHOLINERGIC NEURON POPULATIONS

Genetic diversity in cholinergic populations has consequential influences on their functional properties and integration within neuronal networks. For instance, there is documented diversity in cholinergic striatal activity, with higher levels of CIN baseline activity in the dorsomedial part compared to the ventrolateral part of the striatum (Figure 3A). The presence of a gradient of the phosphorylated ribosomal protein S6 (p-rpS6), a specific marker of cholinergic activity across the striatum (Matamales et al., 2016; Bertran-Gonzalez et al., 2012), suggests that the regulation of striatal output *via* cholinergic cell activity is heterogeneous within the structure. Several characteristics contribute to the functional features of cholinergic neurons.

## Cholinergic Neurons Are Segregated Into Morphological Subgroups

A number of studies have found evidence for morphological diversity among cholinergic neurons in the brain. In addition to diversity between interneurons and projection neurons in different structures (Figure 1C), diversity within a single population or structure has also been found. For instance, olfactory bulb CINs in the mitral and plexiform cell layers can be segregated into three subsets: locally projecting, bipolar projecting, and non-bipolar projecting (Krosnowski et al., 2012). Similarly, VIP/ChAT-expressing cortical interneurons are also categorized into different morphological subtypes: bipolar, bi-tufted, and multipolar interneurons (Li et al., 2018). However, there is no established genetic or functional correlation for the diversity in these structures. In the striatum, some studies have described a relationship between molecular expression and morphological characteristics in CINs (Figure 3A). In particular, the absence of Gbx2 expression leads to abnormal neurite outgrowth and an increase in the complexity of the dendritic field of CINs (Chen et al., 2010). A correlation between the expression of the Lhx6 transcription factor and CINs morphology has also been recently reported (Lozovaya et al., 2018). The Lhx6-negative CINs present a more complex and vast dendritic arborization, compared to the Lhx6-expressing which are dual cholinergic/GABAergic interneurons (CGINs; Figure 3A). These examples of morphological diversity in cholinergic neurons indicate possible heterogeneity in their connectivity and the role they play within the local and distant circuitry.

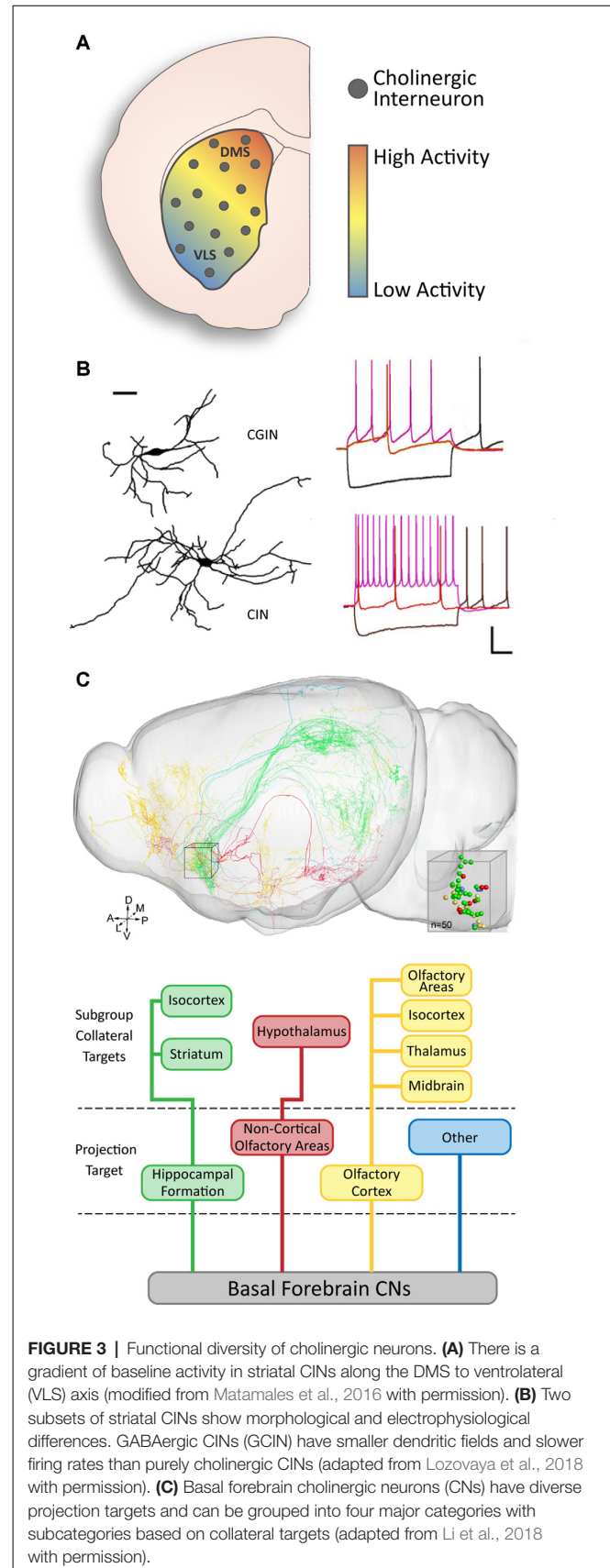


**FIGURE 3 |** Functional diversity of cholinergic neurons. **(A)** There is a gradient of baseline activity in striatal CINs along the DMS to ventrolateral (VLS) axis (modified from Matamales et al., 2016 with permission). **(B)** Two subsets of striatal CINs show morphological and electrophysiological differences. GABAergic CINs (GCIN) have smaller dendritic fields and slower firing rates than purely cholinergic CINs (adapted from Lozovaya et al., 2018 with permission). **(C)** Basal forebrain cholinergic neurons (CNS) have diverse projection targets and can be grouped into four major categories with subcategories based on collateral targets (adapted from Li et al., 2018 with permission).

## Electrophysiological Properties Differentiate Cholinergic Cell Subtypes

Another critical aspect of circuit integration and formation during development is the electrophysiological properties of cholinergic neurons. In addition to their molecular and morphological characteristics, several cholinergic cell subtypes have been sorted in various brain structures based on their electrophysiological properties. For instance, basal forebrain cholinergic projection neurons are segregated into two subtypes, early firing and late firing (Unal et al., 2012). The early firing neurons (70%) are more excitable, as well as adaptive and susceptible to a depolarization block. The late firing neurons (30%), whilst less excitable, are able to maintain tonic firing at lower frequencies. As the basal forebrain is made up of four main regions, the functional diversity can be partly attributed to neuron location. For example, cholinergic neurons in the NB have properties consistent with early firing neurons (López-Hernández et al., 2017) whereas cholinergic neurons in the medial septal region have been found to display low frequency spiking properties (Simon et al., 2006).

Cholinergic neurons in the PPN are also functionally diverse and have been categorized into four groups. This is based on the neurons having low threshold spiking, a transient outward potassium current (known as A-current), both of these properties, or none. In addition, it has also been found that cells with A-current can be either early or late firing (Baksa et al., 2019). The diversity in functional properties of cholinergic neurons is important as they are tonically firing and thus different characteristics could lead to different ACh release patterns, altering circuit activity.

In local cholinergic circuitry, the cortical bipolar VIP+/ChAT+ interneurons have been characterized as mostly tonically firing with little to no adaptation, with a subset (approximately 12%) of stuttered firing neurons (von Engelhardt et al., 2007). Similarly, striatal CINs have also been found to show diversity in their functional properties (Lozovaya et al., 2018). CGINs have a higher sag amplitude following a hyperpolarizing current, a lower frequency of spontaneous tonic firing, and a more prominent pause response than the CINs. This functional cell diversity implies a fine control of information processing from cholinergic neuron subtypes.

## Heterogeneity in Connectivity Underlies Cholinergic Neuron Diversity

Cholinergic neurons have the ability to modulate the activity of other neurons, therefore, facilitating higher-order processing in numerous nuclei (for review, see Teles-Grilo Ruivo and Mellor, 2013). Their specific and extensive pattern of connectivity is fundamental to their role, yet is different between different populations. The cholinergic projection neurons in the basal forebrain innervate various cortical and subcortical regions. Their organization into subgroups is defined by the cortical region that they target (Zaborszky et al., 2015); whereas the heterogeneity of their outputs is reciprocated in the inputs they received from different areas (Zheng et al., 2018; for review, see Zaborszky et al., 2018). It was recently found that

the connectivity pattern of cholinergic neurons can be even more complex. For example, within a single region of the basal forebrain, cholinergic neurons can be segregated by their main target region as well as the target locations of their collaterals (Li et al., 2018; **Figure 3C**). However, we still do not have a full understanding of the intricacies that underpin this system.

It is known that the cortical and thalamic innervation of the striatum follows an approximate topographical gradient, whereby the dorsomedial striatum (DMS) and dorsolateral striatum (DLS) receive inputs from different cortical, thalamic, and brainstem regions (McGeorge and Faull, 1989; Berendse et al., 1992; Bolam et al., 2000; Dautan et al., 2014; Assous et al., 2019). In addition, the dorsal striatum receives more excitatory innervation than the ventral striatum (Assous et al., 2019), indicating that neuronal activity in these regions may be modulated differently. These trends may also extend to influencing CINs, as they receive afferents from the cortex and thalamus (Doig et al., 2014; Klug et al., 2018). DMS CINs have higher levels of activity than those in the DLS (Matamales et al., 2016; **Figure 3A**).

In addition, a pathway from the PPN to the striatum has been reported, and interestingly consists of cholinergic and glutamatergic afferents that target striatal CINs (Dautan et al., 2014, 2016; Assous et al., 2019). Similarly, inputs from the parafascicular nucleus to the striatum form a topographic map and have also been shown to target CINs (Mandelbaum et al., 2019). Whilst extra-striatal sources of innervation onto CINs have been determined, whether they differently target and influence CIN subtypes is not known.

Striatal CINs are also heavily innervated by the local striatal network. They receive various inhibitory inputs from GABAergic neuron types (English et al., 2011; Straub et al., 2016), as well as the projecting SPNs (for review, see Abudukeyoumu et al., 2019). Moreover, CINs receive dense synaptic inputs from other CINs, forming microcircuitry that then modulates the overall striatal output *via* dense innervation of the spiny projection neurons (English et al., 2011; Straub et al., 2016; Abudukeyoumu et al., 2019). CINs virtually target all cells within the striatum (for review, see Lim et al., 2014). They primarily send connections to neuropeptide Y-expressing interneurons, projection neurons, weak inputs to parvalbumin-expressing interneurons (English et al., 2011; Straub et al., 2016) and likely target tyrosine hydroxylase-expressing interneurons (for review, see Tepper et al., 2018). The assortment of inputs and outputs of CINs may be reliant on their diverse identity. In conclusion, this aspect of striatal network connectivity is yet to be investigated and must be taken into account for future studies of the connectivity pattern of cholinergic cell subtypes.

Despite cholinergic neurons being primarily characterized by their release of ACh, there is a great deal of evidence supporting that some cell subtypes have the ability to co-release different neurotransmitters. For instance, cholinergic neurons from the basal forebrain (Takács et al., 2018) and the medial septum co-release gamma-Aminobutyric acid (GABA) and ACh (Desikan et al., 2018) and express synthesis enzymes for both neurotransmitters (Saunders et al., 2015; Granger et al., 2016).

GABAergic identity has also been reported in cortical CINs through their co-expression of glutamic acid decarboxylase (GAD) and cholinergic marker ChAT (von Engelhardt et al., 2007), as expected due to their initial characterization as inhibitory interneurons. Striatal CINs with GABAergic identity defined by *Lhx6* expression co-release GABA alongside ACh (Lozovaya et al., 2018). On the other hand, the expression of a vesicular glutamate transporter VGLUT3 has been shown in cholinergic axon terminals in the striatum (Gras et al., 2008; Higley et al., 2011; Nelson et al., 2014), implying the potential for co-release of Glutamate and ACh in all striatal CINs. If co-release mechanisms are shown to have a functional influence, they must be regulated to maintain normal circuit activity and may have a role in pathology.

## DISCUSSION

### Cholinergic Cell Diversity Is Established During Development

To understand the organizational logic of cholinergic neurons in circuitry, it is necessary to decipher the biological basis of their cellular diversity. As we have reviewed, the genetic, spatial, and temporal framework of cholinergic cell development provides a foundation for discovering and classifying subpopulations. There have been challenges to the exploration of cell specification due to technological limitations, however, the development of new techniques in the field of molecular genetics (single-cell RNA sequencing, patch-sequencing, optogenetics, and pharmacogenetics) has enabled the exposure of hidden neuronal diversity within cholinergic populations (Fuzik et al., 2016; Liu et al., 2018; Muñoz-Manchado et al., 2018).

It is well understood that the maturation of neuronal circuits requires tightly controlled gene expression cascades (Dehorter et al., 2012; Novak et al., 2013). The function and co-expression pattern of different markers that segregate cholinergic cell populations remain ambiguous. In particular, the role of *Er81* (Dehorter et al., 2015) and *Zic4* proteins (Magno et al., 2017) in striatal-fated CINs are currently unknown (Figure 2B). Cholinergic cell diversity is a consequence of different embryonic origins and exposure to transcriptional programs during maturation. As we have outlined, seemingly uniform populations of cholinergic neurons having common properties can be derived from multiple embryonic structures (Figure 2A), with unique chemical and morphological traits arising at distinct time points during development. It is likely that chemically, spatially and temporally-restricted domains give rise to unique neuronal populations. Since MGE-derived neurons are generated at different embryonic stages (Mi et al., 2018; Sandberg et al., 2018) and CINs proliferate along a caudal-rostral axis (Semba et al., 1988), future research may reveal which proliferation domains generate cholinergic cell subtypes. Subsequent to proliferation, cells use different migratory pathways that require the expression of specific receptors to detect chemoattractive and chemorepulsive cues (Wichterle et al., 2003; Gelman et al., 2012; Villar-Cerviño et al., 2015; Touzot et al., 2016). Therefore, development of cholinergic neurons that requires the accurate

modulation of distinct transcriptional programs needs to be further investigated.

As the complex mechanisms behind neuronal development continue to be revealed, the vital role of activity-dependent processes is central to our understanding. These processes seem to be present throughout the developing brain, however, the transcriptional programs appear to be unique to specific neuronal cell-types (for review, see Dehorter et al., 2017; Yap and Greenberg, 2018). Similar mechanisms are also present in adulthood, modulating the output of neuronal circuitry (Dehorter et al., 2015). If we consider this in context of recently discovered striatal cholinergic subpopulations (Magno et al., 2017; Lozovaya et al., 2018), it is possible that different activity-induced processes tune cholinergic activity in specific ways (Krishnaswamy and Cooper, 2009), delineating further subtypes. However, research into the activity-dependent homeostatic specification of cholinergic neurons are, to the best of our knowledge, very limited (Borodinsky et al., 2004). As a result, studies into this field promise to highlight the fundamental mechanisms of cholinergic cell function.

### Functional Complexity of Neuronal Networks Depends on Cholinergic Cell Diversity

Complex neuronal networks are necessary for higher-order processing and require various cell types and connections. We must consider that genetically-diverse CINs may fit into the striatal network in unique ways. For instance, *Lhx6*-positive and negative CINs in the striatum display functional differences (Lozovaya et al., 2018). Although they share several major common intrinsic membrane properties, *Lhx6*-positive CINs display higher sag amplitudes in response to hyperpolarizing pulses than *Lhx6*-negative CINs, lower spontaneous spiking frequency, and smaller dendritic arbors (Figure 3B). Therefore, there is the possibility that they form different connections, and integrate differently in the network.

The striatum has neurochemically diverse regions that are formed during development and may contribute to the formation of subnetworks. The striosome and matrix regions are three-dimensional, interlocked structures constituting neurochemically and morphologically distinct domains, which emerge during development and also have an important role in the mature striatum (Hagimoto et al., 2017; for review, see Brimblecombe and Cragg, 2017). Evidence has shown that early-born striatal cells migrate to striosomes and connect preferentially with limbic circuits, whereas late-born cells populate the matrix and receive dominant input from the neocortex (Crittenden et al., 2017; Hamasaki and Goto, 2019). In addition, CIN dendritic fields preferentially occupy the matrix compartments, alongside higher levels of cholinergic markers, suggesting that cholinergic neurons development is also dependent on the striosome-matrix structure (Crittenden et al., 2017). However, the correlation between CIN diversity and the compartmentalized structure of the striatum remains to be explored.

As we have described, cholinergic neurons can present different morphological and electrophysiological properties (**Figure 1B**). They are known to innervate other structures with different patterns of connectivity (Li et al., 2018; **Figure 3C**), and also receive inputs from various structures and cell types (for review, see Lim et al., 2014). It is thus crucial to determine whether cholinergic cell subtypes exhibit different morphological features (i.e., axonal and dendritic fields) or innervation patterns to ultimately fully characterize their involvement in various microcircuits.

Cholinergic transmission can mediate disparate actions *via* integration of postsynaptic signals (Calabresi et al., 2000). It is necessary to consider the function and distribution of postsynaptic receptors that are scattered across various cells and receptors with different signaling capacities that can be co-expressed in the same cell type. Increased understanding of the specific neuron types responsive to ACh and their functional connectivity is necessary to obtain a phenomenological understanding of neuromodulation and behavior both at the cellular and circuit levels. Interplay between ACh and other neurotransmitters are central for basal ganglia function (for review, see Bonsi et al., 2011), and ACh-dopamine (DA) coupling has been extensively studied, as their reciprocal interaction largely contributes to the control of the striatal output. For example, DA has a fundamental role in the striatum (Tritsch et al., 2012; for review, see Cools, 2011), as it controls the pause in CIN firing (Zhang et al., 2018), both in the medial and lateral areas. There are regional differences in the dopaminergic control of striatal CINs. It has been described that the pause of these cells in the DLS is shorter than in the DMS, *via* a mechanism of DA-glutamate co-transmission (Chuhma et al., 2018). Moreover, activation of glutamatergic receptors by cortical and thalamic inputs might lead to distinct integration strategies from CINs subtypes in the striatum (Kosillo et al., 2016).

CINs are fundamental to the integration of somatosensory information and motor-related signals (for review, see Robbe, 2018). There is a functional dissociation between the DMS, which is responsible for goal-directed actions, and the DLS, supporting procedural learning such as habit formation (Okada et al., 2018). There are also differences in the sensitivity of tonically active neurons to rewarding events between dorsal and ventral striatum (Marche et al., 2017). Determining whether responses of cholinergic cell types vary is an interesting topic for future studies utilizing *in vivo* optogenetics, calcium imaging or electrophysiological approaches.

Our understanding of the role of cholinergic subpopulations within pathological conditions is currently limited, however, a

study reported unique roles of striatal CINs and GABA/ACh co-expressing striatal interneurons (CGINs; **Figure 3B**) in PD (Lozovaya et al., 2018). It shows that DA deprivation specifically strengthens CGIN-CGIN network and abolishes both GABAergic inhibition and pause response in CGINs. Future studies should focus on distinguishing between the different cholinergic subpopulations on the basis of their embryonic origin, molecular profile and connectivity, when analyzing cholinergic network dysfunction in disease conditions.

## CONCLUSION

Despite significant research into cholinergic neurons, the recent discovery of diverse subpopulations has reinforced the notion that our understanding of these cells remains incomplete. In this review, we have combined the current literature surrounding cholinergic neurons in the brain with a specific focus on the newfound diversity within cholinergic population of the striatum. Whereas similarities between cholinergic populations predicated that neurons were relatively functionally homogenous, studies show genetic, morphological and electrophysiological properties in striatal cholinergic subpopulations. This diversity likely underpins their specific function in normal and pathological conditions. Future studies into cholinergic cell subpopulations aiming at understanding their development, morphology and activity are necessary to ultimately determine the implications of this new-found cell diversity in health and disease.

## AUTHOR CONTRIBUTIONS

All authors contributed to the writing of the manuscript, and all have approved it for publication.

## FUNDING

Some of the research in this review and its writing were supported by the Australian National University and the National Health and Medical Research Council (APP1144145).

## ACKNOWLEDGMENTS

Images in **Figure 3B** comes from Lozovaya et al. (2018). Images included are encompassed under the Creative Commons license: <http://creativecommons.org/licenses/by/4.0/>. Images in **Figure 3C** comes from Li et al. (2018). Permission has been granted for the use of the material.

## REFERENCES

- Abudukeyoumu, N., Hernandez-Flores, T., Garcia-Munoz, M., and Arbutnot, G. W. (2019). Cholinergic modulation of striatal microcircuits. *Eur. J. Neurosci.* 49, 604–622. doi: 10.1111/ejn.13949
- Albert-Gascó, H., García-Avilés, A., Moustafa, S., Sánchez-Sarasua, S., Gundlach, A. L., Olucha-Bordonau, F. E., et al. (2017). Central relaxin-3 receptor (RXFP3) activation increases ERK phosphorylation in septal cholinergic neurons and impairs spatial working memory. *Brain Struct. Funct.* 222, 449–463. doi: 10.1007/s00429-016-1227-8
- Allaway, K. C., and Machold, R. (2017). Developmental specification of forebrain cholinergic neurons. *Dev. Biol.* 421, 1–7. doi: 10.1016/j.ydbio.2016.11.007
- Aoki, S., Liu, A. W., Akamine, Y., Zucca, A., Zucca, S., and Wickens, J. R. (2018). Cholinergic interneurons in the rat striatum modulate substitution of habits. *Eur. J. Neurosci.* 47, 1194–1205. doi: 10.1111/ejn.13820

- Aoki, S., Liu, A. W., Zucca, A., Zucca, S., and Wickens, J. R. (2015). Role of striatal cholinergic interneurons in set-shifting in the rat. *J. Neurosci.* 35, 9424–9431. doi: 10.1523/JNEUROSCI.0490-15.2015
- Assous, M., Dautan, D., Tepper, J. M., and Mena-Segovia, J. (2019). Pedunculopontine glutamatergic neurons provide a novel source of feedforward inhibition in the striatum by selectively targeting interneurons. *J. Neurosci.* 39, 4727–4737. doi: 10.1523/JNEUROSCI.2913-18.2019
- Atallah, H. E., McCool, A. D., Howe, M. W., and Graybiel, A. M. (2014). Neurons in the ventral striatum exhibit cell-type-specific representations of outcome during learning. *Neuron* 82, 1145–1156. doi: 10.1016/j.neuron.2014.04.021
- Baksa, B., Kovács, A., Bayasgalan, T., Szentesi, P., Koszeghy, Á., Szücs, P., et al. (2019). Characterization of functional subgroups among genetically identified cholinergic neurons in the pedunculopontine nucleus. *Cell. Mol. Life Sci.* 76, 2799–2815. doi: 10.1007/s00018-019-03025-4
- Ballinger, E. C., Ananth, M., Talmage, D. A., and Role, L. W. (2016). Basal forebrain cholinergic circuits and signaling in cognition and cognitive decline. *Neuron* 91, 1199–1218. doi: 10.1016/j.neuron.2016.09.006
- Bennett, B. D., Callaway, J. C., and Wilson, C. J. (2000). Intrinsic membrane properties underlying spontaneous tonic firing in neostriatal cholinergic interneurons. *J. Neurosci.* 20, 8493–8503. doi: 10.1523/JNEUROSCI.20-22-08493.2000
- Berendse, H. W., Galis-de Graaf, Y., and Groenewegen, H. J. (1992). Topographical organization and relationship with ventral striatal compartments of prefrontal corticostriatal projections in the rat. *J. Comp. Neurol.* 316, 314–347. doi: 10.1002/cne.903160305
- Bertran-Gonzalez, J., Chieng, B. C., Laurent, V., Valjent, E., and Balleine, B. W. (2012). Striatal cholinergic interneurons display activity-related phosphorylation of ribosomal protein S6. *PLoS One* 7:e53195. doi: 10.1371/journal.pone.0053195
- Bolam, J. P., Hanley, J. J., Booth, P. A., and Bevan, M. D. (2000). Synaptic organisation of the basal ganglia. *J. Anat.* 196, 527–542. doi: 10.1046/j.1469-7580.2000.19640527.x
- Bonsi, P., Cuomo, D., Martella, G., Madeo, G., Schirinzii, T., Puglisi, F., et al. (2011). Centrality of striatal cholinergic transmission in basal ganglia function. *Front. Neuroanat.* 5:6. doi: 10.3389/fnana.2011.00006
- Bordia, T., Zhang, D., Perez, X. A., and Quirk, M. (2016). Striatal cholinergic interneurons and D2 receptor-expressing GABAergic medium spiny neurons regulate tardive dyskinesia. *Exp. Neurol.* 286, 32–39. doi: 10.1016/j.expneurol.2016.09.009
- Borodinsky, L. N., Root, C. M., Cronin, J. A., Sann, S. B., Gu, X., and Spitzer, N. C. (2004). Activity-dependent homeostatic specification of transmitter expression in embryonic neurons. *Nature* 429, 523–530. doi: 10.1038/nature02518
- Bradfield, L. A., Bertran-Gonzalez, J., Chieng, B., and Balleine, B. W. (2013). The thalamostriatal pathway and cholinergic control of goal-directed action: interlacing new with existing learning in the striatum. *Neuron* 79, 153–166. doi: 10.1016/j.neuron.2013.04.039
- Breunig, J. J., Haydar, T. F., and Rakic, P. (2011). Neural stem cells: historical perspective and future prospects. *Neuron* 70, 614–625. doi: 10.1016/j.neuron.2011.05.005
- Brimblecombe, K. R., and Cragg, S. J. (2017). The striosome and matrix compartments of the striatum: a path through the labyrinth from neurochemistry toward function. *ACS Chem. Neurosci.* 8, 235–242. doi: 10.1021/acschemneuro.6b00333
- Calabresi, P., Centonze, D., Gubellini, P., Pisani, A., and Bernardi, G. (2000). Acetylcholine-mediated modulation of striatal function. *Trends Neurosci.* 23, 120–126. doi: 10.1016/s0166-2236(99)01501-5
- Ceci, M. L., Pedraza, M., and de Carlos, J. A. (2012). The embryonic septum and ventral pallidum, new sources of olfactory cortex cells. *PLoS One* 7:e44716. doi: 10.1371/journal.pone.0044716
- Chen, L., Chatterjee, M., and Li, J. Y. (2010). The mouse homeobox gene Gbx2 is required for the development of cholinergic interneurons in the striatum. *J. Neurosci.* 30, 14824–14834. doi: 10.1523/JNEUROSCI.3742-10.2010
- Cheng, J., Umschweif, G., Leung, J., Sagi, Y., and Greengard, P. (2019). HCN2 channels in cholinergic interneurons of nucleus accumbens shell regulate depressive behaviors. *Neuron* 101, 662.e5–672.e5. doi: 10.1016/j.neuron.2018.12.018
- Cho, H. H., Cargnin, F., Kim, Y., Lee, B., Kwon, R. J., Nam, H., et al. (2014). Isl1 directly controls a cholinergic neuronal identity in the developing forebrain and spinal cord by forming cell type-specific complexes. *PLoS Genet.* 10:e1004280. doi: 10.1371/journal.pgen.1004280
- Chuhma, N., Mingote, S., Yetnikoff, L., Kalmbach, A., Ma, T., Ztaou, S., et al. (2018). Dopamine neuron glutamate cotransmission evokes a delayed excitation in lateral dorsal striatal cholinergic interneurons. *Elife* 7:e39786. doi: 10.7554/elife.39786
- Cools, R. (2011). Dopaminergic control of the striatum for high-level cognition. *Curr. Opin. Neurobiol.* 21, 402–407. doi: 10.1016/j.conb.2011.04.002
- Crittenden, J. R., Lacey, C. J., Weng, F. J., Garrison, C. E., Gibson, D. J., Lin, Y., et al. (2017). Striatal cholinergic interneurons modulate spike-timing in striosomes and matrix by an amphetamine-sensitive mechanism. *Front. Neuroanat.* 11:20. doi: 10.3389/fnana.2017.00020
- Dautan, D., Hacıoğlu Bay, H., Bolam, J. P., Gerdjikov, T. V., and Mena-Segovia, J. (2016). Extrinsic sources of cholinergic innervation of the striatal complex: a whole-brain mapping analysis. *Front. Neuroanat.* 10:1. doi: 10.3389/fnana.2016.00001
- Dautan, D., Huerta-Ocampo, I., Witten, I. B., Deisseroth, K., Bolam, J. P., Gerdjikov, T., et al. (2014). A major external source of cholinergic innervation of the striatum and nucleus accumbens originates in the brainstem. *J. Neurosci.* 34, 4509–4518. doi: 10.1523/JNEUROSCI.5071-13.2014
- Dehorter, N., Ciceri, G., Bartolini, G., Lim, L., del Pino, I., and Marín, O. (2015). Tuning of fast-spiking interneuron properties by an activity-dependent transcriptional switch. *Science* 349, 1216–1220. doi: 10.1126/science.aab3415
- Dehorter, N., Marichal, N., Marín, O., and Berninger, B. (2017). Tuning neural circuits by turning the interneuron knob. *Curr. Opin. Neurobiol.* 42, 144–151. doi: 10.1016/j.conb.2016.12.009
- Dehorter, N., Vinay, L., Hammond, C., and Ben-Ari, Y. (2012). Timing of developmental sequences in different brain structures: physiological and pathological implications. *Eur. J. Neurosci.* 35, 1846–1856. doi: 10.1111/j.1460-9568.2012.08152.x
- Desikan, S., Koser, D. E., Neitz, A., and Monyer, H. (2018). Target selectivity of septal cholinergic neurons in the medial and lateral entorhinal cortex. *Proc. Natl. Acad. Sci. U S A* 115, E2644–E2652. doi: 10.1073/pnas.1716531115
- Doig, N. M., Magill, P. J., Apicella, P., Bolam, J. P., and Sharott, A. (2014). Cortical and thalamic excitation mediate the multiphasic responses of striatal cholinergic interneurons to motivationally salient stimuli. *J. Neurosci.* 34, 3101–3117. doi: 10.1523/JNEUROSCI.4627-13.2014
- Du, T., Xu, Q., Ocbina, P. J., and Anderson, S. A. (2008). NKX2.1 specifies cortical interneuron fate by activating Lhx6. *Development* 135, 1559–1567. doi: 10.1242/dev.015123
- Elshatory, Y., and Gan, L. (2008). The LIM-homeobox gene Islet-1 is required for the development of restricted forebrain cholinergic neurons. *J. Neurosci.* 28, 3291–3297. doi: 10.1523/JNEUROSCI.5730-07.2008
- English, B. A., Hahn, M. K., Gizer, I. R., Mazei-Robison, M., Steele, A., Kurnik, D. M., et al. (2009). Choline transporter gene variation is associated with attention-deficit hyperactivity disorder. *J. Neurodev. Disord.* 1, 252–263. doi: 10.1007/s11689-009-9033-8
- English, D. F., Ibanez-Sandoval, O., Stark, E., Tecuapetla, F., Buzsáki, G., Deisseroth, K., et al. (2011). GABAergic circuits mediate the reinforcement-related signals of striatal cholinergic interneurons. *Nat. Neurosci.* 15, 123–130. doi: 10.1038/nn.2984
- Faust, T. W., Assous, M., Shah, F., Tepper, J. M., and Koos, T. (2015). Novel fast adapting interneurons mediate cholinergic-induced fast GABA<sub>A</sub> inhibitory postsynaptic currents in striatal spiny neurons. *Eur. J. Neurosci.* 42, 1764–1774. doi: 10.1111/ejn.12915
- Fishell, G., and Heintz, N. (2013). The neuron identity problem: form meets function. *Neuron* 80, 602–612. doi: 10.1016/j.neuron.2013.10.035
- Flames, N., Pla, R., Gelman, D. M., Rubenstein, J. L., Puelles, L., and Marín, O. (2007). Delineation of multiple subpallial progenitor domains by the combinatorial expression of transcriptional codes. *J. Neurosci.* 27, 9682–9695. doi: 10.1523/jneurosci.2750-07.2007
- Fragkouli, A., van Wijk, N. V., Lopes, R., Kessar, N., and Pachnis, V. (2009). LIM homeodomain transcription factor-dependent specification of bipotential MGE progenitors into cholinergic and GABAergic striatal interneurons. *Development* 136, 3841–3851. doi: 10.1242/dev.038083
- French, I. T., and Muthusamy, K. A. (2018). A review of the pedunculopontine nucleus in Parkinson's disease. *Front. Aging Neurosci.* 10:99. doi: 10.3389/fnagi.2018.00099

- Fuzik, J., Zeisel, A., Mate, Z., Calvigioni, D., Yanagawa, Y., Szabo, G., et al. (2016). Integration of electrophysiological recordings with single-cell RNA-seq data identifies neuronal subtypes. *Nat. Biotechnol.* 34, 175–183. doi: 10.1038/nbt.3443
- Gelman, D., Griveau, A., Dehorter, N., Teissier, A., Varela, C., Pla, R., et al. (2011). A wide diversity of cortical GABAergic interneurons derives from the embryonic preoptic area. *J. Neurosci.* 31, 16570–16580. doi: 10.1523/jneurosci.4068-11.2011
- Gelman, D. M., Marin, O., and Rubenstein, J. L. R. (2012). “The generation of cortical interneurons,” in *Jasper’s Basic Mechanisms of the Epilepsies*, eds J. L. Noebels, M. Avoli, M. A. Rogawski, R. W. Olsen and A. V. Delgado-Escueta (Bethesda, MD: National Center for Biotechnology Information (US)), 1171–1186
- Goldberg, J. A., and Reynolds, J. N. (2011). Spontaneous firing and evoked pauses in the tonically active cholinergic interneurons of the striatum. *Neuroscience* 198, 27–43. doi: 10.1016/j.neuroscience.2011.08.067
- Goldberg, J. A., and Wilson, C. J. (2005). Control of spontaneous firing patterns by the selective coupling of calcium currents to calcium-activated potassium currents in striatal cholinergic interneurons. *J. Neurosci.* 25, 10230–10238. doi: 10.1523/jneurosci.2734-05.2005
- Granger, A. J., Mulder, N., Saunders, A., and Sabatini, B. L. (2016). Cotransmission of acetylcholine and GABA. *Neuropharmacology* 100, 40–46. doi: 10.1016/j.neuropharm.2015.07.031
- Gras, C., Amilhon, B., Lepicard, E. M., Poirel, O., Vinatier, J., Herbin, M., et al. (2008). The vesicular glutamate transporter VGLUT3 synergizes striatal acetylcholine tone. *Nat. Neurosci.* 11, 292–300. doi: 10.1038/nn2052
- Hagimoto, K., Takami, S., Murakami, F., and Tanabe, Y. (2017). Distinct migratory behaviors of striosome and matrix cells underlying the mosaic formation in the developing striatum. *J. Comp. Neurol.* 525, 794–817. doi: 10.1002/cne.24096
- Hamasaki, T., and Goto, S. (2019). Parallel emergence of a compartmentalized striatum with the phylogenetic development of the cerebral cortex. *Brain Sci.* 9:E90. doi: 10.3390/brainsci9040900
- Hampel, H., Mesulam, M. M., Cuello, A. C., Farlow, M. R., Giacobini, E., Grossberg, G. T., et al. (2018). The cholinergic system in the pathophysiology and treatment of Alzheimer’s disease. *Brain* 141, 1917–1933. doi: 10.1093/brain/awy132
- Higley, M. J., Gittis, A. H., Oldenburg, I. A., Balthasar, N., Seal, R. P., Edwards, R. H., et al. (2011). Cholinergic interneurons mediate fast VGLUT3-dependent glutamatergic transmission in the striatum. *PLoS One* 6:e19155. doi: 10.1371/journal.pone.0019155
- Higley, M. J., and Picciotto, M. R. (2014). Neuromodulation by acetylcholine: examples from schizophrenia and depression. *Curr. Opin. Neurobiol.* 29, 88–95. doi: 10.1016/j.conb.2014.06.004
- Hoch, R. V., Clarke, J. A., and Rubenstein, J. L. (2015a). Fgf signaling controls the telencephalic distribution of Fgf-expressing progenitors generated in the rostral patterning center. *Neural Dev.* 10:8. doi: 10.1186/s13064-015-0037-7
- Hoch, R. V., Lindtner, S., Price, J. D., and Rubenstein, J. L. (2015b). OTX2 transcription factor controls regional patterning within the medial ganglionic eminence and regional identity of the septum. *Cell Rep.* 12, 482–494. doi: 10.1016/j.celrep.2015.06.043
- Hyde, T. M., and Crook, J. M. (2001). Cholinergic systems and schizophrenia: primary pathology or epiphenomena? *J. Chem. Neuroanat.* 22, 53–63. doi: 10.1016/s0891-0618(01)00101-6
- Jabaudon, D. (2017). Fate and freedom in developing neocortical circuits. *Nat. Commun.* 8:16042. doi: 10.1038/ncomms16042
- Jeong, J. H., Woo, Y. J., Chua, S. Jr., and Jo, Y. H. (2016). Single-cell gene expression analysis of cholinergic neurons in the arcuate nucleus of the hypothalamus. *PLoS One* 11:e0162839. doi: 10.1371/journal.pone.0162839
- Kao, C. F., and Lee, T. (2010). Birth time/order-dependent neuron type specification. *Curr. Opin. Neurobiol.* 20, 14–21. doi: 10.1016/j.conb.2009.10.017
- Karvat, G., and Kimchi, T. (2014). Acetylcholine elevation relieves cognitive rigidity and social deficiency in a mouse model of autism. *Neuropsychopharmacology* 39, 831–840. doi: 10.1038/npp.2013.274
- Klug, J. R., Engelhardt, M. D., Cadman, C. N., Li, H., Smith, J. B., Ayala, S., et al. (2018). Differential inputs to striatal cholinergic and parvalbumin interneurons imply functional distinctions. *Elife* 7:e35657. doi: 10.7554/elifesciences.35657
- Kosillo, P., Zhang, Y. F., Threlfell, S., and Cragg, S. J. (2016). Cortical control of striatal dopamine transmission via striatal cholinergic interneurons. *Cereb. Cortex* doi: 10.1093/cercor/bhw252 [Epub ahead of print].
- Krishnaswamy, A., and Cooper, E. (2009). An activity-dependent retrograde signal induces the expression of the high-affinity choline transporter in cholinergic neurons. *Neuron* 61, 272–286. doi: 10.1016/j.neuron.2008.11.025
- Krosnowski, K., Ashby, S., Sathyanesan, A., Luo, W., Ogura, T., and Lin, W. (2012). Diverse populations of intrinsic cholinergic interneurons in the mouse olfactory bulb. *Neuroscience* 213, 161–178. doi: 10.1016/j.neuroscience.2012.04.024
- Li, X., Yu, B., Sun, Q., Zhang, Y., Ren, M., Zhang, X., et al. (2018). Generation of a whole-brain atlas for the cholinergic system and mesoscopic projectome analysis of basal forebrain cholinergic neurons. *Proc. Natl. Acad. Sci. U S A* 115, 415–420. doi: 10.1073/pnas.1703601115
- Lim, S. A., Kang, U. J., and McGehee, D. S. (2014). Striatal cholinergic interneuron regulation and circuit effects. *Front. Synaptic Neurosci.* 6:22. doi: 10.3389/fnsyn.2014.00022
- Liodis, P., Denaxa, M., Grigoriou, M., Akufo-Addo, C., Yanagawa, Y., and Pachnis, V. (2007). Lhx6 activity is required for the normal migration and specification of cortical interneuron subtypes. *J. Neurosci.* 27, 3078–3089. doi: 10.1523/jneurosci.3055-06.2007
- Liu, Q., Herring, C. A., Sheng, Q., Ping, J., Simmons, A. J., Chen, B., et al. (2018). Quantitative assessment of cell population diversity in single-cell landscapes. *PLoS Biol.* 16:e2006687. doi: 10.1371/journal.pbio.2006687
- Lopes, R., Verhey van Wijk, N., Neves, G., and Pachnis, V. (2012). Transcription factor LIM homeobox 7 (Lhx7) maintains subtype identity of cholinergic interneurons in the mammalian striatum. *Proc. Natl. Acad. Sci. U S A* 109, 3119–3124. doi: 10.1073/pnas.1109251109
- López, A. J., Jia, Y., White, A. O., Kwapis, J. L., Espinoza, M., Hwang, P., et al. (2019). Medial habenula cholinergic signaling regulates cocaine-associated relapse-like behavior. *Addict. Biol.* 24, 403–413. doi: 10.1111/adb.12605
- López-Hernández, G. Y., Ananth, M., Jiang, L., Ballinger, E. C., Talmage, D. A., and Role, L. W. (2017). Electrophysiological properties of basal forebrain cholinergic neurons identified by genetic and optogenetic tagging. *J. Neurochem.* 142, 103–110. doi: 10.1111/jnc.14073
- Lozovaya, N., Eftekhari, S., Cloarec, R., Gouty-Colomer, L. A., Dufour, A., Riffault, B., et al. (2018). GABAergic inhibition in dual-transmission cholinergic and GABAergic striatal interneurons is abolished in Parkinson disease. *Nat. Commun.* 9:1422. doi: 10.1038/s41467-018-03802-y
- Macintosh, F. C. (1941). The distribution of acetylcholine in the peripheral and the central nervous system. *J. Physiol.* 99, 436–442. doi: 10.1113/jphysiol.1941.sp003913
- Magno, L., Barry, C., Schmidt-Hieber, C., Theodotou, P., Hausser, M., and Kessaris, N. (2017). NKX2-1 is required in the embryonic septum for cholinergic system development, learning, and memory. *Cell Rep.* 20, 1572–1584. doi: 10.1016/j.celrep.2017.07.053
- Mamaligas, A. A., and Ford, C. P. (2016). Spontaneous synaptic activation of muscarinic receptors by striatal cholinergic neuron firing. *Neuron* 91, 574–586. doi: 10.1016/j.neuron.2016.06.021
- Mandelbaum, G., Taranda, J., Haynes, T. M., Hochbaum, D. R., Huang, K. W., Hyun, M., et al. (2019). Distinct cortical-thalamic-striatal circuits through the parafascicular nucleus. *Neuron* 102, 636.e7–652.e7. doi: 10.1016/j.neuron.2019.02.035
- Marche, K., Martel, A. C., and Apicella, P. (2017). Differences between dorsal and ventral striatum in the sensitivity of tonically active neurons to rewarding events. *Front. Syst. Neurosci.* 11:52. doi: 10.3389/fnsys.2017.00052
- Marin, O., Anderson, S. A., and Rubenstein, J. L. (2000). Origin and molecular specification of striatal interneurons. *J. Neurosci.* 20, 6063–6076. doi: 10.1523/jneurosci.20-16-06063.2000
- Markowitz, J. E., Gillis, W. F., Beron, C. C., Neufeld, S. Q., Robertson, K., Bhagat, N. D., et al. (2018). The striatum organizes 3D behavior via moment-to-moment action selection. *Cell* 174, 44.e17–58.e17. doi: 10.1016/j.cell.2018.04.019
- Martos, Y. V., Braz, B. Y., Beccaria, J. P., Murer, M. G., and Belforte, J. E. (2017). Compulsive social behavior emerges after selective ablation of striatal cholinergic interneurons. *J. Neurosci.* 37, 2849–2858. doi: 10.1523/jneurosci.3460-16.2017



- Matamales, M., Götze, J., and Bertran-Gonzalez, J. (2016). Quantitative imaging of cholinergic interneurons reveals a distinctive spatial organization and a functional gradient across the mouse striatum. *PLoS One* 11:e0157682. doi: 10.1371/journal.pone.0157682
- Maurice, N., Liberge, M., Jaouen, F., Ztaou, S., Hanini, M., Camon, J., et al. (2015). Striatal cholinergic interneurons control motor behavior and basal ganglia function in experimental Parkinsonism. *Cell Rep.* 13, 657–666. doi: 10.1016/j.celrep.2015.09.034
- McGeorge, A. J., and Faull, R. L. (1989). The organization of the projection from the cerebral cortex to the striatum in the rat. *Neuroscience* 29, 503–537. doi: 10.1016/0306-4522(89)90128-0
- Mena-Segovia, J., and Bolam, J. P. (2017). Rethinking the pedunculopontine nucleus: from cellular organization to function. *Neuron* 94, 7–18. doi: 10.1016/j.neuron.2017.02.027
- Mesulam, M. M., Mufson, E. J., Wainer, B. H., and Levey, A. I. (1983). Central cholinergic pathways in the rat: an overview based on an alternative nomenclature (Ch1-Ch6). *Neuroscience* 10, 1185–1201. doi: 10.1016/0306-4522(83)90108-2
- Mi, D., Li, Z., Lim, L., Li, M., Moissidis, M., Yang, Y., et al. (2018). Early emergence of cortical interneuron diversity in the mouse embryo. *Science* 360, 81–85. doi: 10.1126/science.aar6821
- Mincses, V., Pinto, L., Dan, Y., and Chiba, A. A. (2017). Cholinergic shaping of neural correlations. *Proc. Natl. Acad. Sci. U S A* 114, 5725–5730. doi: 10.1073/pnas.1621493114
- Mori, T., Yuxing, Z., Takaki, H., Takeuchi, M., Iseki, K., Hagino, S., et al. (2004). The LIM homeobox gene, *L3/Lhx8*, is necessary for proper development of basal forebrain cholinergic neurons. *Eur. J. Neurosci.* 19, 3129–3141. doi: 10.1111/j.0953-816x.2004.03415.x
- Mufson, E. J., Martin, T. L., Mash, D. C., Wainer, B. H., and Mesulam, M. M. (1986). Cholinergic projections from the parabrachial nucleus (Ch8) to the superior colliculus in the mouse: a combined analysis of horseradish peroxidase transport and choline acetyltransferase immunohistochemistry. *Brain Res.* 370, 144–148. doi: 10.1016/0006-8993(86)91114-5
- Muñoz-Manchado, A. B., Bengtsson Gonzales, C., Zeisel, A., Munguba, H., Bekkouche, B., Skene, N. G., et al. (2018). Diversity of interneurons in the dorsal striatum revealed by single-cell RNA sequencing and PatchSeq. *Cell Rep.* 24, 2179.e7–2190.e7. doi: 10.1016/j.celrep.2018.07.053
- Nagy, J., Kobilak, J., Berzensyi, S., Abraham, Z., Avci, H. X., Bock, I., et al. (2017). Altered neurite morphology and cholinergic function of induced pluripotent stem cell-derived neurons from a patient with Kleefstra syndrome and autism. *Transl. Psychiatry* 7:e1179. doi: 10.1038/tp.2017.144
- Nelson, A. B., Bussert, T. G., Kreitzer, A. C., and Seal, R. P. (2014). Striatal cholinergic neurotransmission requires VGLUT3. *J. Neurosci.* 34, 8772–8777. doi: 10.1523/jneurosci.0901-14.2014
- Nóbrega-Pereira, S., Gelman, D., Bartolini, G., Pla, R., Pierani, A., and Marin, O. (2010). Origin and molecular specification of globus pallidus neurons. *J. Neurosci.* 30, 2824–2834. doi: 10.1523/jneurosci.4023-09.2010
- Novak, G., Fan, T., O'Dowd, B. F., and George, S. R. (2013). Striatal development involves a switch in gene expression networks, followed by a myelination event: implications for neuropsychiatric disease. *Synapse* 67, 179–188. doi: 10.1002/syn.21628
- Okada, K., Nishizawa, K., Fukabori, R., Kai, N., Shiota, A., Ueda, M., et al. (2014). Enhanced flexibility of place discrimination learning by targeting striatal cholinergic interneurons. *Nat. Commun.* 5:3778. doi: 10.1038/ncomms4778
- Okada, K., Nishizawa, K., Setogawa, S., Hashimoto, K., and Kobayashi, K. (2018). Task-dependent function of striatal cholinergic interneurons in behavioural flexibility. *Eur. J. Neurosci.* 47, 1174–1183. doi: 10.1111/ejn.13768
- Oswald, M. J., Oorschot, D. E., Schulz, J. M., Lipski, J., and Reynolds, J. N. (2009). IH current generates the afterhyperpolarisation following activation of subthreshold cortical synaptic inputs to striatal cholinergic interneurons. *J. Physiol.* 587, 5879–5897. doi: 10.1113/jphysiol.2009.177600
- Pepeu, G., and Grazia Giovannini, M. (2017). The fate of the brain cholinergic neurons in neurodegenerative diseases. *Brain Res.* 1670, 173–184. doi: 10.1016/j.brainres.2017.06.023
- Petzold, A., Valencia, M., Pal, B., and Mena-Segovia, J. (2015). Decoding brain state transitions in the pedunculopontine nucleus: cooperative phasic and tonic mechanisms. *Front. Neural Circuits* 9:68. doi: 10.3389/fnirc.2015.00068
- Pombero, A., Bueno, C., Saglietti, L., Rodenas, M., Guimera, J., Bulfone, A., et al. (2011). Pallial origin of basal forebrain cholinergic neurons in the nucleus basalis of Meynert and horizontal limb of the diagonal band nucleus. *Development* 138, 4315–4326. doi: 10.1242/dev.069534
- Robbe, D. (2018). To move or to sense? Incorporating somatosensory representation into striatal functions. *Curr. Opin. Neurobiol.* 52, 123–130. doi: 10.1016/j.conb.2018.04.009
- Rudy, B., Fishell, G., Lee, S., and Hjerling-Leffler, J. (2011). Three groups of interneurons account for nearly 100% of neocortical GABAergic neurons. *Dev. Neurobiol.* 71, 45–61. doi: 10.1002/dneu.20853
- Sandberg, M., Taher, L., Hu, J., Black, B. L., Nord, A. S., and Rubenstein, J. L. R. (2018). Genomic analysis of transcriptional networks directing progression of cell states during MGE development. *Neural Dev.* 13:21. doi: 10.1186/s13064-018-0119-4
- Saunders, A., Granger, A. J., and Sabatini, B. L. (2015). Corelease of acetylcholine and GABA from cholinergic forebrain neurons. *Elife* 4:e06412. doi: 10.7554/elife.06412
- Scarr, E., Gibbons, A. S., Neo, J., Udawela, M., and Dean, B. (2013). Cholinergic connectivity: it's implications for psychiatric disorders. *Front. Cell. Neurosci.* 7:55. doi: 10.3389/fncel.2013.00055
- Semba, K., Vincent, S. R., and Fibiger, H. C. (1988). Different times of origin of choline acetyltransferase- and somatostatin-immunoreactive neurons in the rat striatum. *J. Neurosci.* 8, 3937–3944. doi: 10.1523/jneurosci.08-10-03937.1988
- Shimo, Y., and Hikosaka, O. (2001). Role of tonically active neurons in primate caudate in reward-oriented saccadic eye movement. *J. Neurosci.* 21, 7804–7814. doi: 10.1523/jneurosci.21-19-07804.2001
- Simon, A. P., Poindessous-Jazat, F., Dutar, P., Epelbaum, J., and Bassant, M. H. (2006). Firing properties of anatomically identified neurons in the medial septum of anesthetized and unanesthetized restrained rats. *J. Neurosci.* 26, 9038–9046. doi: 10.1523/jneurosci.1401-06.2006
- Smith, R., Chung, H., Rundquist, S., Maat-Schieman, M. L., Colgan, L., Englund, E., et al. (2006). Cholinergic neuronal defect without cell loss in Huntington's disease. *Hum. Mol. Genet.* 15, 3119–3131. doi: 10.1093/hmg/ddl252
- Straub, C., Saulnier, J. L., Begue, A., Feng, D. D., Huang, K. W., and Sabatini, B. L. (2016). Principles of synaptic organization of GABAergic interneurons in the striatum. *Neuron* 92, 84–92. doi: 10.1016/j.neuron.2016.09.007
- Sussell, L., Marin, O., Kimura, S., and Rubenstein, J. L. (1999). Loss of *Nkx2.1* homeobox gene function results in a ventral to dorsal molecular respecification within the basal telencephalon: evidence for a transformation of the pallidum into the striatum. *Development* 126, 3359–3370.
- Takács, V. T., Cserép, C., Schlingloff, D., Pósfai, B., Szonyi, A., Sos, K. E., et al. (2018). Co-transmission of acetylcholine and GABA regulates hippocampal states. *Nat. Commun.* 9:2848. doi: 10.1038/s41467-018-05136-1
- Tasic, B., Menon, V., Nguyen, T. N., Kim, T. K., Jarsky, T., Yao, Z., et al. (2016). Adult mouse cortical cell taxonomy revealed by single cell transcriptomics. *Nat. Neurosci.* 19, 335–346. doi: 10.1038/nn.4216
- Tasic, B., Yao, Z., Graybiel, L. T., Smith, K. A., Nguyen, T. N., Bertagnoli, D., et al. (2018). Shared and distinct transcriptomic cell types across neocortical areas. *Nature* 563, 72–78. doi: 10.1038/s41586-018-0654-5
- Taylor, P., and Brown, J. H. (1999). "Synthesis, storage and release of acetylcholine," in *Basic Neurochemistry: Molecular, Cellular and Medical Aspects* 6th Edn., eds G. J. Siegel, B. W. Agranoff and R. W. Alberts (Philadelphia, PA: Lippincott-Raven), 213–242
- Teles-Grilo Ruivo, L. M., and Mellor, J. R. (2013). Cholinergic modulation of hippocampal network function. *Front. Synaptic Neurosci.* 5:2. doi: 10.3389/fnsyn.2013.00002
- Tepper, J. M., Koós, T., Ibanez-Sandoval, O., Tecuapetla, F., Faust, T. W., and Assouf, M. (2018). Heterogeneity and diversity of striatal gabaergic interneurons: update 2018. *Front. Neuroanat.* 12:91. doi: 10.3389/fnana.2018.00091
- Terry, A. V. Jr. (2008). Role of the central cholinergic system in the therapeutics of schizophrenia. *Curr. Neuropharmacol.* 6, 286–292. doi: 10.2174/157015908785777247
- Touzot, A., Ruiz-Reig, N., Vitalis, T., and Studer, M. (2016). Molecular control of two novel migratory paths for CGE-derived interneurons in the developing mouse brain. *Development* 143, 1753–1765. doi: 10.1242/dev.131102

- Tritsch, N. X., Ding, J. B., and Sabatini, B. L. (2012). Dopaminergic neurons inhibit striatal output through non-canonical release of GABA. *Nature* 490, 262–266. doi: 10.1038/nature11466
- Unal, C. T., Golowasch, J. P., and Zaborszky, L. (2012). Adult mouse basal forebrain harbors two distinct cholinergic populations defined by their electrophysiology. *Front. Behav. Neurosci.* 6:21. doi: 10.3389/fnbeh.2012.00021
- Villar-Cerviño, V., Kappeler, C., Nóbrega-Pereira, S., Henkemeyer, M., Rago, L., Nieto, M. A., et al. (2015). Molecular mechanisms controlling the migration of striatal interneurons. *J. Neurosci.* 35, 8718–8729. doi: 10.1523/JNEUROSCI.4317-14.2015
- Vogt, D., Hunt, R. F., Mandal, S., Sandberg, M., Silberberg, S. N., Nagasawa, T., et al. (2014). Lhx6 directly regulates Arx and CXCR7 to determine cortical interneuron fate and laminar position. *Neuron* 82, 350–364. doi: 10.1016/j.neuron.2014.02.030
- von Engelhardt, J., Eliava, M., Meyer, A. H., Rozov, A., and Monyer, H. (2007). Functional characterization of intrinsic cholinergic interneurons in the cortex. *J. Neurosci.* 27, 5633–5642. doi: 10.1523/JNEUROSCI.4647-06.2007
- Wamsley, B., and Fishell, G. (2017). Genetic and activity-dependent mechanisms underlying interneuron diversity. *Nat. Rev. Neurosci.* 18, 299–309. doi: 10.1038/nrn.2017.30
- Wichterle, H., Alvarez-Dolado, M., Erskine, L., and Alvarez-Buylla, A. (2003). Permissive corridor and diffusible gradients direct medial ganglionic eminence cell migration to the neocortex. *Proc. Natl. Acad. Sci. U S A* 100, 727–732. doi: 10.1073/pnas.242721899
- Yamanaka, K., Hori, Y., Minamimoto, T., Yamada, H., Matsumoto, N., Enomoto, K., et al. (2018). Roles of centromedian parafascicular nuclei of thalamus and cholinergic interneurons in the dorsal striatum in associative learning of environmental events. *J. Neural Transm.* 125, 501–513. doi: 10.1007/s00702-017-1713-z
- Yap, E. L., and Greenberg, M. E. (2018). Activity-regulated transcription: bridging the gap between neural activity and behavior. *Neuron* 100, 330–348. doi: 10.1016/j.neuron.2018.10.013
- Zaborszky, L., Csordas, A., Mosca, K., Kim, J., Gielow, M. R., Vadasz, C., et al. (2015). Neurons in the basal forebrain project to the cortex in a complex topographic organization that reflects corticocortical connectivity patterns: an experimental study based on retrograde tracing and 3D reconstruction. *Cereb. Cortex* 25, 118–137. doi: 10.1093/cercor/bht210
- Záborszky, L., Gombkoto, P., Varsanyi, P., Gielow, M. R., Poe, G., Role, L. W., et al. (2018). Specific basal forebrain-cortical cholinergic circuits coordinate cognitive operations. *J. Neurosci.* 38, 9446–9458. doi: 10.1523/JNEUROSCI.1676-18.2018
- Zeisel, A., Hochgerner, H., Lönnerberg, P., Johnsson, A., Memic, F., van der Zwan, J., et al. (2018). Molecular architecture of the mouse nervous system. *Cell* 174, 999.e22–1014.e22. doi: 10.1016/j.cell.2018.06.021
- Zeisel, A., Muñoz-Manchado, A. B., Codeluppi, S., Lönnerberg, P., La Manno, G., Jureus, A., et al. (2015). Brain structure. Cell types in the mouse cortex and hippocampus revealed by single-cell RNA-seq. *Science* 347, 1138–1142. doi: 10.1126/science.aaa1934
- Zhang, Y. F., Reynolds, J. N. J., and Cragg, S. J. (2018). Pauses in cholinergic interneuron activity are driven by excitatory input and delayed rectification, with dopamine modulation. *Neuron* 98, 918.e3–925.e3. doi: 10.1016/j.neuron.2018.04.027
- Zhao, Y., Marin, O., Hermes, E., Powell, A., Flames, N., Palkovits, M., et al. (2003). The LIM-homeobox gene Lhx8 is required for the development of many cholinergic neurons in the mouse forebrain. *Proc. Natl. Acad. Sci. U S A* 100, 9005–9010. doi: 10.1073/pnas.1537759100
- Zheng, Y., Feng, S., Zhu, X., Jiang, W., Wen, P., Ye, F., et al. (2018). Different subgroups of cholinergic neurons in the basal forebrain are distinctly innervated by the olfactory regions and activated differentially in olfactory memory retrieval. *Front. Neural Circuits* 12:99. doi: 10.3389/fncir.2018.00099
- Zhou, K., Cherra, S. J. III., Goncharov, A., and Jin, Y. (2017). Asynchronous cholinergic drive correlates with excitation-inhibition imbalance via a neuronal Ca<sup>2+</sup> sensor protein. *Cell Rep.* 19, 1117–1129. doi: 10.1016/j.celrep.2017.04.043
- Ztaou, S., Maurice, N., Camon, J., Guiraudie-Capraz, G., Kerkerian-Le Goff, L., Beurrier, C., et al. (2016). Involvement of striatal cholinergic interneurons and M1 and M4 muscarinic receptors in motor symptoms of Parkinson's disease. *J. Neurosci.* 36, 9161–9172. doi: 10.1523/JNEUROSCI.0873-16.2016
- Zucca, S., Zucca, A., Nakano, T., Aoki, S., and Wickens, J. (2018). Pauses in cholinergic interneuron firing exert an inhibitory control on striatal output *in vivo*. *Elife* 7:e32510. doi: 10.7554/eLife.32510

**Conflict of Interest Statement:** The authors declare that the research was conducted in the absence of any commercial or financial relationships that could be construed as a potential conflict of interest.

Copyright © 2019 Ahmed, Knowles and Dehorter. This is an open-access article distributed under the terms of the Creative Commons Attribution License (CC BY). The use, distribution or reproduction in other forums is permitted, provided the original author(s) and the copyright owner(s) are credited and that the original publication in this journal is cited, in accordance with accepted academic practice. No use, distribution or reproduction is permitted which does not comply with these terms.

## **Appendix B: Research Paper (Ahmed et al. 2021)**

Original Research Paper published in Journal of Neuroscience

**N. Y. Ahmed\***, Y. Ranjbar-Slamloo\*, A. S. Al Abed, L. Gao, Y. Sontani, R. C.-H. c.-G. A, E. Arabzadeh and N. Dehorter (2021). "Er81 Transcription Factor Fine-Tunes Striatal Cholinergic Interneuron Activity and Drives Habit Formation." J Neurosci 41(20): 4392-4409.

\*Equally contributed

# Er81 Transcription Factor Fine-Tunes Striatal Cholinergic Interneuron Activity and Drives Habit Formation

Noorya Yasmin Ahmed,\* Yadollah Ranjbar-Slamloo,\* Alice Shaam Al Abed, Lingxiao Gao, Yovina Sontani, Alexandre RCom-H'cheo-Gauthier, Ehsan Arabzadeh, and Nathalie Dehorter

Eccles Institute of Neuroscience, John Curtin School of Medical Research, Australian National University, Canberra, Australian Capital Territory 2601, Australia

The molecular mechanisms tuning cholinergic interneuron (CIN) activity, although crucial for striatal function and behavior, remain largely unexplored. Previous studies report that the *Etv1/Er81* transcription factor is vital for regulating neuronal maturation and activity. While *Er81* is known to be expressed in the striatum during development, its specific role in defining CIN properties and the resulting consequences on striatal function is unknown. We report here that *Er81* is expressed in CINs and its specific ablation leads to prominent changes in their molecular, morphologic, and electrophysiological features. In particular, the lack of *Er81* amplifies intrinsic delayed-rectifier and hyperpolarization-activated currents, which subsequently alters the tonic and phasic activity of CINs. We further reveal that *Er81* expression is required for normal CIN pause and time-locked responses to sensorimotor inputs in awake mice. Overall, this study uncovers a new cell type-specific control of CIN function in the striatum which drives habit formation in adult male mice.

**Key words:** interneuron; tuning; striatum; activity; habit

## Significance Statement

Although previous studies have shown that cholinergic interneurons drive striatal activity and habit formation, the underlying molecular mechanisms controlling their function are unknown. Here we reveal that key cholinergic interneuron physiological properties are controlled by *Er81*, a transcription factor regulating neuronal activity and development in a cell-specific manner. Moreover, our findings uncover a link between the *Er81*-dependent molecular control of cholinergic interneuron function and habit formation in mice. These insights will contribute to the future enhancement of our understanding of disorders that involve behavioral inflexibility, such as autism and addiction.

## Introduction

Cholinergic interneurons (CINs) constitute only 1%–2% of all striatal neurons but are the main source of acetylcholine in the striatum and play a crucial role in regulating habitual behavior (Aoki et al., 2018). As the specific timing of CIN firing could be essential for habit regulation, it is crucial to understand how fine-tuned CIN activity contributes to striatal function. Unique morphological and electrophysiological features (Lim et al.,

2014) underpin CIN function in controlling the striatal output neurons (Mamaligas and Ford, 2016; Gritton et al., 2019). CINs fire tonically and display phasic responses to stimuli, which consist of pauses preceded by a transient rise and followed by a “rebound” of CIN activity (Apicella, 2017). The pause in CIN firing is fundamental for striatal processing of information and behavior (Zucca et al., 2018). The tonic and phasic activity of CINs is governed by both synaptic inputs and the intrinsic inward (Z. Zhao et al., 2016) and delayed rectifier currents (Wilson and Goldberg, 2006), referred to as  $I_h$  and  $I_{sAHP}$ , respectively. In particular, pause expression is mediated by the slow  $Kv7$ -dependent potassium current  $I_{Kr}$  in response to excitatory inputs and is regulated by dopamine (Straub et al., 2014; Zhang et al., 2018) and GABA (Lozovaya et al., 2018). The role of molecular factors in regulating the pause of CINs and in controlling the acquisition of these properties during maturation remains unexplored.

Recent findings suggest that developmental differentiation factors induce some degree of functional diversity among CINs, thus enabling them to acquire unique properties (Ahmed et al., 2019). Notably, the LIM homeodomain transcription factor *Lhx6*, which

Received Apr. 23, 2020; revised Mar. 28, 2021; accepted Apr. 2, 2021.

Author contributions: Y.R.-S., N.Y.A., A.S.A.A., L.G., Y.S., A.R.-H.G., and N.D. performed research; Y.R.-S., N.Y.A., A.S.A.A., L.G., Y.S., A.R.-H.G., and E.A. analyzed data; Y.R.-S. and N.D. wrote the first draft of the paper; Y.R.-S., N.Y.A., A.S.A.A., Y.S., and N.D. edited the paper; Y.R.-S., N.Y.A., and N.D. wrote the paper; N.Y.A., L.G., E.A., and N.D. designed research.

The authors declare no competing financial interests.

This work was supported by National Health and Medical Research Council Grant APP1144145 and the Australian National University. We thank Prof. Silvia Arber and Prof. Oscar Marin for the *Er81* antibody and *Er81* conditional mutant mice; and Prof. John Bekkers and Prof. Bernard Balleine for critical comments on the manuscript.

\*N.Y.A. and Y.R.-S. contributed equally to this work.

Correspondence should be addressed to Nathalie Dehorter at [nathalie.dehorter@anu.edu.au](mailto:nathalie.dehorter@anu.edu.au).

<https://doi.org/10.1523/JNEUROSCI.0967-20.2021>

Copyright © 2021 the authors

is required for GABAergic interneuron specification, segregates a subtype of GABAergic CIN with distinct functional properties (Lozovaya et al., 2018). The ETS transcription factor ETV1/Er81 plays specific roles in maturation (Abe et al., 2011; Ding et al., 2016), identity (Cave et al., 2010), and the establishment of synaptic connections (Arber et al., 2000; Hippenmeyer et al., 2005). Er81 also regulates cell excitability by controlling the expression of a potassium channel subunit in adult cortical interneurons (Dehorter et al., 2015). In the striatum, it is expressed in subclasses of interneurons (Mi et al., 2018; Nóbrega-Pereira et al., 2008), but its specific cellular distribution and function in CINs are unknown. We hypothesized that Er81 plays a fundamental role in determining key features of maturing striatal CINs and in controlling their function. Using molecular, electrophysiological, and behavioral approaches, we reveal that the Er81 transcription factor is necessary to set major functional properties of CINs. We unravel its role as a key contributing factor for pause expression, regulation of striatal activity, and habitual behavior.

## Materials and Methods

**Mice.** We generated *Er81<sup>+/+</sup>*; *ChAT-Cre* (control; ChAT: choline acetyltransferase) and *Er81<sup>flox/flox</sup>*; *ChAT-Cre* (*Er81* conditional KO [cKO]) mice by crossing *Er81<sup>flox/flox</sup>* mice (generous gift by Prof Marin at the MRC, London) with *ChAT-Cre* mice (#006410 *ChAT-IRES-Cre* from The Jackson Laboratory). We also generated *Er81<sup>+/+</sup>*; *ChAT-Cre*; *RCE-GFP* (control) and *Er81<sup>flox/flox</sup>*; *ChAT-Cre*; *RCE-GFP* (*Er81* cKO) mice by crossing *Er81<sup>+/+</sup>*; *ChAT-Cre* or *Er81<sup>flox/flox</sup>*; *ChAT-Cre* with *Er81<sup>+/+</sup>*; *RCE-GFP* or *Er81<sup>flox/flox</sup>*; *RCE-GFP* (kindly supplied by Prof Marin at the MRC, London). We used the *Er81<sup>+/+</sup>*; *Nkx2.1-CreER*; *RCE-GFP* (control) and *Er81<sup>flox/flox</sup>*; *Nkx2.1-Cre*; *RCE-GFP* (*Er81* cKO) mice for the analysis of the CIN morphology. *Lhx6-Cre*; *RCE-GFP* mice were used to analyze Er81 expression regarding the Lhx6 phenotype of CINs. All experiments were conducted with approval from the Australian National University Animal Experimentation Ethics Committee (protocol numbers A 2016/14, A2018/43, and A2018/66). All efforts were made to minimize suffering and reduce the number of animals. Only male mice were used in this study.

**In vitro electrophysiological recordings.** We used *Er81<sup>+/+</sup>*; *ChAT-Cre*; *RCE-GFP* (control) and *Er81<sup>flox/flox</sup>*; *ChAT-Cre*; *RCE-GFP* (*Er81* mutant) mice at P6–7 or P30–P60 for slice electrophysiology experiments. Mice were deeply anesthetized with isoflurane and perfused with ice-cold oxygenated ACSF containing the following (in mM): 248 sucrose, 3 KCl, 0.5 CaCl<sub>2</sub>, 4 MgCl<sub>2</sub>, 1.25 NaH<sub>2</sub>PO<sub>4</sub>, 26 NaHCO<sub>3</sub>, and 1 glucose, saturated with 95% O<sub>2</sub> and 5% CO<sub>2</sub>. The animals were then decapitated, and brain was removed and placed in ice cold oxygenated sucrose-based cutting solution. Sagittal slices of 400 μm were cut using a VT1200S vibratome (Leica Microsystems). Slices were then maintained at room temperature in ACSF containing the following (in mM): 124 NaCl, 3 KCl, 2 CaCl<sub>2</sub>, 1 MgCl<sub>2</sub>, 1.25 NaH<sub>2</sub>PO<sub>4</sub>, 26 NaHCO<sub>3</sub>, and 10 glucose saturated with 95% O<sub>2</sub> and 5% CO<sub>2</sub>. For patch-clamp recordings in whole-cell configuration, slices were transferred to a chamber and continuously superfused with ACSF at 34°C. GFP-expressing cholinergic cells located in the dorsal striatum were visualized by infrared-differential interference optics with a 40× water-immersion objective. For targeting GFP-expressing neurons, slices were illuminated by blue light through the objective. Microelectrodes (4–6 MΩ) were pulled from borosilicate glass (1.5 mm outer diameter × 0.86 inner diameter) using a vertical P10 puller (Narishige).

For voltage-clamp recordings, a cesium gluconate-based intracellular solution was used containing the following (in mM): 120 Cs-gluconate, 13 CsCl, 1 CaCl<sub>2</sub>, 10 HEPES, and 10 EGTA (pH 7.2–7.4, 275–285 mOsm). We used the cesium-gluconate solution to measure spontaneous and miniature GABA<sub>A</sub> currents at the reversal potential for glutamatergic (10 mV) events and glutamatergic currents at –60 mV. For current-clamp recordings, we used a potassium-gluconate-based intracellular solution containing the following (in mM): 140 K-gluconate, 10 HEPES, 2

NaCl, 4 KCl, 4 ATP, and 0.4 GTP. Neurobiotin (2–5 mg/ml) was added for postrecording immunocytochemistry. Electrophysiological signals were low-pass filtered online at 10 kHz with a Multiclamp 700B (Molecular Devices) amplifier and acquired at a 20 kHz sampling rate with a LIH 8 + 8 (HEKA) data acquisition board and WinWCP software (created by John Dempster, University of Strathclyde). Circuit capacitance was corrected after gigaseal formation. Series resistance and liquid junction potential were not corrected. Cell-attached spikes were recorded for at least 60 s, after gigaseal formation in voltage-clamp mode. Following break-in, the test pulse was monitored for a few seconds to ensure a stable, low access resistance ( $R_a < 20 \text{ M}\Omega$ ). In whole-cell configuration, spontaneous firing of the CINs was recorded for 60 s and then a current pulse of 200 pA was delivered for 3 s to obtain slow afterhyperpolarization (sAHP). An additional 60 s of spontaneous activity was recorded following the pulse. Then, a current-steps protocol (–200 pA to 225 pA, 25 pA steps, 3 s duration and 7 s intervals) was applied to obtain membrane properties and excitability of the cells. In voltage-clamp mode, membrane potential was held at –60 mV. Hyperpolarizing voltage pulses (–120 mV to –70 mV, 10 mV steps, 3 s duration and 7 s intervals) were applied to measure  $I_h$ . To measure delayed rectifier or  $I_{sAHP}$  currents, depolarizing voltage pulses were applied (–50 mV to –20 mV, 10 mV steps, 3 s duration and 7 s intervals). To measure postsynaptic currents (PSCs), the voltage was held at –60 mV for EPSCs or 10 mV for IPSCs. PSC rise and decay times were calculated as the intervals between 20% and 100% of the PSC peak before and after the peak, respectively.

Electrophysiological data were analyzed in MATLAB using custom-written codes. Spontaneous action potential (AP) before the first current pulse was taken to examine tonic activity of CINs. Threshold was detected based on the positive peaks occurring >10 mV/ms in the first derivative of the membrane potential trace. The AP width was defined as the interval between the first and second threshold crossings. The AHP amplitude and its peak delay were obtained at the minimum potential relative to the AP threshold within a 200 ms interval after the second threshold crossing of the AP. To plot the grand average APs, the traces were aligned to the AP threshold. A biexponential function was fit to the AHP to calculate rise and decay time constants. To characterize membrane potential dynamics following depolarization, APs were removed by linearly interpolating from 30 ms before the AP threshold to 100 ms after second threshold crossing point of the AP. The early component of sAHP was calculated by averaging 1 s of the  $V_m$  following the offset of the current pulse, and the late component was averaged from 1.5 to 4.5 s after the pulse offset, relative to the resting membrane potential. To plot the grand average trace of membrane potentials, the traces of the cells were aligned to the resting membrane potential. Input resistance ( $R_{in}$ ) was calculated at the minimum of the voltage response ( $V_{min}$  to –200 pA pulse) before the sag in  $V_m$  appeared. Sag ratio was calculated based on the following formula:  $Sag\ ratio = (V_{min} - V_{steady}) / (V_{min} - V_{rest})$ , where  $V_{min}$  was the minimum of the voltage during the pulse,  $V_{steady}$  was the average of membrane potential at 2.5–3 s after the onset of the current pulse, and  $V_{rest}$  was the medium of the membrane potential within 500 ms preceding the onset of the current pulse. APs were converted to 0 and 1 arrays based on their peak time and then averaged across neurons in 40 μs bins and smoothed with a 40 ms window to obtain instantaneous AP rates (see Figs. 2B, 3C). AP rate was calculated as the average over the pulse (see Fig. 2C). Statistical tests on the instantaneous firing rates were applied on intervals where the effect was consistently maintained. Adaptation index was calculated as the range of the interspike intervals divided by their minimum.

In voltage-clamp mode, hyperpolarizing and depolarizing voltage pulses were delivered to characterize inward rectifier ( $I_h$ ) and delayed rectifier ( $I_{sAHP}$ ) currents, respectively. To calculate  $I_{sAHP}$  (tail current), the current at 4–5 s following the offset of the voltage step was subtracted and a 4 s window following the offset was averaged across time.  $I_h$  was quantified by subtracting the positive peak of the current and then averaging from this peak to up to 2.9 s. Postsynaptic currents were isolated using a manual threshold and applying principal component analysis in MATLAB.

**In vivo recordings.** Adult *Er81<sup>flox/flox</sup>*; *ChAT-Cre* and *Er81<sup>+/+</sup>*; *ChAT-Cre* mice (P60–P80) were used for *in vivo* extracellular array recordings.

Animals were kept in individual cages and provided with *ad libitum* food and water. Before the surgical operation, anesthesia was induced by 3% isoflurane and the head was mounted on a stereotaxic device (Stoelting). Local anesthetic was applied to the scalp (Lignocaine, Lmx4) and eye gel (Viscotears from Novartis) to both eyes. The skull was exposed and cleared from fascia. A thin layer of tissue adhesive (Vetbond; 3M) was applied on the skull. A custom-made head bar was then glued to the skull and secured by dental cement. The cement was applied all over the skull, except the area of intended craniotomy, which was filled with silicon sealant (Kwik-Kast, WPI) at the end of the surgery. Animals were injected with 5 mg/kg of carprofen and 0.86 ml/kg of penicillin (intraperitoneal injections) and placed on a warm heating pad to recover from anesthesia. The animals were returned to their home cage and allowed 6 d of recovery from surgery. Then the mice were head-fixed for three sessions of 15–90 min over 3 d to habituate. On the following day, the mice were anesthetized with 3% isoflurane and two small craniotomies (<1 mm in diameter) were drilled (0.0–0.4 mm from bregma, 2.5 mm lateral) on both sides; and the dura was left intact, and the craniotomy was filled with silicon sealant. The first recording session started at least 3 h after the recovery from anesthesia. The recording probe was moved down to a depth of ~1.2 mm (distance of the tip from the dura) followed by ~0.1–0.2 mm advancement after each recording, with an active search for tonically active neurons when advancing the electrodes. This was repeated up to a depth of ~4 mm. In the second recording session (24 h later), the opposite craniotomy was used for recording.

At the end of second recording session, the mice were perfused transcardially and the brain was removed for histologic verification.

To obtain sensory driven responses in striatum, a bilateral train of air puffs (10 pulses of 200 ms/cycle) was applied to the whisker arrays during each recording using a Pico spritzer (Parker Instruments) device. The pressure was adjusted to generate visible movements of the whiskers allowing the puffers to be placed in front of the animal, out of the reach of the whiskers. The puff train was repeated every 10 s for 20 trials per recording. Electrophysiological data were acquired using 32 channel NeuroNexus double linear arrays (A1x32-Poly2-10 mm-50s-177, NeuroNexus) coupled with Cereplex Direct data acquisition system (BlackRock Microsystems). A high-speed imaging system (Mikrotron) was used to film the top view of the head at 250 frame/s during electrophysiological acquisition.

The depth of recording at each electrode site was calculated using the probe guidelines (A1x32-Poly2-10mm-50s-177). The whole span of recording depth for individual channels across animals was 0.37–4.20 mm. Based on histology data, we estimated the boundary between cortex and striatum to be at ~2 mm. We limited our analysis of striatal cells to 2.0–3.0 mm of depth. Cells were sorted and analyzed using custom written codes in MATLAB as follows. For every channel, 1.5 ms event waveforms were detected at 1 ms spaced peaks which exceeded 5 times root-mean-square of the high-pass filtered signal (at 300 Hz). Mean spike rates across trials were smoothed by a 16.7 ms averaging window. The width of the average spike waveforms of each cell was calculated at half-amplitude to exclude 10% widest sorted waveforms from control and *Er81* cKO conditions. For classification of different cell types, putative FS cells defined by a narrow spike waveform (maximum width = 0.475 ms) (Dorst et al., 2020) were discarded alongside artifacts by excluding the narrowest 20%. Spiny projection neurons (SPNs) and CIN were both defined by wider waveforms (Dorst et al., 2020). CINs were separated from SPNs by their average spontaneous firing rate in quiet state (with a threshold at 1 Hz, to distinguish low and high spontaneous activity) (English et al., 2011), their evoked response (i.e., the direction of the change in firing rate during 2 s of air puff stimulation compared with the spontaneous activity) and the proportion of long ISIs (i.e., ISI > 2 s, PropISI), as described by Benhamou et al. (2014). CINs typically respond to sensorimotor inputs (Benhamou et al., 2014; Gritton et al., 2019) through suppression or pause of their ongoing tonic activity with cortical and thalamic inputs (Ding et al., 2010; Doig et al., 2014) or with salient sensory stimuli (Aosaki et al., 1994; Apicella et al., 1997, 2009; Ravel et al., 2003; Morris et al., 2004; Thorn and Graybiel, 2014). Moreover, CIN responses to sensorimotor inputs can also be heterogeneous (Benhamou et al., 2014; Gritton et al., 2019). These criteria divided

the units into four groups: (1) excited SPNs with spontaneous firing rate < 1 Hz, (2) inhibited SPNs with spontaneous firing rate < 1 Hz, (3) inhibited CINs with spontaneous firing rate  $\geq$  1 Hz and small propISIs (<30%), and (4) excited CINs/other interneurons (Beatty et al., 2012) with spontaneous firing rate  $\geq$  1 Hz and small propISIs (<30%). All ISIs were computed based on the spontaneous activity (i.e., activity during quiet states). We sorted the data in each group based on the extent of change in firing rate ( $\delta$  firing rate) during stimulus presentation (see Fig. 6D,E). We then segregated the sorted responses into 10 equal-sized fractions based on the total cell number in each group, to ensure that similarly responsive neurons are considered when comparing the changes in firing rate between the control and *Er81* cKO conditions. In order to include the head and whisker motions in the analysis, MATLAB's foreground detection algorithm was used to obtain a motion index (average of the image in binary foreground images). Spike triggered averaging (STA) of the motion index was then performed for each cell and the resulting STA was normalized within the interval (–3 to 3 s). Correlations between firing rate and the air puff and motion were calculated using cross-correlation analysis in MATLAB. For a smooth estimation of the firing rate, spike times were convolved by a leaky integrator function ( $dy/dt = -y$ ). Onsets of the air puffs were also convolved by the same function. The peaks of cross-correlations were chosen within a  $\pm 2$  s lag. Since there was no genotype effect on the lag of the peak, we used the peak cross-correlation to analyze the strength of correlations between the variables.

**Immunohistochemistry.** Animals were perfused transcardially with 0.01 M PBS to eliminate blood and extraneous material followed by 4% PFA under isoflurane anesthesia. Brains were left incubated for 2–5 h in PFA. The fixative was then removed from tissues by 3 washes in PBS. Tissues were sectioned at 60  $\mu$ m using a Leica 1000S vibratome and kept in a cryoprotective ethylene glycol solution at  $-20^{\circ}\text{C}$  until processed for immunofluorescence.

Sections were first washed and permeabilized; then nonspecific binding sites were blocked by immersing the tissue in 10% normal donkey serum, 2% BSA in PBS-T for 2 h. Tissues were then stained using the following primary antibodies overnight: mouse anti- $\beta$  galactosidase (1:1000; Promega), rabbit anti-*Er81* (1:5000; generous gift from Prof Silvia Arber; KO-validated) (Dehorter et al., 2015), chicken anti-GFP (1:3000; Aves Lab), mouse anti-parvalbumin (PV, 1:3000; Sigma Millipore), goat anti-ChAT (1:200; Merck), guinea pig anti-vGluT1 and -vGluT2 (1:2000; Chemicon) and anti-vGluT3 (1:2000; Merck), mouse anti-Lhx6 (1:X; Santa Cruz Biotechnology), rabbit anti-mgluR5 (1:50; Alomone Labs), sheep anti-Neuropeptide Y (1:1000; Merck), rabbit anti-KCNQ2 and anti-HCN2 (1:200; Thermo Fisher Scientific), mouse anti-c-Fos (1:500; Santa Cruz Biotechnology) or rabbit anti-p-Ser240-244-S6rp (1:500; Cell Signaling Technology). After 3 washes with 15 min intervals, we added anti-rabbit, anti-chicken, anti-mouse, anti-goat Alexa-488, -555, or -647 (1:200; Invitrogen) secondary antibodies for 2–3 h or anti-guinea pig biotinylated (1:200; Jackson ImmunoResearch Laboratories), anti-sheep biotinylated (1:200; Invitrogen) followed by streptavidin 555 or 647 for 1. After 3 washes with 15 min intervals, slices were stain for 10 min with DAPI (5  $\mu\text{M}$ ; Sigma Millipore), mounted on Livingstone slides, and then covered with Mowiol (Sigma Millipore) and coverslip (Thermo Fisher Scientific).

After patch-clamp recordings, slices were immediately fixed in 4% PFA for 2–5 h, rinsed in PBS (3 times, 30 min intervals), and kept overnight at  $4^{\circ}\text{C}$ . The same procedure as described above was performed for immunostaining. Images were acquired by a Nikon A1 confocal laser scanning microscope. Stained sections of control and mutant mice were imaged during the same imaging session; and laser power, photomultiplier gain, pinhole, and detection filter settings were kept constant. Immunofluorescence signals were quantified using ImageJ or MATLAB using routine particle analysis procedures to obtain soma or nuclear masks. The signal within masks was normalized to the background. The background masks were obtained by segmentation of thick fibers passing the striatum. To quantify the percent of  $\beta$ Gal-positive cells, the Cartesian distances between the weighted centroids of the ChAT<sup>+</sup> nuclei masks and  $\beta$ Gal masks (threshold at mean + 0.4 SD) were calculated. If the nucleus mask was within 5  $\mu\text{m}$  of a  $\beta$ Gal mask, the cell was considered as ChAT<sup>+</sup>  $\beta$ Gal<sup>+</sup>.

**Western blot.** Brains were dissected in ACSF, and the striatum and cortex were extracted. Tissues were placed in lysis buffer with 1%  $\beta$ -mercaptoethanol (Sigma Millipore) before storage at  $-80^{\circ}\text{C}$ . Total protein was extracted using the AllPrep DNA/RNA/Protein Mini Kit (QIAGEN, #80004) according to the manufacturer's instructions, including DNase treatment. The pellets were suspended in ALO buffer and then stored at  $-20^{\circ}\text{C}$ . We extracted the striatum and cortex and homogenized by handheld homogenizer, at 1:5 g/ml (50 mM Tris-HCl, pH 7.4, 0.32 M sucrose, 5 mM EDTA, 1% Triton X-100, 1% protease inhibitor cocktail) and then stored at  $-80^{\circ}\text{C}$ ; 20  $\mu\text{l}$  of each sample was run on 8%–16% Mini-PROTEAN TGX Stain-Free Gels (200V, 30 min), transferred to a PVDF membrane (340 mA, 70 min). The membrane was then blocked (1 h, 3% BSA in TBS-T), incubated overnight with primary antibody overnight with the guinea-pig anti-vGluT3 (Merck; 1:2000), goat anti-ChAT (Merck; 1:500), mouse anti-Lhx6 (Santa Cruz Biotechnology; 1:500), then washed (3 washes with 5 min intervals, TBS-T) before incubation with HRP-conjugated secondary antibody for 2 h (Bio-Rad, 1:1000). After 3 washes with 5 min intervals with TBS-T, we developed with Clarity Western ECL Blotting Substrates (Bio-Rad). Membranes were imaged by ChemiDoc MP System (Bio-Rad). For reprobing, blots were stripped with harsh stripping buffer for 30 min, then reblocked and probed  $\beta$ -tubulin for 1 h with the mouse anti- $\beta$ -tubulin (1:1000; Sigma Millipore). Bands were analyzed by area under curve relative to tubulin loading controls (Image Lab software).

**FACS.** Mice were rapidly decapitated, and brain slices were prepared as for electrophysiological recordings. Dorsal striatum was dissected and placed in ACSF, in a 15 ml tube with 10 ml digestion buffer (0.5  $\times$  g Trehalose and 10 mg Pronase, 1 mg DNase I, 50  $\mu\text{l}$   $\text{MgCl}_2$  1 M in oxygenated ACSF; Sigma Millipore) at  $37^{\circ}\text{C}$  for 30 min with inversion every 10 min. Tissues were allowed to settle on ice for 1 min, digestion buffer was removed, and the pellet was washed with 2 ml washing buffer (10 ml ACSF, 0.5  $\times$  g Trehalose, 1 mg DNase I, 50  $\mu\text{l}$   $\text{MgCl}_2$  1 M in oxygenated ACSF) at  $4^{\circ}\text{C}$ . To dissociate the cells, we resuspended the tissue in 1 ml wash buffer and triturated 12–15 times with 1 ml pipette. Tubes were placed on ice, large tissue pieces were allowed to settle, and  $\sim 500$   $\mu\text{l}$  of cloudy suspension containing dissociated cells was transferred to a 1.5 ml tube on ice. This process was repeated for the remaining 500  $\mu\text{l}$  suspension with 200  $\mu\text{l}$  pipette 12–15 times and pooled into the 1.5 ml tubes on ice. The last cells were removed by adding 200  $\mu\text{l}$  to the original tube. The cell suspension was filtered through a 70- $\mu\text{m}$ -tick mesh filter into a snap cap tube and 200  $\mu\text{l}$  DAPI 5  $\mu\text{M}$  was added to exclude dead cells. FACS Melody software was used for cell sorting. Cells were collected in 350  $\mu\text{l}$  of lysis buffer with 1%  $\beta$ -mercaptoethanol before storage at  $-80^{\circ}\text{C}$  for RNA extraction.

**qRT-PCR.** Total RNA was extracted using the RNeasy Micro kit (QIAGEN) according to the manufacturer's instructions, including DNase treatment. RNA concentration and purity were determined using the Nanodrop spectrophotometer (Thermo Fisher Scientific). RNA was reverse-transcribed into cDNA using SuperScriptIII First Strand Synthesis System (Invitrogen) with random hexanucleotides according to the manufacturer's instructions. cDNA was analyzed using real time qPCR, in technical triplicates using TaqManGene Expression Assay. Reactions were performed on a MicroAmp Optical 384-Well Reaction Plate with Bar code (Applied Biosystems). Each 10  $\mu\text{l}$  reaction included 5  $\mu\text{l}$  of TaqMan 2 $\times$  Universal PCR Master Mix (Applied Biosystems), 0.5  $\mu\text{l}$  of TaqMan probes gene expression assay, and 4.5  $\mu\text{l}$  of cDNA (5 ng total). PCRs were monitored using the 7900HT real time PCR system (Applied Biosystems). Amplification conditions were activation of AmpErase UNG for 2 min at  $50^{\circ}\text{C}$ , activation of AmpliTaq Gold Enzyme for 10 min at  $95^{\circ}\text{C}$ , followed by 40 cycles of denaturation at  $95^{\circ}\text{C}$  for 15 s, annealing at  $60^{\circ}\text{C}$  for 1 min, and extension at  $60^{\circ}\text{C}$  for 1 min. Relative quantification of mRNA level was performed using the comparative cycle threshold ( $C_T$ ) following the manufacturer's instructions (ABI). Results were normalized relative to the level of *GAPDH* (Mm99999915\_g1 from Thermo Fisher Scientific) using  $2^{-\Delta\Delta C_T}$  method. Primers used are as follows: *Gapdh* (Mm99999915\_g1); *Er81/Etv1* (Mm00514804\_m1); *Lhx6* (Mm01333348\_m1); *Isl1* (Mm00517585\_m1); *ChAT* (Mm01221880\_m1); *Slc5a7* (Mm00452075\_m1); *Grm5* (Mm00690332\_m1); *Kcnq2* (Mm00440080\_m1); *Hcn2* (Mm00468538\_

m1); *Gad2* (Mm00484623\_m1); *Zic4* (Mm00657066\_m1); *Ache* (Mm00477274\_g1); and *Lhx7* (Mm00802919\_m1). The changes in the level of gene expression by age were quantified as relative mRNA expression ( $\Delta C_T$ ) normalized to P30. The fold expression value of the genes of *Er81* cKO is obtained by deducting the *Er81* cKO value with the average of the control value of the same age. Two-sample *t* test was used for statistical analysis.

**Morphology and synaptic bouton analysis.** *Er81*<sup>+/+</sup>; *Nkx2.1-CreER*; *RCE-GFP* and *Er81*<sup>f/f</sup>; *Nkx2.1-CreER*; *RCE-GFP* P0 mouse pups were injected with low-titer tamoxifen (Sigma Millipore, 25  $\mu\text{l}$  of 10 mg/ml solution in corn oil, i.p.) to induce GFP expression and *Er81* cKO in MGE-derived interneurons *Nkx2.1*. Brains were removed after deep anesthesia under 3%–4% isoflurane, and PBS followed by 4% PFA was transcardially perfused. We then proceeded to the immunohistochemistry to select *Nkx2.1-GFP/ChAT*<sup>+</sup> interneurons. Images were acquired using a Nikon A1 Confocal microscope and the Nikon Instruments Elements software. Image stacks were acquired for morphologic reconstruction with 20 $\times$  objective. Images of neurons were acquired using with 60 $\times$  objective and 2 $\times$  scanning zoom for bouton analysis (stacks of 20–25  $\mu\text{m}$  with 1  $\mu\text{m}$  resolution) on the soma, proximal dendrites (<50  $\mu\text{m}$  from the soma), and distal dendrites (>90  $\mu\text{m}$  from the soma) (Hjorth et al., 2020). Parameters were kept consistent across WT and cKO slices. Morphologic quantification was done using the Surface and Filament tools in the IMARIS software. The automatic component of the filament tool reconstructed the dendritic field of the neuron with the dendrite beginning point set to 15  $\mu\text{m}$  and the end point set to 1  $\mu\text{m}$ . The volume of dendritic spread was found by using the Convex Hull Xtension of IMARIS. Bouton analysis was done using the Surface and Spots tools in IMARIS. The surface of the neuron soma or dendrite was reconstructed. A colocalization channel was created to identify individual boutons. This channel was then passed by a threshold to filter weak colocalizations. The brightest 30% of colocalized particles were chosen as boutons. Spots outside 1.5  $\mu\text{m}$  of the neuron surface were also excluded. Bouton density was calculated as the number of boutons divided by the surface area of the soma.

**Behavioral task.** Six-week-old *ChAT-Cre*; *Er81*<sup>+/+</sup> (control) and *ChAT-Cre*; *Er81*<sup>flox/flox</sup> (*Er81* cKO) mice were caged in standardized room conditions under a 12:12 light: dark cycle with *ad libitum* food and water. Starting 5 d before the behavioral task and throughout the training, mice were maintained under a mild water restriction (2 h ON/22 h OFF) with *ad libitum* food access. Mice were then trained in an arena (40 cm length  $\times$  27 cm width  $\times$  25 cm height) made of transparent Plexiglas, divided into three 9 cm corridors, and placed on top of a DigiGait apparatus (Mouse Specifics) where a camera recorded the ventral view of the animal in the middle corridor. The outer corridors were equipped with dispensers to deliver a drop of 10% sucrose in correct trials. We used custom-written MATLAB programs to automatically deliver rewards on lick detection through capacitance sensors, to monitor mouse behavior and to extract the data.

At the beginning of a session, mice were placed at the starting point of the middle corridor and had to go through one of the one-way gates to choose between the two outer corridors. If the choice was correct, the mouse could collect the reward automatically delivered by the dispenser. The mouse could then go back to the start area through a second one-way gate to start the next trial. Before acquisition, mice were habituated to the apparatus over a period of 6 d during which they were allowed to move freely in the maze, with both dispensers delivering the reward. To complete the habituation session, mice had to complete 10 trials, one trial being defined as running from the start site to one of the outer corridors, then back to the start site. If 10 trials were not completed after 40 min, the session was terminated.

During the acquisition phase, each mouse was required to complete 20 trials per session and one session a day for 3 d. Only one side contained the reward. The rewarding side (left or right) was homogenized within an experimental group and balanced between groups. On day 4, corresponding to reversal 1, the side containing the reward was switched for each mouse. Mice were then exposed to the new side for 10 consecutive sessions (day 4 to day 13). From day 14, corresponding to reversal 2, the reward sides were switched again. Mice were tested for 3 d. After

the training in day 14, some of the mice were removed from training for immunohistochemistry analyses. These mice displayed similar performance to those that fully completed the task (day 14:  $n = 5$  control and 4 *Er81* cKO mice; behavior vs cFos groups:  $F_{(3,21)} = 1.5$ ,  $p = 0.244$ ; one-way ANOVA; data not shown). Performance was defined as the percentage choice of the reward side, regardless of reward collection by the animal.

**Statistical analysis.** All statistical tests were conducted in MATLAB (The MathWorks), GraphPad Prism 8, and R, except for behavior (see below). When comparing two groups, data were passed to Shapiro–Wilk normality test to determine suitability for a parametric test. If the data passed this test, an independent two-tailed *t* test was applied; otherwise, a Wilcoxon rank sum test was performed. Pearson's correlation strength ( $\rho$ ) and *p* values were computed using MATLAB's *corr* function with its inbuilt *t* test. *p* values < 0.05 were considered statistically significant. We used one-way ANOVAs to analyze three or more groups of data. Two-way ANOVAs were used to analyze the interactions between two independent variables. All these tests were followed by Bonferroni's multiple comparisons test for pairwise comparisons when dealing with three or more groups. A random permutation test was performed by shuffling the STAs of the cells in the control and *Er81* cKO groups to compute 95% CI and determine the statistical significance of the differences between STAs in the control and the *Er81* cKO condition. For behavior, statistical analyses were performed with the StatView software, using two-way ANOVA to investigate statistical significance of interaction between repeated measures of daily performance and genotype, followed by Bonferroni's multiple comparisons test when appropriate. Statistical significance of performance against chance level (50%) was analyzed using two-tailed one-sample analyses.

Data are presented as mean  $\pm$  SEM. Exact *p* values are reported in the text. Individual points in each graph represent the samples used for the statistical analysis.

## Results

### Er81 is expressed in striatal cholinergic interneurons

We first analyzed the expression of the *Er81* transcription factor from birth to adulthood. We found that both mRNA ( $n = 8$  mice per group,  $F_{(5)} = 31.39$ ,  $p = 7.38 \times 10^{-11}$ , one-way ANOVA; P6 vs P30:  $p = 4.54 \times 10^{-9}$ , Bonferroni's multiple comparisons test; Fig. 1A) and protein levels (P6;  $n = 4$  mice vs P30;  $n = 6$  mice,  $t_{(8)} = 5.10$ ,  $p = 9.28 \times 10^{-4}$ , two-sample *t* test; Fig. 1B) significantly drop from postnatal day 6 (P6) to P30 in the total striatum. In CINs specifically, we observed a similar decrease in *Er81* protein levels from P6 to P30 (P6;  $n = 12$  mice vs P30;  $n = 10$  mice,  $t_{(20)} = 4.49$ ,  $p = 2.23 \times 10^{-4}$ , two-sample *t* test; Fig. 1C). To further determine the proportion of CINs expressing *Er81* at any stage during development, we utilized  $\beta$ -galactosidase staining, which perdures long after being synthesized (Dehorter et al., 2015). We found that most CINs ( $62 \pm 7\%$ ,  $n = 106$  cells) in the *Er81<sup>nlacZ/+</sup>* mice express  $\beta$ -galactosidase (and therefore *Er81*) in the striatum, unlike cholinergic cells in the basal forebrain ( $6 \pm 2\%$ ,  $n = 89$ ,  $z = 6.79$ ,  $p = 1.48 \times 10^{-11}$ , Wilcoxon rank sum test; Fig. 1D,E). As it has been shown that the LIM homeodomain transcription factor *Lhx6* segregates GABAergic CINs (Lozovaya et al., 2018), we next examined whether *Er81* expression was based on *Lhx6* segregation. We found that *Er81* is expressed in both *Lhx6*-positive and *Lhx6*-negative CINs (Fig. 1F,G), and was expressed at similar levels ( $Lhx6^+$ ;  $n = 154$  cells,  $Lhx6^-$ ;  $n = 110$  cells, 5 mice,  $z = 0.31$ ,  $p = 0.755$ , Wilcoxon rank sum test; data not shown). Thus, *Er81* and *Lhx6* expressions segregate different subgroups of CINs. To reveal a potential role of *Er81* in CIN maturation and/or function, we specifically removed *Er81* using cKO (*ChAT-Cre; Er81<sup>fl/fl</sup>* and control mice: *ChAT-Cre; Er81<sup>+/+</sup>*; Fig. 2A). We did not observe any change in cholinergic cell density within the striatum at P2 (while cells are

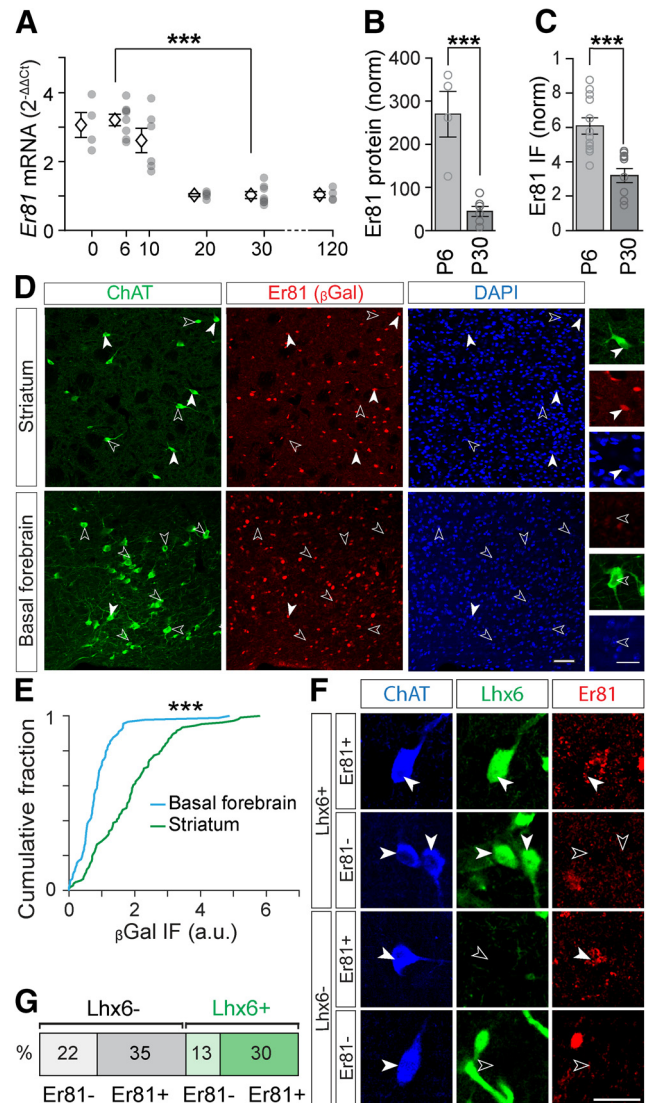


**Figure 1.** Expression of *Er81* in cholinergic interneurons. **A**, Postnatal expression of *Er81* mRNA from P0 to P120 in the dorsal striatum. Data normalized to P30. Stars represent Bonferroni's test result. **B**, *Er81* protein levels in P6 and P30 in the dorsal striatum quantified by Western blot. **C**, *Er81* protein levels in CINs of the striatum at P6 and P30. *Er81* immunofluorescence (IF) is normalized to the background of the images. **D**, *Er81* expression in *ChAT*<sup>+</sup> neurons in the striatum marked with  $\beta$ Gal at P30 (top row). Lack of *Er81* expression in *ChAT*<sup>+</sup> neurons in basal forebrain (bottom row). Scale bars: 50  $\mu$ m; Inset, 25  $\mu$ m. **E**, Cumulative distribution of the  $\beta$ Gal-expressing *ChAT*<sup>+</sup> cells in the striatum and basal forebrain. **F**, Immunostaining for *ChAT* (blue), *Lhx6* (GFP, green), and *Er81* (red). Scale bar, 30  $\mu$ m. **G**, Classification of CINs into four groups based on *Er81* and *Lhx6* expressions. \*\*\* $p < 0.001$ .

migrating) and P30 (when cells are established in the structure) between control and *Er81* cKO conditions, suggesting that the specific deletion of *Er81* does not affect CIN neurogenesis and migration (P2 control;  $n = 4011$  cells, 6 mice, P2 *Er81* cKO;  $n = 1050$  cells, 6 mice,  $t_{(10)} = 0.17$ ,  $p = 0.871$ , P30 control;  $n = 1084$  cells, 6 mice, P30 *Er81* cKO;  $n = 1050$  cells, 6 mice,  $t_{(10)} = 0.28$ ,  $p = 0.784$ , two-sample *t* tests; Fig. 2B).

### Cholinergic interneuron molecular and morphological properties change in the absence of *Er81*

We assessed the molecular properties of the CINs related to the presence of *Er81* in the striatum. First, we quantified the percentage of CINs expressing *Lhx6* protein (control;  $49 \pm 4\%$ ,  $n = 213$



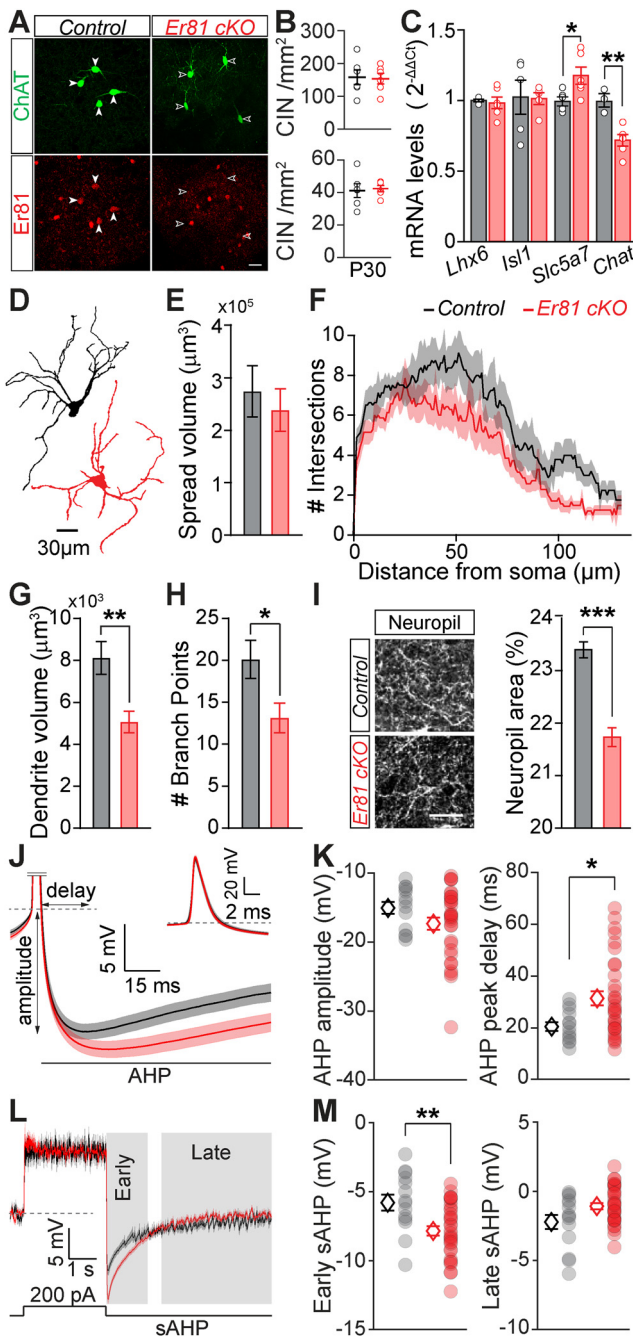


**Figure 2.** Alterations of the CIN properties in the absence of Er81. **A**, ChAT<sup>+</sup> interneurons in P30 striatum of a control (*Chat-Cre; Er81<sup>+/+</sup>*, left) and an *Er81* cKO (*Chat-Cre; Er81<sup>fl/fl</sup>*, right) mouse. Scale bar, 25  $\mu$ m. **B**, CIN density in the dorsal striatum at P2 (top) and P30 (bottom) in the *Er81* cKO compared with the control condition. **C**, Expression of key molecular markers of cholinergic cells in control and *Er81* cKO conditions. *Lhx6*, LIM homeobox 6; *Isl1*, *Isl1*; *Slc5a7*, choline transporter; *Chat*, choline acetyltransferase. **D**, Morphologic reconstruction of soma and dendrites of control (black) and *Er81* cKO (red) CINs at P30. **E**, Volume of dendritic spread in the control and the *Er81* cKO CINs. **F**, Sholl analysis representing the complexity of the dendritic field in the control and the *Er81* cKO. **G**, Total dendritic volume in the control and the *Er81* cKO CINs. **H**, Number of dendritic branch points in the control and the *Er81* cKO CINs. **I**, Left, ChAT<sup>+</sup> neuropil. Right, Quantification of the area occupied by ChAT<sup>+</sup> neuropil in the striatum. **J**, Grand average AHP waveforms ( $\pm$ SEM) in the control (black) and the *Er81* cKO (red). Inset, The AP. Dashed line indicates the AP threshold. AHP delay and amplitude were determined from individual APs. **K**, AHP amplitude (left) and AHP peak delay (right) in the control and the *Er81* cKO mice. Each dot represents the average AHP amplitude per cell. **L**, Average membrane potential ( $\pm$ SEM) during and after a 200 pA current injection. Individual traces were aligned to the resting membrane potential (dashed line). Gray shadings represent early and late phases of the slow AHP. **M**, Average of the early (left) and the

cells, 5 mice, *Er81* cKO;  $41 \pm 7\%$ ,  $n = 196$  cells, 5 mice,  $z = 0.42$ ,  $p = 0.676$ , Wilcoxon rank sum test; data not shown) as well as the *Lhx6* protein levels (control;  $0.48 \pm 0.049$  a.u.,  $n = 213$  cells, 5 mice; *Er81* cKO;  $0.50 \pm 0.078$  a.u.,  $n = 196$  cells, 5 mice,  $t_{(8)} = 0.18$ ,  $p = 0.858$ , two-sample  $t$  test; data not shown) and mRNA levels (control;  $n = 5$  mice, *Er81* cKO;  $n = 6$  mice,  $t_{(9)} = 0.37$ ,  $p = 0.716$ , two-sample  $t$  test; Fig. 2C) and found that they were not different between the control and the *Er81* cKO CINs at P30. This result reinforces the idea that striatal cholinergic population is molecularly diverse, and that *Er81* and *Lhx6* expression marks different CIN subgroups. We then analyzed other key markers to determine the effect *Er81* may have, as a transcriptional regulator, on CIN GABAergic identity throughout development. We found no change in *GAD2* (glutamic acid decarboxylase 2) and *Lhx6* mRNA at P6 (*Lhx6*, control;  $n = 8$  mice, *Er81* cKO;  $n = 6$ ;  $z = 1.87$ ,  $p = 0.061$ , Wilcoxon rank sum test; *GAD2*, control;  $n = 6$  mice, *Er81* cKO;  $n = 5$  mice,  $t_{(9)} = 0.43$ ,  $p = 0.674$ , two-sample  $t$  test; data not shown). These results suggest that *Er81* deletion does not affect the GABAergic cell identity of the CINs. We then quantified the expression of genes associated with striatal cholinergic cell identity, using FACS to select GFP-expressing CINs, followed by qPCR. We found only a select number of genes with altered expression following *Er81* ablation. At developmental stages, only the LIM homeodomain transcription factor *Isl1* (*Isl1*), which is necessary for CIN identity (Allaway and Machold, 2017), displayed an increase in mRNA expression (P6; 5 mice per group,  $t_{(8)} = 2.44$ ,  $p = 0.040$ ; Fig. 2C; P30; 5 mice per group,  $t_{(8)} = 0.12$ ,  $p = 0.906$ , two-sample  $t$  tests; data not shown). Other factors, such as the LIM homeodomain transcription factor *Lhx7* (Lopes et al., 2012) (P6; control;  $n = 9$  mice, *Er81* cKO;  $n = 4$  mice,  $t_{(11)} = 0.29$ ,  $p = 0.780$ , two-sample  $t$  test; data not shown), *Zic4* (Magno et al., 2017) (P6;  $n = 12$  mice per group,  $t_{(22)} = 0.04$ ,  $p = 0.966$ , two-sample  $t$  test; data not shown), acetylcholine esterase *Ache* (P6; control;  $n = 11$  mice; *Er81* cKO;  $n = 9$  mice,  $t_{(18)} = 0.190$ ,  $p = 0.851$ , two-sample  $t$  test; data not shown), and choline transporter *Slc5a7* (P6; control;  $n = 6$  mice; *Er81* cKO;  $n = 5$  mice,  $t_{(9)} = 0.16$ ,  $p = 0.878$ , two-sample  $t$  test; data not shown) mRNA levels showed no developmental changes following the KO. However, in adult stages, only *Slc5a7* expression was upregulated in the cKO condition (P30; control;  $n = 5$  mice, *Er81* cKO;  $n = 6$  mice,  $t_{(9)} = 2.40$ ,  $p = 0.040$ , two-sample  $t$  test; Fig. 2C). The main marker of cholinergic identity, choline acetyltransferase (*Chat*) mRNA and protein expressions significantly increased in the *Er81* cKO at P6 (mRNA; control;  $n = 10$  mice, *Er81* cKO;  $n = 9$  mice;  $2.03 \pm 0.19$ ,  $t_{(17)} = 4.84$ ,  $p = 1.52 \times 10^{-4}$ , protein; control;  $n = 4$  mice, *Er81* cKO;  $n = 5$  mice,  $t_{(7)} = 4.0$ ,  $p = 0.005$ , two-sample  $t$  test; data not shown). On the other hand, *Chat* mRNA level was lower (control;  $n = 3$  mice, *Er81* cKO;  $n = 6$  mice,  $t_{(7)} = 4.3$ ,  $p = 0.004$ , two-sample  $t$  test; Fig. 2C) and *Chat* protein levels were unchanged at P30 in the *Er81* cKO conditions (control;  $n = 4$  mice; *Er81* cKO;  $n = 4$  mice,  $z = 0.14$ ,  $p = 0.886$ , Wilcoxon rank sum test; data not shown), indicative of early maturation of the CINs. As *Er81* incites a number of molecular changes during developmental stages and in particular in dendritogenesis (Abe et al., 2011; Willardsen et al., 2014; Ding et al., 2016), we analyzed CIN dendritic properties and ChAT<sup>+</sup> neuropil area. While the overall spread and the number of

late phase of the slow AHP (right) in the two conditions. \* $p < 0.05$ ; \*\* $p < 0.01$ ; \*\*\* $p < 0.001$ .

**Table 1. Correlation between CIN physiological parameters and the Er81 expression levels at P6 and P30<sup>a</sup>**

rho	P6		P30			
	p	n	rho	p	n	
Resting membrane potential (mV)	−0.533	0.113	10	0.280	0.405	11
Membrane capacitance (pF)	−0.206	0.500	13	0.286	0.302	15
Membrane resistance (MΩ)	0.174	0.570	13	−0.327	0.234	15
AP threshold (mV)	−0.712	0.021*	10	0.337	0.310	11
AP amplitude (mV)	0.303	0.395	10	0.008	0.982	11
AP rise to peak (ms)	−0.377	0.283	10	−0.217	0.522	11
AP fall to threshold	0.195	0.589	10	0.102	0.766	11
AHP amplitude (mV)	0.162	0.654	10	0.137	0.688	11
AHP peak delay (ms)	0.279	0.435	10	0.280	0.405	11
AHP rise time constant (ms)	0.634	0.049*	10	−0.187	0.582	11
AHP decay time constant (ms)	−0.158	0.662	10	0.029	0.932	11
Spontaneous AP rate (whole-cell)	0.683	0.029*	10	0.353	0.287	11
Spontaneous AP rate (cell-attached)	0.345	0.569	5	0.442	0.321	7
Evoked AP rate (Hz)	0.109	0.765	10	0.469	0.146	11
First AP latency (ms)	0.269	0.452	10	−0.162	0.634	11
Early sAHP amplitude (mV)	−0.174	0.631	10	0.406	0.215	11
Late sAHP amplitude (mV)	−0.202	0.575	10	0.437	0.179	11
AP recovery time (s)	−0.332	0.382	10	−0.531	0.141	11
sEPSC frequency (Hz)	−0.254	0.426	12	−0.138	0.542	22
sEPSC amplitude (pA)	−0.357	0.254	12	0.067	0.767	22
sIPSC frequency (Hz)	−0.257	0.445	11	−0.250	0.486	10
sIPSC amplitude (pA)	−0.234	0.489	11	0.474	0.166	10
I <sub>h</sub> (pA)	0.375	0.256	11	−0.172	0.574	13
I <sub>sAHP</sub> (pA)	−0.324	0.434	8	0.633	0.251	5

<sup>a</sup>I<sub>h</sub>, Hyperpolarization-activated current; I<sub>sAHP</sub>, delayed rectifier current. \*p < 0.05.

dendritic intersections measured by Sholl analysis were unchanged (control; *n* = 8 cells, 3 mice, *Er81* cKO; *n* = 7 cells, 3 mice, spread volume:  $t_{(13)} = 0.55$ ,  $p = 0.591$ , two-sample *t* test; Sholl: two-way ANOVA,  $F_{(1,13, \text{genotype})} = 2.68$ ,  $p = 0.126$ ,  $F_{(150,1950, \text{interaction})} = 0.61$ ,  $p = 0.999$ ; Fig. 2D–F), the dendritic volume and number of branch points showed a significant reduction in the absence of *Er81* (dendrite volume;  $t_{(13)} = 3.18$ ,  $p = 0.007$ , number of branch points;  $t_{(13)} = 2.37$ ,  $p = 0.034$ ; Fig. 2G and H). In addition, CIN axonal projections were significantly decreased in the *Er81* cKO condition (ChAT neuropil area; control; *n* = 4 mice, *Er81* cKO; *n* = 3 mice,  $t_{(5)} = 7.06$ ,  $p = 8.8 \times 10^{-4}$ ; Fig. 2I). Together, these results show that *Er81* regulates key developmental genes and the morphologic complexity of the striatal CINs.

### ***Er81* deletion in cholinergic interneurons induces an increase in I<sub>h</sub> and I<sub>sAHP</sub> currents**

To determine how the *Er81* transcription factor regulates CIN functional properties, we performed *in vitro* whole-cell patch-clamp recordings from GFP-labeled ChAT-positive (ChAT<sup>+</sup>) neurons in control (*ChAT-cre; RCE-GFP; Er81<sup>+/+</sup>*) and *Er81* cKO mice (*ChAT-Cre; RCE-GFP; Er81<sup>fl/fl</sup>* mice). While we could not find any correlation between the expression of *Er81* and most of the CIN basic membrane properties at P6 and P30 in control conditions (Table 1), we did observe changes after *Er81* deletion from CINs at P6 (Table 2) and P30 (Table 3). In particular, the AHP phase of the APs was altered in the *Er81* cKO condition at P30, with significantly slower AHP kinetics (Table 3) compared with the control (P30; control; *n* = 13 cells, 4 mice, *Er81* cKO; *n* = 31 cells, 4 mice, AHP amplitude;  $z = 1.4$ ,  $p = 0.150$ , Wilcoxon rank sum test, AHP peak delay;  $z = 2.28$ ,  $p = 0.023$ ; Fig. 2J,K) but not at P6 (AHP amplitude; control; *n* = 13 cells, 4 mice, *Er81* cKO; *n* = 10 cells, 3 mice,  $z = 0.28$ ,  $p = 0.780$ , AHP peak

delay;  $z = 0.71$ ,  $p = 0.476$ , Wilcoxon rank sum tests; data not shown). The absence of *Er81* also led to a significant amplification of the early component of the induced sAHP, whereas the late component amplitude was not affected by *Er81* deletion (P30; control; *n* = 14 cells, 4 mice, *Er81* cKO; *n* = 33 cells, 4 mice; two-way ANOVA,  $F_{(1,45, \text{genotype})} = 0.56$ ,  $p = 0.459$ ,  $F_{(1,45, \text{interaction})} = 40.2$ ,  $p = 9.7 \times 10^{-8}$ , followed by Bonferroni's multiple comparisons test; early sAHP;  $p = 0.003$ , late sAHP;  $p = 0.126$ ; Fig. 2L,M). Analysis of sAHP at P6 stage did not reveal any difference between the control and the *Er81* cKO conditions (control; *n* = 13 cells, 4 mice, *Er81* cKO; *n* = 9 cells, 3 mice, two-way ANOVA,  $F_{(1,20, \text{genotype})} = 0.005$ ,  $p = 0.944$ ,  $F_{(1,20, \text{interaction})} = 0.011$ ,  $p = 0.918$ , followed by Bonferroni's multiple comparisons test; early sAHP;  $p > 0.999$ , late sAHP;  $p > 0.999$ ; data not shown). The preceding depolarization was not significantly different between the two groups at either stage (Tables 2, 3). To further analyze CIN physiological properties, we recorded the evoked firing responses and the tail currents responsible for sAHP (Wilson and Goldberg, 2006). CINs exhibited less persistent evoked firing in the *Er81* cKO mice (Fig. 3A). While the control CINs maintained a high rate of activity during stimulation, the instantaneous firing rate of the P30 *Er81* cKO cells quickly dropped (control; *n* = 16 cells, 5 mice, *Er81* cKO; *n* = 31 cells, 4 mice, two-way ANOVA;  $F_{(1,45, \text{genotype})} = 5.7$ ,  $p = 0.021$ ,  $F_{(1,45, \text{interaction})} = 3.1$ ,  $p = 0.084$ , followed by Bonferroni's multiple comparison test; 0–0.1 s;  $p = 0.470$ , 0.1–3 s;  $p = 0.008$ ; Fig. 3B). We did not observe such a difference at P6 (control; *n* = 16 cells, 5 mice, *Er81* cKO; *n* = 17 cells, 4 mice, two-way ANOVA;  $F_{(1,31, \text{genotype})} = 0.87$ ,  $p = 0.358$ ,  $F_{(1,31, \text{interaction})} = 0.12$ ,  $p = 0.728$ , followed by Bonferroni's multiple comparison test; 0–0.1 s;  $p = 0.696$ , 0.1–3 s;  $p > 0.999$ ; data not shown). Furthermore, the average firing rate of the CINs remained unchanged at P6 (control; *n* = 16 cells, 5 mice, *Er81* cKO; *n* = 17 cells, 4 mice, two-way ANOVA;  $F_{(1,31, \text{genotype})} = 0.52$ ,  $p = 0.477$ ,  $F_{(9,279, \text{interaction})} = 0.81$ ,  $p = 0.611$ ; data not shown) but was consistently lower in the *Er81* cKO conditions for all current intensities at P30 (control; *n* = 16 cells, 5 mice, *Er81* cKO; *n* = 31 cells, 4 mice, two-way ANOVA;  $F_{(1,45, \text{genotype})} = 13.7$ ,  $p = 5.7 \times 10^{-4}$ ,  $F_{(9,405, \text{interaction})} = 8.69$ ,  $p = 5.7 \times 10^{-12}$ ; Fig. 3C). Together, our results indicate that the initial responsiveness of the CINs is not altered, but their overall excitability is reduced because of stronger firing rate adaptations in the absence of *Er81* at P30 (control; *n* = 16 cells, 5 mice, *Er81* cKO; *n* = 31 cells, 4 mice, two-way ANOVA;  $F_{(1,45, \text{genotype})} = 8.6$ ,  $p = 0.005$ ,  $F_{(9,405, \text{interaction})} = 6.7$ ,  $p = 5.9 \times 10^{-9}$ ; Fig. 3D) but not at P6 (control; *n* = 16 cells, 5 mice, *Er81* cKO; *n* = 17 cells, 4 mice, two-way ANOVA;  $F_{(1,31, \text{genotype})} = 0.43$ ,  $p = 0.515$ ,  $F_{(9,279, \text{interaction})} = 0.48$ ,  $p = 0.884$ ; data not shown). It has been shown that CIN firing rate is controlled by I<sub>sAHP</sub>, which is composed of a large calcium-dependent delayed rectifier current (Wilson and Goldberg, 2006; Zhang et al., 2018) and the cadmium-insensitive, voltage-dependent IKr (Zhang et al., 2018). Therefore, the observed differences (Fig. 3B) might be because of an increase in I<sub>sAHP</sub> in the *Er81* cKO conditions. To test this, we applied a depolarizing pulse in voltage-clamp mode to activate I<sub>sAHP</sub> with both of its components (Wilson and Goldberg, 2006), which was maintained for a few seconds after the voltage pulse (Fig. 3E). We found that the amplitude of I<sub>sAHP</sub> remains unchanged at P6 (control; *n* = 9 cells, 5 mice, *Er81* cKO; *n* = 10 cells, 3 mice, two-way ANOVA;  $F_{(1,17, \text{genotype})} = 0.16$ ,  $p = 0.693$ ,  $F_{(3,51, \text{interaction})} = 0.45$ ,  $p = 0.721$ ; data not shown), but is significantly larger in the *Er81* cKO compared with the control CINs at P30 (control; *n* = 14 cells, 3 mice, *Er81* cKO; *n* = 22 cells, 4 mice, two-way ANOVA;  $F_{(1,34, \text{genotype})} = 6.0$ ,  $p = 0.019$ ,  $F_{(9,405, \text{interaction})} =$

**Table 2. Intrinsic properties of striatal CINs in the *Er81* cKO and the control mice at P6**

P6	Ctl	<i>n</i>	<i>Er81</i> cKO	<i>n</i>	represent Wilcoxon rank sum test, and	Statistic <sup>d</sup>	<i>p</i>
Resting membrane potential (mV)	−49.18 ± 1.03	13	−47.10 ± 1.49	9		$t_{(20)} = 1.19$	0.248
Membrane capacitance (pF)	63.06 ± 3.76	16	63.22 ± 4.41	17		$t_{(31)} = 0.03$	0.979
Membrane resistance (MΩ)	209.72 ± 13.37	16	217.19 ± 15.24	17		$t_{(31)} = 0.37$	0.716
AP threshold (mV)	−37.95 ± 1.03	13	−34.82 ± 1.36	9		$z = 1.90$	0.062
AP amplitude (mV)	60.24 ± 2.53	13	62.94 ± 3.15	9		$t_{(20)} = 0.67$	0.508
AP rise to peak (ms)	1.15 ± 0.07	13	1.14 ± 0.11	9		$t_{(20)} = 0.09$	0.929
AP fall to threshold (ms)	3.07 ± 0.13	13	3.14 ± 0.24	9		$z = 0.20$	0.841
AHP rise time constant (ms)	3.79 ± 0.45	13	3.28 ± 0.44	9		$t_{(20)} = 0.77$	0.449
AHP decay time constant (ms)	737.2 ± 184.6	13	381.0 ± 75.1	9		$z = 0.67$	0.504
Spontaneous AP rate (Hz, whole-cell)	1.29 ± 0.19	13	3.34 ± 0.50	9		$t_{(20)} = 4.32$	$3.3 \times 10^{-4}$
Spontaneous AP rate (Hz, cell-attached)	1.04 ± 0.28	8	1.07 ± 0.23	16		$z = 0.09$	0.927
First AP latency (ms)	3.79 ± 0.21	13	3.93 ± 0.49	9		$z = 0.67$	0.503
AP recovery time (s)	7.91 ± 2.77	12	4.01 ± 1.03	9		$z = 1.31$	0.189
Preceding depolarization (mV)	29.27 ± 2.63	13	25.92 ± 3.18	9		$t_{(20)} = 0.81$	0.425

<sup>a</sup>*z* statistics represent Wilcoxon rank sum test, and *t* statistics represent two-sample *t* test.

**Table 3. Intrinsic properties of striatal CINs in the *Er81* cKO and the control mice at P30**

P30	Control	<i>n</i>	<i>Er81</i> cKO	<i>n</i>	Statistic <sup>d</sup>	<i>p</i>
Resting membrane potential (mV)	−48.20 ± 1.32	14	−48.90 ± 0.79	33	$t_{(45)} = 0.52$	0.608
Membrane capacitance (pF)	111.81 ± 11.85	16	121.03 ± 8.80	31	$z = 0.82$	0.412
Membrane resistance (MΩ)	92.39 ± 6.66	16	86.57 ± 4.79	31	$z = 0.94$	0.346
AP threshold (mV)	−39.14 ± 0.81	13	−38.90 ± 0.80	32	$z = 0.14$	0.890
AP amplitude (mV)	64.18 ± 2.38	13	66.22 ± 1.47	32	$z = 1.01$	0.310
AP rise to peak (ms)	0.70 ± 0.06	13	0.68 ± 0.03	32	$z = 0.30$	0.764
AP fall to threshold (ms)	2.88 ± 0.26	13	2.71 ± 0.13	32	$t_{(43)} = 0.66$	0.512
AHP rise time constant (ms)	3.70 ± 0.26	13	5.52 ± 0.57	32	$z = 2.09$	0.037*
AHP decay time constant (ms)	257.90 ± 30.82	13	670.88 ± 127.88	32	$z = 1.46$	0.143
Spontaneous AP rate (Hz, whole-cell)	3.69 ± 1.03	13	2.91 ± 0.44	32	$z = 0.23$	0.822
Spontaneous AP rate (Hz, cell-attached)	7.09 ± 1.72	11	5.43 ± 0.80	16	$t_{(25)} = 0.97$	0.341
First AP latency (ms)	4.98 ± 0.90	14	4.34 ± 0.35	33	$z = 0.05$	0.963
AP recovery time (s)	5.23 ± 1.35	11	9.41 ± 2.03	27	$z = 0.71$	0.479
Preceding depolarization (mV)	9.88 ± 0.96	14	10.37 ± 0.60	33	$z = 0.00$	1.000

<sup>a</sup>*z* statistics represent Wilcoxon rank sum test, and *t* statistics represent two-sample *t* test. \**p* < 0.05.

6.7,  $p = 5.9 \times 10^{-9}$ ; Fig. 3F,G). In order to decipher the molecular mechanisms behind this regulation, we first analyzed the expression of previously identified  $I_{K_r}$  mediators in CINs, such as the KCNQ2/3 hetero-tetramer channels (Zhang et al., 2018) and the metabotropic glutamate receptor 5 (mGluR5), which can amplify  $I_{sAHP}$  by raising intracellular calcium concentration (Reiner and Levitz, 2018). We found a significant decrease in *Kcnq2* mRNA but not the channel protein levels (mRNA; control;  $n = 6$  mice, *Er81* cKO;  $n = 5$  mice,  $t_{(9)} = 4.8$ ,  $p = 9.6 \times 10^{-4}$ , two-sample *t* test, Fig. 3H; protein; control;  $n = 5$  mice, 260 CINs, *Er81* cKO;  $n = 4$  mice, CINs,  $t_{(7)} = 1.1$ ,  $p = 0.302$ , two-sample *t* test, Fig. 3I,J). Interestingly, *Grm5* mRNA levels were also decreased, whereas the mGluR5 protein level was increased in the *Er81* cKO (mRNA; control;  $n = 7$  mice, *Er81* cKO;  $n = 6$  mice,  $t_{(11)} = 4.14$ ,  $p = 0.002$ , two-sample *t* test, Fig. 3K; protein; control;  $n = 5$  mice, 264 CINs, *Er81* cKO;  $n = 4$  mice, 211 CINs,  $t_{(7)} = 6.2$ ,  $p = 4.3 \times 10^{-4}$ , two-sample *t* test, Fig. 3L,M). These results demonstrate that *Er81* deletion could alter  $I_{sAHP}$  current via elevated mGluR5 at P30. *Er81* deletion did not cause any significant change in AHPs,  $I_{sAHP}$ , or their associated properties at P6. We conclude that the ablation of *Er81* expression has an impact on cell maturation, which leads to permanent changes in cell properties in mature state. This is different from direct transcriptional control observed in PV interneurons (Dehorter et al., 2015).

A large inward rectifier current ( $I_h$ ) is associated with a longer pause in CIN firing and a reduction in spontaneous activity

(Wilson and Goldberg, 2006). However, despite a larger  $I_{sAHP}$  current in *Er81* cKO condition (Fig. 2F), we saw no difference in the AP recovery time and baseline firing rates (Table 3), suggesting that the overall duration of the pause in CIN firing is unlikely to be affected by *Er81* deletion. Consistently, we also observed that a counter current is engaged to balance CIN activity in the absence of *Er81*, as the late sAHP showed no difference between the two groups (Fig. 2L). We examined the prominent inward rectifying  $I_h$  current that contributes to rebound activity following hyperpolarization and the tonic firing of the CINs (Bennett et al., 2000). While we could not see any difference between control and *Er81* cKO conditions in CINs at P6 (sag ratio: control;  $n = 16$  cells, 5 mice; *Er81* cKO;  $n = 17$  cells, 4 mice; two-way ANOVA;  $F_{(1,31, genotype)} = 0.002$ ,  $p = 0.960$ ,  $F_{(7,217, interaction)} = 0.35$ ,  $p = 0.927$ ; rebound firing: two-way ANOVA,  $F_{(1,31, genotype)} = 0.037$ ,  $p = 0.849$ ,  $F_{(1,31, interaction)} = 0.52$ ,  $p = 0.475$ , followed by Bonferroni's multiple comparisons test; 3–3.23 s;  $p > 0.999$ , 3.23–5 s;  $p > 0.999$ ; data not shown), we found that both sag ratio and rebound firing were enhanced at P30 in *Er81* cKO CINs (control;  $n = 16$  cells, 5 mice, *Er81* cKO;  $n = 31$  cells, 4 mice, sag ratio:  $F_{(1,45, genotype)} = 7.1$ ,  $p = 0.010$ ,  $F_{(7,315, current)} = 9.5$ ,  $p = 2.2 \times 10^{-4}$ ,  $F_{(7,315, interaction)} = 5.1$ ,  $p = 1.7 \times 10^{-5}$ , two-way ANOVA; rebound firing:  $F_{(1,45, genotype)} = 2.4$ ,  $p = 0.125$ ,  $F_{(1,45, interaction)} = 6.0$ ,  $p = 0.0178$ , two-way ANOVA, followed by Bonferroni's multiple comparisons test: 3–3.23 s;  $p = 1.000$ , 3.23–5 s;  $p = 0.029$ ; Fig. 4A–C). Consistently, we found the  $I_h$  current amplitude unchanged in the *Er81* cKO compared with the control CINs at P6 (control;  $n = 13$  cells, 5 mice,

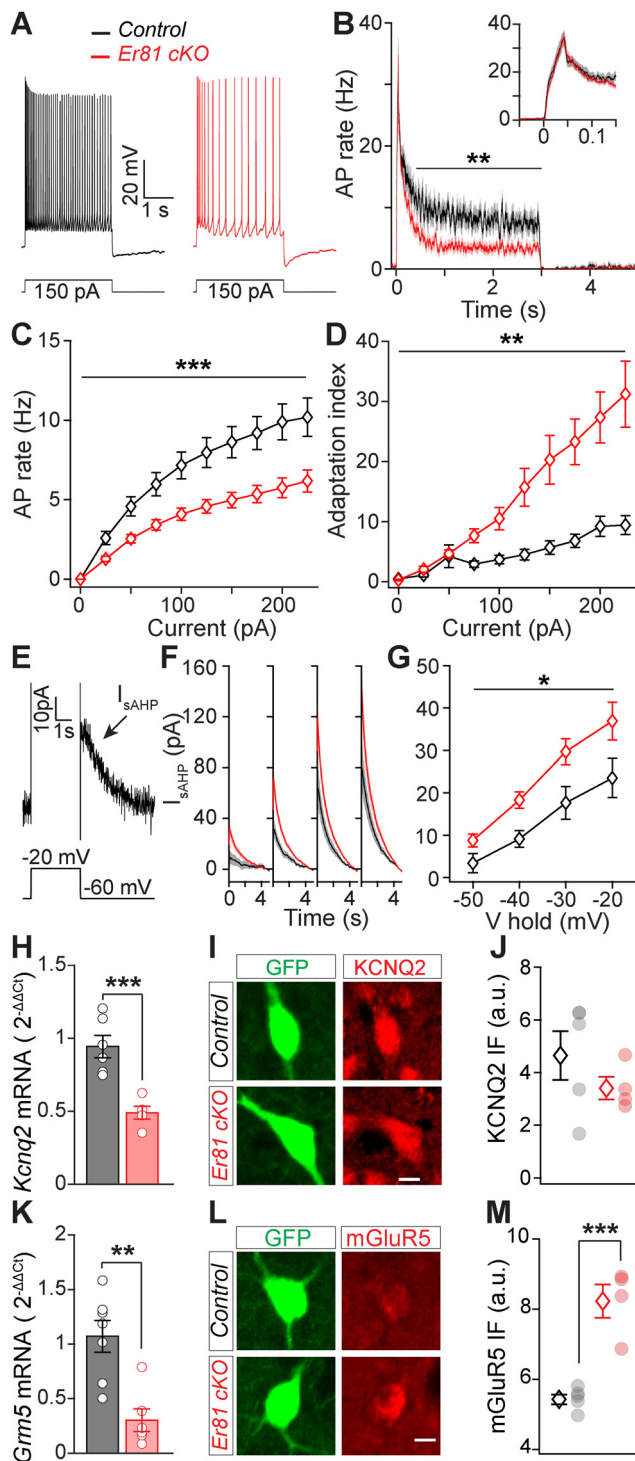


**Figure 3.** Reduced CIN excitability and enhanced delayed rectifier current  $I_{sAHP}$  following *Er81* deletion. **A**, Representative responses of P30 CINs to a 150 pA positive current pulse in the control and the *Er81* cKO conditions. **B**, Average AP rate across all positive current pulses. Inset, Time-expanded view of the early response. **C**, Average AP rate during positive current steps. Stars represent genotype effect. **D**, Adaptation index as a function of the current step amplitude. Stars represent genotype effect. **E**, Example trace of the putative  $I_{sAHP}$  following a depolarizing voltage pulse. **F**, Mean traces of  $I_{sAHP}$  ( $\pm$  SEM) as a function of time at different holding potentials ( $-50$  to  $-20$  mV, 10 mV steps). **G**, Average  $I_{sAHP}$  as a function of the holding potential. Stars represent genotype effect. **H**, *Kcnq2* mRNA expression levels in the striatum of control and *Er81* cKO mice. **I**, Representative image of a ChAT-GFP cell (green) stained for KCNQ2 protein (red) in control and *Er81* cKO. Scale bar, 10  $\mu$ m. **J**, Average KCNQ2 protein expression levels in control and *Er81* cKO CINs. **K**, *Gm5* mRNA expression levels in the striatum of the control and the *Er81* cKO mice. **L**, Representative image of a ChAT-GFP

*Er81* cKO;  $n = 11$  cells, 4 mice, two-way ANOVA;  $F_{(1,22, genotype)} = 0.17$ ,  $p = 0.678$ ,  $F_{(5,110, interaction)} = 0.08$ ,  $p = 0.996$ , followed by Bonferroni's multiple comparisons test;  $p > 0.999$  at all holding potentials; data not shown) and increased at P30 (control;  $n = 18$  cells, 4 mice, *Er81* cKO;  $n = 22$  cells, 4 mice, two-way ANOVA;  $F_{(1,38, genotype)} = 1.6$ ,  $p = 0.215$ ,  $F_{(7,315, interaction)} = 5.1$ ,  $p = 1.7 \times 10^{-5}$ , followed by Bonferroni's multiple comparisons test;  $V_{hold} = -80$  mV;  $p = 0.012$ ;  $V_{hold} = -70$  mV;  $p = 0.003$ ; Fig. 4D–F). We next analyzed the expression of the main channel subunits underlying the enhanced  $I_h$  current, that is, the hyperpolarization activated cyclic nucleotide-gated potassium and sodium channel 1 and 2 (HCN1 and HCN2) (Z. Zhao et al., 2016). However, we did not find any difference in the expression of either HCN2 or HCN1 between the *Er81* cKO and the control CINs (*Hcn2* mRNA; control;  $n = 5$  mice, *Er81* cKO;  $n = 4$  mice,  $t_{(7)} = 0.9$ ,  $p = 0.391$ ; HCN2 protein; control;  $n = 5$  mice, 350 cells, *Er81* cKO;  $n = 4$  mice, 270 cells,  $t_{(7)} = 0.9$ ,  $p = 0.391$ , two-sample  $t$  test; HCN1 protein; control;  $n = 5$  mice, 60 cells, *Er81* cKO;  $n = 4$  mice, 55 cells,  $z = 0.9$ ,  $p = 0.391$ , Wilcoxon rank sum test; Fig. 4G–J). These results show that, rather than a quantitative change in the channel subunits underlying  $I_h$ , their function is likely enhanced in the absence of *Er81*. Together, we demonstrate that the absence of *Er81* affects the two major intrinsic currents  $I_{sAHP}$  and  $I_h$  in the striatal CINs, through mGluR5 upregulation.

#### Rewiring of cholinergic interneurons in the absence of *Er81*

Changes in the functional properties of CINs are likely to affect their synaptic integration within the striatal microcircuit. To test whether the deletion of *Er81* alters CIN synaptic profile, we performed *in vitro* patch-clamp recordings of the sEPSCs and sIPSCs onto CINs at P6 and P30. We did not observe any significant changes in the frequency and amplitude of sEPSCs in the absence of *Er81* at either postnatal stage (P6, control;  $n = 12$  cells, 6 mice, *Er81* cKO;  $n = 14$ , 3 mice, rate;  $z = 0.9$ ,  $p = 0.368$ , Wilcoxon rank sum test, amplitude;  $t_{(24)} = 0.5$ ,  $p = 0.624$ , two-sample  $t$  test, rise time;  $z = 0.3$ ,  $p = 0.777$ , decay time;  $z = 0.7$ ,  $p = 0.456$ , Wilcoxon rank sum tests; data not shown; P30, control;  $n = 22$  cells, 9 mice, *Er81* cKO;  $n = 20$  cells, 4 mice, rate;  $z = 1.8$ ,  $p = 0.076$ , Wilcoxon rank sum test, amplitude;  $t_{(40)} = 0.8$ ,  $p = 0.451$ , two-sample  $t$  test, rise time;  $z = 1.2$ ,  $p = 0.222$ , decay time;  $z = 1.1$ ,  $p = 0.284$ , Wilcoxon rank sum tests; Fig. 5A–D). As CINs receive excitatory inputs from both the cortex and thalamus (Ding et al., 2010), we examined whether pathway-specific inputs were modified in the absence of *Er81*. Bouton analyses revealed no significant changes in the density of the cortical vesicular glutamate transporter type 1 (vGluT1) and thalamic vesicular glutamate transporter type 2 (vGluT2) positive boutons (Doig et al., 2014) on the somas of CINs in the absence of *Er81* at either postnatal stages (P30 somas; vGluT1; control;  $n = 15$  cells, 3 mice, *Er81* cKO;  $n = 15$  cells, 3 mice,  $t_{(28)} = 1.98$ ,  $p = 0.058$ , vGluT2; control;  $n = 10$  cells, 3 mice, *Er81* cKO;  $n = 10$  cells, 3 mice,  $t_{(18)} = 0.10$ ,  $p = 0.924$ , Fig. 5E–H, P6 somas; vGluT1; control;  $n = 12$  cells, 3 mice, *Er81* cKO;  $n = 12$  cells, 3 mice,  $t_{(22)} = 1.09$ ,  $p = 0.288$ ,  $n = 12$  cells, 3 mice in each condition, vGluT2; control;  $n = 14$  cells, 3 mice, *Er81* cKO;  $n = 10$  cells, 3 mice,  $t_{(22)} = 1.05$ ,  $p = 0.306$ , two-sample  $t$  tests; data not shown). In addition, we found a homogeneous distribution of both transporters across proximal and

←

cell (green) stained for mGluR5 protein (red) in control and *Er81* cKO. Scale bar, 10  $\mu$ m. **M**, Average mGluR5 protein expression levels in control and *Er81* cKO CINs. \* $p < 0.05$ . \*\* $p < 0.01$ . \*\*\* $p < 0.001$ .

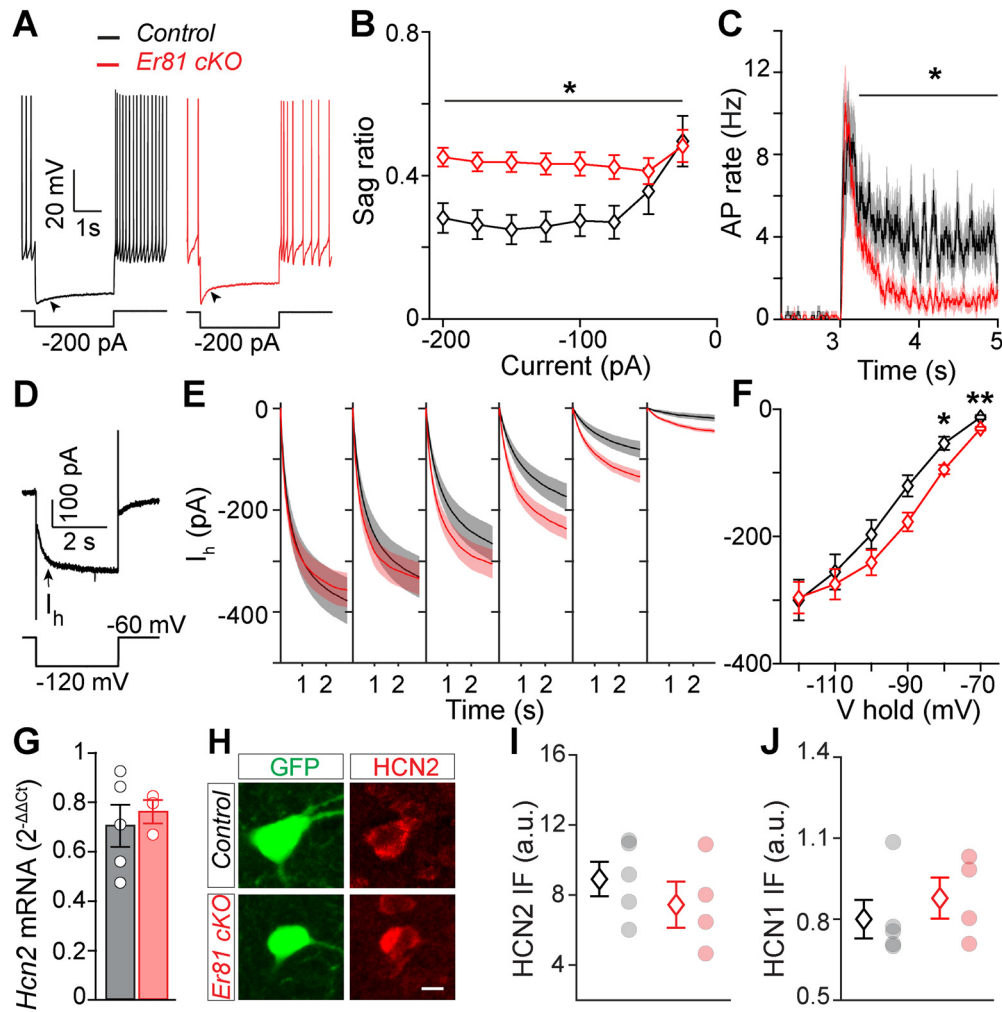


**Figure 4.** Increase in the  $I_h$  in CINs following *Er81* deletion. **A**, Representative responses of P30 CINs to a negative current pulse in the control and the *Er81* cKO conditions. Arrowheads indicate the voltage sag. **B**, Average sag ratio at different current steps. Stars represent genotype effect. **C**, Rebound firing at the end of negative current steps. **D**, Example voltage-clamp trace showing the slowly activated  $I_h$  (arrow) during a hyperpolarizing voltage pulse. **E**, Traces of  $I_h$  averaged across CINs at different holding potentials ( $-70$  to  $-110$  mV, 10 mV steps). **F**, Time-averaged  $I_h$  across CINs at different holding potentials. Stars represent Bonferroni's test result. **G**, *Hcn2* mRNA expression levels in the striatum of control and *Er81* cKO mice. **H**, Representative image of a ChAT-GFP cell (green) expressing HCN2 protein in control and *Er81* cKO. Scale bar, 10  $\mu$ m. **I**, Expression of HCN2 protein in the CINs of control and the *Er81* cKO group. **J**, Expression of HCN1 protein in the CINs of control and the *Er81* cKO group. a.u.: arbitrary units. \* $p < 0.05$ . \*\* $p < 0.01$ .

distal segments of CIN dendrites in P30 WT conditions (vGluT1:  $n = 16$  proximal, 9 distal dendrites, vGluT2:  $n = 13$  proximal, 10 distal dendrites, 6 mice; two-way ANOVA:  $F_{(1,20, \text{Transporter})} = 0.90$ ,  $p = 0.355$ ,  $F_{(1,20, \text{Dendrite segment})} = 0.01$ ,  $p = 0.913$ ,  $F_{(1,20, \text{Interaction})} = 1.36$ ,  $p = 0.258$ ; data not shown), and this was unchanged in the KO (WT vs cKO,  $n = 4$  mice; vGluT1:  $n = 17$  proximal dendrites,  $t_{(8)} = 0.87$ ,  $p = 0.406$ ; 8 distal dendrites,  $t_{(8)} = 0.18$ ,  $p = 0.860$ ; vGluT2:  $n = 14$  proximal dendrites,  $t_{(8)} = 0.97$ ,  $p = 0.362$ ; 6 distal dendrites,  $t_{(8)} = 0.73$ ,  $p = 0.487$ ; two-sample  $t$  tests; data not shown). Recordings of sIPSCs showed similar frequency but significantly larger amplitude and decay time in the *Er81* cKO compared with the control cells at P30 (control;  $n = 16$  cells, 4 mice, *Er81* cKO;  $n = 24$  cells, 5 mice, rate;  $z = 0.37$ ,  $p = 0.709$ , amplitude;  $z = 3.55$ ,  $p = 3.9 \times 10^{-4}$ , rise time;  $z = 0.94$ ,  $p = 0.348$ , Wilcoxon rank sum test, decay time;  $t_{(38)} = 3.70$ ,  $p = 6.8 \times 10^{-4}$ , two-sample  $t$  test; Fig. 5I–L), with no changes at P6 (control;  $n = 12$  cells, 3 mice, *Er81* cKO;  $n = 12$  cells, 3 mice, rate;  $z = 0.20$ ,  $p = 0.840$ , amplitude;  $z = 0.38$ ,  $p = 0.707$ , rise time;  $t_{(22)} = 1.05$ ,  $p = 0.305$ , decay time;  $z = 0.26$ ,  $p = 0.795$ , Wilcoxon rank sum tests; data not shown). Since interneurons expressing the neuropeptide Y (NPY<sup>+</sup>) are the principal inhibitory sources to CINs

(English et al., 2011; Szydlowski et al., 2013; Straub et al., 2016) and PV neurons are the most common type of inhibitory interneuron in the striatum, we determined whether NPY<sup>+</sup> and PV<sup>+</sup> bouton densities onto CINs were altered in the absence of *Er81*. We observed a higher density of NPY<sup>+</sup> boutons in the *Er81* cKO compared with control mice at P6 (control;  $n = 14$  cells, 3 mice, *Er81* cKO;  $n = 11$  cells, 3 mice,  $t_{(23)} = 2.43$ ,  $p = 0.023$ , two-sample  $t$  test; data not shown) with no change in NPY<sup>+</sup> boutons on the soma or dendrites at P30 (soma, control;  $n = 15$  cells, 4 mice; *Er81* cKO;  $n = 14$  cells, 3 mice,  $t_{(27)} = 0.58$ ,  $p = 0.567$ , two-sample  $t$  tests; Fig. 5M,N; dendrites, control;  $n = 9$  cells, 3 mice, *Er81* cKO;  $n = 9$  cells, 3 mice,  $t_{(16)} = 0.46$ ,  $p = 0.650$ , two-sample  $t$  tests; data not shown). We also found denser PV<sup>+</sup> boutons on the *Er81* cKO CIN somas compared with controls at P30 (control;  $n = 12$  cells, 3 mice, *Er81* cKO;  $n = 12$  cells, 3 mice,  $t_{(22)} = 2.18$ ,  $p = 0.040$ ; Fig. 5O,P), but not in dendrites (control;  $n = 12$  cells, 3 mice; *Er81* cKO;  $n = 12$  cells, 3 mice,  $t_{(22)} = 0.34$ ,  $p = 0.738$ ; data not shown). As *Er81* deletion affects cholinergic neuropil (Fig. 2F), we expected that CIN output to other striatal cell types would also be altered. We found that the density of boutons expressing the specific CIN synaptic terminal marker vGluT3

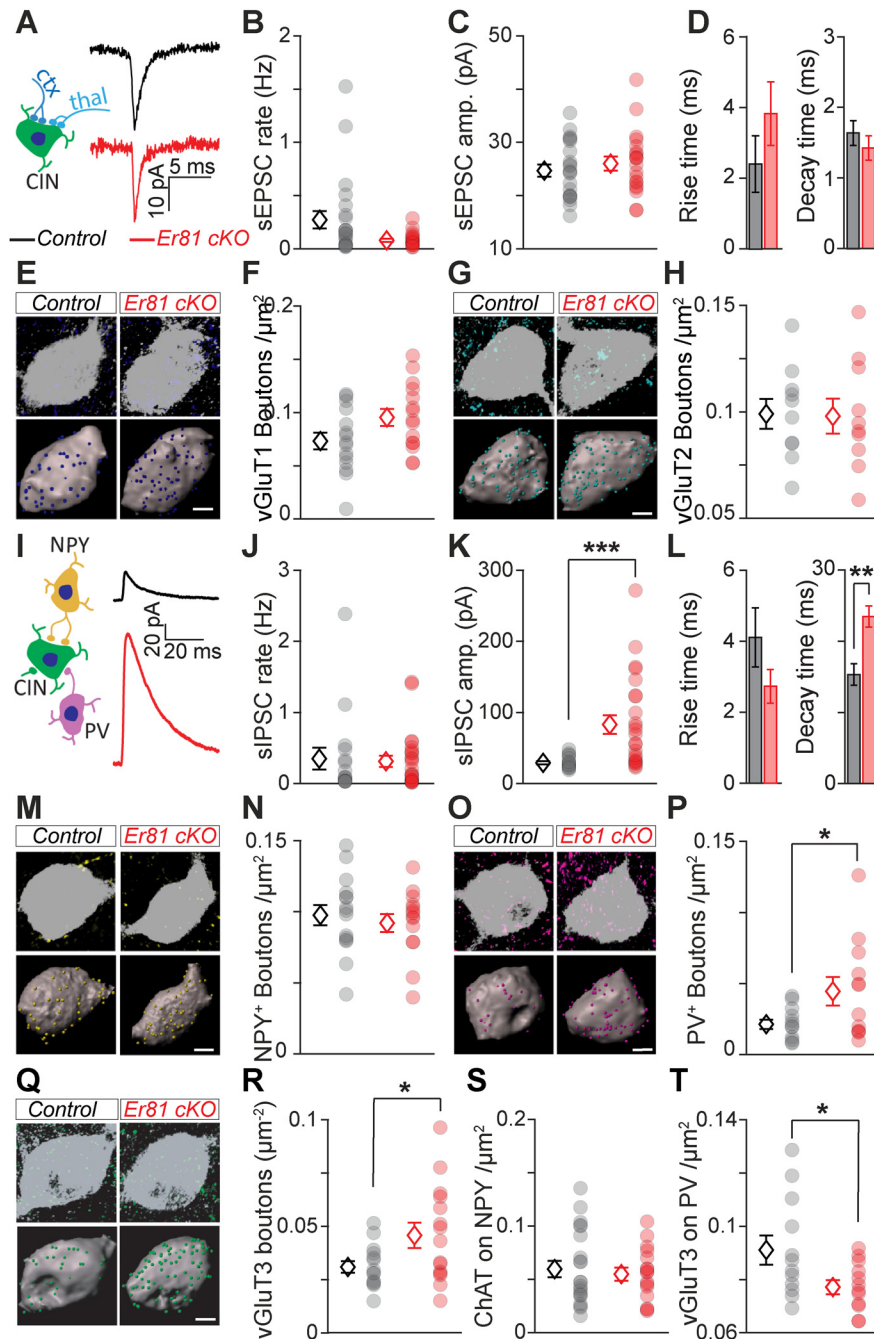


**Figure 5.** Rewiring of the CINs in the absence of Er81. **A**, Left, Excitatory inputs to CINs from cortex (ctx, dark blue) and thalamus (thal, light blue). Right, Average sEPSC traces of a control and *Er81* cKO CIN. **B–D**, Rate (**B**), amplitude (**C**), rise time (**D**, left), and decay time (**D**, right) of sEPSCs in control and *Er81* cKO CINs. **E**, Top, Control and *Er81* cKO CINs (ChAT, gray) with vesicular glutamate transporter 1 (vGluT1, dark blue, cortical boutons). Bottom, 3D reconstruction of control and *Er81* cKO CINs soma (gray) and vGluT1 boutons (spots). **F**, vGluT1 bouton density on control and *Er81* cKO CINs. **G**, Control and *Er81* cKO CINs (ChAT, gray) with vGluT2 boutons (light blue, thalamic boutons). Details as in **E**. **H**, vGluT2 bouton density on control and *Er81* cKO CINs. **I**, Left, Schematic of local inhibitory inputs to CINs from NPY<sup>+</sup> (yellow) and PV<sup>+</sup> (magenta) interneurons. Right, Average spontaneous sIPSC traces of a control and *Er81* cKO CIN. **J–L**, Rate (**J**), amplitude (**K**), rise time (**L**, left), and decay time (**L**, right) of sIPSCs in control and *Er81* cKO CINs. **M**, Control and *Er81* cKO CINs with NPY<sup>+</sup> boutons (yellow). Details as in **E**. **N**, NPY<sup>+</sup> bouton density on control and *Er81* cKO CINs. **O**, Control and *Er81* cKO CINs with PV<sup>+</sup> boutons (magenta). Details as in **E**. **P**, PV<sup>+</sup> bouton density on control and *Er81* cKO CINs. **Q**, Control and *Er81* cKO CINs with vGluT3<sup>+</sup> boutons (green, cholinergic boutons). Details as in **E**. **R**, vGluT3<sup>+</sup> bouton density on control and *Er81* cKO CINs. **S**, ChAT<sup>+</sup> bouton density on NPY<sup>+</sup> interneurons in control and *Er81* cKO conditions. **T**, ChAT bouton density on PV<sup>+</sup> interneurons in control and *Er81* cKO conditions. Diamonds represent averages. Circles represent individual neurons. Scale bars, 5  $\mu$ m. \* $p$  < 0.05. \*\* $p$  < 0.01. \*\*\* $p$  < 0.001.

(Gras et al., 2008; Higley et al., 2011; Nelson et al., 2014) was increased at P30 (soma, control;  $n = 14$  cells, 3 mice, *Er81* cKO;  $n = 15$  cells, 3 mice,  $t_{(27)} = 2.24$ ,  $p = 0.033$ ; Fig. 5Q,R; dendrites, control;  $n = 12$  cells, 3 mice, *Er81* cKO;  $n = 12$  cells, 3 mice,  $t_{(22)} = 1.53$ ,  $p = 0.141$ , two-sample  $t$  tests; data not shown) but not at P6 (control;  $n = 16$  cells, 3 mice, *Er81* cKO;  $n = 7$  cells, 3 mice,  $t_{(21)} =$

0.13,  $p = 0.899$ , two-sample  $t$  tests; data not shown) on neighbor CINs in the absence of Er81. On the contrary, vGluT3 bouton density onto NPY<sup>+</sup> interneurons was reduced at P6 (control;  $n = 17$  cells, 3 mice, *Er81* cKO;  $n = 12$  cells, 3 mice,  $t_{(27)} = 2.47$ ,  $p = 0.020$ , two-sample  $t$  tests; data not shown) but not at P30 (control;  $n = 21$  cells, 4 mice, *Er81* cKO;  $n = 16$  cells, 3 mice,

$z = 0.11$ ,  $p = 0.915$ ; Fig. 5S) and was significantly reduced onto P30 PV-expressing interneurons in the *Er81* cKO condition (control;  $n = 12$  cells, 3 mice, *Er81* cKO;  $n = 12$  cells, 3 mice,  $t_{(22)} = 2.29$ ,  $p = 0.032$ , two-sample  $t$  test; Fig. 5T). Overall, these results suggest that the increase in IPSC amplitude of mature CINs lacking *Er81* is because of a stronger connection with PV and/or CIN interneurons. Such changes in the circuitry are likely to influence the *in vivo* activity of these neurons and the striatal network.

### Changes in spike timing of striatal cholinergic interneurons alter striatal sensorimotor processing

CINs have a key role in striatal function by controlling the output neurons (Mamaligas and Ford, 2016) and modulating their GABAergic (English et al., 2011), glutamatergic (Mamaligas et al., 2019), and dopaminergic inputs (Threlfell et al., 2012; Kosillo et al., 2016; Brimblecombe et al., 2018). It is unknown how fine-tuning of the CIN firing impacts sensorimotor processing. We anticipated that alterations in CIN properties will have a crucial impact on striatal function. To address that, we performed *in vivo* multielectrode array recordings from the dorsal striatum, which receives somatotopically organized sensory and motor inputs from the cortex (Robbe, 2018). We coupled our recordings to whisker stimulation in awake adult mice (Fig. 6A), taking advantage of the whiskers as mobile sensors to study movement-related neuronal activities in a head-fixed configuration. In the first step, we excluded from analysis the putative fast spiking cells characterized by narrow spikes (Mallet et al., 2005; Lee et al., 2017; Dorst et al., 2020) and potential artifacts (see Materials and Methods; Fig. 6B, black). This exclusion based on waveform resulted in 731 cells from 3 control and 732 cells from 4 *Er81* cKO mice (Fig. 6B, teal). We then identified putative SPNs and CINs by the following three criteria: spontaneous activity ( $<1$  Hz or  $>1$  Hz, respectively) (English et al., 2011; Sharott et al., 2012), phasic responses to sensorimotor stimuli, as captured by  $\delta$  firing rate (Inokawa et al., 2010), and the proportion of ISIs  $> 2$  s (PropISI  $> 30\%$  or  $< 30\%$ , respectively; Fig. 6C, right) (Benhamou et al., 2014). Figure 6D, E illustrates the response profile of all recorded cells based on these segregations. Group 1 ( $n = 267$  cells in control and 366 cells in *Er81* cKO mice) represents putative SPNs (pSPNs, Fig. 6D) and Group 3 ( $n = 150$  cells in control and 111 cells in *Er81* cKO mice) represents putative CINs (pCINs; Fig. 6E). Group 2 ( $n = 260$  cells in control and 200 cells in *Er81* cKO mice) and Group 4 ( $n = 54$  cells in control and 55 cells in *Er81* cKO mice) represent more heterogeneous cell populations of pSPNs and pCINs, respectively, with other putative interneurons, such as low-threshold spiking interneurons (Sharott et al., 2009; Beatty et al., 2012).

In the *Er81* cKO mice, we found significantly larger responses to the stimulus in Group 1 compared with the control (pSPNs;  $n = 267$  control cells;  $n = 366$ , *Er81* cKO cells; two-way ANOVA,  $F_{(1,623, \text{genotype})} = 138.1$ ,  $p = 6.11 \times 10^{-29}$ ,  $F_{(9,623, \text{interaction})} = 35.9$ ,  $p = 3.57 \times 10^{-51}$ ; Fig. 6D, top) and a weaker response in Group 2 (pSPNs and other interneurons;  $n = 260$  control cells, *Er81* cKO;  $n = 200$  *Er81* cKO cells, two-way ANOVA,  $F_{(1,458, \text{genotype})} = 14.6$ ,  $p = 1.49 \times 10^{-4}$ ,  $F_{(9,458, \text{interaction})} = 6.058$ ,  $p = 4.72 \times 10^{-8}$ ; Fig. 6D, bottom). In contrast, cells in Group 3 (pCINs) exhibited a stronger inhibition/pause responses in the *Er81* cKO condition, compared with the control ( $n = 150$  control cells;  $n = 111$  *Er81* cKO cells; two-way ANOVA,  $F_{(1,255, \text{genotype})} = 70.5$ ,  $p = 3.26 \times 10^{-15}$ ,  $F_{(9,255, \text{interaction})} = 5.3$ ,  $p = 1.42 \times 10^{-6}$ ; Fig. 6E, top). Cells in group 4 (pCINs and other putative interneurons) displayed a stronger response to stimulus in the *Er81* cKO compared

with the control condition ( $n = 54$  control cells;  $n = 55$  *Er81* cKO cells; two-way ANOVA,  $F_{(1,107, \text{genotype})} = 108.4$ ,  $p = 5.95 \times 10^{-18}$ ,  $F_{(9,107, \text{interaction})} = 11.0$ ,  $p = 5.18 \times 10^{-12}$ ; Fig. 6E, bottom).

Interestingly, the quiet state firing rate was significantly reduced in Groups 1 and 2 (pSPNs; Group 1: control;  $0.27 \pm 0.018$  Hz, *Er81* cKO;  $0.20 \pm 0.013$  Hz, two-way ANOVA;  $F_{(1,623, \text{genotype})} = 10.4$ ,  $p = 0.001$ ,  $F_{(9,623, \text{interaction})} = 0.9$ ,  $p = 0.494$ ; Group 2: control;  $0.45 \pm 0.050$ , *Er81* cKO;  $0.34 \pm 0.020$ ; two-way ANOVA;  $F_{(1,458, \text{genotype})} = 22.8$ ,  $p = 2.44 \times 10^{-6}$ ,  $F_{(9,458, \text{interaction})} = 0.7$ ,  $p = 0.729$ ; data not shown), while the quiet state firing rate of the putative CINs was higher in the absence of *Er81* (Group 3: control;  $2.19 \pm 0.261$  Hz, *Er81* cKO;  $2.90 \pm 0.180$  Hz, two-way ANOVA;  $F_{(1,255, \text{genotype})} = 16.4$ ,  $p = 6.88 \times 10^{-5}$ ,  $F_{(9,255, \text{interaction})} = 1.1$ ,  $p = 0.352$ ; Group 4: control;  $1.86 \pm 0.122$ , *Er81* cKO;  $2.45 \pm 0.217$ , two-way ANOVA;  $F_{(1,107, \text{genotype})} = 5.5$ ,  $p = 0.021$ ,  $F_{(9,107, \text{interaction})} = 0.6$ ,  $p = 0.799$ ; data not shown).

These results reveal that an increase in pCIN inhibition (Group 3) in the absence of *Er81* leads to enhanced excitation of the pSPNs (Group 1) during stimulation, and an elevated firing rate of pCINs during quiet states (Group 3) leads to a reduced firing rate of pSPNs (Group 1). This is consistent with the fact that CINs are known to suppress SPN activity (English et al., 2011; Zucca et al., 2018).

To further investigate the activity profile of these four groups, we analyzed neuronal activity relative to the movement. As head-fixed awake mice voluntarily move (Ranjbar-Slamloo and Arabzadeh, 2019), striatal cell firing could be affected by movement as well as the sensory stimulus. We thus analyzed how the snout and whiskers behaved during the course of stimulation. We found that the overall motion index was different, revealing a higher motor activity of the *Er81* cKO mice compared with control ( $n = 21$  recordings from 3 control mice;  $1.76 \pm 5 \times 10^{-4}$  a.u.;  $n = 23$  recordings from 4 *Er81* cKO mice;  $2.16 \pm 7 \times 10^{-4}$  a.u.,  $t_{(42)} = 4.5$ ,  $p = 0.003$ , two-sample  $t$  test; data not shown). We then performed a reverse correlation analysis to examine the coupling between spikes and movements. The STA motions showed a larger peak at spike time in the putative SPN groups of the *Er81* cKO mice compared with control (Group 1,  $n = 267$  control cells;  $n = 366$  *Er81* cKO cells,  $F_{(1,631, \text{genotype})} = 13.3$ ,  $p = 2.86 \times 10^{-4}$ ; Group 2,  $n = 260$  control cells;  $n = 200$  *Er81* cKO cells;  $F_{(1,458, \text{genotype})} = 6.3$ ,  $p = 0.012$ , two-way ANOVA; Fig. 6F). This indicates enhanced temporal precision of the putative output neuron activity encoding motion. Magnitude of the STA near spike time was also larger in the putative CINs, indicating a better temporal alignment of the spikes to the onset of the movement in the *Er81* cKO mice (Group 3;  $n = 150$  control cells;  $n = 111$  *Er81* cKO cells;  $F_{(1,259, \text{genotype})} = 4.0$ ,  $p = 0.045$ , Fig. 6H, left; Group 4;  $n = 54$  control cells;  $n = 55$  *Er81* cKO cells,  $F_{(1,107, \text{genotype})} = 10.0$ ,  $p = 2.0 \times 10^{-3}$ , two-way ANOVA, Fig. 6H, right). Together with the enhanced suppression (i.e., more reliable pause) during stimulus, these results show that striatal neurons are more effectively recruited by the sensorimotor inputs in the absence of *Er81*.

To further examine the relative contributions of the stimulus and the motion in generating spikes in the absence of *Er81*, we performed cross-correlation analysis between the firing rate, motion, and puff stimulation. In putative SPNs (Group 1), positive spike-motion correlations were on average stronger in the absence of *Er81*, whereas the corresponding spike-puff correlations were not affected (control;  $n = 233$  cells, *Er81* cKO;  $n = 317$  cells, spike-puff correlations;  $z = 0.37$ ,  $p = 0.714$ , spike-motion correlations;  $z = 6.6$ ,  $p = 4.9 \times 10^{-11}$ , Wilcoxon rank sum tests;

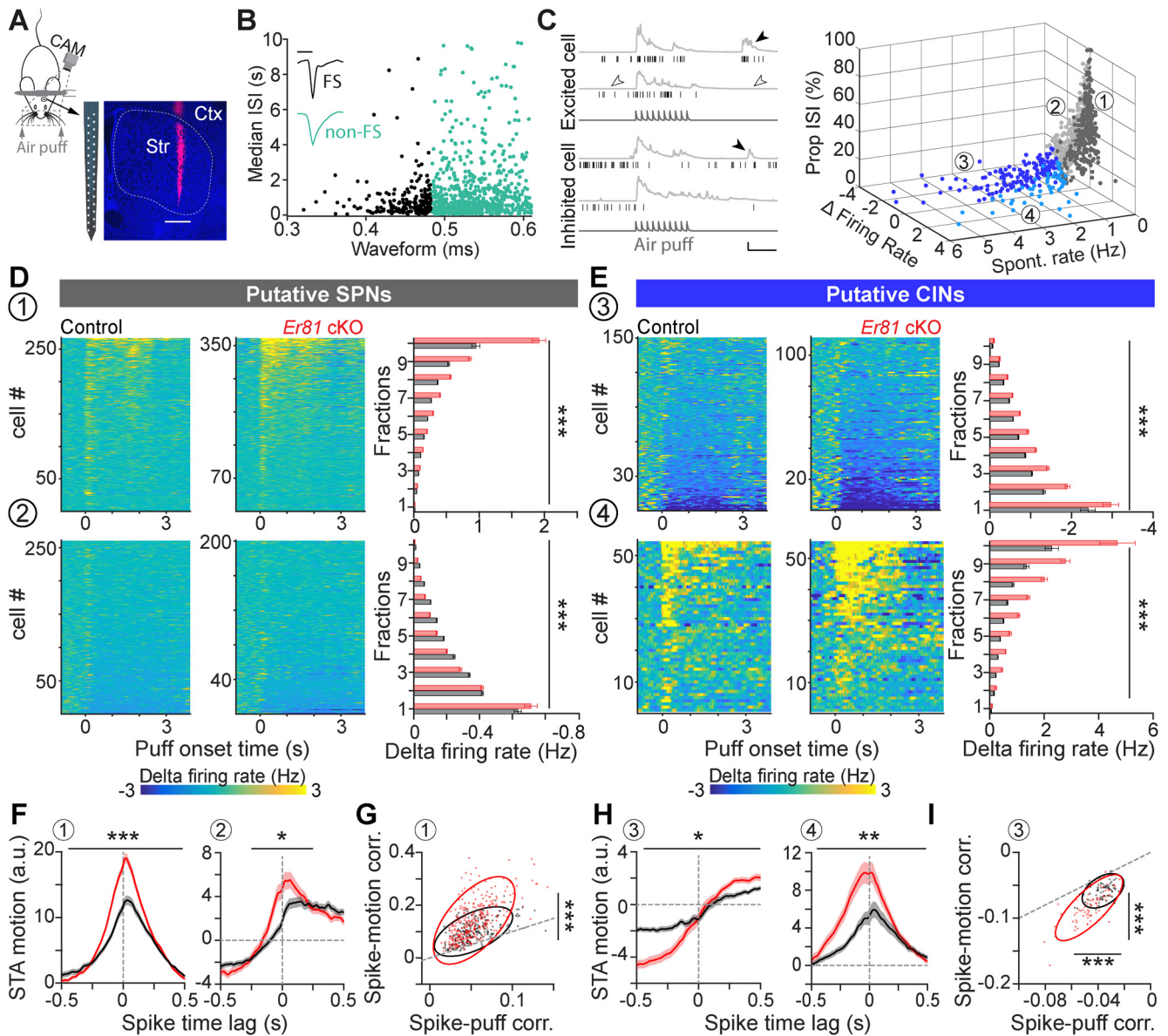


**Figure 6.** Enhanced inhibitory response of striatal CINs in the absence of *Er81*. **A**, Head-fixed awake recording by multi-electrode arrays. Track of the recording array marked by Dil (magenta). Str, Striatum; Ctx, cortex. Scale bar, 0.5 mm. **B**, Units classified into FS (black) and non-FS cells (teal) based on their spike waveform and median ISIs. Inset, Representative traces (scale bars, 0.5 ms; normalized amplitudes). **C**, Left, Example trials showing spike raster (black) and the combined movements of the whiskers and nose quantified as motion index (light gray) for one excited cell and one inhibited cell. Dark gray traces at the bottom represent air puff trains. Filled arrowheads indicate the bouts of voluntary movement. Empty arrowheads indicate quiet states (scale bars, 1 s, 10 a.u.). Right, 3D scatter plot separating striatal neuron subtypes into four groups (1–4), based on spontaneous firing rate (spontaneous rate, quantified in quiet states), evoked firing rate (firing rate during air puff presentation, normalized to the activity before the stimulus) and proportion of ISIs > 2 s (propISIs). Threshold for  $\delta$  firing rate: 0; threshold for spontaneous rate: 1 Hz. **D**, Top, Normalized spiking activity in Group 1 (putative SPNs; left, control; middle, *Er81* cKO; right). Bar plots represent average ( $\pm$ SEM) of the evoked activity within fractions of the sorted data for each genotype (gray, control; red, *Er81* cKO). Bottom, Normalized spiking activity in Group 2 (SPNs and other cell types, bar plots as in top). Stars represent genotype effect. **E**, Top, Normalized spiking activity of the putative CINs (Group 3, bar plots as in **D**). Bottom, Normalized spiking activity of Group 4 (putative CINs and other interneurons, bar plots as in **D**). Stars represent genotype effect. **F**, STA (average STA across cells  $\pm$  SEM, normalized within 3 s from the spike time) of the motion index corresponding to the putative SPNs (left, Group 1) and Group 2 (right). **G**, Strength of correlations between the spiking activity of the putative SPNs and the air puff (x axis) or motion (y axis). Dots represent individual cells with positive correlation regarding both variables. The ellipses are the first contours of the fitted Gaussian mixture models. Dashed line indicates the line of equality. **H**, Average STA across the putative CINs (left, Group 2) and Group 4 (right). Vertical dashed lines indicate the spike time. Horizontal dashed lines extend zeros. **I**, Strength of correlations between the spiking activity of putative CINs and the air puff (x axis) or motion (y axis). Dots represent individual cells with a negative correlation regarding both variables. Ellipses represent the first contours of the fitted Gaussian mixture models. Dashed line indicates the line of equality. \* $p$  < 0.05. \*\* $p$  < 0.01. \*\*\* $p$  < 0.001.

Fig. 6G). On the other hand, negative correlations in the putative CINs (Group 3) were significantly larger in the *Er81* cKO compared with the control mice (control;  $n = 74$  cells, *Er81* cKO;  $n = 69$  cells, spike-puff correlations;  $z = 5.5$ ,  $p = 3.0 \times 10^{-8}$ , Wilcoxon rank sum test, spike-motion correlations;  $t_{(141)} = 8.0$ ,  $p = 5.1 \times 10^{-13}$ , two-sample  $t$  test; Fig. 6I). Interestingly, we also found that spike-motion correlations were consistently higher

than spike-puff correlations (Fig. 6G,I). Together, our results suggest that neurons were mostly tuned to the voluntary movements, rather than the stimulus. They indicate that physiological changes in the *Er81* cKO mice lead to higher motor activity and a more effective modulation of cell activity in the striatum. These data imply that the putative CIN population producing phasic responses during movement are more responsive to sen-



sorimotor inputs in the absence of Er81, and cause a higher excitation of the putative output neurons.

### Er81 is a molecular regulator of habit formation

Striatal CINs are crucial for cognitive flexibility (Okada et al., 2014, 2018; Aoki et al., 2018). To assess the impact of Er81 on striatal-dependent behaviors, we designed a reversal learning task, allowing the concomitant assessment of cognitive flexibility and habit formation in the *Er81* cKO mice. In the first part of the training, both control and *Er81* cKO mice were able to discriminate the rewarded corridor of the maze (day 3: control; 66.4% of correct answers,  $n = 17$  mice, *Er81* cKO; 68.9% of correct answers,  $n = 17$  mice; two-way ANOVA,  $F_{(2,64)}$ , days 1–3  $\times$  genotype = 0.567;  $p = 0.570$ ; Fig. 7A), and switch to the opposite side after a first reversal on day 4 (day 4: control; 42.8%, *Er81* cKO: 43.5%;  $n = 17$ ; two-way ANOVA,  $F_{(1,32)}$ , days 3–4  $\times$  genotype = 0.762;  $p = 0.9509$ ; Fig. 7A). *Er81* cKO mice hence displayed normal learning capacities (days 1–3) as well as intact cognitive flexibility (days 4–13; two-way ANOVA,  $F_{(9,207)}$ , days 4–13  $\times$  genotype = 1.559;  $p = 0.1294$ ). After they reached their performance plateau, mice were then overtrained for 5 d, to induce habit formation (Balleine et al., 2009; Lingawi and Balleine, 2012) (day 13: control; 85.6%,  $n = 12$  mice, *Er81* cKO; 83.6%,  $n = 13$  mice; one-way ANOVA,  $F_{(1,23, \text{genotype})} = 0.19$ ,  $p = 0.669$ ; Fig. 7A). As the strategy used (goal-directed or habitual) cannot be revealed during training (Balleine and Ostlund, 2007), we assessed whether mice were engaged in goal-directed or habitual behavior by performing a second reversal (day 14). This step aims to change the action–outcome contingency to probe behavior: an animal persisting on choosing the nonrewarding side would reveal its previous engagement in an automatic, habitual behavior. During this session, control mice displayed performance significantly below chance level (controls: 25.4%; controls vs 50%:  $t_{(11)} = 6.6$ ,  $p = 2.1 \times 10^{-5}$ ; one-sample analysis;  $n = 12$  mice; Fig. 7A, right) and significantly lower compared with the first reversal (day 4; one-way ANOVA,  $F_{(1,11)}$ , day 4 vs day 14 in controls = 10.1,  $p = 0.009$ ). Together, these results confirm that control mice were successfully engaged in habitual behavior, through their inability to flexibly shift to the new rewarded side (Dickinson et al., 1995; Yin et al., 2004). Interestingly, *Er81* cKO mice performed significantly higher compared with controls during the second reversal (day 14; one-way ANOVA,  $F_{(1,23, \text{genotype})} = 4.3$ ,  $p = 0.045$ , controls: 25.4%;  $n = 12$  and *Er81* cKO; 34.7%;  $n = 13$ ; Fig. 7A, right). To further analyze this session, we compared the first five trials to the last five trials of this session. While both groups performed similarly at the beginning of the session (controls: 13.3% and *Er81* cKO: 20.0%; one-way ANOVA,  $F_{(1,23, \text{genotype})} = 1.5$ ,  $p = 0.234$ ; Fig. 7B, Trials 1–5), only control mice remained significantly below chance level at the end of the session (controls: 31.7%; controls vs 50%, one-sample analysis:  $t_{(11)} = -2.6$ ,  $p = 0.027$ ; Fig. 7B, Trials 16–20). In contrast, *Er81* cKO mice displayed rapid improvement of their performance, reaching chance level by the end of the session (*Er81* cKO: 49.2%;  $n = 13$ ). This result was further confirmed by the following session (day 15) during which *Er81* cKO mice performed significantly above chance level, unlike controls (*Er81* cKO vs 50%;  $n = 9$ , one-sample analysis;  $t_{(8)} = 3.6$ ,  $p = 0.005$ ; Fig. 7A, right). Moreover, analysis of the performance across the second reversal (days 13–16) demonstrates a significant difference between the control and *Er81* cKO mice (two-way ANOVA,  $F_{(3,39)}$ , days 13–16  $\times$  genotype = 3.0;  $p = 0.040$ ), unlike the first reversal (two-way ANOVA,  $F_{(3,69)}$ , days 3–6  $\times$  genotype = 0.4;  $p = 0.727$ ). Together, these results demonstrate that mice lacking Er81 display intact goal-directed actions and an impairment of habit formation. These mice also showed

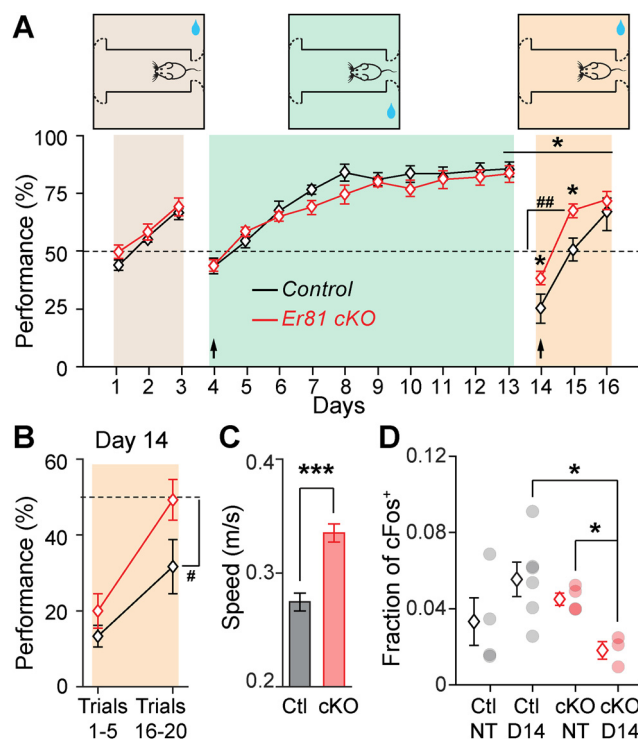


**Figure 7.** *Er81* cKO mice exhibit disrupted habitual behavior. **A**, Reversal learning task in a 3 corridors arena (top). Dashed curve indicates one-way gate. Blue droplet represents sucrose reward. Performance of the mice in each session (bottom; control in black vs *Er81* cKO in red). Arrows indicate the days of reversal.  $##p < 0.01$ , statistical comparison with the chance level (performance at 50%, dashed line). Horizontal line indicates interaction between performance and genotype. **B**, Average performance across the first 5 trials and last 5 trials of day 14.  $#p < 0.05$ , statistical comparison with the chance level (performance at 50%, dashed line). **C**, Average locomotion speed of control and *Er81* cKO mice in the middle corridor. **D**, Fraction of the cells expressing cFos in nontrained (NT) and day 14 of training (D14) in the control and the *Er81* cKO.  $*p < 0.05$ .  $***p < 0.001$ .

general hyperactivity as they move faster in the middle corridor ( $n = 13$  control mice;  $n = 12$  *Er81* cKO mice;  $z = 4.8$ ,  $p = 1.05 \times 10^{-6}$ , Wilcoxon rank sum test; Fig. 7C), which is consistent with the higher motion index of the snout and whiskers in the head-fixed experiments. Considering the differential role of the dorsomedial and dorsolateral striatum in cognitive flexibility and habit formation, respectively (Packard and Knowlton, 2002), we then analyzed the changes in striatal activity associated with the paradigm. Expression of the cellular activity marker cFos in the dorsal striatum revealed an alteration of the task-induced activity of the output neurons in the *Er81* cKO mice (Fig. 7D). While training had no effect on cFos expression in controls, the *Er81* deletion induced a drastic hypoactivation of the striatum in trained mice, compared with nontrained mice (two-way ANOVA,  $F_{(1,13, \text{interaction})} = 6.8$ ;  $p = 0.022$ ; day 14:  $F_{(1,7, \text{genotype})} = 7.5$ ;  $p = 0.029$ ). This result suggests that the striatum in *Er81* cKO does not adapt properly to the behavioral demand, which could underlie the mice inability to form habits. This is further supported by the analysis of the cFos expression in the dorsomedial striatum (DMS) versus dorsolateral striatum (DLS). We found a significant decrease of cFos expression in the DLS of *Er81* cKO mice compared with controls (day 14; one-way ANOVA,  $F_{(1,6, \text{genotype})} = 7.3$ ;  $p = 0.036$ ) and compared with day 4 (day 4 vs day 14 in *Er81* cKO: one-way ANOVA,  $F_{(1,8)} = 8.5$ ;  $p = 0.019$ ; data not shown). This specific DLS hypoactivation could therefore underpin the observed lack of habit formation; conversely, the intact DMS activity could explain the use of cognitive flexibility in

*Er81* cKO. Overall, our results indicate that the fine-tuned activity of CINs by *Er81* is crucial for striatal function and habit formation.

## Discussion

Here, by using *in vitro* and *in vivo* assessments, we find that the *Er81* transcription factor has an age-dependent effect on some CIN physiological properties, thus demonstrating that *Er81* contributes to CIN microcircuit formation and fine-tuned activity. We also show that *Er81* controls *in vivo* striatal neuron responses and their correlation to sensorimotor inputs. Finally, we reveal that proper CIN maturation through *Er81* function is required for normal habit acquisition in mice.

### Control of the cholinergic interneuron identity

The functional implications of molecular heterogeneity in striatal CINs are at present not well understood (Magno et al., 2017; Lozovaya et al., 2018; Munoz-Manchado et al., 2018). CINs originate from distinct areas of the subpallium which give rise to heterogeneous populations of cholinergic cells in the forebrain (Ahmed et al., 2019). These areas are further divided into subdomains, based on the combinatorial expression of multiple transcription factors, such as *Lhx6*, *Lhx7*, *Isl1*, and *Er81* (Flames et al., 2007; He et al., 2016). The temporal order of expression of these transcription factors and their interactions is crucial for normal development of cholinergic neurons (Y. Zhao et al., 2003; Allaway and Machold, 2017; Ahmed et al., 2019). In this study, we identified *Er81* as a molecular controller of key CIN properties and described how its expression affects other transcription factors. Future fate-mapping investigations will determine more specifically the proportion of *Er81*-expressing striatal CINs that may originate from different sources (i.e., MGE, POa, and septum).

In the mature cortex, *Er81* directly regulates the functional diversity of cortical PV-expressing interneurons (Dehorter et al., 2015). While *Er81* expression is strong and mostly nuclear in the cortical PV interneurons, it remains weak and cytoplasmic in the CINs of the striatum. This suggests that *Er81* works through different mechanisms in the CINs than in the PV interneurons (Dehorter et al., 2015), likely through protein-protein interactions or regulation of translational processes. However, while the molecular targets may be different, *Er81* seems to have a common role in neuronal function across different cell types, regulating excitability and spike timing (i.e., the phasic activity of the striatal CINs and the firing latency in the cortical [Dehorter et al., 2015] and striatal PV interneurons [unpublished data]). Moreover, the role of *Er81* in the dopaminergic (Flames and Hobert, 2009; Cave et al., 2010) and serotonergic cell fates (Lloret-Fernández et al., 2018) and here, in cholinergic cell identity, suggests a general regulatory mechanism of *Er81* on the emergence of functional neuromodulatory systems in the developing brain. CINs are neurochemically complex as they corelease GABA (Saunders et al., 2015; Granger et al., 2016) and glutamate (Higley et al., 2011) alongside acetylcholine, to provide both potent inhibition (Zucca et al., 2018) or excitation (Koos and Tepper, 2002; Tepper et al., 2018) within the striatum. As we found changes in the molecular properties of the CINs (acetylcholine transporter, *Isl1*, and *ChAT*), corelease with other neurotransmitters might be also affected by *Er81* deletion and ultimately alter the neurochemical function of the CINs. Our study therefore emphasizes the need to further investigate the molecular factors determining the identity and the functional diversity of striatal CINs.

### Mechanisms regulating tonic and phasic activity of the striatal cholinergic interneurons

Intrinsic electrophysiological properties are responsible for maintaining tonic activity of striatal CINs (Bennett et al., 2000). Together with synaptic inputs (Franklin and Frank, 2015; Klug et al., 2018), they also contribute to the phasic response to stimuli (Zhang et al., 2018). The role of molecular factors in the maturation of these properties was unknown. For the first time, our findings link the *Er81* transcription factor with intrinsic currents and plasticity-related receptors, such as mGluR5, and provide a basis to determine which molecular factors contribute to the emergence of the unique properties of striatal CINs. Elevated  $I_{sAHP}$  and  $I_h$  currents, together with larger inhibitory inputs on CINs, explain the sharper firing dynamics and higher correlations of the putative CINs activity with sensorimotor inputs *in vivo* in the absence of *Er81* (Bennett et al., 2000; Wilson and Goldberg, 2006; Zhang et al., 2018). KCNQ2/3 and HCN2 channels in CINs underlie the  $I_{sAHP}$  and the  $I_h$ , respectively. While our results show no difference in their expression in the absence of *Er81*, these voltage-sensitive channels could be modulated by second messengers, such as phosphatidylinositol-4,5-bisphosphate and calcium for KCNQ2/3 (Wilson and Goldberg, 2006; Falkenburger et al., 2010; Kim et al., 2016), and cAMP for HCN2 (Z. Zhao et al., 2016; Alvarez-Baron et al., 2018). We propose that the enhanced  $I_{sAHP}$  in the *Er81* cKO cells is because of a higher intracellular calcium concentration mediated through mGluR5 (Niswender and Conn, 2010). It is also likely that different potassium channel subtypes underlie  $I_{sAHP}$  as the current can be divided into two calcium-sensitive components (Wilson and Goldberg, 2006) and a calcium-insensitive component (Zhang et al., 2018). We also suggest that enhanced cAMP signaling leads to the increase in the  $I_h$  current. Lower CIN excitability in the absence of *Er81* can indeed result in a decreased acetylcholine recruitment at the CIN membrane, reduced M2 muscarinic receptor activity and consequently, to higher levels of intracellular cAMP (Z. Zhao et al., 2016; Alvarez-Baron et al., 2018). We propose that the changes in CIN activity in the absence of *Er81* modify their connectivity and morphology via homeostatic compensations during maturation.

### Cholinergic interneuron activity modulates striatal sensorimotor plasticity and learning

To probe striatal deficits in *Er81* cKO mice, we designed a mixed, striatum-dependent behavioral paradigm, consisting of a within-subject reversal learning task. We first assessed cognitive flexibility (day 4) and then overtrained mice in the second stage (day 9 to day 13) to force habit formation (Lingawi and Balleine, 2012). This was followed by a second reversal (day 14), allowing the assessment of the strategy used by the mice during the second stage. Overall, extensive training leads to automatic choice of the designated reward side, and the reversal of the rewarded side induces a change in action-outcome contingency. Insensitivity to such a change reveals habit behavior (Balleine et al., 2009; Bergstrom et al., 2018). Here, control mice displayed an inability to shift to the new rewarded side after the second reversal, demonstrating that they were engaged in habitual behavior. In contrast, *Er81* cKO mice displayed rapid improvement of their performance after the second reversal, demonstrating that they displayed intact cognitive flexibility and were not engaged in habit formation during the second stage. While our results support that *Er81* is required for habitual behavior, differences in reversal between control and *Er81* cKO mice may not exclusively originate from an inability to form habits and may also be

explained by differences in reward sensitivity, persistence, or general cognitive flexibility. Future studies should specifically target habit formation or cognitive flexibility to further understand the impact of Er81.

Our study also reveals that developmental alterations of striatal CINs strongly impact the process of integration of sensorimotor information, which is critical for the acquisition and the update of adaptive actions (Markowitz et al., 2018; Robbe, 2018). It also highlights the significance of cholinergic signaling for movement control and learning. Putative striatal CINs better encode motion and display enhanced phasic responses in the *Er81* cKO mice. In particular, at the onset of movement, spikes are more time-locked to the events and less jittered. This also enhanced the timing of putative output neurons which directly encode CIN firing (Mamaligas and Ford, 2016). Enhanced timing of the striatal cells indicates that spike timing-dependent plasticity could be affected by the *Er81* deletion (Cui et al., 2018), via a metabotropic glutamate receptor-induced LTD or a NMDA receptor-induced LTP (Fino et al., 2008). However, the mechanisms of spike timing-dependent plasticity have been poorly investigated in the CINs as of yet (Perrin and Venance, 2019). More investigation is therefore required to better understand how CIN alterations impact intrinsic, synaptic, and structural plasticity and overall, the striatal function. CINs control habit formation via the synchronization and strengthening of the activity of the striatal output neurons (O'Hare et al., 2016; Gritton et al., 2019). Strong pauses have been shown to emerge during learning in response to reward-associated stimuli but not to neutral stimuli (Morris et al., 2004). Adaptable CIN responses to sensorimotor inputs (Aosaki et al., 1994) are required for suppression of competing actions and the expression of habitual behavior. We reveal a notable increase in the recruitment of CINs following the ablation of the *Er81* transcription factor. Previous studies showed that manipulation of CINs in both the DMS and DLS modulates cognitive flexibility after several days of training (Bradfield et al., 2013; Okada et al., 2014; Aoki et al., 2015). In particular, the activity of the CINs in the DLS is necessary for habit substitution (Aoki et al., 2018). Consistently, we have found that elevated CIN function in the DLS (increased quiet state firing and increased inhibition in response to sensorimotor inputs in the cKO) is correlated with decreased habit formation. We uncover a crucial molecular mechanism underlying this relationship and demonstrate, for the first time, that the *Er81* transcription factor underlies the functional tuning of CIN activity and habitual behavior. However, the involvement of the DMS in these conditions is yet to be elucidated. Moreover, it would be of major interest to study the *Er81* transcription factor as a potential target to manipulate set-shifting capacities, known to contribute to the pathophysiology and cognitive defects commonly observed in disorders where repetitive behaviors are debilitating (Lewis and Kim, 2009), such as autism (Karvat and Kimchi, 2014), obsessive-compulsive disorder (Xu et al., 2015; Martos et al., 2017), and addiction (Graybiel and Grafton, 2015).

## References

- Abe H, Okazawa M, Nakanishi S (2011) The *Etv1/Er81* transcription factor orchestrates activity-dependent gene regulation in the terminal maturation program of cerebellar granule cells. *Proc Natl Acad Sci USA* 108:12497–12502.
- Ahmed NY, Knowles R, Dehorter N (2019) New insights into cholinergic neuron diversity. *Front Mol Neurosci* 12:204.
- Allaway KC, Machold R (2017) Developmental specification of forebrain cholinergic neurons. *Dev Biol* 421:1–7.
- Alvarez-Baron CP, Klenchin VA, Chanda B (2018) Minimal molecular determinants of isoform-specific differences in efficacy in the HCN channel family. *J Gen Physiol* 150:1203–1213.
- Aoki S, Liu AW, Zucca A, Zucca S, Wickens JR (2015) Role of striatal cholinergic interneurons in set-shifting in the rat. *J Neurosci* 35:9424–9431.
- Aoki S, Liu AW, Akamine Y, Zucca A, Zucca S, Wickens JR (2018) Cholinergic interneurons in the rat striatum modulate substitution of habits. *Eur J Neurosci* 47:1194–1205.
- Aosaki T, Tsubokawa H, Ishida A, Watanabe K, Graybiel AM, Kimura M (1994) Responses of tonically active neurons in the primate's striatum undergo systematic changes during behavioral sensorimotor conditioning. *J Neurosci* 14:3969–3984.
- Apicella P (2017) The role of the intrinsic cholinergic system of the striatum: what have we learned from TAN recordings in behaving animals? *Neuroscience* 360:81–94.
- Apicella P, Legallet E, Trouche E (1997) Responses of tonically discharging neurons in the monkey striatum to primary rewards delivered during different behavioral states. *Exp Brain Res* 116:456–466.
- Apicella P, Deffains M, Ravel S, Legallet E (2009) Tonic active neurons in the striatum differentiate between delivery and omission of expected reward in a probabilistic task context. *Eur J Neurosci* 30:515–526.
- Arber S, Ladle DR, Lin JH, Frank E, Jessell TM (2000) *ETS* gene *Er81* controls the formation of functional connections between group Ia sensory afferents and motor neurons. *Cell* 101:485–498.
- Balleine BW, Ostlund SB (2007) Still at the choice-point: action selection and initiation in instrumental conditioning. *Ann NY Acad Sci* 1104:147–171.
- Balleine BW, Liljeholm M, Ostlund SB (2009) The integrative function of the basal ganglia in instrumental conditioning. *Behav Brain Res* 199:43–52.
- Beatty JA, Sullivan MA, Morikawa H, Wilson CJ (2012) Complex autonomous firing patterns of striatal low-threshold spike interneurons. *J Neurophysiol* 108:771–781.
- Benhamou L, Kehat O, Cohen D (2014) Firing pattern characteristics of tonically active neurons in rat striatum: context dependent or species divergent? *J Neurosci* 34:2299–2304.
- Bennett BD, Callaway JC, Wilson CJ (2000) Intrinsic membrane properties underlying spontaneous tonic firing in neostriatal cholinergic interneurons. *J Neurosci* 20:8493–8503.
- Bergstrom HC, Lipkin AM, Lieberman AG, Pinard CR, Gunduz-Cinar O, Brockway ET, Taylor WW, Nonaka M, Bukalo O, Wills TA, Rubio FJ, Li X, Pickens CL, Winder DG, Holmes A (2018) Dorsolateral striatum engagement interferes with early discrimination learning. *Cell Rep* 23:2264–2272.
- Bradfield LA, Bertran-Gonzalez J, Chieng B, Balleine BW (2013) The thalamostriatal pathway and cholinergic control of goal-directed action: interlacing new with existing learning in the striatum. *Neuron* 79:153–166.
- Brimblecombe KR, Threlfell S, Dautan D, Kosillo P, Mena-Segovia J, Cragg SJ (2018) Targeted activation of cholinergic interneurons accounts for the modulation of dopamine by striatal nicotinic receptors. *eNeuro* 5:ENEURO.0397-17.2018.
- Cave JW, Akiba Y, Banerjee K, Bhosle S, Berlin R, Baker H (2010) Differential regulation of dopaminergic gene expression by *Er81*. *J Neurosci* 30:4717–4724.
- Cui Y, Prokin I, Mendes A, Berry H, Venance L (2018) Robustness of STDP to spike timing jitter. *Sci Rep* 8:8139.
- Dehorter N, Ciceri G, Bartolini G, Lim L, del Pino I, Marín O (2015) Tuning of fast-spiking interneuron properties by an activity-dependent transcriptional switch. *Science* 349:1216–1220.
- Dickinson A, Balleine B, Watt A, Gonzalez F, Boakes RA (1995) Motivational control after extended instrumental training. *Anim Learn Behav* 23:197–206.
- Ding B, Cave JW, Dobner PR, Mullikin-Kilpatrick D, Bartzokis M, Zhu H, Chow CW, Gronostajski RM, Kilpatrick DL (2016) Reciprocal autoregulation by NFI occupancy and *ETV1* promotes the developmental expression of dendrite-synapse genes in cerebellar granule neurons. *Mol Biol Cell* 27:1488–1499.
- Ding JB, Guzman JN, Peterson JD, Goldberg JA, Surmeier DJ (2010) Thalamic gating of corticostriatal signaling by cholinergic interneurons. *Neuron* 67:294–307.
- Doig NM, Magill PJ, Apicella P, Bolam JP, Sharott A (2014) Cortical and thalamic excitation mediate the multiphasic responses of striatal cholinergic interneurons to motivationally salient stimuli. *J Neurosci* 34:3101–3117.

- Dorst MC, Tokarska A, Zhou M, Lee K, Stagkourakis S, Broberger C, Masmanidis S, Silberberg G (2020) Polysynaptic inhibition between striatal cholinergic interneurons shapes their network activity patterns in a dopamine-dependent manner. *Nat Commun* 11:5113.
- English DF, Ibanez-Sandoval O, Stark E, Tecuapetla F, Buzsaki G, Deisseroth K, Tepper JM, Koos T (2011) GABAergic circuits mediate the reinforcement-related signals of striatal cholinergic interneurons. *Nat Neurosci* 15:123–130.
- Falkenburger BH, Jensen JB, Hille B (2010) Kinetics of PIP2 metabolism and KCNQ2/3 channel regulation studied with a voltage-sensitive phosphatase in living cells. *J Gen Physiol* 135:99–114.
- Fino E, Deniau JM, Venance L (2008) Cell-specific spike-timing-dependent plasticity in GABAergic and cholinergic interneurons in corticostriatal rat brain slices. *J Physiol* 586:265–282.
- Flames N, Hobert O (2009) Gene regulatory logic of dopamine neuron differentiation. *Nature* 458:885–889.
- Flames N, Pla R, Gelman DM, Rubenstein JL, Puelles L, Marin O (2007) Delineation of multiple subpallial progenitor domains by the combinatorial expression of transcriptional codes. *J Neurosci* 27:9682–9695.
- Franklin NT, Frank MJ (2015) A cholinergic feedback circuit to regulate striatal population uncertainty and optimize reinforcement learning. *Elife* 4:e12029.
- Granger AJ, Mulder N, Saunders A, Sabatini BL (2016) Cotransmission of acetylcholine and GABA. *Neuropharmacology* 100:40–46.
- Gras C, Amilhon B, Lepicard EM, Poirel O, Vinatier J, Herbin M, Dumas S, Tzavara ET, Wade MR, Nomikos GG, Hanoun N, Saurini F, Kemel ML, Gasnier B, Giros B, El Mestikawy S (2008) The vesicular glutamate transporter VGLUT3 synergizes striatal acetylcholine tone. *Nat Neurosci* 11:292–300.
- Graybiel AM, Grafton ST (2015) The striatum: where skills and habits meet. *Cold Spring Harb Perspect Biol* 7:a021691.
- Gritton HJ, Howe WM, Romano MF, DiFeliceantonio AG, Kramer MA, Saligrama V, Bucklin ME, Zemel D, Han X (2019) Unique contributions of parvalbumin and cholinergic interneurons in organizing striatal networks during movement. *Nat Neurosci* 22:586–597.
- He M, Tucciarone J, Lee S, Nigro MJ, Kim Y, Levine JM, Kelly SM, Kruglikov I, Wu P, Chen Y, Gong L, Hou Y, Osten P, Rudy B, Huang ZJ (2016) Strategies and tools for combinatorial targeting of GABAergic neurons in mouse cerebral cortex. *Neuron* 92:555.
- Higley MJ, Gittis AH, Oldenburg IA, Balhasar N, Seal RP, Edwards RH, Lowell BB, Kreitzer AC, Sabatini BL (2011) Cholinergic interneurons mediate fast VGLUT3-dependent glutamatergic transmission in the striatum. *PLoS One* 6:e19155.
- Hippenmeyer S, Vrieseling E, Sigrist M, Portmann T, Laengle C, Ladle DR, Arber S (2005) A developmental switch in the response of DRG neurons to ETS transcription factor signaling. *PLoS Biol* 3:e159.
- Hjorth JJJ, Kozlov A, Carannante I, Frost Nylén J, Lindroos R, Johansson Y, Tokarska A, Dorst MC, Suryanarayana SM, Silberberg G, Hellgren Kotaleski J, Grillner S (2020) The microcircuits of striatum in silico. *Proc Natl Acad Sci USA* 117:9554–9565.
- Inokawa H, Yamada H, Matsumoto N, Muranishi M, Kimura M (2010) Juxtacellular labeling of tonically active neurons and phasically active neurons in the rat striatum. *Neuroscience* 168:395–404.
- Karvat G, Kimchi T (2014) Acetylcholine elevation relieves cognitive rigidity and social deficiency in a mouse model of autism. *Neuropsychopharmacology* 39:831–840.
- Kim KS, Duignan KM, Hawryluk JM, Soh H, Tzingounis AV (2016) The voltage activation of cortical KCNQ channels depends on global PIP2 levels. *Biophys J* 110:1089–1098.
- Klug JR, Engelhardt MD, Cadman CN, Li H, Smith JB, Ayala S, Williams EW, Hoffman H, Jin X (2018) Differential inputs to striatal cholinergic and parvalbumin interneurons imply functional distinctions. *Elife* 7:e35657.
- Koos T, Tepper JM (2002) Dual cholinergic control of fast-spiking interneurons in the neostriatum. *J Neurosci* 22:529–535.
- Kosillo P, Zhang YF, Threlfell S, Cragg SJ (2016) Cortical control of striatal dopamine transmission via striatal cholinergic interneurons. *Cereb Cortex* 26:4160–4169.
- Lee K, Holley SM, Shobe JL, Chong NC, Cepeda C, Levine MS, Masmanidis SC (2017) Parvalbumin interneurons modulate striatal output and enhance performance during associative learning. *Neuron* 93:1451–1463.
- Lewis M, Kim SJ (2009) The pathophysiology of restricted repetitive behavior. *J Neurodev Disord* 1:114–132.
- Lim SA, Kang UJ, McGehee DS (2014) Striatal cholinergic interneuron regulation and circuit effects. *Front Synaptic Neurosci* 6:22.
- Lingawi NW, Balleine BW (2012) Amygdala central nucleus interacts with dorsolateral striatum to regulate the acquisition of habits. *J Neurosci* 32:1073–1081.
- Lloret-Fernández C, Maicas M, Mora-Martínez C, Artacho A, Jimeno-Martin Á, Chirivella L, Weinberg P, Flames N (2018) A transcription factor collective defines the HSN serotonergic neuron regulatory landscape. *Elife* 7:e32785.
- Lopes R, Verhey van Wijk N, Neves G, Pachnis V (2012) Transcription factor LIM homeobox 7 (Lhx7) maintains subtype identity of cholinergic interneurons in the mammalian striatum. *Proc Natl Acad Sci USA* 109:3119–3124.
- Lozovaya N, Eftekhari S, Cloarec R, Gouty-Colomer LA, Dufour A, Riffault B, Billon-Grand M, Pons-Bennaceur A, Oumar N, Burnashev N, Ben-Ari Y, Hammond C (2018) GABAergic inhibition in dual-transmission cholinergic and GABAergic striatal interneurons is abolished in Parkinson disease. *Nat Commun* 9:1422.
- Magno L, Barry C, Schmidt-Hieber C, Theodotou P, Häusser M, Kessaris N (2017) NKX2-1 is required in the embryonic septum for cholinergic system development, learning, and memory. *Cell Rep* 20:1572–1584.
- Mallet N, Le Moine C, Charpier S, Gonon F (2005) Feedforward inhibition of projection neurons by fast-spiking GABA interneurons in the rat striatum in vivo. *J Neurosci* 25:3857–3869.
- Mamaligas AA, Ford CP (2016) Spontaneous synaptic activation of muscarinic receptors by striatal cholinergic neuron firing. *Neuron* 91:574–586.
- Mamaligas AA, Barcomb K, Ford CP (2019) Cholinergic transmission at muscarinic synapses in the striatum is driven equally by cortical and thalamic inputs. *Cell Rep* 28:1003–1014.
- Markowitz JE, Gillis WF, Beron CC, Neufeld SQ, Robertson K, Bhagat ND, Peterson RE, Peterson E, Hyun M, Linderman SW, Sabatini BL, Datta SR (2018) The striatum organizes 3D behavior via moment-to-moment action selection. *Cell* 174:44–58.e17.
- Martos YV, Braz BY, Beccaria JP, Murer MG, Belforte JE (2017) Compulsive social behavior emerges after selective ablation of striatal cholinergic interneurons. *J Neurosci* 37:2849–2858.
- Mi D, Li Z, Lim L, Li M, Moissidis M, Yang Y, Gao T, Hu TX, Pratt T, Price DJ, Sestan N, Marin O (2018) Early emergence of cortical interneuron diversity in the mouse embryo. *Science* 360:81–85.
- Morris G, Arkadir D, Nevet A, Vaadia E, Bergman H (2004) Coincident but distinct messages of midbrain dopamine and striatal tonically active neurons. *Neuron* 43:133–143.
- Munoz-Manchado AB, Bengtsson Gonzales C, Zeisel A, Munguba H, Bekkouche B, Skene NG, Lonnerberg P, Ryge J, Harris KD, Linnarsson S, Hjerling-Leffler J (2018) Diversity of interneurons in the dorsal striatum revealed by single-cell RNA sequencing and PatchSeq. *Cell Rep* 24:2179–2190.e2177.
- Nelson AB, Bussert TG, Kreitzer AC, Seal RP (2014) Striatal cholinergic neurotransmission requires VGLUT3. *J Neurosci* 34:8772–8777.
- Niswender CM, Conn PJ (2010) Metabotropic glutamate receptors: physiology, pharmacology, and disease. *Annu Rev Pharmacol Toxicol* 50:295–322.
- Nóbrega-Pereira S, Kessaris N, Du T, Kimura S, Anderson SA, Marin O (2008) Postmitotic Nkx2-1 controls the migration of telencephalic interneurons by direct repression of guidance receptors. *Neuron* 59:733–745.
- O'Hare JK, Ade KK, Sukharnikova T, Van Hooser SD, Palmeri ML, Yin HH, Calakos N (2016) Pathway-specific striatal substrates for habitual behavior. *Neuron* 89:472–479.
- Okada K, Nishizawa K, Fukabori R, Kai N, Shiota A, Ueda M, Tsutsui Y, Sakata S, Matsushita N, Kobayashi K (2014) Enhanced flexibility of place discrimination learning by targeting striatal cholinergic interneurons. *Nat Commun* 5:3778.
- Okada K, Nishizawa K, Setogawa S, Hashimoto K, Kobayashi K (2018) Task-dependent function of striatal cholinergic interneurons in behavioural flexibility. *Eur J Neurosci* 47:1174–1183.
- Packard MG, Knowlton BJ (2002) Learning and memory functions of the basal ganglia. *Annu Rev Neurosci* 25:563–593.
- Perrin E, Venance L (2019) Bridging the gap between striatal plasticity and learning. *Curr Opin Neurobiol* 54:104–112.

- Ranjbar-Slamloo Y, Arabzadeh E (2019) Diverse tuning underlies sparse activity in layer 2/3 vibrissal cortex of awake mice. *J Physiol* 597:2803–2817.
- Ravel S, Legallet E, Apicella P (2003) Responses of tonically active neurons in the monkey striatum discriminate between motivationally opposing stimuli. *J Neurosci* 23:8489–8497.
- Reiner A, Levitz J (2018) Glutamatergic signaling in the central nervous system: ionotropic and metabotropic receptors in concert. *Neuron* 98:1080–1098.
- Robbe D (2018) To move or to sense? Incorporating somatosensory representation into striatal functions. *Curr Opin Neurobiol* 52:123–130.
- Saunders A, Granger AJ, Sabatini BL (2015) Corelease of acetylcholine and GABA from cholinergic forebrain neurons. *Elife* 52:e06412.
- Sharott A, Moll CK, Engler G, Denker M, Grun S, Engel AK (2009) Different subtypes of striatal neurons are selectively modulated by cortical oscillations. *J Neurosci* 29:4571–4585.
- Sharott A, Doig NM, Mallet N, Magill PJ (2012) Relationships between the firing of identified striatal interneurons and spontaneous and driven cortical activities in vivo. *J Neurosci* 32:13221–13236.
- Straub C, Tritsch NX, Hagan NA, Gu C, Sabatini BL (2014) Multiphasic modulation of cholinergic interneurons by nigrostriatal afferents. *J Neurosci* 34:8557–8569.
- Straub C, Saulnier JL, Begue A, Feng DD, Huang KW, Sabatini BL (2016) Principles of synaptic organization of GABAergic interneurons in the striatum. *Neuron* 92:84–92.
- Szydlowski SN, Pollak Dorocic I, Planert H, Carlen M, Meletis K, Silberberg G (2013) Target selectivity of feedforward inhibition by striatal fast-spiking interneurons. *J Neurosci* 33:1678–1683.
- Tepper JM, Koos T, Ibanez-Sandoval O, Tecuapetla F, Faust TW, Assous M (2018) Heterogeneity and diversity of striatal GABAergic interneurons: update 2018. *Front Neuroanat* 12:91.
- Thorn CA, Graybiel AM (2014) Differential entrainment and learning-related dynamics of spike and local field potential activity in the sensorimotor and associative striatum. *J Neurosci* 34:2845–2859.
- Threlfell S, Lalic T, Platt NJ, Jennings KA, Deisseroth K, Cragg SJ (2012) Striatal dopamine release is triggered by synchronized activity in cholinergic interneurons. *Neuron* 75:58–64.
- Willardsen M, Hutcheson DA, Moore KB, Vetter ML (2014) The ETS transcription factor *Etv1* mediates FGF signaling to initiate proneural gene expression during *Xenopus laevis* retinal development. *Mech Dev* 131:57–67.
- Wilson CJ, Goldberg JA (2006) Origin of the slow afterhyperpolarization and slow rhythmic bursting in striatal cholinergic interneurons. *J Neurophysiol* 95:196–204.
- Xu M, Kobets A, Du JC, Lenington J, Li L, Banasr M, Duman RS, Vaccarino FM, DiLeone RJ, Pittenger C (2015) Targeted ablation of cholinergic interneurons in the dorsolateral striatum produces behavioral manifestations of Tourette syndrome. *Proc Natl Acad Sci USA* 112:893–898.
- Yin HH, Knowlton BJ, Balleine BW (2004) Lesions of dorsolateral striatum preserve outcome expectancy but disrupt habit formation in instrumental learning. *Eur J Neurosci* 19:181–189.
- Zhang YF, Reynolds JN, Cragg SJ (2018) Pauses in cholinergic interneuron activity are driven by excitatory input and delayed rectification, with dopamine modulation. *Neuron* 98:918–925.e913.
- Zhao Y, Marin O, Hermes E, Powell A, Flames N, Palkovits M, Rubenstein JL, Westphal H (2003) The LIM-homeobox gene *Lhx8* is required for the development of many cholinergic neurons in the mouse forebrain. *Proc Natl Acad Sci USA* 100:9005–9010.
- Zhao Z, Zhang K, Liu X, Yan H, Ma X, Zhang S, Zheng J, Wang L, Wei X (2016) Involvement of HCN channel in muscarinic inhibitory action on tonic firing of dorsolateral striatal cholinergic interneurons. *Front Cell Neurosci* 10:71.
- Zucca S, Zucca A, Nakano T, Aoki S, Wickens J (2018) Pauses in cholinergic interneuron firing exert an inhibitory control on striatal output in vivo. *Elife* 7:e32510.

## **Appendix C: Research Paper (Ahmed et al. 2023)**

Original Research Paper published in Frontiers in Cell Developmental Biology

**N. Y. Ahmed**, R. Knowles, L. Liu, Y. Yan, X. Li, U. Schumann, Y. Wang, Y. Sontani, N. Reynolds, R. Natoli, J. Wen, I. Del Pino, D. Mi and N. Dehorter (2023). "Developmental deficits of MGE-derived interneurons in the *Cntnap2* knockout mouse model of autism spectrum disorder." *Front Cell Dev Biol* 11: 1112062.



## OPEN ACCESS

EDITED BY  
Ilaria Parenti,  
University Hospital Essen, Germany

REVIEWED BY  
Yuri Bozzi,  
University of Trento, Italy  
Bernadette Basilico,  
Institute of Science and Technology  
Austria (IST Austria), Austria

\*CORRESPONDENCE  
Nathalie Dehorter,  
✉ nathalie.dehorter@anu.edu.au

SPECIALTY SECTION  
This article was submitted to Molecular  
and Cellular Pathology,  
a section of the journal  
Frontiers in Cell and Developmental  
Biology

RECEIVED 30 November 2022

ACCEPTED 17 January 2023

PUBLISHED 01 February 2023

CITATION  
Ahmed NY, Knowles R, Liu L, Yan Y, Li X,  
Schumann U, Wang Y, Sontani Y,  
Reynolds N, Natoli R, Wen J, Del Pino I,  
Mi D and Dehorter N (2023),  
Developmental deficits of MGE-derived  
interneurons in the *Cntnap2* knockout  
mouse model of autism  
spectrum disorder.  
*Front. Cell Dev. Biol.* 11:1112062.  
doi: 10.3389/fcell.2023.1112062

COPYRIGHT  
© 2023 Ahmed, Knowles, Liu, Yan, Li,  
Schumann, Wang, Sontani, Reynolds,  
Natoli, Wen, Del Pino, Mi and Dehorter.  
This is an open-access article distributed  
under the terms of the [Creative Commons  
Attribution License \(CC BY\)](#). The use,  
distribution or reproduction in other  
forums is permitted, provided the original  
author(s) and the copyright owner(s) are  
credited and that the original publication in  
this journal is cited, in accordance with  
accepted academic practice. No use,  
distribution or reproduction is permitted  
which does not comply with these terms.

# Developmental deficits of MGE-derived interneurons in the *Cntnap2* knockout mouse model of autism spectrum disorder

Noorya Yasmin Ahmed<sup>1</sup>, Rhys Knowles<sup>1</sup>, Lixinyu Liu<sup>1</sup>, Yiming Yan<sup>2</sup>, Xiaohan Li<sup>2</sup>, Ulrike Schumann<sup>1</sup>, Yumeng Wang<sup>1</sup>, Yovina Sontani<sup>1</sup>, Nathan Reynolds<sup>1</sup>, Riccardo Natoli<sup>1</sup>, Jiayu Wen<sup>1</sup>, Isabel Del Pino<sup>3</sup>, Da Mi<sup>2</sup> and Nathalie Dehorter<sup>1\*</sup>

<sup>1</sup>The Australian National University, The John Curtin School of Medical Research, Canberra, ACT, Australia, <sup>2</sup>Tsinghua-Peking Center for Life Sciences, IDG/McGovern Institute for Brain Research, School of Life Sciences, Tsinghua University, Beijing, China, <sup>3</sup>Institute of Neurosciences, Spanish National Research Council (CSIC), Sant Joan d'Alacant, Spain

Interneurons are fundamental cells for maintaining the excitation-inhibition balance in the brain in health and disease. While interneurons have been shown to play a key role in the pathophysiology of autism spectrum disorder (ASD) in adult mice, little is known about how their maturation is altered in the developing striatum in ASD. Here, we aimed to track striatal developing interneurons and elucidate the molecular and physiological alterations in the *Cntnap2* knockout mouse model. Using Stereo-seq and single-cell RNA sequencing data, we first characterized the pattern of expression of *Cntnap2* in the adult brain and at embryonic stages in the medial ganglionic eminence (MGE), a transitory structure producing most cortical and striatal interneurons. We found that *Cntnap2* is enriched in the striatum, compared to the cortex, particularly in the developing striatal cholinergic interneurons. We then revealed enhanced MGE-derived cell proliferation, followed by increased cell loss during the canonical window of developmental cell death in the *Cntnap2* knockout mice. We uncovered specific cellular and molecular alterations in the developing Lhx6-expressing cholinergic interneurons of the striatum, which impacts interneuron firing properties during the first postnatal week. Overall, our work unveils some of the mechanisms underlying the shift in the developmental trajectory of striatal interneurons which greatly contribute to the ASD pathogenesis.

## KEYWORDS

interneuron, maturation, striatum, autism, CNTNAP2

## Introduction

Interneurons are vital cells that regulate the balance between excitation and inhibition in the brain (Dehorter et al., 2017; Antoine et al., 2019) and are required to shape functional circuits during development (Fuccillo, 2016). Deficits to interneurons have been identified in both human patients and in mouse models of neurodevelopmental disorders such as Autism Spectrum Disorder (ASD). Interneuron dysfunction supports behavioural traits including impaired social interactions and repetitive behaviours (Fuccillo, 2016; Contractor et al., 2021). Therefore, these cells present interesting targets for therapeutic interventions (Selimbeyoglu et al., 2017). Yet, how the maturation of interneurons is affected at

embryonic and early postnatal stages in this condition has remained poorly investigated and as such, the cellular mechanisms contributing to ASD pathophysiology is still unknown.

Most of the interneurons fated to the cortex and striatum derive from a transitory embryonic brain structure, the Medial Ganglionic Eminence (MGE; (Penagarikano et al., 2011; Vogt et al., 2017; Knowles et al., 2021), where they express specific molecules, such as the Lim Homeodomain Lhx6 and NK2 homeobox 1 (Nkx2.1) transcription factors (Knowles et al., 2021). Between embryonic day (E) 12.5 and postnatal day (P) 10, a combination of innate genetic programs (Yap and Greenberg, 2018), external environmental cues, and neuronal activity shape interneuron specification and facilitate the establishment of functional cells (Babij and De Marco Garcia, 2016; Mayer et al., 2018; Wong et al., 2018). The ASD risk gene Contactin-associated protein-like 2 (Cntnap2/CASPR2), first shown to be altered in patients presenting with severe autism features (Strauss et al., 2006), is a transmembrane scaffolding protein and a cell adhesion protein of the neurexin family which coordinates several processes that are critical for the maturation of neuronal circuits (Benamer et al., 2020), including myelination (Scott et al., 2017), cell excitability (Poliak et al., 1999) and synapse development (Varea et al., 2015). Whilst Cntnap2 cell-autonomously affects adult interneuron functioning (Vogt et al., 2017; Antoine et al., 2019) and has been shown to be expressed from E14 in the MGE (Penagarikano et al., 2011; Vogt et al., 2017), the specific pattern of expression in the brain, as well as its influence on interneuron development have remained poorly investigated; in particular, how the absence of Cntnap2 perturbs the maturation of the MGE-derived interneurons.

Although they account for ~5% of the total neuronal population, striatal interneurons are functionally diverse and consist of two main cell types, i.e. the Lhx6-expressing GABAergic interneurons and the Lhx6-expressing cholinergic interneurons (Lozovaya et al., 2018; Ahmed et al., 2021). These two populations precisely regulate the striatal output neurons and present with characteristic electrophysiological profiles. The Lhx6-expressing GABAergic interneurons are fast-spiking cells, characterized by short duration action potentials with large and rapid kinetics (Tepper et al., 2010), whilst the cholinergic cells are tonic active neurons that display adaptation and prominent after-hyperpolarizations (Ahmed et al., 2019).

Here, we hypothesized that the developmental trajectory of these striatal interneurons is perturbed in the Cntnap2 Knockout (KO) mouse model of ASD (Penagarikano et al., 2011). We analyzed the cellular and molecular developmental alterations of the developing MGE-derived interneurons of the striatum at embryonic and early postnatal stages, in control and Cntnap2 KO mice. We show that interneuron production, migration and integration in the developing striatum are affected in the Cntnap2 KO mouse model, likely contributing to ASD-related pathogenesis.

## Material and methods

### Mice

*Lhx6-iCre;td-Tomato* ("Control") and *Cntnap2<sup>-/-</sup>; Lhx6-iCre; td-Tomato* ("Cntnap2 KO") male and female mice (*Cntnap2<sup>-/-</sup>*, Jackson ID: #017482, (Tepper et al., 2010)) were used. To track MGE-derived cells through the stages of embryonic development, we also utilized the inducible *Nkx2.1CreER:TdTomato* and *Nkx2.1CreER:TdTomato*:

*Cntnap2<sup>-/-</sup>* mice. Tamoxifen in corn oil (40 mg/ml) was used to orally gavage pregnant female mice at E12.5 (3.3 µL/g, 30 mg/kg) to induce cre expression.

Timed matings were used to generate embryonic tissue for collection. Detection of a plug was considered embryonic day (E) 0.5. Embryonic tissue was collected at E12.5, E14.5, and E15.5 (a minimum of three embryos), and postnatal tissue was collected at postnatal day (P) 0, 4, 6, 10, and 30. All procedures were conducted in accordance with the Australian National University Animal Experimentation Ethics Committee (protocol numbers A2019/46 & A2021/43).

### Spatial transcriptomics (Stereo-seq)

To unbiasedly determine the expression pattern of *Cntnnpa2* in the adult mouse brain, we employed Spatial Enhanced Resolution Omics-Sequencing (Stereo-seq) technology from BGI, in beta testing (V1.0, not commercially available). This analysis combines whole transcriptome information with nanoscale resolution. Upon interaction with tissue section, cDNA is synthesized *in situ* from mRNA captured by the chip probes. The spatial transcriptomic profile of the section was performed by cDNA sequencing with cell spatial coordinates.

An adult (P30+) brain was extracted and embedded and frozen in optimal cutting temperature compound (OCT), then sectioned sagittally *via* cryostat at a thickness of 10 µm. Tissue was mounted onto STOmics-GeneExpression-S1 chips (1 cm<sup>2</sup>), which are patterned grids of probes containing spatial coordinates. A permeabilization analysis was first performed to determine the optimal permeabilization time: tissue on the chip was fixed in methanol, then incubated at 37°C for various lengths of time (0–30 min) in Permeabilization Reagent (BGI, 0.01N HCl and PR Enzyme). Reverse transcription was then performed at 42°C for 1 + hours. The whole chip was then imaged (AxioScan Slide Scanner), and the permeabilization time with the strongest fluorescence signal with the lowest signal diffusion was selected. The gene expression experiment was then performed with duplicates. The tissue was fixed as before, permeabilized, and the reverse transcription performed. The tissue was removed from the chip, and cDNA Release Mix was added to the chip and incubated at 55°C for 3 + hours. The quality of the generated cDNA library was checked *via* Bioanalyser, after which we proceeded with one library (F2). Library preparation and sequencing was done at the WEHI core facility using the DNBSEQ-G400RS FCL PE100 kit and sequencer.

### Mapping the raw data

Stereo-seq Analysis Workflow (SAW) software (Chen et al., 2021) was used to process the sequencing information. The coordinate ID (CID) sequences were mapped to the designed coordinates on the chip with a mismatch tolerance of 1 bp. The Molecular ID (MID) sequences with a quality score greater than 10 were kept. cDNA sequences were mapped to the reference genome (mm10) by STAR (Dobin et al., 2013). We obtained an expression profile matrix with 70901 units and 18191 features using a bin size 50×50 DNA nanoball (DNBs).

### Unsupervised clustering

We used the *stereopy* packages (Chen et al., 2021) to perform the normalisation and unsupervised clustering. In the bin 50×50 DNBs



expression matrix, the low-quality units with fewer than 100 genes and more than 10% mitochondria gene level were filtered out. The low-abundance genes that were expressed in fewer than 10 cells were removed. On the filtered cells, the expression matrix was normalised, and PCA was analyzed. Next, the Gaussian smoothing (Shen et al., 2022) method was performed to make the expression value closer to reality. On the smoothed values, we performed dimensionality reduction with the function “*stereo.tl.pca*”. The clusters were identified using the functions “*stereo.tl.neighbors*” and “*stereo.tl.leiden*”.

### Clustering annotation

We extracted the top marker genes expressed in each cluster based on the most significant adjusted p-values using “*sc.findmarker*” function from *Scanpy* (Wolf et al., 2018). The clusters were annotated based on the known marker expression and spatial localisation of clusters in the brain. Tissue identities were assigned based on the above information.

### Differential expression and pathway enrichment analysis

Differential expression (DE) analysis was conducted pairwise between clusters using the function “*FindMarker*” from Seurat (Stuart, 2019). The p-values and the adjusted p-values, and log<sub>2</sub> fold-changes were calculated between two clusters. The differentially expressed genes were selected with a adjusted p-values smaller than 0.01, log<sub>2</sub> fold-change greater than 1. *ClusterProfiler* (Yu et al., 2012) was used to find enriched Gene Ontology (GO) terms from the DE genes.

### Hotspot module analysis

Hotspot analysis (DeTomaso and Yosef, 2021) was carried out on the normalised data to identify the spatially functional modules with informative genes. Within each identified module, GO enrichment analysis was performed using *ClusterProfiler* (Yu et al., 2012).

### Analysis of published single-cell RNA sequencing data

Using the available single-cell RNA-sequencing data from Mi et al., 2018, we performed t-Distributed Stochastic Neighbor Embedding (t-SNE) analysis to visualize data in a two dimensional map, as in (22). We generated plots containing E12.5 and E14.5 MGE neurons, along with histograms showing the regional and temporal identities of cells. We made feature plots for *Cntnap2* expression in E12.5 and E14.5 MGE neurons and a heatmap plot in which we classified cell clusters into three classes (*i.e.* cortical interneurons, striatal interneurons and cholinergic neurons), according to the marker gene expression pattern. We then compared *Cntnap2* levels across three cell classes.

### Tissue collection

Pregnant females were cervically dislocated and the embryos were removed from the mother, and placed into ice-cold 0.01M phosphate buffered saline (PBS). E12-14 embryos were decapitated, and the brain was dissected and placed into 4% paraformaldehyde (PFA) for

overnight fixation. Considering the larger size of the E15 embryos and to ensure adequate fixation we performed cardiac perfusion on E15.5 embryos. The arm of the embryo was removed to reveal the heart and the animal was perfused with 1 ml 0.01M PBS followed by 3 ml 4% PFA. The brain was then removed and fixed overnight in 4% PFA. Brains were then washed in 0.01M PBS for 5 h to remove the fixative. Embryonic tissue was embedded in 4% Bacto-Agar in 0.01M PBS heated to 37°C, allowed to cool, and then sectioned at 60 µm using a Leica 1000S vibratome and kept in a cryoprotective ethylene glycol solution at -20°C until further processing for immunohistochemistry.

Postnatal mice (P0-P30) were deeply anaesthetised on ice (P0-P4) or with 4–4.5% isoflurane (P6-P30) and perfused transcardially with 0.01M PBS followed by 4% PFA. Brains were post-fixed for 2–5 h in 4% PFA. The fixative was then washed from tissues 3 times for 30 min each with 0.01M PBS. Tissue was sectioned at 60 µm using a Leica 1000S vibratome and kept in a cryoprotective ethylene glycol solution at -20°C until further processing for immunohistochemistry.

### Immunohistochemistry

Sections were first washed twice for 5 min in 0.01M PBS and permeabilised twice for 5 min with 0.25% TritonX. Non-specific binding sites were then blocked by immersing the tissue in a blocking solution (10% Normal Donkey Serum, 0.25% TritonX, 2% Bovine Serum Albumin in 0.01M PBS), for 2 h at room temperature. Slices were then incubated in primary antibodies added to blocking solution overnight at 4°C on a shaker. The following day, slices were left at room temperature for 1 h on a shaker and were washed 3 times for 15 min each with 0.01M PBS. Slices were then stained with fluorescence conjugated or biotinylated secondary antibodies in blocking solution for 2–3 h and then washed 3 times for 15 min each with 0.01M PBS. This was repeated for those requiring tertiary antibodies for 1 h. Slices were then incubated with 5 µM DAPI (Sigma) for 10 min and washed 4 times for 5 min each with PBS. The slices were mounted on Livingstone slides submerged in gelatine, allowed to dry, covered with Mowiol (Sigma) and a coverslip (Thermofisher).

The following primary antibodies were used: mouse anti-Tuj1 (1:500, Biologend), rabbit anti-Ki67 (1:500, Abcam), mouse anti-Lhx6 (1:300; Santa Cruz), goat anti-ChAT (1:200; Merck), rabbit anti-mgluR5 (1:50; Alomone), rabbit anti-cleaved Caspase-3 (1:200, Cell Signalling), rabbit anti-NMDAR2C (1:100, ThermoFisher); and secondary antibodies: donkey anti-rabbit 488 (1:200, Molecular Probes), anti-goat and anti-mouse Alexa 488, 555 or 647 (1:200; Life Technologies), and streptavidin 647 (1:200, Jackson).

To mark proliferating cells at specific developmental time points, pregnant female mice were injected intraperitoneally with 5-ethynyl 2'-deoxyuridine (EdU) dissolved in distilled water (5 mg/ml; 30 mg/kg). To label the EdU that was incorporated into the DNA of proliferating cells at the time of IP injection, the Click-It® EdU Imaging Kit from Invitrogen was used, with slight modifications. To label nuclei, DAPI was used. In addition, washes were completed in 1x PBS instead of 3% BSA. To perform staining of EdU, tissue was washed in 1x PBS. The tissue was washed in 500 µL of 0.5% Triton for 15 min. The reaction cocktail was prepared, according to the Click-iT® protocol. The triton solution was removed from the wells and replaced with the reaction cocktail solution for 30 min. The reaction cocktail was removed and replaced with blocking solution for 2 h at RT.

## Confocal imaging

Immunostained slices were imaged with a Nikon A1 confocal microscope controlled with the NIS-elements advanced imaging software or a Leica SP5 confocal microscope controlled by LAS AF. Images were collected at 4x, 10x, 20x, 40x, and 63x. To ensure consistency in imaging, the same confocal microscope was used within a data set and the parameters for offset, pinhole, gain and laser intensity were kept constant for each experimental set.

## Image analysis

Image analysis was largely completed using Fiji/ImageJ. To count Lhx6+ and Nkx2.1 + cells, a custom-made code was used to run multiple threshold events at different threshold values, whilst simultaneously completing image processing and detecting particles of the appropriate size and circularity. The code was modified for a number of parameters including the lower and upper threshold, number of thresholds, minimum and maximum cell size, and circularity, dependent on the dataset being analyzed. During analysis of control and experimental conditions, all parameters were kept consistent. VZ thickness was measured by creating a straight line on Fiji at the apex of the MGE spanning from the ventricular wall to the VZ/SVZ border, which was defined by Tuj1 immunostaining. The SVZ thickness was approximated by measuring from the VZ/SVZ border at the apex of the MGE through to the mantle, which was defined by either the higher level of Tuj1 and/or the lack of Ki67 cells.

To measure the thickness of the migratory streams, masks surrounding the superficial and deep migrating postmitotic cells were created on ImageJ manually. The width of the middle of the mask was measured in  $\mu\text{m}$ . The same masks were used for automated cell counting to quantify the total density of Nkx2.1 + cells.

The size of the postnatal striatum was quantified from low magnification images containing the whole striatum; the contour was traced and the area measured. The thickness of the postnatal PFC was measured as a line perpendicular to the midline, spanning across all cortical layers. Rostro-caudal coordinates were kept consistent between control and knockout conditions.

## Fluorescence activated cell sorting (FACS)

Mice were rapidly decapitated, the brain was removed and placed in an ice cold oxygenated sucrose-based cutting solution. 400  $\mu\text{m}$  coronal slices were cut using a Leica VT1200S vibratome. The dorsal striatum was dissected from slices in an Artificial Cerebrospinal Fluid (ACSF) containing (in mM): 124 NaCl, 3 KCl, 2 CaCl<sub>2</sub>, 1 MgCl<sub>2</sub>, 1.25 NaH<sub>2</sub>PO<sub>4</sub>, 26 NaHCO<sub>3</sub> and 10 glucose saturated with 95% O<sub>2</sub> and 5% CO<sub>2</sub>. Tissue was disrupted using micro-knife and transferred to a 15 ml tube containing 10 ml digestion buffer (0.5g Trehalose and 10 mg Pronase, 1 mg DNase I, 50  $\mu\text{L}$  MgCl<sub>2</sub> 1M in oxygenated ACSF; Sigma) at 37°C for 30 min with inversion every 10 min. The tissue was allowed to settle on ice for 1 min, the digestion buffer was removed and the pellet was washed with 2 ml washing buffer (10 ml ACSF, 0.5 g Trehalose, 1 mg DNase I, 50  $\mu\text{L}$  MgCl<sub>2</sub> 1M in oxygenated ACSF) at 4°C. To dissociate the cells,

the tissue was resuspended in 1 ml wash buffer and triturated 12–15 times with 1 ml pipette. Tubes were placed on ice, large tissue pieces were allowed to settle, and ~500  $\mu\text{L}$  of cloudy suspension containing dissociated cells was transferred to a 1.5 ml tube on ice. This process was repeated for the remaining 500  $\mu\text{L}$  suspension with 200  $\mu\text{L}$  pipette 12–15 times and pooled in to the 1.5 ml tubes on ice. The last cells were removed by adding 200  $\mu\text{L}$  to the original tube. The cell suspension was filtered through a 70  $\mu\text{m}$  thick mesh filter into a snap cap tube and 200  $\mu\text{L}$  DAPI 5  $\mu\text{M}$  was added to exclude dead cell. The cells were sorted on a BD FACSMelody Cell Sorter. The neuronal population was gated ensuring myelin and other debris were excluded by FSC/SSC profile. Doublets were then excluded by FSC-W/FSC-H and SSC-W/SSC-H. Dead cells shown as DAPI positive cells were also excluded. The Lhx6+ cell population was sorted by gating on TdTomato + signal above negative background from TdTomato negative mice. A fraction of the sorted cells were checked for purity by running some of the sorted cells back into the cell sorter, and were determined as 99% pure. The remaining cells were sorted into 350  $\mu\text{L}$  RLT buffer (RNeasy Microkit; Qiagen) with 1%  $\beta$ -Mercaptoethanol. Sorted cells were immediately frozen on dry ice and placed at -80°C until further processing.

## Quantitative real time polymerase chain reaction (qRT-PCR)

Total RNA was extracted using the RNeasy Micro kit (Qiagen) for FACS sorted cells and some tissue samples and the RNeasy Mini Kit (Qiagen) for other tissue samples according to manufacturer's instructions, including DNase treatment for some samples. RNA concentration and purity were determined using the Nanodrop spectrophotometer (Thermo Fisher Scientific). RNA was reverse transcribed into cDNA using SuperScriptIII First Strand Synthesis System (Invitrogen) with random hexanucleotides according to manufacturer instructions. cDNA was analyzed using real time qPCR, in technical triplicates using TaqMan™ Gene Expression Assay. Reactions were performed on a MicroAmp™ Optical 96- or 384-Well Reaction Plate with Barcode (Applied Biosystems). Each 10  $\mu\text{L}$  reaction (performed on 384-well plates) contained 5  $\mu\text{L}$  of TaqMan™ universal PCR Master Mix (Applied Biosystems), 0.5  $\mu\text{L}$  of Taqman probes gene expression assay and 4.5  $\mu\text{L}$  of cDNA (10 ng RNA). Each 20  $\mu\text{L}$  reaction (performed on 96-well plates) contained 10  $\mu\text{L}$  of TaqMan™ universal PCR Master Mix (Applied Biosystems), 1  $\mu\text{L}$  of Taqman probes gene expression assay and 4  $\mu\text{L}$  of cDNA (10 ng RNA), and 5  $\mu\text{L}$  of RNase free water. PCRs were monitored using the 7900HT Real-Time PCR system (Applied Biosystems) or the StepOnePlus™ Real-Time PCR system (Applied Biosystems). The reaction cycle involved incubation at 50°C for 2 min, at 95°C for 10 min to allow for AmpliTaq Gold DNA 57 Polymerase activation and then cycled 40 times at 95°C for 15 s (denaturation) and 60°C for 1 min (annealing and extension). Analysis was performed by comparing the experimental Ct values against those for the reference housekeeping gene Gapdh. A  $1/\Delta\text{Ct}$  value was calculated to represent differences between conditions. The following Taqman primers were used: Lhx6 (Mm01333348\_m1), ChAT (Mm01221880\_m1), Grin2C (Mm00439180\_m1), Grin2D (Mm00433822\_m1), Grin 1 (Mm00433790\_m1), Grin2A (Mm00433802\_m1), Grin2B (Mm00433820\_m1), Lhx8 (Mm00802919\_m1), Gbx2

(Mm00494578\_m1), Zic4 (Mm00657066\_m1), Grm5 (Mm00690332\_m1).

## Electrophysiology

Postnatal mice were deeply anaesthetised with 4–4.5% isoflurane and transcardially perfused with an ice-cold oxygenated, sucrose-based artificial cerebrospinal fluid (ACSF) containing (in mM): 248 sucrose, 3 KCl, 0.5 CaCl<sub>2</sub>, 4 MgCl<sub>2</sub>, 1.25 NaH<sub>2</sub>PO<sub>4</sub>, 26 NaHCO<sub>3</sub>, and 1 glucose, saturated with 95% O<sub>2</sub> and 5% CO<sub>2</sub>. The animals were then decapitated, the brain was removed and placed in ice cold oxygenated sucrose-based ACSF cutting solution. 400 µm coronal slices were sectioned using a Leica VT1200S vibratome. Slices were then placed into room temperature ACSF containing (in mM): 124 NaCl, 3 KCl, 2 CaCl<sub>2</sub>, 1 MgCl<sub>2</sub>, 1.25 NaH<sub>2</sub>PO<sub>4</sub>, 26 NaHCO<sub>3</sub> and 10 glucose saturated with 95% O<sub>2</sub> and 5% CO<sub>2</sub>, where they were maintained until recording.

Slices were transferred to a chamber and continuously perfused with ACSF at 34°C. Red fluorescent protein (TdTomato) expressing Lhx6 cells located in the dorsal striatum were visualized by infrared-differential interference optics with a ×40 water-immersion objective. For targeting TdTomato expressing neurons, slices were illuminated by green light through the objective. Microelectrodes (4–6 MΩ) were pulled from borosilicate glass (1.5 mm outer diameter × 0.86 inner diameter) using a vertical P10 puller (Narishige).

For current-clamp recordings, we targeted *Lhx6-iCre;td-Tomato*-positive (Lhx6+) CINs, based on the large size of their soma and typical tonic firing properties (Ahmed et al., 2019), and putative Lhx6+ fast-spiking GABAergic cells and discarded the somatostatin cells, which present with elongated soma shape, very high input resistance (>600 MΩ), low threshold spike (LTS), and typical AHP kinetics and rebound firing (Tepper et al., 2010). We used a potassium-gluconate-based intracellular solution containing (in mM): 140 K-gluconate, 10 HEPES, 2 NaCl, 4 KCl, 4 ATP, and 0.4 GTP. Neurobiotin (2–5 mg/ml) was added for post-recording immunocytochemistry. For voltage-clamp recordings, a cesium gluconate-based intracellular solution was used containing (in mM): 120 Cs-gluconate, 13 CsCl, 1 CaCl<sub>2</sub>, 10 HEPES, and 10 EGTA (pH 7.2–7.4, 275–285 mOsm). We used the cesium-gluconate solution to measure spontaneous and miniature GABA<sub>A</sub> currents at the reversal potential for glutamatergic (+10 mV) events and glutamatergic currents at -60 mV.

Electrophysiological signals were low-pass filtered on-line at 10 kHz with a Multiclamp 700B (Axon Instruments) amplifier and acquired at a 20-kHz sampling rate with a LIH 8 + 8 (HEKA) data acquisition board and WinWCP software (created by John Dempster, University of Strathclyde). Circuit capacitance was corrected after gigaseal formation. Series resistance and liquid junction potential were not corrected. Following break-in, the test pulse was monitored for a few seconds to ensure a stable, low access resistance (Ra <20MΩ). To measure postsynaptic currents, the voltage was held at -70 mV for AMPA/KA or +10 mV for GABA<sub>A</sub> events under NBQX and +40 mV under NBQX 10µM, GABAZINE 10µM and 4-AP (10µM; Sigma). PSC rise and decay times were calculated as the intervals between 20 and 100 percent of the PSC peak before and after the peak respectively. Event detection was set to 1.5 times the background noise. Electrophysiological data were analyzed in Easy

Electrophysiology. Threshold was detected based on the positive peaks occurring above 10 mV/ms in the first derivative of the membrane potential. A 500 m ramp was used to analyze the rheobase, which was characterized as the lowest current inject to elicit an action potential.

After patch clamp recordings, slices were immediately fixed in 4% PFA for 2–5 h, rinsed in PBS (3 times, 30 min intervals) and kept overnight at 4°C. The same procedure as described above, was performed for immunostaining with 15' washes.

## Morphology

Images stacks (delta 1) for morphological reconstruction were acquired using a Nikon A1 Confocal microscope (×40 objective) and the Nikon Instruments Elements software. Morphological quantification was done using the Surface and Filament tools in the IMARIS software. The automatic component of the filament tool reconstructed the dendritic field of the neuron with the dendrite beginning point set to 15 µm and the end point set to 1 µm. The volume of dendritic spread was found by using the Convex Hull Xtension of IMARIS.

## Statistics

All statistical analysis was completed using 'Prism 8' by GraphPad. If normally distributed, significance between data sets was examined with a parametric students t-test.

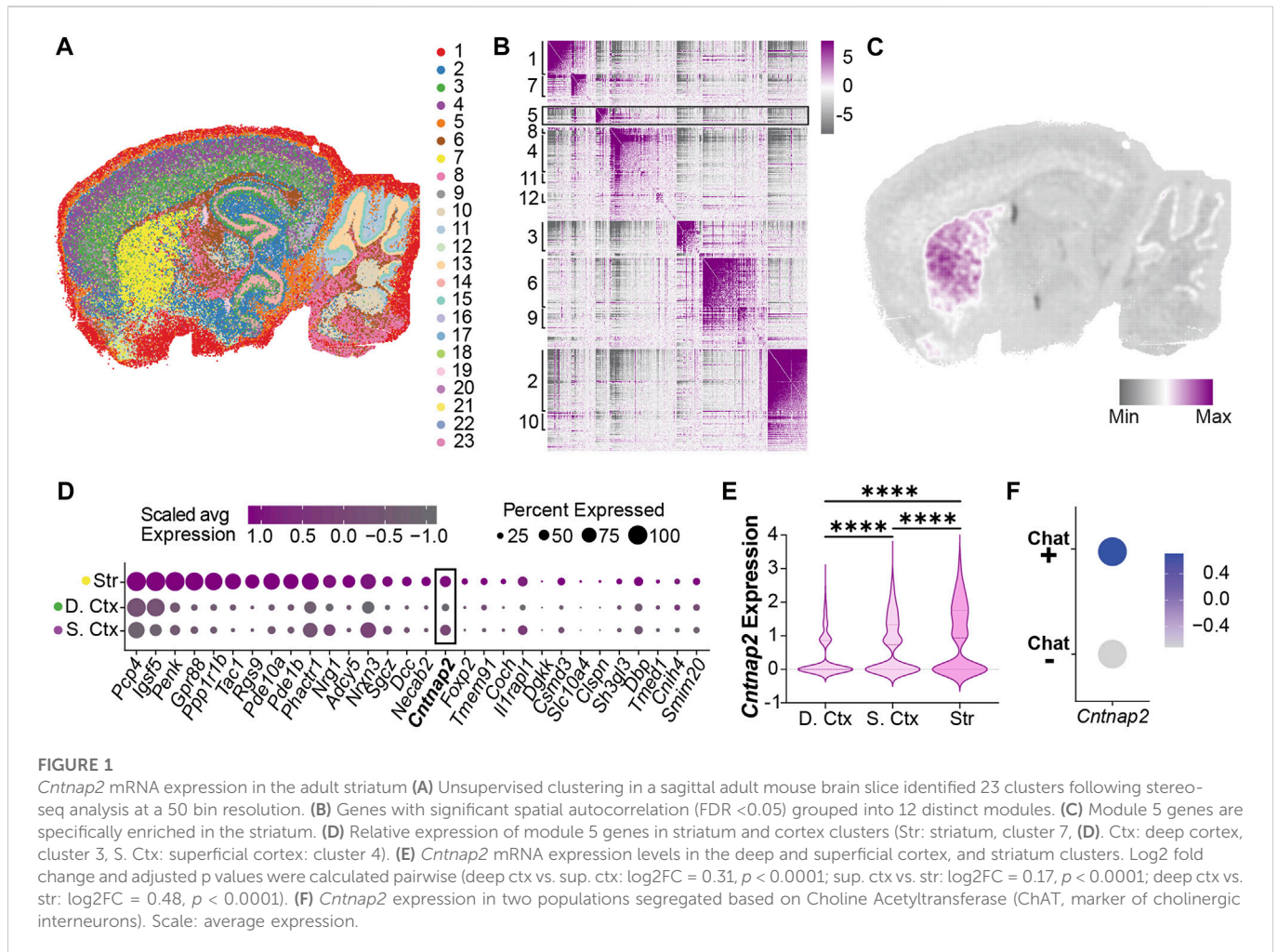
Datasets with three groups were tested using a one-way ANOVA. Datasets with two variables were tested with a two-way ANOVA with Bonferroni *post hoc* multiple comparisons. Individual data values were considered outliers if they extended beyond the mean ± 2.5x standard deviation. A critical α value of 0.05 was employed to determine significance, which is signified by  $p < 0.05^*$ ;  $p < 0.01^{**}$ ;  $p < 0.001^{***}$ ;  $p < 0.0001^{****}$ . Error bars in all graphs show the standard error of the mean.

## Results

### Expression of *Cntnap2* in the mouse brain

*Cntnap2/Caspr2* is known to be ubiquitously expressed throughout the brain (Poliak et al., 1999) and its absence in the *Cntnap2* KO mouse model and in humans has been shown to trigger behavioral characteristics of ASD (Penagarikano et al., 2011; Scott et al., 2017). Yet, the intricacies of *Cntnap2* expression during brain development are not well characterized.

To examine this, we performed spatial transcriptomics (Stereo-seq) on adult brain tissue to map *Cntnap2* mRNA expression to anatomical locations. Unbiased clustering found 23 clusters that mapped onto known brain regions (Figure 1A), such as the striatum (cluster 7), deep layers of the cortex (cluster 3) and superficial layers of the cortex (cluster 4). Further clustering of spatially defined co-expressed genes generated 12 distinct modules (Figure 1B, Supplementary Figure S1A), revealing that the striatum (Figure 1C; Module 5) displays an individual genetic profile involving known biological pathways such as learning, cognition and locomotor



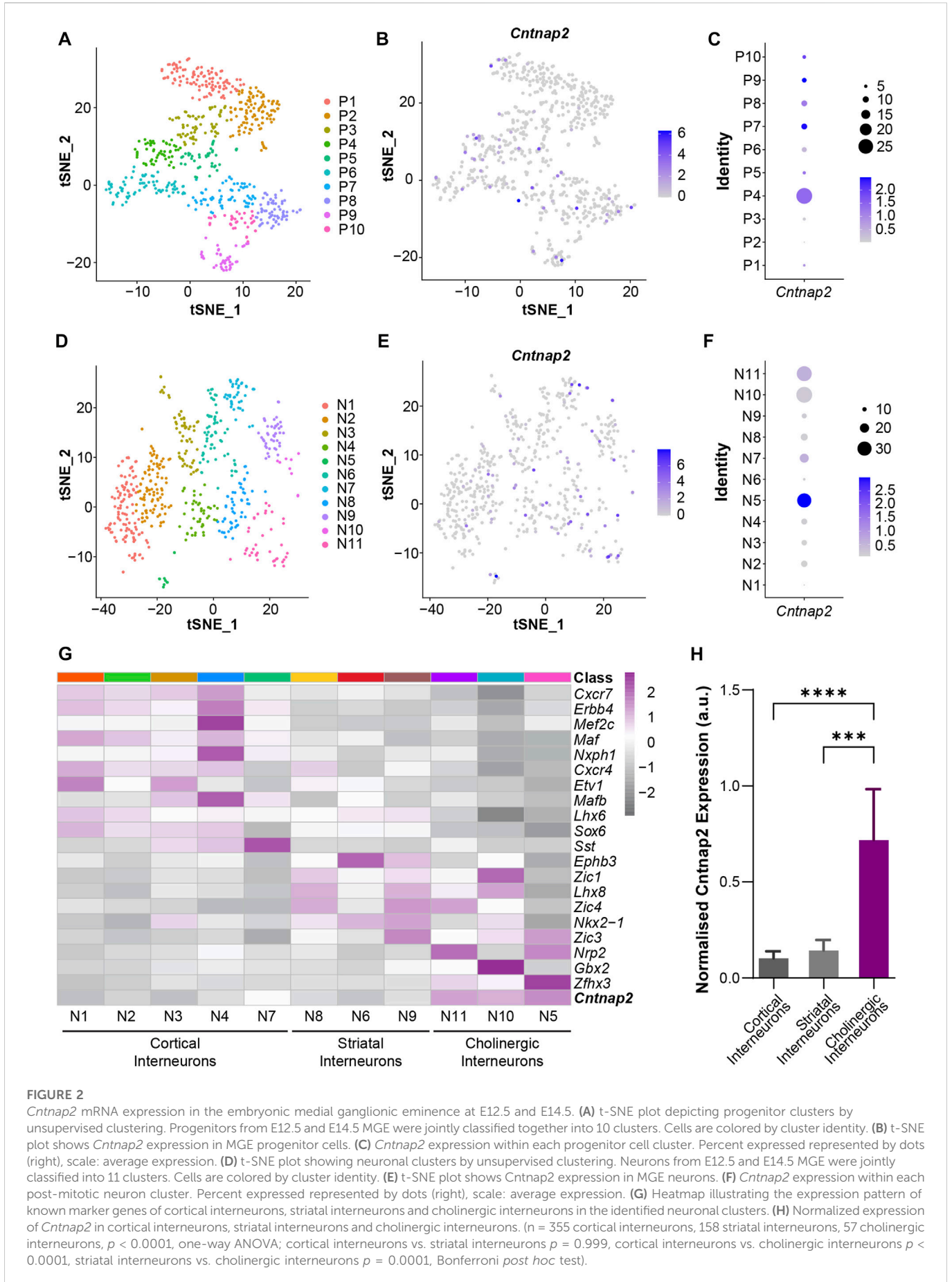
behaviour (Supplementary Figure S1B). Furthermore, we found in this module an enriched expression of *Cntnap2* (Figure 1D; Supplementary Figure S1C). When compared to cortical regions (deep vs. superficial layers), the striatum showed significantly higher levels of *Cntnap2* (Figures 1D, E). Interestingly, we also found that striatal cholinergic interneurons, expressing Choline Acetyltransferase (ChAT) presented higher *Cntnap2* levels, compared to the rest of the striatal ChAT-negative population (Figure 1F).

To confirm whether this feature originates from brain development, we investigated *Cntnap2* expression at embryonic stages. *Cntnap2*/Caspr2 protein expression has been detected in the mouse brain as early as E14 (Penagarikano et al., 2011). However, its expression pattern in the embryonic ganglionic eminences is largely unknown. To this end, we used a published single-cell RNA-sequencing dataset of embryonic mouse ganglionic eminences (Mi et al., 2018) and performed new analyses on progenitors and postmitotic neurons of E12.5 and E14.5 MGE. We used unsupervised clustering to classify MGE progenitors into 10 transcriptionally distinctive clusters (P1-P10) with characteristic regional and temporal patterns (Figure 2A; Supplementary Figures S2A–F), and *Cntnap2* expression was quantified across these clusters (Figure 2B). We found that *Cntnap2* was highly expressed in some E12.5 and E14.5 clusters

(e.g., P4, P7, P9, Figure 2C), corresponding to progenitor cell populations allocated primarily in the ventricular zone (VZ; P9) and subventricular zone (SVZ; P4 & P7) and of the MGE (Supplementary Figure S2F). Unsupervised clustering analysis also revealed 11 postmitotic neuron clusters (N1-N11; Figure 2D), and we observed *Cntnap2* expression in some of these clusters (Figures 2E, F). We also found that *Cntnap2* expression is particularly enriched in cell clusters annotated as cholinergic neurons, compared to cortical and striatal interneurons (Figures 2G, H). Overall, these data indicate that *Cntnap2* is expressed in a subset of progenitors and postmitotic neurons of embryonic MGE and remains enriched in the MGE-derived cholinergic interneurons of the striatum in adult. We hypothesized that this specific pattern of expression could underlie some precise alterations to striatal cells in the absence of *Cntnap2*. Specifically, we questioned whether there would be a change to MGE cell proliferation in the *Cntnap2* KO mouse model of autism, potentially contributing to ASD aetiology.

## MGE proliferation in the *Cntnap2* KO mice

We examined the density of the proliferation marker Ki67 in the MGE, at “early” (E12.5) and “late” (E14.5 & E15.5) embryonic stages,



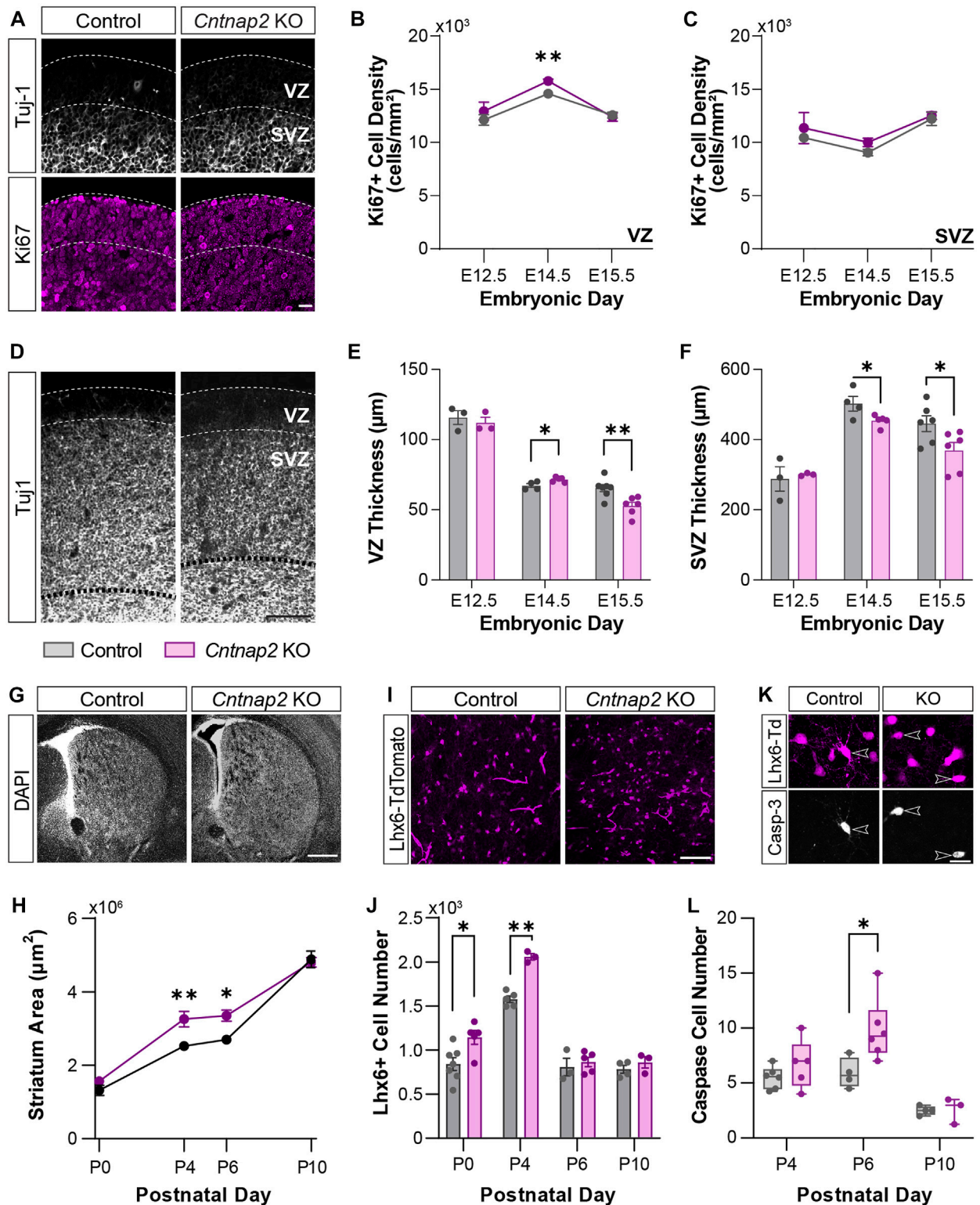


**FIGURE 3**

MGE-derived interneuron cell numbers at early stages of development. (A) Ki67-positive progenitor cells (magenta) in the VZ and SVZ of the MGE delineated by Tuj-1 staining (white), in Control and the *Cntnap2* knockout, scale: 50 μm. (B) Ki67-positive cell density in the VZ (E12.5: n = 3 Control, 3 KO, *p* = 0.440; E14.5: n = 4 Control, 5 KO, *p* = 0.001; E15.5: n = 6 Control, 5 KO, *p* = 0.718) and (C) in the SVZ of the MGE across embryonic stages (E12.5: n = 3 Control, 3 KO, *p* = 0.578; E14.5: n = 4 Control, 5 KO, *p* = 0.106; E15.5: n = 6 Control, 5 KO, *p* = 0.686). (D) Thickness of the VZ and SVZ in the MGE, shown by Tuj-1 staining, scale: 100 μm. (E) Quantification of the thickness of the VZ (E12.5: n = 3 Control, 3 KO, *p* = 0.584; E14.5: n = 4 Control, 5 KO, *p* = 0.027; E15.5: n = 7 Control, 6 KO, *p* = 0.005) and (F) SVZ (E12.5: n = 3 Control, 3 KO, *p* = 0.739; E14.5: n = 4 Control, 5 KO, *p* = 0.046; E15.5: n = 6 Control, 6 KO, *p* = 0.040) across embryonic stages. (G) DAPI staining of the striatum in Control and *Cntnap2* KO, scale: 500 μm. (H) Quantification of the striatum area across early postnatal stages in Control and *Cntnap2* KO (P0: n = 8 Control, 5 KO, *p* = 0.195; P4: n = 5 Control, 3 KO, *p* = 0.007; P6: n = 3 Control, 5 KO, *p* = 0.027; P10: n = 4 Control, 4 KO, *p* = 0.768). (I) Lhx6 positive interneurons in the striatum, scale: 100 μm. (J) The number of Lhx6 positive interneurons in the Control and *Cntnap2* KO (Continued)

**FIGURE 3 (Continued)**

striatum across early postnatal stages (P0: n = 7 Control, 5 KO,  $p = 0.019$ ; P4: n = 5 Control, 3 KO,  $p = 0.0001$ ; P6: n = 3 Control, 5 KO,  $p = 0.606$ ; P10: n = 4 Control, 3 KO,  $p = 0.343$ ). (K) Expression of the cell death marker Caspase-3 in striatal Lhx6 positive interneurons, scale: 20  $\mu\text{m}$ . (L) Quantification of Lhx6 positive interneurons expressing Caspase-3 across early postnatal stages in the Control and *Cntnap2* KO conditions (P4: n = 6 Control, 5 KO,  $p = 0.259$ ; P6: n = 4 Control, 5 KO,  $p = 0.033$ ; P10: n = 4 Control, 3 KO,  $p = 0.898$ ). Unless otherwise specified, a Student's t-test was used to determine significance,  $p < 0.05$ \*,  $p < 0.01$ \*\*\*,  $p < 0.001$ \*\*\*,  $p < 0.0001$ \*\*\*\*.

in the control and *Cntnap2* KO mice (Figure 3A). We observed that the number of progenitor cells in the VZ proliferative region were transiently increased at E14.5, with no changes at E12.5 or E15.5 (Figure 3B) and in the SVZ (Figure 3C). To confirm this was not a result of cells remaining in the cell cycle and/or accumulating in the VZ, we labelled cells with EdU 1 h prior to immunostaining (Flomerfelt and Gress, 2016). We observed no changes to the density or proportion of EdU<sup>+</sup> cells expressing Ki67 (i.e., cells that were in DNA synthesis (S) phase an hour prior; Supplementary Figures S3A–E). During the late stages of MGE development (>E14), cell-division is biased towards neurogenic divisions and is correlated with a reduction in the size of the VZ and SVZ progenitor pools (Turrero Garcia and Harwell, 2017). We wondered whether this process was altered in the *Cntnap2* KO condition, as alterations in progenitor cells has been reported in ASD (Satterstrom et al., 2020). Whilst no changes were seen in the VZ and SVZ size at E12.5, we found that the thickness of the VZ was significantly larger at E14.5, and sharply decreased by E15.5 (Figures 3D, E). On the other hand, the SVZ remained smaller at both E14.5 and E15.5 (Figures 3D, F). Together, this indicates a short period of enhanced VZ proliferation around E14.5, which is coupled to a larger VZ size and higher density of progenitor cells. This is followed by a rapid change to a more “mature” state of the VZ and SVZ, which decrease in size earlier than in control conditions at E15.5. Interestingly, we found that this was associated with a large increase in the number of interneurons migrating towards the cortex (Supplementary Figures S3F–H). We next wanted to assess whether the enhanced proliferation and migration contribute to changes in the early postnatal brain.

## MGE-derived interneuron cell number in the *Cntnap2* KO mice at perinatal stages

Previous studies have shown either no change or a decrease to GABAergic and cholinergic interneuron populations in adulthood (Penagarikano et al., 2011; Lauber et al., 2018). To reconcile this with the embryonic increase in proliferation and migration we observed, we first quantified the morphological differences in the early postnatal mouse brain. Indeed, enlargement in total brain volume have been reported in ASD patients (Sacco et al., 2015). Yet, such deficits were not studied in the *Cntnap2* KO mice. Here, we found that the striatum size is enlarged in the *Cntnap2* KO condition, compared to control, specifically at P4 and P6, then rectified by P10 (Figures 3G, H). This was associated with a marked increase in the absolute number of striatal interneurons at early postnatal stages, labelled with the specific marker of MGE-derived precursors and interneurons, LIM homeobox 6 (Lhx6) transcription factor (Liodis et al., 2007); Figures 3I, J) between P0 and P4. However, striatal Lhx6 interneuron number is normalized from P6 in the *Cntnap2* KO mice (Supplementary Figure S3I), and no changes in cortical Lhx6<sup>+</sup> cell density and prefrontal cortex thickness was observed (Supplementary Figures S3J–L).

Since the first postnatal week corresponds to a critical period for brain development, with notable cell death episodes (Wong et al., 2018; Sreenivasan et al., 2022), we hypothesized that changes to apoptosis were responsible for the restoration of cell number. As previously described in the striatum, Lhx6<sup>+</sup> cell death occurs around P6 (Sreenivasan et al., 2022). Quantification of the marker Caspase-3 across early postnatal stages within the Lhx6<sup>+</sup> interneuron population showed a 49% cell loss at P6 in control conditions, as previously reported (Sreenivasan et al., 2022), and an increase to 58% cell loss in the *Cntnap2* KO mice (Figures 3K, L). More cell death was also seen in the neocortex in the *Cntnap2* KO mice, compared to controls (data not shown). Together, these findings show that in the absence of *Cntnap2*, an embryonic increase in cell proliferation in the MGE leads to an increase in interneuron numbers at early postnatal stages, which is compensated for by additional cell death to rectify this back to control levels. As previously described (Vogt et al., 2017), we did not find any differences in the number of MGE-derived cells in the adult striatum (n = 3 control and n = 3 KO; data not shown). However, alterations to cellular development during embryonic and early postnatal periods are likely to trigger morpho-functional modifications that could contribute to ASD aetiology. Therefore, we next analyzed whether the properties of the striatal Lhx6<sup>+</sup> interneurons were modified at these stages.

## Morpho-functional properties of the MGE-derived striatal interneurons in the *Cntnap2* KO mice

Analysis of spatial transcriptomics and single-cell RNA sequencing data indicated higher levels of *Cntnap2* in putative MGE-derived cholinergic neuron populations (Figure 1 and Figure 2), potentially suggesting that *Cntnap2* plays a specific role in CINs. To determine whether this population was preferentially altered following *Cntnap2* deletion, and likely contribute to the ASD-related alterations, we quantified the proportion of the Lhx6<sup>+</sup> interneurons expressing ChAT at early postnatal stages. At P0, there was a greater proportion of interneurons that were cholinergic in the *Cntnap2* KO condition (Figures 4A, B) and correspondingly, this proportion was decreased at P6, specifically in the dorsolateral striatum (DLS; Figure 4C). This decrease was specific to the Lhx6<sup>+</sup> cholinergic cell population, as we did not find any alterations in the cholinergic Lhx6-negative cells in the striatum (Supplementary Figures S4A, B).

We next wondered whether the molecular profile of these cells was changed. We first analyzed the molecular profile of Lhx6-expressing interneurons by qRT-PCR, at embryonic and perinatal stages in the control and *Cntnap2* KO mice. Whilst we found that expression levels of genes related to cholinergic identity such as *ChAT*, *Lhx8*, *Gbx2* and *Zic4* (Ahmed et al., 2019) remain unchanged between the two conditions in the MGE and the postnatal striatum (P6: Figure 4D and Supplementary Figure S4C), we observed increased levels of

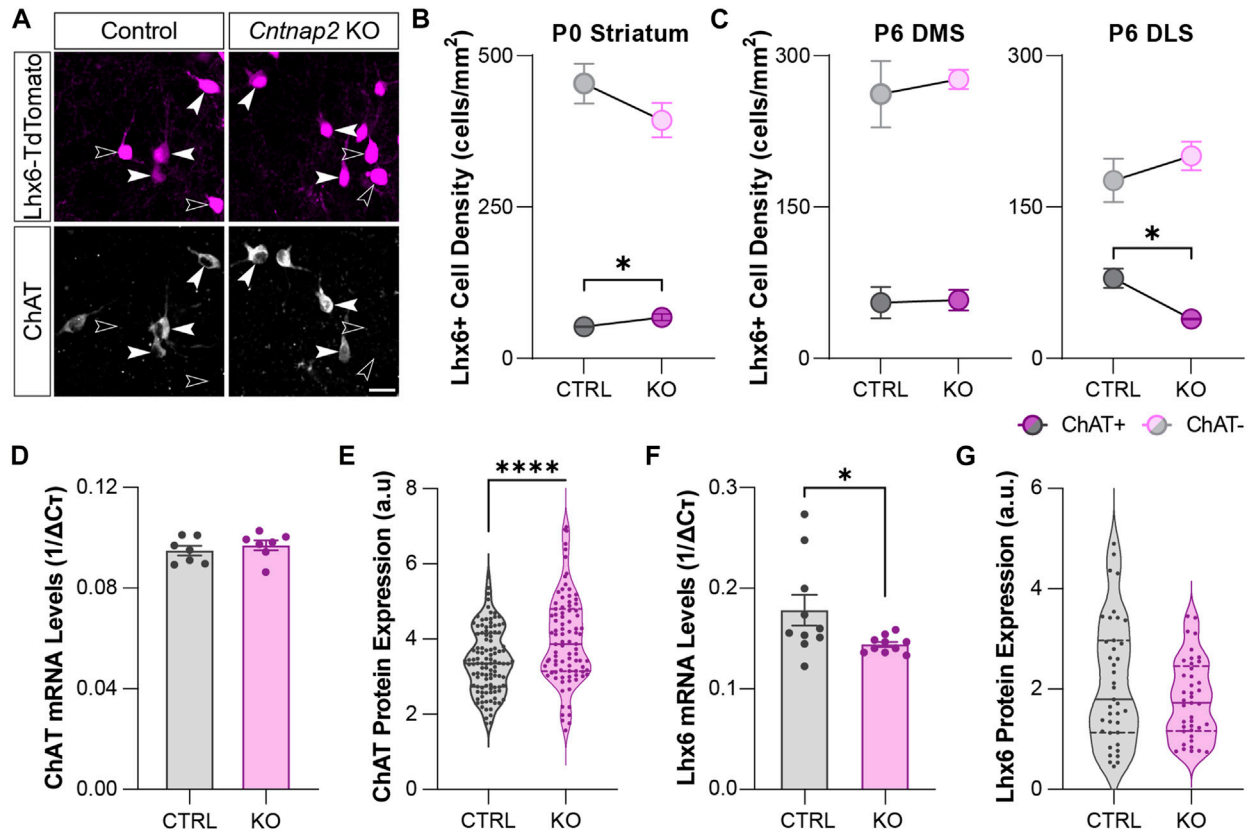


FIGURE 4

Molecular identity of the developing striatal Lhx6+ interneurons in Control and *Cntnap2* KO mice (A) Expression of the cholinergic marker ChAT in the Lhx6+ interneurons of the striatum at P6, scale: 20  $\mu$ m. (B) Density of ChAT positive and ChAT negative Lhx6+ interneurons in the Control and *Cntnap2* KO striatum at P0 (n = 5 Control, 3 KO,  $p = 0.043$  ChAT+,  $p = 0.259$  ChAT-). (C) Density of ChAT positive and ChAT negative Lhx6+ interneurons in the Control and *Cntnap2* KO at P6, in the dorsomedial (DMS, n = 3 Control, 4 KO,  $p = 0.893$  ChAT+,  $p = 0.644$  ChAT-) and dorsolateral (DLS, n = 3 KO,  $p = 0.016$  ChAT+,  $p = 0.398$  ChAT-) striatum. (D) Relative ChAT mRNA expression in the striatum in Control and *Cntnap2* KO conditions at P6 (n = 7 Control, 7 KO,  $p = 0.465$ ). (E) Normalized ChAT protein levels in striatal cholinergic interneurons, in Control and *Cntnap2* KO conditions (n = 110 cells, 4 Control, 91 cells, 3 KO,  $p = 0.00005$ ). (F) Relative *Lhx6* mRNA expression in the striatum, in Control and *Cntnap2* KO conditions at P6 (n = 10 Control, 10 KO,  $p = 0.041$ ). (G) Normalized Lhx6 protein levels in striatal interneurons, in Control and *Cntnap2* KO conditions (n = 40 cells, 4 Control, 42 cells, 3 KO,  $p = 0.129$ ). Unless otherwise specified, a Student's t-test was used to determine significance,  $p < 0.05$ :\*,  $p < 0.01$ :\*\*,  $p < 0.001$ :\*\*\*,  $p < 0.0001$ :\*\*\*\*.

ChAT protein within striatal cholinergic Lhx6+ interneurons at P6 (Figure 4E), but not cholinergic Lhx6-negative interneurons (Supplementary Figure S4D). We also quantified a decrease in *Lhx6* mRNA levels (Figure 4F), with no change to the Lhx6 protein expression levels in the Lhx6+ cells at P6 (Figure 4G). This data suggests different post-transcriptional control of the striatal Lhx6+ interneurons in the *Cntnap2* KO mice, compared to controls.

We then performed *in vitro* whole-cell patch clamp recording of the Lhx6+ cells in the P6 striatum, to assess whether the electrical and morphological features of those cells were altered in the absence of *Cntnap2*. We separated Lhx6+ CINs and GABAergic neurons in the control and *Cntnap2* KO mice, based on their firing properties and *post hoc* staining (Supplementary Figure S5A; Tables 1, 2). The Lhx6+ CINs display spontaneous tonic activity in current-clamp mode (Ahmed et al., 2019) which appears reduced (Figures 5A, B) and far more irregular in the *Cntnap2* KO condition (Figure 5C). This was also reflected in evoked firing rates upon current injection, which were also significantly decreased (Figures 5D, E), whilst the input resistance was lower (Table 1). Sag ratio and spike adaptation were similar in control and KO Lhx6+ CINs (Table 1), suggesting similar level of maturation of the conductances. Reduced firing frequency was also observed in the

adult CINs, suggesting persistent developmental alterations in the *Cntnap2* KO conditions (Reynolds et al., unpublished).

Because cell activity regulates morphological development and *Cntnap2* has been reported to stabilize interneuron dendritic arbors (Gao et al., 2018), we next investigated whether cell morphology was affected in the *Cntnap2* KO condition. We performed morphological analysis of the striatal Lhx6+ CINs to verify whether their development at P6 was impaired in the absence of *Cntnap2* (Figure 5F). We found that Lhx6+ CINs were more complex at proximal dendrites (*i.e.* ~ 50  $\mu$ m from the soma; Figure 5G), and presented increased branching and dendritic segments (Supplementary Figures S4E–H).

We also checked the electrophysiological properties of the putative Lhx6+ GABAergic interneurons (that are negative for ChAT immunostaining; Supplementary Figure S5A). Whilst most of the basic intrinsic properties remained unchanged (Table 2), we found a significant increase in the rheobase (Supplementary Figure S5B), associated with a lower firing at intermediate depolarizing steps, but not at maximum firing (Supplementary Figures S5C, D). The morphological characteristics were also changed, with more complex arborization at distal dendrites (*i.e.* >50  $\mu$ m from the soma) and larger volume of spread (Supplementary Figures S5E, J).



**TABLE 1** Intrinsic properties of Lhx6+ striatal cholinergic interneurons in the control and *Cntnap2* KO mice at P6.

Lhx6+ cholinergic interneurons					
Property	Control		KO		<i>p</i>
	Mean	n	Mean	n	
Resting membrane potential (mV)	-44.90 ± 1.55	16	-47.44 ± 2.27	12	0.368
Input resistance (MΩ)	551.24 ± 60.17	14	408.61 ± 23.79	12	0.049
Membrane capacitance (pF)	596.63 ± 59.82	14	802.39 ± 125.74	12	0.135
Sag ratio	0.27 ± 0.03	10	0.30 ± 0.07	7	0.676
Spike adaptation index	0.60 ± 0.05	14	0.60 ± 0.05	11	0.926
Latency to first spike (ms)	19.64 ± 3.13	14	21.59 ± 3.22	11	0.671
Action potential threshold (mV)	-35.59 ± 1.18	15	-36.58 ± 1.97	12	0.655
Action potential amplitude (mV)	51.95 ± 2.13	15	50.13 ± 3.62	12	0.654
Action potential rise time (ms)	1.07 ± 0.09	15	0.77 ± 0.06	12	0.017
Action potential decay (ms)	2.05 ± 0.01	15	2.02 ± 0.02	12	0.229
Action potential halfwidth (ms)	2.71 ± 0.16	15	2.50 ± 0.14	12	0.347
Action potential fast AHP (mV)	9.02 ± 1.23	15	6.11 ± 1.35	12	0.126
Action potential medium AHP (mV)	-13.77 ± 1.22	15	-13.78 ± 1.00	12	0.993

AHP: Afterhyperpolarization. Statistics from two-sample Student's *t*-test.

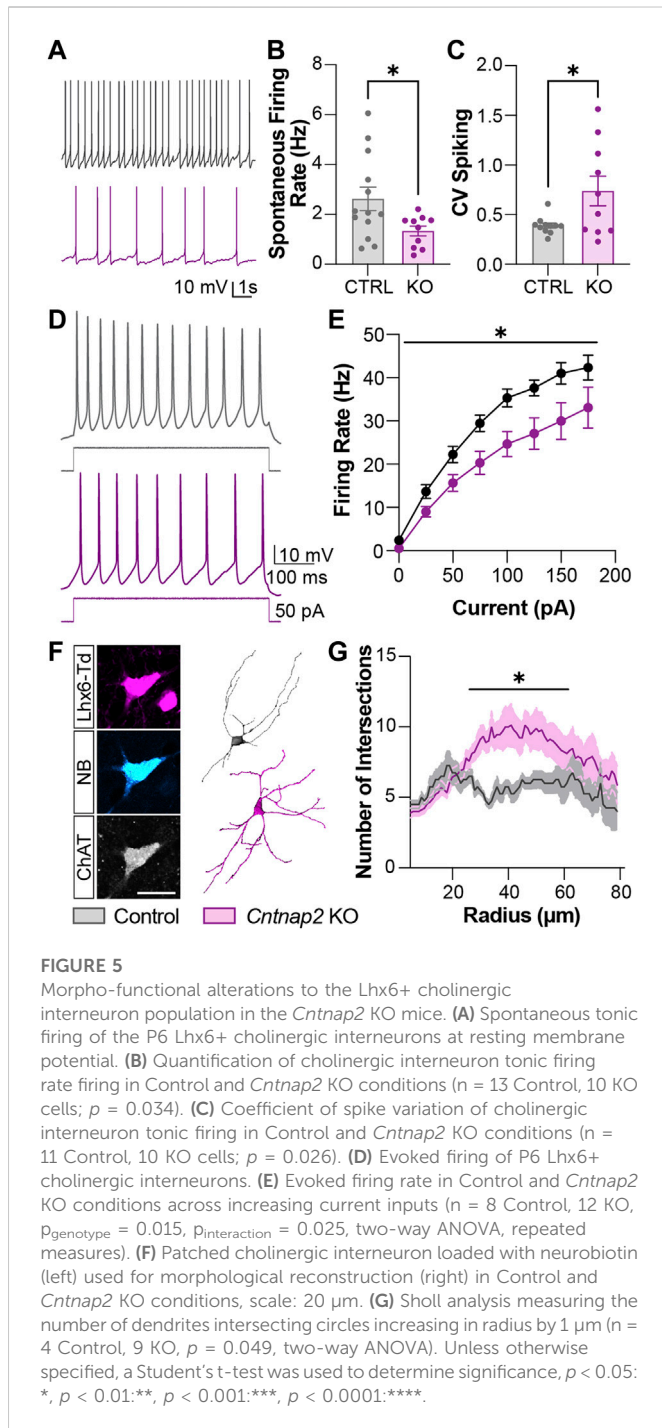
**TABLE 2** Intrinsic properties of Lhx6+ striatal GABAergic fast-spiking interneurons in the control and *Cntnap2* KO mice at P6.

Lhx6+ putative fast spiking interneurons					
Property	Control		KO		<i>p</i>
	Mean	n	Mean	n	
Resting membrane potential (mV)	-54.45 ± 1.50	22	-53.98 ± 3.09	13	0.880
Input resistance (MΩ)	780.28 ± 75.02	19	406.55 ± 47.03	14	0.0005
Membrane capacitance (pF)	805.33 ± 126.76	19	1064.36 ± 273.87	14	0.357
Latency to first spike (ms)	270.01 ± 35.37	6	315.87 ± 25.58	10	0.303
Action potential threshold (mV)	-35.49 ± 1.43	19	-32.45 ± 1.91	11	0.184
Action potential amplitude (mV)	48.15 ± 1.80	19	44.59 ± 3.43	11	0.320
Action potential rise time (ms)	0.72 ± 0.05	19	0.59 ± 0.05	11	0.078
Action potential decay (ms)	1.80 ± 0.05	19	1.59 ± 0.09	11	0.031
Action potential halfwidth (ms)	1.74 ± 0.12	19	1.22 ± 0.11	11	0.006
Action potential fast AHP (mV)	-2.69 ± 1.72	19	-10.89 ± 1.09	11	0.002
Action potential medium AHP (mV)	-13.15 ± 0.92	19	-15.37 ± 0.70	11	0.105

AHP: Afterhyperpolarization. Statistics from two-sample Student's *t*-test.

To further characterize the changes in synaptic connectivity in the *Cntnap2* KO mice, we performed voltage-clamp recordings of the inhibitory and excitatory inputs onto Lhx6+ interneurons at P6. We found that cells receive similar GABAergic and  $\alpha$ -Amino-3-hydroxy-5-methyl-4-isoxazolepropionic acid (AMPA)/Kainate-driven glutamate inputs (Supplementary Figures S6A–J) in control and

*Cntnap2* KO mice. However, Lhx6+ interneurons receive more N-methyl-D-aspartate (NMDA) receptor-driven glutamate inputs at P6 in the KO condition (Supplementary Figures S6K–O). This was associated with a shift in the expression of glutamate receptors such as the metabotropic receptor mgluR5 (Supplementary Figures S6P, Q), and glutamate receptor NR2 C & D subunits (Supplementary



Figures S6R, S), but not NR1 and NR2 A & B subunits (data not shown). Overall, these results reveal lower cell excitability and altered synaptic connectivity in the Lhx6+ interneuron population of the P6 striatum in the *Cntnap2* KO mice.

## Discussion

From early prenatal stages through childhood, the striatum undergoes an avalanche of developmental events that shape network formation (Dehorter et al., 2012; Dehorter and Del

Pino, 2020). Yet, how the maturation of the striatal interneurons is sculpted in ASD has remained poorly investigated. Here, we demonstrated that the developmental trajectory of striatal MGE-derived interneurons is perturbed in the *Cntnap2* KO mouse model of ASD from embryonic stages. In particular, we uncovered enhanced proliferation of neural progenitor cells, followed by an early maturation of the VZ and SVZ of the MGE, and accumulation of cells in the migratory stream. This led to transitory changes to the developing brain size, and heightened postnatal cell loss (20% increase) during the canonical window of developmental cell death in the striatum [around P6; (Sreenivasan et al., 2022)]. These alterations were associated with intrinsic perturbations to interneuron physiological properties, neuronal differentiation and connectivity that are likely to support striatal-related impairments described in the *Cntnap2* KO mice model (Scott et al., 2017).

## Altered proliferation and migration of the striatal cholinergic interneurons following *Cntnap2* deletion

Using high-resolution spatial transcriptomics (Stereo-seq) and scRNAseq data from the MGE, we described the spatial pattern of expression of *Cntnap2* in the adult brain and at embryonic stages in the MGE, where we could detect some *Cntnap2*+ cells, as early as E12. We reveal that *Cntnap2* expression is enriched in the progenitor cells, as well as post-mitotic neurons of the striatum and in particular, in the MGE-derived cholinergic interneurons. Since we observed a shift in the proportion of Lhx6+ CINs produced, and enhanced cell-specific cell death in the *Cntnap2* KO mice, we established that deletion of *Cntnap2* preferentially affected these cells. Considering *Cntnap2* is known to control processes that occur in more developed cells (e.g., myelination, synapse maintenance...), it was interesting to find *Cntnap2* in progenitor cells. Does *Cntnap2* regulate neural progenitor cell physiology? Some of our data from *in vitro* patch clamp recordings at E16 suggest that the basic electrical properties of the progenitor cells are unchanged in the *Cntnap2* KO condition (Data not shown). However, the *Cntnap2* protein expression levels and precise subcellular distribution of the potassium channel subunits Kv1.2 (Poliak et al., 1999; Scott et al., 2017) remain to be determined, to fully appreciate the functional impact *Cntnap2* has on different embryonic cell types. Since *Cntnap2* is expressed ubiquitously in the developing brain, it will be necessary to use a conditional mutant to better analyze the specific intricacies of *Cntnap2* that may affect cell function and early cell communication. Overall, our results emphasize the importance of further study how a human disease risk gene such as *Cntnap2* regulates interneuron development. Indeed, *Cntnap2* is expressed in the MGE progenitors cells in humans (Satterstrom et al., 2020), and in future sub-pallial cholinergic and GABAergic neurons (Shi et al., 2021), suggesting that potential therapeutic interventions could be conducted from embryonic stages to rectify the altered developmental trajectory in ASD, but also a range of neurodevelopmental disorders such as schizophrenia, intellectual disability, dyslexia, epilepsy and attention-deficit hyperactivity disorder (Rodenas-Cuadrado et al., 2014; Poot, 2015).

## Readjustment of normal cell number during the first postnatal week

Disruption of cholinergic interneurons (CINs) in the striatum generate network and behavioral modifications significant to ASD (Rapanelli et al., 2017a; Caubit et al., 2022). Yet, how developing CINs are impacted in ASD has been poorly explored. By uncovering preferential and specific developmental modifications of the striatal interneuron maturation at embryonic and early postnatal stages, we demonstrate that the MGE-derived Lhx6<sup>+</sup> CINs, which represent at least 50% of the striatal cholinergic contingent (Magno et al., 2017), are primarily affected by the absence of *Cntnap2*, suggesting that these cells substantially contribute to the ASD-related alterations observed in the *Cntnap2* KO conditions. Whether this is the case for ASD in general will need to be further assessed by examining the alterations of MGE-derived cholinergic interneurons in other ASD mouse models. In addition, investigating the specific role of *Cntnap2* in CINs vs. other striatal cells with conditional mutants will be essential to delineate the specific role of CINs in ASD pathophysiology.

Evidence shows *in utero* alterations in ASD (Satterstrom et al., 2020), with enlargement of the brain size and cell number (Bonnet-Brilhault et al., 2018). Concurrently, we found an expansion of the MGE proliferative zone around E14.5, and a shift in Lhx6<sup>+</sup> cell migration, exemplified by an early reduction of the VZ proliferative zone in the MGE, and enlarged cortical migratory stream. However, there is still no rationale about whether alterations in the scaffold protein *Cntnap2* can lead to migration abnormalities in these interneurons (Rapanelli et al., 2017b). Striatal cell migration is tightly regulated (Villar-Cervino et al., 2015), and genetic and environmental factors that perturb cell migration and distribution result in improper cell positioning, and E/I imbalances in ASD (Guo and Anton, 2014; de la Torre-Ubieta et al., 2016). There are reciprocal mechanisms at play in the developing brain, whereby interneuron migration influences principal cell generation (Silva et al., 2018), and activity of the principal cells affects interneuron cell survival (Wong et al., 2018). In addition, it has been shown that cell-intrinsic properties of interneuron migration controls the flow of interneurons invading the cortex and also impairs the generation of age-matched projection neurons of the upper cortical layers (Silva et al., 2018). Indeed, previous studies have shown a redirection of late-born cortical interneurons from upper layers to deeper layers in the *Cntnap2* knockout (Penagarikano et al., 2011). This is reflected in our findings with the increase in thickness of the superficial migratory stream which underlies the increase in Lhx6<sup>+</sup> cell density in the deep layers of the prefrontal cortex at early developmental stages. Cell numbers in the PFC at later developmental stages were unchanged, consistent with recent studies (Scott et al., 2017; Lauber et al., 2018).

Further study is required to decipher the mechanisms underlying the involvement of specific striatal CINs, which are known to support the pathophysiology of ASD (Caubit et al., 2022), and how changes in cell number and positioning—although transitory—influence other striatal interneurons and output neurons, either directly or by compensatory mechanisms, and the establishment of functional neuronal assemblies within the striatum. Indeed, any alterations in developing interneuron function is expected to alter the excitation-inhibition balance and, overall striatal activity, to ultimately impact activity-dependent mechanisms such as perinatal network oscillations that are fundamental to build functional circuitries (Dehorter et al., 2012). A reduction in inhibitory power in different neuronal circuits

(e.g., striatum vs. cortex) is expected to have distinctive impact on the excitation-inhibition balance. For example, there are no glutamatergic neurons in the striatum, compared to the cortex. This could explain why morphological alterations in the cortical GABAergic interneurons (Gao et al., 2018) are different compared to the striatal GABAergic interneurons (Supplementary Figure S5). In terms of a mechanism, a possibility is that interneurons could adjust their polarity in response to region-specific chemotactic cues (Rodenas-Cuadrado et al., 2014) to populate their final location, affecting cell morphological architecture. However, we also cannot discard that migration of the striatal output neurons, also affected in the *Cntnap2* KO condition, could directly participate to this phenotype. Employing a conditional knockout for *Cntnap2* will address these questions and tease apart the cellular and brain region specificity of the impact of *Cntnap2* in developing cell migration and connectivity.

During the first two postnatal weeks, massive cell death event [i.e., up to 50% cell death; (Wong et al., 2018)] occurs in the brain. During this key period, inactive MGE-derived interneurons are more likely to die than active neurons (Denaxa et al., 2018; Wong et al., 2018). With the marked reduction of striatal cell number and increase in caspase-positive cells detected between P4 and P6, our data reveals that apoptosis is enhanced in the MGE-derived cells of the *Cntnap2* KO mice. Whilst the canonical window of developmental cell death does not appear to be shifted in this condition, the extent of cell loss appeared increased. Interestingly, the final number of CINs is regulated by the activity of the striatal output neurons, also called spiny projection neurons (SPN). When the SPN activity is increased, CIN survival is diminished (Sreenivasan et al., 2022). Therefore, we speculate that loss of striatal CIN in the *Cntnap2* KO mice may be due to an increase in SPN activity, probably driven by an early maturation of the cortico-striatal pathway, reported in ASD mouse models (Peixoto et al., 2016). Future directions will require to study the mechanisms supporting this process, such as the involvement of molecules such as the phosphatase and tensin homolog deleted on chromosome 10 (PTEN), which controls cell death (Wong et al., 2018), and the role of its interactor Tau (Tai et al., 2020). Together with the substantial loss in MGE-derived interneurons in the *Cntnap2* KO mice, we found a large decrease in the excitability of the Lhx6<sup>+</sup> interneurons of the striatum. We hypothesize that changes in early cell activities also provide a feedback loop that represents a homeostatic mechanism for fine-tuning the number of interneurons (Denaxa et al., 2018), and contribute to the striatal apoptotic process. Whether these mechanisms are conserved in other interneuron types coming from the pre-optic area, septal neuroepithelium (which give rise to 50% of the CINs (Magno et al., 2017)), caudal ganglionic eminence (Ahmed et al., 2019), and other proliferative regions (e.g., cortical VZ, lateral ganglionic eminence), to contribute to the overall phenotype observed in this study, will need to be further investigated in *Cntnap2* conditional mutants.

## Striatal interneuron function and network activity

*Cntnap2* is known to play a role in cell firing properties, influencing latency of adult cell firing, *via* loss of the potassium channel subunit Kv1.2 (Vogt et al., 2017). Here, we unveiled key physiological cell deficits during a key perinatal period (Dehorter et al., 2012), during which activity-dependent mechanisms

dynamically adjust the number of interneurons in developing circuits, and ultimately establish the correct proportions of neural connections in a structure to be functional (Wong et al., 2018). In other words, these critical early neural activities are thought to represent checkpoints that ensure the proper formation of neuronal circuits (Dehorter et al., 2012). In this study, we observed a reduction in cell excitability, associated with increased expression of the metabotropic glutamate receptor mgluR5 and a decrease in the expression of the NMDA NR2 C/D subunits in the *Cntnap2* KO mice, which mediate large synaptic currents in interneurons (von Engelhardt et al., 2015), confers different sensitivity of the receptors to ligands (Williams et al., 1993), and provide a critical source of Ca<sup>2+</sup> entry via trophic glutamate signaling (Paoletti et al., 2013), which could add to the impact on synaptogenesis and their well-described role in potentiation (i.e., LTP/LTD; (Luscher and Malenka, 2012)). In addition, NMDA receptor-dependent and voltage-gated calcium channels activation are also known trigger calcium influx that promotes cell survival (Desfeux et al., 2010). They also mediate transcriptional cascades to control gene expression during the development of MGE-derived interneurons. In particular, specific loss of NMDA receptors in the MGE has been shown to result in a downregulation of diverse transcriptional, synaptogenesis and membrane excitability regulatory programs (Mahadevan et al., 2021). In addition, we found less NMDA-driven inputs onto Lhx6<sup>+</sup> interneurons and larger dendritic complexity, overall indicating an early maturation of the glutamatergic processing in these cells (Peixoto et al., 2016). We propose that these qualitative changes in striatal interneuron physiology will impact global neural activity levels and the formation of specific synaptic connections, as seen in other ASD mouse models (Cheyne et al., 2019; Bitzenhofer et al., 2021). A better understanding of the functional link between the early alterations in the developing interneurons, and the establishment of operative neuronal assemblies is required to appreciate the consequent behavioral deficits (i.e., repetitive movements) that are contingent to the malfunction of the mature striatal network in ASD (Penagarikano et al., 2011). For example, calcium imaging recordings should determine how shifting interneuron excitability shapes synapse-driven early network oscillations, such as the giant depolarizing potentials (Dehorter et al., 2011) to control the emergence of functional circuitry in the mature striatum (Dehorter et al., 2012).

The current literature lacks an understanding of the intricate alterations to interneuron development in ASD and how this could contribute autism aetiology. Together, this study forms the basis to further explore the mechanisms underlying deficits of the developing interneurons in ASD. These findings emphasize the importance of considering targeting developing interneurons to restore normal developmental brain trajectory in ASD.

## Data availability statement

The datasets presented in this study can be found in online repositories. The names of the repository/repositories and accession number(s) can be found below: Gene Expression Omnibus accession number: GSE222383 and GSE109796.

## Ethics statement

The animal study was reviewed and approved by Australian National University Animal Experimentation Ethics Committee (protocol numbers A2019/46 & A2021/43).

## Author contributions

Conceptualization: ND. Methodology: NA, RK, and ND. Formal analysis: NA, YW, YS, RK, NR, LL, YY, XL, US, RN, JW, and IDP. Interpretation: NA, RK, RN, JW, DM, and ND. Data curation: NA, RK, YS, RN, US, and IDP. Writing—original-draft: NA and ND. Writing—review and editing: NA, RK, NR, DM, IDP, and ND. Visualization: NYA and ND. Supervision: ND. Resources: DM, JW, RN, and ND. Project administration: ND. Funding acquisition: ND.

## Funding

This work was supported by The Australian National University (Futures Scheme 2017-2021) and a National Health and Medical research Council (NHMRC) Project Grant (APP1144145) to ND, and the STI2030-Major Projects (2021ZD0202300, 2021ZD0202301) and the Ministry of Science and Technology of China (2021ZD0202300) to DM.

## Acknowledgments

We are very grateful to Xiaohuan Sun, BGI Australia, Jiyoti Verma, Decode Science Australia, and Barry Thompson's lab for helping with the Stereo-seq approach at the ANU.

## Conflict of interest

The authors declare that the research was conducted in the absence of any commercial or financial relationships that could be construed as a potential conflict of interest.

## Publisher's note

All claims expressed in this article are solely those of the authors and do not necessarily represent those of their affiliated organizations, or those of the publisher, the editors and the reviewers. Any product that may be evaluated in this article, or claim that may be made by its manufacturer, is not guaranteed or endorsed by the publisher.

## Supplementary material

The Supplementary Material for this article can be found online at: <https://www.frontiersin.org/articles/10.3389/fcell.2023.1112062/full#supplementary-material>

## References

- Ahmed, N. Y., Knowles, R., and Dehorter, N. (2019). New insights into cholinergic neuron diversity. *Front. Mol. Neurosci.* 12, 204. doi:10.3389/fnmol.2019.00204
- Ahmed, N. Y., Ranjbar-Slamloo, Y., Abed, A. S. A., Gao, L., Sontani, Y., H'Cheo-Gauthier, A. R., et al. (2021). Er81 transcription factor fine-tunes striatal cholinergic interneuron activity and drives habit formation. *J. Neurosci.* 41, 4392–4409. doi:10.1523/JNEUROSCI.0967-20.2021
- Antoine, M. W., Langberg, T., Schnepel, P., and Feldman, D. E. (2019). Increased excitation-inhibition ratio stabilizes synapse and circuit excitability in four autism mouse models. *Neuron* 101 (4), 648–661. doi:10.1016/j.neuron.2018.12.026
- Babji, R., and De Marco Garcia, N. (2016). Neuronal activity controls the development of interneurons in the somatosensory cortex. *Front. Biol. Beijing* 11 (6), 459–470. doi:10.1007/s11515-016-1427-x
- Benamer, N., Vidal, M., Balia, M., and Angulo, M. C. (2020). Myelination of parvalbumin interneurons shapes the function of cortical sensory inhibitory circuits. *Nat. Commun.* 11 (1), 5151. doi:10.1038/s41467-020-18984-7
- Bitzenhofer, S. H., Popplau, J. A., Chini, M., Marquardt, A., and Hanganu-Opatz, I. L. (2021). A transient developmental increase in prefrontal activity alters network maturation and causes cognitive dysfunction in adult mice. *Neuron* 109 (8), 1350–1364. e6. doi:10.1016/j.neuron.2021.02.011
- Bonnet-Brilhault, F., Rajerison, T. A., Paillet, C., Guimard-Brunault, M., Saby, A., Ponson, L., et al. (2018). Autism is a prenatal disorder: Evidence from late gestation brain overgrowth. *Autism Res.* 11 (12), 1635–1642. doi:10.1002/aur.2036
- Caubit, X., Gubellini, P., Roubertoux, P. L., Carlier, M., Molitor, J., Chabbert, D., et al. (2022). Targeted Tshz3 deletion in corticostriatal circuit components segregates core autistic behaviors. *Transl. Psychiatry* 12 (1), 106. doi:10.1038/s41398-022-01865-6
- Cheyne, J. E., Zabouri, N., Baddeley, D., and Lohmann, C. (2019). Spontaneous activity patterns are altered in the developing visual cortex of the Fmr1 knockout mouse. *Front. Neural Circuits* 13, 57. doi:10.3389/fncir.2019.00057
- Contractor, A., Ethell, I. M., and Portera-Cailliau, C. (2021). Cortical interneurons in autism. *Nat. Neurosci.* 24 (12), 1648–1659. doi:10.1038/s41593-021-00967-6
- de la Torre-Ubieta, L., Won, H., Stein, J. L., and Geschwind, D. H. (2016). Advancing the understanding of autism disease mechanisms through genetics. *Nat. Med.* 22 (4), 345–361. doi:10.1038/nm.4071
- Dehorter, N., and Del Pino, I. (2020). Shifting developmental trajectories during critical periods of brain formation. *Front. Cell. Neurosci.* 14, 283. doi:10.3389/fncel.2020.00283
- Dehorter, N., Michel, F. J., Marissal, T., Rotrou, Y., Matrot, B., Lopez, C., et al. (2011). Onset of pup locomotion coincides with loss of NR2C/D-Mediated cortico-striatal EPSCs and dampening of striatal network immature activity. *Front. Cell. Neurosci.* 5, 24. doi:10.3389/fncel.2011.00024
- Dehorter, N., Vinay, L., Hammond, C., and Ben-Ari, Y. (2012). Timing of developmental sequences in different brain structures: Physiological and pathological implications. *Eur. J. Neurosci.* 35 (12), 1846–1856. doi:10.1111/j.1460-9568.2012.08152.x
- Dehorter, N., Marichal, N., Marin, O., and Berninger, B. (2017). Tuning neural circuits by turning the interneuron knob. *Curr. Opin. Neurobiol.* 42, 144–151. doi:10.1016/j.conb.2016.12.009
- Denaxa, M., Neves, G., Rabinowitz, A., Kemlo, S., Liadis, P., Burrone, J., et al. (2018). Modulation of apoptosis controls inhibitory interneuron number in the cortex. *Cell. Rep.* 22 (7), 1710–1721. doi:10.1016/j.celrep.2018.01.064
- Desfeux, A., El Ghazi, F., Jegou, S., Legros, H., Marret, S., Laudenbach, V., et al. (2010). Dual effect of glutamate on GABAergic interneuron survival during cerebral cortex development in mice neonates. *Cereb. Cortex* 20 (5), 1092–1108. doi:10.1093/cercor/bhp181
- Flomerfelt, F. A., and Gress, R. E. (2016). Analysis of cell proliferation and homeostasis using EdU labeling. *Methods Mol. Biol.* 1323, 211–220. doi:10.1007/978-1-4939-2809-5\_18
- Fuccillo, M. V. (2016). Striatal circuits as a common node for autism pathophysiology. *Front. Neurosci.* 10, 27. doi:10.3389/fnins.2016.00027
- Gao, R., Pigué, N. H., Melendez-Zaidi, A. E., Martin-de-Saavedra, M. D., Yoon, S., Forrest, M. P., et al. (2018). CNTNAP2 stabilizes interneuron dendritic arbors through CASK. *Mol. Psychiatry* 23, 1832–1850. doi:10.1038/s41380-018-0027-3
- Guo, J., and Anton, E. S. (2014). Decision making during interneuron migration in the developing cerebral cortex. *Trends Cell. Biol.* 24 (6), 342–351. doi:10.1016/j.tcb.2013.12.001
- Knowles, R., Dehorter, N., and Ellender, T. (2021). From progenitors to progeny: Shaping striatal circuit development and function. *J. Neurosci.* 41 (46), 9483–9502. doi:10.1523/JNEUROSCI.0620-21.2021
- Lauber, E., Filice, F., and Schwaller, B. (2018). Dysregulation of parvalbumin expression in the Cntnap2<sup>-/-</sup> mouse model of autism spectrum disorder. *Front. Mol. Neurosci.* 11, 262. doi:10.3389/fnmol.2018.00262
- Liadis, P., Denaxa, M., Grigoriou, M., Akufo-Addo, C., Yanagawa, Y., and Pachnis, V. (2007). Lhx6 activity is required for the normal migration and specification of cortical interneuron subtypes. *J. Neurosci.* 27 (12), 3078–3089. doi:10.1523/JNEUROSCI.3055-06.2007
- Lozovaya, N., Eftekhari, S., Cloarec, R., Gouty-Colomer, L. A., Dufour, A., Riffault, B., et al. (2018). GABAergic inhibition in dual-transmission cholinergic and GABAergic striatal interneurons is abolished in Parkinson disease. *Nat. Commun.* 9 (1), 1422. doi:10.1038/s41467-018-03802-y
- Luscher, C., and Malenka, R. C. (2012). NMDA receptor-dependent long-term potentiation and long-term depression (LTP/LTD). *Cold Spring Harb. Perspect. Biol.* 4 (6), a005710. doi:10.1101/cshperspect.a005710
- Magno, L., Barry, C., Schmidt-Hieber, C., Theodotou, P., Hausser, M., and Kessaris, N. (2017). NKX2-1 is required in the embryonic septum for cholinergic system development, learning, and memory. *Cell. Rep.* 20 (7), 1572–1584. doi:10.1016/j.celrep.2017.07.053
- Mahadevan, V., Mitra, A., Zhang, Y., Yuan, X., Peltekian, A., Chittajallu, R., et al. (2021). NMDARs drive the expression of neuropsychiatric disorder risk genes within GABAergic interneuron subtypes in the juvenile brain. *Front. Mol. Neurosci.* 14, 712609. doi:10.3389/fnmol.2021.712609
- Mayer, C., Hafemeister, C., Bandler, R. C., Machold, R., Batista Brito, R., Jaglin, X., et al. (2018). Developmental diversification of cortical inhibitory interneurons. *Nature* 555 (7697), 457–462. doi:10.1038/nature25999
- Mi, D., Li, Z., Lim, L., Li, M., Moissidis, M., Yang, Y., et al. (2018). Early emergence of cortical interneuron diversity in the mouse embryo. *Science* 360 (6384), 81–85. doi:10.1126/science.aar6821
- Paoletti, P., Bellone, C., and Zhou, Q. (2013). NMDA receptor subunit diversity: Impact on receptor properties, synaptic plasticity and disease. *Nat. Rev. Neurosci.* 14 (6), 383–400. doi:10.1038/nrn3504
- Peixoto, R. T., Wang, W., Cronney, D. M., Kozorovitskiy, Y., and Sabatini, B. L. (2016). Early hyperactivity and precocious maturation of corticostriatal circuits in Shank3B<sup>-/-</sup> mice. *Nat. Neurosci.* 19 (5), 716–724. doi:10.1038/nn.4260
- Penagarikano, O., Abrahams, B. S., Herman, E. I., Winden, K. D., Gdalyahu, A., Dong, H., et al. (2011). Absence of CNTNAP2 leads to epilepsy, neuronal migration abnormalities, and core autism-related deficits. *Cell* 147 (1), 235–246. doi:10.1016/j.cell.2011.08.040
- Poliak, S., Gollan, L., Martinez, R., Custer, A., Einheber, S., Salzer, J. L., et al. (1999). Caspr2, a new member of the neuixin superfamily, is localized at the juxtaparanodes of myelinated axons and associates with K<sup>+</sup> channels. *Neuron* 24 (4), 1037–1047. doi:10.1016/s0896-6273(00)81049-1
- Poot, M. (2015). Connecting the CNTNAP2 networks with neurodevelopmental disorders. *Mol. Syndromol.* 6 (1), 7–22. doi:10.1159/000371594
- Rapanelli, M., Frick, L. R., Xu, M., Groman, S. M., Jindachomthong, K., Tamamaki, N., et al. (2017). Targeted interneuron depletion in the dorsal striatum produces autism-like behavioral abnormalities in male but not female mice. *Biol. Psychiatry* 82 (3), 194–203. doi:10.1016/j.biopsych.2017.01.020
- Rapanelli, M., Frick, L. R., and Pittenger, C. (2017). The role of interneurons in autism and tourette syndrome. *Trends Neurosci.* 40 (7), 397–407. doi:10.1016/j.tins.2017.05.004
- Rodenas-Cuadrado, P., Ho, J., and Vernes, S. C. (2014). Shining a light on CNTNAP2: Complex functions to complex disorders. *Eur. J. Hum. Genet.* 22 (2), 171–178. doi:10.1038/ejhg.2013.100
- Sacco, R., Gabriele, S., and Persico, A. M. (2015). Head circumference and brain size in autism spectrum disorder: A systematic review and meta-analysis. *Psychiatry Res.* 234 (2), 239–251. doi:10.1016/j.psychres.2015.08.016
- Satterstrom, F. K., Kosmicki, J. A., Wang, J., Breen, M. S., De Rubeis, S., An, J. Y., et al. (2020). Large-scale exome sequencing study implicates both developmental and functional changes in the neurobiology of autism. *Cell* 180 (3), 568–584.e23. doi:10.1016/j.cell.2019.12.036
- Scott, R., Sanchez-Aguilera, A., van Elst, K., Lim, L., Dehorter, N., Bae, S. E., et al. (2017). Loss of Cntnap2 causes axonal excitability deficits, developmental delay in cortical myelination, and abnormal stereotyped motor behavior. *Cereb. Cortex* 29, 586–597. doi:10.1093/cercor/bhx341
- Selimbeyoglu, A., Kim, C. K., Inoue, M., Lee, S. Y., Hong, A. S. O., Kauvar, I., et al. (2017). Modulation of prefrontal cortex excitation/inhibition balance rescues social behavior in CNTNAP2-deficient mice. *Sci. Transl. Med.* 9 (401), eaah6733. doi:10.1126/scitranslmed.aah6733
- Shi, Y., Wang, M., Mi, D., Lu, T., Wang, B., Dong, H., et al. (2021). Mouse and human share conserved transcriptional programs for interneuron development. *Science* 374 (6573), eabj6641. doi:10.1126/science.abj6641
- Silva, C. G., Peyre, E., Adhikari, M. H., Tielens, S., Tanco, S., Van Damme, P., et al. (2018). Cell-intrinsic control of interneuron migration drives cortical morphogenesis. *Cell* 172 (5), 1063–1078. doi:10.1016/j.cell.2018.01.031
- Sreenivasan, V., Serafeimidou-Pouliou, E., Exposito-Alonso, D., Bercsenyi, K., Bernard, C., Bae, S. E., et al. (2022). Input-specific control of interneuron numbers in nascent striatal networks. *Proc. Natl. Acad. Sci. U. S. A.* 119 (20), e2118430119. doi:10.1073/pnas.2118430119
- Strauss, K. A., Puffenberger, E. G., Huentelman, M. J., Gottlieb, S., Dobrin, S. E., Parod, J. M., et al. (2006). Recessive symptomatic focal epilepsy and mutant contactin-associated protein-like 2. *N. Engl. J. Med.* 354 (13), 1370–1377. doi:10.1056/NEJMoa052773

- Tai, C., Chang, C. W., Yu, G. Q., Lopez, I., Yu, X., Wang, X., et al. (2020). Tau reduction prevents key features of autism in mouse models. *Neuron* 106 (3), 421–437. doi:10.1016/j.neuron.2020.01.038
- Tepper, J. M., Tecuapetla, F., Koos, T., and Ibanez-Sandoval, O. (2010). Heterogeneity and diversity of striatal GABAergic interneurons. *Front. Neuroanat.* 4, 150. doi:10.3389/fnana.2010.00150
- Turrero Garcia, M., and Harwell, C. C. (2017). Radial glia in the ventral telencephalon. *FEBS Lett.* 591 (24), 3942–3959. doi:10.1002/1873-3468.12829
- Varea, O., Martin-de-Saavedra, M. D., Kopeikina, K. J., Schurmann, B., Fleming, H. J., Fawcett-Patel, J. M., et al. (2015). Synaptic abnormalities and cytoplasmic glutamate receptor aggregates in contactin associated protein-like 2/Caspr2 knockout neurons. *Proc. Natl. Acad. Sci. U. S. A.* 112 (19), 6176–6181. doi:10.1073/pnas.1423205112
- Villar-Cervino, V., Kappeler, C., Nobrega-Pereira, S., Henkemeyer, M., Rago, L., Nieto, M. A., et al. (2015). Molecular mechanisms controlling the migration of striatal interneurons. *J. Neurosci.* 35 (23), 8718–8729. doi:10.1523/JNEUROSCI.4317-14.2015
- Vogt, D., Cho, K. K. A., Shelton, S. M., Paul, A., Huang, Z. J., Sohal, V. S., et al. (2017). Mouse *Cntnap2* and human *CNTNAP2* ASD alleles cell autonomously regulate PV+ cortical interneurons. *Cereb. Cortex* 28, 1–12. doi:10.1093/cercor/bhx248
- von Engelhardt, J., Bocklisch, C., Tonges, L., Herb, A., Mishina, M., and Monyer, H. (2015). GluN2D-containing NMDA receptors mediate synaptic currents in hippocampal interneurons and pyramidal cells in juvenile mice. *Front. Cell. Neurosci.* 9, 95. doi:10.3389/fncel.2015.00095
- Williams, K., Russell, S. L., Shen, Y. M., and Molinoff, P. B. (1993). Developmental switch in the expression of NMDA receptors occurs *in vivo* and *in vitro*. *Neuron* 10 (2), 267–278. doi:10.1016/0896-6273(93)90317-k
- Wong, F. K., Bercsenyi, K., Sreenivasan, V., Portales, A., Fernandez-Otero, M., and Marin, O. (2018). Pyramidal cell regulation of interneuron survival sculpts cortical networks. *Nature* 557 (7707), 668–673. doi:10.1038/s41586-018-0139-6
- Yap, E. L., and Greenberg, M. E. (2018). Activity-regulated transcription: Bridging the gap between neural activity and behavior. *Neuron* 100 (2), 330–348. doi:10.1016/j.neuron.2018.10.013

## **Appendix D: Details of contributions**

### **Chapter 2:**

**Figure 2.3:** Data in panels A-G contributed to an honours thesis (Noorya Ahmed, 2018).

**Figure 2.4:** Electrophysiological recordings (B-C) were performed and analysed by Yadollah Ranjbar Slamloo (YRS). Data in panels D-M contributed to an honours thesis (Noorya Ahmed, 2018), except for distal dendrite measures in panels E & G.

**Figure 2.5:** Data in panels B & C contributed to an honours thesis (Noorya Ahmed, 2018).

### **Chapter 3:**

**Figure 3.5:** Analysis code for open field mouse tracking was modified by Rebekah Parkinson (RP).

**Figure 3.6:** DigiGait experimentation and analysis (panels D-I) was done by RP. NA contributed to the experimental procedures.

**Figure 3.10:** Cell counting in adult mice was performed by Melissa Ritchie (MR) and Lachlan Kimpton (LK), under supervision from NA, on images collected by NA, MR, LK.

### **Chapter 4:**

**Figure 4.2:** Stereo-seq was done in collaboration with Ulrike Schumann (US) and Lixinyu Liu (LL). Tissue collection was done by NA and US, tissue processing and experimental procedure was done by US, analysis was done by LL, with contributions and direction from NA.

**Figure 4.3:** Lhx6 cell counting was done in collaboration with Rhys Knowles (RK). NA performed all experimental processes and preliminary analyses, RK performed the cell counting via an ImageJ/Fiji macro.

**Figure 4.4:** Cholinergic interneuron cell counting was done in collaboration with Yovina Sontani (YS). YS performed cell counting at P0, NA performed cell counting at P6.

**Figure 4.5:** mRNA and protein analyses were done with YS and Yumeng Wang (YW).

**Figure 4.7 & 4.8:** CIN electrophysiology data was contributed to by Nathan Reynolds (NR) and Isabel del Pino (IDP). Both contributed to electrophysiology recordings of CINs and PV-INs, all analysis was done by NA.

**Figure 4.9:** Recordings were contributed to by IDP and NR. Initial analysis of EPSC characteristics (panel F-J) was performed by NR, with later modifications by NA. Panels P-S were generated by YW and YS.

## Appendix E: Electrophysiology Result Tables

The following tables correspond to electrophysiology data presented in this thesis. Statistical tests displayed were Student's t-tests or (#) non-parametric Mann-Whitney tests.

**Table 4: Intrinsic properties of *Lhx6*+ striatal cholinergic interneurons in control and *Lhx6-Er81* cKO mice at P5-7**

Lhx6+ Cholinergic Interneurons P5-7					
Property	Control		<i>Er81</i> cKO		<i>p</i>
	Mean	n	Mean	n	
Resting membrane potential (mV)	-48.37 ± 1.43	9	-46.88 ± 1.69	7	0.5095
Input resistance (MΩ)	474.43 ± 59.05	9	412.13 ± 102.6	7	0.5872
Membrane capacitance (pF)	767.24 ± 123.66	9	650.02 ± 78.98	7	0.4683
Sag ratio	0.17 ± 0.03	9	0.22 ± 0.05	7	0.4698 <sup>#</sup>
Spike adaptation index	0.44 ± 0.07	9	0.44 ± 0.07	7	0.9906
Spontaneous firing rate (Hz)	1.56 ± 0.42	8	1.08 ± 0.23	6	0.3779
Coefficient of Spike Variation	0.72 ± 0.21	8	0.50 ± 0.14	6	0.4069
Action potential threshold (mV)	-34.38 ± 2.25	9	-36.65 ± 1.76	7	0.4591
Action potential amplitude (mV)	50.74 ± 2.68	9	51.53 ± 2.76	7	0.8416
Action potential rise time (ms)	0.94 ± 0.07	9	1.13 ± 0.13	7	0.2080
Action potential decay (ms)	3.10 ± 0.07	9	3.12 ± 0.06	7	0.8247
Action potential halfwidth (ms)	2.74 ± 0.18	9	2.97 ± 0.15	7	0.3781
Action potential fast AHP (mV)	2.46 ± 1.34	9	3.01 ± 1.16	7	0.8665
Action potential medium AHP (mV)	-13.56 ± 2.79	9	-11.96 ± 1.07	7	>0.9999

**Table 5: Intrinsic properties of *Lhx6*+ striatal cholinergic interneurons in control and *Lhx6-Er81* cKO mice at P30+**

Lhx6+ Cholinergic Interneurons P30+					
Property	Control		<i>Er81</i> cKO		<i>p</i>
	Mean	n	Mean	n	
Resting membrane potential (mV)	-44.10 ± 1.80	7	-45.24 ± 1.59	5	0.6628
Input resistance (MΩ)	181.70 ± 36.33	7	289.75 ± 99.33	5	0.2727
Membrane capacitance (pF)	655.73 ± 76.73	7	1729.70 ± 528.04	5	0.0371
Sag ratio	0.13 ± 0.05	7	0.06 ± 0.03	5	0.3352
Spike adaptation index	0.52 ± 0.11	7	0.55 ± 0.08	5	0.7986
Spontaneous firing rate (Hz)	3.83 ± 1.46	7	5.71 ± 1.92	5	0.4458
Coefficient of Spike Variation	0.67 ± 0.13	7	0.44 ± 0.15	5	0.2670
Action potential threshold (mV)	-44.89 ± 1.36	7	-40.13 ± 1.83	5	0.0588
Action potential amplitude (mV)	55.18 ± 5.10	7	53.71 ± 6.58	5	0.8608
Action potential rise time (ms)	0.64 ± 0.08	7	0.67 ± 0.15	5	0.8593
Action potential decay (ms)	2.86 ± 0.17	7	2.44 ± 0.29	5	0.2067
Action potential halfwidth (ms)	2.06 ± 0.26	7	1.66 ± 0.19	5	0.2726
Action potential fast AHP (mV)	0.26 ± 1.99	7	-6.12 ± 1.46	5	0.0381
Action potential medium AHP (mV)	-7.38 ± 0.53	7	-11.66 ± 0.73	5	0.0007



**Table 6: Intrinsic properties of Lhx6+ striatal GABAergic fast spiking interneurons in control and Lhx6-Er81 cKO mice at P5-7**

Lhx6+ Putative Fast Spiking Interneurons P5-7					
Property	Control		Er81 cKO		p
	Mean	n	Mean	n	
Resting membrane potential (mV)	-57.07 ± 1.69	12	-60.12 ± 1.82	11	0.2334
Input resistance (MΩ)	453.83 ± 46.09	13	281.12 ± 34.08	13	0.0060
Membrane capacitance (pF)	601.65 ± 128.60	13	794.85 ± 93.29	13	0.2358
Rheobase (pA)	23.61 ± 3.64	13	57.04 ± 7.35	13	0.0010 <sup>#</sup>
Latency to first spike (ms)	127.82 ± 24.55	13	113.92 ± 18.68	13	0.8798 <sup>#</sup>
Maximum firing frequency (Hz)	53.69 ± 3.57	13	62.00 ± 4.48	13	0.1599
Action potential threshold (mV)	-32.51 ± 1.56	13	-33.51 ± 0.92	13	0.5861
Action potential amplitude (mV)	42.87 ± 3.26	13	40.58 ± 3.06	13	0.6129
Action potential rise time (ms)	0.82 ± 0.07	13	0.81 ± 0.06	13	0.9532
Action potential decay (ms)	2.25 ± 0.14	13	2.36 ± 0.13	13	0.5553
Action potential halfwidth (ms)	1.73 ± 0.18	13	1.72 ± 0.11	13	0.6866 <sup>#</sup>
Action potential fast AHP (mV)	-8.34 ± 1.15	13	-7.24 ± 0.66	13	0.4147
Action potential medium AHP (mV)	-10.65 ± 0.86	13	-9.33 ± 0.86	13	0.1389 <sup>#</sup>

**Table 7: Intrinsic properties of Lhx6+ striatal GABAergic parvalbumin positive/fast spiking interneurons in control and Lhx6-Er81 cKO mice at P30+**

Lhx6+ Putative Fast Spiking Interneurons/ PV+ Interneurons P30+					
Property	Control		Er81 cKO		p
	Mean	n	Mean	n	
Resting membrane potential (mV)	-65.39 ± 2.85	11	-68.87 ± 1.68	12	0.2949
Input resistance (MΩ)	205.40 ± 31.27	23	222.38 ± 34.15	18	0.7850 <sup>#</sup>
Membrane capacitance (pF)	1246.00 ± 516.90	23	556.65 ± 94.76	18	0.7063 <sup>#</sup>
Rheobase (pA)	164.09 ± 48.22	9	178.29 ± 59.62	7	0.8541
Latency to first spike (ms)	192.66 ± 49.57	9	335.68 ± 52.78	7	0.0704
Maximum firing frequency (Hz)	141.50 ± 11.39	16	159.11 ± 9.38	9	0.3058
Action potential threshold (mV)	-38.86 ± 1.52	23	-36.01 ± 1.70	18	0.2192
Action potential amplitude (mV)	47.01 ± 1.94	23	44.47 ± 2.06	18	0.3787
Action potential rise time (ms)	0.34 ± 0.03	23	0.36 ± 0.03	18	0.3283 <sup>#</sup>
Action potential decay (ms)	0.85 ± 0.10	23	0.96 ± 0.10	18	0.0806 <sup>#</sup>
Action potential halfwidth (ms)	0.59 ± 0.06	23	0.67 ± 0.06	18	0.1067 <sup>#</sup>
Action potential fast AHP (mV)	-7.40 ± 0.77	23	-8.92 ± 0.68	18	0.1602
Action potential medium AHP (mV)	-7.72 ± 0.57	23	-8.80 ± 0.54	18	0.1850

**Table 8: Intrinsic properties of striatal parvalbumin positive in control and PV-Er81 cKO mice at 30+**

Fast Spiking Interneurons/ PV+ Interneurons P30+					
Property	Control		Er81 cKO		p
	Mean	n	Mean	n	
Resting membrane potential (mV)	-72.90 ± 1.59	6	-73.12 ± 0.95	7	0.9090
Rheobase (pA)	202.85 ± 18.52	4	219.25 ± 37.57	7	0.9273 <sup>#</sup>
Latency to first spike (ms)	377.21 ± 28.36	6	270.49 ± 24.55	7	0.0167
Maximum firing frequency (Hz)	152.25 ± 23.94	8	145.43 ± 20.10	7	0.9795 <sup>#</sup>
Action potential threshold (mV)	-31.18 ± 2.65	7	-29.48 ± 4.23	7	> 0.9999 <sup>#</sup>
Action potential amplitude (mV)	46.31 ± 4.98	7	39.44 ± 5.97	7	0.3946
Action potential rise time (ms)	0.58 ± 0.14	7	0.85 ± 0.24	7	0.3518
Action potential decay (ms)	0.75 ± 0.10	7	1.07 ± 0.11	7	0.0495
Action potential halfwidth (ms)	0.55 ± 0.06	7	0.90 ± 0.20	7	0.0728 <sup>#</sup>

**Table 9: Intrinsic properties of Pet+ serotonergic neurons of the dorsal raphe nucleus in control and *Pet-Er81* cKO female mice at P60+**

<i>Pet+</i> Serotonergic Neurons in Female Mice P60+					
Property	Control		<i>Er81</i> cKO		<i>p</i>
	Mean	n	Mean	n	
Resting membrane potential (mV)	-58.67 ± 2.59	5	-57.20 ± 3.64	9	0.7865
Input resistance (MΩ)	529.05 ± 42.52	5	402.59 ± 37.71	9	0.0992 <sup>#</sup>
Sag ratio	0.09 ± 0.02	5	0.02 ± 0.02	9	0.0247
Rheobase (pA)	14.20 ± 5.80	5	37.28 ± 10.51	9	0.1119 <sup>#</sup>
Spike adaptation index	0.40 ± 0.03	5	0.45 ± 0.04	9	0.4107
Action potential threshold (mV)	-40.46 ± 1.37	5	-34.09 ± 1.59	9	0.0203
Action potential amplitude (mV)	62.22 ± 5.17	5	47.45 ± 5.68	9	0.1117
Action potential rise time (ms)	0.52 ± 0.03	5	0.66 ± 0.07	9	0.1722
Action potential decay (ms)	1.90 ± 0.06	5	2.01 ± 0.27	9	0.7713
Action potential halfwidth (ms)	1.80 ± 0.10	5	1.44 ± 0.12	9	0.0621
Action potential fast AHP (mV)	-5.93 ± 1.04	5	-13.59 ± 1.83	9	0.0124
Action potential medium AHP (mV)	-25.71 ± 1.19	5	-21.01 ± 2.09	9	0.1397

**Table 10: Intrinsic properties of Pet+ serotonergic neurons of the dorsal raphe nucleus in control and *Pet-Er81* cKO male mice at P60+**

<i>Pet+</i> Serotonergic Neurons in Male Mice P60+					
Property	Control		<i>Er81</i> cKO		<i>p</i>
	Mean	n	Mean	n	
Resting membrane potential (mV)	-57.54 ± 3.10	12	-60.51 ± 3.24	10	0.6223
Input resistance (MΩ)	454.73 ± 33.59	12	580.35 ± 69.81	10	0.1536
Sag ratio	0.05 ± 0.01	12	0.04 ± 0.01	10	0.5802
Rheobase (pA)	24.47 ± 4.80	11	16.39 ± 3.79	9	0.1943 <sup>#</sup>
Spike adaptation index	0.42 ± 0.04	12	0.39 ± 0.03	10	0.5646
Action potential threshold (mV)	-38.16 ± 0.87	12	-36.91 ± 0.80	10	0.3500
Action potential amplitude (mV)	58.87 ± 4.33	12	60.19 ± 3.63	10	0.9229 <sup>#</sup>
Action potential rise time (ms)	0.58 ± 0.05	12	0.65 ± 0.06	9	0.2276 <sup>#</sup>
Action potential decay (ms)	1.99 ± 0.18	12	1.86 ± 0.12	10	0.6525
Action potential halfwidth (ms)	1.49 ± 0.12	12	1.72 ± 0.17	10	0.2778
Action potential fast AHP (mV)	-13.86 ± 1.13	12	-12.12 ± 2.33	10	0.8718 <sup>#</sup>
Action potential medium AHP (mV)	-20.84 ± 1.55	12	-26.10 ± 1.37	10	0.0221

**Table 11: Intrinsic properties of Lhx6+ striatal cholinergic interneurons in control and *Cntnap2* KO mice at P5-7**

Lhx6+ Cholinergic Interneurons P5-7					
Property	Control		<i>Cntnap2</i> KO		<i>p</i>
	Mean	n	Mean	n	
Resting membrane potential (mV)	-44.90 ± 1.55	16	-47.44 ± 2.27	12	0.368
Input resistance (MΩ)	551.24 ± 60.17	14	408.61 ± 23.79	12	0.049
Membrane capacitance (pF)	596.63 ± 59.82	14	802.39 ± 125.74	12	0.135
Sag ratio	0.27 ± 0.03	10	0.30 ± 0.07	7	0.676
Spike adaptation index	0.60 ± 0.05	14	0.60 ± 0.05	11	0.926
Latency to first spike (ms)	19.64 ± 3.13	14	21.59 ± 3.22	11	0.671
Action potential threshold (mV)	-35.59 ± 1.18	15	-36.58 ± 1.97	12	0.655
Action potential amplitude (mV)	51.95 ± 2.13	15	50.13 ± 3.62	12	0.654
Action potential rise time (ms)	1.07 ± 0.09	15	0.77 ± 0.06	12	0.017
Action potential decay (ms)	2.05 ± 0.01	15	2.02 ± 0.02	12	0.229
Action potential halfwidth (ms)	2.71 ± 0.16	15	2.50 ± 0.14	12	0.347
Action potential fast AHP (mV)	9.02 ± 1.23	15	6.11 ± 1.35	12	0.126
Action potential medium AHP (mV)	-13.77 ± 1.22	15	-13.78 ± 1.00	12	0.993

**Table 12: Intrinsic properties of Lhx6+ striatal GABAergic fast spiking interneurons in control and *Cntnap2* KO mice at P5-7**

Lhx6+ Putative Fast Spiking Interneurons P5-7					
Property	Control		<i>Cntnap2</i> KO		<i>p</i>
	Mean	n	Mean	n	
Resting membrane potential (mV)	-54.45 ± 1.50	22	-53.98 ± 3.09	13	0.880
Input resistance (MΩ)	780.28 ± 75.02	19	406.55 ± 47.03	14	0.0005
Membrane capacitance (pF)	805.33 ± 126.76	19	1064.36 ± 273.87	14	0.357
Latency to first spike (ms)	270.01 ± 35.37	6	315.87 ± 25.58	10	0.303
Action potential threshold (mV)	-35.49 ± 1.43	19	-32.45 ± 1.91	11	0.184
Action potential amplitude (mV)	48.15 ± 1.80	19	44.59 ± 3.43	11	0.320
Action potential rise time (ms)	0.72 ± 0.05	19	0.59 ± 0.05	11	0.078
Action potential decay (ms)	1.80 ± 0.05	19	1.59 ± 0.09	11	0.031
Action potential halfwidth (ms)	1.74 ± 0.12	19	1.22 ± 0.11	11	0.006
Action potential fast AHP (mV)	-2.69 ± 1.72	19	-10.89 ± 1.09	11	0.002
Action potential medium AHP (mV)	-13.15 ± 0.92	19	-15.37 ± 0.70	11	0.105

# Appendix F: Fiji/ImageJ Macros

## 1. Macro for the analysis of Er81 expression in neurons

```
// This macro will analyze Er81 expression in individual whole cells,
//and will then give average nuclear (based on DAPI staining) and cytoplasmic
Er81 expression (i.e. one number for the whole image).
//Expected staining: 1. DAPI 2. GFP (cellular marker) 3. Er81
//Code works based on results being copied and pasted as it is running.
Dialogue boxes will tell you when to paste data into your spreadsheet,
//you can then press OK to progress the macro.

Original=getTitle();
print(Original);
run("Clear Results");
run("Set Measurements...", "mean redirect=None decimal=3");
selectWindow("Log");
print("\\Clear");
print(Original);
selectWindow("Log");
filename = getInfo("log");
String.copy(filename);
print("\\Clear");
waitForUser("Filename is copied, please paste into spreadsheet.\nPress OK to
continue.");
selectWindow(Original);
run("Duplicate...", "duplicate");
imageTitle=getTitle();
run("Split Channels");
selectWindow("C3-"+imageTitle)
run("Duplicate...", " ");
run("Despeckle");
run("Remove Outliers...", "radius=2.5 threshold=50 which=Bright");
Er81=getTitle()
selectWindow("C2-"+imageTitle)
run("Duplicate...", " ");
run("Despeckle");
run("Remove Outliers...", "radius=2.5 threshold=50 which=Bright");
run("Remove Outliers...", "radius=2.5 threshold=50 which=Dark");
run("Duplicate...", " ");
//Percentage threshold code
percentage = 95.00;
nBins = 256;
resetMinAndMax();
getHistogram(values, counts, nBins);
// find cumulative sum
nPixels = 0;
for (i = 0; i<counts.length; i++)
nPixels += counts[i];
nBelowThreshold = nPixels * percentage / 100;
sum = 0;
for (i = 0; i<counts.length; i++) {
sum = sum + counts[i];
if (sum >= nBelowThreshold) {
setThreshold(values[0], values[i]);
print(values[0]+"-"+values[i]+" : "+sum/nPixels*100+"%");
i = 99999999; //break
}
}
run("Convert to Mask");
run("Remove Outliers...", "radius=10 threshold=50 which=Dark");

run("Invert");

run("Analyze Particles...", "size=60-Infinity add");

selectWindow(Er81);
run("Duplicate...", " ");
roiManager("Show All without labels");

roiManager("Measure");
roiManager("Show None");
FinalEr81=getTitle();
selectWindow("Results");
String.copyResults();

waitForUser("Er81 expression in whole cells has been copied.\nPlease paste
results into spreadsheet, then press OK to continue.");
run("Clear Results");

//DAPI

selectWindow("C1-"+imageTitle)
run("Duplicate...", " ");
run("Despeckle");

//Percentage threshold code for DAPI MASK
percentage = 85.00;
nBins = 256;
resetMinAndMax();
getHistogram(values, counts, nBins);
// find cumulative sum
nPixels = 0;
for (i = 0; i<counts.length; i++)
nPixels += counts[i];
nBelowThreshold = nPixels * percentage / 100;
sum = 0;
for (i = 0; i<counts.length; i++) {
sum = sum + counts[i];
if (sum >= nBelowThreshold) {
setThreshold(values[0], values[i]);
print(values[0]+"-"+values[i]+" : "+sum/nPixels*100+"%");
i = 99999999; //break
}
}
run("Convert to Mask");
run("Remove Outliers...", "radius=10 threshold=50 which=Dark");

roiManager("Show All");
roiManager("Combine");

run("Clear Outside");

roiManager("Show None");
run("Select None");
Cytoplasm=getTitle();
//white = cytoplasm

selectWindow("C1-"+imageTitle)
run("Duplicate...", " ");
run("Despeckle");

//Percentage threshold code for DAPI MASK

percentage = 85.00;
nBins = 256;
resetMinAndMax();
getHistogram(values, counts, nBins);
// find cumulative sum
nPixels = 0;
for (i = 0; i<counts.length; i++)
nPixels += counts[i];
nBelowThreshold = nPixels * percentage / 100;
sum = 0;
for (i = 0; i<counts.length; i++) {
sum = sum + counts[i];
if (sum >= nBelowThreshold) {
setThreshold(values[0], values[i]);
print(values[0]+"-"+values[i]+" : "+sum/nPixels*100+"%");
i = 99999999; //break
}
}
run("Convert to Mask");
run("Remove Outliers...", "radius=10 threshold=50 which=Dark");

run("Invert");

roiManager("Show All");
roiManager("Combine");

run("Clear Outside");

roiManager("Show None");
run("Select None");
Nucleus=getTitle();

wait(2000);

//Delete PET cells from final Er81 image for background
selectWindow(FinalEr81);
roiManager("Show All");
roiManager("Combine");
run("Clear");
roiManager("Show None");
run("Select None");

selectWindow("ROI Manager");
run("Close");

selectWindow(Nucleus);
run("Create Selection");
run("Make Inverse");
run("Copy");
selectWindow(Er81);
run("Duplicate...", " ");
run("Paste");
run("Make Inverse");
run("Measure");
run("Select None");

selectWindow(Cytoplasm);
run("Create Selection");
run("Make Inverse");
run("Copy");
selectWindow(Er81);
run("Duplicate...", " ");
run("Paste");
run("Make Inverse");
run("Measure");
run("Select None");

selectWindow("Results")
String.copyResults();

waitForUser("Nuclear and Cytoplasmic Er81 has been copied.\nPlease paste
results into spreadsheet, then press OK to continue.\n1: Nuclear Er81, 2:
Cytoplasmic Er81");
run("Clear Results");

selectWindow(FinalEr81);

makeRectangle(1, 1, 49, 49);
run("Measure");
makeRectangle(1, 970, 49, 49);
run("Measure");
makeRectangle(970, 1, 49, 49);
run("Measure");
selectWindow("Results")
String.copyResults();

waitForUser("Er81 Background copied. Please paste results into spreadsheet,
press OK to continue.");
run("Clear Results");
run("Close All")
```

## 2. Macro for the analysis of neuropil area

```

imageTitle=getTitle();
imageTitle=File.nameWithoutExtension();
run("Duplicate...", "duplicate");
//use VGLuT3 Channel to remove holes
run("Stack to Images");
//Select first image pair and map out dark VGLuT3 areas
selectWindow(imageTitle+"-1-0002")
//Percentage threshold code
percentage = 35.00;
nBins = 256;
resetMinAndMax();
getHistogram(values, counts, nBins);
// find culmulative sum
nPixels = 0;
for (i = 0; i<counts.length; i++)
    nPixels += counts[i];
nBelowThreshold = nPixels * percentage / 100;
sum = 0;
for (i = 0; i<counts.length; i++) {
    sum = sum + counts[i];
    if (sum >= nBelowThreshold) {
        setThreshold(values[0], values[i]);
        print(values[0]+"-"+values[i]+": "+sum/nPixels*100+"%");
        i = 99999999;//break
    }
}
//Analyse dark areas
run("Analyze Particles...", "size=10-Infinity summarize add");
roiManager("Combine");
run("Copy");
selectWindow(imageTitle+"-1-0001")
run("Paste");
run("Clean", "slice");
run("Make Inverse");
//Measure area of interest for percentage.
run("Measure");
selectWindow("ROI Manager");
run("Close");
selectWindow(imageTitle+"-1-0001")
run("Select None");
//Threshold for neuropil
percentage = 90.00;
nBins = 256;
resetMinAndMax();
getHistogram(values, counts, nBins);
// find culmulative sum
nPixels = 0;
for (i = 0; i<counts.length; i++)
    nPixels += counts[i];
nBelowThreshold = nPixels * percentage / 100;
sum = 0;
for (i = 0; i<counts.length; i++) {
    sum = sum + counts[i];
    if (sum >= nBelowThreshold) {
        setThreshold(values[0], values[i]);
        print(values[0]+"-"+values[i]+": "+sum/nPixels*100+"%");
        i = 99999999;//break
    }
}
run("Convert to Mask");
run("Remove Outliers...", "radius=0.75 threshold=50 which=Bright");
run("Invert");
run("Create Selection");
run("Measure");
selectWindow(imageTitle+"-1-0001")
close()
selectWindow(imageTitle+"-1-0002")
close()

//move to second image
selectWindow(imageTitle+"-1-0004")
//Percentage threshold code
percentage = 35.00;
nBins = 256;
resetMinAndMax();
getHistogram(values, counts, nBins);
// find culmulative sum
nPixels = 0;
for (i = 0; i<counts.length; i++)
    nPixels += counts[i];
nBelowThreshold = nPixels * percentage / 100;
sum = 0;
for (i = 0; i<counts.length; i++) {
    sum = sum + counts[i];
    if (sum >= nBelowThreshold) {
        setThreshold(values[0], values[i]);
        print(values[0]+"-"+values[i]+": "+sum/nPixels*100+"%");
        i = 99999999;//break
    }
}
//Analyse dark areas
run("Analyze Particles...", "size=10-Infinity summarize add");
roiManager("Combine");
run("Copy");
selectWindow(imageTitle+"-1-0003")
run("Paste");
run("Clean", "slice");
run("Make Inverse");
//Measure area of interest for percentage.
run("Measure");
selectWindow("ROI Manager");
run("Close");
selectWindow(imageTitle+"-1-0003")
run("Select None");
//Threshold for neuropil
percentage = 90.00;
nBins = 256;
resetMinAndMax();
getHistogram(values, counts, nBins);
// find culmulative sum
nPixels = 0;
for (i = 0; i<counts.length; i++)
    nPixels += counts[i];
nBelowThreshold = nPixels * percentage / 100;
sum = 0;
for (i = 0; i<counts.length; i++) {
    sum = sum + counts[i];
    if (sum >= nBelowThreshold) {
        setThreshold(values[0], values[i]);
        print(values[0]+"-"+values[i]+": "+sum/nPixels*100+"%");
        i = 99999999;//break
    }
}
run("Convert to Mask");
run("Remove Outliers...", "radius=0.75 threshold=50 which=Bright");
run("Invert");
run("Create Selection");
run("Measure");
selectWindow(imageTitle+"-1-0005")
close()
selectWindow(imageTitle+"-1-0006")
close()

selectWindow("Results");
String_copyResults();
close();
run("Close All");
selectWindow("Results");
run("Close");

//Threshold for neuropil
percentage = 90.00;
nBins = 256;
resetMinAndMax();
getHistogram(values, counts, nBins);
// find culmulative sum
nPixels = 0;
for (i = 0; i<counts.length; i++)
    nPixels += counts[i];
nBelowThreshold = nPixels * percentage / 100;
sum = 0;
for (i = 0; i<counts.length; i++) {
    sum = sum + counts[i];
    if (sum >= nBelowThreshold) {
        setThreshold(values[0], values[i]);
        print(values[0]+"-"+values[i]+": "+sum/nPixels*100+"%");
        i = 99999999;//break
    }
}
run("Convert to Mask");
run("Remove Outliers...", "radius=0.75 threshold=50 which=Bright");
run("Invert");
run("Create Selection");
run("Measure");
selectWindow(imageTitle+"-1-0003")
close()
selectWindow(imageTitle+"-1-0004")
close()

//move to third image
selectWindow(imageTitle+"-1-0006")
//Percentage threshold code
percentage = 35.00;
nBins = 256;
resetMinAndMax();
getHistogram(values, counts, nBins);
// find culmulative sum
nPixels = 0;
for (i = 0; i<counts.length; i++)
    nPixels += counts[i];
nBelowThreshold = nPixels * percentage / 100;
sum = 0;
for (i = 0; i<counts.length; i++) {
    sum = sum + counts[i];
    if (sum >= nBelowThreshold) {
        setThreshold(values[0], values[i]);
        print(values[0]+"-"+values[i]+": "+sum/nPixels*100+"%");
        i = 99999999;//break
    }
}
//Analyse dark areas
run("Analyze Particles...", "size=10-Infinity summarize add");
roiManager("Combine");
run("Copy");
selectWindow(imageTitle+"-1-0005")
run("Paste");
run("Clean", "slice");
run("Make Inverse");
//Measure area of interest for percentage.
run("Measure");
selectWindow("ROI Manager");
run("Close");
selectWindow(imageTitle+"-1-0005")
run("Select None");
//Threshold for neuropil
percentage = 90.00;
nBins = 256;
resetMinAndMax();
getHistogram(values, counts, nBins);
// find culmulative sum
nPixels = 0;
for (i = 0; i<counts.length; i++)
    nPixels += counts[i];
nBelowThreshold = nPixels * percentage / 100;
sum = 0;
for (i = 0; i<counts.length; i++) {
    sum = sum + counts[i];
    if (sum >= nBelowThreshold) {
        setThreshold(values[0], values[i]);
        print(values[0]+"-"+values[i]+": "+sum/nPixels*100+"%");
        i = 99999999;//break
    }
}
run("Convert to Mask");
run("Remove Outliers...", "radius=0.75 threshold=50 which=Bright");
run("Invert");
run("Create Selection");
run("Measure");
selectWindow(imageTitle+"-1-0005")
close()
selectWindow(imageTitle+"-1-0006")
close()

selectWindow("Results");
String_copyResults();
close();
run("Close All");
selectWindow("Results");
run("Close");

```

## References

- Abbott, A. E., A. C. Linke, A. Nair, A. Jahedi, L. A. Alba, C. L. Keown, I. Fishman and R. A. Muller (2018). "Repetitive behaviors in autism are linked to imbalance of corticostriatal connectivity: a functional connectivity MRI study." *Soc Cogn Affect Neurosci* **13**(1): 32-42.
- Abe, H., M. Okazawa and S. Nakanishi (2011). "The Etv1/Er81 transcription factor orchestrates activity-dependent gene regulation in the terminal maturation program of cerebellar granule cells." *Proc Natl Acad Sci U S A* **108**(30): 12497-12502.
- Abrahams, B. S. and D. H. Geschwind (2008). "Advances in autism genetics: on the threshold of a new neurobiology." *Nat Rev Genet* **9**(5): 341-355.
- Abudukeyoumu, N., T. Hernandez-Flores, M. Garcia-Munoz and G. W. Arbutnott (2019). "Cholinergic modulation of striatal microcircuits." *Eur J Neurosci* **49**(5): 604-622.
- Ahmed, N. Y., R. Knowles and N. Dehorter (2019). "New Insights Into Cholinergic Neuron Diversity." *Front Mol Neurosci* **12**: 204.
- Ahmed, N. Y., R. Knowles, L. Liu, Y. Yan, X. Li, U. Schumann, Y. Wang, Y. Sontani, N. Reynolds, R. Natoli, J. Wen, I. Del Pino, D. Mi and N. Dehorter (2023). "Developmental deficits of MGE-derived interneurons in the Cntnap2 knockout mouse model of autism spectrum disorder." *Front Cell Dev Biol* **11**: 1112062.
- Ahmed, N. Y., Y. Ranjbar-Slamloo, A. S. Al Abed, L. Gao, Y. Sontani, R. C.-H. c.-G. A, E. Arabzadeh and N. Dehorter (2021). "Er81 Transcription Factor Fine-Tunes Striatal Cholinergic Interneuron Activity and Drives Habit Formation." *J Neurosci* **41**(20): 4392-4409.
- Aishworiya, R., T. Valica, R. Hagerman and B. Restrepo (2022). "An Update on Psychopharmacological Treatment of Autism Spectrum Disorder." *Neurotherapeutics* **19**(1): 248-262.
- Ajram, L. A., J. Horder, M. A. Mendez, A. Galanopoulos, L. P. Brennan, R. H. Wichers, D. M. Robertson, C. M. Murphy, J. Zinkstok, G. Ivin, M. Heasman, D. Meek, M. D. Tricklebank, G. J. Barker, D. J. Lythgoe, R. A. E. Edden, S. C. Williams, D. G. M. Murphy and G. M. McAlonan (2017). "Shifting brain inhibitory balance and connectivity of the prefrontal cortex of adults with autism spectrum disorder." *Transl Psychiatry* **7**(5): e1137.
- Akula, S. K., K. B. McCullough, C. Weichselbaum, J. D. Dougherty and S. E. Maloney (2020). "The trajectory of gait development in mice." *Brain Behav* **10**(6): e01636.
- Alarcon, M., B. S. Abrahams, J. L. Stone, J. A. Duvall, J. V. Perederiy, J. M. Bomar, J. Sebat, M. Wigler, C. L. Martin, D. H. Ledbetter, S. F. Nelson, R. M. Cantor and D. H. Geschwind (2008). "Linkage, association, and gene-expression analyses identify CNTNAP2 as an autism-susceptibility gene." *Am J Hum Genet* **82**(1): 150-159.
- Alegre-Cortes, J., M. Saez, R. Montanari and R. Reig (2021). "Medium spiny neurons activity reveals the discrete segregation of mouse dorsal striatum." *Elife* **10**.
- Allene, C. and R. Cossart (2010). "Early NMDA receptor-driven waves of activity in the developing neocortex: physiological or pathological network oscillations?" *J Physiol* **588**(Pt 1): 83-91.
- Allene, C., M. A. Picardo, H. Becq, G. Miyoshi, G. Fishell and R. Cossart (2012). "Dynamic changes in interneuron morphophysiological properties mark the maturation of hippocampal network activity." *J Neurosci* **32**(19): 6688-6698.
- Anderson, A. G., A. Kulkarni, M. Harper and G. Konopka (2020). "Single-Cell Analysis of Foxp1-Driven Mechanisms Essential for Striatal Development." *Cell Rep* **30**(9): 3051-3066 e3057.
- Andreae, L. C. and J. Burrone (2014). "The role of neuronal activity and transmitter release on synapse formation." *Curr Opin Neurobiol* **27**(100): 47-52.

- Antoine, M. W., T. Langberg, P. Schnepel and D. E. Feldman (2019). "Increased Excitation-Inhibition Ratio Stabilizes Synapse and Circuit Excitability in Four Autism Mouse Models." Neuron **101**(4): 648-661 e644.
- Aosaki, T., M. Miura, T. Suzuki, K. Nishimura and M. Masuda (2010). "Acetylcholine-dopamine balance hypothesis in the striatum: an update." Geriatr Gerontol Int **10 Suppl 1**: S148-157.
- Arber, S., D. R. Ladle, J. H. Lin, E. Frank and T. M. Jessell (2000). "ETS gene Er81 controls the formation of functional connections between group Ia sensory afferents and motor neurons." Cell **101**(5): 485-498.
- Arumugam, H., X. Liu, P. J. Colombo, R. A. Corriveau and A. B. Belousov (2005). "NMDA receptors regulate developmental gap junction uncoupling via CREB signaling." Nat Neurosci **8**(12): 1720-1726.
- Assous, M., D. Dautan, J. M. Tepper and J. Mena-Segovia (2019). "Pedunculopontine Glutamatergic Neurons Provide a Novel Source of Feedforward Inhibition in the Striatum by Selectively Targeting Interneurons." J Neurosci **39**(24): 4727-4737.
- Assous, M., J. Kaminer, F. Shah, A. Garg, T. Koos and J. M. Tepper (2017). "Differential processing of thalamic information via distinct striatal interneuron circuits." Nat Commun **8**: 15860.
- Atallah, H. E., A. D. McCool, M. W. Howe and A. M. Graybiel (2014). "Neurons in the ventral striatum exhibit cell-type-specific representations of outcome during learning." Neuron **82**(5): 1145-1156.
- Aznavour, N., N. Mechawar, K. C. Watkins and L. Descarries (2003). "Fine structural features of the acetylcholine innervation in the developing neostriatum of rat." J Comp Neurol **460**(2): 280-291.
- Bahrami, F. and N. Yousefi (2011). "Females are more anxious than males: a metacognitive perspective." Iran J Psychiatry Behav Sci **5**(2): 83-90.
- Balleine, B. W., M. Liljeholm and S. B. Ostlund (2009). "The integrative function of the basal ganglia in instrumental conditioning." Behav Brain Res **199**(1): 43-52.
- Bang, D., K. T. Kishida, T. Lohrenz, J. P. White, A. W. Laxton, S. B. Tatter, S. M. Fleming and P. R. Montague (2020). "Sub-second Dopamine and Serotonin Signaling in Human Striatum during Perceptual Decision-Making." Neuron **108**(5): 999-1010 e1016.
- Banghart, M. R., S. Q. Neufeld, N. C. Wong and B. L. Sabatini (2015). "Enkephalin Disinhibits Mu Opioid Receptor-Rich Striatal Patches via Delta Opioid Receptors." Neuron **88**(6): 1227-1239.
- Barettino, C., A. Ballesteros-Gonzalez, A. Aylon, X. Soler-Sanchis, L. Orti, S. Diaz, I. Reillo, F. Garcia-Garcia, F. J. Iborra, C. Lai, N. Dehorter, X. Leinekugel, N. Flames and I. Del Pino (2021). "Developmental Disruption of Erbb4 in Pet1+ Neurons Impairs Serotonergic Sub-System Connectivity and Memory Formation." Front Cell Dev Biol **9**: 770458.
- Bassett, D. S., C. H. Xia and T. D. Satterthwaite (2018). "Understanding the Emergence of Neuropsychiatric Disorders With Network Neuroscience." Biol Psychiatry Cogn Neurosci Neuroimaging **3**(9): 742-753.
- Bel, C., K. Oguievetskaia, C. Pitaval, L. Goutebroze and C. Faivre-Sarrailh (2009). "Axonal targeting of Caspr2 in hippocampal neurons via selective somatodendritic endocytosis." J Cell Sci **122**(Pt 18): 3403-3413.
- Belousov, A. B. and J. D. Fontes (2013). "Neuronal gap junctions: making and breaking connections during development and injury." Trends Neurosci **36**(4): 227-236.
- Ben-Ari, Y. (2002). "Excitatory actions of gaba during development: the nature of the nurture." Nat Rev Neurosci **3**(9): 728-739.
- Ben-Ari, Y. (2012). "The Yin and Yen of GABA in Brain Development and Operation in Health and Disease." Front Cell Neurosci **6**: 45.

- Ben-Ari, Y. and E. Lemonnier (2021). "Using bumetanide to treat autism appears promising but further clinical trials are needed to confirm this approach." *Acta Paediatr* **110**(5): 1395-1397.
- Ben-Ari, Y., M. A. Woodin, E. Sernagor, L. Cancedda, L. Vinay, C. Rivera, P. Legendre, H. J. Luhmann, A. Bordey, P. Wenner, A. Fukuda, A. N. van den Pol, J. L. Gaiarsa and E. Cherubini (2012). "Refuting the challenges of the developmental shift of polarity of GABA actions: GABA more exciting than ever!" *Front Cell Neurosci* **6**: 35.
- Berendse, H. W., Y. Galis-de Graaf and H. J. Groenewegen (1992). "Topographical organization and relationship with ventral striatal compartments of prefrontal corticostriatal projections in the rat." *J Comp Neurol* **316**(3): 314-347.
- Bernacer, J., L. Prensa and J. M. Gimenez-Amaya (2007). "Cholinergic interneurons are differentially distributed in the human striatum." *PLoS One* **2**(11): e1174.
- Bertran-Gonzalez, J., B. C. Chieng, V. Laurent, E. Valjent and B. W. Balleine (2012). "Striatal cholinergic interneurons display activity-related phosphorylation of ribosomal protein S6." *PLoS One* **7**(12): e53195.
- Block, A., M. M. Ahmed, A. R. Dhanasekaran, S. Tong and K. J. Gardiner (2015). "Sex differences in protein expression in the mouse brain and their perturbations in a model of Down syndrome." *Biol Sex Differ* **6**: 24.
- Blomeley, C. P. and E. Bracci (2009). "Serotonin excites fast-spiking interneurons in the striatum." *Eur J Neurosci* **29**(8): 1604-1614.
- Blundell, J., C. A. Blaiss, M. R. Etherton, F. Espinosa, K. Tabuchi, C. Walz, M. F. Bolliger, T. C. Sudhof and C. M. Powell (2010). "Neurologin-1 deletion results in impaired spatial memory and increased repetitive behavior." *J Neurosci* **30**(6): 2115-2129.
- Bolam, J. P., J. J. Hanley, P. A. Booth and M. D. Bevan (2000). "Synaptic organisation of the basal ganglia." *J Anat* **196** ( Pt 4): 527-542.
- Bonsi, P., D. Cuomo, J. Ding, G. Sciamanna, S. Ulrich, A. Tscherter, G. Bernardi, D. J. Surmeier and A. Pisani (2007). "Endogenous serotonin excites striatal cholinergic interneurons via the activation of 5-HT<sub>2C</sub>, 5-HT<sub>6</sub>, and 5-HT<sub>7</sub> serotonin receptors: implications for extrapyramidal side effects of serotonin reuptake inhibitors." *Neuropsychopharmacology* **32**(8): 1840-1854.
- Borodinsky, L. N., Y. H. Belgacem, I. Swapna, O. Visina, O. A. Balashova, E. B. Sequerra, M. K. Tu, J. B. Levin, K. A. Spencer, P. A. Castro, A. M. Hamilton and S. Shim (2015). "Spatiotemporal integration of developmental cues in neural development." *Dev Neurobiol* **75**(4): 349-359.
- Borodinsky, L. N., C. M. Root, J. A. Cronin, S. B. Sann, X. Gu and N. C. Spitzer (2004). "Activity-dependent homeostatic specification of transmitter expression in embryonic neurons." *Nature* **429**(6991): 523-530.
- Bosco, A., C. Bureau, P. Affaticati, P. Gaspar, L. Bally-Cuif and C. Lillesaar (2013). "Development of hypothalamic serotonergic neurons requires Fgf signalling via the ETS-domain transcription factor Etv5b." *Development* **140**(2): 372-384.
- Boulting, G. L., E. Duresi, B. Ataman, M. A. Sherman, K. Mei, D. A. Harmin, A. C. Carter, D. R. Hochbaum, A. J. Granger, J. M. Engreitz, S. Hrvatin, M. R. Blanchard, M. G. Yang, E. C. Griffith and M. E. Greenberg (2021). "Activity-dependent regulome of human GABAergic neurons reveals new patterns of gene regulation and neurological disease heritability." *Nat Neurosci* **24**(3): 437-448.
- Bourin, M. and M. Hascoet (2003). "The mouse light/dark box test." *Eur J Pharmacol* **463**(1-3): 55-65.
- Brimblecombe, K. R. and S. J. Cragg (2017). "The Striosome and Matrix Compartments of the Striatum: A Path through the Labyrinth from Neurochemistry toward Function." *ACS Chem Neurosci* **8**(2): 235-242.



- Budry, L., C. Couture, A. Balsalobre and J. Drouin (2011). "The Ets factor Etv1 interacts with Tpit protein for pituitary pro-opiomelanocortin (POMC) gene transcription." J Biol Chem **286**(28): 25387-25396.
- Burrows, E. L., L. Koyama, C. May, E. L. Hill-Yardin and A. J. Hannan (2020). "Environmental enrichment modulates affiliative and aggressive social behaviour in the neuroligin-3 R451C mouse model of autism spectrum disorder." Pharmacol Biochem Behav **195**: 172955.
- Burrows, E. L., L. Laskaris, L. Koyama, L. Churilov, J. C. Bornstein, E. L. Hill-Yardin and A. J. Hannan (2015). "A neuroligin-3 mutation implicated in autism causes abnormal aggression and increases repetitive behavior in mice." Mol Autism **6**: 62.
- Busch, R. M., S. Srivastava, O. Hogue, T. W. Frazier, P. Klaas, A. Hardan, J. A. Martinez-Agosto, M. Sahin, C. Eng and C. Developmental Synaptopathies (2019). "Neurobehavioral phenotype of autism spectrum disorder associated with germline heterozygous mutations in PTEN." Transl Psychiatry **9**(1): 253.
- Butt, S. J., I. Cobos, J. Golden, N. Kessar, V. Pachnis and S. Anderson (2007). "Transcriptional regulation of cortical interneuron development." J Neurosci **27**(44): 11847-11850.
- Butt, S. J., M. Fuccillo, S. Nery, S. Noctor, A. Kriegstein, J. G. Corbin and G. Fishell (2005). "The temporal and spatial origins of cortical interneurons predict their physiological subtype." Neuron **48**(4): 591-604.
- Butt, S. J., V. H. Sousa, M. V. Fuccillo, J. Hjerling-Leffler, G. Miyoshi, S. Kimura and G. Fishell (2008). "The requirement of Nkx2-1 in the temporal specification of cortical interneuron subtypes." Neuron **59**(5): 722-732.
- Caillard, O., H. Moreno, B. Schwaller, I. Llano, M. R. Celio and A. Marty (2000). "Role of the calcium-binding protein parvalbumin in short-term synaptic plasticity." Proc Natl Acad Sci U S A **97**(24): 13372-13377.
- Calabresi, P., B. Picconi, A. Tozzi, V. Ghiglieri and M. Di Filippo (2014). "Direct and indirect pathways of basal ganglia: a critical reappraisal." Nat Neurosci **17**(8): 1022-1030.
- Calderoni, S., M. Bellani, A. Y. Hardan, F. Muratori and P. Brambilla (2014). "Basal ganglia and restricted and repetitive behaviours in Autism Spectrum Disorders: current status and future perspectives." Epidemiol Psychiatr Sci **23**(3): 235-238.
- Cameron, W. E., P. A. Nunez-Abades, I. A. Kerman and T. M. Hodgson (2000). "Role of potassium conductances in determining input resistance of developing brain stem motoneurons." J Neurophysiol **84**(5): 2330-2339.
- Campanac, E., C. Gassel, A. Baude, S. Rama, N. Ankri and D. Debanne (2013). "Enhanced intrinsic excitability in basket cells maintains excitatory-inhibitory balance in hippocampal circuits." Neuron **77**(4): 712-722.
- Canali, G., M. Garcia, B. Hivert, D. Pinatel, A. Goullancourt, K. Oguievetskaia, M. Saint-Martin, J. A. Girault, C. Faivre-Sarrailh and L. Gouttebroze (2018). "Genetic variants in autism-related CNTNAP2 impair axonal growth of cortical neurons." Hum Mol Genet **27**(11): 1941-1954.
- Canitano, R. and R. Palumbi (2021). "Excitation/Inhibition Modulators in Autism Spectrum Disorder: Current Clinical Research." Front Neurosci **15**: 753274.
- Carey, C., N. Singh, J. T. Dunn, T. Sementa, M. A. Mendez, H. Velthuis, A. C. Pereira, C. M. Pretzsch, J. Horder, S. Hader, D. J. Lythgoe, D. G. Rotaru, A. Gee, D. Cash, M. Veronese, D. Murphy and G. McAlonan (2022). "From bench to bedside: The mGluR5 system in people with and without Autism Spectrum Disorder and animal model systems." Transl Psychiatry **12**(1): 395.
- Carlsson, M. and A. Carlsson (1988). "A Regional Study of Sex-Differences in Rat-Brain Serotonin." Progress in Neuro-Psychopharmacology & Biological Psychiatry **12**(1): 53-61.

- Cases, O., T. Vitalis, I. Seif, E. De Maeyer, C. Sotelo and P. Gaspar (1996). "Lack of barrels in the somatosensory cortex of monoamine oxidase A-deficient mice: role of a serotonin excess during the critical period." *Neuron* **16**(2): 297-307.
- Caubit, X., P. Gubellini, J. Andrieux, P. L. Roubertoux, M. Metwaly, B. Jacq, A. Fatmi, L. Had-Aissouni, K. Y. Kwan, P. Salin, M. Carlier, A. Lieden, E. Rudd, M. Shinawi, C. Vincent-Delorme, J. M. Cuisset, M. P. Lemaître, F. Abderrehamane, B. Duban, J. F. Lemaître, A. S. Woolf, D. Bockenhauer, D. Severac, E. Dubois, Y. Zhu, N. Sestan, A. N. Garratt, G. Lydia Kerkerian-Le and L. Fasano (2016). "TSHZ3 deletion causes an autism syndrome and defects in cortical projection neurons." *Nat Genet* **48**(11): 1359-1369.
- Caubit, X., P. Gubellini, P. L. Roubertoux, M. Carlier, J. Molitor, D. Chabbert, M. Metwaly, P. Salin, A. Fatmi, Y. Belaidouni, L. Brosse, L. Kerkerian-Le Goff and L. Fasano (2022). "Targeted Tshz3 deletion in corticostriatal circuit components segregates core autistic behaviors." *Transl Psychiatry* **12**(1): 106.
- Cavaccini, A., M. Gritti, A. Giorgi, A. Locarno, N. Heck, S. Migliarini, A. Bertero, M. Mereu, G. Margiani, M. Trusel, T. Catelani, R. Marotta, M. A. De Luca, J. Caboche, A. Gozzi, M. Pasqualetti and R. Tonini (2018). "Serotonergic Signaling Controls Input-Specific Synaptic Plasticity at Striatal Circuits." *Neuron* **98**(4): 801-816 e807.
- Celada, P., M. V. Puig and F. Artigas (2013). "Serotonin modulation of cortical neurons and networks." *Front Integr Neurosci* **7**: 25.
- Cellot, G. and E. Cherubini (2014). "GABAergic signaling as therapeutic target for autism spectrum disorders." *Front Pediatr* **2**: 70.
- Chang, H. T. and H. Kita (1992). "Interneurons in the rat striatum: relationships between parvalbumin neurons and cholinergic neurons." *Brain Res* **574**(1-2): 307-311.
- Charnay, Y. and L. Leger (2010). "Brain serotonergic circuitries." *Dialogues Clin Neurosci* **12**(4): 471-487.
- Cheadle, L., S. A. Rivera, J. S. Phelps, K. A. Ennis, B. Stevens, L. C. Burkly, W. A. Lee and M. E. Greenberg (2020). "Sensory Experience Engages Microglia to Shape Neural Connectivity through a Non-Phagocytic Mechanism." *Neuron* **108**(3): 451-468 e459.
- Chen, L., M. Chatterjee and J. Y. Li (2010). "The mouse homeobox gene Gbx2 is required for the development of cholinergic interneurons in the striatum." *J Neurosci* **30**(44): 14824-14834.
- Chen, Q. Y., X. H. Li, J. S. Lu, Y. Liu, J. A. Lee, Y. X. Chen, W. Shi, K. Fan and M. Zhuo (2021). "NMDA GluN2C/2D receptors contribute to synaptic regulation and plasticity in the anterior cingulate cortex of adult mice." *Mol Brain* **14**(1): 60.
- Chen, S. Y., K. M. Lu, H. A. Ko, T. H. Huang, J. H. Hao, Y. T. Yan, S. L. Chang, S. M. Evans and F. C. Liu (2020). "Parcellation of the striatal complex into dorsal and ventral districts." *Proc Natl Acad Sci U S A* **117**(13): 7418-7429.
- Chesselet, M. F., J. L. Plotkin, N. Wu and M. S. Levine (2007). "Development of striatal fast-spiking GABAergic interneurons." *Prog Brain Res* **160**: 261-272.
- Cho, H. H., F. Cargnin, Y. Kim, B. Lee, R. J. Kwon, H. Nam, R. Shen, A. P. Barnes, J. W. Lee, S. Lee and S. K. Lee (2014). "Isl1 directly controls a cholinergic neuronal identity in the developing forebrain and spinal cord by forming cell type-specific complexes." *PLoS Genet* **10**(4): e1004280.
- Chou, S. M., K. X. Li, M. Y. Huang, C. Chen, Y. H. Lin King, G. G. Li, W. Zhou, C. F. Teo, Y. N. Jan, L. Y. Jan and S. B. Yang (2021). "Kv1.1 channels regulate early postnatal neurogenesis in mouse hippocampus via the TrkB signaling pathway." *Elife* **10**.
- Clipperton-Allen, A. E., O. S. Cohen, M. Aceti, A. Zucca, J. Levy, J. Ellegood, J. P. Lerch and D. T. Page (2019). "Pten haploinsufficiency disrupts scaling across brain areas during development in mice." *Transl Psychiatry* **9**(1): 329.

- Condorelli, D. F., R. Parenti, F. Spinella, A. Trovato Salinaro, N. Belluardo, V. Cardile and F. Cicirata (1998). "Cloning of a new gap junction gene (Cx36) highly expressed in mammalian brain neurons." *Eur J Neurosci* **10**(3): 1202-1208.
- Contractor, A., I. M. Ethell and C. Portera-Cailliau (2021). "Cortical interneurons in autism." *Nat Neurosci* **24**(12): 1648-1659.
- Cooper, C. D., J. A. Newman, H. Aitkenhead, C. K. Allerston and O. Gileadi (2015). "Structures of the Ets Protein DNA-binding Domains of Transcription Factors Etv1, Etv4, Etv5, and Fev: DETERMINANTS OF DNA BINDING AND REDOX REGULATION BY DISULFIDE BOND FORMATION." *J Biol Chem* **290**(22): 13692-13709.
- Courchesne, E. (2002). "Abnormal early brain development in autism." *Mol Psychiatry* **7 Suppl 2**: S21-23.
- Courchesne, E. (2004). "Brain development in autism: early overgrowth followed by premature arrest of growth." *Ment Retard Dev Disabil Res Rev* **10**(2): 106-111.
- Courchesne, E., C. M. Karns, H. R. Davis, R. Ziccardi, R. A. Carper, Z. D. Tigue, H. J. Chisum, P. Moses, K. Pierce, C. Lord, A. J. Lincoln, S. Pizzo, L. Schreibman, R. H. Haas, N. A. Akshoomoff and R. Y. Courchesne (2001). "Unusual brain growth patterns in early life in patients with autistic disorder: an MRI study." *Neurology* **57**(2): 245-254.
- Cover, K. K. and B. N. Mathur (2021). "Axo-axonic synapses: Diversity in neural circuit function." *J Comp Neurol* **529**(9): 2391-2401.
- Crepel, V., D. Aronov, I. Jorquera, A. Represa, Y. Ben-Ari and R. Cossart (2007). "A parturition-associated nonsynaptic coherent activity pattern in the developing hippocampus." *Neuron* **54**(1): 105-120.
- Crockett, M. J., A. Apergis-Schoute, B. Herrmann, M. D. Lieberman, U. Muller, T. W. Robbins and L. Clark (2013). "Serotonin modulates striatal responses to fairness and retaliation in humans." *J Neurosci* **33**(8): 3505-3513.
- Cruz, C. D. and F. Cruz (2007). "The ERK 1 and 2 pathway in the nervous system: from basic aspects to possible clinical applications in pain and visceral dysfunction." *Curr Neuropharmacol* **5**(4): 244-252.
- Culotta, L. and P. Penzes (2020). "Exploring the mechanisms underlying excitation/inhibition imbalance in human iPSC-derived models of ASD." *Mol Autism* **11**(1): 32.
- Cummings, K., A. Watkins, C. Jones, R. Dias and A. Welham (2022). "Behavioural and psychological features of PTEN mutations: a systematic review of the literature and meta-analysis of the prevalence of autism spectrum disorder characteristics." *J Neurodev Disord* **14**(1): 1.
- Damodaran, S., R. C. Evans and K. T. Blackwell (2014). "Synchronized firing of fast-spiking interneurons is critical to maintain balanced firing between direct and indirect pathway neurons of the striatum." *J Neurophysiol* **111**(4): 836-848.
- Das, A. T., L. Tenenbaum and B. Berkhout (2016). "Tet-On Systems For Doxycycline-inducible Gene Expression." *Curr Gene Ther* **16**(3): 156-167.
- Daubert, E. A. and B. G. Condrón (2010). "Serotonin: a regulator of neuronal morphology and circuitry." *Trends Neurosci* **33**(9): 424-434.
- Dautan, D., I. Huerta-Ocampo, I. B. Witten, K. Deisseroth, J. P. Bolam, T. Gerdjikov and J. Mena-Segovia (2014). "A major external source of cholinergic innervation of the striatum and nucleus accumbens originates in the brainstem." *J Neurosci* **34**(13): 4509-4518.
- Dbouk, H. A., R. M. Mroue, M. E. El-Sabban and R. S. Talhouk (2009). "Connexins: a myriad of functions extending beyond assembly of gap junction channels." *Cell Commun Signal* **7**: 4.
- De Marco Garcia, N. V., T. Karayannis and G. Fishell (2011). "Neuronal activity is required for the development of specific cortical interneuron subtypes." *Nature* **472**(7343): 351-355.

- De Marco Garcia, N. V., R. Priya, S. N. Tuncdemir, G. Fishell and T. Karayannis (2015). "Sensory inputs control the integration of neurogliaform interneurons into cortical circuits." Nat Neurosci **18**(3): 393-401.
- de Wit, J. and A. Ghosh (2016). "Specification of synaptic connectivity by cell surface interactions." Nat Rev Neurosci **17**(1): 22-35.
- Deans, A. E., Y. Z. Wadghiri, O. Aristizabal and D. H. Turnbull (2015). "3D mapping of neuronal migration in the embryonic mouse brain with magnetic resonance microimaging." Neuroimage **114**: 303-310.
- Dehorter, N., G. Ciceri, G. Bartolini, L. Lim, I. del Pino and O. Marin (2015). "Tuning of fast-spiking interneuron properties by an activity-dependent transcriptional switch." Science **349**(6253): 1216-1220.
- Dehorter, N. and I. Del Pino (2020). "Shifting Developmental Trajectories During Critical Periods of Brain Formation." Front Cell Neurosci **14**: 283.
- Dehorter, N., F. J. Michel, T. Marissal, Y. Rotrou, B. Matrot, C. Lopez, M. D. Humphries and C. Hammond (2011). "Onset of Pup Locomotion Coincides with Loss of NR2C/D-Mediated Cortico-Striatal EPSCs and Dampening of Striatal Network Immature Activity." Front Cell Neurosci **5**: 24.
- Dehorter, N., L. Vinay, C. Hammond and Y. Ben-Ari (2012). "Timing of developmental sequences in different brain structures: physiological and pathological implications." Eur J Neurosci **35**(12): 1846-1856.
- Dekkers, M. P., V. Nikolettou and Y. A. Barde (2013). "Cell biology in neuroscience: Death of developing neurons: new insights and implications for connectivity." J Cell Biol **203**(3): 385-393.
- Del Pino, I., B. Rico and O. Marin (2018). "Neural circuit dysfunction in mouse models of neurodevelopmental disorders." Curr Opin Neurobiol **48**: 174-182.
- Denaxa, M., G. Neves, A. Rabinowitz, S. Kemlo, P. Liodis, J. Burrone and V. Pachnis (2018). "Modulation of Apoptosis Controls Inhibitory Interneuron Number in the Cortex." Cell Rep **22**(7): 1710-1721.
- Di Maria, V., M. Moindrot, M. Ryde, A. Bono, L. Quintino and M. Ledri (2020). "Development and Validation of CRISPR Activator Systems for Overexpression of CB1 Receptors in Neurons." Front Mol Neurosci **13**: 168.
- Di Martino, A., D. A. Fair, C. Kelly, T. D. Satterthwaite, F. X. Castellanos, M. E. Thomason, R. C. Craddock, B. Luna, B. L. Leventhal, X. N. Zuo and M. P. Milham (2014). "Unraveling the miswired connectome: a developmental perspective." Neuron **83**(6): 1335-1353.
- Di, Y., Z. Diao, Q. Zheng, J. Li, Q. Cheng, Z. Li, S. Fang, H. Wang, C. Wei, Q. Zheng, Y. Liu, J. Han, Z. Liu, J. Fan, W. Ren and Y. Tian (2022). "Differential Alterations in Striatal Direct and Indirect Pathways Mediate Two Autism-like Behaviors in Valproate-Exposed Mice." J Neurosci **42**(41): 7833-7847.
- Dillman, A. A. and M. R. Cookson (2014). "Transcriptomic changes in brain development." Int Rev Neurobiol **116**: 233-250.
- Ding, B., J. W. Cave, P. R. Dobner, D. Mullikin-Kilpatrick, M. Bartzokis, H. Zhu, C. W. Chow, R. M. Gronostajski and D. L. Kilpatrick (2016). "Reciprocal autoregulation by NFI occupancy and ETV1 promotes the developmental expression of dendrite-synapse genes in cerebellar granule neurons." Mol Biol Cell **27**(9): 1488-1499.
- Ding, S. L., J. J. Royall, P. Lesnar, B. A. C. Facer, K. A. Smith, Y. Wei, K. Brouner, R. A. Dalley, N. Dee, T. A. Dolbeare, A. Ebbert, I. A. Glass, N. H. Keller, F. Lee, T. A. Lemon, J. Nyhus, J. Pendergraft, R. Reid, M. Sarreal, N. V. Shapovalova, A. Szafer, J. W. Phillips, S. M. Sunkin, J. G. Hohmann, A. R. Jones, M. J. Hawrylycz, P. R. Hof, L. Ng, A. Bernard

- and E. S. Lein (2022). "Cellular resolution anatomical and molecular atlases for prenatal human brains." J Comp Neurol **530**(1): 6-503.
- Dixon, C., P. Sah, J. W. Lynch and A. Keramidas (2014). "GABAA receptor alpha and gamma subunits shape synaptic currents via different mechanisms." J Biol Chem **289**(9): 5399-5411.
- Doig, N. M., P. J. Magill, P. Apicella, J. P. Bolam and A. Sharott (2014). "Cortical and thalamic excitation mediate the multiphasic responses of striatal cholinergic interneurons to motivationally salient stimuli." J Neurosci **34**(8): 3101-3117.
- Dorst, M. C., A. Tokarska, M. Zhou, K. Lee, S. Stagkourakis, C. Broberger, S. Masmanidis and G. Silberberg (2020). "Polysynaptic inhibition between striatal cholinergic interneurons shapes their network activity patterns in a dopamine-dependent manner." Nat Commun **11**(1): 5113.
- Duflocq, A., F. Chareyre, M. Giovannini, F. Couraud and M. Davenne (2011). "Characterization of the axon initial segment (AIS) of motor neurons and identification of a para-AIS and a juxtapara-AIS, organized by protein 4.1B." BMC Biol **9**: 66.
- Dunn, A. R. and C. C. Kaczorowski (2019). "Regulation of intrinsic excitability: Roles for learning and memory, aging and Alzheimer's disease, and genetic diversity." Neurobiol Learn Mem **164**: 107069.
- Egger, G., K. M. Roetzer, A. Noor, A. C. Lionel, H. Mahmood, T. Schwarzbraun, O. Boright, A. Mikhailov, C. R. Marshall, C. Windpassinger, E. Petek, S. W. Scherer, W. Kaschnitz and J. B. Vincent (2014). "Identification of risk genes for autism spectrum disorder through copy number variation analysis in Austrian families." Neurogenetics **15**(2): 117-127.
- Ehlinger, D. G., J. C. Burke, C. G. McDonald, R. F. Smith and H. C. Bergstrom (2017). "Nicotine-induced and D1-receptor-dependent dendritic remodeling in a subset of dorsolateral striatum medium spiny neurons." Neuroscience **356**: 242-254.
- Eid, W. and W. Abdel-Rehim (2019). "Genome-wide analysis of ETV1 targets: Insights into the role of ETV1 in tumor progression." J Cell Biochem **120**(6): 8983-8991.
- English, D. F., O. Ibanez-Sandoval, E. Stark, F. Tecuapetla, G. Buzsaki, K. Deisseroth, J. M. Tepper and T. Koos (2011). "GABAergic circuits mediate the reinforcement-related signals of striatal cholinergic interneurons." Nat Neurosci **15**(1): 123-130.
- Eugenin, E. A., D. Basilio, J. C. Saez, J. A. Orellana, C. S. Raine, F. Bukauskas, M. V. Bennett and J. W. Berman (2012). "The role of gap junction channels during physiologic and pathologic conditions of the human central nervous system." J Neuroimmune Pharmacol **7**(3): 499-518.
- Ewald, R. C. and H. T. Cline (2009). NMDA Receptors and Brain Development. Biology of the NMDA Receptor. A. M. Van Dongen. Boca Raton (FL).
- Fatemi, S. H., T. J. Reutiman, T. D. Folsom and P. D. Thuras (2009). "GABA(A) receptor downregulation in brains of subjects with autism." J Autism Dev Disord **39**(2): 223-230.
- Faust, T. E., G. Gunner and D. P. Schafer (2021). "Mechanisms governing activity-dependent synaptic pruning in the developing mammalian CNS." Nat Rev Neurosci **22**(11): 657-673.
- Favuzzi, E. and B. Rico (2018). "Molecular diversity underlying cortical excitatory and inhibitory synapse development." Curr Opin Neurobiol **53**: 8-15.
- Ferguson, B. R. and W. J. Gao (2018). "PV Interneurons: Critical Regulators of E/I Balance for Prefrontal Cortex-Dependent Behavior and Psychiatric Disorders." Front Neural Circuits **12**: 37.
- Ferrer, I., E. Bernet, E. Soriano, T. del Rio and M. Fonseca (1990). "Naturally occurring cell death in the cerebral cortex of the rat and removal of dead cells by transitory phagocytes." Neuroscience **39**(2): 451-458.
- Filice, F., K. J. Vorckel, A. O. Sungur, M. Wöhr and B. Schwaller (2016). "Reduction in parvalbumin expression not loss of the parvalbumin-expressing GABA interneuron

- subpopulation in genetic parvalbumin and shank mouse models of autism." Mol Brain **9**: 10.
- Fishell, G. and B. Rudy (2011). "Mechanisms of inhibition within the telencephalon: "where the wild things are"." Annu Rev Neurosci **34**: 535-567.
- Fiszman, M. L., L. N. Borodinsky and J. H. Neale (1999). "GABA induces proliferation of immature cerebellar granule cells grown in vitro." Brain Res Dev Brain Res **115**(1): 1-8.
- Flames, N. and O. Hobert (2009). "Gene regulatory logic of dopamine neuron differentiation." Nature **458**(7240): 885-889.
- Flames, N., R. Pla, D. M. Gelman, J. L. Rubenstein, L. Puelles and O. Marin (2007). "Delineation of multiple subpallial progenitor domains by the combinatorial expression of transcriptional codes." J Neurosci **27**(36): 9682-9695.
- Flavell, S. W. and M. E. Greenberg (2008). "Signaling mechanisms linking neuronal activity to gene expression and plasticity of the nervous system." Annu Rev Neurosci **31**: 563-590.
- Fleiss, B., S. A. Rivkees and P. Gressens (2019). "Early origins of neuropsychiatric disorders." Pediatr Res **85**(2): 113-114.
- Fox, S. E., P. Levitt and C. A. Nelson, 3rd (2010). "How the timing and quality of early experiences influence the development of brain architecture." Child Dev **81**(1): 28-40.
- Fragkouli, A., N. V. van Wijk, R. Lopes, N. Kessar and V. Pachnis (2009). "LIM homeodomain transcription factor-dependent specification of bipotential MGE progenitors into cholinergic and GABAergic striatal interneurons." Development **136**(22): 3841-3851.
- Fricker, M., A. M. Tolkovsky, V. Borutaite, M. Coleman and G. C. Brown (2018). "Neuronal Cell Death." Physiol Rev **98**(2): 813-880.
- Fuccillo, M. V. (2016). "Striatal Circuits as a Common Node for Autism Pathophysiology." Front Neurosci **10**: 27.
- Fukuda, T. (2009). "Network architecture of gap junction-coupled neuronal linkage in the striatum." J Neurosci **29**(4): 1235-1243.
- Gadsby, D. C., A. L. Wit and P. F. Cranefield (1978). "The effects of acetylcholine on the electrical activity of canine cardiac Purkinje fibers." Circ Res **43**(1): 29-35.
- Galarreta, M. and S. Hestrin (2001). "Electrical synapses between GABA-releasing interneurons." Nat Rev Neurosci **2**(6): 425-433.
- Gandhi, T. and C. C. Lee (2020). "Neural Mechanisms Underlying Repetitive Behaviors in Rodent Models of Autism Spectrum Disorders." Front Cell Neurosci **14**: 592710.
- Gao, R., N. H. Piguél, A. E. Melendez-Zaidi, M. D. Martin-de-Saavedra, S. Yoon, M. P. Forrest, K. Myczek, G. Zhang, T. A. Russell, J. G. Csernansky, D. J. Surmeier and P. Penzes (2018). "CNTNAP2 stabilizes interneuron dendritic arbors through CASK." Mol Psychiatry **23**(9): 1832-1850.
- Gaspar, P., O. Cases and L. Maroteaux (2003). "The developmental role of serotonin: news from mouse molecular genetics." Nat Rev Neurosci **4**(12): 1002-1012.
- Gatto, C. L. and K. Broadie (2010). "Genetic controls balancing excitatory and inhibitory synaptogenesis in neurodevelopmental disorder models." Front Synaptic Neurosci **2**: 4.
- Gelman, D., A. Griveau, N. Dehorter, A. Teissier, C. Varela, R. Pla, A. Pierani and O. Marin (2011). "A wide diversity of cortical GABAergic interneurons derives from the embryonic preoptic area." J Neurosci **31**(46): 16570-16580.
- Ghiretti, A. E. and S. Paradis (2014). "Molecular mechanisms of activity-dependent changes in dendritic morphology: role of RGK proteins." Trends Neurosci **37**(7): 399-407.
- Ghosh, M. and D. D. Pearse (2014). "The role of the serotonergic system in locomotor recovery after spinal cord injury." Front Neural Circuits **8**: 151.
- Gittis, A. H. and A. C. Kreitzer (2012). "Striatal microcircuitry and movement disorders." Trends Neurosci **35**(9): 557-564.

- Gittis, A. H., A. B. Nelson, M. T. Thwin, J. J. Palop and A. C. Kreitzer (2010). "Distinct roles of GABAergic interneurons in the regulation of striatal output pathways." J Neurosci **30**(6): 2223-2234.
- Goodfellow, N. M., M. Benekareddy, V. A. Vaidya and E. K. Lambe (2009). "Layer II/III of the prefrontal cortex: Inhibition by the serotonin 5-HT1A receptor in development and stress." J Neurosci **29**(32): 10094-10103.
- Goos, H., M. Kinnunen, K. Salokas, Z. Tan, X. Liu, L. Yadav, Q. Zhang, G. H. Wei and M. Varjosalo (2022). "Human transcription factor protein interaction networks." Nat Commun **13**(1): 766.
- Graybiel, A. M. and S. T. Grafton (2015). "The striatum: where skills and habits meet." Cold Spring Harb Perspect Biol **7**(8): a021691.
- Greenwood, B. N., P. V. Strong, A. B. Loughridge, H. E. Day, P. J. Clark, A. Mika, J. E. Hellwinkel, K. G. Spence and M. Fleshner (2012). "5-HT2C receptors in the basolateral amygdala and dorsal striatum are a novel target for the anxiolytic and antidepressant effects of exercise." PLoS One **7**(9): e46118.
- Griguoli, M. and E. Cherubini (2017). "Early Correlated Network Activity in the Hippocampus: Its Putative Role in Shaping Neuronal Circuits." Front Cell Neurosci **11**: 255.
- Gritton, H. J., W. M. Howe, M. F. Romano, A. G. DiFeliceantonio, M. A. Kramer, V. Saligrama, M. E. Bucklin, D. Zemel and X. Han (2019). "Unique contributions of parvalbumin and cholinergic interneurons in organizing striatal networks during movement." Nat Neurosci **22**(4): 586-597.
- Guo, J. and E. S. Anton (2014). "Decision making during interneuron migration in the developing cerebral cortex." Trends Cell Biol **24**(6): 342-351.
- Guo, Q., D. Wang, X. He, Q. Feng, R. Lin, F. Xu, L. Fu and M. Luo (2015). "Whole-brain mapping of inputs to projection neurons and cholinergic interneurons in the dorsal striatum." PLoS One **10**(4): e0123381.
- Ha, S., I. J. Sohn, N. Kim, H. J. Sim and K. A. Cheon (2015). "Characteristics of Brains in Autism Spectrum Disorder: Structure, Function and Connectivity across the Lifespan." Exp Neurobiol **24**(4): 273-284.
- Haas, J. S., C. M. Greenwald and A. E. Pereda (2016). "Activity-dependent plasticity of electrical synapses: increasing evidence for its presence and functional roles in the mammalian brain." BMC Cell Biol **17 Suppl 1**(Suppl 1): 14.
- Handen, B. L., C. R. Johnson, S. McAuliffe-Bellin, P. J. Murray and A. Y. Hardan (2011). "Safety and efficacy of donepezil in children and adolescents with autism: neuropsychological measures." J Child Adolesc Psychopharmacol **21**(1): 43-50.
- Hausdorff, J. M. (2009). "Gait dynamics in Parkinson's disease: common and distinct behavior among stride length, gait variability, and fractal-like scaling." Chaos **19**(2): 026113.
- Hazlett, H. C., H. Gu, B. C. Munsell, S. H. Kim, M. Styner, J. J. Wolff, J. T. Elison, M. R. Swanson, H. Zhu, K. N. Botteron, D. L. Collins, J. N. Constantino, S. R. Dager, A. M. Estes, A. C. Evans, V. S. Fonov, G. Gerig, P. Kostopoulos, R. C. McKinstry, J. Pandey, S. Paterson, J. R. Pruett, R. T. Schultz, D. W. Shaw, L. Zwaigenbaum, J. Piven, I. Network, S. Clinical, C. Data Coordinating, C. Image Processing and A. Statistical (2017). "Early brain development in infants at high risk for autism spectrum disorder." Nature **542**(7641): 348-351.
- He, H. Y. and H. T. Cline (2019). "What Is Excitation/Inhibition and How Is It Regulated? A Case of the Elephant and the Wisemen." J Exp Neurosci **13**: 1179069519859371.
- He, S., Z. Li, S. Ge, Y. C. Yu and S. H. Shi (2015). "Inside-Out Radial Migration Facilitates Lineage-Dependent Neocortical Microcircuit Assembly." Neuron **86**(5): 1159-1166.

- Hendricks, T., N. Francis, D. Fyodorov and E. S. Deneris (1999). "The ETS domain factor Pet-1 is an early and precise marker of central serotonin neurons and interacts with a conserved element in serotonergic genes." *J Neurosci* **19**(23): 10348-10356.
- Heumann, D. and G. Leuba (1983). "Neuronal death in the development and aging of the cerebral cortex of the mouse." *Neuropathol Appl Neurobiol* **9**(4): 297-311.
- Hienert, M., G. Gryglewski, M. Stamenkovic, S. Kasper and R. Lanzenberger (2018). "Striatal dopaminergic alterations in Tourette's syndrome: a meta-analysis based on 16 PET and SPECT neuroimaging studies." *Transl Psychiatry* **8**(1): 143.
- Higley, M. J., A. H. Gittis, I. A. Oldenburg, N. Balthasar, R. P. Seal, R. H. Edwards, B. B. Lowell, A. C. Kreitzer and B. L. Sabatini (2011). "Cholinergic interneurons mediate fast VGluT3-dependent glutamatergic transmission in the striatum." *PLoS One* **6**(4): e19155.
- Hippenmeyer, S., E. Vrieseling, M. Sigrist, T. Portmann, C. Laengle, D. R. Ladle and S. Arber (2005). "A developmental switch in the response of DRG neurons to ETS transcription factor signaling." *PLoS Biol* **3**(5): e159.
- Hjorth, J., K. T. Blackwell and J. H. Kotaleski (2009). "Gap junctions between striatal fast-spiking interneurons regulate spiking activity and synchronization as a function of cortical activity." *J Neurosci* **29**(16): 5276-5286.
- Hobert, O., I. Carrera and N. Stefanakis (2010). "The molecular and gene regulatory signature of a neuron." *Trends Neurosci* **33**(10): 435-445.
- Hoch, R. V., J. A. Clarke and J. L. Rubenstein (2015). "Fgf signaling controls the telencephalic distribution of Fgf-expressing progenitors generated in the rostral patterning center." *Neural Dev* **10**: 8.
- Hollenhorst, P. C. (2012). "RAS/ERK pathway transcriptional regulation through ETS/AP-1 binding sites." *Small GTPases* **3**(3): 154-158.
- Hollville, E., S. E. Romero and M. Deshmukh (2019). "Apoptotic cell death regulation in neurons." *FEBS J* **286**(17): 3276-3298.
- Hou, G. and Z. W. Zhang (2017). "NMDA Receptors Regulate the Development of Neuronal Intrinsic Excitability through Cell-Autonomous Mechanisms." *Front Cell Neurosci* **11**: 353.
- Huang, K. W., N. E. Ochandarena, A. C. Philson, M. Hyun, J. E. Birnbaum, M. Cicconet and B. L. Sabatini (2019). "Molecular and anatomical organization of the dorsal raphe nucleus." *Elife* **8**.
- Hunnicutt, B. J., B. C. Jongbloets, W. T. Birdsong, K. J. Gertz, H. Zhong and T. Mao (2016). "A comprehensive excitatory input map of the striatum reveals novel functional organization." *Elife* **5**.
- Hussman, J. P., R. H. Chung, A. J. Griswold, J. M. Jaworski, D. Salyakina, D. Ma, I. Konidari, P. L. Whitehead, J. M. Vance, E. R. Martin, M. L. Cuccaro, J. R. Gilbert, J. L. Haines and M. A. Pericak-Vance (2011). "A noise-reduction GWAS analysis implicates altered regulation of neurite outgrowth and guidance in autism." *Mol Autism* **2**(1): 1.
- Ito-Ishida, A., K. Ure, H. Chen, J. W. Swann and H. Y. Zoghbi (2015). "Loss of MeCP2 in Parvalbumin- and Somatostatin-Expressing Neurons in Mice Leads to Distinct Rett Syndrome-like Phenotypes." *Neuron* **88**(4): 651-658.
- Ito, M. and K. Doya (2015). "Distinct neural representation in the dorsolateral, dorsomedial, and ventral parts of the striatum during fixed- and free-choice tasks." *J Neurosci* **35**(8): 3499-3514.
- Jabaudon, D. (2017). "Fate and freedom in developing neocortical circuits." *Nat Commun* **8**: 16042.
- Jabeen, S. and V. Thirumalai (2018). "The interplay between electrical and chemical synaptogenesis." *J Neurophysiol* **120**(4): 1914-1922.



- Jan, Y. N. and L. Y. Jan (2010). "Branching out: mechanisms of dendritic arborization." Nat Rev Neurosci **11**(5): 316-328.
- Janknecht, R. (1996). "Analysis of the ERK-stimulated ETS transcription factor ER81." Mol Cell Biol **16**(4): 1550-1556.
- Jing, P. B., X. H. Chen, H. J. Lu, Y. J. Gao and X. B. Wu (2022). "Enhanced function of NR2C/2D-containing NMDA receptor in the nucleus accumbens contributes to peripheral nerve injury-induced neuropathic pain and depression in mice." Mol Pain **18**: 17448069211053255.
- Johnson, M. H. (2017). "Autism as an adaptive common variant pathway for human brain development." Dev Cogn Neurosci **25**: 5-11.
- Jones, M. D. and I. Lucki (2005). "Sex differences in the regulation of serotonergic transmission and behavior in 5-HT receptor knockout mice." Neuropsychopharmacology **30**(6): 1039-1047.
- Kalb, R. G. (1994). "Regulation of motor neuron dendrite growth by NMDA receptor activation." Development **120**(11): 3063-3071.
- Kao, C. F. and T. Lee (2010). "Birth time/order-dependent neuron type specification." Curr Opin Neurobiol **20**(1): 14-21.
- Karvat, G. and T. Kimchi (2014). "Acetylcholine elevation relieves cognitive rigidity and social deficiency in a mouse model of autism." Neuropsychopharmacology **39**(4): 831-840.
- Kassam, S. M., P. M. Herman, N. M. Goodfellow, N. C. Alves and E. K. Lambe (2008). "Developmental excitation of corticothalamic neurons by nicotinic acetylcholine receptors." J Neurosci **28**(35): 8756-8764.
- Kasyanov, A. M., V. F. Safiulina, L. L. Voronin and E. Cherubini (2004). "GABA-mediated giant depolarizing potentials as coincidence detectors for enhancing synaptic efficacy in the developing hippocampus." Proc Natl Acad Sci U S A **101**(11): 3967-3972.
- Kawauchi, T. (2015). "Cellular insights into cerebral cortical development: focusing on the locomotion mode of neuronal migration." Front Cell Neurosci **9**: 394.
- Kazdoba, T. M., P. T. Leach, M. Yang, J. L. Silverman, M. Solomon and J. N. Crawley (2016). "Translational Mouse Models of Autism: Advancing Toward Pharmacological Therapeutics." Curr Top Behav Neurosci **28**: 1-52.
- Kepecs, A. and G. Fishell (2014). "Interneuron cell types are fit to function." Nature **505**(7483): 318-326.
- Kernell, D. (1966). "Input resistance, electrical excitability, and size of ventral horn cells in cat spinal cord." Science **152**(3729): 1637-1640.
- Kerschensteiner, D. (2014). "Spontaneous Network Activity and Synaptic Development." Neuroscientist **20**(3): 272-290.
- Khandelwal, N., S. Cavalier, V. Rybalchenko, A. Kulkarni, A. G. Anderson, G. Konopka and J. R. Gibson (2021). "FOXP1 negatively regulates intrinsic excitability in D2 striatal projection neurons by promoting inwardly rectifying and leak potassium currents." Mol Psychiatry **26**(6): 1761-1774.
- Kim, S., H. Kim and J. W. Um (2018). "Synapse development organized by neuronal activity-regulated immediate-early genes." Exp Mol Med **50**(4): 1-7.
- Kim, T., R. A. Capps, K. C. Hamade, W. H. Barnett, D. I. Todorov, E. M. Latash, S. N. Markin, I. A. Rybak and Y. I. Molkov (2019). "The Functional Role of Striatal Cholinergic Interneurons in Reinforcement Learning From Computational Perspective." Front Neural Circuits **13**: 10.
- Klaus, A., H. Planert, J. J. Hjorth, J. D. Berke, G. Silberberg and J. H. Kotaleski (2011). "Striatal fast-spiking interneurons: from firing patterns to postsynaptic impact." Front Syst Neurosci **5**: 57.

- Klug, J. R., M. D. Engelhardt, C. N. Cadman, H. Li, J. B. Smith, S. Ayala, E. W. Williams, H. Hoffman and X. Jin (2018). "Differential inputs to striatal cholinergic and parvalbumin interneurons imply functional distinctions." *Elife* **7**.
- Knowles, R., N. Dehorter and T. Ellender (2021). "From Progenitors to Progeny: Shaping Striatal Circuit Development and Function." *J Neurosci* **41**(46): 9483-9502.
- Ko, K. W., M. N. Rasband, V. Meseguer, R. H. Kramer and N. L. Golding (2016). "Serotonin modulates spike probability in the axon initial segment through HCN channels." *Nat Neurosci* **19**(6): 826-834.
- Kohls, G., L. Antezana, M. G. Mosner, R. T. Schultz and B. E. Yerys (2018). "Altered reward system reactivity for personalized circumscribed interests in autism." *Mol Autism* **9**: 9.
- Kohls, G., B. E. Yerys and R. T. Schultz (2014). "Striatal development in autism: repetitive behaviors and the reward circuitry." *Biol Psychiatry* **76**(5): 358-359.
- Kolb, B. and R. Gibb (2011). "Brain plasticity and behaviour in the developing brain." *J Can Acad Child Adolesc Psychiatry* **20**(4): 265-276.
- Koos, T. and J. M. Tepper (1999). "Inhibitory control of neostriatal projection neurons by GABAergic interneurons." *Nat Neurosci* **2**(5): 467-472.
- Koos, T. and J. M. Tepper (2002). "Dual cholinergic control of fast-spiking interneurons in the neostriatum." *J Neurosci* **22**(2): 529-535.
- Kuo, H. Y. and F. C. Liu (2020). "Pathological alterations in striatal compartments in the human brain of autism spectrum disorder." *Mol Brain* **13**(1): 83.
- Labonte, B., O. Engmann, I. Purushothaman, C. Menard, J. Wang, C. Tan, J. R. Scarpa, G. Moy, Y. E. Loh, M. Cahill, Z. S. Lorsch, P. J. Hamilton, E. S. Calipari, G. E. Hodes, O. Issler, H. Kronman, M. Pfau, A. L. J. Obradovic, Y. Dong, R. L. Neve, S. Russo, A. Kazarskis, C. Tamminga, N. Mechawar, G. Turecki, B. Zhang, L. Shen and E. J. Nestler (2017). "Sex-specific transcriptional signatures in human depression." *Nat Med* **23**(9): 1102-1111.
- Langen, M., D. Bos, S. D. Noordermeer, H. Nederveen, H. van Engeland and S. Durston (2014). "Changes in the development of striatum are involved in repetitive behavior in autism." *Biol Psychiatry* **76**(5): 405-411.
- Langen, M., H. G. Schnack, H. Nederveen, D. Bos, B. E. Lahuis, M. V. de Jonge, H. van Engeland and S. Durston (2009). "Changes in the developmental trajectories of striatum in autism." *Biol Psychiatry* **66**(4): 327-333.
- Lauber, E., F. Filice and B. Schwaller (2018). "Dysregulation of Parvalbumin Expression in the Cntnap2<sup>-/-</sup> Mouse Model of Autism Spectrum Disorder." *Front Mol Neurosci* **11**: 262.
- Lebouc, M., Q. Richard, M. Garret and J. Baufreton (2020). "Striatal circuit development and its alterations in Huntington's disease." *Neurobiol Dis* **145**: 105076.
- Lee, A., H. Choo and B. Jeon (2022). "Serotonin Receptors as Therapeutic Targets for Autism Spectrum Disorder Treatment." *Int J Mol Sci* **23**(12).
- Lemonnier, E., C. Degrez, M. Phelep, R. Tyzio, F. Josse, M. Grandgeorge, N. Hadjikhani and Y. Ben-Ari (2012). "A randomised controlled trial of bumetanide in the treatment of autism in children." *Transl Psychiatry* **2**(12): e202.
- Lenroot, R. K. and P. K. Yeung (2013). "Heterogeneity within Autism Spectrum Disorders: What have We Learned from Neuroimaging Studies?" *Front Hum Neurosci* **7**: 733.
- Lerner, T. N. and A. C. Kreitzer (2011). "Neuromodulatory control of striatal plasticity and behavior." *Curr Opin Neurobiol* **21**(2): 322-327.
- Li, K., K. Figarella, X. Su, Y. Kovalchuk, J. Gorzolka, J. J. Neher, N. Mojtahedi, N. Casadei, U. B. S. Hedrich and O. Garaschuk (2023). "Endogenous but not sensory-driven activity controls migration, morphogenesis and survival of adult-born juxtglomerular neurons in the mouse olfactory bulb." *Cell Mol Life Sci* **80**(4): 98.

- Li, S., P. Mattar, R. Dixit, S. O. Lawn, G. Wilkinson, C. Kinch, D. Eisenstat, D. M. Kurrasch, J. A. Chan and C. Schuurmans (2014). "RAS/ERK signaling controls proneural genetic programs in cortical development and gliomagenesis." *J Neurosci* **34**(6): 2169-2190.
- Li, W. and L. Pozzo-Miller (2020). "Dysfunction of the corticostriatal pathway in autism spectrum disorders." *J Neurosci Res* **98**(11): 2130-2147.
- Lim, L., D. Mi, A. Llorca and O. Marin (2018). "Development and Functional Diversification of Cortical Interneurons." *Neuron* **100**(2): 294-313.
- Lim, M., A. Carollo, D. Dimitriou and G. Esposito (2022). "Recent Developments in Autism Genetic Research: A Scientometric Review from 2018 to 2022." *Genes (Basel)* **13**(9).
- Lim, S. A., U. J. Kang and D. S. McGehee (2014). "Striatal cholinergic interneuron regulation and circuit effects." *Front Synaptic Neurosci* **6**: 22.
- Lin, Y., X. J. Zhang, J. Yang, S. Li, L. Li, X. Lv, J. Ma and S. H. Shi (2023). "Developmental neuronal origin regulates neocortical map formation." *Cell Rep* **42**(3): 112170.
- Liodis, P., M. Denaxa, M. Grigoriou, C. Akufo-Addo, Y. Yanagawa and V. Pachnis (2007). "Lhx6 activity is required for the normal migration and specification of cortical interneuron subtypes." *J Neurosci* **27**(12): 3078-3089.
- Lipton, D. M., B. J. Gonzales and A. Citri (2019). "Dorsal Striatal Circuits for Habits, Compulsions and Addictions." *Front Syst Neurosci* **13**: 28.
- Liu, C., T. Maejima, S. C. Wyler, G. Casadesus, S. Herlitze and E. S. Deneris (2010). "Pet-1 is required across different stages of life to regulate serotonergic function." *Nat Neurosci* **13**(10): 1190-1198.
- Liu, X., Q. Wang, T. F. Haydar and A. Bordey (2005). "Nonsynaptic GABA signaling in postnatal subventricular zone controls proliferation of GFAP-expressing progenitors." *Nat Neurosci* **8**(9): 1179-1187.
- Lloret-Fernandez, C., M. Maicas, C. Mora-Martinez, A. Artacho, A. Jimeno-Martin, L. Chirivella, P. Weinberg and N. Flames (2018). "A transcription factor collective defines the HSN serotonergic neuron regulatory landscape." *Elife* **7**.
- Lo, S. Q., J. C. G. Sng and G. J. Augustine (2017). "Defining a critical period for inhibitory circuits within the somatosensory cortex." *Sci Rep* **7**(1): 7271.
- Long, Z., X. Duan, D. Mantini and H. Chen (2016). "Alteration of functional connectivity in autism spectrum disorder: effect of age and anatomical distance." *Sci Rep* **6**: 26527.
- Lopes-Ramos, C. M., C. Y. Chen, M. L. Kuijjer, J. N. Paulson, A. R. Sonawane, M. Fagny, J. Platig, K. Glass, J. Quackenbush and D. L. DeMeo (2020). "Sex Differences in Gene Expression and Regulatory Networks across 29 Human Tissues." *Cell Rep* **31**(12): 107795.
- Lopes, R., N. Verhey van Wijk, G. Neves and V. Pachnis (2012). "Transcription factor LIM homeobox 7 (Lhx7) maintains subtype identity of cholinergic interneurons in the mammalian striatum." *Proc Natl Acad Sci U S A* **109**(8): 3119-3124.
- Lossi, L., C. Castagna and A. Merighi (2018). "Caspase-3 Mediated Cell Death in the Normal Development of the Mammalian Cerebellum." *Int J Mol Sci* **19**(12).
- LoTurco, J. J., D. F. Owens, M. J. Heath, M. B. Davis and A. R. Kriegstein (1995). "GABA and glutamate depolarize cortical progenitor cells and inhibit DNA synthesis." *Neuron* **15**(6): 1287-1298.
- Lozovaya, N., S. Eftekhari, R. Cloarec, L. A. Gouty-Colomer, A. Dufour, B. Riffault, M. Billon-Grand, A. Pons-Bennaceur, N. Oumar, N. Burnashev, Y. Ben-Ari and C. Hammond (2018). "GABAergic inhibition in dual-transmission cholinergic and GABAergic striatal interneurons is abolished in Parkinson disease." *Nat Commun* **9**(1): 1422.
- Lu, J., T. Wu, B. Zhang, S. Liu, W. Song, J. Qiao and H. Ruan (2021). "Types of nuclear localization signals and mechanisms of protein import into the nucleus." *Cell Commun Signal* **19**(1): 60.

- Lu, P., F. Wang, S. Zhou, X. Huang, H. Sun, Y. W. Zhang, Y. Yao and H. Zheng (2021). "A Novel CNTNAP2 Mutation Results in Abnormal Neuronal E/I Balance." Front Neurol **12**: 712773.
- Lucki, I. (1998). "The spectrum of behaviors influenced by serotonin." Biol Psychiatry **44**(3): 151-162.
- Lugo, J. N., G. D. Smith, E. P. Arbuckle, J. White, A. J. Holley, C. M. Floruta, N. Ahmed, M. C. Gomez and O. Okonkwo (2014). "Deletion of PTEN produces autism-like behavioral deficits and alterations in synaptic proteins." Front Mol Neurosci **7**: 27.
- Luhmann, H. J., A. Sinning, J. W. Yang, V. Reyes-Puerta, M. C. Stüttgen, S. Kirischuk and W. Kilb (2016). "Spontaneous Neuronal Activity in Developing Neocortical Networks: From Single Cells to Large-Scale Interactions." Front Neural Circuits **10**: 40.
- Lunden, J. W., M. Durens, A. W. Phillips and M. W. Nestor (2019). "Cortical interneuron function in autism spectrum condition." Pediatr Res **85**(2): 146-154.
- Macintosh, F. C. (1941). "The distribution of acetylcholine in the peripheral and the central nervous system." J Physiol **99**(4): 436-442.
- Maejima, T., O. A. Masseck, M. D. Mark and S. Herlitze (2013). "Modulation of firing and synaptic transmission of serotonergic neurons by intrinsic G protein-coupled receptors and ion channels." Front Integr Neurosci **7**: 40.
- Magno, L., C. Barry, C. Schmidt-Hieber, P. Theodotou, M. Hausser and N. Kessaris (2017). "NKX2-1 Is Required in the Embryonic Septum for Cholinergic System Development, Learning, and Memory." Cell Rep **20**(7): 1572-1584.
- Mallet, N., A. Leblois, N. Maurice and C. Beurrier (2019). "Striatal Cholinergic Interneurons: How to Elucidate Their Function in Health and Disease." Front Pharmacol **10**: 1488.
- Mamaligas, A. A., K. Barcomb and C. P. Ford (2019). "Cholinergic Transmission at Muscarinic Synapses in the Striatum Is Driven Equally by Cortical and Thalamic Inputs." Cell Rep **28**(4): 1003-1014 e1003.
- Marin, O., S. A. Anderson and J. L. Rubenstein (2000). "Origin and molecular specification of striatal interneurons." J Neurosci **20**(16): 6063-6076.
- Marsh, R., A. J. Gerber and B. S. Peterson (2008). "Neuroimaging studies of normal brain development and their relevance for understanding childhood neuropsychiatric disorders." J Am Acad Child Adolesc Psychiatry **47**(11): 1233-1251.
- Martinez-Cerdeno, V. and S. C. Noctor (2018). "Neural Progenitor Cell Terminology." Front Neuroanat **12**: 104.
- Masi, A., M. M. DeMayo, N. Glozier and A. J. Guastella (2017). "An Overview of Autism Spectrum Disorder, Heterogeneity and Treatment Options." Neurosci Bull **33**(2): 183-193.
- Matamalas, M., J. Gotz and J. Bertran-Gonzalez (2016). "Quantitative Imaging of Cholinergic Interneurons Reveals a Distinctive Spatial Organization and a Functional Gradient across the Mouse Striatum." PLoS One **11**(6): e0157682.
- Mathur, B. N., N. A. Capik, V. A. Alvarez and D. M. Lovinger (2011). "Serotonin induces long-term depression at corticostriatal synapses." J Neurosci **31**(20): 7402-7411.
- McCormick, D. A., D. B. Nestvogel and B. J. He (2020). "Neuromodulation of Brain State and Behavior." Annual Review of Neuroscience **43**(1): 391-415.
- McDevitt, R. A. and J. F. Neumaier (2011). "Regulation of dorsal raphe nucleus function by serotonin autoreceptors: a behavioral perspective." J Chem Neuroanat **41**(4): 234-246.
- McGeorge, A. J. and R. L. Faull (1989). "The organization of the projection from the cerebral cortex to the striatum in the rat." Neuroscience **29**(3): 503-537.
- McGuirt, A. F., M. R. Post, I. Pigulevskiy, D. Sulzer and O. J. Lieberman (2021). "Coordinated Postnatal Maturation of Striatal Cholinergic Interneurons and Dopamine Release Dynamics in Mice." J Neurosci **41**(16): 3597-3609.

- Mi, D., Z. Li, L. Lim, M. Li, M. Moissidis, Y. Yang, T. Gao, T. X. Hu, T. Pratt, D. J. Price, N. Sestan and O. Marin (2018). "Early emergence of cortical interneuron diversity in the mouse embryo." *Science* **360**(6384): 81-85.
- Migliarini, S., G. Pacini, B. Pelosi, G. Lunardi and M. Pasqualetti (2013). "Lack of brain serotonin affects postnatal development and serotonergic neuronal circuitry formation." *Mol Psychiatry* **18**(10): 1106-1118.
- Mills, K. L., A. L. Goddings, L. S. Clasen, J. N. Giedd and S. J. Blakemore (2014). "The developmental mismatch in structural brain maturation during adolescence." *Dev Neurosci* **36**(3-4): 147-160.
- Miterko, L. N., E. P. Lackey, D. H. Heck and R. V. Sillitoe (2018). "Shaping Diversity Into the Brain's Form and Function." *Front Neural Circuits* **12**: 83.
- Moessner, R., C. R. Marshall, J. S. Sutcliffe, J. Skaug, D. Pinto, J. Vincent, L. Zwaigenbaum, B. Fernandez, W. Roberts, P. Szatmari and S. W. Scherer (2007). "Contribution of SHANK3 mutations to autism spectrum disorder." *Am J Hum Genet* **81**(6): 1289-1297.
- Mohajerani, M. H. and E. Cherubini (2006). "Role of giant depolarizing potentials in shaping synaptic currents in the developing hippocampus." *Crit Rev Neurobiol* **18**(1-2): 13-23.
- Molitor, J. (2022). *Dysfunction of striatal cholinergic interneurons as a neural substrate in autism spectrum disorders in relation to Tshz3 gene deletion*. PhD, Aix-Marseille.
- Molyneaux, B. J., P. Arlotta, J. R. Menezes and J. D. Macklis (2007). "Neuronal subtype specification in the cerebral cortex." *Nat Rev Neurosci* **8**(6): 427-437.
- Monteiro, P., B. Barak, Y. Zhou, R. McRae, D. Rodrigues, I. R. Wickersham and G. Feng (2018). "Dichotomous parvalbumin interneuron populations in dorsolateral and dorsomedial striatum." *J Physiol* **596**(16): 3695-3707.
- Motulsky, H. J. and R. E. Brown (2006). "Detecting outliers when fitting data with nonlinear regression - a new method based on robust nonlinear regression and the false discovery rate." *BMC Bioinformatics* **7**: 123.
- Muller, C. L., A. M. J. Anacker and J. Veenstra-VanderWeele (2016). "The serotonin system in autism spectrum disorder: From biomarker to animal models." *Neuroscience* **321**: 24-41.
- Munakata, Y. and J. Pfaffly (2004). "Hebbian learning and development." *Dev Sci* **7**(2): 141-148.
- Munoz-Manchado, A. B., C. Bengtsson Gonzales, A. Zeisel, H. Munguba, B. Bekkouche, N. G. Skene, P. Lonnerberg, J. Ryge, K. D. Harris, S. Linnarsson and J. Hjerling-Leffler (2018). "Diversity of Interneurons in the Dorsal Striatum Revealed by Single-Cell RNA Sequencing and PatchSeq." *Cell Rep* **24**(8): 2179-2190 e2177.
- Nadarajah, B., J. E. Brunstrom, J. Grutzendler, R. O. Wong and A. L. Pearlman (2001). "Two modes of radial migration in early development of the cerebral cortex." *Nat Neurosci* **4**(2): 143-150.
- Nadim, F. and D. Bucher (2014). "Neuromodulation of neurons and synapses." *Curr Opin Neurobiol* **29**: 48-56.
- Nagy, J., J. Kobolak, S. Berzsenyi, Z. Abraham, H. X. Avci, I. Bock, Z. Bekes, B. Hodocsek, A. Chandrasekaran, A. Teglassi, P. Dezso, B. Kovanyi, E. T. Voros, L. Fodor, T. Szel, K. Nemeth, A. Balazs, A. Dinnyes, B. Lendvai, G. Levay and V. Roman (2017). "Altered neurite morphology and cholinergic function of induced pluripotent stem cell-derived neurons from a patient with Kleefstra syndrome and autism." *Transl Psychiatry* **7**(7): e1179.
- Nahar, L., B. M. Delacroix and H. W. Nam (2021). "The Role of Parvalbumin Interneurons in Neurotransmitter Balance and Neurological Disease." *Front Psychiatry* **12**: 679960.

- Nair, S. G., M. M. Estabrook and J. F. Neumaier (2020). "Serotonin regulation of striatal function." Handbook of the Behavioral Neurobiology of Serotonin, 2nd Edition **31**: 321-335.
- Navailles, S. and P. De Deurwaerdere (2011). "Presynaptic control of serotonin on striatal dopamine function." Psychopharmacology (Berl) **213**(2-3): 213-242.
- Nelson, A. B., T. G. Bussert, A. C. Kreitzer and R. P. Seal (2014). "Striatal cholinergic neurotransmission requires VGLUT3." J Neurosci **34**(26): 8772-8777.
- Nishizawa, S., C. Benkelfat, S. N. Young, M. Leyton, S. Mzengeza, C. de Montigny, P. Blier and M. Diksic (1997). "Differences between males and females in rates of serotonin synthesis in human brain." Proc Natl Acad Sci U S A **94**(10): 5308-5313.
- Nobrega-Pereira, S. and O. Marin (2009). "Transcriptional control of neuronal migration in the developing mouse brain." Cereb Cortex **19 Suppl 1**: i107-113.
- Nosaka, D. and J. R. Wickens (2022). "Striatal Cholinergic Signaling in Time and Space." Molecules **27**(4).
- Oh, S., S. Shin, H. Song, J. P. Grande and R. Janknecht (2019). "Relationship between ETS Transcription Factor ETV1 and TGF-beta-regulated SMAD Proteins in Prostate Cancer." Sci Rep **9**(1): 8186.
- Okaty, B. W., M. N. Miller, K. Sugino, C. M. Hempel and S. B. Nelson (2009). "Transcriptional and electrophysiological maturation of neocortical fast-spiking GABAergic interneurons." J Neurosci **29**(21): 7040-7052.
- Okaty, B. W., N. Sturrock, Y. Escobedo Lozoya, Y. Chang, R. A. Senft, K. A. Lyon, O. V. Alekseyenko and S. M. Dymecki (2020). "A single-cell transcriptomic and anatomic atlas of mouse dorsal raphe Pet1 neurons." Elife **9**.
- Oldenburg, I. A. and J. B. Ding (2011). "Cholinergic modulation of synaptic integration and dendritic excitability in the striatum." Curr Opin Neurobiol **21**(3): 425-432.
- Oran, Y. and I. Bar-Gad (2018). "Loss of Balance between Striatal Feedforward Inhibition and Corticostriatal Excitation Leads to Tremor." J Neurosci **38**(7): 1699-1710.
- Oyamada, M., Y. Oyamada and T. Takamatsu (2005). "Regulation of connexin expression." Biochim Biophys Acta **1719**(1-2): 6-23.
- Page, D. T., O. J. Kutti, C. Prestia and M. Sur (2009). "Haploinsufficiency for Pten and Serotonin transporter cooperatively influences brain size and social behavior." Proc Natl Acad Sci U S A **106**(6): 1989-1994.
- Pakhotin, P. and E. Bracci (2007). "Cholinergic interneurons control the excitatory input to the striatum." J Neurosci **27**(2): 391-400.
- Pan, Y. H., N. Wu and X. B. Yuan (2019). "Toward a Better Understanding of Neuronal Migration Deficits in Autism Spectrum Disorders." Front Cell Dev Biol **7**: 205.
- Paxinos, G. and K. B. J. Franklin (2001). The Mouse Brain in Stereotaxic Coordinates. United States of America, Academic Press.
- Peca, J., C. Feliciano, J. T. Ting, W. Wang, M. F. Wells, T. N. Venkatraman, C. D. Lascola, Z. Fu and G. Feng (2011). "Shank3 mutant mice display autistic-like behaviours and striatal dysfunction." Nature **472**(7344): 437-442.
- Peinado, A., R. Yuste and L. C. Katz (1993). "Gap junctional communication and the development of local circuits in neocortex." Cereb Cortex **3**(5): 488-498.
- Peixoto, R. T., L. Chantranupong, R. Hakim, J. Levasseur, W. Wang, T. Merchant, K. Gorman, B. Budnik and B. L. Sabatini (2019). "Abnormal Striatal Development Underlies the Early Onset of Behavioral Deficits in Shank3B(-/-) Mice." Cell Rep **29**(7): 2016-2027 e2014.
- Penagarikano, O., B. S. Abrahams, E. I. Herman, K. D. Winden, A. Gdalyahu, H. Dong, L. I. Sonnenblick, R. Gruver, J. Almajano, A. Bragin, P. Golshani, J. T. Trachtenberg, E. Peles and D. H. Geschwind (2011). "Absence of CNTNAP2 leads to epilepsy, neuronal migration abnormalities, and core autism-related deficits." Cell **147**(1): 235-246.

- Pfisterer, U. and K. Khodosevich (2017). "Neuronal survival in the brain: neuron type-specific mechanisms." Cell Death Dis **8**(3): e2643.
- Piers, T. M., D. H. Kim, B. C. Kim, P. Regan, D. J. Whitcomb and K. Cho (2012). "Translational Concepts of mGluR5 in Synaptic Diseases of the Brain." Front Pharmacol **3**: 199.
- Pinatel, D., B. Hivert, J. Boucraut, M. Saint-Martin, V. Rogemond, L. Zoupi, D. Karageorgos, J. Honorat and C. Faivre-Sarrailh (2015). "Inhibitory axons are targeted in hippocampal cell culture by anti-Caspr2 autoantibodies associated with limbic encephalitis." Front Cell Neurosci **9**: 265.
- Platkiewicz, J. and R. Brette (2010). "A threshold equation for action potential initiation." PLoS Comput Biol **6**(7): e1000850.
- Poliak, S., D. Salomon, H. Elhanany, H. Sabanay, B. Kiernan, L. Pevny, C. L. Stewart, X. Xu, S. Y. Chiu, P. Shrager, A. J. Furley and E. Peles (2003). "Juxtaparanodal clustering of Shaker-like K<sup>+</sup> channels in myelinated axons depends on Caspr2 and TAG-1." J Cell Biol **162**(6): 1149-1160.
- Pollak Dorocic, I., D. Furth, Y. Xuan, Y. Johansson, L. Pozzi, G. Silberberg, M. Carlen and K. Meletis (2014). "A whole-brain atlas of inputs to serotonergic neurons of the dorsal and median raphe nuclei." Neuron **83**(3): 663-678.
- Pommer, S., Y. Akamine, S. N. Schiffmann, A. de Kerchove d'Exaerde and J. R. Wickens (2021). "The Effect of Serotonin Receptor 5-HT1B on Lateral Inhibition between Spiny Projection Neurons in the Mouse Striatum." J Neurosci **41**(37): 7831-7847.
- Poot, M. (2015). "Connecting the CNTNAP2 Networks with Neurodevelopmental Disorders." Mol Syndromol **6**(1): 7-22.
- Poppi, L. A., K. T. Ho-Nguyen, A. Shi, C. T. Daut and M. A. Tischfield (2021). "Recurrent Implication of Striatal Cholinergic Interneurons in a Range of Neurodevelopmental, Neurodegenerative, and Neuropsychiatric Disorders." Cells **10**(4).
- Pouchelon, G., D. Dwivedi, Y. Bollmann, C. K. Agba, Q. Xu, A. M. C. Mirow, S. Kim, Y. Qiu, E. Sevier, K. D. Ritola, R. Cossart and G. Fishell (2021). "The organization and development of cortical interneuron presynaptic circuits are area specific." Cell Rep **37**(6): 109993.
- Prigge, M. B. D., N. Lange, E. D. Bigler, J. B. King, D. C. Dean, 3rd, N. Adluru, A. L. Alexander, J. E. Lainhart and B. A. Zielinski (2021). "A 16-year study of longitudinal volumetric brain development in males with autism." Neuroimage **236**: 118067.
- Quentin, E., A. Belmer and L. Maroteaux (2018). "Somato-Dendritic Regulation of Raphe Serotonin Neurons; A Key to Antidepressant Action." Front Neurosci **12**: 982.
- Radulescu, A., J. Herron, C. Kennedy and A. Scimemi (2017). "Global and local excitation and inhibition shape the dynamics of the cortico-striatal-thalamo-cortical pathway." Sci Rep **7**(1): 7608.
- Rapanelli, M., L. R. Frick, M. Xu, S. M. Groman, K. Jindachomthong, N. Tamamaki, C. Tanahira, J. R. Taylor and C. Pittenger (2017). "Targeted Interneuron Depletion in the Dorsal Striatum Produces Autism-like Behavioral Abnormalities in Male but Not Female Mice." Biol Psychiatry **82**(3): 194-203.
- Rash, J. E., W. A. Staines, T. Yasumura, D. Patel, C. S. Furman, G. L. Stelmack and J. I. Nagy (2000). "Immunogold evidence that neuronal gap junctions in adult rat brain and spinal cord contain connexin-36 but not connexin-32 or connexin-43." Proc Natl Acad Sci U S A **97**(13): 7573-7578.
- Reimann, M. W., A. L. Horlemann, S. Ramaswamy, E. B. Muller and H. Markram (2017). "Morphological Diversity Strongly Constrains Synaptic Connectivity and Plasticity." Cereb Cortex **27**(9): 4570-4585.

- Reiner, O., E. Karzbrun, A. Kshirsagar and K. Kaibuchi (2016). "Regulation of neuronal migration, an emerging topic in autism spectrum disorders." *J Neurochem* **136**(3): 440-456.
- Ren, J., D. Friedmann, J. Xiong, C. D. Liu, B. R. Ferguson, T. Weerakkody, K. E. DeLoach, C. Ran, A. Pun, Y. Sun, B. Weissbourd, R. L. Neve, J. Huguenard, M. A. Horowitz and L. Luo (2018). "Anatomically Defined and Functionally Distinct Dorsal Raphe Serotonin Sub-systems." *Cell* **175**(2): 472-487 e420.
- Ren, J., A. Isakova, D. Friedmann, J. Zeng, S. M. Grutzner, A. Pun, G. Q. Zhao, S. S. Kolluru, R. Wang, R. Lin, P. Li, A. Li, J. L. Raymond, Q. Luo, M. Luo, S. R. Quake and L. Luo (2019). "Single-cell transcriptomes and whole-brain projections of serotonin neurons in the mouse dorsal and median raphe nuclei." *Elife* **8**.
- Riccio, O., G. Potter, C. Walzer, P. Vallet, G. Szabo, L. Vutskits, J. Z. Kiss and A. G. Dayer (2009). "Excess of serotonin affects embryonic interneuron migration through activation of the serotonin receptor 6." *Mol Psychiatry* **14**(3): 280-290.
- Rodenas-Cuadrado, P., J. Ho and S. C. Vernes (2014). "Shining a light on CNTNAP2: complex functions to complex disorders." *Eur J Hum Genet* **22**(2): 171-178.
- Rodenas-Cuadrado, P., N. Pietrafusa, T. Francavilla, A. La Neve, P. Striano and S. C. Vernes (2016). "Characterisation of CASPR2 deficiency disorder--a syndrome involving autism, epilepsy and language impairment." *BMC Med Genet* **17**: 8.
- Rubenstein, J. L. and M. M. Merzenich (2003). "Model of autism: increased ratio of excitation/inhibition in key neural systems." *Genes Brain Behav* **2**(5): 255-267.
- Rutter, M., A. Caspi and T. E. Moffitt (2003). "Using sex differences in psychopathology to study causal mechanisms: unifying issues and research strategies." *J Child Psychol Psychiatry* **44**(8): 1092-1115.
- Rybaczyk, L. A., M. J. Bashaw, D. R. Pathak, S. M. Moody, R. M. Gilders and D. L. Holzschu (2005). "An overlooked connection: serotonergic mediation of estrogen-related physiology and pathology." *BMC Womens Health* **5**: 12.
- Saino-Saito, S., J. W. Cave, Y. Akiba, H. Sasaki, K. Goto, K. Kobayashi, R. Berlin and H. Baker (2007). "ER81 and CaMKIV identify anatomically and phenotypically defined subsets of mouse olfactory bulb interneurons." *J Comp Neurol* **502**(4): 485-496.
- Saint-Martin, M., B. Joubert, V. Pellier-Monnin, O. Pascual, N. Noraz and J. Honnorat (2018). "Contactin-associated protein-like 2, a protein of the neurexin family involved in several human diseases." *Eur J Neurosci* **48**(3): 1906-1923.
- Schilke, E. D., L. Tremolizzo, I. Appollonio and C. Ferrarese (2022). "Tics: neurological disorders determined by a deficit in sensorimotor gating processes." *Neurol Sci* **43**(10): 5839-5850.
- Schilman, E. A., O. Klavir, C. Winter, R. Sohr and D. Joel (2010). "The role of the striatum in compulsive behavior in intact and orbitofrontal-cortex-lesioned rats: possible involvement of the serotonergic system." *Neuropsychopharmacology* **35**(4): 1026-1039.
- Schmittgen, T. D. and K. J. Livak (2008). "Analyzing real-time PCR data by the comparative C(T) method." *Nat Protoc* **3**(6): 1101-1108.
- Schmitz, M. T., K. Sandoval, C. P. Chen, M. A. Mostajo-Radji, W. W. Seeley, T. J. Nowakowski, C. J. Ye, M. F. Paredes and A. A. Pollen (2022). "The development and evolution of inhibitory neurons in primate cerebrum." *Nature* **603**(7903): 871-877.
- Schwartz, R. K., C. M. Thiel, C. P. Muller and J. P. Huston (1998). "Relationship between anxiety and serotonin in the ventral striatum." *Neuroreport* **9**(6): 1025-1029.
- Scott-Van Zeeland, A. A., M. Dapretto, D. G. Ghahremani, R. A. Poldrack and S. Y. Bookheimer (2010). "Reward processing in autism." *Autism Res* **3**(2): 53-67.
- Scott, R., A. Sanchez-Aguilera, K. van Elst, L. Lim, N. Dehorter, S. E. Bae, G. Bartolini, E. Peles, M. J. H. Kas, H. Bruining and O. Marin (2019). "Loss of Cntnap2 Causes Axonal



- Excitability Deficits, Developmental Delay in Cortical Myelination, and Abnormal Stereotyped Motor Behavior." *Cereb Cortex* **29**(2): 586-597.
- Sears, L. L., C. Vest, S. Mohamed, J. Bailey, B. J. Ranson and J. Piven (1999). "An MRI study of the basal ganglia in autism." *Prog Neuropsychopharmacol Biol Psychiatry* **23**(4): 613-624.
- Seibenhener, M. L. and M. C. Wooten (2015). "Use of the Open Field Maze to measure locomotor and anxiety-like behavior in mice." *J Vis Exp*(96): e52434.
- Seiffe, A., M. F. Ramirez, L. Sempe and A. M. Depino (2022). "Juvenile handling rescues autism-related effects of prenatal exposure to valproic acid." *Sci Rep* **12**(1): 7174.
- Selimbeyoglu, A., C. K. Kim, M. Inoue, S. Y. Lee, A. S. O. Hong, I. Kauvar, C. Ramakrishnan, L. E. Fenno, T. J. Davidson, M. Wright and K. Deisseroth (2017). "Modulation of prefrontal cortex excitation/inhibition balance rescues social behavior in CNTNAP2-deficient mice." *Sci Transl Med* **9**(401).
- Semba, K., S. R. Vincent and H. C. Fibiger (1988). "Different times of origin of choline acetyltransferase- and somatostatin-immunoreactive neurons in the rat striatum." *J Neurosci* **8**(10): 3937-3944.
- Semple, B. D., K. Blomgren, K. Gimlin, D. M. Ferriero and L. J. Noble-Haeusslein (2013). "Brain development in rodents and humans: Identifying benchmarks of maturation and vulnerability to injury across species." *Prog Neurobiol* **106-107**: 1-16.
- Shekhar, A., X. Lin, B. Lin, F. Y. Liu, J. Zhang, A. Khodadadi-Jamayran, A. Tsigos, L. Bu, G. I. Fishman and D. S. Park (2018). "ETV1 activates a rapid conduction transcriptional program in rodent and human cardiomyocytes." *Sci Rep* **8**(1): 9944.
- Shekhar, A., X. Lin, F. Y. Liu, J. Zhang, H. Mo, L. Bastarache, J. C. Denny, N. J. Cox, M. Delmar, D. M. Roden, G. I. Fishman and D. S. Park (2016). "Transcription factor ETV1 is essential for rapid conduction in the heart." *J Clin Invest* **126**(12): 4444-4459.
- Shen, K. and P. Scheiffele (2010). "Genetics and cell biology of building specific synaptic connectivity." *Annu Rev Neurosci* **33**: 473-507.
- Simon, P., R. Dupuis and J. Costentin (1994). "Thigmotaxis as an index of anxiety in mice. Influence of dopaminergic transmissions." *Behav Brain Res* **61**(1): 59-64.
- Sin, W. C., K. Haas, E. S. Ruthazer and H. T. Cline (2002). "Dendrite growth increased by visual activity requires NMDA receptor and Rho GTPases." *Nature* **419**(6906): 475-480.
- Soghomonian, J. J., L. Descarries and K. C. Watkins (1989). "Serotonin Innervation in Adult-Rat Neostriatum .2. Ultrastructural Features - a Autoradiographic and Immunocytochemical Study." *Brain Research* **481**(1): 67-86.
- Sohal, V. S. and J. L. R. Rubenstein (2019). "Excitation-inhibition balance as a framework for investigating mechanisms in neuropsychiatric disorders." *Mol Psychiatry* **24**(9): 1248-1257.
- Spencer, W. C. and E. S. Deneris (2017). "Regulatory Mechanisms Controlling Maturation of Serotonin Neuron Identity and Function." *Front Cell Neurosci* **11**: 215.
- Spitzer, N. C. (2006). "Electrical activity in early neuronal development." *Nature* **444**(7120): 707-712.
- Spitzer, N. C. (2017). "Neurotransmitter Switching in the Developing and Adult Brain." *Annu Rev Neurosci* **40**: 1-19.
- Spreafico, R., C. Frassoni, P. Arcelli, M. Selvaggio and S. De Biasi (1995). "In situ labeling of apoptotic cell death in the cerebral cortex and thalamus of rats during development." *J Comp Neurol* **363**(2): 281-295.
- Spruston, N., D. B. Jaffe and D. Johnston (1994). "Dendritic attenuation of synaptic potentials and currents: the role of passive membrane properties." *Trends Neurosci* **17**(4): 161-166.
- Sreenivasan, V., E. Serafeimidou-Pouliou, D. Exposito-Alonso, K. Bercsenyi, C. Bernard, S. E. Bae, F. Oozeer, A. Hanusz-Godoy, R. H. Edwards and O. Marin (2022). "Input-specific

- control of interneuron numbers in nascent striatal networks." Proc Natl Acad Sci U S A **119**(20): e2118430119.
- Stamford, J. A., C. Davidson, D. P. McLaughlin and S. E. Hopwood (2000). "Control of dorsal raphe 5-HT function by multiple 5-HT(1) autoreceptors: parallel purposes or pointless plurality?" Trends Neurosci **23**(10): 459-465.
- Stampanoni Bassi, M., E. Iezzi, L. Gilio, D. Centonze and F. Buttari (2019). "Synaptic Plasticity Shapes Brain Connectivity: Implications for Network Topology." Int J Mol Sci **20**(24).
- Steinbusch, H. W., R. Nieuwenhuys, A. A. Verhofstad and D. Van der Kooy (1981). "The nucleus raphe dorsalis of the rat and its projection upon the caudatoputamen. A combined cytoarchitectonic, immunohistochemical and retrograde transport study." J Physiol (Paris) **77**(2-3): 157-174.
- Stenman, J., H. Toresson and K. Campbell (2003). "Identification of two distinct progenitor populations in the lateral ganglionic eminence: implications for striatal and olfactory bulb neurogenesis." J Neurosci **23**(1): 167-174.
- Stern, E. A., D. Jaeger and C. J. Wilson (1998). "Membrane potential synchrony of simultaneously recorded striatal spiny neurons in vivo." Nature **394**(6692): 475-478.
- Stiles, J. and T. L. Jernigan (2010). "The basics of brain development." Neuropsychol Rev **20**(4): 327-348.
- Straub, C., J. L. Saulnier, A. Begue, D. D. Feng, K. W. Huang and B. L. Sabatini (2016). "Principles of Synaptic Organization of GABAergic Interneurons in the Striatum." Neuron **92**(1): 84-92.
- Straub, C., N. X. Tritsch, N. A. Hagan, C. Gu and B. L. Sabatini (2014). "Multiphasic modulation of cholinergic interneurons by nigrostriatal afferents." J Neurosci **34**(25): 8557-8569.
- Strauss, K. A., E. G. Puffenberger, M. J. Huentelman, S. Gottlieb, S. E. Dobrin, J. M. Parod, D. A. Stephan and D. H. Morton (2006). "Recessive symptomatic focal epilepsy and mutant contactin-associated protein-like 2." N Engl J Med **354**(13): 1370-1377.
- Strong, P. V., J. P. Christianson, A. B. Loughridge, J. Amat, S. F. Maier, M. Fleshner and B. N. Greenwood (2011). "5-hydroxytryptamine 2C receptors in the dorsal striatum mediate stress-induced interference with negatively reinforced instrumental escape behavior." Neuroscience **197**: 132-144.
- Sudhof, T. C. (2018). "Towards an Understanding of Synapse Formation." Neuron **100**(2): 276-293.
- Sun, F., J. Zhou, B. Dai, T. Qian, J. Zeng, X. Li, Y. Zhuo, Y. Zhang, Y. Wang, C. Qian, K. Tan, J. Feng, H. Dong, D. Lin, G. Cui and Y. Li (2020). "Next-generation GRAB sensors for monitoring dopaminergic activity in vivo." Nat Methods **17**(11): 1156-1166.
- Szydłowski, S. N., I. Pollak Dorocic, H. Planert, M. Carlen, K. Meletis and G. Silberberg (2013). "Target selectivity of feedforward inhibition by striatal fast-spiking interneurons." J Neurosci **33**(4): 1678-1683.
- Taber, K. H., J. Salpekar, A. H. Wong and R. A. Hurley (2011). "Developmental origins for neuropsychiatric illness." J Neuropsychiatry Clin Neurosci **23**(1): 1-5.
- Takahashi, H., Y. Takada, N. Nagai, T. Urano and A. Takada (1998). "Extracellular serotonin in the striatum increased after immobilization stress only in the nighttime." Behav Brain Res **91**(1-2): 185-191.
- Tamariz, E. and A. Varela-Echavarría (2015). "The discovery of the growth cone and its influence on the study of axon guidance." Front Neuroanat **9**: 51.
- Tanaka, S. C., N. Schweighofer, S. Asahi, K. Shishida, Y. Okamoto, S. Yamawaki and K. Doya (2007). "Serotonin differentially regulates short- and long-term prediction of rewards in the ventral and dorsal striatum." PLoS One **2**(12): e1333.

- Tang, G., K. Gudsnuk, S. H. Kuo, M. L. Cotrina, G. Rosoklija, A. Sosunov, M. S. Sonders, E. Kanter, C. Castagna, A. Yamamoto, Z. Yue, O. Arancio, B. S. Peterson, F. Champagne, A. J. Dwork, J. Goldman and D. Sulzer (2014). "Loss of mTOR-dependent macroautophagy causes autistic-like synaptic pruning deficits." Neuron **83**(5): 1131-1143.
- Tau, G. Z. and B. S. Peterson (2010). "Normal development of brain circuits." Neuropsychopharmacology **35**(1): 147-168.
- Telley, L., G. Agirman, J. Prados, N. Amberg, S. Fievre, P. Oberst, G. Bartolini, I. Vitali, C. Cadilhac, S. Hippenmeyer, L. Nguyen, A. Dayer and D. Jabaudon (2019). "Temporal patterning of apical progenitors and their daughter neurons in the developing neocortex." Science **364**(6440).
- Tenney, A. P., J. Livet, T. Belton, M. Prochazkova, E. M. Pearson, M. C. Whitman, A. B. Kulkarni, E. C. Engle and C. E. Henderson (2019). "Etv1 Controls the Establishment of Non-overlapping Motor Innervation of Neighboring Facial Muscles during Development." Cell Rep **29**(2): 437-452 e434.
- Tepper, J. M., T. Koos, O. Ibanez-Sandoval, F. Tecuapetla, T. W. Faust and M. Assous (2018). "Heterogeneity and Diversity of Striatal GABAergic Interneurons: Update 2018." Front Neuroanat **12**: 91.
- Tepper, J. M., F. Tecuapetla, T. Koos and O. Ibanez-Sandoval (2010). "Heterogeneity and diversity of striatal GABAergic interneurons." Front Neuroanat **4**: 150.
- Thivierge, J. P. (2008). "Neural diversity creates a rich repertoire of brain activity." Commun Integr Biol **1**(2): 188-189.
- Tien, N. W. and D. Kerschensteiner (2018). "Homeostatic plasticity in neural development." Neural Dev **13**(1): 9.
- Tierney, A. L. and C. A. Nelson, 3rd (2009). "Brain Development and the Role of Experience in the Early Years." Zero Three **30**(2): 9-13.
- Todd, K. L., W. B. Kristan, Jr. and K. A. French (2010). "Gap junction expression is required for normal chemical synapse formation." J Neurosci **30**(45): 15277-15285.
- Tubert, C., I. R. E. Taravini, E. Flores-Barrera, G. M. Sanchez, M. A. Prost, M. E. Avale, K. Y. Tseng, L. Rela and M. G. Murer (2016). "Decrease of a Current Mediated by Kv1.3 Channels Causes Striatal Cholinergic Interneuron Hyperexcitability in Experimental Parkinsonism." Cell Rep **16**(10): 2749-2762.
- Turner, K. M., A. Svegborn, M. Langguth, C. McKenzie and T. W. Robbins (2022). "Opposing Roles of the Dorsolateral and Dorsomedial Striatum in the Acquisition of Skilled Action Sequencing in Rats." J Neurosci **42**(10): 2039-2051.
- Turrero Garcia, M., J. M. Baizabal, D. N. Tran, R. Peixoto, W. Wang, Y. Xie, M. A. Adam, L. A. English, C. M. Reid, S. I. Brito, M. A. Booker, M. Y. Tolstorukov and C. C. Harwell (2020). "Transcriptional regulation of MGE progenitor proliferation by PRDM16 controls cortical GABAergic interneuron production." Development **147**(22).
- Turrero Garcia, M. and C. C. Harwell (2017). "Radial glia in the ventral telencephalon." FEBS Lett **591**(24): 3942-3959.
- Tzimourakas, A., S. Giasemi, M. Mouratidou and D. Karageos (2007). "Structure-function analysis of protein complexes involved in the molecular architecture of juxtaparanodal regions of myelinated fibers." Biotechnol J **2**(5): 577-583.
- Uchino, S. and C. Waga (2013). "SHANK3 as an autism spectrum disorder-associated gene." Brain Dev **35**(2): 106-110.
- Vaccarino, F. M. and K. M. Smith (2009). "Increased brain size in autism--what it will take to solve a mystery." Biol Psychiatry **66**(4): 313-315.
- van Vulpén, E. H. and D. van der Kooy (1998). "Striatal cholinergic interneurons: birthdates predict compartmental localization." Brain Res Dev Brain Res **109**(1): 51-58.

- Vandaele, Y., N. R. Mahajan, D. J. Ottenheimer, J. M. Richard, S. P. Mysore and P. H. Janak (2019). "Distinct recruitment of dorsomedial and dorsolateral striatum erodes with extended training." *Elife* **8**.
- Vandromme, M., C. Gauthier-Rouviere, N. Lamb and A. Fernandez (1996). "Regulation of transcription factor localization: fine-tuning of gene expression." *Trends Biochem Sci* **21**(2): 59-64.
- Varea, O., M. D. Martin-de-Saavedra, K. J. Kopeikina, B. Schurmann, H. J. Fleming, J. M. Fawcett-Patel, A. Bach, S. Jang, E. Peles, E. Kim and P. Penzes (2015). "Synaptic abnormalities and cytoplasmic glutamate receptor aggregates in contactin associated protein-like 2/Caspr2 knockout neurons." *Proc Natl Acad Sci U S A* **112**(19): 6176-6181.
- Vasa, R. A., S. H. Mostofsky and J. B. Ewen (2016). "The Disrupted Connectivity Hypothesis of Autism Spectrum Disorders: Time for the Next Phase in Research." *Biol Psychiatry Cogn Neurosci Neuroimaging* **1**(3): 245-252.
- Vicenzi, S., L. Foa and R. J. Gasperini (2021). "Serotonin functions as a bidirectional guidance molecule regulating growth cone motility." *Cell Mol Life Sci* **78**(5): 2247-2262.
- Villar-Cervino, V., C. Kappeler, S. Nobrega-Pereira, M. Henkemeyer, L. Rago, M. A. Nieto and O. Marin (2015). "Molecular mechanisms controlling the migration of striatal interneurons." *J Neurosci* **35**(23): 8718-8729.
- Virk, M. S., Y. Sagi, L. Medrihan, J. Leung, M. G. Kaplitt and P. Greengard (2016). "Opposing roles for serotonin in cholinergic neurons of the ventral and dorsal striatum." *Proc Natl Acad Sci U S A* **113**(3): 734-739.
- Vitalis, T., O. Cases, S. Passemard, J. Callebert and J. G. Parnavelas (2007). "Embryonic depletion of serotonin affects cortical development." *Eur J Neurosci* **26**(2): 331-344.
- Vogt, D., K. K. A. Cho, S. M. Shelton, A. Paul, Z. J. Huang, V. S. Sohal and J. L. R. Rubenstein (2018). "Mouse Cntnap2 and Human CNTNAP2 ASD Alleles Cell Autonomously Regulate PV+ Cortical Interneurons." *Cereb Cortex* **28**(11): 3868-3879.
- Vogt Weisenhorn, D. M., M. R. Celio and M. Rickmann (1998). "The onset of parvalbumin-expression in interneurons of the rat parietal cortex depends upon extrinsic factor(s)." *Eur J Neurosci* **10**(3): 1027-1036.
- Waclaw, R. R., B. Wang, Z. Pei, L. A. Ehrman and K. Campbell (2009). "Distinct temporal requirements for the homeobox gene Gsx2 in specifying striatal and olfactory bulb neuronal fates." *Neuron* **63**(4): 451-465.
- Wallace, J. A. and J. M. Lauder (1983). "Development of the serotonergic system in the rat embryo: an immunocytochemical study." *Brain Res Bull* **10**(4): 459-479.
- Wan, J., W. Peng, X. Li, T. Qian, K. Song, J. Zeng, F. Deng, S. Hao, J. Feng, P. Zhang, Y. Zhang, J. Zou, S. Pan, M. Shin, B. J. Venton, J. J. Zhu, M. Jing, M. Xu and Y. Li (2021). "A genetically encoded sensor for measuring serotonin dynamics." *Nat Neurosci* **24**(5): 746-752.
- Wang, D. D. and A. R. Kriegstein (2008). "GABA regulates excitatory synapse formation in the neocortex via NMDA receptor activation." *J Neurosci* **28**(21): 5547-5558.
- Wang, H. L., S. Zhang, J. Qi, H. Wang, R. Cachepe, C. A. Mejias-Aponte, J. A. Gomez, G. E. Mateo-Semidey, G. M. J. Beaudoin, C. A. Paladini, J. F. Cheer and M. Morales (2019). "Dorsal Raphe Dual Serotonin-Glutamate Neurons Drive Reward by Establishing Excitatory Synapses on VTA Mesoaccumbens Dopamine Neurons." *Cell Rep* **26**(5): 1128-1142 e1127.
- Wang, L., L. E. Almeida, N. A. Spornick, N. Kenyon, S. Kamimura, A. Khaibullina, M. Nouraie and Z. M. Quezado (2015). "Modulation of social deficits and repetitive behaviors in a mouse model of autism: the role of the nicotinic cholinergic system." *Psychopharmacology (Berl)* **232**(23): 4303-4316.

- Wang, X., A. L. Bey, B. M. Katz, A. Badea, N. Kim, L. K. David, L. J. Duffney, S. Kumar, S. D. Mague, S. W. Hulbert, N. Dutta, V. Hayrapetyan, C. Yu, E. Gaidis, S. Zhao, J. D. Ding, Q. Xu, L. Chung, R. M. Rodriguiz, F. Wang, R. J. Weinberg, W. C. Wetsel, K. Dzirasa, H. Yin and Y. H. Jiang (2016). "Altered mGluR5-Homer scaffolds and corticostriatal connectivity in a Shank3 complete knockout model of autism." Nat Commun **7**: 11459.
- Wang, Z., T. V. Maia, R. Marsh, T. Colibazzi, A. Gerber and B. S. Peterson (2011). "The neural circuits that generate tics in Tourette's syndrome." Am J Psychiatry **168**(12): 1326-1337.
- Waselus, M., J. P. Galvez, R. J. Valentino and E. J. Van Bockstaele (2006). "Differential projections of dorsal raphe nucleus neurons to the lateral septum and striatum." J Chem Neuroanat **31**(4): 233-242.
- Watari, H., A. J. Tose and M. M. Bosma (2013). "Hyperpolarization of resting membrane potential causes retraction of spontaneous Ca(i)(2)(+) transients during mouse embryonic circuit development." J Physiol **591**(4): 973-983.
- West, A. E. and M. E. Greenberg (2011). "Neuronal activity-regulated gene transcription in synapse development and cognitive function." Cold Spring Harb Perspect Biol **3**(6).
- White, L. D. and S. Barone, Jr. (2001). "Qualitative and quantitative estimates of apoptosis from birth to senescence in the rat brain." Cell Death Differ **8**(4): 345-356.
- Whitehouse, A. J., D. V. Bishop, Q. W. Ang, C. E. Pennell and S. E. Fisher (2011). "CNTNAP2 variants affect early language development in the general population." Genes Brain Behav **10**(4): 451-456.
- Wiesel, T. N. and D. H. Hubel (1963). "Single-Cell Responses in Striate Cortex of Kittens Deprived of Vision in One Eye." J Neurophysiol **26**: 1003-1017.
- Wohr, M., D. Orduz, P. Gregory, H. Moreno, U. Khan, K. J. Vorckel, D. P. Wolfer, H. Welzl, D. Gall, S. N. Schiffmann and B. Schwaller (2015). "Lack of parvalbumin in mice leads to behavioral deficits relevant to all human autism core symptoms and related neural morphofunctional abnormalities." Transl Psychiatry **5**(3): e525.
- Wong, F. K., K. Bercsenyi, V. Sreenivasan, A. Portales, M. Fernandez-Otero and O. Marin (2018). "Pyramidal cell regulation of interneuron survival sculpts cortical networks." Nature **557**(7707): 668-673.
- Xenias, H. S., O. Ibanez-Sandoval, T. Koos and J. M. Tepper (2015). "Are striatal tyrosine hydroxylase interneurons dopaminergic?" J Neurosci **35**(16): 6584-6599.
- Yamaguchi, N., J. Xiao, D. Narke, D. Shaheen, X. Lin, E. Offerman, A. Khodadadi-Jamayran, A. Shekhar, A. Choy, S. Y. Wass, D. R. Van Wagoner, M. K. Chung and D. S. Park (2021). "Cardiac Pressure Overload Decreases ETV1 Expression in the Left Atrium, Contributing to Atrial Electrical and Structural Remodeling." Circulation **143**(8): 805-820.
- Yang, J. M., J. Zhang, Y. Q. Yu, S. Duan and X. M. Li (2014). "Postnatal development of 2 microcircuits involving fast-spiking interneurons in the mouse prefrontal cortex." Cereb Cortex **24**(1): 98-109.
- Yap, E. L. and M. E. Greenberg (2018). "Activity-Regulated Transcription: Bridging the Gap between Neural Activity and Behavior." Neuron **100**(2): 330-348.
- Yoneshima, H., S. Yamasaki, C. C. Voelker, Z. Molnar, E. Christophe, E. Audinat, M. Takemoto, M. Nishiwaki, S. Tsuji, I. Fujita and N. Yamamoto (2006). "Er81 is expressed in a subpopulation of layer 5 neurons in rodent and primate neocortices." Neuroscience **137**(2): 401-412.
- Yu, Y. C., R. S. Bultje, X. Wang and S. H. Shi (2009). "Specific synapses develop preferentially among sister excitatory neurons in the neocortex." Nature **458**(7237): 501-504.
- Yu, Y. C., S. He, S. Chen, Y. Fu, K. N. Brown, X. H. Yao, J. Ma, K. P. Gao, G. E. Sosinsky, K. Huang and S. H. Shi (2012). "Preferential electrical coupling regulates neocortical lineage-dependent microcircuit assembly." Nature **486**(7401): 113-117.

- Zarei, M., D. Xie, F. Jiang, A. Bagirov, B. Huang, A. Raj, S. Nagarajan and S. Guo (2022). "High activity and high functional connectivity are mutually exclusive in resting state zebrafish and human brains." BMC Biol **20**(1): 84.
- Zerbi, V., G. D. Ielacqua, M. Markicevic, M. G. Haberl, M. H. Ellisman, A. B. A, A. Frick, M. Rudin and N. Wenderoth (2018). "Dysfunctional Autism Risk Genes Cause Circuit-Specific Connectivity Deficits With Distinct Developmental Trajectories." Cereb Cortex **28**(7): 2495-2506.
- Zhai, S., W. Shen, S. M. Graves and D. J. Surmeier (2019). "Dopaminergic modulation of striatal function and Parkinson's disease." J Neural Transm (Vienna) **126**(4): 411-422.
- Zhang, C., H. Li and R. Han (2020). "An open-source video tracking system for mouse locomotor activity analysis." BMC Res Notes **13**(1): 48.
- Zhang, X. J., Z. Li, Z. Han, K. T. Sultan, K. Huang and S. H. Shi (2017). "Precise inhibitory microcircuit assembly of developmentally related neocortical interneurons in clusters." Nat Commun **8**: 16091.
- Zhao, Y., O. Marin, E. Hermesz, A. Powell, N. Flames, M. Palkovits, J. L. Rubenstein and H. Westphal (2003). "The LIM-homeobox gene Lhx8 is required for the development of many cholinergic neurons in the mouse forebrain." Proc Natl Acad Sci U S A **100**(15): 9005-9010.
- Zhong, J. (2016). "RAS and downstream RAF-MEK and PI3K-AKT signaling in neuronal development, function and dysfunction." Biol Chem **397**(3): 215-222.
- Zhou, Y., T. Kaiser, P. Monteiro, X. Zhang, M. S. Van der Goes, D. Wang, B. Barak, M. Zeng, C. Li, C. Lu, M. Wells, A. Amaya, S. Nguyen, M. Lewis, N. Sanjana, Y. Zhou, M. Zhang, F. Zhang, Z. Fu and G. Feng (2016). "Mice with Shank3 Mutations Associated with ASD and Schizophrenia Display Both Shared and Distinct Defects." Neuron **89**(1): 147-162.
- Zhu, G., L. Du, L. Jin and A. Offenhausser (2016). "Effects of Morphology Constraint on Electrophysiological Properties of Cortical Neurons." Sci Rep **6**: 23086.